

**Univerza v Ljubljani**

**Fakulteta za elektrotehniko**

**Gorazd Pucihar**

**Vsiljena transmembranska napetost in  
elektropermeabilizacija celic v kulturah *in vitro***

**DOKTORSKA DISERTACIJA**

**Ljubljana, 2006**

**Univerza v Ljubljani**

**Fakulteta za elektrotehniko**

**mag. Gorazd Pucihar, univ. dipl. inž. el.**

**Vsiljena transmembranska napetost in  
elektropermeabilizacija celic v kulturah *in vitro***

**DOKTORSKA DISERTACIJA**

**Mentor: docent dr. Tadej Kotnik**

**Somentor: znanstveni svetnik dr. Justin Teissié**

**Ljubljana, 2006**

**University of Ljubljana**

**Faculty of Electrical Engineering**

**Gorazd Pucihar, M.Sc.**

**Induced Transmembrane Voltage and  
Electropermeabilization of Cells in Cultures *in vitro***

**DOCTORAL THESIS**

**Mentor: Assist. Prof. Tadej Kotnik, Ph.D.**

**Co-mentor: Director of Research Justin Teissié, Ph.D.**

**Ljubljana, 2006**

## **DECLARATION**

The author herewith states that the content of the thesis is a result of his own research work supervised by mentors Assistant Professor Tadej Kotnik, Ph.D. and Justin Teissié, Ph.D. Results achieved in collaboration with other colleagues were published in papers presented in the Appendix. The assistance from other colleagues is stated in the Acknowledgements. Published results of other authors are listed in the List of References.

Gorazd Pucihar

## **IZJAVA**

Izjavljam, da sem doktorsko disertacijo izdelal sam, pod mentorstvom doc. dr. Tadeja Kotnika in dr. Justin Teisséja. Rezultati, ki so nastali v sodelovanju z drugimi sodelavci, so bili objavljeni v člankih, zbranih v dodatku. Izkazano pomoč ostalih sodelavcev sem v celoti navedel v zahvali. Že objavljeni dosežki drugih avtorjev so navedeni v spisku literature.

Gorazd Pucihar

## Acknowledgements

First, I would like to thank my mentor, dr. Tadej Kotnik, for his guidance, advices, support and patience during the making of this thesis. I am grateful for the inspiring discussions on science we had, for the time he spent on correcting and improving my papers, for the not so scientific but rather dynamic debates on basketball, stock exchange, politics, music and important existential issues (“*Ah Koto, kam gre ta svet?*”). I would also like to apologize for the argues we had during my studies, which resulted from my doubtful and suspicious nature, and also for the unconventional telephone calls he sometimes received in the crack of dawn.

Special thanks to my co-mentor, dr. Justin Teissié, who was willing to accept me to his laboratory and let me ‘play’ with his machines. I am grateful for numerous discussions on electroporabilization, for the enthusiasm he showed for my results and for helping me getting around in the lab and outside of it. I sincerely apologize for the bad moments I had, which were a result of intense work and the tight time schedules. I had a great time in his lab and I will probably come back, if not for research at least to go skiing to Pyrenees.

My research work began when I joined the Laboratory of Biocybernetics (Ljubljana, Slovenia), supervised by dr. Damijan Miklavčič, when I was still an undergraduate student. He introduced me to the exciting field of Biomedical Engineering and gave me the opportunity to actively participate in the research work of the laboratory, for which I am deeply grateful. With his suggestions, ideas and experience he also actively participated in the progress of this thesis.

Thanks to dr. Lluís M. Mir from the Institute Gustave-Roussy (Villejuif, France) and dr. Ratko Magjarević from the Faculty of Electrical Engineering and Computing (Zagreb, Croatia) for evaluation of the thesis, and to dr. Didier Fournier from the Institute of Pharmacology and Structural Biology (Toulouse, France) for participating in the defense committee.

I also thank to dr. Marie-Pierre Rols, dr. Muriel Golzio, dr. Cyril Favard, dr. Laetitia Hellaudais, Jean-Michel Escoffre, Claire Millot and other people and students working or cooperating with the group of dr. Justin Teissié during my staying at the Institute of Pharmacology and Structural Biology, for the help with cells, chemicals, machines, for interesting discussions and for the hospitality.

This study was performed in a wonderful atmosphere created by my co-workers of the Laboratory of Biocybernetics. Thank you for your help, stimulating discussions and for all the crazy and unforgettable moments we had. Special thanks to Karel Flisar and dr. Marko Puc for building the electropulsation device and a switcher unit.

Thanks to my family, my two brothers and sister for their love and understanding. It was much easier to accomplish the goals with your great support and I am glad that my achievements make you so proud and happy.

This postgraduate study was financed by the Ministry of Higher Education, Science and Technology of Slovenia. Experimental work and staying in France were partly financed by the EGIDE scholarship and the French-Slovenian Scientific Cooperation (PROTEUS and PICS programs).

# Table of contents

<b>I RAZŠIRJENI POVZETEK .....</b>	<b>5</b>
<b>1 Uvod .....</b>	<b>5</b>
1.1 Mirovalna transmembranska napetost.....	5
1.2 Vsiljena transmembranska napetost.....	5
1.3 Elektropermeabilizacija .....	6
1.3.1 Zgodovina elektropermeabilizacije in eksperimentalni rezultati.....	8
1.4 Namen naloge .....	8
1.4.1 Meritve mirovalne transmembranske napetosti .....	8
1.4.2 Meritve vsiljene transmembranske napetosti na posameznih okroglih celicah, posameznih celicah nepravilnih oblik in celičnih skupkih.....	9
1.4.3 Numerični izračuni vsiljene transmembranske napetosti na posameznih okroglih celicah, posameznih celicah nepravilnih oblik in celičnih skupkih .....	10
1.4.4 Opazovanje poteka elektropermeabilizacije na posameznih okroglih celicah, posameznih celicah nepravilnih oblik, celičnih skupkih in gostih celičnih suspenzijah.....	10
<b>2 Materiali in metode .....</b>	<b>10</b>
2.1 Meritve mirovalne transmembranske napetosti .....	10
2.2 Meritve vsiljene transmembranske napetosti na posameznih okroglih celicah, posameznih celicah nepravilnih oblik in celičnih skupkih.....	11
2.2.1 Kalibracija di-8-ANEPPS .....	12
2.3 Numerični izračuni vsiljene transmembranske napetosti na posameznih okroglih celicah, posameznih celicah nepravilnih oblik in celičnih skupkih.....	12
2.3.1 Gradnja tridimenzionalnega modela celice.....	12
2.3.2 Modeliranje celične membrane .....	13
2.3.3 Nastavitve modela in izračuni vsiljene transmembranske napetosti .....	13
2.4 Opazovanje poteka elektropermeabilizacije na posameznih okroglih celicah, posameznih celicah nepravilnih oblik, celičnih skupkih in gostih celičnih suspenzijah.....	14
2.4.1 Permeabilizacija na posameznih okroglih celicah, posameznih celicah nepravilnih oblik in celičnih skupkih .....	14
2.4.2 Kinetika prenosa barvila skozi permeabilizirano membrano .....	15
2.4.3 Elektropermeabilizacija gostih celičnih suspenzij .....	15
<b>3 Rezultati in razprava.....</b>	<b>16</b>
3.1 Meritve mirovalne transmembranske napetosti .....	16
3.2 Meritve in izračuni vsiljene transmembranske napetosti ter permeabilizacija na posameznih okroglih celicah, posameznih celicah nepravilnih oblik in celičnih skupkih .....	17
3.2.1 Okrogla celica.....	17
3.2.2 Celica nepravilne oblike.....	19
3.2.3 Celični skupki in goste celične suspenzije .....	21
3.2.3.1 Goste celične suspenzije.....	24
3.2.3.2 Kinetika prenosa molekul čez permeabilizirano membrano.....	25

<b>4 Zaključek .....</b>	<b>26</b>
4.1 Meritve mirovalne transmembranske napetosti.....	26
4.2 Meritve in izračuni vsiljene transmembranske napetosti ter permeabilizacija na posameznih okroglih celicah .....	26
4.3 Meritve in izračuni vsiljene transmembranske napetosti ter permeabilizacija na posameznih celicah nepravilnih oblik .....	27
4.4 Meritve in izračuni vsiljene transmembranske napetosti ter permeabilizacija na celičnih skupkih .....	27
4.4.1 <i>Elektropermeabilizacija gostih celičnih suspenzij</i> .....	27
4.4.2 <i>Kinetika prenosa molekul čez permeabilizirano membrano</i> .....	27
4.5 Smernice za nadaljnje delo .....	28
<b>5 IZVIRNI PRISPEVKI K ZNANOSTI.....</b>	<b>29</b>
<b>II ABSTRACT.....</b>	<b>31</b>
<b>III RESUMÉ.....</b>	<b>35</b>
<b>1 INTRODUCTION.....</b>	<b>39</b>
1.1 Resting and induced transmembrane voltage .....	39
1.1.1 Resting transmembrane voltage.....	39
1.1.2 Induced transmembrane voltage .....	41
1.2 Measurements of resting and induced transmembrane voltage .....	43
1.2.1 Microelectrodes .....	43
1.2.1.1 <i>Patched electrodes</i> .....	44
1.2.1.2 <i>Patch clamp recordings</i> .....	45
1.2.2 Potentiometric fluorescent dyes.....	46
1.2.2.1 <i>Slow dyes</i> .....	47
1.2.2.2 <i>Fast dyes</i> .....	48
1.2.2.3 <i>Calibration</i> .....	49
1.3 Electropermeabilization .....	50
1.3.1 Theoretical models of electropermeabilization.....	50
1.3.2 A brief history of electropermeabilization and the experimental results .....	51
1.3.3 Parameters that influence cell electropermeabilization .....	52
1.4 Objectives of the study.....	55
1.4.1 Measurements of resting transmembrane voltage.....	56
1.4.2 Measurements of induced transmembrane voltage on single spherical cells, single irregularly shaped cells and cell clusters .....	57
1.4.3 Numerical calculations of induced transmembrane voltage on single spherical cells, single irregularly shaped cells and cell clusters .....	57
1.4.4 Electropermeabilization of single spherical, single irregularly shaped cells, cell clusters, and dense cell suspensions .....	57
<b>2 MATERIALS AND METHODS .....</b>	<b>59</b>
2.1 Cells, media and chemicals .....	59
2.1.1 Cells.....	59
2.1.2 Media .....	59

2.1.3 Chemicals .....	61
2.2 Measurements of resting transmembrane voltage .....	62
2.3 Measurements of induced transmembrane voltage on single spherical cells, single irregularly shaped cells and cell clusters .....	64
2.3.1 Calibration of di-8-ANEPPS .....	66
2.4 Numerical calculations of induced transmembrane voltage on single spherical cells, single irregularly shaped cells and cell clusters .....	67
2.4.1 Construction of a three-dimensional model of a cell .....	67
2.4.2 Modeling the cell membrane .....	68
2.4.3 Settings of the model and subsequent computations of induced transmembrane voltage .....	70
2.4.4 Electrodes .....	71
2.5 Electroporation of single spherical cells, irregularly shaped cells, cell clusters, and dense cell suspensions .....	71
2.5.1 Visualization of electroporation on single spherical cells, irregularly shaped cells and cell clusters .....	71
2.5.2 Kinetics of dye transport through electroporated membrane .....	74
2.5.3 Differences between the imaging system used for following electroporation .....	77
2.5.4 Electroporation of dense cell suspensions .....	77
2.6 Test for gap junctions .....	78
<b>3 MEASUREMENTS OF RESTING TRANSMEMBRANE VOLTAGE .....</b>	<b>81</b>
3.1 Results .....	81
3.2 Discussion .....	82
<b>4 SPHERICAL CELLS .....</b>	<b>85</b>
4.1 Results .....	85
4.1.1 Measurements of induced transmembrane voltage .....	85
4.1.2 Numerical calculations of induced transmembrane voltage .....	86
4.1.3 Visualization of cell electroporation .....	88
4.1.3.1 <i>The influence of pulse parameters on the course of cell electroporation</i> .....	89
4.2 Discussion .....	99
<b>5 IRREGULARLY SHAPED CELLS .....</b>	<b>103</b>
5.1 Results .....	103
5.1.1 Measurements and calculations of induced transmembrane voltage, and permeabilization of irregularly shaped cells .....	104
5.1.2 The influence of electric field orientation on induced transmembrane voltage .....	118
5.1.3 The influence of resting transmembrane voltage on the total membrane voltage .....	120
5.2 Discussion .....	122
<b>6 CELL CLUSTERS AND DENSE CELL SUSPENSIONS .....</b>	<b>125</b>
6.1 Results – Cell clusters .....	125
6.1.1 Measurements and calculations of induced transmembrane voltage on cell clusters and visualization of permeabilization .....	125

6.1.1.1 <i>Induced transmembrane voltage calculated on a cell inside the cluster and on the same cell isolated</i> .....	140
6.1.2 Test for gap junctions .....	141
6.2 Results – Dense cell suspensions .....	144
6.3 Kinetics of transmembrane transport of small molecules after electropermeabilization.....	145
6.3.1 Cell suspensions .....	145
6.3.2 Single cells.....	148
6.3.3 Attached cells .....	149
6.4 Discussion .....	151
6.4.1 Cell clusters .....	151
6.4.2 Kinetics of dye transport.....	154
<b>7 CONCLUSIONS .....</b>	<b>157</b>
7.1 Measurements of resting transmembrane voltage .....	157
7.2 Measurements and calculations of induced transmembrane voltage and visualization of permeabilization on spherical cells .....	157
7.3 Measurements and calculations of induced transmembrane voltage and visualization of permeabilization on irregularly shaped cells.....	158
7.4 Measurements and calculations of induced transmembrane voltage and visualization of permeabilization on cell clusters .....	158
7.4.1 Electropermeabilization of dense cell suspensions.....	159
7.4.2 Kinetics of transmembrane transport of dye molecules after electropermeabilization .....	159
7.5 Guidelines for future work .....	159
<b>8 ORIGINAL SCIENTIFIC CONTRIBUTIONS.....</b>	<b>161</b>
<b>9 REFERENCES.....</b>	<b>163</b>
<b>10 APPENDIX.....</b>	<b>173</b>

# I RAZŠIRJENI POVZETEK

## 1 UVOD

Z električnega vidika predstavlja celična membrana tanek izolacijski sloj, ki loči dve električno prevodni področji – citoplazmo in zunajcelični prostor. Lipidi, ki so glavni gradniki membrane, se v njej organizirajo v dvosloj, v katerem so polarne glave lipidov obrnjene navzven, nepolarni repi pa navznoter. Tudi proteini, ki se nahajajo v membrani, so zgrajeni iz polarnih in nepolarnih področij, v membrano pa se vgradijo tako, da so nepolarni deli v notranjosti membrane, torej v stiku z repi lipidov, polarni deli pa segajo navzven. Zaradi takšne zgradbe voda in v njej raztopljeni ioni obdajajo membrano, v njeno notranjost pa ne morejo oziroma so iz nje hitro izrinjeni.

### 1.1 Mirovalna transmembranska napetost

Na celični membrani je stalno prisotna električna napetost, ki je posledica majhnega primanjkljaja pozitivnih ionov v citoplazmi. Ta primanjkljaj ustvari in vzdržuje sistem črpalk  $Na^+ - K^+$  in trajno prepustnih kanalov  $K^+$ . Napetost, ki ji pravimo mirovalna transmembranska napetost, določa Goldmanova enačba (Alberts et al., 1994):

$$U_{RTV} = \frac{R \cdot T}{F} \ln \frac{q [Na^+]_e + [K^+]_e}{q [Na^+]_i + [K^+]_i} \quad (1.1)$$

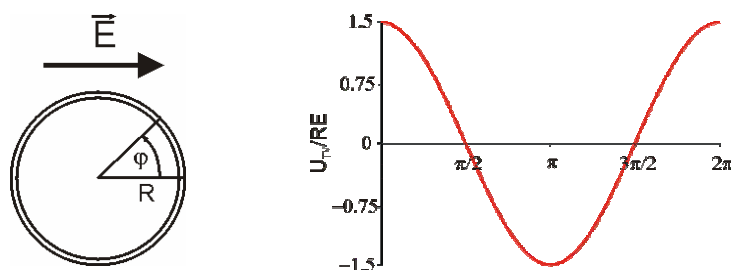
kjer je  $R$  plinska konstanta,  $T$  absolutna temperatura,  $F$  Faradayeva konstanta,  $q$  razmerje prepustnosti membrane za  $Na^+$  in  $K^+$ ,  $[Na^+]_e$ ,  $[K^+]_e$ ,  $[Na^+]_i$ , in  $[K^+]_i$  pa so koncentracije ionov zunaj in znotraj celice.

### 1.2 Vsiljena transmembranska napetost

Vsiljena transmembranska napetost nastane zaradi prerazporeditve ionov v električnem polju. Med trajanjem električnih pulzov se ta napetost prišteje mirovalni, po koncu pulzov pa na membrani ponovno ostane samo mirovalna napetost. Ustaljeno vrednost, ki jo vsiljena napetost na membrani okrogle celice doseže v nekaj mikrosekundah po vklopu enosmernega polja, opisuje Schwanova enačba (Schwan, 1957; Kotnik et al., 1997):

$$U_{ITV} = 1.5RE \cos \varphi, \quad (1.2)$$

kjer je  $E$  jakost zunanjega električnega polja,  $R$  polmer celice,  $\varphi$  pa kot med smerjo polja in daljico, ki poteka od središča celice do obravnavane točke na membrani. Vsiljena membranska napetost se tako za razliko od mirovalne, ki je povsod po membrani enaka, spreminja z lego, kot to določa kosinus v Schwanovi enačbi (Slika 1.1). Schwanova enačba pove tudi, da je vsiljena membranska napetost sorazmerna jakosti zunanjega električnega polja. Če celica ni okrogla, velja Schwanova enačba zanjo le približno. Za nekatere pravilne geometrijske oblike, kot so sferoidi in elipsoidi, lahko izpeljemo natančne izraze, ki veljajo namesto Schwanove enačbe (Kotnik in Miklavčič, 2000a; Gimsa in Wachner, 2001a), pri bolj nepravilnih oblikah celic pa vsiljeno napetost izračunamo numerično (Pucihar et al., 2006).

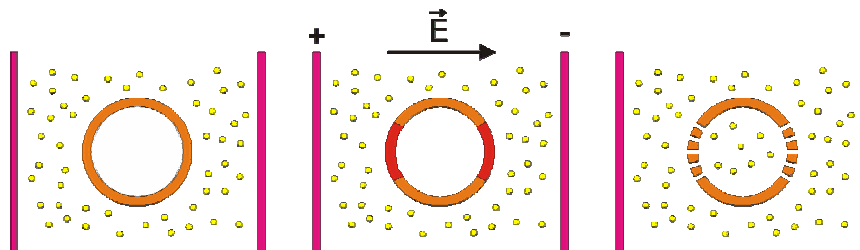


Slika 1.1. (A) Model okrogle celice. (B) Odvisnost vsiljene napetosti od položaja na celični membrani.

### 1.3. Elektropermeabilizacija

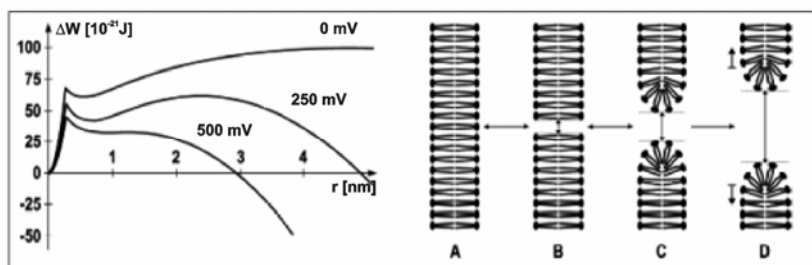
Elektropermeabilizacija je metoda, ki omogoča umetno povečanje prepustnosti membrane s kratkotrajno izpostavitvijo celice dovolj močnemu električnemu polju. Če električno polje ni premočno in ne traja več kot nekaj milisekund, se po koncu izpostavitve prepustnost membrane postopoma zniža na začetno raven, celice pa ohranijo svoje fiziološko delovanje; govorimo o reverzibilni elektropermeabilizaciji. Povišanje prepustnosti nastopi že v nekaj mikrosekundah, okrevanje pa je mnogo počasnejše in se popolnoma zaključi šele po več sekundah ali minutah.

V času povišane prepustnosti membrane je mogoč vnos različnih učinkovin v celico. Manjše molekule, vstopajo vanjo z difuzijo, k pretoku ionov in električno nabitih molekul, predvsem večjih (npr. DNA in proteinov), pa v času delovanja električnega polja prispeva tudi elektroforetska sila, ki jo ustvarja električno polje. Uporaba elektropermeabilizacije za vnos snovi v celico sega danes od temeljnih raziskav v biokemiji in molekularni biologiji, prek uporabnih raziskav v biotehnologiji in farmaciji, do predklinične in klinične uporabe v onkologiji in genski terapiji (Neumann et al., 1999; Teissié et al., 1999). Kombinacija elektropermeabilizacije in kemoterapevtikov (elektrokemoterapija) se je izkazala kot zelo uspešna metoda zdravljenja kožnih in podkožnih tumorjev in se že uveljavlja v kliničnem okolju (Mir in Orłowski, 1999; Heller et al., 1999; Serša et al., 2003; Miklavčič et al., 2005). Uporaba elektropermeabilizacije za vnos DNA (elektrogenska terapija) je še v predklinični fazi, rezultati pa obetajo ponovljivo in predvsem varnejšo alternativo genski transfekciji z virusnimi vektorji (Somari et al., 2000; Šatkauskas et al., 2002; Golzio et al., 2005).



Slika 1.2. Elektropermeabilizacija.

Obstaja več teoretičnih modelov, ki skušajo razložiti, kako izpostavitve električnim pulzom privede do povišane prepustnosti membrane. Med njimi so takšni, ki skušajo pojav razložiti z elektrokompresijo membrane, z denaturacijo membranskih kanalov, pa tudi s tvorbo razpok med lipidnimi mikropodročji. Nobena od naštetih razlag, katerih podrobnejši pregled najdemo v članku Weaverja in Čizmadževa (Weaver in Chizmadzev, 1996), ni našla podpore v eksperimentalnih rezultatih. Danes je najbolj uveljavljen model, ki povišanje prepustnosti membrane pripisuje nastanku hidrofilnih por v membrani (Weaver in Mintzer, 1981; Glaser et al., 1988). Ta model napoveduje, da povišana membranska napetost zmanjšuje energijo, potrebno za nastanek hidrofilnih por, s tem pa povečuje verjetnost takšnega dogodka (Slika 1.3). S tem razloži tudi postopnost in počasnost okrevanja, saj mora vsaka pora za svoje zaprtje spet preseči določen energijski prag. Model elektroporacije predvideva, da je premer hidrofilnih por velikostnega razreda enega nanometra, z naraščanjem membranske napetosti pa stabilnost pore hitro upada, dokler pri nadkritični napetosti reda nekaj sto mV ne pride do ireverzibilne porušitve.



Slika 1.3. Energija membranske pore v odvisnosti od njenega polmera (levo) in skica elektroporacije na molekularnem nivoju (desno). Po zakonih termodinamike minimumi energije pore ustrezajo stabilnim stanjem. Prvi minimum je pri polmeru nič, ko pore ni, torej tedaj, ko membrana ni elektroporirana (desno, A). Koničast maksimum energije, ki sledi, predstavlja prag, pri katerem se pora preoblikuje iz hidrofobne (B) v hidrofilno obliko (C, D). Napetost na membrani ta prag zniža, kar poveča verjetnost nastanka hidrofilnih por. Če ta napetost ni previsoka, sledi še en minimum energije, v katerem se hidrofilna pora ustali (C), to pa omogoči tudi poznejše okrevanje (reverzibilna permeabilizacija). Pri previsoki napetosti ta minimum izgine, pora ob raztezanju več ne doseže stabilnosti (D), okrevanje pa ni več mogoče (ireverzibilna permeabilizacija).

Simulacije molekularne dinamike lipidov v splošnem potrjujejo, da membranska napetost, ki za velikostni razred presega mirovalno vrednost, poviša verjetnost oziroma pogostost nastanka por, pride pa tudi do spontanega oblikovanja hidrofilne notranjosti pore – zaradi

vode in ionov v pori se lipidi v njej reorientirajo tako, da z glavami segajo v njeno notranjost (Tieleman et al., 2003; Leontiadou et al., 2004; Kasson et al., 2004).

### ***1.3.1 Zgodovina elektropermeabilizacije in eksperimentalni rezultati***

Kot prvi je o električni porušitvi celične membrane leta 1958 poročal Stämpfli (Stämpfli, 1958). Približno desetletje kasneje sta Sale in Hamilton objavila serijo člankov, v katerih sta opisala netermično uničevanje mikroorganizmov s kratkimi električnimi pulzi visoke napetosti (Sale in Hamilton, 1967; Hamilton in Sale, 1967; Sale in Hamilton, 1968). Leta 1972 pa sta Neumann in Rosenheck (Neumann in Rosenheck, 1972) pokazala, da lahko električni pulzi povzročijo znatno, a reverzibilno povišanje prepustnosti membrane, ki ga lahko uporabimo za vnos snovi v celico. Njune ugotovitve predstavljajo mejnik v raziskovanju elektropermeabilizacije, saj so vzbudile zanimanje širšega kroga raziskovalcev, eksperimentalni podatki pa so se nato pričeli kopičiti hitreje in bolj sistematično. Prve sistematične raziskave elektropermeabilizacije so temeljile na meritvah električnih lastnosti membrane med izpostavitvijo električnim pulzom. Te meritve so pokazale, da v primeru, ko napetost na membrani preseže določeno kritično vrednost (med 0.2 V in 1 V, odvisno od vrste celic in eksperimentalnih pogojev), že nekaj mikrosekund po začetku električnega pulza zaznamo spremembo prevodnosti in kapacitivnosti membrane (Babakov in Ermishkin, 1966; Neumann in Rosenheck, 1972). Če pulzi niso predolgi, se po njihovem koncu kapacitivnost in prevodnost membrane postopoma vrne v začetno stanje. Več raziskovalcev je poizkušalo elektropermeabilizacijo opazovati pod mikroskopom. Vsi poskusi so bili neuspešni in še danes je nemogoče neposredno opazovati nastanek por med elektropermeabilizacijo (Chang in Reese, 1990). Zato preostane le posredno opazovanje, pri katerem lahko s katerim od potenciometričnih barvil, ki se vgradijo v membrano, opazujemo spremembe membranske napetosti, s katerim od fluorescentnih barvil pa lahko opazujemo pretok snovi skozi membrano. Na ta način so ugotovili, da spremembe membranske napetosti nastopijo že v prvih mikrosekundah po začetku električnih pulzov in da že v manj kot mikrosekundi po začetku pulza membranska napetost dobi komponento kosinusne oblike, kot to predvideva Schwanova enačba. Če je napetost dovolj visoka, se kosinusna porazdelitev na področjih, kjer presega določeno kritično vrednost, v naslednjih nekaj mikrosekundah spet zniža, kar odraža začetek elektroporacije tistega področja membrane (Hibino et al. 1991; Hibino et al., 1993).

### **1.4 Namen naloge**

Kot smo že omenili se elektropermeabilizacija pojavi na tistih področjih celične membrane, kjer vsota vsiljene transmembranske napetosti (VTN) in mirovalne transmembranske napetosti (MTN) preseže kritično vrednost. Pri običajnih primerih uporabe permeabilizacije (npr. vnos molekul DNK v celico) želimo doseči učinkovito in hkrati reverzibilno elektropermeabilizacijo. Zato je največkrat potrebno poskuse načrtovati, kar vključuje tudi približno oceno amplitude VTN na celicah, ki bo povzročila permeabilizacijo. Težava nastopi, kadar želimo poskuse opravljati na tkivih, kjer je celična geometrija bolj zapletena. Poleg tega

so celice v tkivih dovolj blizu skupaj, da vplivajo na porazdelitev električnega polja okrog njih, velikokrat pa so tudi povezane med sabo s prevodnimi kanali oz. presledkovnimi stiki (angl. 'gap junctions'). V takih primerih analitične rešitve za VTN ni mogoče izpeljati, lahko pa jo določimo z numeričnimi metodami. Zaradi zapletene strukture tkiva so numerični modeli večinoma makroskopski, kjer podrobna zgradba tkiva ni upoštevana. Kadar pa so modeli mikroskopski, so večinoma zgrajeni iz preprostih geometrijskih oblik (polkroglja, kvader) in predstavljajo le slab približek realni strukturi. Da bi bolje razumeli kako električno polje deluje na tkivo na ravni posameznih celic (mikroskopski model), ki kot celota določajo makroskopsko obnašanje tkiva, smo zgradili realistične mikroskopske modele celic nepravilnih oblik, skupkov takšnih celic ter gostih celičnih suspenzij. Takšni celični sestavi so po obliki, gostoti in povezavah med celicami, podobni celicam v tkivu. Raziskavo smo začeli z meritvami MTN na celicah, ki smo jih uporabili v nadaljnjih poskusih. Nato smo izračunali VTN na modelih posameznih okroglih celic in celic nepravilnih oblik ter celičnih skupkih in te izračune primerjali z meritvami VTN na istih celicah, ki so bile uporabljene za gradnjo modelov. Na teh celicah smo opazovali tudi potek elektropermeabilizacije in rezultate primerjali z meritvami in izračuni VTN. Z dodatnimi poskusi smo bolj natančno preučili kinetiko pretoka snovi skozi membrano v celice med in po permeabilizaciji. Na koncu smo izračunali še VTN na modelu celic v gostih suspenzijah in te izračune primerjali z deležem permeabiliziranih celic, ki smo ga izmerili na suspenzijah z različnimi gostotami. Naslednji odstavki vsebujejo bolj natančen opis omenjenih poskusov in numeričnih pristopov.

#### **1.4.1 Meritve mirovalne transmembranske napetosti**

Med izpostavitvijo električnemu polju se mirovalni napetosti (MTN) na membrani prišteje še vsiljena napetost (VTN). Ker je MTN znatno nižja od VTN jo ponavadi zanemarimo, in VTN pa vzamemo kot približek celotni napetosti na membrani. V tej raziskavi smo določili velikost MTN na različnih celičnih linijah in ocenili njen prispevek k celotni napetosti. Poleg tega smo MTN izmerili tudi na celicah v zunajceličnih medijih z različno sestavo in prevodnostmi. Meritve smo primerjali z izračuni in predpostavkami, ki smo jih naredili v naši prejšnji raziskavi o vplivu takih medijev na permeabilizacijo celic (**članek 4** v Dodatku, Pucihar et al., 2001).

#### **1.4.2 Meritve vsiljene transmembranske napetosti na posameznih okroglih celicah, posameznih celicah nepravilnih oblik in celičnih skupkih**

Kvantitativne meritve vsiljene transmembranske napetosti (VTN) na posameznih okroglih celicah, celicah nepravilnih oblik in celičnih skupkih so bile narejene s pomočjo potenciometričnega fluorescentnega barvila. S temi meritvami je bilo mogoče preučiti vpliv oblike, gostote in povezav med celicami na porazdelitev VTN na posameznih celicah in celičnih skupkih. Poskusi so pokazali ali se celice v skupkih, kadar jih izpostavimo zunanjemu električnemu polju, obnašajo kot posamezne, med seboj izolirane celice, ali kot med seboj povezana velika celica.

### **1.4.3 Numerični izračuni vsiljene transmembranske napetosti na posameznih okroglih celicah, posameznih celicah nepravilnih oblik in celičnih skupkih**

Glavne težave pri numeričnem modeliranju bioloških celic so povezane z realističnim modeliranjem celice in njene membrane. Modeli, v katerih je celica zgrajena iz preprostih geometrijskih oblik ali iz kombinacije takih oblik, so ponavadi le grobi približki dejanski obliki celice (Fear in Stuchly, 1998a; Fear in Stuchly, 1998b; Cheng et al., 1999; Buitenweg et al., 2003; Valič et al., 2003). Drugo težavo predstavlja celična membrana, ki je za nekaj velikostnih razredov tanjša od dimenzij tipične celice in predstavlja težavo pri graditvi mreže. Poleg tega je enakomerno debelino membrane pri modelih celic nepravilnih oblik težko zagotoviti. Predstavili smo metodo za izgradnjo realističnih 3D modelov celic nepravilnih oblik in celičnih skupkov ter metodo s katero membrano v modelu nadomestimo z robnim pogojem. Ker smo modele zgradili iz slik celic na katerih so bile narejene meritve (glej 1.4.2) smo lahko numerično izračunano VTN primerjali z izmerjeno.

### **1.4.4 Opazovanje poteka elektropermeabilizacije na posameznih okroglih celicah, posameznih celicah nepravilnih oblik, celičnih skupkih in gostih celičnih suspenzijah**

Z uporabo fluorescentnega barvila Propidijev Jodid smo najprej preučili potek permeabilizacije na posameznih celicah in celičnih skupkih. Ti poskusi so pokazali ali se celice v skupkih med elektropermeabilizacijo obnašajo kot posamezne celice ali kot med seboj povezana velika celica. Rezultate permeabilizacije smo nato primerjali z meritvami in izračuni VTN (poglavje 1.4.2 in 1.4.3). Na podlagi teh rezultatov smo poskušali določiti kritično vrednost VTN pri kateri nastopi permeabilizacija. Z opazovanjem vnosa molekul barvila Propidijev Jodid v posamezne celice, celične suspenzije in celice v kulturah, smo spremljali kako hitro po vključitvi polja pride do vnosa molekul v permeabilizirano celico. Na koncu smo določili še učinkovitost permeabilizacije celic v suspenzijah z naraščajočo gostoto celic in dobljene rezultate primerjali s permeabilizacijo v redkih celičnih suspenzijah.

## **2 MATERIALI IN METODE**

### **2.1 Meritve mirovalne transmembranske napetosti**

Uporabili smo potenciometrično fluorescentno barvilo TMRM. Barvilo se na spremembe membranske napetosti odziva v nekaj sekundah, vendar s precejšnjo spremembo v intenziteti fluorescence (60 - 80 % na 100 mV) (Ehrenberg et al., 1988; Farkas et al., 1989). Delovanje barvila temelji na njegovi prerazporeditvi med zunanostjo in notranostjo celice v odvisnosti od napetosti na membrani. Ker se praktično ne vgrajuje v membrano in je intenziteta fluorescence sorazmerna s koncentracijo barvila, lahko MTN določimo z uporabo Nernstove enačbe:

$$U_{RTV} = \frac{R \cdot T}{F} \cdot \ln \frac{F_o}{F_i}, \quad (2.1)$$

kjer sta  $F_o$  in  $F_i$  izmerjeni intenziteti fluorescence zunaj in znotraj celice, medtem ko so  $R$ ,  $T$  in  $F$  standardne termodinamične konstante. Meritve smo izvedli na CHO WTT celicah v suspenziji ter različnih celicah v monoslojih (CHO K1, B16 F1, BHK).

Približno 15-20 minut pred meritvami, smo celicam dodali barvilo TMRM (0.5  $\mu$ M, Sigma-Aldrich, Nemčija) fluorescenco pa smo opazovali s konfokalnim mikroskopom (Zeiss 100M, objektiv  $\times 63$ , vodna imerzija, Zeiss, Nemčija). Barvilo smo vzbujali z laserjem z valovno dolžino 534 nm, njegovo fluorescenco pa zaznali pri valovnih dolžinah  $> 564$  nm. Fluorescenčne slike smo zajemali s sistemom fotopomnoževalk (Zeiss, Nemčija) ter jih obdelali s programskim orodjem FLM 520 (Zeiss, Nemčija). Fluorescenco znotraj celice ( $F_i$ ) smo določili kot povprečno fluorescenco izbranega področja na mestu, kjer se nahaja jedro (Ehrenberg et.al, 1988), fluorescenco zunaj celice ( $F_o$ ) pa s povprečjem intenzitete izbranega področja v neposredni bližini celice.

Pred meritvami MTN na celicah v medijih z različno sestavo in različno električno prevodnostjo smo celicam zamenjali gojišče z izbranim medijem, ki je vseboval 0.5  $\mu$ M TMRM. Postopek smo nato nadaljevali kot smo opisali zgoraj. MTN je bila izmerjena na celicah v gojiščih, treh kalijevih medijih z različnimi prevodnostmi (K-ZAP: 10 mM, 5 mM, 1 mM  $K_2HPO_4/KH_2PO_4$ , 250 mM saharoza, 1 mM  $MgCl_2$ ), treh različnih natrijevih medijih (Na-ZAP: 10 mM, 5 mM, 1 mM  $Na_2HPO_4/NaH_2PO_4$ , 250 mM saharoza, 1 mM  $MgCl_2$ ) ter nizkoprevodnem mediju iz naše prejšnje raziskave (**članek 4** v Dodatku, Pucihar et al. 2001).

## 2.2 Meritve vsiljene transmembranske napetosti na posameznih okroglih celicah, posameznih celicah nepravilnih oblik in celičnih skupkih

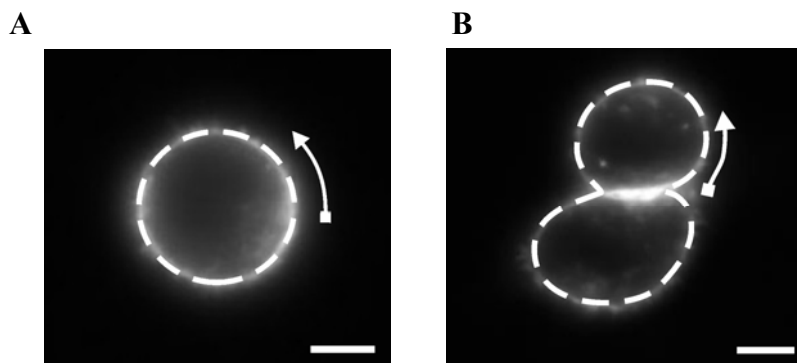
Za meritve VTN smo uporabili hitro potenciometrično fluorescentno barvilo di-8-ANEPPS (Bedlack et al., 1994; Gross et al., 1986; Montana et al., 1989). Barvilo se vgradi v celično membrano, na spremembe napetosti na membrani pa se odzove v nekaj mikrosekundah, vendar s precej nizko spremembo intenzitete fluorescence (5-10 % na 100 mV).

CHO K1 in B16F1 celicam, ki smo jih pred poskusi nasadili na krovna stekelca, smo gojišče zamenjali z medijem SMEM, ki je vseboval 30  $\mu$ M barvila di-8-ANEPPS (Molecular Probes, Leiden, Nizozemska) in 0.05% Pluronske kisline. Po 12 minutah smo raztopino z barvilom odstranili in jo nadomestili z 10 mM K-ZAP medijem. Celice smo izpostavili 100 ms, 40 V pulzu, ki je bil doveden na elektrodi z medsebojno razdaljo 4 mm. Fluorescenčne slike celic oziroma skupkov smo zajeli pred (kontrola) in med pulzom (vzbujanje 490 nm, fluorescenca 605 nm), jih odšteli, razlike v fluorescenci na izbranem področju vzdolž membrane celice pa izrazili v sivinah (Slika 2.1). Z umerjanjem barvila (glej spodaj) smo spremembe fluorescence pretvorili v vrednosti VTN, ki smo jih prikazali na grafu v odvisnosti normalizirane dolžine

loka okrog celice. Slike smo zajeli s CCD kamero (VisiCam 1280, Visitron, Nemčija) pritrjeno na mikroskop (Zeiss AxioVert 200, objektiv  $\times 100$ , in  $\times 63$  oljna imerzija, Zeiss, Nemčija) in jih obdelali z MetaMorph 5.0 (Molecular Devices Corporation, PA, ZDA).

### 2.2.1 Kalibracija di-8-ANEPPS

Celice smo pobarvali z barvilom di-8-ANEPPS kot smo opisali zgoraj. Nato smo raztopino z barvilom zamenjali s kalibracijskim medijem (10 mM Hepes, 140 mM NaCl/KCl, 1  $\mu$ M valinomicin). Koncentracije NaCl in KCl smo spreminjali tako, da smo dobili 3, 10, 50, in 140 mM koncentracijo KCl, ki ustreza membranskim napetostim -99, -68, -27, in 0 mV. Te napetosti smo dobili iz Nernstove enačbe. Pri tem smo privzeli, da znaša znotrajcelična koncentracija  $K^+$  ionov 140 mM (Alberts et al., 1994) in da membranska napetost zaradi valinomicina ustreza ravnotežni napetosti za  $K^+$ . Po 4 min inkubacije v mediju z najnižjo koncentracijo KCl (3 mM) smo zajeli sliko ter medij zamenjali z novim. Na vsaki sliki smo izmerili povprečno sivino izbranega področja okoli celice in te vrednosti pretvorili v relativne spremembe fluorescence. Iz grafa odvisnosti relativnih fluorescenc od membranske napetosti smo dobili kalibracijsko krivuljo, z naklonom 6% / 100 mV.



Slika 2.1. Izbrano področje vzdolž katerega so bile izmerjene vrednosti sivin za (A) okroglo celico, (B) skupek celic. Bela pušica označuje začetek in smer loka. Merilo predstavlja 5  $\mu$ m.

## 2.3 Numerični izračuni vsiljene transmembranske napetosti na posameznih okroglih celicah, posameznih celicah nepravilnih oblik in celičnih skupkih

### 2.3.1 Gradnja tridimenzionalnega modela celice

Tridimenzionalni modeli celic in skupkov so bili zgrajeni iz fluorescenčnih slik prereзов celic (CHO K1 in B16F1), ki so bile pobarvane z barvilom di-8-ANEPPS (glej 2.2). Sivinske slike smo zajeli iz različnih nivojev celice z istim sistemom kot smo ga opisali v poglavju 2.2 in jih nato pretvorili v črno bele slike (Sliki 2.2A in B). S pomočjo programskega paketa Femlab 3.1 (COMSOL Inc., Burlington, MA, ZDA) in Matlabovih funkcij (MathWorks Inc., Natick, MA, ZDA) smo iz črno belih slik določili robove celic (`flim2curve`), jih pretvorili v površine s 35 robovi (`solid2`) ter jih združili v 3D model celice (`loft`) (Sliki 2.2 C in D).

Model smo nato uvozili v okolje Femlab in ga postavili na dno kvadra, da bi posnemal celico, pritrjeno na krovno stekelce. Za gradnjo modela več celic (**članek 5** v Dodatku, Pucihar et al., 2005) ali celičnih skupkov smo opisani postopek ponovili za vsako celico posebej. V primeru celičnih skupkov smo posamezne modele celic nato združili.

### 2.3.2 Modeliranje celične membrane

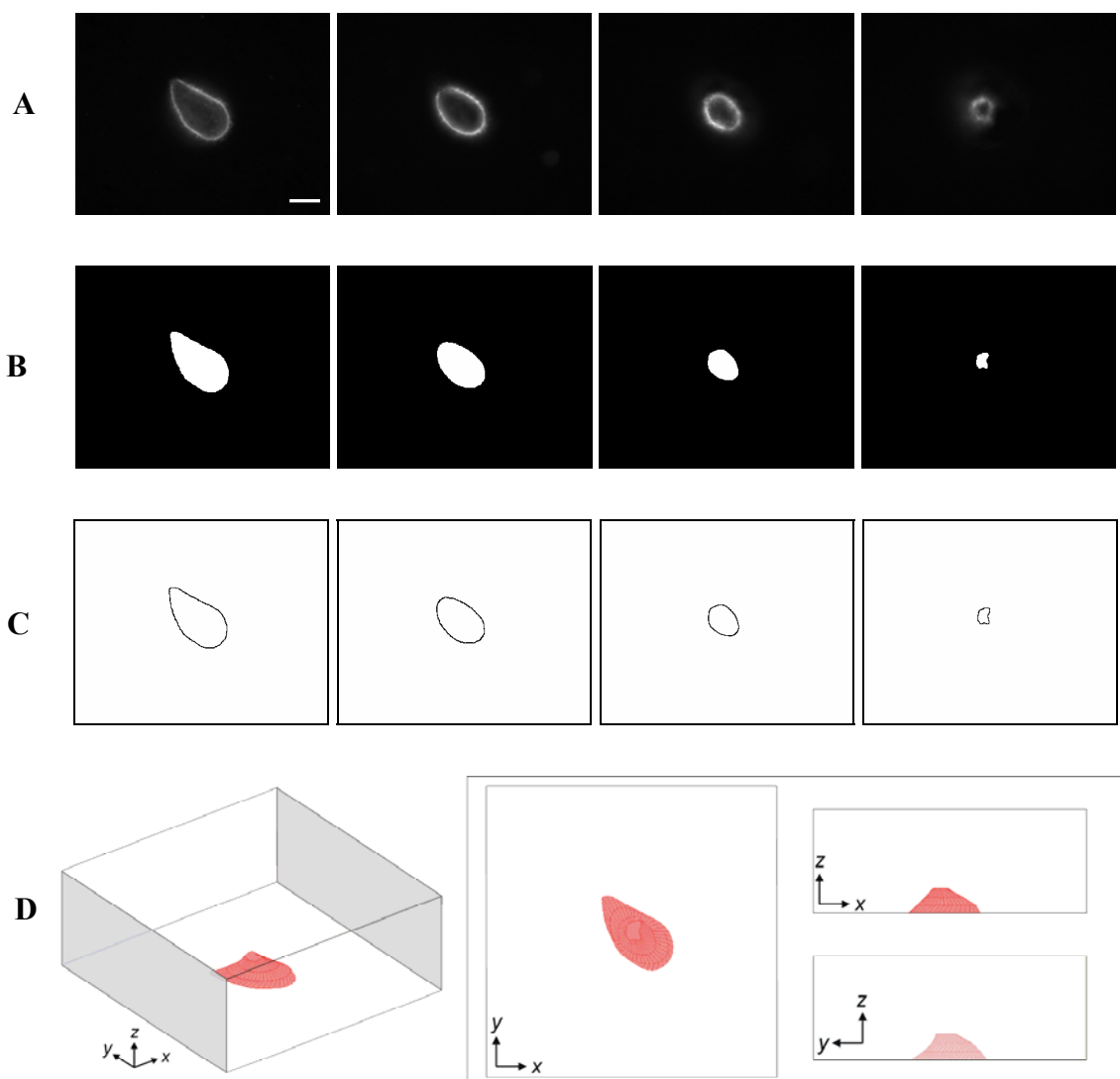
Celična membrana zaradi svoje tankosti predstavlja težavo pri gradnji modelov celic. Kadar nas porazdelitev električnega polja, gostote toka ali električni potencial znotraj membrane ne zanimata, lahko celično membrano nadomestimo s stično ploskvijo med celico in okolico, ki ji pripišemo površinsko specifično prevodnost. Vpliv membrane je namreč enak vplivu ustrezne površinske prevodnosti na stiku med zunanostjo in notranostjo celice. Zaradi nizke prevodnosti membrane, tok teče praktično pravokotno skozi membrano in ga lahko zapišemo:

$$J = \frac{\sigma_m (V_o - V_i)}{d}, \quad (2.2)$$

kjer je  $\sigma_m$  specifična prevodnost membrane ( $5 \times 10^{-7}$  S/m, Gascoyne et al., 1993),  $d$  njena debelina ( $5 \times 10^{-9}$  m, Alberts et al., 1994),  $V_o$ ,  $V_i$  pa električna potenciala zunaj in znotraj celice. Razmerje  $\sigma_m/d$  predstavlja specifično površinsko prevodnost. Kljub temu, da membrane ni v modelu je padec napetosti na stični ploskvi med zunanostjo in notranostjo celice enak VTN na membrani s specifično prevodnostjo  $\sigma_m$  in debelino  $d$ . Bolj natančna razlaga je podana v **članku 5** v Dodatku (Pucihar et al., 2006).

### 2.3.3 Nastavitve modela in izračuni vsiljene transmembranske napetosti

Specifično prevodnost notranosti modela celice smo nastavili na 0.3 S/m (Harris in Kell, 1983), prevodnost kvadra (zunajcelični medij) pa na 0.14 S/m (Rols et al., 1998). Dve nasprotni stranici kvadra sta predstavljali elektrodi z ustreznima električnima potencialoma, tako da smo med elektrodama imeli polje 100 V/cm, enako kot pri poskusih v poglavju 2.2. Ostale stranice kvadra so bile izolirane. Na stični ploskvi med celično zunanostjo in notranostjo smo določili normalno gostoto električnega toka, kot ga določa enačba 2.2. Nato smo zgradili mrežo končnih elementov in izračunali električni potencial zunaj in znotraj celice z metodo končnih elementov s programskim orodjem Femlab. VTN smo določili kot razliko električnih potencialov na obeh straneh membrane ( $VTN = V_i - V_o$ ) ter jo prikazali na grafu v odvisnosti od normalizirane dolžine loka za najnižjo ploskev v modelu.



Slika 2.2. Gradnja 3D modela celice nepravilne oblike. (A) Sivinske slike CHO celice nepravilnih oblik pobarvane z barvilom di-8-ANEPPS. Merilo predstavlja 10  $\mu\text{m}$ . (B) Črno bele slike. (C) Robovi celic. (D) Tridimenzionalni model celice sestavljen iz prerezov. Notranjost kvadra predstavlja zunajcelični medij, sive stranice so elektrode, ostale stranice kvadra so izolirane.

## 2.4 Opazovanje poteka elektropermeabilizacije na posameznih okroglih celicah, posameznih celicah nepravilnih oblik, celičnih skupkih in gostih celičnih suspenzijah

### 2.5.1 Permeabilizacija na posameznih okroglih celicah, posameznih celicah nepravilnih oblik in celičnih skupkih

Poskusi so bili narejeni na celičnih linijah CHO WTT, CHO K1 in B16F1. Celicam smo pred poskusi odstranili gojišče in ga zamenjali s kalijevim pufrom (10 mM K-ZAP) in Propidijevim Jodidom (100  $\mu\text{M}$ , PI, Sigma, Saint Louis, ZDA). Barvilo v osnovi ne prehaja skozi membrano lahko pa vstopi v permeabilizirane celice, kar se odraža v spremembi fluorescence znotraj celic. Spremembo fluorescence smo opazovali z dvema sistemoma za slikanje.

Hitri sistem za zajemanje slik je predstavljala občutljiva, hitra video kamera (LH 750-ULL, Lhesa, Cergy-Pontoise, Francija) pritrjena na mikroskop (Leica DM IRB, Nemčija). Kamera omogoča zvezno zajemanje slik v časovnem intervalu 20 ms, oziroma šest zaporednih slik s hitrostjo 1 slika/3.33 ms. Barvilo smo vzbujali s  $530 \text{ nm} < \lambda > 560 \text{ nm}$ , fluorescenco pa zaznavali pri  $> 580 \text{ nm}$ . Sistem smo uporabili za preučevanje vpliva amplitude pulzov (400, 500, 600, 700 V) in trajanja pulzov (1, 3, 5 ms) na časovni potek permeabilizacije med in takoj po pulzu. Slika, ki smo jo zajeli preden je bil doveden pulz, je služila za kontrolo, nadaljnjih pet slik pa je predstavljalo fluorescenco celice med in po pulzu.

Počasnejši sistem za zajemanje slik je sestavljala počasna CCD kamera z visoko ločljivostjo ( $1024 \times 1280$  točk, VisiCam 1280, Visitron, Nemčija) pritrjena na mikroskop (AxioVert 200, objektiv  $\times 63$  in  $\times 100$ , oljna imerzija, Zeiss, Nemčija). Ta sistem smo uporabili za določanje področij membrane, kjer se je pojavila permeabilizacija, in sicer na istih okroglih celicah, celicah nepravilnih oblik in celičnih skupkih, na katerih smo izmerili in izračunali VTN (glej 2.2 in 2.3). Slike smo zajemali s hitrostjo 1 slika /100 ms. Sliki fluorescence, ki smo jo zajeli tik pred pulzom (kontrola) smo odšteli od slik po dovedenem pulzu z uporabo programskega orodja MetaMorph 5.0 (Molecular Devices Corporation, PA, ZDA).

### ***2.5.2 Kinetika prenosa barvila skozi permeabilizirano membrano***

Za spremljanje prenosa molekul skozi membrano smo ponovno uporabili fluorescentno barvilo Propidijev Jodid. Barvilo smo vzbujali s  $530 \text{ nm} < \lambda > 560 \text{ nm}$ , fluorescenco pa zaznali pri  $> 580 \text{ nm}$ . Celice smo izpostavili pulzu z amplitudami (350, 500, 650, 800 V) in trajanjem (100  $\mu\text{s}$ , 500  $\mu\text{s}$ , 1 ms, 3 ms), spremembe fluorescence pa smo za razliko od prejšnjih poskusov zaznali z občutljivo fotopomnoževalko (FP) pritrjeno na mikroskop. FP je pretvorila fluorescenčni signal v napetostni signal, ki smo ga filtrirali, ojačili ter shranili v zapisovalnik (DL 922, Datalab, VB). Analogni signal iz zapisovalnika smo pretvorili v digitalni (12 bitni A/D) ter ga obdelali s programom Pico (Pico, Francija). Spremembe fluorescence smo spremljali na različnih časovnih intervalih: 400  $\mu\text{s}$  in 2000  $\mu\text{s}$  z 9  $\mu\text{s}$  časovno ločljivostjo, ter 80 ms in 8 sekund s 45  $\mu\text{s}$  oz. 2 ms časovno ločljivostjo. Poskuse smo izvedli na posameznih okroglih CHO WTT celicah, celicah v suspenziji (cca.  $3 \times 10^6$  celic/ml) in celičnih monoslojih.

### ***2.5.3. Elektropermeabilizacija gostih celičnih suspenzij***

Natančen opis celotnega poskusa je podan v **članku 6** v Dodatku (Pucihar et al. – v recenziji). Na kratko, celično suspenzijo smo najprej centrifugirali ( $200 \times g$ , 5 min) ter zamenjali supernatant s kalijevim pufrom (10 mM K-ZAP) in Propidijevim Jodidom (100  $\mu\text{M}$ ), tako da smo dobili suspenzije z gostotami  $400 \times 10^6$ ,  $200 \times 10^6$  in  $10 \times 10^6$  celic/ml. Volumski deleži celic v teh suspenzijah so bili 36%, 18%, in 1%. Suspenziji (100  $\mu\text{l}$ ) med ploščatimi elektrodami smo dovedli vlak pulzov  $8 \times 100 \mu\text{s}$  ali  $10 \times 5 \text{ ms}$  (Jouan, St Herblain, Francija). Delež permeabiliziranih celic in povprečno fluorescenco celic smo določili s histogramov na

pretočnem citometru (FACscan, Becton-Dickinson, ZDA). Okrevanje celic po permeabilizaciji smo določili tako, da smo barvilo dodali suspenziji ob določenih časih po koncu pulzov. Tako smo v redkih suspenzijah barvilo dodali 0 s, 10 s, 30 s, 1 min, 3 min, 5 min in 7 min po vlaku pulzov, v gostih pa 0 s, 3 min in 7 min po vlaku pulzov.

### 3 REZULTATI IN RAZPRAVA

#### 3.1 Meritve mirovalne transmembranske napetosti

Mirovalna napetost (MTN), ki smo jo izmerili na celicah v gojišču in medijih z različno sestavo in prevodnostjo, je prikazana v Tabeli 3.1. Meritve kažejo, da je v fizioloških razmerah (celice v gojišču) in v kalijevem mediju (10 mM K-ZAP) MTN nizka in znaša med -4 in -35 mV na celicah v suspenzijah in med -18 in -27 mV na pritrjenih celicah. Po podatkih iz literature naj bi bile tako nizke vrednosti MTN posledica gojenja celic v kulturah, kjer se le-te stalno delijo (Cone 1971). Na nekaterih celičnih linijah (npr. CHO) pa so podobno nizke napetosti izmerili tudi drugi raziskovalci (Gamper et al, 2005). Naše meritve kažejo, da pri poskusih permeabilizacije vsiljena napetost predstavlja dober približek celotni napetosti na membrani, MTN pa lahko zanemarimo (Valič et al., 2003).

MTN se v medijih z vedno nižjo prevodnostjo zmanjšuje, toda manj kot bi pričakovali na podlagi teoretičnih izračunov (Goldmanova enačba). Ti npr. kažejo, da bi morala biti MTN v 10 mM K-ZAP mediju okrog -50 mV. Razloge za odstopanje lahko delno pripišemo napačni oceni znotrajcelične koncentracije  $K^+$ . Možno pa je tudi, da uporabljen metoda meritve MTN ni primerna za naše poskuse.

**Tabela 3.1. Meritve mirovalne napetosti na različnih celičnih linijah (CHO WTT, B16F1, BHK). MTN so podane v milivoltih in predstavljene kot povprečja  $\pm$  SD (N > 25). \*Sestava gojišča je bila različna za različne celične linije.**

	CHO suspenzije	CHO pritrjene	B16F1 pritrjene	BHK pritrjene
*Gojišče	-4,0 $\pm$ 5,3	-18.6 $\pm$ 10.6	-19.8 $\pm$ 5.0	-18.1 $\pm$ 12.3
m1 (KZAP 10 mM)	-34.6 $\pm$ 13.3	-25.5 $\pm$ 12.8	-26.7 $\pm$ 4.4	-23.3 $\pm$ 8.9
m2 (KZAP 5 mM)	-40.5 $\pm$ 9.0	-20.6 $\pm$ 11.7	-27.7 $\pm$ 5.2	-35.2 $\pm$ 10.3
m3 (KZAP 1 mM)	-52.5 $\pm$ 11.0	-32.1 $\pm$ 9.9	-28.0 $\pm$ 5.2	-39.0 $\pm$ 6.7
m4 (NaZAP 10 mM)	-41.5 $\pm$ 10.2	-43.8 $\pm$ 12.9	-35.1 $\pm$ 4.5	-31.6 $\pm$ 6.9
m5 (NaZAP 5 mM)	-43.4 $\pm$ 12.3	-42.8 $\pm$ 22.1	-33.4 $\pm$ 2.8	-35.3 $\pm$ 7.2
m6 (NaZAP 1 mM)	-47.9 $\pm$ 12.2	-41.2 $\pm$ 21.2	-32.7 $\pm$ 4.5	-43.8 $\pm$ 9.1
m7	-52.2 $\pm$ 13.8	-96.6 $\pm$ 49.8	-35.4 $\pm$ 6.6	-51.7 $\pm$ 9.3

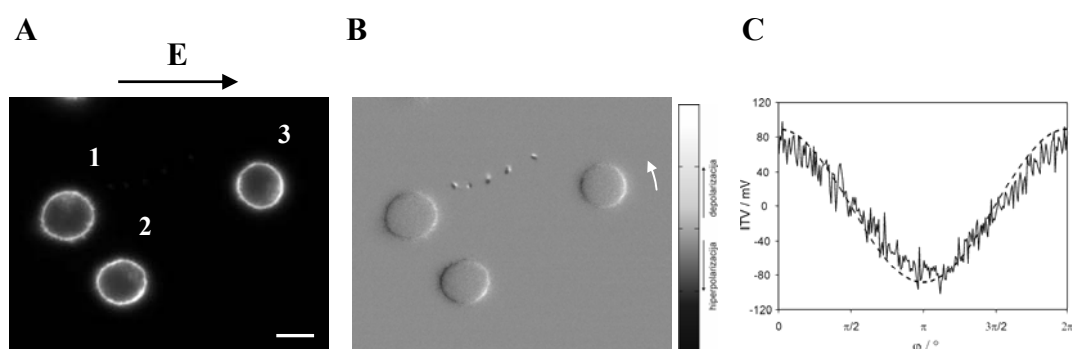
### 3.2 Meritve in izračuni vsiljene transmembranske napetosti ter permeabilizacija na posameznih okroglih celicah, posameznih celicah nepravilnih oblik in celičnih skupkih

Zaradi učinkovitejše predstavitve in lažje primerjave rezultatov, bomo meritve in izračune vsiljene napetosti ter potek elektropermeabilizacije prikazali skupaj na različnih celičnih sestavih. Tako bodo najprej predstavljeni rezultati na posameznih okroglih celicah, nato na posameznih celicah nepravilnih oblik in na koncu še na celičnih skupkih.

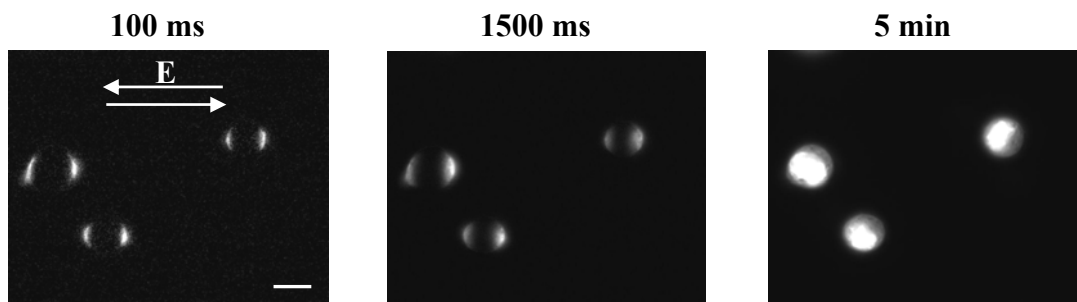
#### 3.2.1 Okrogla celica

Fluorescenčne slike treh približno okroglih celic med izpostavitvijo električnemu polju 100 V/cm so prikazane na Sliki 3.1A, medtem ko Slika 3.1B prikazuje spremembe v intenziteti fluorescence. Bela barva na tej sliki predstavlja zvišanje intenzitete fluorescence glede na kontrolo (depolarizacija), medtem ko črna barva predstavlja znižanje fluorescence (hiperpolarizacija). Vsiljena napetost (VTN), izmerjena na celici 3, je prikazana na Sliki 3.1C in se spreminja s kosinusno funkcijo po obodu celice med približno +80 mV in -80 mV. Izmerjena VTN se dobro ujema z numerično izračunano (prekinjena črta na Sliki 3.1C) na modelu iste celice.

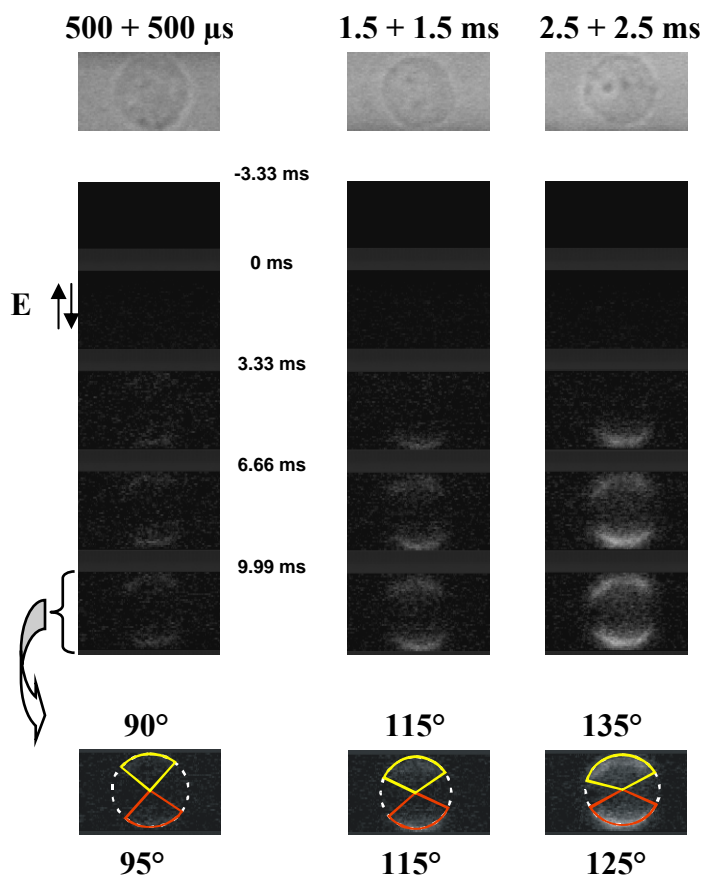
Celice, predstavljene na Sliki 3.1, smo nato elektropermeabilizirali s pravokotnim bipolarnim pulzom amplitude 260 V (650 V/cm) in trajanjem 750 + 750  $\mu$ s. Rezultati na Sliki 3.2 kažejo, da barvilo vstopi v celice na tistih področjih membrane, ki so obrnjena proti elektrodam, oziroma tam, kjer je absolutna vrednost VTN najvišja. To se ujema z opažanji ostalih raziskovalcev (Hibino et al., 1991; Tekle et al., 1991; Hibino et al., 1993; Tekle et al., 1994; Gabriel et al., 1999).



Slika 3.1. (A) Fluorescenčne slike CHO K1 celic pobarvanih z barvilom di-8-ANEPPS. (B) Spremembe fluorescence, ki jih dobimo z odštevanjem kontrolne slike celic od slike s poljem. Območje sivin na sliki je premaknjeno za 50 %. Bela puščica kaže smer in začetek meritev vsiljene napetosti. Skala predstavlja 10  $\mu$ m. (C) Porazdelitev vsiljene napetosti na membrani celice 3 v odvisnosti od položaja na membrani. Celice smo izpostavili pulzu z amplitudo 40 V (polje 100 V/cm) in trajanjem 100 ms. Spremembe fluorescence smo pretvorili v napetost s kalibracijsko krivuljo (6 % spremembe fluorescence ustreza 100 mV). Prekinjena črta prikazuje numerično izračunano VTN na isti celici.



Slika 3.2. Elektropermeabilizacija celic. (A) Fluorescenca 100 ms, (B) 1500 ms in (C) 5 min po pulzu. Slike so odštete od kontrolne slike, ki je bila posneta pred pulzom. Kontrast na slikah je avtomatsko izboljššan. Celice smo izpostavili pravokotnemu bipolarnemu pulzu z amplitudo 260 V (650 V/cm) in trajanjem 750 + 750  $\mu$ s. Za opazovanje permeabiliziranih področij membrane smo celični suspenziji pred permeabilizacijo dodali fluorescentno barvilo Propidijev Jodid (100  $\mu$ M). Merilo predstavlja 10  $\mu$ m.



Slika 3.3. Spremembe fluorescence med in po elektropermeabilizaciji. Okroglo celico smo izpostavili pravokotnemu bipolarnemu pulzu z amplitudo 500 V (1000 V/cm) in različnim trajanjem (500  $\mu$ s + 500  $\mu$ s, 1.5 ms + 1.5 ms in 2.5 ms + 2.5 ms). Prva slika predstavlja fazni kontrast, druga slika je fluorescenca celice pred pulzom (-3.33 ms), ostale slike so fluorescenca med (0 ms) in po pulzu. Kontrolo (-3.33 ms) smo odšteli od slik s pulzom. Puščice kažejo kdaj je bil doveden pulz in njegovo smer. Zadnjo sliko iz vsakega poskusa (9.99 ms) smo uporabili za določitev polarne kota permeabilizacije (rdeče in rumene črte).

Z merilnim sistemom, ki je omogočal zajemanje slik z visoko časovno ločljivostjo (3.33 ms), smo permeabilizacijo preučevali med in takoj po pulzu. Celice smo izpostavili pravokotnemu bipolarnemu pulzu z amplitudo 500 V (1000 V/cm) in trajanjem 500 + 500  $\mu$ s, 1.5 + 1.5 ms in 2.5 + 2.5 ms. Časovni poteki permeabilizacije za posamezne dolžine pulzov so prikazani na Sliki 3.3. Permeabilizacijo, ki se odraža kot sprememba fluorescence celice, opazimo 6.66 ms po začetku pulza in sicer le na eni strani celice, s časom pa postane fluorescentna tudi druga stran celice. Ta opažanja so verjetno posledica elektroforetske sile s katero električni pulz deluje na nabite molekule barvila. Meritve polarnega kota permeabilizacije na koncu opazovanega časovnega intervala kažejo, da je permeabilizacija približno simetrična, velikost polarnega kota pa narašča z dolžino pulza. Na podlagi teh rezultatov je mogoče oceniti velikost kritične VTN pri kateri pride do elektropermeabilizacije ( $VTN_c = 1.5 \cdot R \cdot E \cdot \cos \varphi$ , kjer je  $\varphi$  polovica polarnega kota permeabilizacije), vendar so taki izračuni pravilni le pri krajših pulzih. Rezultati na Sliki 3.3 namreč kažejo, da se polarni kot pri daljših pulzih poveča.

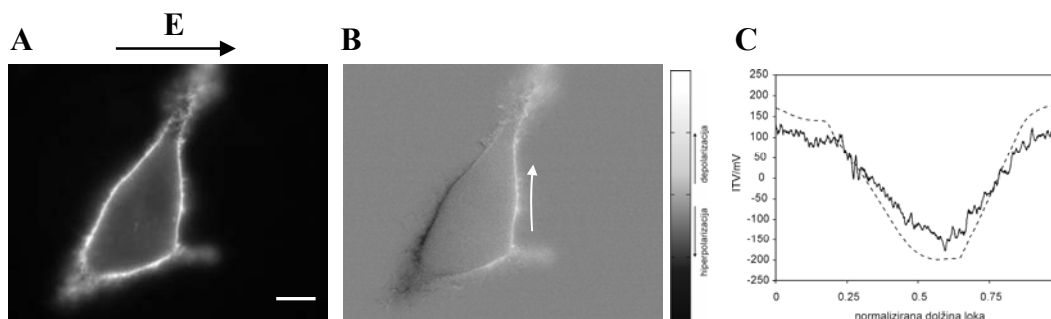
### 3.2.2 Celica nepravilne oblike

Nekateri rezultati meritev in izračunov vsiljene transmembranske napetosti (VTN) ter podroben opis gradnje modela celic nepravilnih oblik so opisani že v **članku 5** v Dodatku (Pucihar et al., 2006). Na tem mestu bomo naredili nekaj dodatnih meritev in izračunov na drugi celici nepravilne oblike ter jih primerjali z rezultati permeabilizacije, česar v članku nismo naredili.

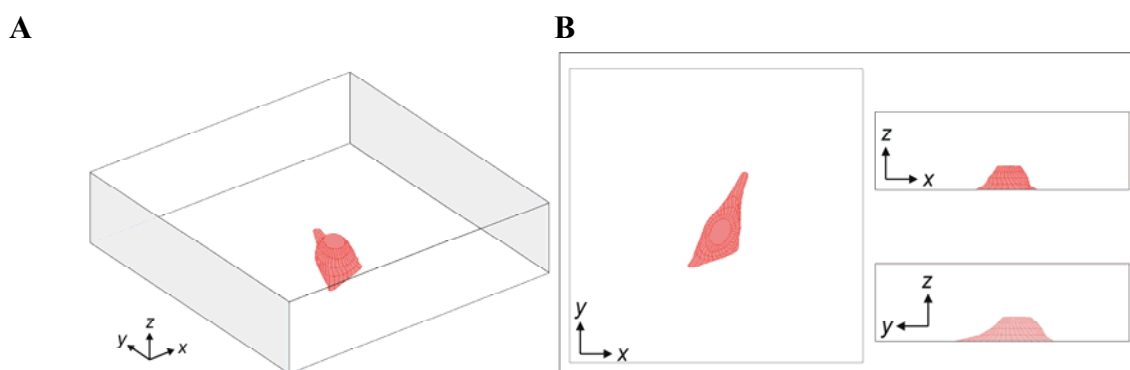
Fluorescenčne slike celice nepravilne oblike (B16F1) med izpostavitvijo zunanemu polju so prikazane na Sliki 4.1A, medtem ko Slika 4.1B prikazuje razlike v intenziteti fluorescence. Izmerjena VTN se po obodu celice spreminja, in sicer med približno 130 in -170 mV (Slika 4.1C).

S pomočjo fluorescenčnih slik, posnetih na različnih nivojih celice, smo zgradili 3D model celice (Slika 4.2). Model zgrajen na tak način predstavlja znatno bolj realistično podobo celice kot pa običajni modeli celic zgrajeni iz preprostih geometrijskih oblik, npr. krogla, sferoid (Buitenweg et al., 2003; Fear in Stuchly 1998a; Huang et al., 2004; Valič et al., 2003). Poenostavljene modele sicer lahko uporabimo za izračune na celicah v suspenzijah, medtem ko niso primerni za modele celic, ki rastejo v posodah ali v tkivih saj so te celice izrazito nepravilnih oblik. Poleg tega metoda gradnje realističnega modela omogoča neposredno primerjavo meritev z izračuni. Membrano v modelu celice smo nadomestili z robnim pogojem, kar znatno zmanjša število končnih elementov v modelu in posledično skrajša čas potreben za izračun problema. Z modelom smo nato izračunali porazdelitev električnega potenciala zunaj in znotraj celice (Slika 4.3A). VTN smo izračunali kot razliko med potencialoma na obeh straneh membrane ( $VTN = V_i - V_o$ , Slika 4.3B) in jo za najnižji nivo celice prikazali s prekinjeno črto na Sliki 4.1C. Primerjava z izmerjeno VTN pokaže, da se napetosti sicer kvalitativno ujemata, medtem ko lahko opazimo odstopanja v njihovih

amplitudah. Nekaj razlogov za odstopanja smo navedli že v članku in vključujejo razlike v naklonu kalibracijske krivulje za različne celice, razlike med dejanskimi in privzetimi parametri modela (npr. prevodnost membrane) in sistem za zajemanje in merjenje, ki ni bil najbolj primeren.

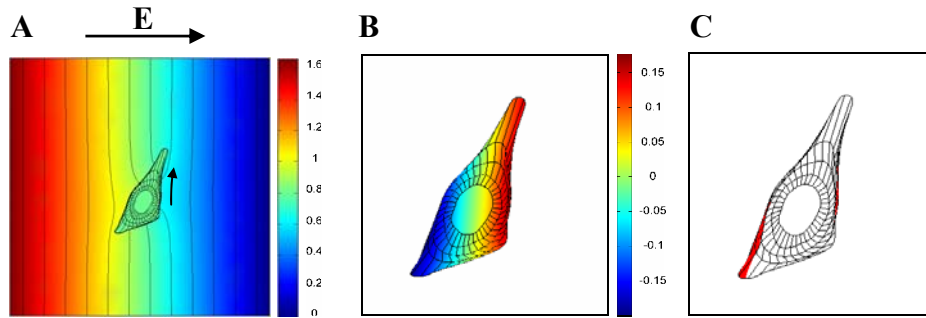


Slika 4.1. (A) Fluorescenčna slika B16F1 celice nepravilne oblike. Merilo predstavlja 10  $\mu\text{m}$ . (B) Spremembe fluorescence, ki jih dobimo z odštevanjem kontrolne slike celic od slike s poljem. Območje sivin na sliki je premaknjeno za 50 %. Bela puščica kaže smer in začetek meritev vsiljene napetosti. (C) Porazdelitev VTN na membrani celice v odvisnosti od normalizirane dolžine loka. Celico smo izpostavili pulzu z amplitudo 40 V (polje 100 V/cm) in trajanjem 100 ms. Spremembe fluorescence smo pretvorili v napetost s kalibracijsko krivuljo (6 % spremembe fluorescence ustreza 100 mV). Prekinjena črta prikazuje numerično izračunano VTN na isti celici (glej Sliko 4.2).

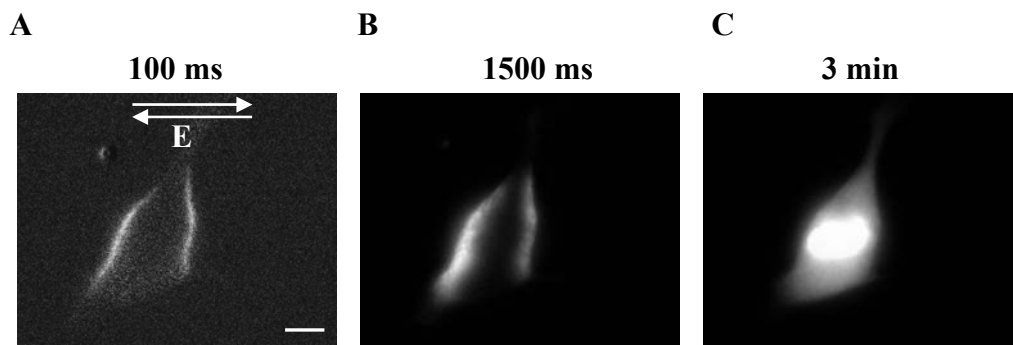


Slika 4.2. Numerični model celice nepravilne oblike prikazane na Sliki 4.1. (A) 3D model celice pritrjene na krovno stekelce. Kvader z velikostjo  $166 \times 166 \times 42 \mu\text{m}$  predstavlja zunajcelični medij s prevodnostjo 0.14 S/m, sive stranice so elektrode. Potencial ene elektrode smo postavili na 1.66 V in druge na 0 V (polje 100 V/cm). Preostale stranice so izolirane. Notranjost celice ima prevodnost 0.3 S/m; membrana je modelirana kot robni pogoj. (B) Trije stranski pogledi.

V prisotnosti fluorescentnega barvila Propidijev Jodid smo iste celice izpostavili pravokotnemu bipolarnemu pulzu z amplitudo 260 V (650 V/cm) in trajanjem 750 +750  $\mu\text{s}$  (Slika 4.4). Spremembe fluorescence smo zaznali na obeh straneh membrane celice 100 ms po pulzu. Področja, kjer smo zaznali porast fluorescence (Slika 4.4C), smo primerjali z izračuni VTN (prikazana na površini modela celice na Sliki 4.3B). Ugotovili smo, da se fluorescenčna področja ujemajo s področji membrane, kjer je absolutna vrednost VTN najvišja (rdeče obarvana površina celice na Sliki 4.3C prikazuje področja, kjer absolutna vrednost VTN presega poljubno izbran prag 15% njene največje vrednosti).



Slika 4.3. Izračuni vsiljene transmembranske napetosti. (A) Porazdelitev električnega potenciala v x-y ravnini, prikazana za najnižji nivo celice. Črne črte so ekvipotencialke, puščica nakazuje začetek in smer loka po katerem smo merili potencial. Merilo je v voltih. (B) VTN izračunana kot razlika med potencialoma na obeh straneh membrane ( $VTN = V_i - V_o$ ) in prikazana na površini povečanega modela celice. Za najnižji nivo celice smo VTN predstavili že na Sliki 4.1C s prekinjeno črto. (C) Področja membrane celice, kjer je absolutna vrednost VTN največja (rdeče obarvana površina prikazuje področja, kjer absolutna vrednost VTN presega 15% njene največje vrednosti).

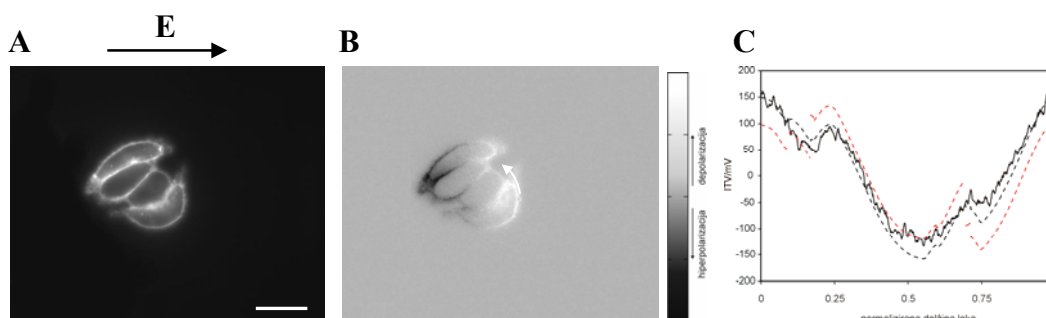


Slika 4.4. Elektropermeabilizacija celic. (A) Fluorescenca 100 ms, (B) 1500 ms in (C) 5 min po pulzu. Slike so odštete od kontrolne slike, ki je bila posneta pred pulzom. Kontrast na slikah je avtomatsko izboljšán. Celice smo izpostavili pravokotnemu bipolarnemu pulzu z amplitudo 260 V (650 V/cm) in trajanjem 750 + 750  $\mu$ s. Za opazovanje permeabiliziranih področij membrane smo celični suspenziji pred permeabilizacijo dodali fluorescentno barvilo Propidijev Jodid (100  $\mu$ M). Merilo predstavlja 10  $\mu$ m.

### 3.2.3 Celični skupki in goste celične suspenzije

Da bi bolje razumeli kako zunanje električno polje vpliva na celice v tkivih, poskusi opravljene na posameznih okroglih celicah in posameznih celicah nepravilnih oblik ne zadostujejo. Celice v tkivih so namreč izrazito nepravilnih oblik, so dovolj blizu skupaj, da vplivajo na porazdelitev električnega polja okrog njih, velikokrat pa so tudi povezane med sabo s prevodnimi kanali oz. presledkovnimi stiki (angl. 'gap junctions'). Zato smo v nadaljevanju uporabili bolj zapletene celične sestave: celične skupke in goste celične suspenzije. Začeli bomo s predstavitvijo poskusov na celičnih skupkih na koncu pa bomo prikazali še rezultate na suspenzijah.

Primer skupka štirih CHO celic je prikazan na Sliki 5.1. Celice smo izpostavili električnemu polju ( $75 \text{ V/cm}$ ,  $50 \text{ ms}$ ) in izmerili vsiljeno transmembransko napetost (VTN) na zunanjem sloju membrane skupka. Kot kažejo rezultati, se del skupka, ki je obrnjen proti pozitivni elektrodi hiperpolarizira, drugi del skupka pa depolarizira. Meritve VTN se ujemajo z izračuni na modelu istega skupka (polna in prekinjena črta na Sliki 5.1C), če so celice v skupku modelirane kot električno povezane. Ti poskusi kažejo, da se pri parametrih pulzov uporabljenih pri meritvah VTN, celice v skupku obnašajo kot velika celica. To se ujema tudi z opažanji drugih raziskovalcev, ki pa, za razliko od naše študije, niso naredili kvantitativnih meritev VTN (Gross et al, 1986; Hassan et al., 2002). Da električne povezave med celicami uporabljenimi v poskusih dejansko obstajajo smo se prepričali s testom za prisotnost presledkovnih stikov.

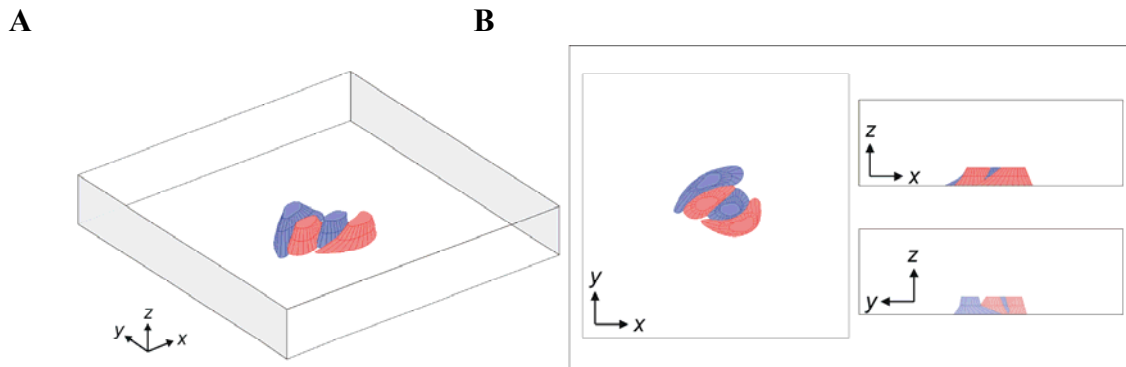


**Slika 5.1.** (A) Fluorescenčna slika skupka štirih CHO celic. (B) Spremembe fluorescence, ki jih dobimo z odštevanjem kontrolne slike celic od slike s poljem. Območje sivin na sliki je premaknjeno za 50 %. Bela puščica kaže smer in začetek meritev vsiljene napetosti. (C) Porazdelitev vsiljene napetosti na zunanjih membranah skupka v odvisnosti od normalizirane dolžine loka. Skupke smo izpostavili pravokotnemu pulzu z amplitudo  $19 \text{ V}$  (polje  $75 \text{ V/cm}$ ) in trajanjem  $50 \text{ ms}$ . Spremembe fluorescence smo pretvorili v napetost s kalibracijsko krivuljo ( $6 \%$  spremembe fluorescence ustreza  $100 \text{ mV}$ ). Prekinjena črta prikazuje numerično izračunano VTN na modelu istega skupka za primer ko so celice električno povezane (črna črta) in za primer, ko so med seboj izolirane (rdeča črta) (glej Sliko 5.2). Merilo predstavlja  $20 \mu\text{m}$ .

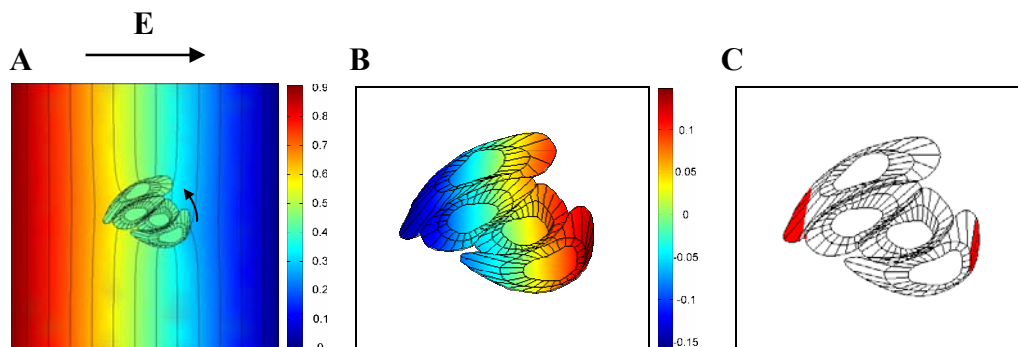
Električno povezane celice v skupku smo modelirali tako, da smo membranam na stiku celic pripisali znatno višjo prevodnost kot pa membranam na preostalih delih celic. Za primerjavo smo celice modelirali tudi kot električno izolirane. V tem primeru je bila prevodnost membrane na stiku podobna kot na preostalih delih membrane. Izračun porazdelitve električnega potenciala zunaj in znotraj celice za primer električno povezanih in električno izoliranih celic je prikazan na Slikah 5.3A in 5.4A, VTN na celicah v skupku pa na Slikah 5.3B in 5.4B.

Skupek celic smo nato v prisotnosti barvila Propidijev Jodid izpostavili pravokotnemu bipolarnemu pulzu z amplitudo  $260 \text{ V}$  ( $1050 \text{ V/cm}$ ) in trajanjem  $750 \mu\text{s} + 750 \mu\text{s}$ . Fluorescenco smo opazili na obeh straneh vsake posamezne celice v skupku (Slika 5.5). Ta opažanja se ne ujemajo z izračuni VTN na električno povezanih celicah (Slike 5.3B in C), so pa v skladu z izračuni na električno izoliranih celicah (Sliki 5.4B in C). Kot kaže, se celice v skupkih, pri parametrih pulzov uporabljenih pri permeabilizaciji, obnašajo kot bi bile med

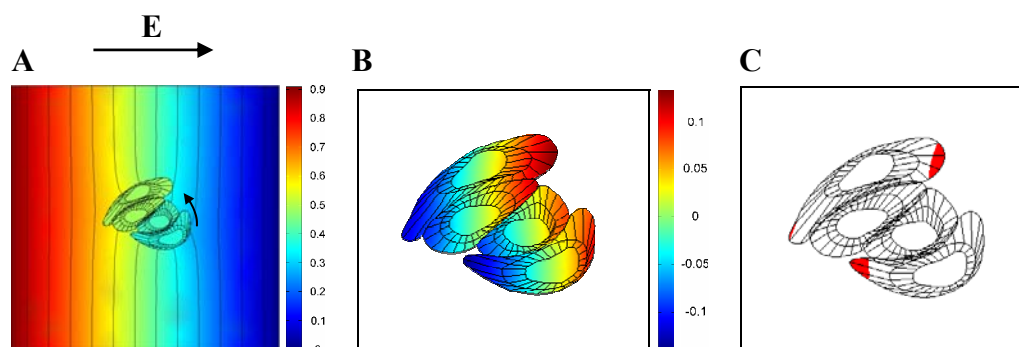
sabo izolirane, saj se vsaka celica permeabilizira posebej. To je ravno v nasprotju z opažanji pri meritvah VTN, kjer so se celice obnašale kot ena velika celica (primerjaj Sliko 5.1B in 5.5A). Takšno obnašanje celic v skupku bi lahko bilo posledica vpliva parametrov električnih pulzov na delovanje ali strukturo presledkovnih stikov med celicami. Možno pa je, da je za izmerjene rezultate odgovoren nek drug pojav.



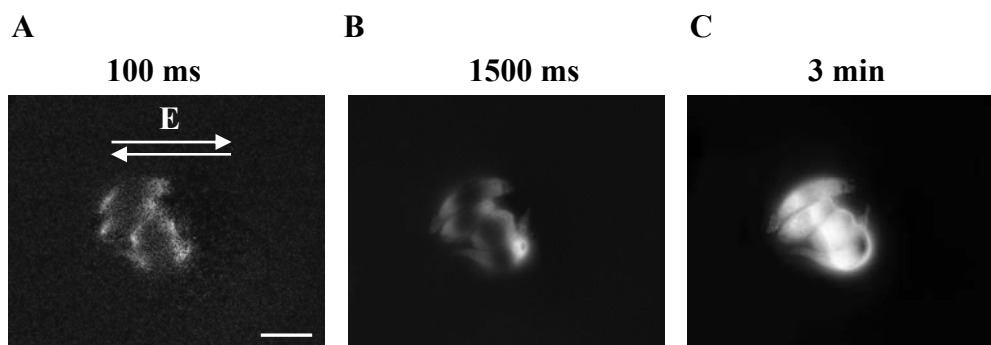
Slika 5.2. Numerični model skupka štirih celic prikazanega na Sliki 5.1. (A) 3D model skupka na krovnem stekelcu. Kvader z velikostjo  $121 \times 121 \times 35 \mu\text{m}$  predstavlja zunajcelični medij s prevodnostjo  $0.14 \text{ S/m}$ , sive stranice so elektrode. Potencial ene elektrode smo postavili na  $0.91 \text{ V}$  in druge na  $0 \text{ V}$  (polje  $75 \text{ V/cm}$ ). Preostale stranice so izolirane. Notranjost celic v skupku ima prevodnost  $0.3 \text{ S/m}$ ; membrane so modelirane kot robni pogoji. Kadar smo celice v skupku modelirali kot električno povezane smo membranam na stiku celic pripisali  $1000 \times$  višjo prevodnost kot ostalim membranam. Kadar smo želeli model električno izoliranih celic pa so imele membrane na stiku za polovico nižjo prevodnost kot preostale membrane. (B) Trije stranski pogledi.



Slika 5.3. Izračuni vsiljene transmembranske napetosti za primer električno povezanih celic v skupku. (A) Porazdelitev električnega potenciala v  $x$ - $y$  ravnini, prikazana za najnižji nivo skupka. Črne črte so ekvipotencialke, puščica nakazuje začetek in smer loka po katerem smo merili potencial. Merilo je v voltih. (B) VTN izračunana kot razlika med potencialoma na obeh straneh membrane ( $VTN = V_i - V_o$ ) in prikazana na površini povečanega modela skupka. Za najnižji nivo skupka smo VTN predstavili že na Sliki 5.1C s prekinjeno črto. (C) Področja membrane skupka, kjer je absolutna vrednost VTN največja (rdeče obarvana površina prikazuje področja, kjer absolutna vrednost VTN presega 15% njene največje vrednosti).



Slika 5.4. Izračuni vsiljene napetosti za primer električno izoliranih celic v skupku. (A) Porazdelitev električnega potenciala v x-y ravnini, prikazana za najnižji nivo skupka. (B) VTN izračunana kot razlika med potencialoma na obeh straneh membrane ( $VTN = V_i - V_o$ ) in prikazana na površini povečanega modela skupka. (C) Področja membrane skupka, kjer je absolutna vrednost VTN največja (rdeče obarvana površina prikazuje področja, kjer absolutna vrednost VTN presega 15% njene največje vrednosti).

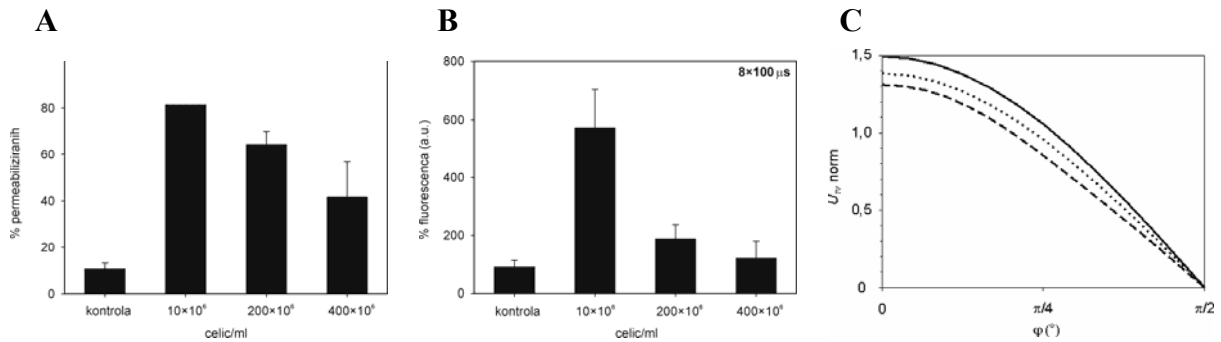


Slika 5.5. Elektropermeabilizacija celičnega skupka. (A) Fluorescenca 100 ms, (B) 1500 ms in (C) 5 min po pulzu. Slike so odštete od kontrolne slike, ki je bila posneta pred pulzom. Kontrast na slikah je avtomatsko izboljššan. Skupek smo izpostavili pravokotnemu bipolarnemu pulzu z amplitudo 260 V (1040 V/cm) in trajanjem 750 + 750  $\mu$ s. Za opazovanje permeabiliziranih področij membrane smo celični suspenziji pred permeabilizacijo dodali fluorescentno barvilo Propidijev Jodid (100  $\mu$ M).

### 3.2.3.1 Goste celične suspenzije

Rezultati izračunov vsiljene transmembranske napetosti na celicah v gostih suspenzijah in deleža permeabiliziranih celic so natančno opisani v **članku 6** v Dodatku (Pucihar et al., v recenziji), zato bomo tukaj podali le najpomembnejše rezultate.

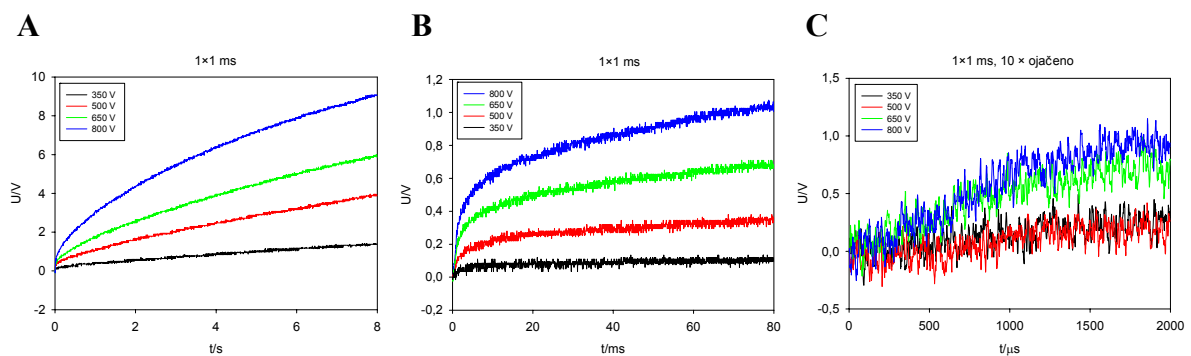
Z naraščajočo gostoto celic v suspenziji (od  $10 \times 10^6$  celic/ml do  $400 \times 10^6$  celic/ml) se delež permeabiliziranih celic zmanjša za približno 50% (Slika 5.6 A). Glavni razlog za razlike je sprememba lokalnega polja okrog celic, ki povzroči zmanjšanje VTN na celicah (Slika 5.6C). Fluorescenca celic, ki predstavlja vnos Propidijevega Jodida, se prav tako zmanjša z gostoto celic, vendar bolj kot bi pričakovali na podlagi izmerjenih deležev permeabiliziranih celic (Slika 5.6B). Na dodatno zmanjšanje fluorescence verjetno vpliva napihovanje celic med in po permeabilizaciji, ki zmanjša dostopnost barvila do celic in difuzijo barvila v celice.



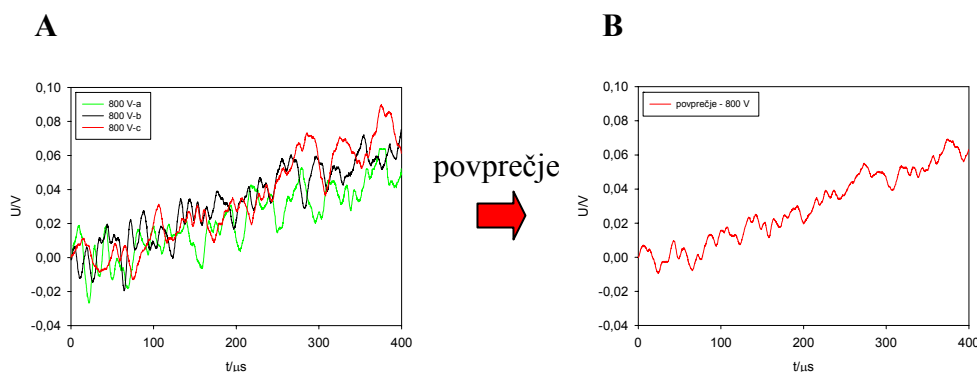
Slika 5.6. (A) Elektropermeabilizacija in (B) fluorescenca v odvisnosti od gostote celic pri izpostavitvi  $8 \times 100 \mu\text{s}$ ,  $700 \text{ V/cm}$  pulzom. Stolpec predstavlja povprečje treh meritev  $\pm$  SD. (C) VTN na celici v suspenziji pri različnih volumskih deležih celic. 1% - polna črta, 18% - točkasta črta, 36% - prekinjena črta. VTN je normalizirana na radij celice in električno polje. Zaradi simetrije je prikazana le četrtina celotnega poteka.

### 3.2.3.2 Kinetika prenosa molekul čez permeabilizirano membrano

Spremljali smo vnos molekule Propidijevga Jodida v CHO WTT celice med in po pulzu. Ko barvilo vstopi v celico začne močneje fluorescirati, kar lahko zaznamo z občutljivo fotopomnoževalko (FP). Ker FP optični signal pretvori v napetostnega so rezultati meritev prikazani kot spremembe napetosti s časom. Primer kinetike vnosa barvila pri permeabilizaciji z 1 ms pulzom različnih amplitud je prikazan na Sliki 5.7. Meritve na različnih časovnih intervalih kažejo, da permeabilizacija z višjimi amplitudami povzroči povečan vnos barvila v celico. Fluorescenca v prvih deset milisekundah po pulzu najprej hitro naraste, nadaljnje naraščanje pa je počasnejše (slika 5.7B). Opazovanje na časovnem intervalu  $2000 \mu\text{s}$  pokaže, da je dinamika naraščanja med in takoj po pulzu različna, kar lahko pripišemo elektroforetski sili, s katero zunanje polje deluje na molekule barvila (Slika 5.7C). Rezultati kinetike na časovnem intervalu  $400 \mu\text{s}$  (pri višji občutljivosti fotopomnoževalke in višji koncentraciji barvila) kažejo, da barvilo vstopi v celico že  $100 \mu\text{s}$  po začetku pulza (Slika 5.8).



Slika 5.7. Vpliv amplitude pulzov na časovni potek fluorescence po elektropermeabilizaciji. (A) 8 s, (B) 80 ms, (C) 2 ms interval zajemanja. CHO WTT celice v suspenziji s  $100 \mu\text{M}$  Propidijevim Jodidom smo izpostavili pravokotnemu 1 ms pulzu z amplitudami 350, 500, 650, in 800 V ( $700 - 1600 \text{ V/cm}$ ). Pulz je bil doveden ob času 0 s. Rezultati prikazani pod C so  $10 \times$  ojačeni. Fluorescenco smo zaznali s fotopomnoževalko.



**Slika 5.8. (A) Časovni potek fluorescence izmerjen pri povečani občutljivosti fotopomnoževalke in 1 mM koncentraciji Propidijevega Jodida. Prikazani so rezultati treh ponovitev in (B) njihovo povprečje. CHO WTT celice smo izpostavili pravokotnemu 1 ms pulzu z amplitudo 800 V (1600 V/cm).**

## 4 ZAKLJUČEK

### 4.1 Meritve mirovalne transmembranske napetosti

Meritve mirovalne napetosti (MTN) na različnih linijah so pokazale, da je v fizioloških razmerah MTN približno -20 mV. Pri poskusih permeabilizacije torej vsiljena napetost predstavlja dober približek celotni napetosti na membrani, MTN pa lahko zanemarimo. MTN je v medijih z nižjo prevodnostjo vedno bolj negativna, vendar manj kot bi pričakovali na podlagi teoretičnih izračunov.

### 4.2 Meritve in izračuni vsiljene transmembranske napetosti ter permeabilizacija na posameznih okroglih celicah

Meritve vsiljene napetosti (VTN) na okroglih celicah se ujemajo s teoretičnim zapisom VTN (Schwanova enačba), ki predvideva kosinusno porazdelitev VTN na membrani celice, meritve pa se ujemajo tudi z numerično izračunano VTN.

Primerjava izmerjene in izračunane VTN z meritvami permeabilizacije so potrdile, da se permeabilizacija pojavi na tistih področjih membrane, kjer je absolutna vrednost VTN največja – na področjih, ki so obrnjena proti elektrodam. Polarni kot permeabilizacije se povečuje z amplitudo in trajanjem pulza. Izračuni kritične VTN s pomočjo meritev kritičnega kota so torej mogoči le pri uporabi krajših pulzov. Tudi v tem primeru pa je tako določena kritična VTN verjetno le grob približek pravi vrednosti.

### **4.3 Meritve in izračuni vsiljene transmembranske napetosti ter permeabilizacija na posameznih celicah nepravilnih oblik**

Vsiljena napetost (VTN) izmerjena na posameznih celicah nepravilnih oblik se kvalitativno ujema z izračunano, medtem ko lahko opazimo odstopanja v njihovih amplitudah.

Predstavili smo metodo za izgradnjo realističnega modela celice nepravilnih oblik na osnovi fluorescenčnih slik prereзов celice. To omogoča določiti VTN na istih celicah na katerih smo izvedli meritve. Pokazali smo, kako lahko membrano v modelu celice nadomestimo z robnim pogojem, kar znatno zmanjša število končnih elementov v modelu in posledično skrajša čas potreben za izračun problema.

Elektropermeabilizacija se vedno pojavi na tistih področjih membrane celice, kjer je absolutna vrednost VTN največja.

### **4.4 Meritve in izračuni vsiljene transmembranske napetosti ter permeabilizacija na celičnih skupkih**

Meritve VTN se ujemajo z izračuni na modelu istega skupka, če so celice v skupku modelirane kot električno povezane. Ti poskusi kažejo, da se pri parametrih pulzov uporabljenih pri meritvah VTN, celice v skupku obnašajo kot velika celica - del skupka, ki je obrnjen proti pozitivni elektrodi se hiperpolarizira, drugi del skupka pa depolarizira.

Nasprotno pa se pri parametrih pulzov uporabljenih pri permeabilizaciji, celice v skupkih obnašajo kot bi bile med sabo izolirane - vsaka celica se permeabilizira posebej. Področja permeabilizacije se ujemajo področji, kjer je izračunana absolutna vrednost VTN največja, če so izračuni narejeni za primer električno izoliranih celic.

#### **4.4.1 Elektropermeabilizacija gostih celičnih suspenzij**

Z višanjem gostote celic v suspenziji se delež permeabiliziranih celic znatno zmanjša. Glavni razlog za razlike je sprememba lokalnega polja okrog celic, ki povzroči zmanjšanje VTN na celicah. Fluorescenca celic se zmanjša bolj kot bi pričakovali na podlagi deležev permeabiliziranih celic. Na dodatno zmanjšanje fluorescence verjetno vpliva napihovanje celic, ki zmanjša dostopnost barvila do celic in difuzijo v celice.

#### **4.4.2 Kinetika prenosa molekul čez permeabilizirano membrano**

Permeabilizacija z višjimi amplitudami ali pa trajanjem pulza poveča vnos barvila v celico. Vnos v prvih milisekundah po pulzu najprej hitro naraste, nadaljnje naraščanje pa je počasnejše. Hitrost vnosa med in takoj po pulzu je zaradi elektroforetskega prispevka pulza različna. Prenos molekul barvila čez membrano opazimo že 100  $\mu$ s po začetku pulza.

### 4.5 Smernice za nadaljnje delo

- Preveriti pravilnost meritev MTN na celicah v nizkoprevodnih medijih z uporabo drugih fluorescentnih barvil (npr. barvilo DiBAC) in mikroelektrodami.
- Meritve VTN pri nadkritičnih amplitudah pulzov s hitro in občutljivo kamero. S tako kamero, ki je sedaj na voljo v našem laboratoriju, in fluorescentnim indikatorjem za kalcijeve ione Fluo3AM, bi bilo mogoče hkratno merjenje VTN in spremljanje poteka permeabilizacije.
- Meritve VTN in spremljanje permeabilizacije na celičnih skupkih z zaprtimi medceličnimi povezavami (gap junctions) in primerjava z rezultati na skupkih z odprtimi povezavami.
- Razširitev obstoječega monoslojnega numeričnega modela celičnega skupka na model skupka z več sloji celic.
- Izgradnja dinamičnega numeričnega modela VTN in permeabilizacije.
- Primerjava meritev kinetike prenosa skozi permeabilizirano membrano z obstoječimi teoretičnimi modeli.

## 5 IZVIRNI PRISPEVKI K ZNANOSTI

### **Meritve mirovalne transmembranske napetosti na celicah v različnih medijih**

Z uporabo fluorescentnega barvila TMRM smo izmerili mirovalno napetost na različnih celičnih linijah (CHO, B16F1 in BHK) in v medijih z različnimi zunajceličnimi prevodnostmi. Ugotovili smo, da je amplituda mirovalne napetosti nizka in da jo lahko pri poskusih permeabilizacije zanemarimo. Meritve mirovalne napetosti smo primerjali tudi s teoretično izračunanimi vrednostmi in ugotovili odstopanja, predvsem v primerih, ko se celice nahajajo v medijih z nizko prevodnostjo.

### **Meritve vsiljene transmembranske napetosti na posameznih celicah nepravilnih oblik in celičnih skupkih**

Kvantitativne meritve vsiljene transmembranske napetosti (VTN) na celicah nepravilnih oblik in celičnih skupkih so pomembne za razumevanje poteka elektropermeabilizacije v tkivu. Meritve VTN so bile do sedaj narejene le na okroglih celicah, medtem ko je bil na celicah nepravilnih oblik in na celičnih skupkih potek VTN določen le slikovno. VTN smo merili s fluorescentnim barvilom di-8-ANEPPS, fluorescenčne slike celic pa zajeli s sistemom za slikanje s fluorescenčnim mikroskopom. Pokazali smo, da je vsiljena napetost po absolutni vrednosti najvišja na tistih področjih celic, ki so obrnjeni proti elektrodam, medtem ko se skupek celic pri teh meritvah obnaša kot ena velika celica - del skupka, ki je obrnjen proti pozitivni elektrodi se hiperpolarizira, drugi del skupka pa depolarizira.

### **Numerični izračuni vsiljene transmembranske napetosti na posameznih celicah nepravilnih oblik in celičnih skupkih**

Z uporabo metode končnih elementov smo VTN numerično izračunali na modelih celic nepravilnih oblik in skupkov dveh oziroma štirih takih celic. Modele smo zgradili na osnovi realne geometrije celic, ki smo jo dobili z večnivojskimi mikroskopskimi posnetki celic na katerih so bile narejene meritve ITV. Tako je bilo mogoče primerjati meritve z numeričnimi izračuni. Pokazali smo, kako lahko celično membrano v modelu celice nadomestimo z robnim pogojem, kar znatno zmanjša število končnih elementov v modelu in posledično skrajša čas potreben za izračun problema.

### **Opazovanje poteka elektropermeabilizacije na posameznih celicah in celičnih skupkih**

Potek elektropermeabilizacije na posameznih celicah nepravilnih oblik in celičnih skupkih smo spremljali s fluorescentnim barvilom propidijev jodid. Na področju elektropermeabilizacije postane membrana med drugim prepustna tudi za molekule barvila, kar zaznamo kot dvig fluorescence, ki se najprej pojavi v okolici permeabiliziranega področja membrane. Z opazovanjem permeabilizacije na istih celicah, na katerih smo izmerili in

izračunali VTN, smo pokazali, da pride do elektropermeabilizacije le na tistih področjih membrane, kjer je absolutna vrednost VTN največja. Na ta način je bilo mogoče določiti tudi pragovno vrednost VTN, ki jo moramo preseči, da dosežemo elektropermeabilizacijo. Ugotovili smo, da se med elektropermeabilizacijo celice v skupkih obnašajo kot bi bile med seboj izolirane - vsaka celica v skupku se permeabilizira posebej.

## II ABSTRACT

When a biological cell is exposed to an external electric field, induced transmembrane voltage (ITV) forms on its membrane. During the exposure, ITV superimposes to the native or resting transmembrane voltage (RTV) and when the sum of both voltages exceeds some threshold value, the permeability of the cell membrane in these regions transiently increases. This phenomenon is termed electropermeabilization. In many applications of electropermeabilization an efficient and at the same time reversible permeabilization is essential (e.g. DNA electrotransfer). Thus, a careful planning of the experiment, which involves the estimation of the amplitude of ITV leading to cell permeabilization, is required. The problem arises in case of tissues, where cell geometry is more complicated, cells are close enough to affect the electric field around each other, and they are often connected with pathways between them. In all these cases, an analytical description of ITV is in general not attainable and numerical methods are often the only feasible approach. Due to the complexity of tissue structure, numerical models are either macroscopic, where detailed cell structure is not considered, or in case of microscopic models, the models are constructed using simple geometrical shapes (semi-spheres, cubes). To better understand how the electric field interacts with tissues on a microscopic (single cell) level, which in turn determines the macroscopic behavior of the tissue, we constructed realistic microscopic models of irregularly shaped cells, clusters of such cells, and dense suspensions. Regarding the shape, density and connections between cells, these cell assemblies are in their complexity close to tissues. First, the amplitude of resting transmembrane voltage of cells used in the study was determined. Next, calculations of ITV were performed on models of single spherical, single attached cells, and cell clusters and they were compared to measurements of ITV on the same cells, from which the models were constructed. The course of electropermeabilization of these cells was then monitored and the results were compared with measurements and calculations of ITV. In a separate experiment, a detailed investigation of kinetics of molecular transport into cells after permeabilization was performed. Similarly, for dense cell suspensions, the ITV calculated on a model of suspension was compared with the fraction of permeabilized cells measured in suspensions with increasing cell densities.

Measurements of resting transmembrane voltage (RTV) were performed by means of a slow potentiometric fluorescent dye TMRM on different cell lines in culture media and media with progressively decreasing conductivities. ITV was measured on single spherical cells, single irregularly shaped cells, and cell clusters with a fast potentiometric fluorescent dye di-8-ANEPPS. The cross-section fluorescence images of the same cells on which the measurements of ITV were performed, were used to construct realistic numerical models of cells and the ITV on these models was then calculated with finite elements method. Finite-thickness, nonzero-conductivity cell membrane in the model was replaced by a boundary condition in which a specific surface conductivity was assigned to the interface between the cell interior and the exterior. Electropermeabilization of cells was followed by monitoring the

changes in intracellular fluorescence of membrane-impermeant fluorescent dye Propidium Iodide.

Measurements of RTV showed that in physiological conditions (cells in culture medium) and in the presence of pulsing buffer, RTV on investigated cell lines is low (between -4 and -35 mV for suspended cells and between -18 and -27 mV for attached cells). Therefore, in experiments involving electropermeabilization ITV can be used as a rough approximate of the total voltage on the membrane, while RTV can be neglected. RTV in cells in media with decreasing conductivities gradually decreased, but less than expected from theoretical calculations. This was partly attributed to overestimated intracellular concentration of potassium. However, it is also possible that the method for measuring RTV, although reported as efficient, was not suitable for these experiments.

Measurements of ITV on single spherical cells, single attached cells, and cell clusters were in qualitative agreement with results of numerical calculations, while in some cases discrepancies in measured and calculated amplitudes could be observed. This was attributed to variations of the slope of calibration curve, the differences between the actual and implemented parameters of the model, physiological state of cells, and experimental setup. In addition, we observed that at pulse parameters used in measurements of ITV, cells in clusters behaved as electrically connected, i.e. a cluster acted as one giant cell.

Numerical calculations on models of cells where cell membrane was replaced with a boundary condition resulted in considerably lower number of mesh elements and consequently shorter time needed to solve the problem. We also demonstrated that calculations of ITV on simplified models of irregularly shaped cells can lead to considerable deviations from ITV calculated on a realistic model. Electric field orientation affects the amplitude and distribution of calculated ITV and consequently permeabilization. Namely, cells oriented with their longer axis parallel to the field are more likely to get permeabilized than the same cells oriented perpendicularly to the field.

Comparison of measured and calculated ITVs with observations of electropermeabilization on single spherical and single attached cells confirmed that permeabilization occurs in those regions of the membrane, where the absolute value of ITV is the highest (the regions facing the electrodes). Additional experiments performed on single spherical cells showed that during and immediately after the pulse, the fluorescence from cells increases asymmetrically if unipolar pulses were delivered, while symmetrical fluorescence was observed for bipolar pulses. These observations were attributed to electrophoretic effect of the pulse. On a longer time scale, asymmetry in fluorescence was still observed, even for bipolar pulses, and we did not find any reasonable explanation for that. Critical value of ITV, at which permeabilization occurs, was calculated from the polar angle of permeabilization measured immediately after the pulse and was found to be approximately 450 mV, in agreement with reported critical thresholds. Permeabilization results obtained on cell clusters showed that cells in clusters, at

pulse parameters used in these experiments, behaved as electrically insulated and were permeabilized individually. This is in contradiction to what we observed during measurements of ITV (i.e. with longer, low voltage pulses), where cells in clusters behaved as electrically connected, and was assumed to be the result of opening and closing of gap junctions at different pulse parameters.

Measurements of kinetics of membrane transport showed that electropermeabilization with progressively increasing pulse amplitudes or pulse durations results in increased dye transport into cells. A sharp increase was observed milliseconds after the onset of a pulse, followed by a moderate additional fluorescence increase. Results measured on a time interval of 400  $\mu$ s revealed that the transport across the permeabilized membrane can be detected within 100  $\mu$ s after the onset of the pulse. Besides, different dynamics of fluorescence increase was observed during and immediately after the pulse.

Experiments carried out on dense cell suspensions showed that with increasing cell density (from  $10 \times 10^6$  cells/ml to  $400 \times 10^6$  cells/ml) the fraction of permeabilized cells decreased by approximately 50%. We attributed this to the changes in the local electric field, which lead to a decrease in the amplitude of ITV. The uptake of Propidium Iodide also decreased with cell density, but by a larger amount than expected from permeabilization results. We supposed that the additional decrease in fluorescence was mainly due to cell swelling after permeabilization, which reduced extracellular dye availability to the permeabilized membrane and hindered the dye diffusion into the cells. Resealing of cells appeared to be slower in dense suspensions, which can also be attributed to cell swelling resulting from electropermeabilization.



### III RÉSUMÉ

L'exposition d'une cellule à un champ électrique peut produire diverses réponses physiques et chimiques. La plupart de ces réponses sont associées à la modification du voltage transmembranaire produit par le champ électrique appliqué. Alors que le voltage transmembranaire du repos (RTV) est présent sur la membrane cellulaire à tout moment, l'exposition de la cellule à un champ électrique induit une composante additionnelle : le voltage transmembranaire induit (ITV), qui se superpose au voltage de repos. Ce phénomène conduit à l'électroperméabilisation lorsque le potentiel résultant devient supérieur à une valeur critique. Dans la majorité des applications de l'électroperméabilisation une perméabilisation efficace et réversible est indispensable. Ainsi, perméabiliser une cellule biologique de manière efficace demande une organisation minutieuse d'expériences, il est aussi très important de connaître la valeur d'ITV seuil pour l'électroperméabilisation d'une cellule. Le problème se complique au niveau des tissus en raison de la complexité de la géométrie de la cellule, de la proximité entre les cellules, ce qui a des effets sur le champ électrique autour ces cellules, ainsi qu'en raison des connexions entre elles. Dans toutes ces cases, l'analyse de l'ITV de manière analytique est impossible, et pour cette raison afin de calculer la valeur d'ITV il faut utiliser une méthode numérique. En raison de la complexité de la structure du tissu, on a créé des modélisations soit au niveau macroscopique (où la structure de la cellule exacte n'était pas examinée), soit au niveau microscopique (où la structure cellulaire était représentée sous formes géométriques simplifiées, telles que les demi-sphères et les carrés). Afin de mieux comprendre l'influence du champ électrique sur les tissus biologiques au niveau microscopique, ce qui par conséquent détermine les propriétés du tissu au niveau macroscopique, on a construit les trois modèles suivants : le modèle d'une cellule avec une forme irrégulière, le modèle de groupe de telles cellules et le modèle d'une dense suspension de cellules. Le choix de la forme, de la densité et des connexions entre des cellules, conduisent à des modèles de groupes de cellules ressemblant aux tissus biologiques. Premièrement, l'amplitude du RTV chez les cellules examinées dans cette étude était déterminée. Deuxièmement, le ITV était d'abord calculé sur les modèles : d'une cellule sphérique, des cellules liées et des groupes des cellules, ensuite les résultats obtenus ainsi étaient comparés aux valeurs du ITV mesurées sur la même cellule qui représente la base pour la modélisation. La cinétique de l'électroperméabilisation des cellules était suivie et les résultats ainsi obtenus étaient comparés aux prédictions d'ITV obtenues par des calculs et des mesures. Dans une expérience séparée, la pénétration moléculaire au sein des cellules, qui avaient été électroperméabilisées, était examinée expérimentalement.

De même, pour les suspensions cellulaires denses, l'ITV calculé sur les modèles de suspension a été comparé aux fractions de cellules électroperméabilisées obtenues dans les suspensions denses de cellules.

Le voltage transmembranaire de repos (RTV) est mesuré par imagerie de fluorescence avec la sonde potentiométrique lente TMRM sur des lignées de cellules dans le milieu de culture et dans sept milieux de la conductivité décroissante. L'ITV a été mesuré par imagerie de fluorescence en utilisant la sonde rapide di-8-ANEPPS, sur une seule cellule sphérique, sur une cellule avec une forme irrégulière et sur un groupe des cellules. La création des modèles des cellules, sur lesquelles l'ITV a été mesuré, a été basée sur les photographies numériques des cellules, qui ont été obtenues par imagerie de fluorescence sous microscope. Ensuite, l'ITV a été calculé par la méthode des éléments finis. Les particularités des modélisations telles que l'épaisseur et la conductivité de la membrane sont introduites par la définition de la valeur de la conductivité spécifique entre l'extérieur et l'intérieur de la cellule. L'électroperméabilisation des cellules a été examinée par imagerie de fluorescence avec la sonde fluorescente iodure de propidium (PI) que ne traverse pas librement la membrane sur des temps courts.

Les résultats de RTV montrent que dans les conditions physiologiques (les cellules dans le milieu de culture) et aussi dans le milieu d'électroperméabilisation, la valeur de RTV chez les lignes cellulaires examinée est basse (entre -4 et -35 mV pour les cellules en suspension et entre -18 et -27 mV pour les cellules en monocouche). Pour cette raison dans les expériences où l'électroperméabilisation est présente, on peut utiliser la valeur du ITV comme une estimation approximative de la valeur du voltage membranaire total, tandis que le RTV peut être négligé. Chez les cellules dans des solutions de faible conductivité, la valeur du RTV décroît progressivement de manière qui n'était pas prévue par la théorie. Cette décroissance du RTV est partialement due à une surestimation de la concentration intracellulaire du potassium. Cependant, il est aussi possible que la méthode utilisée pour mesurer le RTV n'était pas la plus adéquate dans le cadre de cette étude, alors que son efficacité était valide dans des travaux antérieurs.

Les mesures de ITV sur une seule cellule sphérique, sur une seule cellule attachée, et sur des cellules groupées sont en adéquation avec les résultats numériques, tandis que dans des cas plus complexes des déviations des amplitudes mesurées et calculées apparaissent. Cela est dû à des variations de l'inclinaison de courbe de la calibration, à des différences entre les paramètres réels et les paramètres du modèle, à l'état physiologique des cellules et à la configuration expérimentale. En outre, on a observé que en utilisant les mêmes paramètres utilisés pour mesurer l'ITV, les cellules groupées se sont comportées comme électriquement connectées l'une à l'autre, c'est-à-dire comme si un groupe des cellules a les propriétés d'une seule cellule géante.

Les calculs obtenues de manière numérique sur les modèles des cellules avec la membrane remplacé par une condition de limite ont besoin de considérablement moins d'éléments dans le modèle, et par conséquent le temps pour obtenir les résultats du modèle est considérablement réduit. On a également montré que le calcul du ITV sur les modèles simplifiées des cellules de forme irrégulière peut être confrontés à des déviations

considérables du ITV calculé par rapport à un modèle plus réel. L'orientation du champ électrique change l'amplitude et la distribution du ITV, par conséquence la perméabilisation change aussi. En bref, la perméabilisation d'une cellule sphéroïdale dont le plus long axe est parallèle avec le champ électrique est plus probable que la perméabilisation d'une cellule où il est perpendiculaire au champ.

La comparaison des ITVs mesuré et calculé avec des observations d'électroperméabilisation sur une seule cellule sphérique et sur une seule cellule attachée a confirmé que le perméabilisation se produit dans les régions de la membrane, où la valeur absolue d'ITV est la plus haute (soit les régions faisant face aux électrodes). Les expériences additionnelles sur les cellules sphériques ont prouvé que pendant et juste après l'impulsion, la fluorescence des cellules augmente de manière asymétrique si des impulsions unipolaires étaient fournies, alors qu'une augmentation de la fluorescence symétrique était observée avec des impulsions bipolaires. Ces observations ont été attribuées à l'effet électrophorétique de l'impulsion. Sur une plus longue échelle de temps, l'asymétrie dans la fluorescence était toujours observée, même pour des impulsions bipolaires, et nous n'avons trouvé aucune explication raisonnable pour cela. La valeur critique d'ITV, auquel la perméabilisation se produit, a été calculée à partir de l'angle polaire du perméabilisation mesuré juste après l'impulsion, et a été évalué de l'ordre de 450 mV, en accord avec les seuils critiques rapportés. Les résultats de perméabilisation obtenus sur des cellules groupées ont prouvé que ces cellules, aux paramètres d'impulsion utilisés dans ces expériences, se sont comportées comme isolées électriquement et perméabilisées individuellement. C'est en contradiction à ce qu'on a observé pendant les mesures d'ITV, où les cellules groupées se sont comportées comme électriquement reliées. Ceci a pu être le résultat d'ouverture et de fermeture des jonctions d'espace en fonction des paramètres d'impulsion.

Les mesures de la cinétique du transport membranaire ont prouvé que avec des amplitudes d'impulsion, ou avec de durées d'impulsion progressivement croissantes, le transport de colorant dans des cellules augmente aussi. Une hausse forte était observée quelques millisecondes après le début de l'impulsion, suivi d'une augmentation additionnelle modérée de fluorescence. Les résultats mesurés sur un intervalle de temps de 400  $\mu$ s ont indiqué que le transport à travers la membrane perméabilisée peut être détecté à moins de 100  $\mu$ s après le début de l'impulsion. En outre, une dynamique différente d'augmentation de la fluorescence pendant et après l'impulsion a été observée.

Les expériences sur les suspensions denses de cellules ont prouvé qu'avec l'augmentation de la densité de cellules (de  $10 \times 10^6$  cells/ml à  $400 \times 10^6$  cells/ml) la fraction des cellules perméabilisées a diminuée approximativement de 50%. Nous avons attribué ceci aux variations du champ électrique local, qui mènent à une diminution de l'amplitude d'ITV. La prise de l'iodure de propidium a également diminué avec la densité croissante de cellules, mais avec une plus grande ampleur que prévu à partir des résultats de la perméabilisation. Nous avons supposé que la diminution additionnelle de la fluorescence était principalement

due au gonflement de cellules après le perméabilisation, qui a restreint la disponibilité extracellulaire de colorant à la membrane perméabilisée, et a gêné la diffusion de colorant dans les cellules. Le récupération des cellules a semblé être plus lente dans les suspensions denses, en accord avec les prédictions liées au gonflement de cellules résultant de l'électroperméabilisation.

# 1 INTRODUCTION

## 1.1 Resting and induced transmembrane voltage

From the electrical point of view, cell membrane presents a thin insulating layer, which divides two electrically conductive compartments - the cytoplasm and the extracellular medium. Cell membrane is mainly composed of lipid molecules, which organize themselves to form a bilayer (the hydrophilic heads are oriented towards the outside environment while the hydrophobic tails are oriented to the inside of the membrane). Proteins, which can also be found in the membrane, incorporate into the membrane with their nonpolar regions in contact with lipid chains, and polar regions oriented outwards. Such membrane structure prevents the water to enter the membrane. The phospholipid bilayer also contains cholesterol, which makes the bilayer stronger, more flexible and more permeable (Figure 1.1).

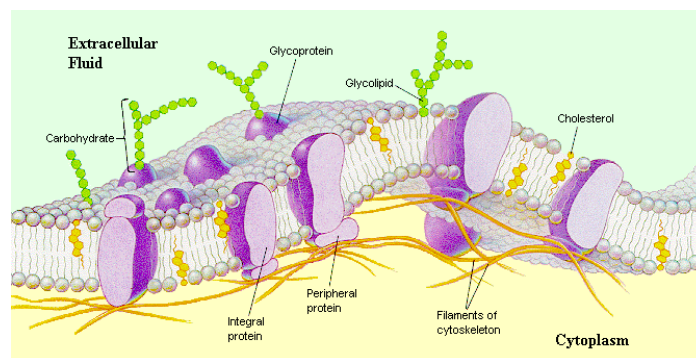


Figure 1.1. The cell membrane (Chiras, 2002).

### 1.1.1 Resting transmembrane voltage

When a biological cell is in its physiological state, a small voltage, termed resting transmembrane voltage (RTV), is constantly present on its membrane. In most cells this voltage is negative, i.e. inside of the cell is more negative with respect to the outside (between -30 and -90 mV). For RTV to occur a concentration gradient of ions must exist across the membrane and the membrane must contain ion selective channels (e.g.  $K^+$  and  $Na^+$  channels). The RTV is a consequence of the interplay of a system of active  $Na^+-K^+$  pumps and  $K^+$  channels. In every cycle the  $Na^+-K^+$  pump transfers 3  $Na^+$  ions out of the cell and 2  $K^+$  ions into the cell for every ATP hydrolyzed. This changes the intracellular and extracellular concentrations of  $Na^+$  and  $K^+$  ions inside the cell and at the same time contributes to the electric potential difference across the membrane. The  $K^+$  channels allow  $K^+$  to leak out of the cell but at sufficiently negative RTV this leakage stops as the concentration gradient is equilibrated by electric potential gradient in the opposite direction (Alberts et al., 2004).

In equilibrium, the electrochemical potentials for the ion  $S$  on both sides of the membrane must be equal ( $i$  and  $o$  stand for the inside and outside of the membrane, respectively):

$$Z_S \cdot F \cdot V_i + R \cdot T \cdot \ln[S]_i = Z_S \cdot F \cdot V_o + R \cdot T \cdot \ln[S]_o, \quad (1.1)$$

In Eq. 1.1,  $Z_S$  is the valence of the  $S$ ,  $F$  is the Faraday's constant,  $V$  is electric potential,  $R$  is the gas constant,  $T$  is the temperature, and  $[S]$  the concentration of ion  $S$ . This equation explains that for the equilibrium of the ion  $S$  across cell membrane, the work needed to transfer the ion outside the cell equals to the work needed to transfer the ion inside the cell through the membrane. If we define the membrane voltage  $U_m$  as a difference of electric potentials inside and outside the cell, we obtain the *Nernst equation* (Alberts et al., 1994):

$$U_m = V_i - V_o = \frac{R \cdot T}{Z_S \cdot F} \cdot \ln \frac{[S]_o}{[S]_i}. \quad (1.2)$$

This voltage is often referred to as the *equilibrium voltage* for the ion  $S$ . In case of two ions (for example  $\text{Na}^+$  and  $\text{K}^+$ ) we can write:

$$U_m = \frac{R \cdot T}{F} \cdot \ln \frac{[\text{Na}^+]_o}{[\text{Na}^+]_i} = \frac{R \cdot T}{F} \cdot \ln \frac{[\text{K}^+]_o}{[\text{K}^+]_i}. \quad (1.3)$$

For the most important ions found in the cell, Eq. 1.3 can be expressed in the form of *Gibbs-Donnan* equilibrium:

$$\frac{[\text{K}^+]_o}{[\text{K}^+]_i} = \frac{[\text{Na}^+]_o}{[\text{Na}^+]_i} = \frac{[\text{Cl}^-]_i}{[\text{Cl}^-]_o} = \left( \frac{[\text{Ca}^{2+}]_o}{[\text{Ca}^{2+}]_i} \right)^2. \quad (1.4)$$

By applying Eq. 1.4 to ions in most biological cells, we find that in most cases the Gibbs-Donnan equilibrium does not hold; the ions are not always in equilibrium (Table 1.1) and the Nernst equation is therefore not always suitable for determining RTV on the cell membrane.

**Table 1.1. Concentration of the most representative ions inside and outside the mammalian cell (Alberts et al, 1994).  $X^-$  denotes the large, negatively charged proteins.**

Ion concentrations in mmol/l		
	outside	inside
$\text{Na}^+$	150	12
$\text{K}^+$	4	142
$\text{Cl}^-$	120	6
$X^-$	34	148

In order to determine RTV on the membrane, we must take into account the flow of ions through the membrane (via passive and active membrane protein channels), which are responsible for the development and the maintenance of resting voltage. If RTV is constant, i.e. time invariant, then the sum of all currents flowing through the membrane must equal zero. For two most important ions,  $\text{Na}^+$  and  $\text{K}^+$ , we can write the following equation:

$$J_K + J_{Na} = 0 \quad (1.5)$$

For the ion  $S$  the current  $J_S$  through the membrane can be derived by accounting for the electrical and diffusion force that act on an ion inside the membrane:

$$J_S = -D_S \frac{d[S]}{dx} - k \cdot D_S \cdot [S] \frac{dV}{dx} \quad k = \frac{Z_S \cdot F}{R \cdot T}, \quad (1.6)$$

with  $D_S$  a diffusion constant and the other parameters the same as above. By integrating the Eq. 1.6 over the thickness of the membrane  $d$  and defining the permeability of the membrane  $P_S$  as  $D_S/d$ , we obtain:

$$J_S = f(V) \cdot P_S \cdot ([S]_i \cdot e^{k \cdot U_m} - [S]_o) \quad f(V) = \frac{d}{\int_0^d e^{k \cdot U_m} dx} \quad (1.7)$$

By inserting Eq. 1.7 into Eq. 1.5, the function of the potential inside the membrane ( $f(V)$ ) falls out of the equation, and we finally obtain *Goldman's equation*, which denotes resting transmembrane voltage on the membrane. For given intracellular and extracellular ion concentrations and their membrane permeability coefficients  $P$  the equation yields:

$$U_{RTV} = \frac{R \cdot T}{F} \ln \frac{P_{Na} \cdot [Na^+]_o + P_K \cdot [K^+]_o}{P_{Na} \cdot [Na^+]_i + P_K \cdot [K^+]_i} \quad (1.8)$$

### 1.1.2 Induced transmembrane voltage

When a biological cell is exposed to an external electric field, the induced transmembrane voltage (ITV) forms on its membrane. During the field exposure, ITV superimposes to resting, while after the exposure only resting voltage remains on the membrane. Transmembrane voltage occurs as a consequence of the ion redistribution in the electric field and for a spherical cell with radius  $R$  can be calculated using Schwan's equation (Schwan, 1957; Kotnik et al., 1997):

$$U_{ITV} = f_s RE \cos \varphi \quad (1.9)$$

where  $\varphi$  is the angle between the direction of the field and the line connecting the center of the cell and the point of interest on the membrane (Figure 1.2A), and  $f_s$  is a function reflecting the electric and dimensional properties of the cell and the surrounding medium (Kotnik et al., 1997):

$$f_s = \frac{3\lambda_o \left[ 3dR^2\lambda_i + (3d^2R - d^3)(\lambda_m - \lambda_i) \right]}{2R^3(\lambda_m + 2\lambda_o) \left( \lambda_m + \frac{1}{2}\lambda_i \right) - 2(R-d)^3(\lambda_o - \lambda_m)(\lambda_i - \lambda_m)} \quad (1.10)$$

In Eq. 1.10,  $\lambda_o$ ,  $\lambda_i$ , and  $\lambda_m$  are the specific conductivities of the extracellular medium, cytoplasm and the membrane, respectively, and  $d$  is the thickness of the membrane. Under physiological conditions, where  $\lambda_m$  is at least five orders of magnitude smaller than both  $\lambda_o$  and  $\lambda_i$ ,  $f_s$  is very close to the value of 3/2, and the Schwan's equation is often written as:

$$U_{ITV} = 1.5RE \cos \varphi \quad (1.11)$$

In contrast to the RTV, the ITV varies with the position on the cell membrane (Figure 1.2B), is proportional to the electric field, and is also influenced by cell geometry and electrical characteristics of the medium surrounding the cell.

The response of the ITV to a step change of a DC field can be calculated as:

$$U_{ITV} = f_s RE \cos \varphi (1 - e^{-t/\tau}), \quad (1.12)$$

where  $\tau$  is the time constant of the membrane:

$$\tau = \frac{Rc_m}{\frac{2\lambda_o\lambda_i}{2\lambda_o + \lambda_i} + \frac{R}{d}\lambda_m}, \quad (1.13)$$

and  $c_m = \varepsilon_m / d$  is the membrane capacitance, with  $\varepsilon_m$  denoting the membrane permittivity. The Eq. 1.13 is valid also in case of rectangular pulses (Figure 1.2C), while for electric fields with shapes different from rectangular, different solutions for ITV were derived. For the cases of triangular, trapezoidal, exponential, sine modulated pulses and for trains of such pulses, the solutions and the complete derivations of the ITV can be found in (Kotnik et al, 1998).

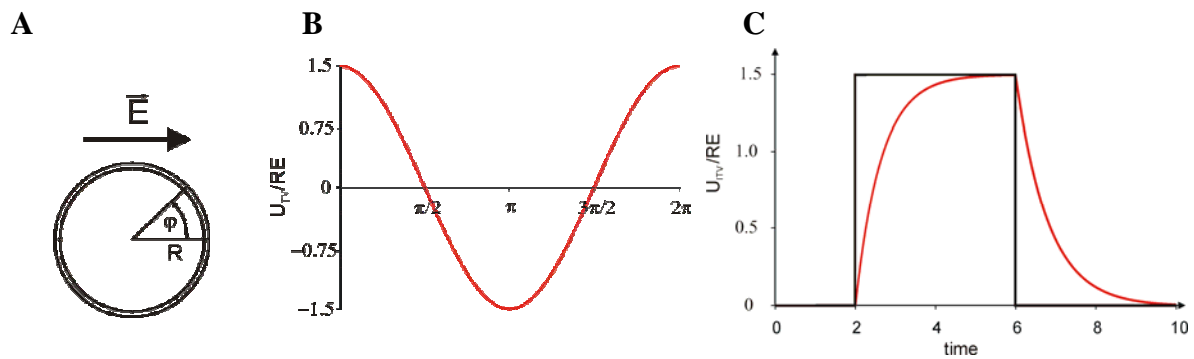


**Figure 1.2.** (A) The model of the cell. (B) The dependence of the ITV on the position on the cell membrane. (C) The time response of induced transmembrane voltage to a rectangular pulse.

For some regular geometrical shapes, such as spheroids and ellipsoids, the exact analytical solutions were derived, which are used instead of the Schwan's equation, while for more complicated cell geometries, an analytical description is in general not attainable. ITV in these cases can be assessed only experimentally or numerically (Gross, et al., 1986; Bedlack et al., 1994; Pucihar et al., 2006).

## 1.2 Measurements of resting and induced transmembrane voltage

Membrane voltage can be measured by using microelectrodes (which can be classical microelectrodes or patch-clamp) or potentiometric fluorescent dyes. While resting voltage can be measured with both methods, induced voltage is usually measured by means of potentiometric dyes, because the microelectrodes distort the electric field distribution around the cell and therefore directly affect the value of induced voltage. The following paragraphs contain a brief description of the most commonly used microelectrodes and fluorescent dyes.

### 1.2.1 Microelectrodes

Microelectrodes were introduced in 1949 by Ling and Gerard to measure the membrane voltage of frog muscle fibres (Ling and Gerard, 1949). The electrodes are made of glass tubes filled with a conductive electrolyte solution (usually 3M KCl, VanDuijn et al., 1988), which provides electrical contact between the cell interior and the voltmeter (Figure 1.3). The reference electrode, which is in the extracellular medium, is usually an Ag/AgCl electrode. The electrodes for intracellular recordings of mammalian cells have to be very fine tipped in order to impale membranes of living cells. To determine the tip diameter, which should be in the order of  $\mu\text{m}$  or less, electrical measurements of the ohmic resistance are usually employed and generally, the resistances range from 20 to 500 M $\Omega$ . Sharp and small tip makes microelectrodes different in shape and size to those used for patch-clamp recording (see

below). While the temporal resolution of the membrane voltage measured with microelectrodes is high, the spatial resolution is their limiting factor.

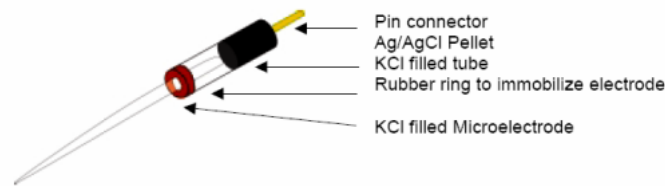


**Figure 1.3. Microelectrode.**

### ***1.2.1.1 Patched electrodes***

In comparison with standard microelectrodes, the patch electrodes have larger tips and are filled with isotonic solutions (e.g. Ringer's, Tyrode's solutions). The advantage of the patch clamp over the microelectrodes is that they can be used to measure the membrane voltage on cells, which are very thin (e.g. in tissues) and are difficult to impale by the microelectrode.

The patch clamp technique was introduced initially by Cole in the late 1930's and was exploited by Hodgkin and Huxley in the late 1940's (Cole 1968; Hodgkin 1951). Nowadays, patch-clamp recording is the leading method for studying the behavior of ion channels. In 1976, Neher and Sakmann (Neher and Sakmann, 1976) first used the cell-attached configuration of the patch-clamp technique to resolve current flow through single acetylcholine-activated cation channels in frog skeletal muscle. Subsequent improvements of the technique produced a range of methods for the high resolution recording of current flow through ion channels in both intact cells and excised membrane patches (Hamill et al., 1981). With patch clamp techniques, real-time measurements of currents with amplitudes of 200 fA flowing through a single channel are possible. *On-cell patch* is obtained when a glass patch-pipette forms high resistance electrical seal ( $\geq 10 \text{ G}\Omega$ ) with cell membrane (Figure 1.4A). Membrane patches can be excised from cells to form either the excised *inside-out* or *outside-out* configurations (Figures 1.4B and D). Alternatively, the membrane patch can be destroyed to establish the *whole-cell* configuration (Figure 1.4C). This configuration is equivalent to intracellular recording with sharp microelectrodes and is also used to measure membrane voltage. The different configurations of the patch-clamp technique permit precise control of the composition of the solutions on either side of the cell membrane. As a result, the regulation of ion channels can be investigated simply by adding ion channel modulators into either the bath or pipette solutions while the selectivity of ion channels can be determined by manipulating the ionic composition of these solutions.

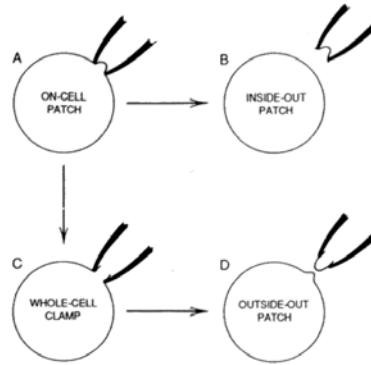


**Figure 1.4.** Patch clamp configurations. (A) On cell patch, (B) inside-out patch, (C) whole-cell clamp, (D) outside-out patch.

### 1.2.1.2 Patch clamp recordings

In general, two patch-clamp recordings are possible, the *voltage clamp* and the *current clamp*. When the membrane voltage is held (clamped) at a constant value and the current that flows through the membrane is measured, the technique is called *voltage-clamp*. Basic voltage clamping involves two electrodes, one to control the cell membrane voltage, and the other to measure the current response of the cell (Figure 1.5). The membrane voltage is recorded by a unity-gain buffer amplifier (A1) connected to the voltage recording electrode (E1). The membrane voltage  $U_m$  is compared with the reference voltage ( $U_{ref}$ ) in a high gain differential amplifier (A2) and the difference drives the current through the cell via electrode E2 until the membrane voltage ( $U_m$ ) and the reference voltage ( $U_{ref}$ ) are the same.

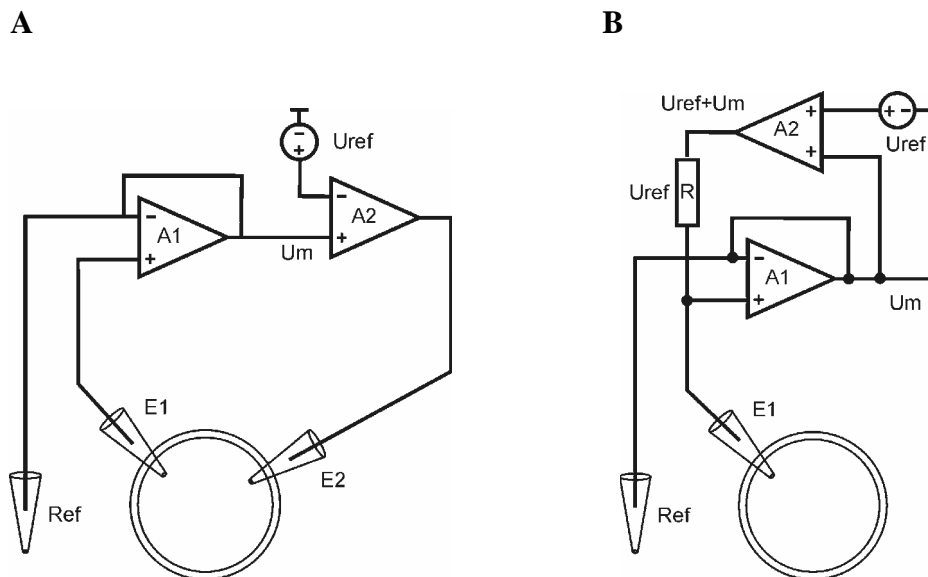


**Figure 1.5.** (A) Voltage clamp and (B) current clamp.

In *current-clamp experiment*, the amplifier controls the current and measures the change in membrane voltage caused by the applied current. Usually the current is passed to stimulate a cell or modify its resting voltage during intracellular voltage recording (Neher et al. 1978; Hamill et al., 1981). This allows the detection and measurement of action potentials in excitable cells such as neurons. One of the possible realizations of current clamp (a current source) is shown in Figure 1.5B. The voltage across the resistor  $R$  is equal to the reference voltage  $U_{ref}$  regardless of the value of the membrane voltage  $U_m$ . Thus, the current through the resistor and through the pipette to the cell can be adjusted by changing the  $R$  or  $U_{ref}$  ( $I = U_{ref}/R$ ). The membrane voltage can be measured by using only the voltage follower  $AI$ .

### 1.2.2 Potentiometric fluorescent dyes

One of the possibilities to measure the membrane voltage on cells, organelles and vesicles that are too small to be studied with microelectrodes is to use dye molecules as potentiometric optical probes. By using different imaging techniques, these probes can be employed to map variations in membrane voltage across excitable cells and perfused organs, with spatial resolution that is not achievable using microelectrodes. Potentiometric probes include the cationic carbocyanines and rhodamines, the anionic oxonols and merocyanine 540 and the styryl dyes. Based on their response mechanism, probes can be divided into two categories:

- *Slow-response probes (or redistribution probes)* exhibit voltage-dependent changes in their transmembrane distribution that are accompanied by a fluorescence change (Sims et al., 1974). The magnitude of their optical response is up to 100% fluorescence change per 100 mV. Slow-response probes, which include cationic carbocyanines and rhodamines, and anionic oxonols, are suitable for detecting changes in resting membrane voltage of nonexcitable cells caused by respiratory activity, ion-channel permeability, drug binding and other factors (Loew et al., 1982; Cohen et al., 1974; Waggoner, 1998).
- *Fast-response probes* (usually styrylpyridinium dyes) operate by means of a change in their electronic structure, and consequently their fluorescence properties, in response to a change in the surrounding electric field (membrane voltage) (Grinvald et al., 1982; Grinvald et al., 1983). Their optical response is sufficiently fast to detect transient (millisecond or microsecond) potential changes in excitable cells, including single neurons, cardiac cells, and intact brains (Bedlack et al., 1992; Knisley et al., 1993; Bedlack et al., 1994; Cheng et al., 1999). In addition, they can be used to study the changes in membrane voltage on nonexcitable cells, caused by the exposure of cells to electromagnetic fields (Gross et al., 1986; Ehrenberg et al., 1987; Lojewska et al., 1989). The amplitude of the voltage-dependent fluorescence change of fast probes is often small, 2–10% of the fluorescence change per 100 mV.

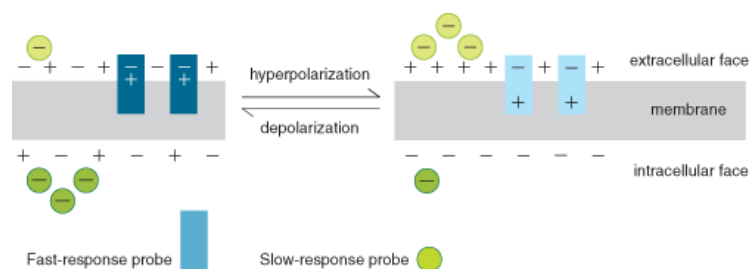


**Figure 1.6. Response mechanisms of membrane voltage probes. Slow-response probes are lipophilic anions or cations that are translocated across membranes by an electrophoretic mechanism. Fluorescence changes associated with transmembrane redistribution result from sensitivity of the probe to intracellular and extracellular environments. Fast-response probes undergo electric field-driven changes of intramolecular charge distribution that produce corresponding changes in the spectral profile or intensity of their fluorescence. Thus, potentiometric response speed directly reflects the time constants of the underlying processes - fast intramolecular redistribution of electrons versus relatively slow transmembrane movement of entire molecules.**

### 1.2.2.1 Slow dyes

#### *Carbocyanines*

- Indo- (DiI), thia- (DiS) and oxa- (DiO) carbocyanines with short alkyl tails (<7 carbon atoms) were among the first potentiometric fluorescent probes developed. These cationic dyes accumulate on hyperpolarized membranes and are translocated into the lipid bilayer. Aggregation within the membrane interior results in decreased fluorescence and absorption shifts, although the amplitude and even the direction of the fluorescence response is dependent on the concentration of the dye and its structural characteristics (Sims et al., 1974). DiOC<sub>6</sub>(3) and DiOC<sub>5</sub>(3) have been the most widely used carbocyanine dyes for membrane voltage measurements (Novo et al., 1999; Remani et al., 1999; Shapiro, 2000). The indocarbocyanine DiIC<sub>1</sub>(5) was used to measure mitochondrial potential in apoptotic cells. Carbocyanine dyes, particularly thiacyanines such as DiSC<sub>3</sub>(5), can inhibit respiration and may therefore be cytotoxic (Anderson et al., 1993).
- *JC-1*: JC-1 (5,5',6,6'-tetrachloro-1,1',3,3'-tetraethylbenzimidazolylcarbocyanine iodide) exists as a green-fluorescent monomer at low concentrations or at low membrane voltage. However, at higher concentrations or higher voltages, JC-1 forms red-fluorescent "J-aggregates". Because J-aggregate formation increases with applied membrane voltage, this phenomenon can be used for membrane voltage measurements. Ratiometric measurements are possible by combining signals from the green-fluorescent JC-1 monomer (emission at 529 nm) and the red-fluorescent J-aggregate (emission at 590 nm), with excitation at 485 nm. A review by Chen and Smiley describes the properties of JC-1 and its use for investigating mitochondrial potentials in live cells (Chen and Smiley, 1993). The most widely implemented application for JC-1 is the detection of mitochondrial depolarization occurring in apoptosis (Reers et al, 1991; Smiley et al., 1991).

### *Rhodamine Probes*

- Rhodamine 123 is widely used as a structural marker for mitochondria and as an indicator of mitochondrial activity (Johnson et al., 1981; Smiley et al., 1991; Scaduto et al., 1999). TMRM and TMRE, the methyl and ethyl esters of tetramethylrhodamine are closely related to rhodamine 123. They were developed by Loew and colleagues (Ehrenberg et al., 1988; Farkas et al., 1989; Loew et al., 1992) and follow the Nernstian distribution closely, requiring only minor corrections for the nonspecific binding. Because the fluorescence of TMRM and TMRE is relatively insensitive to the environment, their transmembrane distribution can be directly related to the membrane voltage using the Nernst equation. These dyes were also used for measuring the mitochondrial membrane voltage (Farkas et al., 1989).

### *Oxonols*

- Oxonol V and Oxonol VI: The anionic bis-isoxazolone oxonols accumulate in the cytoplasm of depolarized cells by a Nernst equilibrium-dependent uptake from the extracellular solution (Smith and Chance, 1979). DiBAC Dyes (DiBAC<sub>4</sub>(3), DiSBAC<sub>2</sub>(3), DiBAC<sub>4</sub>(5)), usually referred to as "bis-oxonols", enter depolarized cells, where they bind to intracellular proteins or membranes and exhibit enhanced fluorescence and red spectral shifts. Voltage-dependent fluorescence changes generated by DiBAC<sub>4</sub>(3) are typically ~100% per 100 mV (Epps et al., 1994).

### *Merocyanines*

- Merocyanine 540 was among the first fluorescent dyes to be used as a potentiometric probe (Wagoner 1988), however, its use has declined mostly because of its high phototoxicity. Merocyanine 540 exhibits a biphasic kinetic response to membrane polarization changes. It binds to the surface of polarized membranes in a perpendicular orientation, reorienting as the membrane depolarizes to form nonfluorescent dimers with altered absorption spectra (Dragsten and Webb, 1978). This fast (microseconds) reorientation is followed by a slower response caused by an increased dye uptake (milliseconds to seconds). Merocyanine 540 is also a useful probe of lipid packing because it binds preferentially to membranes with highly disordered lipids (Stillwell et al., 1993). Fluorescence of merocyanine 540 is sensitive to heat-induced changes in the organization of membrane lipids (Kumar et al., 1990).

### **1.2.2.2 Fast dyes**

#### *Styryl Dyes*

The ANEP (AminoNaphthylEthenylPyridinium) dyes developed by Loew and co-workers are among the most sensitive of the styryl fast-response probes (Loew et al., 1978; Loew et al., 1979; Loew et al., 1985). Di-4-ANEPPS and di-8-ANEPPS, exhibit uniform 10% per 100 mV changes in fluorescence intensity in a variety of tissue, cell and model membrane systems. The response time of these dyes is in a microsecond time range. The styryl dyes exhibit good

photostability and low toxicity, and are essentially nonfluorescent in aqueous solutions. Both di-4-ANEPPS and di-8-ANEPPS respond to increases in membrane potential (hyperpolarization) with a decrease in fluorescence excited at approximately 440 nm and an increase in fluorescence excited at 530 nm. These excitation spectral shifts permit the use of ratiometric methods (Montana et al., 1989; Hayashi et al., 1996). Potential-dependent fluorescence emission ratio measurements (ratio of emission intensities at 560 nm and 620 nm after excitation at 475 nm) have also been reported using both dyes (Knisley et al., 2000; Kao et al., 2001). Styryl dyes can be used on nonexcitable cells to measure the changes in membrane voltage during the electric field exposure (Gross et al. 1986; Ehrenberg et al., 1987; Loew, 1992). In fact, di-4 ANEPPS was used to experimentally demonstrate, for the first time, the validity of the Schwan's equation on biological membranes (Gross et al., 1986).

### *RH Dyes*

Originally synthesized by Rina Hildesheim, the RH dyes include an extensive series of dialkylaminophenylpolyenylpyridinium dyes that are mainly used for functional imaging of neurons (Grinvald et al., 1983; Denk et al., 1994). Currently, the most widely used RH dyes are RH 414, RH 795 and RH 237. The RH 421 probe has yielded the most sensitive response recorded for a fast potentiometric probe, exhibiting a more than 20% fluorescence change per 100 mV on neuroblastoma cells (Grinvald et al., 1983; Grinvald et al., 1988). The RH dyes exhibit varying degrees of fluorescence excitation and emission spectral shifts in response to membrane voltage changes. RH 292 proved to be very successful for measuring voltage changes of sea urchin eggs exposed to high external electric fields (Hibino et al., 1991; Hibino et al., 1993). Using a pulsed laser, synchronized to both the field pulse and the video acquisition system, the authors were able to monitor the changes in membrane voltage at submicrosecond time resolution.

### ***1.2.2.3 Calibration***

Changes of fluorescence and absorption obtained with potentiometric dyes for any given voltage change can depend on the dye-to-cell ratio, the total concentration of the dye, and the type of cell. Thus there is no universal calibration curve, which would relate fluorescence to millivolts of membrane voltage. The calibration curve is obtained by setting the membrane voltage to different values and determining the dye absorbance or fluorescence at these voltages (Wagonner, 1988). However, it is not always possible to experimentally establish a membrane voltage that is known with confidence (mostly because the ionic concentrations within the cell are not accurately determined). Generally, valinomycin is used to induce a  $K^+$  equilibrium voltage, which is given by the Nernst equation, and it is assumed that the  $K^+$  conductance in the presence of valinomycin is much larger than the other ionic conductances of the cell membrane so that the others are negligible. The internal  $K^+$  concentration of the cells must be determined, and calibration is completed by measuring the fluorescence or absorbance of cells in the presence of valinomycin in a number of separated experiments, each with a different external  $K^+$  concentration.

### 1.3 Electroporation

During the exposure of the cell to the electric field, the induced component of the transmembrane voltage superimposes to the resting component. When the sum of both voltages exceeds some critical value (the exact value depends on the cell type and experimental conditions (Tsong, 1991; Teissié and Rols, 1993; Bier et al. 1999; Miklavčič et al., 2000), the permeability of the cell membrane in those regions increases significantly. This phenomenon is termed electroporation or electropermeabilization (Tsong, 1991; Barnett and Weaver, 1991; Weaver and Chizmadzhev, 1996; Teissié et al., 1999; Neumann et al., 1999). While the first term corresponds to the increase in the membrane permeability in general, the second term assumes that the increased permeability is related to the occurrence of hydrophilic pores in the membrane. Provided that the parameters of the electric field (amplitude, duration, number of pulses, frequency) are moderate, the increased permeability is reversible, and cells return to their initial state a few minutes after the exposure (reversible electroporation). During the state of high permeability it is possible to deliver membrane-impermeant ions and small molecules (e.g. drugs, DNA) into the cell. Small molecules enter the cell with diffusion, while the transport of ions and electrically charged molecules (such as proteins and DNA) is driven by electrophoretic force caused by the electric field. Electroporation is finding an increasing use in biochemistry, molecular biology, and many fields of medicine (Neumann et al., 1999; Teissié et al., 1999). It has already become an established method in oncology for electrochemotherapy of tumors (Mir and Orlowski, 1999; Heller et al., 1999; Serša et al., 2003; Miklavčič et al., 2005), and holds great promises in gene therapy (Somari et al., 2000; Šatkauskas et al., 2002; Golzio et al., 2005).

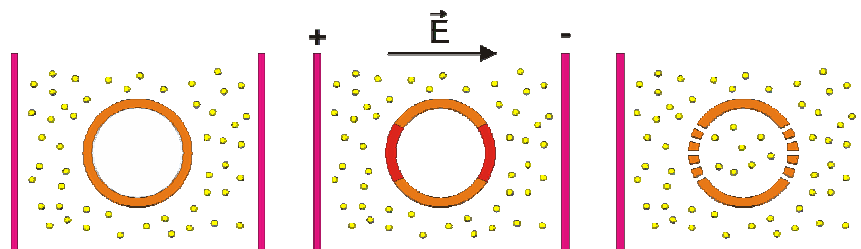
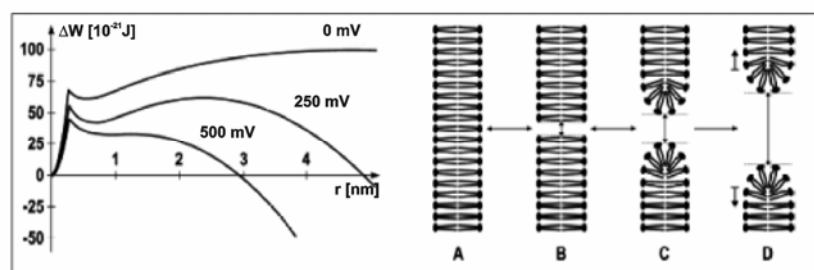


Figure 1.7. Electroporation.

#### 1.3.1 Theoretical models of electroporation

To explain the increase in permeability of the cell membrane due to electric field exposure, many models of electroporation were proposed. These include electrocompression model, denaturation of membrane channels, formation of cracks between lipid microdomains, etc. However, none of the mentioned models has confirmed the experimental observations (Weaver and Chizmadzhev, 1996). The most widely accepted model nowadays is the model of electroporation, which attributes the increase in membrane permeability to the occurrence of hydrophilic pores in the membrane (Weaver and Mintzer, 1981; Glaser et al., 1988).

Electroporation model predicts that the increased membrane voltage decreases the energy necessary for formation of hydrophilic pores and consequently increases the probability of this event (Figure 1.8). It also explains the slow resealing because each pore must exceed a certain energy threshold for its closure. Model of electroporation predicts that the diameter of a hydrophilic pore is in the order of 1 nm, and that the stability of the pore decreases rapidly with the increase in membrane voltage. At a supracritical voltage of a few hundreds of mV, irreversible breakdown occurs, which is in agreement with experimental observations. Many improvements to the existing model of electroporation were proposed, which include the influence of membrane conductivity, membrane curvature, osmotic pressure and ion concentration of the cytoplasm and extracellular medium (Barnett and Weaver, 1991; Freeman et al., 1994; Neumann et al., 1999; DeBruin and Krassowska, 1999). Recently, it became possible to perform computer simulations of the molecular dynamics of lipids, i.e. their movement within the bilayer surrounded by ion solution. The simulations confirm the influence of the increase in membrane voltage on the increase in the probability of the pore formation (Tieleman et al., 2003; Leontiadou et al., 2004; Kasson et al., 2004). The pores in molecular simulations are less regularly shaped than those depicted in Figure 1.8, but are stable and close with the decrease in the membrane voltage.



**Figure 1.8.** Energy of membrane pore as a function of its radius (left) and a schematic drawing of electroporation (right). According to the laws of thermodynamics, the minimum pore energy corresponds to a stable state. The first minimum is at pore radius zero, when membrane is not permeabilized (right - A). The sharp maximum of pore energy represents the threshold at which a hydrophobic pore (right - B) transforms into a hydrophilic pore (right - C). By increasing the voltage on the membrane, this threshold decreases, thereby increasing the probability of the occurrence of hydrophilic pore. At moderate voltages the hydrophilic pore stabilizes in the second energy minimum (right - C), while at still higher voltages this minimum disappears and the pore expands (right - D) until the membrane ruptures – irreversible permeabilization.

### 1.3.2 A brief history of electropermeabilization and the experimental results

The first report on the electrical breakdown of the cell membrane was published in 1958 by Stämpfli (Stämpfli, 1958). Approximately a decade later, Sale and Hamilton published a series of papers, describing the nonthermal killing of microorganisms with short, high voltage electric pulses (Sale and Hamilton, 1967; Hamilton and Sale, 1967; Sale and Hamilton, 1968). In 1972 Neumann and Rosenheck demonstrated that electric pulses cause considerable but reversible increase in the membrane permeability, which could be used for

the uptake of membrane impermeable molecules to cells (Neumann and Rosenheck, 1972). This paper presents a milestone in the research of electropermeabilization, because it initiated the interest of other researchers and research groups.

First systematic studies of electropermeabilization were based on the measurements of electric characteristics of the membrane during the exposure to electric pulses. Changes in membrane conductance and membrane capacitance were detected already a few microseconds after the onset of the supracritical electric field (Babakov and Ermishkin, 1966; Neumann and Rosenheck, 1972). These measurements showed that membrane conductivity increases by more than thousandfold, while the increase in the capacitance is only a few percents, showing that the electrocompression of the membrane is not playing a significant role in electropermeabilization. Under moderate electric field parameters, the membrane capacitance and the membrane conductivity gradually returned to their initial values.

Some researchers attempted to investigate the electropermeabilization under the microscope to visualize the pores predicted by the electroporation theory (Chang and Reese, 1990). However, these attempts all failed and even today it is still impossible to directly observe the changes in the lipid bilayer during electropermeabilization. Only indirect observations of the phenomenon are possible, for example, by using potentiometric fluorescent dyes to monitor the changes in the transmembrane voltage, or by using water soluble fluorescent dyes to observe the flow of molecules through the membrane. Fast potentiometric fluorescent dyes are used for observing the membrane voltage, because the changes in the voltage occur within microseconds after the onset of the electric pulse. If the voltage is sufficiently high, the cosine dependence on the areas, where the voltage is higher than the critical value, decreases in the next few microseconds, showing the onset of electropermeabilization of that area of the membrane (Hibino et al. 1991; Hibino et al., 1993).

With the measurements of the polarization of absorbed and reflected light it is possible to estimate the orientation of lipid heads in the membrane. Kakorin with co-workers (Kakorin et al., 1996) used this principle to demonstrate that the changes in the polarization of the light occur in the first microseconds after the onset of the pulse. Their measurements also show that during the time when the changes occur, water enters into bilayer, which they attributed to the occurrence of the hydrophilic pores (transformation from B to C in Figure 1.8). These pores should occupy between 0.02 to 0.2% of the total surface of the membrane, depending on the intensity of electropermeabilization.

### **1.3.3 Parameters that influence cell electropermeabilization**

When electropermeabilization is performed on a large cell population, one usually aims to obtain the highest possible fraction of permeabilized cells that also recover after the electric field exposure. Besides, the uptake of molecules to permeabilized cells should be as high as possible. In general, the intensity of permeabilization (and consequently the uptake of

molecules), increases with increasing amplitude of the external electric field, duration of pulses and their number. However, with the increase of each of these parameters, the fraction of cells that do not survive the treatment also increases. Through years of systematic experimental work of different research groups, the outlines regarding the voltage, duration and number of pulses were obtained, at which the optimal ratio between the fraction of permeabilized and viable cells is achieved (Rols and Teissié, 1990; Rols and Teissié, 1998; Canatella et al., 2001; Kotnik et al., 2001; Kotnik et al., 2003). In experimental conditions *in vitro*, the most usual pulse protocol for the uptake of small molecules is  $8 \times 100 \mu\text{s}$  or  $10 \times 100 \mu\text{s}$ , with a pulse frequency of 1 Hz. An example of such study *in vitro*, namely, the study of the shape of electric pulses, on the permeabilization, cell viability, and molecular uptake can be found in **paper 1** in the Appendix (Kotnik et al., 2003).

The pulse protocol  $8 \times 100 \mu\text{s}$ , 1 Hz, is also used in experiments *in vivo*, like for example electrochemotherapy, where the chemotherapeutic agents (bleomycin or cisplatin) are delivered to cutaneous or subcutaneous tumors (Mir et al., 1998; Serša et al., 2000; Čemažar et al., 2001). Recently, we proposed the use of high frequency pulses instead of standard 1 Hz pulse protocol for *in vivo* electrochemotherapy, in order to reduce muscle contractions associated to electric pulse delivery. First, we showed that the uptake of small molecules, with size similar to chemotherapeutics, into permeabilized cells *in vitro* remains at a similar level when pulse frequency increased from 1 Hz to 8300 Hz (Pucihar et al., 2002). Second, we demonstrated that the efficiency of electrochemotherapy with high frequency pulses remains at a similar level regardless of the pulse frequency (in the range from 1 Hz to 5000 Hz), while the number of muscle contractions with pulse frequencies higher than 100 Hz decreases considerably. The results of these two studies are described in detail in **paper 2** - *in vitro* study (Pucihar et al., 2002) and in **paper 3** - *in vivo* study (Miklavčič et al., 2005), in the Appendix.

Electropermeabilization can also be used to deliver larger, charged molecules (e.g. DNA) into cells. In this case, the uptake is achieved mainly by the electrophoretic force of the electric pulses, rather than by the diffusion of molecules. The pulse protocols used in gene therapy therefore consist of a short, high voltage permeabilizing pulses followed by longer, low voltage electrophoretic pulses (few milliseconds) (Klenchin et al., 1991; Sukharev et al., 1992; Šatkauskas et al., 2002; Šatkauskas et al., 2005).

Besides the parameters of electric pulses, electrical and physiological parameters of the cell and medium surrounding it also influence cell permeabilization. These include the temperature, conductivity of the extracellular medium, osmotic pressure, cytoskeleton and pH.

During the permeabilizing pulse, currents as high as few amperes can flow through cell suspension, but due to the short duration of the pulse, the increase in the temperature of the suspension is in most cases around  $1^\circ\text{C}$ . Some researchers use low conductivity media and in

this case, the temperature rise is even lower, approximately 0.1°C. While the preincubation temperature between 4°C and 37°C does not have a significant effect on cell survival or transfection efficiency, higher postincubation temperature considerably increases cell survival after permeabilization and also increases the transfection efficiency (Rols et al., 1994).

Conductivity of extracellular medium affects the amplitude of RTV and ITV (see Eqs. 1.8 and 1.10) and also the time constant of induced voltage (Eq. 1.13, Kotnik et al., 1997). We demonstrated that electropermeabilization of cells surrounded by media with progressively decreasing conductivities, results in increased survival of cells after permeabilization, while the fraction of cell permeabilization was less affected (Lojewska et al., 1989; Djuzenova et al. 1996; Pucihar et al, 2001). These results were attributed to the decrease in the amplitude of induced voltage and an increase in resting voltage on cells in low conductivity media. More details on this study can be found in **paper 4** in the Appendix (Pucihar et al., 2001).

Osmotic pressure of the pulsing medium affects the transfection efficiency, fusion of cells, and the uptake of molecules to permeabilized cells, while permeabilization and survival of cells are not affected considerably. The postpulse change in osmolarity of the medium influences the cell recovery, the transfection efficiency and the fusion index (Rols and Teissie, 1990; Golzio et al., 1998).

Altering the cell cytoskeleton, either with drugs such as colchicine, or by high temperature shock, was associated with a decrease in the stability of the electro-induced permeated structures. These experiments showed that the cytoskeleton has an important role in electropermeabilization recovery (Rols and Teissié, 1992).

Electropermeabilization of cells in a medium with neutral pH (pH = 7.0) yields the highest cell survival and transfection efficiency, while increasing or decreasing the pH value of the pulsing medium considerably decreases both cell survival and transfection efficiency (Xie and Tsong, 1992).

## 1.4 Objectives of the study

Despite increasing use of electroporation in different areas of biology and medicine, the events on the molecular scale that result in the increase in membrane permeability are still not completely understood. For biological cells, the mechanisms of electroporation are better understood in isolated cells or diluted cell suspensions than in tissues, where irregular shapes of cells, their mutual electric shielding, and perhaps connections between them (e.g. gap junctions) could play a role. To improve understanding of tissue electroporation, the researchers often use – both in theoretical analysis and in experiments – simple models of tissues, such as dense cell suspensions, cell pellets or multicellular spheroids (Abidor et al., 1993; Abidor et al., 1994; Susil et al., 1998; Pavlin et al., 2002; Schmeer et al., 2004; Canatella et al., 2004). These studies suggest that if cells are relatively close to each other, they respond to electric field differently from isolated cells. Indeed, in two recent theoretical studies the authors showed that the amplitude of transmembrane voltage induced on spherical cells progressively decreased when cells were brought closer together (Susil et al., 1998; Pavlin et al., 2002). In addition, an experimental study on multicellular spheroids showed that the uptake of molecules into cells after permeabilization in such spheroids is lower and spatially more heterogeneous than the uptake into isolated cells (Canatella et al., 2004). The observed differences in uptake were partly attributed to heterogeneous field strength caused by the proximity of neighboring cells.

In many applications of electroporation an efficient and at the same time reversible permeabilization is essential (e.g. DNA electrotransfer). Thus, a careful planning of the experiment, which involves the estimation of the amplitude of ITV leading to cell permeabilization, is required. It was demonstrated experimentally that induced transmembrane voltage (ITV) determines the regions of the membrane where electroporation occurs (Hibino et al., 1991; Hibino et al., 1993). Namely, increased permeability is observed only in regions of the membrane where ITV exceeds a critical value. As already stated, ITV is proportional to the electric field, varies with the position on the cell membrane, and is influenced by cell geometry and physiological characteristics of the medium surrounding the cell (Eqs. 1.9 and 1.10). For an isolated cell of simple shape, such as a cylinder, a sphere, or an ellipsoid, ITV can be described analytically (Schwan, 1957; Kotnik et al., 1997; Kotnik et al., 2000a; Kotnik and Miklavčič 2000; Gimsa and Wachner, 2001a; Gimsa and Wachner, 2001b). The analytical solution also holds for dilute suspensions of cells. However, in tissues the cell geometry is more complicated, cells are close enough to affect the electric field around each other, and they are often connected with pathways between them. In all these cases, an analytical description is in general not attainable and ITV can be determined either experimentally (e.g. with potentiometric fluorescent dyes (Gross et al., 1986; Montana et al., 1989; Loew, 1992; Knisley et al., 1993; Bedlack et al., 1994; Hassan et al., 2002) or numerically (Miller and Henriquez, 1988; Fear and Stuchly, 1998a; Fear and Stuchly, 1998b; Susil et al., 1998; Pavlin et al., 2002; Valič et al., 2003; Gowrishankar and Weaver, 2003; Stewart et al., 2004).

The experimental approach, which is simple and efficient with suspended cells or with cells growing in monolayers, is of limited use in tissues, where only the surface and a thin layer beneath it are directly accessible to standard microscopy techniques. For determination of ITV on cells in tissues, the numerical methods are thus often the only feasible approach. Due to complexity of the tissue structure, numerical models are either macroscopic, where the average or bulk electric properties (e.g. bulk conductivity or permittivity) are assigned to different types of tissues while detailed cell structure is not considered, or in case of microscopic models, the models are constructed using simple geometrical shapes (hemispheres, cubes). To better understand how the electric field interacts with tissues on a microscopic (single cell) level, which in turn determines the macroscopic behavior of the tissue, we constructed realistic microscopic models of irregularly shaped cells, clusters of such cells, and dense suspensions. Regarding the shape, density and connections between cells, these cell assemblies are in their complexity close to tissues and could provide new insights into the course of tissue permeabilization. First, the amplitude of RTV of cells used in the study was determined. Next, calculations of ITV were performed on models of single spherical, single attached cells, and cell clusters and they were compared to measurements of ITV on the same cells, from which the models were constructed. The course of electropermeabilization of these cells was then followed and the results were compared with measurements and calculations of ITV. In a separate experiment, a detailed investigation of kinetics of molecular transport into cells after permeabilization was performed. Similarly, for dense cell suspensions, the ITV calculated on a model of suspension was compared with fraction of permeabilized cells measured in suspensions with increasing cell densities. The following paragraphs contain more detailed information on these experimental and numerical approaches.

### **1.4.1 Measurements of resting transmembrane voltage**

When a biological cell is exposed to an external electric field induced transmembrane voltage (ITV) forms on its membrane. During the exposure, ITV superimposes to the native or resting transmembrane voltage (RTV) and when the sum of both voltages exceeds a critical value, the permeability of the cell membrane in these regions transiently increases. Because resting voltage is considerably smaller than ITV it is usually neglected and ITV is taken as a rough estimate of the total membrane voltage. In this study, however, resting voltage was experimentally determined and its contribution to the total membrane voltage was evaluated.

In addition, RTV was measured in cells in extracellular media with progressively decreasing conductivities. The measurements were compared to theoretical predictions from our previous study on the influence of such media on cell permeabilization (**paper 4** in the Appendix, Pucihar et al., 2001).

#### **1.4.2 Measurements of induced transmembrane voltage on single spherical cells, single irregularly shaped cells and cell clusters**

Quantitative measurements of induced transmembrane voltage on cells of spherical shape, irregular shape and cell clusters were performed by means of a potentiometric fluorescent dye. With these measurements it was possible to investigate the influence of cell shape, cell density, and pathways between cells on the distribution of ITV on a single cell and cell clusters. Namely, the measurements of ITV made it possible to determine, whether cells in clusters, when exposed to electric field, behaved as individual cells, or rather as one giant cell. ITV in this case was determined on cell membranes of the outermost layer of the cluster.

#### **1.4.3 Numerical calculations of induced transmembrane voltage on single spherical cells, single irregularly shaped cells and cell clusters.**

The main problems of numerical methods are related to realistic modeling of a cell and its membrane. The models in which the cell is built with simple geometric shape or by combining several simple geometric shapes are usually only rough approximations of the real cell shape (Fear and Stuchly, 1998a; Fear and Stuchly, 1998b; Cheng et al., 1999; Buitenweg et al., 2003; Valič et al., 2003). The other problem is the cell membrane, which is over a thousandfold thinner than the dimensions of a typical cell and presents a difficulty in mesh generation. Also, the uniform thickness of the membrane is a realistic condition that is very hard to meet in building a finite-elements model of an irregularly shaped cell. A method to construct 3D numerical models of irregularly shaped cells and cell clusters was presented. Because the model was constructed from images of cells on which the experiment was carried out (see 1.4.2), it was possible to compare numerically calculated ITV with measured ITV.

#### **1.4.4 Electroporation of single spherical, single irregularly shaped cells, cell clusters, and dense cell suspensions**

In this part of the study, we investigated the course of permeabilization of single spherical cells, single irregularly shaped cells, and cell clusters by means of fluorescent dye Propidium Iodide. These observations showed whether cells in clusters behaved as individual cells or as an interconnected giant cell. The results of permeabilization could be compared with experimentally and numerically determined ITV (see 1.4.2 and 1.4.3), because the experiments and calculations were performed on the same cell clusters. This analysis was also used to determine the critical value of ITV where electroporation occurs. By visualizing the fast events, e.g. the entrance of molecules of Propidium Iodide into individual cells, cells in suspension, and cell monolayers, we determined the onset of the transport of molecules through the permeabilized membrane and followed the kinetic of transport during and after the pulse. Besides, the efficiency of permeabilization of cells in suspensions with increasing cell densities was investigated and compared to permeabilization of cells in dilute suspensions.



## 2 MATERIALS AND METHODS

### 2.1 Cells, media and chemicals

#### 2.1.1 Cells

CHO K1 – Chinese Hamster Ovary cells were grown at 37°C, 5% CO<sub>2</sub> in flasks in culture medium (HAM-F12, Sigma-Aldrich, Steinheim, Germany) with added Fetal calf serum (8%, Sigma-Aldrich, Steinheim, Germany), antibiotics (crystacillin 200 units/ml, gentamicin 16 µg/ml) and L-glutamine (0.15 mg/ml, Sigma-Aldrich, Steinheim, Germany).

CHO WTT - Chinese Hamster Ovary cells were grown at 37°C, 5% CO<sub>2</sub> in culture medium (CM1MEM 40-01, Eurobio, France) with added Fetal calf serum (8%, Boehringer, Germany), antibiotics (penicillin 100 units/ml, streptomycin 100 µg/ml) and L-glutamine (1.16 mg/ml, Sigma-Aldrich, Steinheim, Germany). Cells were kept in suspension by gentle, continuous agitation (100 rpm) in spinner flasks.

B16 F1 – Mouse Melanoma cells were grown at 37°C, 5% CO<sub>2</sub> in flasks in culture medium (EMEM, Sigma-Aldrich, Steinheim, Germany) with added Fetal calf serum (8%, Sigma-Aldrich, Steinheim, Germany), antibiotics (crystacillin 200 units/ml, gentamicin 16 µg/ml) and L-glutamine (1.16 mg/ml, Sigma-Aldrich, Steinheim, Germany).

BHK – Baby Hamster Kidney cells were grown at 37°C, 5% CO<sub>2</sub> in flasks in culture medium (Glasgow MEM, BHK 21, Gibco, USA) with added Fetal calf serum (8%, Boehringer, Germany), antibiotics (penicillin 100 units/ml, streptomycin 100 µg/ml) and L-glutamine (0.3 mg/ml, Sigma-Aldrich, Steinheim, Germany).

V79 - Chinese Hamster Lung Fibroblasts were grown in flasks in culture medium (EMEM, Sigma-Aldrich, Steinheim, Germany) with added Fetal calf serum (8%, Sigma-Aldrich, Steinheim, Germany), antibiotics (crystacillin 200 units/ml, gentamicin 16 µg/ml) and L-glutamine (1.16 mg/ml, Sigma-Aldrich, Steinheim, Germany) at 37°C, 5% CO<sub>2</sub>.

#### 2.1.2 Media

Culture media were used only for cell cultivation, while the experiments were performed in the following media:

- *Pulsing buffer* (10 mM K-ZAP): Consisted of 10 mM KH<sub>2</sub>PO<sub>4</sub>/K<sub>2</sub>HPO<sub>4</sub>, 250 mM sucrose and 1 mM MgCl<sub>2</sub>. This buffer was added to cells before measurements of induced transmembrane voltage and before electropermeabilization.

- *Calibration buffer*: 10 mM Hepes buffer (pH 7.5, Merck, Darmstadt, Germany) with varying concentrations of NaCl and KCl (140 mM NaCl/KCl). The buffer was used to calibrate di-8-ANEPPS.
- *SMEM*: Spinner's modification of Eagle's MEM (SMEM, Gibco, USA). Basically a Ca<sup>2+</sup> depleted version of EMEM, which was used for washing the cells before experiments and for incubation with di-8-ANEPPS.
- *Media used for measurements of resting transmembrane voltage*: The components of the media are given in Table 2.1 and 2.2. Medium m1 is a potassium pulsing buffer 10 mM K-ZAP, while m2 and m3 are its 2 - times and 10 - times diluted variants. Medium m4 is a sodium pulsing buffer 10 mM Na-ZAP, while m5 and m6 are its 2 - times and 10 - times diluted variants. Medium m7 is a low conductivity medium used in our previous study (**paper 4** in Appendix - Pucihar et al., 2001).

**Table 2.1. Composition of culture media. Besides the components given in table, media also contain amino acids, vitamins, Phenol Red, antibiotics, L-glutamine and Fetal calf serum. More detailed information on composition can be found in Sigma catalog (Cat. No. 21430-20), Eurobio catalog (Cat. No. CM1MEM40-01) and Gibco catalog (Cat. No. N4888). pH was measured with pH meter (Minisis, Tacusel Electronique, France), calibrated with buffer with pH 7.0. Conductivity was measured with HI 8820 (Hamma Instruments, France), calibrated in different calibrating solutions (HI 7030 - 12880  $\mu$ S/cm, HI 7031 - 1413  $\mu$ S/cm, HI 7033 - 84  $\mu$ S/cm). Osmolarity was measured with osmometer (Osmomat 030, Gonotec, Germany) calibrated with 9.4 g/l NaCl. Measurements were performed at 25°C.**

	Culture medium (CHO K1)	Culture medium (CHO WTT)	Culture medium (B16F1, V79)	Culture medium (BHK)
	(mg/l)	(mg/l)	(mg/l)	(mg/l)
NaCl	7599	6800	6800	6400
KCl	224	400	400	400
NaHCO <sub>3</sub>	1176	2200	2200	2750
NaH <sub>2</sub> PO <sub>4</sub>	142	122	122	
Na <sub>2</sub> HPO <sub>4</sub>				108
KH <sub>2</sub> PO <sub>4</sub>				
K <sub>2</sub> HPO <sub>4</sub>				
MgCl <sub>2</sub> 6H <sub>2</sub> O	123			
MgSO <sub>4</sub> 7H <sub>2</sub> O		200	98	98
CaCl <sub>2</sub> 2H <sub>2</sub> O	441	266	265	265
Sucrose				
D-Glucose	1802	1000	1000	4500
pH	7.6	7.5	7.55	7.5
Conductivity (S/m)	1.55	1.43	1.55	1.5
Osmolarity (mOsm/kg H <sub>2</sub> O)	315	320	315	315

Table 2.2. Composition of the other media used in measurements of resting transmembrane voltage. m1: 10 mM K-ZAP, m2: 5 mM K-ZAP, m3: 1 mM K-ZAP, m4: 10 mM Na-ZAP, m5: 5 mM Na-ZAP, m6: 1 mM Na-ZAP, m7: low conductivity medium from paper 4 (Pucihar et al., 2001). pH was measured with pH meter (Minisis, Tacusel Electronique, France), calibrated with buffer with pH 7.0. Conductivity was measured with HI 8820 (Hanna Instruments, France), calibrated in different calibrating solutions (HI 7030 - 12880  $\mu\text{S}/\text{cm}$ , HI 7031 - 1413  $\mu\text{S}/\text{cm}$ , HI 7033 - 84  $\mu\text{S}/\text{cm}$ ). Osmolarity was measured with osmometer (Osmomat 030, Gonotec, Germany) calibrated with 9.4 g/l NaCl. Measurements were performed at 25°C.

	m1	m2	m3	m4	m5	m6	m7
	K-ZAP	K-ZAP	K-ZAP	Na-ZAP	Na-ZAP	Na-ZAP	
	10 mM	5 mM	1 mM	10 mM	5 mM	1 mM	
	(mg/l)						
NaCl							
KCl							
NaHCO <sub>3</sub>							
NaH <sub>2</sub> PO <sub>4</sub>				240	120	24	
Na <sub>2</sub> HPO <sub>4</sub>				1136	568	113.6	33.75
KH <sub>2</sub> PO <sub>4</sub>	272	136	27.2				8.49
K <sub>2</sub> HPO <sub>4</sub>	1392	696	139.2				
MgCl <sub>2</sub> 6H <sub>2</sub> O	203	101.5	20.3	203	101.5	20.3	2.85
MgSO <sub>4</sub> 7H <sub>2</sub> O							
CaCl <sub>2</sub> 2H <sub>2</sub> O							
Sucrose	85500	85500	85500	85500	85500	85500	90000
D-Glucose							
pH	7.35	7.4	7.35	7.35	7.45	7.35	7.25
Conductivity (S/m)	0.17	0.09	0.021	0.13	0.076	0.017	0.0049
Osmolality (mOsm/kg H <sub>2</sub> O)	320	303	300	320	302	300	303

### 2.1.3 Chemicals

#### *Fluorescent dyes*

- di-8-ANEPPS: for measurements of induced transmembrane voltage (Molecular Probes, Leiden, Netherlands).
- Propidium Iodide: to monitor permeabilization (Sigma, Saint Louis, USA).
- TMRM: for measurements of resting transmembrane voltage (Sigma-Aldrich, Steinheim, Germany).
- FITC dextran: to determine the contribution of the out of the focus fluorescence in measurements of resting transmembrane voltage (FD 40, Sigma, USA).
- Lucifer Yellow: to test for the existence of gap junctions (Sigma, Saint Louis, USA).

### *Other chemicals*

- Valinomycin: potassium ionophore used for calibration of di-8-ANEPPS (Sigma-Aldrich, Steinheim, Germany).
- Pluronic acid: to facilitate the di-8-ANEPPS incorporation into cell membrane (Molecular Probes, Leiden, Netherlands).
- Lindane: gap junction inhibitor (Sigma-Aldrich, Steinheim, Germany).

## 2.2 Measurements of resting transmembrane voltage

*These experiments were performed at the Institute of Pharmacology and Structural Biology (IPBS), Toulouse, France.*

Resting transmembrane voltage (RTV) was measured by using potentiometric fluorescent dye TMRM. The dye is characterized as slow, because it responds to changes of the membrane voltage on time scale of minutes. Its change in fluorescence intensity is reported to be in the range from 60 to 80 % per 100 mV (Ehrenberg et al., 1988; Farkas et al., 1989). The dye is distributed between cell interior and exterior depending on the membrane voltage. Because its binding to the membrane and cellular constituents is low, and because the intensity of its fluorescence is proportional to the concentration of the dye, RTV can, in general, be determined from the Nernst equation by replacing the concentrations with the corresponding fluorescence intensities:

$$U_{RTV} = \frac{R \cdot T}{F} \cdot \ln \frac{F_o}{F_i} \quad (2.1)$$

where  $F_o$  and  $F_i$  are the measured intensities of fluorescence outside and inside the cell, respectively. The measurements must be performed with a confocal microscope to reduce the contribution of out of focus fluorescence. This contribution was evaluated by using a large fluorescent molecule, a FITC - dextran (FD 40, Sigma, USA), which can not enter the cell, due to its size. The fluorescence of dextran was measured inside and outside of cell by exciting the dye with 488 nm laser and detecting the emission with long pass filter at 534 nm. The ratio of FITC - dextran fluorescence inside and outside the cell ( $R_{DEX} = F_{DEXi}/F_{DEXo}$ ) was never higher than 0.05 in all experiments. Taking into account the out-of-focus fluorescence, Eq. 2.1 yields (Ehrenberg et.al, 1988):

$$U_{RTV} = \frac{R \cdot T}{F} \ln \frac{F_o \cdot (1 - R_{DEX})}{F_i - F_o \cdot R_{DEX}} \quad (2.2)$$

The experiments were performed on suspended CHO WTT cells, and attached CHO WTT, B16F1, and BHK cells. Prior to experiments, part of the suspension (CHO cells) was taken from the spinner (usually  $1 \times 10^6$  cells/ml), and the fluorescent dye TMRM (Sigma-Aldrich,

Germany) was added in an amount leading to  $0.5 \mu\text{M}$  of the dye in suspension. For the measurements of resting voltage on the attached cells, the cells were plated in Lab-Tec plastic chambers ( $1 \times 10^5$  cells/ml). Approximately 24 hours later the culture medium was replaced with a fresh medium containing  $0.5 \mu\text{M}$  of TMRM.

After 15 to 20 minutes of incubation at room temperature, fluorescence of dye was observed under the fluorescence confocal microscope (Zeiss 100M, objective  $\times 63$ , water immersion, Zeiss, Germany). The dye was excited with laser light at 534 nm and emission was detected with long-pass filter at 564 nm. The fluorescence images were acquired with a system of photomultiplier tubes (Zeiss, Germany) mounted under the microscope and the images were converted to 12-bit greyscale images using FLM 520 software (Zeiss, Germany). The fluorescence inside the cell –  $F_i$ , was determined by averaging the intensities within a region of interest, positioned above the nucleus of the cell (Ehrenberg et.al, 1988). Similarly, the fluorescence outside the cell -  $F_o$ , was obtained by averaging the intensity within a region positioned in the cell vicinity (see Figure 2.1). RTV was then determined from Eq. 2.2.

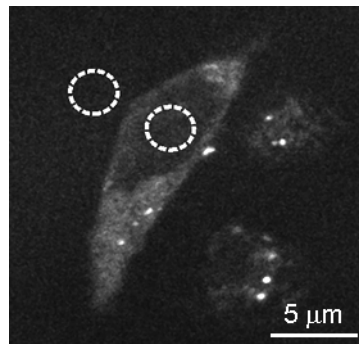


**Figure 2.1.** Attached CHO cell stained with  $0.5 \mu\text{M}$  TMRM dye. The circles mark the regions where the average fluorescence was measured.

We also investigated the influence of composition and conductivity of the extracellular medium on the amplitude of RTV. The basic components of all investigated media are given in Tables 2.1 and 2.2 above. Culture medium depends on the cell line used. Medium m1 is a potassium buffer used as a pulsing medium for electroporation of cells (10 mM K-ZAP), while m2 and m3 are the twofold and tenfold diluted variants of m1. Medium m4 is a sodium buffer also used as a pulsing medium (10 mM Na-ZAP), while m5 and m6 are the twofold and tenfold diluted variants of m4. Medium m7 is one of the low conductivity media used in our previous study (**paper 4** in Appendix - Pucihar et al., 2001). Cells in suspension were centrifuged ( $200 \times g$ , 5 min, Jouan C 500 centrifuge, France) and supernatant was replaced with a given medium. The procedure was repeated two to three times. For attached cells, the medium was replaced by pipetting and the procedure was repeated three times. The subsequent protocol (addition of dye, incubation, acquisition, measurements...) were the same as described in the preceding paragraphs.

### 2.3 Measurements of induced transmembrane voltage on single spherical cells, single irregularly shaped cells and cell clusters

*These experiments were performed in Laboratory of Biocybernetics, Faculty of Electrical Engineering, University of Ljubljana, Slovenia.*

To experimentally determine induced transmembrane voltage (ITV) on single spherical cells, single irregular shaped cells and cell clusters, we used di-8-ANEPPS, a fast potentiometric fluorescent dye. The dye binds to the cell membrane, which causes a considerable increase in its fluorescence. With the change in ITV, the fluorescence of the dye then varies linearly (Bedlack et al., 1994; Gross et al., 1986; Montana et al., 1989). The linear response of the dye was found for voltages ranging from  $-280$  mV to  $+140$  mV (Cheng et al., 1999), as well as from  $0$  to  $+250$  mV (Lojewska et al., 1989).

CHO K1 and B16F1 cells were grown on cover glasses in culture medium. When cells attached to the glass (usually after 2 to 4 hours to obtain spherical attached cells, 6 to 8 hours for single irregularly shaped cells and 24 to 35 hours for cell clusters), the culture medium was replaced with SMEM medium containing  $30 \mu\text{M}$  of di-8-ANEPPS and 0.05% of Pluronic. Pluronic was added to facilitate dye incorporation into the membrane. After staining for 12 min at  $4^\circ\text{C}$ , the cells were washed thoroughly with pure SMEM to remove the excess dye. Before the experiments, SMEM was replaced with an isoosmotic pulsing buffer (10 mM K-ZAP). Cells (single cells or cell clusters) were then exposed to a voltage of 40 V applied for duration of 100 ms (unless stated otherwise) on two parallel wire electrodes with a 4 mm distance between them (voltage-to-distance ratio 100 V/cm). The polarity of the voltage was then reversed using a custom-made switcher and the same experiment was repeated. Before and during the pulse, the fluorescence image of the lowermost level of a cell or a cell cluster was acquired, with excitation at 490 nm and emission detected at 605 nm (D605/55m, Chroma, Rockingham, USA). Excitation light was generated with a monochromator system (PolyChrome IV, Visitron, Germany). The exposition of cells to fluorescence was controlled with electronic shutter and was also synchronized with electric pulses and image acquisition. The procedure was repeated ten times (five acquisitions for each polarity of the electric field), with a 2 s delay between pulses. The control image was then subtracted from the corresponding pulse image and the corrected images were averaged to increase the signal-to-noise ratio. The changes in fluorescence of the dye in the membrane were quantified by measurements of grey levels along the region of interest, which was a 5 pixel wide line encircling the cell at the site of the membrane (Figure 2.2). For cell clusters, the region of interest was a line encircling the outermost membranes of cells in cluster. Using a calibration curve obtained in a separate experiment (see below), fluorescence changes were transformed to the values of induced transmembrane voltage, which were plotted on a graph as a function of the normalized arc length. The images were acquired using a cooled CCD camera (VisiCam 1280, Visitron, Germany) mounted on a fluorescence microscope (Zeiss AxioVert

200, objective  $\times 63$  or  $\times 100$ , oil immersion, Zeiss, Germany) and processed with MetaMorph 5.0 software (Molecular Devices Corporation, PA, USA). Schematic presentation of the system and the photo of the system are presented in Figure 2.3.

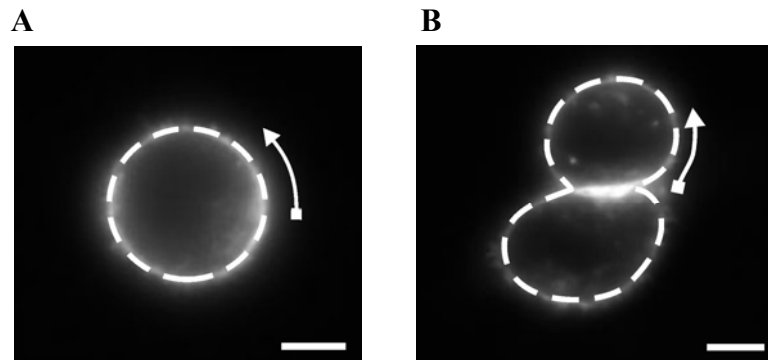


Figure 2.2. Region of interest along which the grey levels were measured for (A) a single cell and (B) cell cluster. White arrow marks the start and the direction of the path. Bar represents 5  $\mu\text{m}$ .

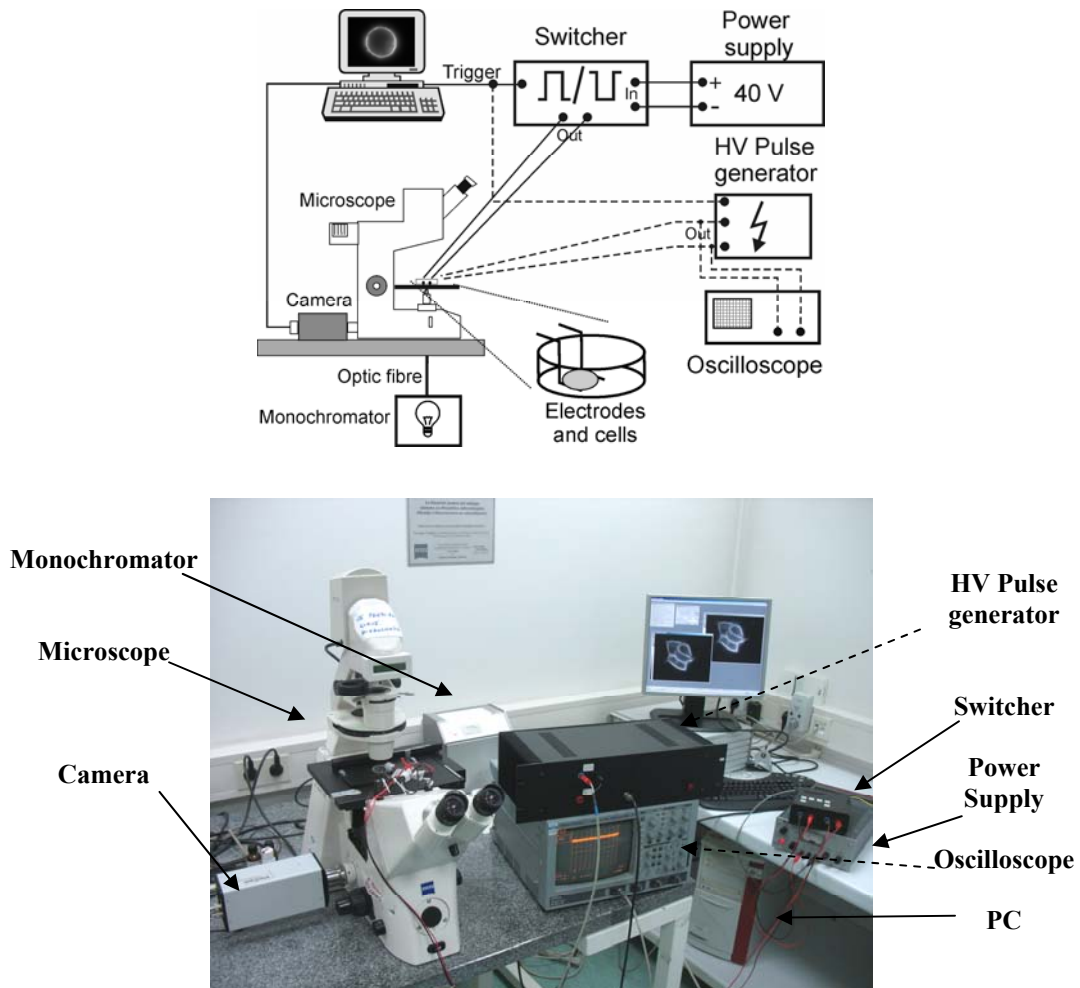
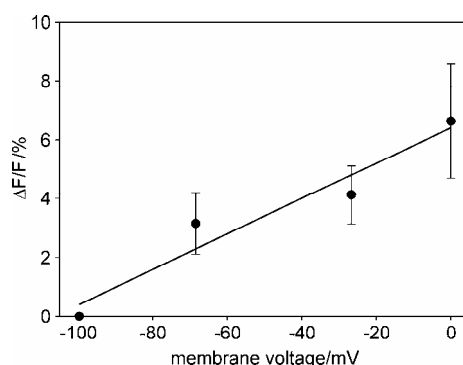


Figure 2.3. Simplified schematic presentation of the imaging system for measurements of induced transmembrane voltage (top) and the photo of the setup (bottom). Permeabilization was performed by adding a high voltage pulse generator to the existing setup (dashed lines).

### 2.3.1 Calibration of di-8-ANEPPS

CHO K1 cells were grown and stained with di-8-ANEPPS as described above. After washing, SMEM was replaced with the calibrating medium consisting of 10 mM Hepes buffer, 140 mM NaCl/KCl and 1  $\mu$ M valinomycin, a potassium ionophore. The concentrations of NaCl and KCl were adjusted to obtain 3, 10, 50, and 140 mM concentrations of KCl, corresponding to membrane voltages of -99, -68, -27, and 0 mV, respectively. The voltages were obtained using the Nernst equation, assuming the intracellular  $K^+$  concentration of 140 mM (Alberts et al., 1994) and considering that the membrane voltage corresponds to  $K^+$  equilibrium in the presence of valinomycin. After 4 minutes of incubation in the calibration medium with the lowest KCl concentration (3 mM), the fluorescence image was acquired (excitation 490 nm, emission 605 nm) with the imaging system shown in Figure 2.3, and the medium was replaced with another one with higher KCl concentration. This procedure was repeated until 140 mM  $K^+$  concentration was reached. The average grey value of the whole line (region of interest) encircling the cell at the site of the membrane was determined for each image acquired. These values were then transformed to relative changes of di-8-ANEPPS fluorescence and were plotted versus the voltage. The measurements were performed on three cells from different cover glasses and the results are presented in Figure 2.4 as the mean  $\pm$  SD. Linear regression was performed on the measured values to obtain the calibration curve with a slope of 6% / 100 mV.



**Figure 2.4. Calibration curve for di-8-ANEPPS.** The measurements represent the mean of the relative changes in the fluorescence ( $\Delta F/F \pm$  SD (N = 3)). The slope of the calibration curve (6% / 100 mV) was determined from the linear regression curve.

## 2.4 Numerical calculations of induced transmembrane voltage on single spherical cells, single irregularly shaped cells and cell clusters

*These experiments were performed in Laboratory of Biocybernetics, Faculty of Electrical Engineering, University of Ljubljana, Slovenia.*

### 2.4.1 Construction of a three-dimensional model of a cell

The calculations of induced transmembrane voltage (ITV) were performed on 3D models of single spherical cells, single irregularly shaped cells, and cell clusters. While a sphere was used as a model of a spherical cell, 3D models of single attached cells and cell clusters were constructed from a sequence of microscopic fluorescence images representing cross-sections of a cell attached to the cover glass. Mostly, the models in the study were built from CHO and B16 cells, but the method can be applied to other cell types. Fluorescence images were obtained by staining the cell or a cluster with fluorescent dye di-8-ANEPPS (see Section 2.3). The dye emits a strong fluorescence when it binds to the membrane, therefore making the cell edges visible. The cross-sections were obtained by shifting the focus on a fluorescence microscope (Zeiss AxioVert 200, objective  $\times 63$  or  $\times 100$ , oil immersion, Zeiss, Germany) in constant steps of 1  $\mu\text{m}$  from the bottom to the top of the cell (Figure 2.5A). The images were acquired using the same system as described in Section 2.3 and shown in Figure 2.3 and converted from greyscale (8 bit) to black and white images (1 bit) in Corel PhotoPaint 11.0 (Corel Corp., Ottawa, Canada) (Figure 2.5A and B). Subsequent processing was performed on a PC equipped with a 2.8 GHz Pentium IV processor and 1 GB RAM. Using FEMLAB 3.1 package (COMSOL Inc., Burlington, MA, USA) with MATLAB 6.5 (MathWorks Inc., Natick, MA, USA), the contours of the cell were detected using `flim2curve` (Figure 2.4C), transformed to solid planes with 35 edges with `solid2`, and the planes were connected into a 3D object using `loft` to obtain the model of the cell. This model was then imported to the FEMLAB workspace, where it was positioned to the bottom of a rectangular block, thereby mimicking the cell attached with its bottom to the cover glass (Figure 2.5D). To construct a model of several cells, or a cell cluster, this procedure was repeated for each cell separately (an example for two distant irregularly shaped cells can be found in **paper 5** in Appendix, Pucihar et al., 2006). In case of a cell cluster, individual cells were, after they were imported to FEMLAB, merged together to form a cluster.

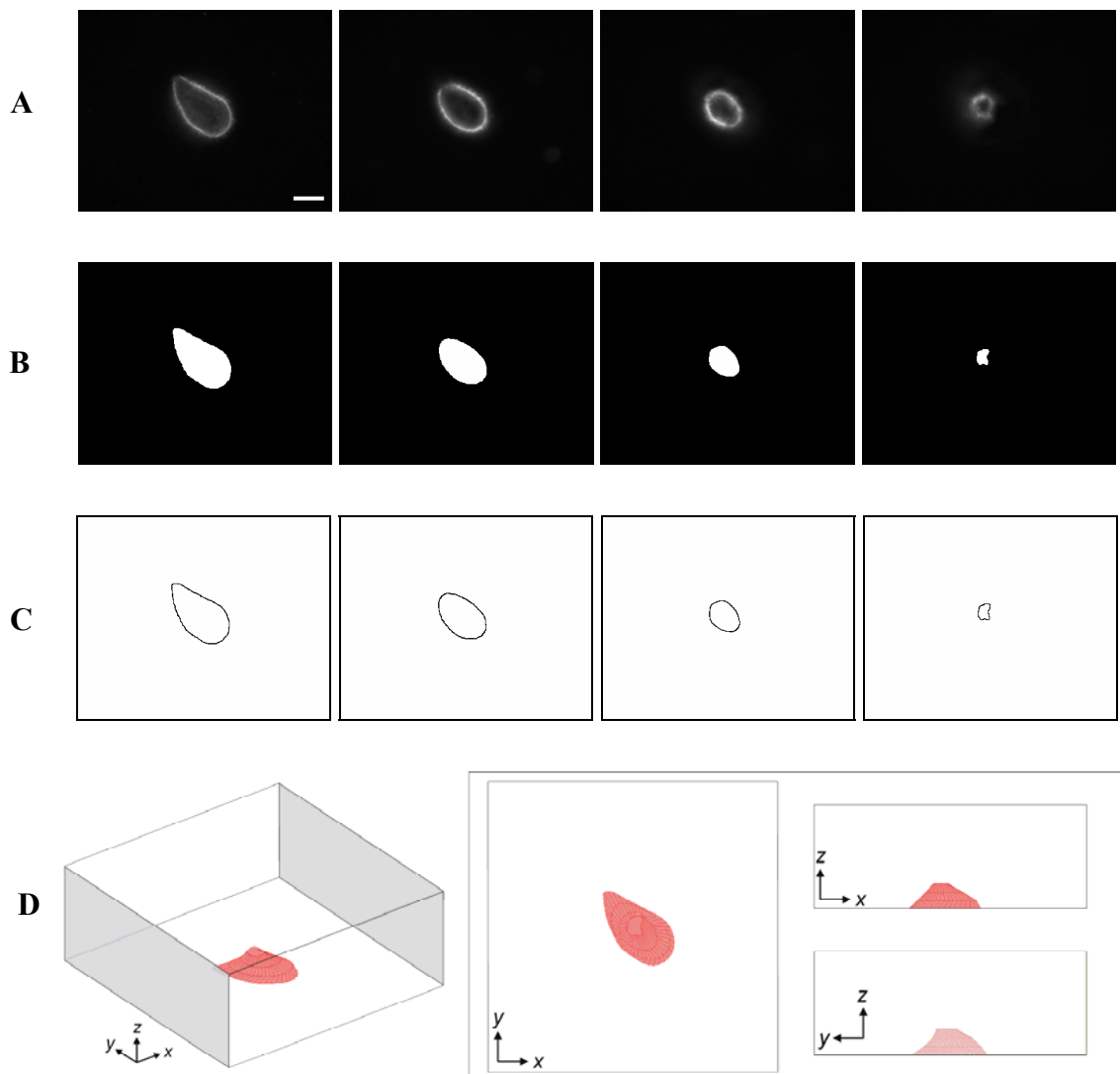


**Figure 2.5.** Construction of a 3D model of an irregularly shaped cell. (A) Fluorescence images (8 bit) of an irregularly shaped CHO cell stained with di-8-ANEPPS. The images represent four cross-sections of the cell, acquired from bottom to the top of the cell in  $2\ \mu\text{m}$  steps. Bar represents  $10\ \mu\text{m}$ . (B) Black and white (1 bit) images. (C) The corresponding contour of the cell edge for a given cross-section. (D) The three-dimensional geometry of the cell model constructed from the cross-sections. The interior of the rectangular block represents the extracellular medium, the grey-shaded faces are the electrodes, and the other four faces are insulating.

#### 2.4.2 Modeling the cell membrane

Direct incorporation of a realistic cell membrane (i.e. a layer of very small, yet non-zero thickness surrounding the cell) into the model is technically very problematic. Unless the distribution of the electric field, current density, and/or electric potential *within the membrane* is of interest, this can be avoided. Namely, the effect of the membrane on these electric quantities in the cell interior and exterior is equivalent to the effect of a corresponding surface conductivity assigned to the interface between the interior and the exterior. More precisely, as

the specific conductivity of the membrane – typically about  $5 \times 10^{-7}$  S/m (Gascoyne et al., 1993) – is at least five orders of magnitude lower than the specific conductivities of the media surrounding it, the current flows through the membrane practically orthogonally to its surface. Consequently, in the membrane the total current density is virtually equal to its normal component alone ( $J$ ), which is given by

$$J = \frac{\sigma_m (V_o - V_i)}{d}, \quad (2.3)$$

where  $\sigma_m$  is the specific membrane conductivity,  $d$  is the membrane thickness and  $V_o$ ,  $V_i$  are the electric potentials at the outer and inner surface of the membrane, respectively. Here  $J$ ,  $V_o$ , and  $V_i$  are functions varying with the position on the membrane, while  $\sigma_m$  and  $d$  are constants. For the purpose of determining ITV, the events inside the membrane layer are not relevant, and the ratio  $\sigma_m/d$  can be treated as a single entity — the specific surface conductivity,  $\kappa_m = \sigma_m/d$ . The interface between the cell interior (the cytoplasm) and the cell exterior is then characterized by

$$J = \kappa_m (V_o - V_i). \quad (2.4)$$

Despite the membrane as such being absent from the model, the drop of electric potential at such an interface is equivalent to ITV on a membrane with a specific conductivity  $\sigma_m$  and thickness  $d$ . In models constructed in this way, the mesh of finite elements is generated without difficulty, as very small elements corresponding to the membrane itself are avoided (Figure 2.6). More details can be found in **paper 5** in Appendix (Pucihar et al., 2006).

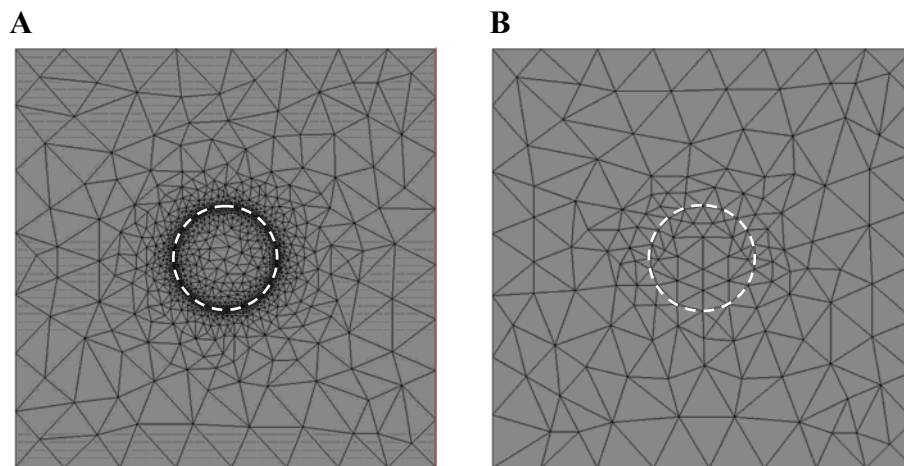


**Figure 2.6.** Comparison of mesh for a model of a spherical cell with radius  $10 \mu\text{m}$ . A cross-section through the center of the cell is shown. (A) Membrane with thickness of  $0.3 \mu\text{m}$  was incorporated in the model, which is still about 70 times thicker than the real membrane. Number of mesh elements was 199000. (B) Membrane was modeled as a boundary condition. Number of mesh elements was 3746. More details can be found in **paper 5** in Appendix (Pucihar et al., 2006).

### 2.4.3 Settings of the model and subsequent computations of induced transmembrane voltage

The computation of the functions  $J$ ,  $V_o$  and  $V_i$  was performed in FEMLAB by introducing two application modes, the cell exterior (extracellular medium) being active in the first, and the cell interior (cytoplasm) in the second mode. Both application modes were of a static current density type. For models containing several cells, an additional application mode active in the cytoplasm of each cell was introduced, and the functions  $J_1, J_2, \dots$  and  $V_o, V_{i1}, V_{i2}, \dots$  were computed.

The specific conductivity of the cell interior was set to 0.3 S/m, a typical conductivity of the cell cytoplasm (Harris and Kell, 1983), and the specific conductivity of the rest of the block (the cell exterior) was set to 0.14 S/m, which is a typical value of the low conductivity extracellular medium, 10 mM K-ZAP (Rols et al., 1998). Two of the opposite vertical faces of the block were modeled as electrodes, which was done by assigning fixed electric potentials to both electrodes (one was usually set to ground) to obtain the voltage-to-distance ratio of 100 V/cm, the same as in experiments in Section 2.3. The remaining four faces of the block were modeled as insulating surfaces, the bottom one representing the cover glass. At the boundary surface between the cell interior and exterior, the normal component of the current density was set corresponding to Eq. 2.3 with a negative sign ( $-J$ ) in the mode corresponding to the cell exterior, and with a positive sign in the mode corresponding to the cytoplasm (or, with several cells, in all such modes). The specific surface conductivity was set at  $\kappa_m = 100 \text{ S/m}^2$ , which is the ratio between a specific membrane conductivity of  $5 \times 10^{-7} \text{ S/m}$  and a membrane thickness of 5 nm (Alberts et al., 1994). In case of cell clusters, individual cells in cluster were modeled as either electrically insulated or electrically connected. When cells were modeled as electrically insulated, the specific conductivity of the contact surface was, due to the double thickness of the membrane on the contact, set to half of the initial specific conductivity ( $\kappa_m = 50 \text{ S/m}^2$ ). When cells were modeled as electrically connected (e.g. via gap junctions), a 1000 times higher specific surface conductivity was assigned to the contact surface ( $\kappa_m = 50000 \text{ S/m}^2$ ), which proved to be enough to obtain a roughly constant value of electric potential inside the whole cluster. Higher conductivities yielded essentially the same results, while at lower conductivities, substantial variations of intracellular electric potential was obtained.

After the mesh was generated, the electric potential was computed using finite elements method with FEMLAB's stationary nonlinear *Conjugate gradients* solver with *Algebraic multigrid* preconditioner. ITV was calculated as the difference between electric potentials on the two sides of the boundary surface separating the inside and outside of the cell, i.e. as  $\text{ITV} = V_i - V_o$ . ITV was then plotted as a function of relative arc length.

#### 2.4.4 Electrodes

Electrodes used in most of our experiments (measurements of induced transmembrane voltage, electropermeabilization) were made of two 0.8 mm Pt/Ir (90/10) wires separated by 4 mm (unless stated otherwise). To verify if the electric field ( $E$ ) between the electrodes corresponds to the electric field calculated from the voltage-to-distance ratio ( $E = U/d$ ), we constructed a model where the electrodes were positioned at the bottom of the dish filled with extracellular medium. The electric field distribution for the case of 40 V applied to the electrodes with 4 mm distance between them is shown in Figure 2.7A. The results show that the field distribution is inhomogeneous; the highest field is obtained in the vicinity of the electrodes. However, cells are located at the bottom of the dish (dashed line in Figure 2.7A) and are considerably smaller than the dimensions of the electrodes. A plot of electric field distribution on the bottom of the dish between the electrodes show that considerable deviations from the  $U/d$  ratio of 100 V/cm (red line in Figure 2.7B) occur in the vicinity of the electrodes, while in the middle between them (denoted by a dashed box) the field is close to the  $U/d$  ratio (the error is within 6% of that value). On the basis of these computations we decided to perform experiments on cells, located in the middle between the electrodes, in the region marked with dashed line.

### 2.5 Electropermeabilization of single spherical cells, irregularly shaped cells, cell clusters, and dense cell suspensions

*The majority of these experiments were performed at the Institute of Pharmacology and Structural Biology (IPBS), Toulouse, France. The experiment with the slow acquisition system was performed in Laboratory of Biocybernetics, Faculty of Electrical Engineering, University of Ljubljana, Slovenia.*

#### 2.5.1 Visualization of electropermeabilization on single spherical cells, irregularly shaped cells and cell clusters

Cells (CHO WTT, CHO K1, and B16F1) were grown and prepared as described in Sections 2.1 and 2.3. Prior to experiments, the culture medium was replaced with pulsing buffer (10 mM K-ZAP), which contained 100  $\mu$ M of fluorescent dye Propidium Iodide (PI, Sigma, Saint Louis, USA). The dye is essentially membrane impermeant, but can enter the electropermeabilized cells. Because its fluorescence increases several fold upon binding to DNA or mRNA, it can be used to detect electropermeabilization of cells. The electrodes (Figure 2.7) were positioned to the bottom of Lab-Tec plastic chamber or cover glass (depending on the experiment), where cells were grown. A pulse with a given amplitude and duration (depending on the experiment, see below for details) was delivered to the electrodes, and fluorescence from cells was monitored. Two imaging systems were used to monitor permeabilization, a fast system with a fast, sensitive camera, and a slow system with a slow, high resolution camera.

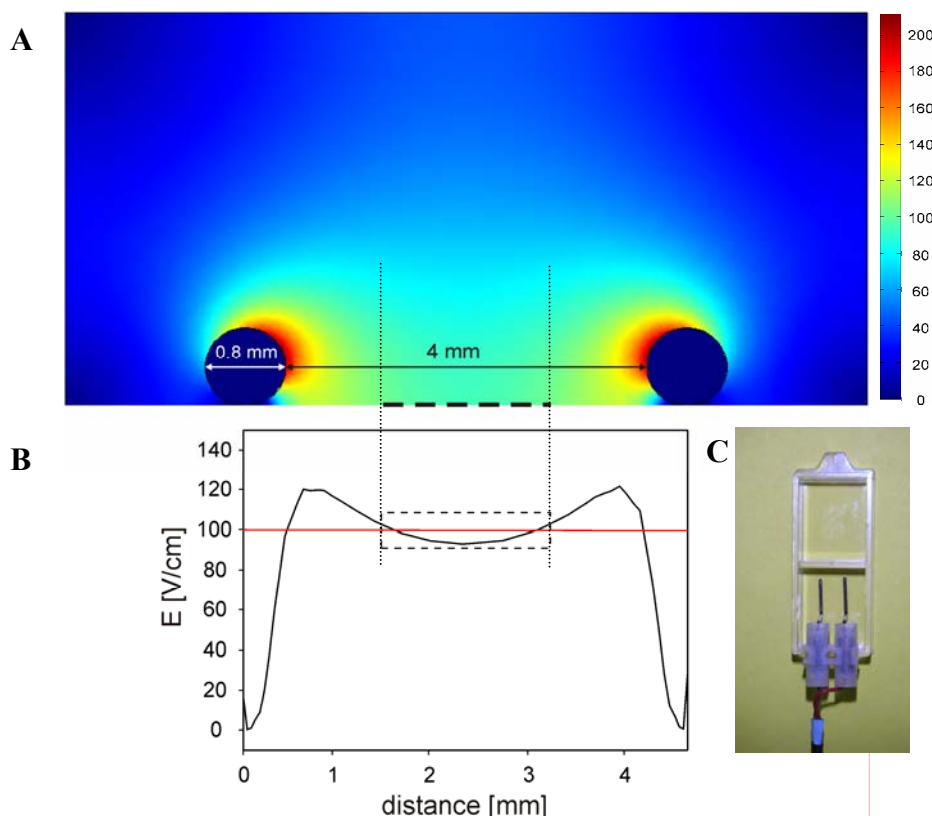


**Figure 2.7.** Computations of electric field distribution between the electrodes. Electrodes were two Pt/Ir wires with 0.8 mm diameter and 4 mm distance between them. (A) Electric field distribution in the model of electrodes positioned to the bottom of the dish. The electrodes (blue circles) were modeled as highly conductive, while the conductivity of the surroundings was set to 0.14 S/m to model the extracellular medium. Dashed line presents the region where the experiments were performed on cells. Bar scale is in V/cm. (B) The graph of electric field distribution on the bottom of the dish between the electrodes, where the cells are located. Red line denotes the voltage-to-distance ratio ( $U/d = 100$  V/cm). Dashed square shows the variations in the electric field from the  $U/d$  ratio in the region where the experiments were performed. (C) The photo (top view) of the electrodes.

The fast imaging system comprised of a sensitive, fast video camera (LH 750-ULL, Lhesa, Cergy-Pontoise, France) mounted on a fluorescence microscope (Leica DM IRB, Germany). The camera allowed real-time acquisition of fluorescence images within 20 ms video frame, i.e. six consecutive images of 3.33 ms each. The fluorescence of the cell was observed under  $\times 63$ , 1.4 NA oil immersion objective (Leitz, Wetzlar, Germany) after passing the light from the xenon light source through the filter (Leitz N2 block filter, excitation:  $530 \text{ nm} < \lambda > 560 \text{ nm}$ ; emission  $> 580 \text{ nm}$ ). The gain of the camera was manually adjusted to obtain the fluorescence signal from the nonpermeabilized cells just above the background. The system was used to investigate the influence of pulse duration (1 ms, 3 ms, 5 ms) and pulse amplitude (400 V, 500 V, 600 V, 700 V) on the time course of electroporation on a single spherical cell. Irregularly shaped cells or cell clusters could not be observed because they were too large to fit to the imaging area. The first image was acquired immediately before the pulse delivery and represented the control image of the selected cell, while the other five

images represented the fluorescence of the cell during and after the pulse. Using the frame-grabber board (IP 8, Matrox, Québec, Canada), the images were transferred to a PC, where the video signal was converted to the 8-bit grey scale image. The control image was then subtracted from the fluorescence images of the cell recorded during and after the pulse using Optimas 4.02 software (Bioscan, Edmonds, WA). The same system also allowed slower acquisition with 10 images/s, which was used on spherical cells to observe permeabilization on a longer time scale (2 seconds). The scheme of the system and the photo are shown in Figure 2.8 while more details on the system can be found in (Gabriel and Teissie, 1998).

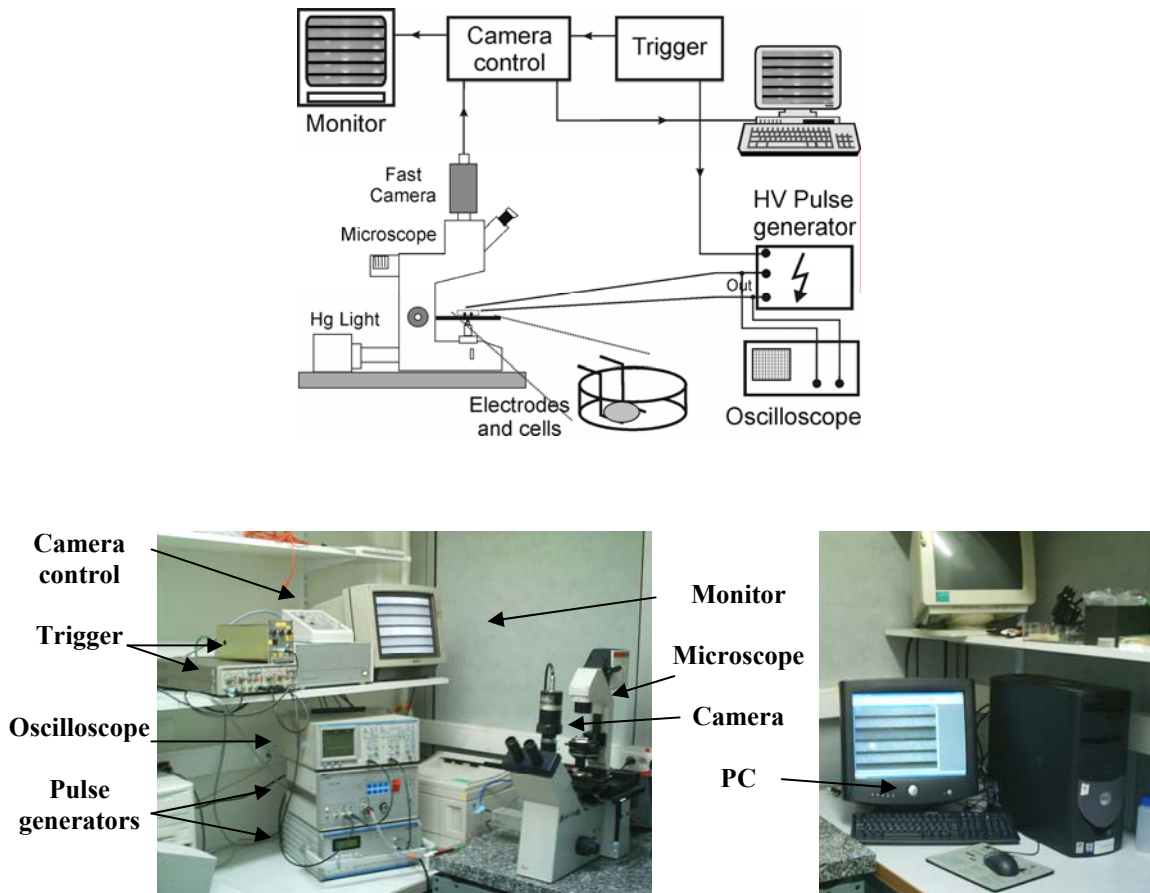


**Figure 2.8.** Simplified schematic presentation of the fast imaging system (top) and the photo of the setup (bottom). More details can be found in (Gabriel and Teissie, 1998).

The slow imaging system was the same as described in Section 2.3 and comprised of a slow, high resolution, cooled, CCD camera (12 bit, 1024×1280 pixels, VisiCam 1280, Visitron, Germany) mounted on a fluorescence microscope (Zeiss AxioVert 200, objective ×63, oil immersion, Zeiss, Germany) (Figure 2.3). The system was used to determine the permeabilized regions of the cell membrane on the same spherical cells, irregularly shaped cells, and cell clusters on which induced transmembrane voltage was measured and computed (see Sections 2.3 and 2.4). All this could not be performed with a fast system described above, due to its low resolution, low dynamic range and the lack of electronic shutter control (the dye for measuring ITV is likely to photobleach). The permeabilized regions were determined by

acquiring 20 images with a rate of 1 image per 100 ms. The fluorescence of PI was excited at 515 nm and emission detected from the band pass filter centered at 605 nm (D605/55m, Chroma, Rockingham, USA). Excitation light was generated from a monochromator system (PolyChrome IV, Visitron, Germany). The fluorescence image before the pulse (the control) was subtracted from the images after the pulse delivery. The images were acquired and processed with MetaMorph 5.0 software (Molecular Devices Corporation, PA, USA).

### 2.5.2 Kinetics of dye transport through electropermeabilized membrane

To monitor the kinetics of molecular transport through the cell membrane during and after electropermeabilization, we used a membrane-impermeable fluorescent dye Propidium iodide, because its fluorescence considerably increases when the dye enters into the cell. Changes in fluorescence were detected with a sensitive photomultiplier tube (PM tube) mounted on a fluorescence microscope (Leitz Fluovert, Germany) (Figure 2.9). Cells (CHO, WTT) were observed under  $\times 63$ , 1.4 NA oil immersion objective (Leitz, Wetzlar, Germany) after passing the light through the filter (Leitz N2 block filter, excitation:  $530 \text{ nm} < \lambda > 560 \text{ nm}$ ; emission  $> 580 \text{ nm}$ ). A single pulse of various durations (100  $\mu\text{s}$ , 500  $\mu\text{s}$ , 1 ms, 3 ms) and amplitudes (350 V, 500 V, 650 V, and 800 V) was delivered to cells and the change in fluorescence after electropermeabilization was detected with PM tube. The optical signal entering the PM tube was transformed to a voltage signal, which was amplified and filtered with a custom made amplifier and stored in a transient recorder (DL 922, Datalab, UK). The onset of the pulse was synchronized with the start of acquisition of the chart recorder. The analog signal from the recorder was then transformed to a digital signal using the 12 bit A/D converter and processed on a PC using the Pico software (Pico, France). The system allowed detection of fluorescence changes occurring during and after permeabilization with a high sensitivity and high speed but without spatial resolution. The main difference from the fast system described above (comprising of fast camera) is the continuous acquisition, which can last from 200  $\mu\text{s}$  up to 8 s, with a sampling rate of 2000 points in each range. This translates into time resolutions ranging from 100 ns (for 200  $\mu\text{s}$  acquisition) to 1 ms (for 8 s acquisition). In practice, the sensitive measurements of the fluorescence changes required high amplifications of the signal and filtering of the noise, which eventually resulted in reliable time resolutions ranging into few tens of microseconds. Four different time intervals were chosen to observe the change in fluorescence caused by the dye uptake into cells. The shortest acquisitions lasted 400  $\mu\text{s}$  and 2000  $\mu\text{s}$  with a 9  $\mu\text{s}$  time resolution, and were used either to determine the onset of dye transport through the membrane or to compare the transport during and after the pulse. Longer acquisitions, 80 ms (with 45  $\mu\text{s}$  time resolution) and 8 s (with 2 ms time resolution), were used to observe the kinetics of the dye uptake after electropermeabilization. The experiments were performed on single spherical cells, suspended cells (approximately  $3 \times 10^6$  cells/ml) and confluent cell monolayers (CHO WTT).

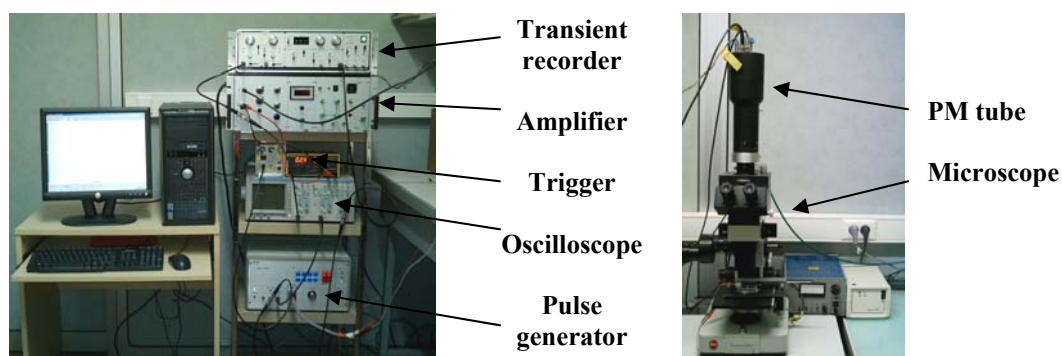
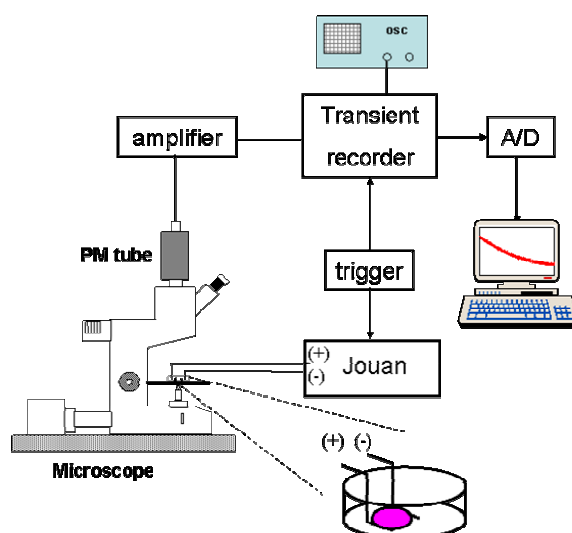


**Figure 2.9.** Simplified schematic presentation of the fast imaging system with photomultiplier tube and the photo of the setup.

Before we carried out the experiments, we first analyzed the measuring system in terms of noise and speed of response. The noise, resulting from light source, electronics and surroundings could be filtered out by using different rise times of the response of the amplifier. An example of noise from a solution of Propidium Iodide without cells, measured on time interval of 8 seconds and using different rise times (3, 9, 45, and 100  $\mu\text{s}$ ) is shown in Figure 2.10. Longer rise times decreased the noise but at the same time also decreased the speed of the response of the measuring system (Figure 2.11). From these two figures it is also evident that the signal during the 8 s acquisition is stable and that a delay of the electronics on a step change of the signal is approximately 2  $\mu\text{s}$  (Figure 2.11 –  $1 \times 10 \mu\text{s}$  LED). On the basis of the measurements presented on these two figures, we decided to use rise times of 9  $\mu\text{s}$  and 45  $\mu\text{s}$  in the experiments. We assumed that at these rise times, the response to the change in fluorescence would be sufficiently fast, while the level of noise would be acceptable. Therefore, observations on long time intervals (8 s and 80 ms) were done with 45  $\mu\text{s}$  rise time, while on short time intervals (2 ms and 400  $\mu\text{s}$ ) a 9  $\mu\text{s}$  rise time was used. The noise from solution of PI and cells measured with these two rise times is shown on different time intervals in Figure 2.12 and is somehow larger than the noise measured in pure solution of PI.

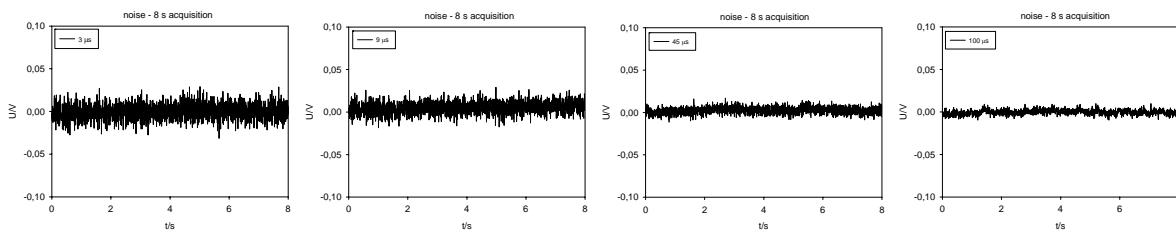


Figure 2.10. Noise from a solution of 100  $\mu\text{M}$  Propidium Iodide measured on a time interval of 8 s and different rise times of the amplifier (3, 9, 45, and 100  $\mu\text{s}$ ).

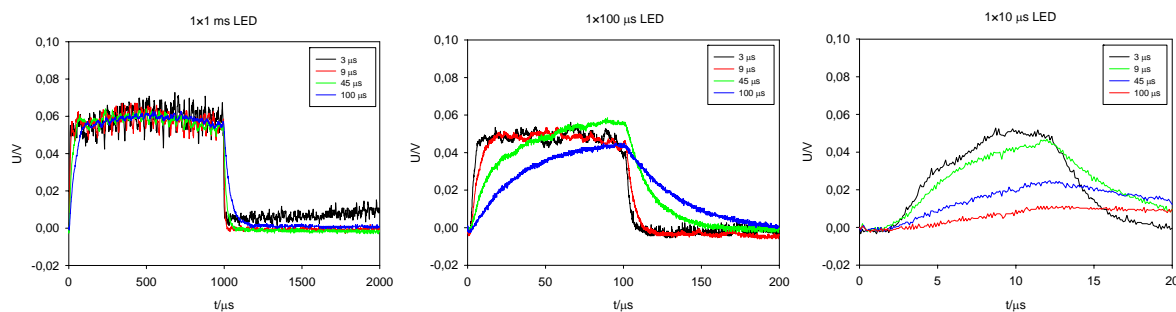


Figure 2.11. Response of the measuring system on a step change of light signal produced by LED.

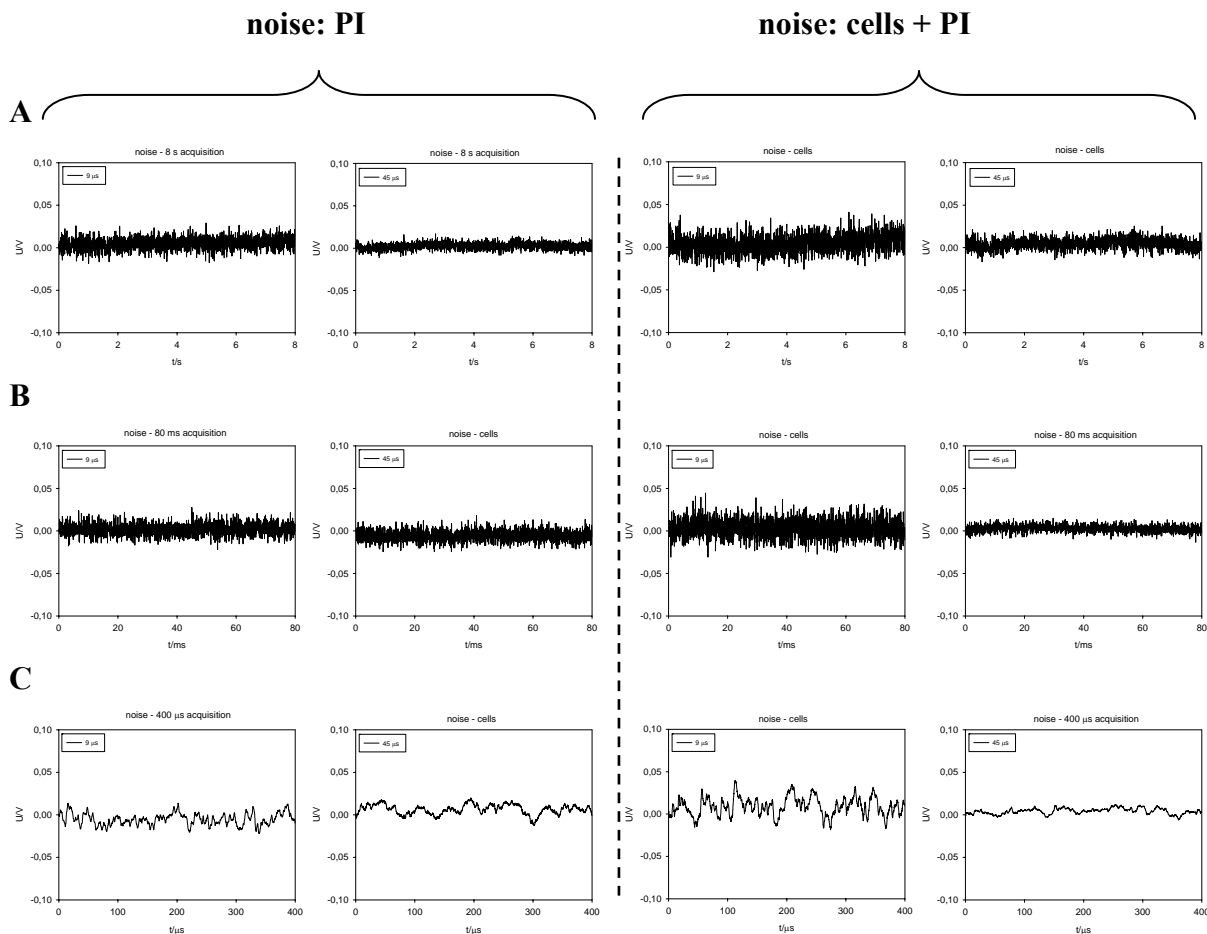
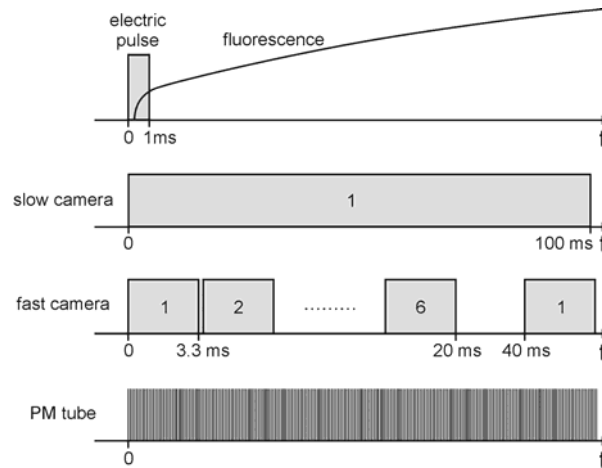


Figure 2.12. Comparison of noise in the absence (left) and presence of cells (right) in solution of 100  $\mu\text{M}$  Propidium Iodide measured on time intervals of (A) 8 s, (B) 80 ms, (C) 400  $\mu\text{s}$  at two rise times of the amplifier (9 and 45  $\mu\text{s}$ ). Electroporation pulse was not delivered.

### 2.5.3 Differences between the imaging systems used for following electroporation

The main differences between the imaging systems used (fast system with camera, slow system with camera, and fast system with PM tube) are depicted in the Figure 2.13.



**Figure 2.13.** The comparison of the imaging systems used for investigation of the course of electroporation. Slow system acquires 1 image on 100 ms. Fast system with camera acquires 1 image in 3.3 ms, but only 6 consecutive images. Fast system with photomultiplier tube (PM tube) continuously acquires data with  $\mu\text{s}$  resolution. Note that imaging system with slow and fast camera acquire images of cells, while the fast system with PM tube transforms the fluorescence change into a voltage signal (with this system we do not have a spatial resolution).

### 2.5.4. Electroporation of dense cell suspensions

*These experiments were performed at the Institute of Pharmacology and Structural Biology (IPBS), Toulouse, France.*

A detailed description of cell preparation and handling is given in **paper 6** in Appendix (Pucihar et al. – in review) and was in some parts similar as described in Section 2.3. Before experiments, the suspension was centrifuged ( $200 \times g$ , 5 min) and the supernatant was replaced with pulsing buffer (10 mM K-ZAP), which contained  $100 \mu\text{M}$  of propidium iodide, to obtain cell density of  $400 \times 10^6$  cells/ml. When the buffer was added, the volume of the pellet was taken into account and was thus subtracted from the calculated volume. A part of the suspension with  $400 \times 10^6$  cells/ml was then further diluted with the same dye-containing buffer to obtain cell densities of  $200 \times 10^6$  and  $10 \times 10^6$  cells/ml. The volume fractions of cells in these cell densities were approximately 36%, 18%, and 1%, respectively. Cells were kept at  $4^\circ\text{C}$  before exposure to electric pulses.

Cell suspension ( $100 \mu\text{l}$ ) was placed between two parallel plate electrodes placed 5 mm apart, connected to Jouan electropulsator (Jouan, St Herblain, France). The suspensions were exposed to  $8 \times 100 \mu\text{s}$  and  $10 \times 5 \text{ ms}$  rectangular pulses, delivered with 1 Hz repetition

frequency. After electroporation, cells were incubated for 7 minutes at 25°C and then resuspended in 1 ml of D-PBS (Gibco, USA). The percentage of permeabilized cells and the mean fluorescence intensity of cells were determined from the histograms obtained by flow cytometry (FACScan, Becton-Dickinson, USA).

Resealing of cells after electroporation was assayed by adding the Propidium Iodide to cell suspension at specific times after pulse delivery. The experiments were first performed in  $10 \times 10^6$  cells/ml suspension, where the dye was added 0 s, 10 s, 30 s, 1 min, 3 min, 5 min, and 7 min after permeabilization. From the results, the times at which roughly 0%, 50%, and 100% of the cells resealed were determined and at these specific times (0 s, 3 min, 7 min), the resealing of cells in  $400 \times 10^6$  cells/ml suspension was measured. In dense suspension, the resealing was measured only at three specific times because a very large number of cells were required in the experiments with dense suspensions. After permeabilization the cells were incubated for 7 min at 25°C, except for the cells to which the dye was added 7 min after pulsation, which were incubated for additional 2 min. The subsequent cell handling and the detection of permeabilization were the same as described above.

### 2.6 Test for gap junctions

*The experiments were performed in Laboratory of Biocybernetics, Faculty of Electrical Engineering, University of Ljubljana, Slovenia.*

Cells in tissues are usually connected with small pathways called gap junctions. These are small protein channels which allow the flow of ions between adjacent cells. Such pathways could affect the distribution of the induced transmembrane voltage on cells in a cluster and consequently the cell permeabilization. To verify if cells in our experiments were forming gap junctions, we used the so-called 'Scrape-loading test' (El-Fouly et al., 1987). In brief, a small, membrane-impermeant fluorescent dye Lucifer Yellow is added to the cell culture. A part of the culture is then damaged to allow the dye to enter the cells. If gap junctions exist between the cells, the dye crosses from damaged cells through gap junctions to the intact ones, making them fluorescent.

Three different cell lines (CHO K1, B16F1, V79) were plated on small petri dishes ( $1 \times 10^5$  cells/ml) in culture medium. 24 - 48 hours later the culture medium was replaced by SMEM containing 100  $\mu$ M of the fluorescent dye Lucifer Yellow (Sigma, Saint Louis, USA). A sharp blade from a scalpel or the tip of a surgical needle was used to scratch a few cells from the bottom of the petri dish. After 5 minutes of incubation, the dye was carefully washed away with pure SMEM and fluorescence from cells was then observed under the microscope (Zeiss AxioVert 200, objective  $\times 20$ , or  $\times 40$ , Zeiss, Germany). The dye was excited with 425 nm and emission detected from the band pass filter centered at 605 nm (D605/55m, Chroma, Rockingham, USA). The images were acquired using a cooled CCD camera (VisiCam 1280, Visitron, Germany) mounted on a fluorescence microscope (Zeiss AxioVert 200, objective

×20, Zeiss, Germany) and processed with MetaMorph 5.0 software (Molecular Devices Corporation, PA, USA). The acquisition of images lasted 1 s.

To inhibit the gap junctions, a 1  $\mu$ M concentration of gap junction inhibitor Lindane was added to cell culture 24 h before the experiments. The concomitant cell handling, dye addition and fluorescence observation were the same as described above.



## 3 MEASUREMENTS OF RESTING TRANSMEMBRANE VOLTAGE

### 3.1 Results

Resting transmembrane voltage (RTV) was measured using a fluorescent dye TMRM (Ehrenberg et al., 1988; Farkas et al., 1989) for three different cell lines (CHO, B16F1 and BHK). The voltage was measured in culture medium and seven other media with different composition and conductivities. In case of CHO cells, RTV was measured in suspended and attached cells, while for other cell lines the RTV was measured only on attached cells. The results of measurements are presented in Table 3.1. Resting voltage of attached cells measured in culture medium is approximately -20 mV for all investigated cell lines. For suspended CHO cells, RTV is even less negative, with the mean value of -4 mV. With decreasing potassium concentration in the extracellular medium, RTV of suspended CHO, attached CHO and BHK cells became slightly more negative, while for B16F1 cells the voltage remained practically the same. Decreasing sodium concentration caused more negative RTV of suspended CHO and BHK cells, while almost no change was observed for attached CHO and B16F1 cells. The most negative resting voltages were measured in presence of a low conductivity medium m7, and they varied considerably between cell lines. For example, in attached CHO cells RTV was approximately -96 mV, while in B16F1 cells RTV was approximately -35 mV.

**Table 3.1. Measurements of resting transmembrane voltage on different cell lines (CHO WTT - Chinese Hamster ovary cells, B16F1 - Mouse Melanoma cells, BHK - Baby Hamster Kidney cells). The measurements are given in millivolts and are presented as a mean  $\pm$  SD (N > 25). \* Culture medium was different for each cell line.**

	CHO suspended	CHO attached	B16F1 attached	BHK attached
* Culture medium	-4,0 $\pm$ 5,3	-18.6 $\pm$ 10.6	-19.8 $\pm$ 5.0	-18.1 $\pm$ 12.3
m1 (K-ZAP 10 mM)	-34.6 $\pm$ 13.3	-25.5 $\pm$ 12.8	-26.7 $\pm$ 4.4	-23.3 $\pm$ 8.9
m2 (K-ZAP 5 mM)	-40.5 $\pm$ 9.0	-20.6 $\pm$ 11.7	-27.7 $\pm$ 5.2	-35.2 $\pm$ 10.3
m3 (K-ZAP 1 mM)	-52.5 $\pm$ 11.0	-32.1 $\pm$ 9.9	-28.0 $\pm$ 5.2	-39.0 $\pm$ 6.7
m4 (Na-ZAP 10 mM)	-41.5 $\pm$ 10.2	-43.8 $\pm$ 12.9	-35.1 $\pm$ 4.5	-31.6 $\pm$ 6.9
m5 (Na-ZAP 5 mM)	-43.4 $\pm$ 12.3	-42.8 $\pm$ 22.1	-33.4 $\pm$ 2.8	-35.3 $\pm$ 7.2
m6 (Na-ZAP 1 mM)	-47.9 $\pm$ 12.2	-41.2 $\pm$ 21.2	-32.7 $\pm$ 4.5	-43.8 $\pm$ 9.1
m7	-52.2 $\pm$ 13.8	-96.6 $\pm$ 49.8	-35.4 $\pm$ 6.6	-51.7 $\pm$ 9.3

### 3.2 Discussion

Resting transmembrane voltage (RTV) in nonexcitable cells is in general difficult to measure with direct contact techniques because these cells are smaller than nerve and muscle cells and therefore more difficult to impale with microelectrodes. In such cases, fluorescent dyes present an alternative to microelectrodes and were also used in our study to measure RTV of three different cell lines: CHO, B16F1, and BHK.

Although cells in this study originated from different tissues types (ovary cells, kidney cells, and tumor cells, respectively), the values of RTV measured in attached cells in culture medium were rather high and similar (between -18.1 and -19.8 mV), while suspended CHO cells had even less negative RTV (-4 mV). As reported in literature, such low negative values of RTV are not unusual for cultured cells (Cone 1971). Namely, RTV of mature (nonexcitable) somatic cells (liver, lung, connective tissue) is generally found to be in the range of -50 to -60 mV, but it increases to approximately -10 mV upon adaptation of cells to continuous proliferation in culture, and remains at this level as long as active proliferation continues (Cone 1971). This characteristic increase in RTV is reported to be a general phenomenon, occurring for different cell types. For CHO cells, RTV was indeed measured in the range from -5 to -10 mV (Gamper et al, 2005), while for tumor cells (such as B16F1) the RTV was found in the range of -10 to -20 mV (Cone 1971; Niemtow 1985; Vodovnik et al., 1992). In contrast, the RTV of transfected type of BHK cells was measured to be approximately -50 mV (McDonald et al., 1972; Potapova et al., 1990). Substantial variations of RTV from the mean values can be observed from results presented in Table 3.1 for all examined cell types. They most probably reflect RTV on cells in different phases of cell cycle. Namely, it was demonstrated that RTV varies considerably during the cell cycle (Cone 1971; Sachs et al., 1974; Stambrok et al., 1974).

Measurements of RTV in cells in media with decreasing concentration of potassium and sodium ions show a decrease in RTV towards more negative values, but to a lesser extent than expected from theory (see below). In case of B16F1 cells, the changes in RTV were even hardly noticeable. For given external  $[X]_o$  and internal  $[X]_i$  ion concentrations, and their membrane permeabilities  $P_X$ , RTV can be calculated with Goldman equation (Hodgkin and Katz 1949; Alberts et al., 1994):

$$U_{RTV} = \frac{RT}{F} \ln \frac{[K]_o + p[Na]_o}{[K]_i + p[Na]_i}, \quad p = P_{Na} / P_K \quad (3.1)$$

where  $R$  is the gas constant,  $T$  is the temperature and  $F$  is the Faraday's constant ( $RT/F =$  appr. 25.3 mV). For cells in media with decreasing potassium ion concentrations (m1, m2 and m3) the above equation reduces to Nernst equation for potassium ions. If we consider external potassium concentrations of 18 mM, 9 mM and 1.8 mM for m1, m2, m3, respectively

(calculated from Table 2.2 in Materials and Methods Section by assuming that molecules  $K_2HPO_4$  and  $KH_2PO_4$  completely dissolve in water) and 130 mM internal potassium concentration (Williams 1970), we can calculate RTV in cells in such potassium media (Table 3.2). Similar calculations can be performed also for media with decreasing sodium ion concentrations by considering the internal concentration of sodium of 15 mM (Williams 1970).

**Table 3.2. Theoretically calculated resting transmembrane voltages for potassium media.  $[K]_o = 18$  mM (m1),  $[K]_o = 9$  mM (m2),  $[K]_o = 1.8$  mM (m3),  $[K]_i = 130$  mM.**

	RTV/mV
<b>m1</b> (KZAP 10 mM)	-50 mV
<b>m2</b> (KZAP 5 mM)	-68 mV
<b>m3</b> (KZAP 1 mM)	-108 mV

The calculated RTVs are substantially more negative than measured RTVs (Table 3.1). This can be partially attributed to overestimated intracellular concentration of potassium used in calculations. The 130 mM internal potassium concentration holds for cell in physiological conditions (in culture medium), while the calculations were performed for media with progressively decreasing ionic concentrations. It was shown by several authors that changing the extracellular concentration of ions also alter the intracellular ion concentration (McDonald et al., 1972; Cone 1971; Lezzi 1970). Besides, it was shown that ion permeability coefficients depend on RTV (Williams 1970; Baker et al., 1971). Because cells in our experiments were incubated in each medium for at least 20 minutes, it is reasonable to believe that the internal potassium (and also sodium) concentration was different from the one in culture medium. However, until the exact concentrations of ions inside cells in these media are determined, we can only speculate about the reasons for observed discrepancies. They can also be due to the fact that the chosen method for measuring RTV, although reported as efficient (Ehrenberg et al., 1988; Farkas et al., 1989) is not suitable for these experiments. Namely, with different method and different fluorescent dye, di-BAC<sub>4</sub>(3), RTV in CHO cells in 10 mM K-ZAP medium was measured to be approximately -50 mV, in agreement with theoretical predictions in Table 3.2 (Valič et al., 2003).

In one of our previous papers (**paper 4** in Appendix, Pucihar et al., 2001) we predicted that RTV of cells in media with progressively decreasing conductivities should also decrease. Measurements of RTV presented here are in qualitative agreement with predictions from the paper, i.e. RTV decreased with decreasing extracellular medium conductivity. Quantitative comparisons, however, are difficult because experiments were not performed on the same cell lines; Chinese Hamster lung fibroblasts (DC3F) were used in the abovementioned paper and these cells are not accessible in our laboratory any longer. Regardless, if we compare the

calculated RTV for one of the media from the paper, which was also used in the present study (medium m7, RTV = -159 mV), with measured RTV in the same medium (between -37 mV and -100 mV), we again obtain considerable differences, which most probably arise due to the same reasons as discussed above (overestimated intracellular potassium concentration, changes of ion permeability coefficients, the proper method).

During external electric field exposure (e.g. during electropermeabilization), induced transmembrane voltage (ITV) forms on the cell membrane. This voltage superimposes to the resting transmembrane voltage and together they form the total transmembrane voltage (ITV+RTV). In electropermeabilization experiments ITV exceeds few hundred millivolts, therefore, RTV is usually neglected and ITV is taken as a rough estimate of total transmembrane voltage (Valič et al., 2004). On the basis of measurements of RTV in culture medium and 10 mM K-ZAP medium, we can conclude that such approximation is reasonable. Therefore, in the following sections, the RTV will be neglected in the analysis of the data. We will, however, demonstrate in one example to what extent the total transmembrane voltage changes if RTV is considered.

## 4 SPHERICAL CELLS

### 4.1 Results

#### 4.1.1 Measurements of induced transmembrane voltage

Measurements of induced transmembrane voltage (ITV) were performed by means of potentiometric fluorescent dye di-8-ANEPPS. The fluorescence images of three almost spherical cells stained with the dye are shown in Figure 4.1A. The cells were exposed to a voltage of 40 V, corresponding to electric field 100 V/cm, which was delivered consecutively in two opposite directions. After subtraction of the control image, the changes in the fluorescence become clearly visible (Figure 4.1B). The grey color in these 8-bit figures has the intensity of 128 and represents no change in the fluorescence from the fluorescence in the control, while the white and the black colors characterize an increase (cell depolarization) and a decrease in fluorescence (cell hyperpolarization), respectively.

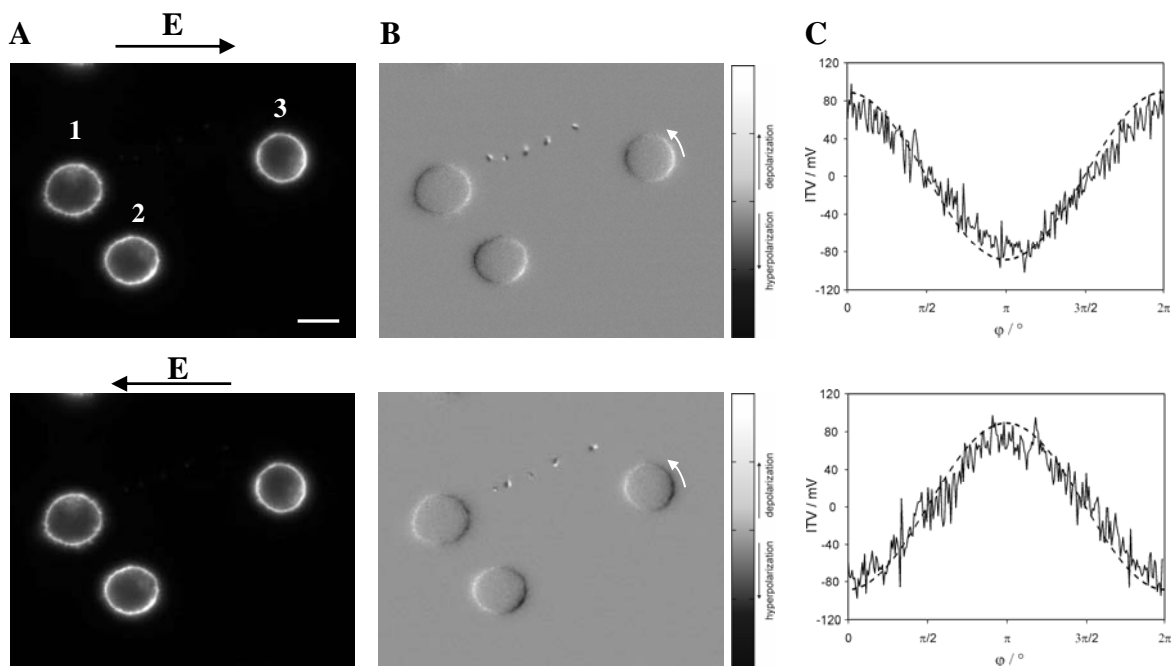


**Figure 4.1.** Measurements of induced transmembrane voltage (ITV) on a spherical CHO cell. First row shows the results for the electric field  $E$  directed to the right and the second row for the opposite direction. (A) The 8-bit fluorescence images of cells stained with di-8-ANEPPS and acquired during the exposure to 40 V (100 V/cm), 100 ms rectangular pulse. The brightness of the image was automatically enhanced. Bar represents 10  $\mu\text{m}$ . (B) Changes in fluorescence of cells obtained by subtracting the control image (not shown) from the image with pulse and shifting the grayscale range by 50%. White arrow shows the path along which ITV was measured. The brightness of the image was automatically enhanced. (C) ITV for cell 3 as a function of angle. Solid curve – measured values, dashed curve – numerically calculated values (see below). The changes in fluorescence were transformed to ITV by using a calibration curve (6 % change in fluorescence corresponding to 100 mV).

The changes in fluorescence shown in Figure 4.1B were transformed into values of ITV by using a calibration curve (6% change in fluorescence corresponding to 100 mV; see Section 2.3.1 in Materials in Methods). For cell 3, the distribution of ITV along the perimeter is shown in Figure 4.1C for both field directions. According to these results, ITV changes with a cosine function along the perimeter of the cell between approximately +80 and -80 mV, and has a zero value at the poles of the cell ( $90^\circ$  and  $270^\circ$ ). The maximal and minimal values of ITV were obtained in regions of the cell facing the electrodes. The change in the orientation of the electric field results in a change in the polarity of ITV, which changes in the same range and again with a cosine function. The dashed lines in Figure 4.1C show the numerically computed ITV for the model of the same cell (see Section 4.1.2 below for details).

ITV was also measured for cells exposed to different external pulse amplitudes: 20, 30, and 40 V, corresponding to electric fields of 50, 75 and 100 V/cm. An example of such measurements performed on cell 1 is shown in Figure 4.2. With increasing pulse amplitudes, the absolute value of ITV increases almost linearly. Namely, the absolute values, obtained at the poles of the cell ( $0^\circ$  and  $180^\circ$ ) increase from approximately 40 mV for a 20 V pulse to 70 mV for a 30 V pulse and to approximately 90 mV for a 40 V pulse, while at  $90^\circ$  and  $270^\circ$  ITVs are zero. The dashed lines give the numerically computed ITV for the same cell (see Section 4.1.2 below for details).

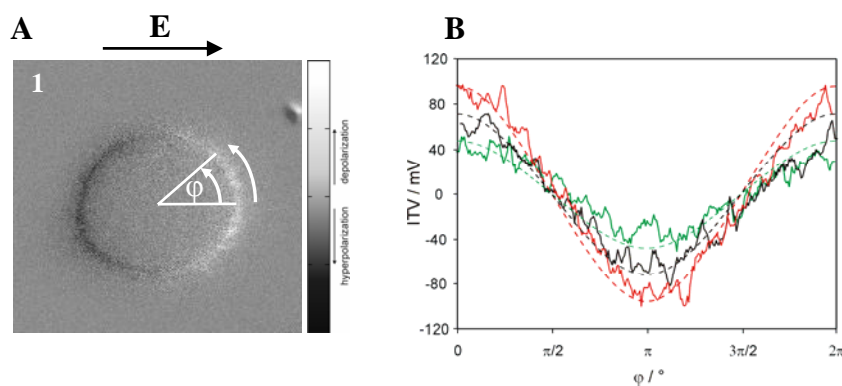


**Figure 4.2.** The distribution of ITV as a function of angle  $\phi$ . (A) Magnified fluorescence image of the cell of interest (cell 1). White arrow shows the path along which ITV was measured. (B) Measured ITVs for cell 1 at different pulse amplitudes: 20 V – Green, 30 V – Black, 40 V – Red. The changes in the fluorescence were transformed to ITV by using the calibration curve (6 % change in fluorescence corresponding to 100 mV). The corresponding dashed curves represent the numerically calculated ITV for the same cell.

#### 4.1.2 Numerical calculations of induced transmembrane voltage

Numerical calculations were performed on the model of the same cell on which the experiment in Section 4.1.1 was carried out. A sphere with radius corresponding to the radius of a cell ( $5.6 \mu\text{m}$  for cell 3 and  $6.5 \mu\text{m}$  for cell 1) was constructed and placed to the bottom of

a  $50 \times 50 \times 30 \mu\text{m}$  cube, which represented the extracellular medium (Figure 4.3A). The two opposing sides of the cube, colored in grey, represented the electrodes to which the electric potential was assigned, while the other faces of the cube were insulating. The voltage of 0.5 V was applied to the electrodes to mimic the same conditions as in the experiments in Section 4.1 (electric field 100 V/cm). A bottom of the sphere was cut to model the cell partially attached to the cover glass (Figure 4.3B). The membrane was modeled as a boundary condition (see Section 2.4.2 in Materials and Methods). The calculated distribution of electric potential around and inside the cell is presented in Figure 4.3C in the x-y plane crossing the center of the cell. The dark red color represents electrical potential of 0.5 V and the dark blue color the potential of 0 V. The electric potential outside the cell changes with position on the cell membrane while the potential inside the cell is constant and has the value of 0.25 V. ITV was determined as a difference of electric potentials on both sides of the cell membrane ( $ITV = V_i - V_o$ ). For cell 3, the numerically calculated ITV changes between approximately +89 mV and -89 mV, and is presented with dashed curves in Figure 4.1C together with experimentally measured ITV.

A similar procedure was performed for cell 1 to compute ITV at different external pulse amplitudes and the results of these computations are shown with dashed curves in Figure 4.2B.

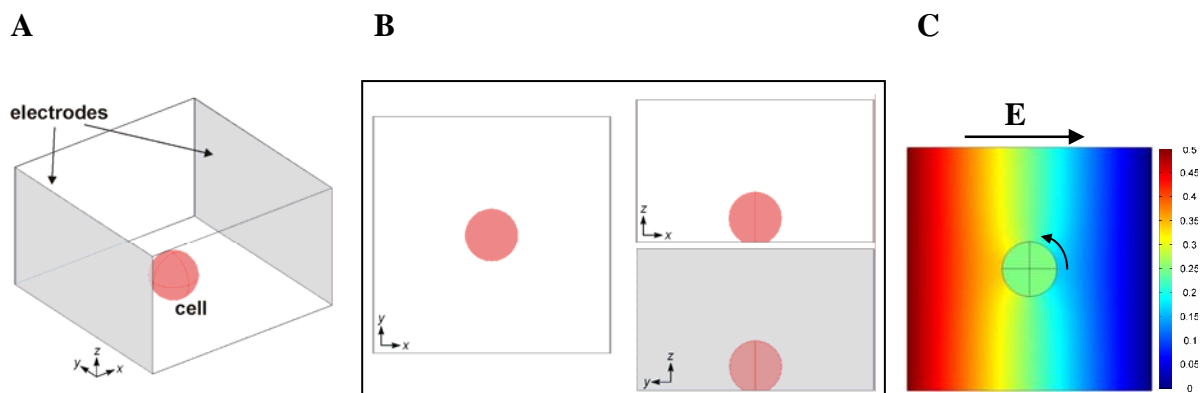


**Figure 4.3** Numerical calculations of ITV. (A) 3D model of a cell 3. The cell is modeled as a sphere with a radius of  $5.6 \mu\text{m}$ , while the cube with dimensions  $50 \times 50 \times 30 \mu\text{m}$  represents the extracellular medium with conductivity of  $0.14 \text{ S/m}$ . The inside of the sphere was assigned a conductivity of  $0.3 \text{ S/m}$ ; the membrane was modeled as a boundary condition. The opposing grey sides of the cube are the electrodes, one set to  $0.5 \text{ V}$  and the other to the ground ( $100 \text{ V/cm}$ ). The remaining faces of the cube are insulating. (B) The three side views of the model. (C) The computed distribution of the electric potential around and inside the cell in the x-y plane through the center of the cell. The arrow marks the path along which the potential was measured. ITV was determined as the difference between the potentials on both sides of the membrane ( $ITV = V_i - V_o$ ).

### 4.1.3 Visualization of cell electropermeabilization

After measurements of induced transmembrane voltage, the same spherical CHO cells from Section 4.1.1 (Figure 4.1A) were electropermeabilized with a single 260 V (650 V/cm) rectangular bipolar pulse (750 + 750  $\mu$ s). The interpulse delay was approximately 3  $\mu$ s. The permeabilization was followed by observing the change in fluorescence emanating from cells after adding a fluorescent dye Propidium Iodide to the suspension. The dye fluorescence increases upon entering the cell interior. The first image, acquired 100 ms after the pulse delivery, shows that the dye enters the cell in the regions of the membrane facing the electrodes (Figure 4.4) and the increase in fluorescence seems symmetrical. Namely, for cell 1, the polar angles of the cell membrane, where increased fluorescence is observed are 65° and 70°, for cell 2, 70° and 70°, and for cell 3, 75° and 70° respectively (Figure 4.5). Five minutes after permeabilization the whole cell interior becomes fluorescent, mostly the nuclear regions of the cell, where many binding sites for the dye are available (Figure 4.4).

In the following subsections the course of permeabilization on spherical cells will be investigated in more detail.

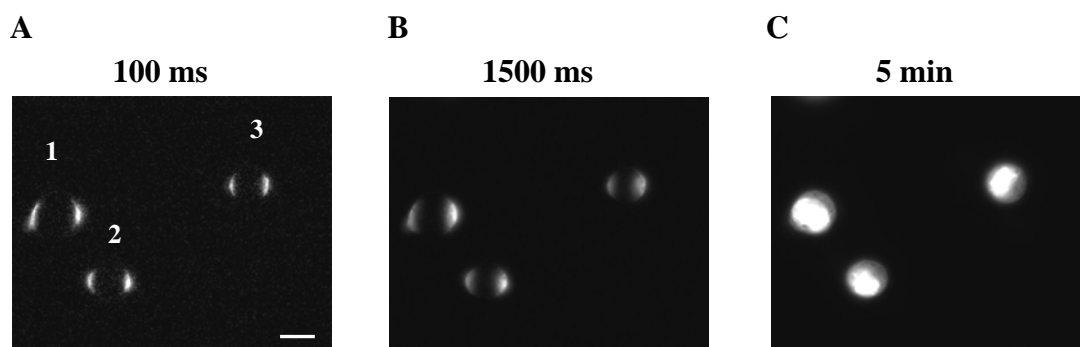


**Figure 4.4** Visualization of cell electropermeabilization. (A) Fluorescence of the cells 100 ms, (B) 1500 ms, and (C) 5 min after the pulse delivery. The images are corrected for the background fluorescence. The cells were exposed to a single 260 V (650 V/cm) rectangular bipolar pulse (750 + 750  $\mu$ s). Propidium Iodide was added to suspension before the pulse was applied to visualize the permeabilized regions. Bar represents 10  $\mu$ m.

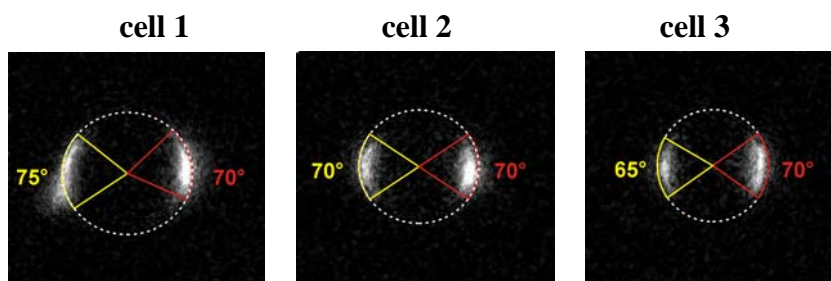


**Figure 4.5** Determination of the polar angles of the cell membrane where permeabilization occurs. The cells are the same as in Figure 4.1. The dashed white curve outlines the cell, while the yellow and red curves are the polar angles of the permeabilized regions. The cell was permeabilized with a single 260 V (650 V/cm) rectangular bipolar pulse (750  $\mu$ s + 750  $\mu$ s).

#### ***4.1.3.1 The influence of pulse parameters on the course of cell electropermeabilization***

The effect of different pulse amplitudes, durations and pulse shape on permeabilization of spherical CHO cells was investigated. Permeabilization was monitored by following the dye uptake into cells during and after permeabilization on two time scales: a short time scale (13.33 ms) with 3.33 ms time resolution, and a long time scale (1.5 s) with 100 ms time resolution.

##### ***Short time scale observations***

###### ***Unipolar pulses***

First, we investigated the influence of pulse amplitudes on cell electropermeabilization. A single, unipolar, rectangular pulse with 1 ms duration and amplitudes of 400, 500, 600, and 700 V (800 V/cm - 1400 V/cm) was delivered to cells. The increase in fluorescence was detected within the first 3.33 ms after the onset of the electric pulse (denoted with an arrow in Figure 4.6), demonstrating permeabilization of the cell membrane. After pulse delivery the intensity of the fluorescence gradually increased with time, indicating the dye uptake into the cells, but only on the side of the cell facing the positive electrode. The polar angle of permeabilization increased with time after permeabilization and with pulse amplitude (graph in Figure 4.6 and Table 4.1). At the end of the investigated time interval the polar angles were 95°, 115°, 130°, and 145°, for 400, 500, 600, and 700 V pulse, respectively.

Next, we investigated the influence of pulse durations on cell permeabilization. A single, unipolar, rectangular 500 V (1000 V/cm) pulse with durations of 1, 3, and 5 ms was applied and changes in fluorescence were monitored. Again, we detected an increase in fluorescence within 3.33 ms after the onset of the electric pulse, demonstrating electropermeabilization of the cell (Figure 4.7). The increase in fluorescence was observed only on the side of the cell facing the positive electrode. The polar angle of permeabilization increased with time and with increasing pulse durations (graph in Figure 4.7 and Table 4.1). At the end of the investigated time interval the polar angles were 115°, 140°, and 155°, for 1, 3, and 5 ms pulse, respectively.

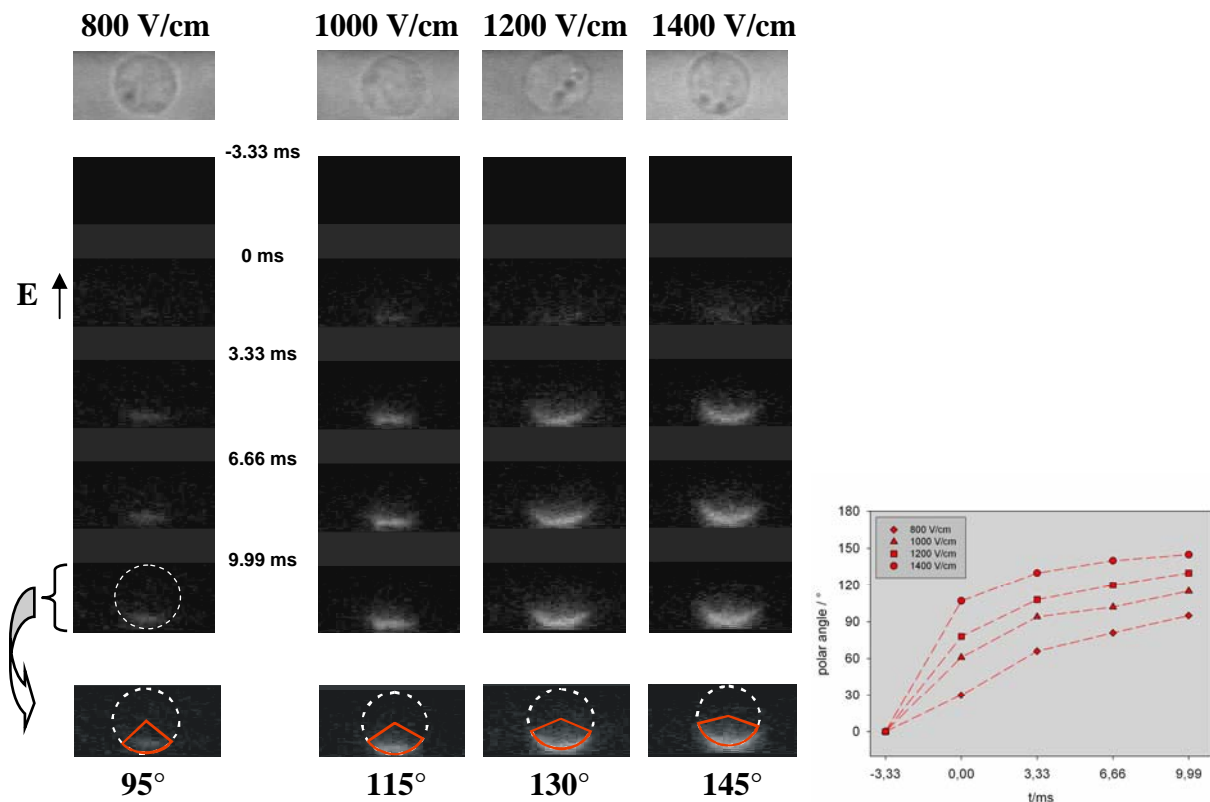


**Figure 4.6** Changes in fluorescence from cells after electroporation observed on a time scale of 13.33 ms. CHO cells were exposed to a single unipolar rectangular pulse with 1 ms duration and pulse amplitudes of 400 V (800 V/cm), 500 V (1000 V/cm), 600 V (1200 V/cm), and 700 V (1400 V/cm). The first image is the phase contrast of the cell, the second (-3.33 ms) is the fluorescence of the cell before the pulse, the following images are the fluorescence of the cell during (0 ms) and after the pulse. The control image (-3.33 ms) was subtracted from the pulse and post-pulse images. The pulse was applied at time 0 - marked with an arrow. The polar angles of permeabilization were measured within each time frame for all investigated pulse parameters and are presented with red symbols in the graph.

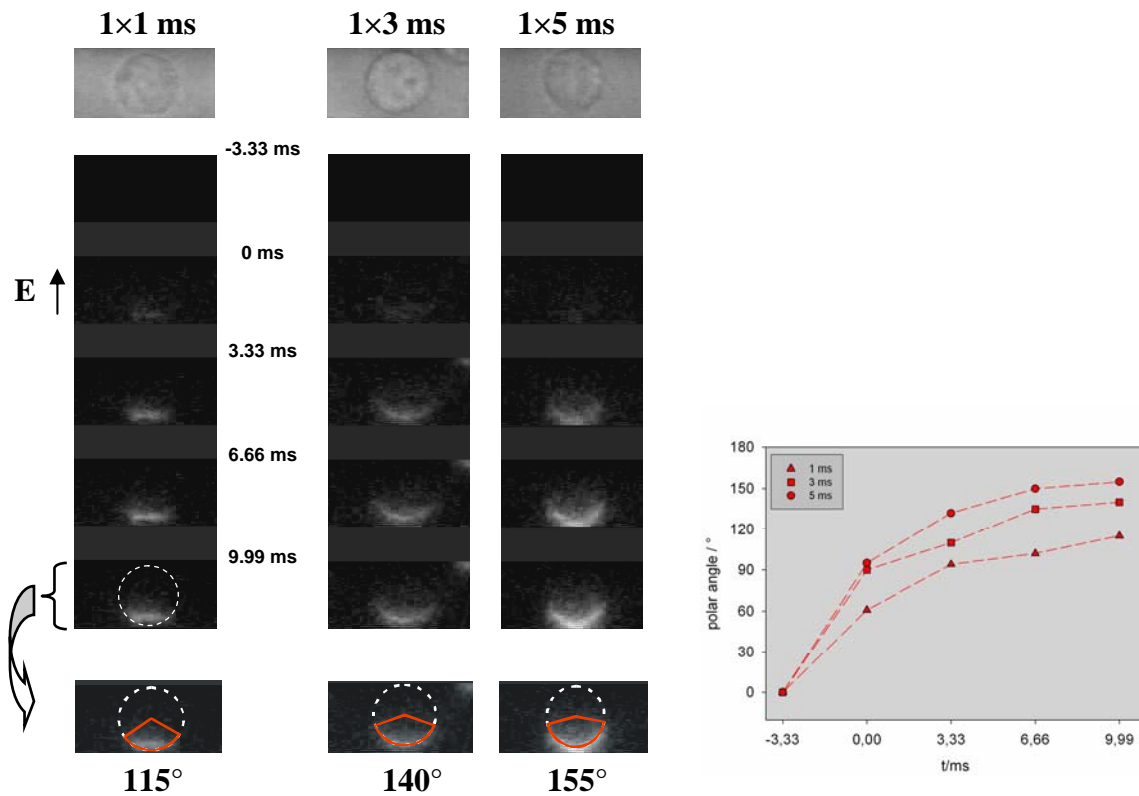


**Figure 4.7** Changes in fluorescence from cells after electropermeabilization, observed on a time scale of 13.33 ms. CHO cells were exposed to a single, unipolar, 500 V (1000 V/cm) rectangular pulse with durations of 1, 3, and 5 ms. The first image is the phase contrast of the cell, the second (-3.33 ms) is the fluorescence of the cell before the pulse, the following images are the fluorescence during (0 ms) and after the pulse. The control image (-3.33 ms) was subtracted from the pulse and post-pulse images. The pulse was applied at time 0 - marked with an arrow. The polar angles of permeabilization were measured within each time frame for all investigated pulse parameters and are presented with red symbols in the graph.

In some of the experiments presented above, relatively long pulse durations (e.g. 5 ms) and high pulse amplitudes (1400 V/cm) were used. Such pulses could cause cell movement, which could affect the data presented above. In addition, cells after permeabilization increase in size (cell swelling), and this increase could occur already within the investigated time interval. The possible changes in cell position and shape during and after the pulse application were examined by exposing the cells to the same electric pulses as before, and acquiring the transmission light images instead of fluorescence images.

The results for different pulse amplitudes are presented in Figure 4.8. For the pulse amplitudes investigated (1×1 ms pulse, 800 V/cm – 1400 V/cm) we did not observe any considerable changes in cell position or cell size/shape, at least in the investigated time interval (13.33 ms).

The results for different pulse durations (1000 V/cm, 1, 3, and 5 ms) are shown in Figure 4.9. No considerable changes in cell position or cell shape were observed for a 1 ms pulse. However, for longer pulses (3 ms and 5 ms), we detected cell elongation in the direction of

the electric field during the pulse application, which was also followed by an increase in cell size (cell swelling). The latter was the most pronounced for 5 ms pulse (Figure 4.9).

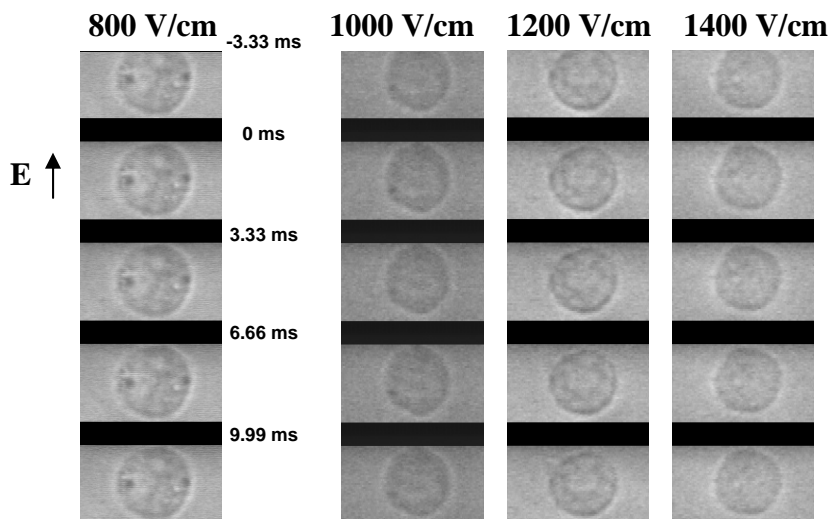


**Figure 4.8.** Transmission light observations of the changes in cell position and cell shape during and after permeabilization. A single 1 ms pulse with amplitudes 800, 1000, 1200, and 1400 V/cm was applied at time 0 ms (black arrow).

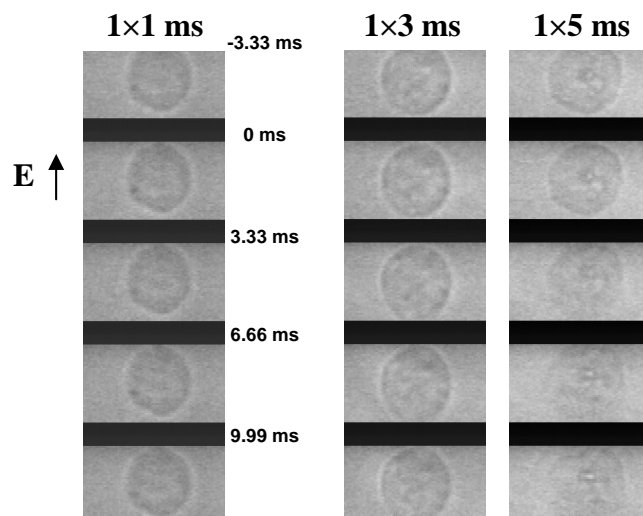


**Figure 4.9.** Transmission light observations of the changes in cell position and cell shape during and after permeabilization. A single 1000 V/cm pulse with durations 1, 3, and 5 ms was applied at time 0 ms (black arrow).

***Bipolar pulses***

Cells were exposed to a single rectangular bipolar pulse with the same cumulative duration as the unipolar pulse used in the above experiments.

To investigate the influence of pulse amplitudes on cell permeabilization, a single rectangular bipolar 1.5 + 1.5 ms pulse with amplitudes of 800 and 1000 V/cm was applied to the cell. Unfortunately, 1000 V/cm was the upper amplitude generated by our bipolar pulse generator. The changes in fluorescence during and after pulse application are shown in Figure 4.10. According to results for the 800 V/cm bipolar pulse, 3.33 ms after pulse, a symmetrical increase in fluorescence on both sides of the cell can be observed, while for a 1000 V/cm pulse, fluorescence from only one side of the cell is visible within this time frame. With time, both sides of the cell become symmetrically fluorescent (graph of Figure 4.10 and Table 4.2). In comparison to results for a 3 ms unipolar pulse of the same amplitude, the fluorescence intensities for a bipolar pulse are lower (compare Figures 4.6 and 4.10).

A similar experiment was also repeated for different durations of the bipolar pulse. A single rectangular bipolar pulse with amplitude of 1000 V/cm and durations 500 + 500  $\mu$ s, 1.5 + 1.5 ms and 2.5 + 2.5 ms was delivered to the cell. The durations of the bipolar pulses were chosen to have the same cumulative durations as the unipolar pulse in the above experiments (i.e. 1, 3, and 5 ms). While a symmetrical fluorescence increase after permeabilization was observed for a 500 + 500  $\mu$ s bipolar pulse, fluorescence for 1.5 + 1.5 ms and 2.5 + 2.5 ms pulses first occurred only on one side of the cell, but became roughly symmetrical by the end of the observed time interval (graph of Figure 4.11 and Table 4.2). With increasing pulse durations the polar angles of permeabilization increased.

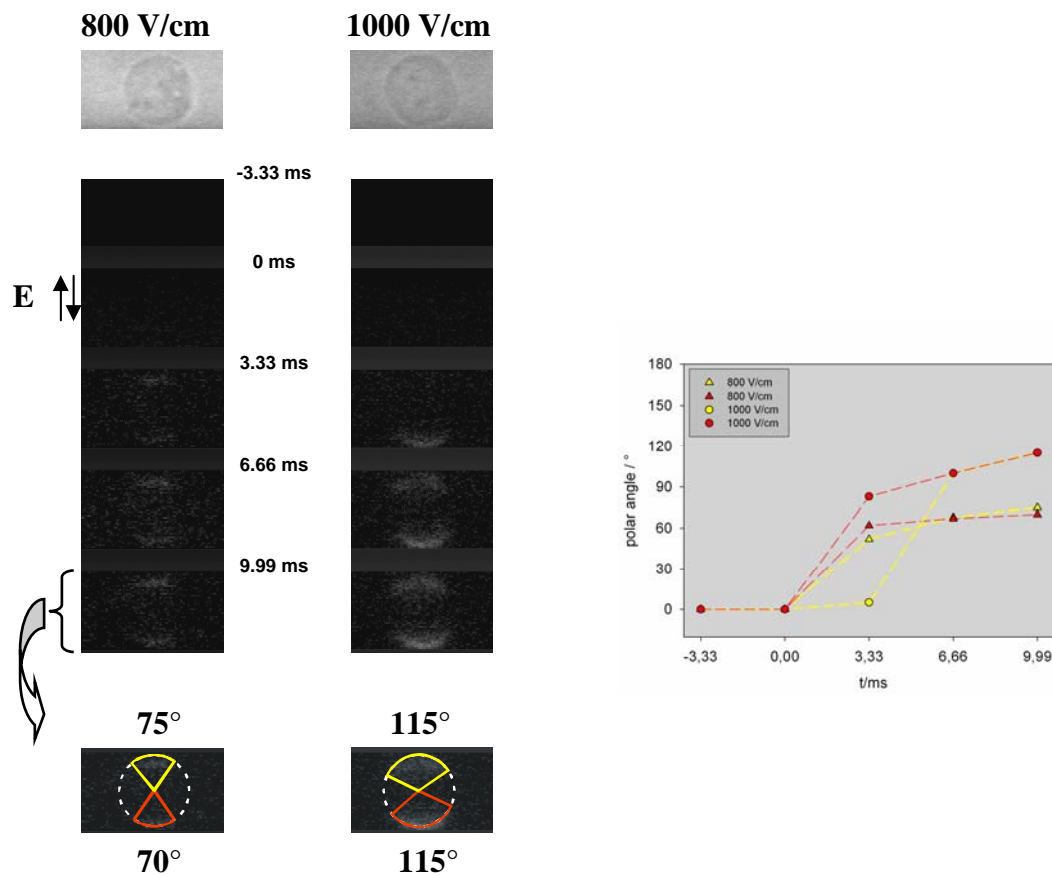


**Figure 4.10** Changes in fluorescence from cells after electropermeabilization, observed on a time scale of 13.33 ms. A single spherical cell was exposed to a 1.5 + 1.5 ms bipolar, rectangular pulse with amplitudes of 400 V (800 V/cm) and 500 V (1000 V/cm). The first image is the phase contrast of the cell, the second (-3.33 ms) is the fluorescence of the cell before the pulse, the following images are the fluorescence of the cell during (0 ms) and after the pulse. The control image (-3.33 ms) was subtracted from the pulse and post-pulse images. The time when the pulse was applied is marked with an arrow. The polar angles of permeabilization were measured within each time frame for all investigated pulse parameters and are presented with red and yellow symbols in the graph.

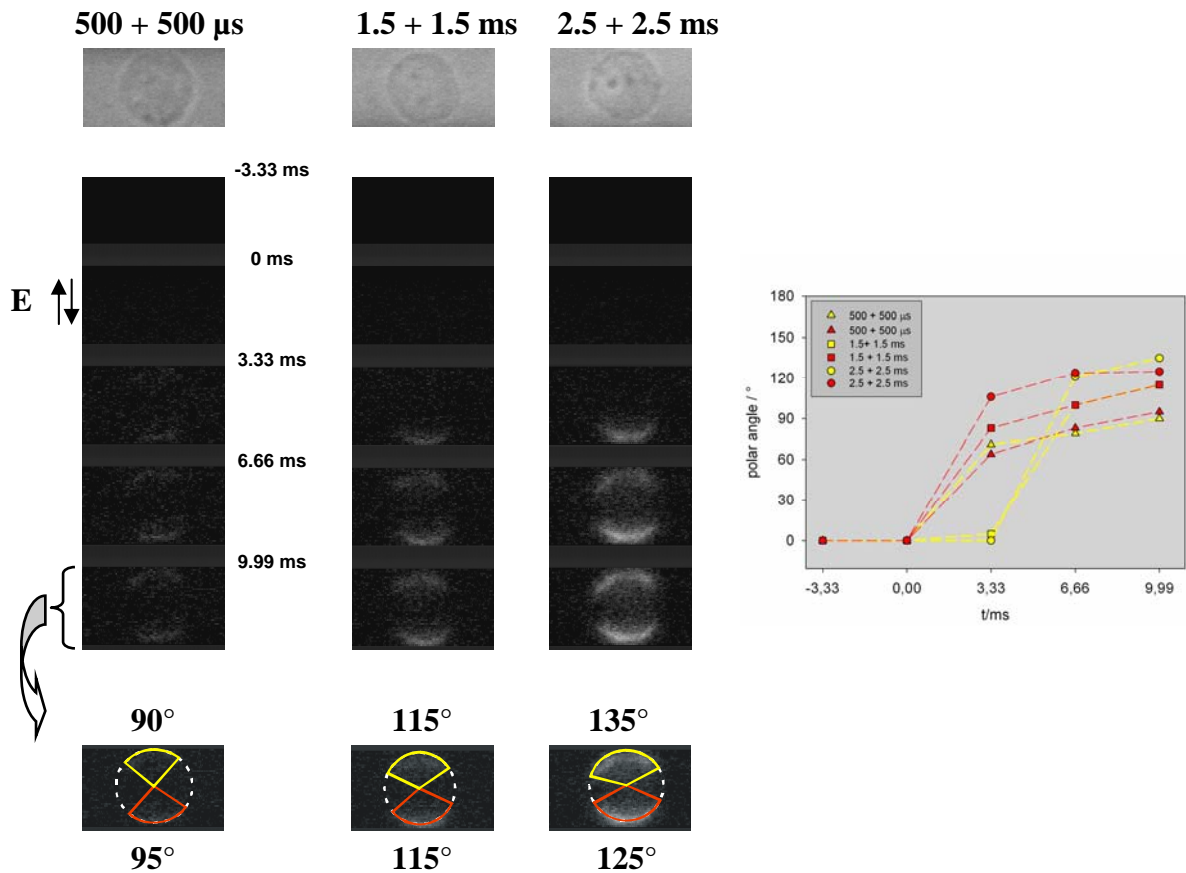


**Figure 4.11.** Changes in fluorescence from cells after electroporation, observed on a time scale of 16.67 ms. A single spherical cell was exposed to a 1000 V/cm bipolar, rectangular pulse with duration of 500 + 500  $\mu$ s, 1.5 + 1.5 ms, and 2.5 + 2.5 ms. The first image is the phase contrast of the cell, the second (-3.33 ms) is the fluorescence of the cell before the pulse and the following images are the fluorescence of the cell during (0 ms) and after the pulse. The control image (-3.33 ms) was subtracted from the pulse and post-pulse images. The time when the pulse was applied is marked with an arrow. The polar angles of permeabilization were measured within each time frame for all investigated pulse parameters and are presented with red and yellow symbols in the graph.

**Table 4.1.** Polar angles of permeabilization at different parameters of unipolar pulses.

	time	800 V/cm	1000 V/cm	1200 V/cm	1400 V/cm	1 $\times$ 1 ms	1 $\times$ 3 ms	1 $\times$ 5 ms
		<b>unipolar</b>	-3.33 ms	0°	0°	0°	0°	0°
	0 ms	30°	61°	78°	107°	61°	95°	90°
	3.33 ms	66°	94°	108°	130°	94°	110°	132°
	6.66 ms	81°	102°	120°	140°	102°	135°	150°
	9.99 ms	95°	115°	130°	145°	115°	140°	155°

**Table 4.2.** Polar angles of permeabilization at different parameters of bipolar pulses.

	time	800 V/cm	1000 V/cm	500 + 500 $\mu$ s	1.5 + 1.5 ms	2.5 + 2.5 ms
		<b>bipolar</b>	-3.33 ms	0/0°	0/0°	0/0°
	0 ms	0/0°	0/0°	0/0°	0/0°	0/0°
	3.33 ms	52/62°	5/83°	71/64°	0/94°	0/106°
	6.66 ms	68/67°	100/100°	79/83°	98/102°	121/124°
	9.99 ms	75/70°	115/115°	90/95°	115/115°	135/125°

### *Long time scale observations*

#### *Unipolar pulse*

The dye uptake after electropermeabilization was monitored on a time scale of 1.5 seconds with 100 ms time resolution. A single 500 V/cm unipolar, rectangular pulse with durations 100  $\mu$ s, 250  $\mu$ s, 500  $\mu$ s, and 1 ms was applied to CHO cells in suspension and the change in fluorescence was observed (pulse amplitudes were not investigated in this part of the study). The first column in Figure 4.12 shows the phase contrast of cells, while the second and third columns show the fluorescence images acquired 100 ms and 1.5 s after the pulse, respectively. Electropermeabilization with pulses with increasing pulse durations increased the intensity of fluorescence from cells, which indicates a larger uptake of dye to cells. Also, the fluorescence at a given pulse duration increases with time. While only the part of the cell facing the positive electrode is fluorescent 100 ms after the pulse, an increase in fluorescence from the opposite side of the cell can be observed 1.5 s after the pulse (Figure 4.12, second and third column).

Observations of the fluorescence with pulse durations shorter than 100  $\mu$ s were not possible, at least within the investigated time interval, because of the low signal-to-noise ratio. The results with pulse durations longer than 1 ms were essentially the same, except for the higher fluorescence from the cells.

#### *Bipolar pulse*

Similar experiments were performed with 500 V/cm bipolar pulses, with durations 250 + 250  $\mu$ s, 500 + 500  $\mu$ s, 1.5 + 1.5 ms, and 2.5 + 2.5 ms. The results are presented in Figure 4.13 in the same form as for unipolar pulses (phase contrast and two fluorescence images). Again, the fluorescence from the cells increases with time after pulse application, and also with increasing pulse durations. We first observe a symmetrical increase in fluorescence from the sides of the cells facing the electrodes (100 ms after the pulse delivery) for all investigated pulse durations. However, 1.5 s after the pulse, the fluorescence from the cells becomes asymmetrical (at least for pulses shorter than 2.5 + 2.5 ms), with higher fluorescence from the side of the cell, facing the positive electrode at the end of the bipolar pulse (Figure 4.13).

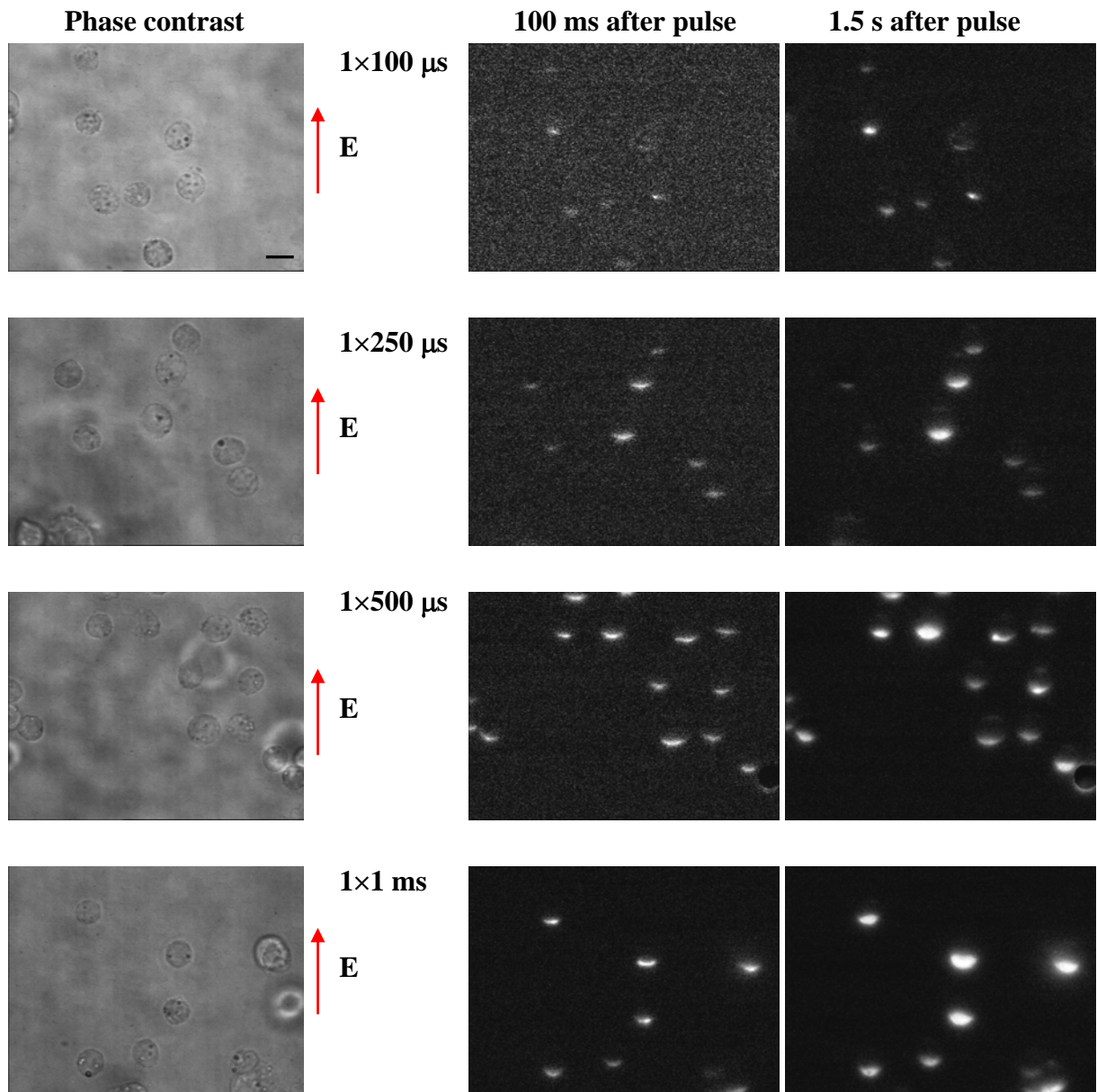


**Figure 4.12.** Changes in cell fluorescence after electropermeabilization observed on a time scale of 1.5 s. Cell suspension was permeabilized with 500 V/cm unipolar pulse with durations 100  $\mu\text{s}$ , 250  $\mu\text{s}$ , 500  $\mu\text{s}$ , and 1 ms. The first column shows the phase contrast, the second and the third columns are fluorescence images 100 ms and 1.5 s after the pulse, respectively. The fluorescence image acquired before pulse was subtracted from the fluorescence images. Bar represents 10  $\mu\text{m}$ .

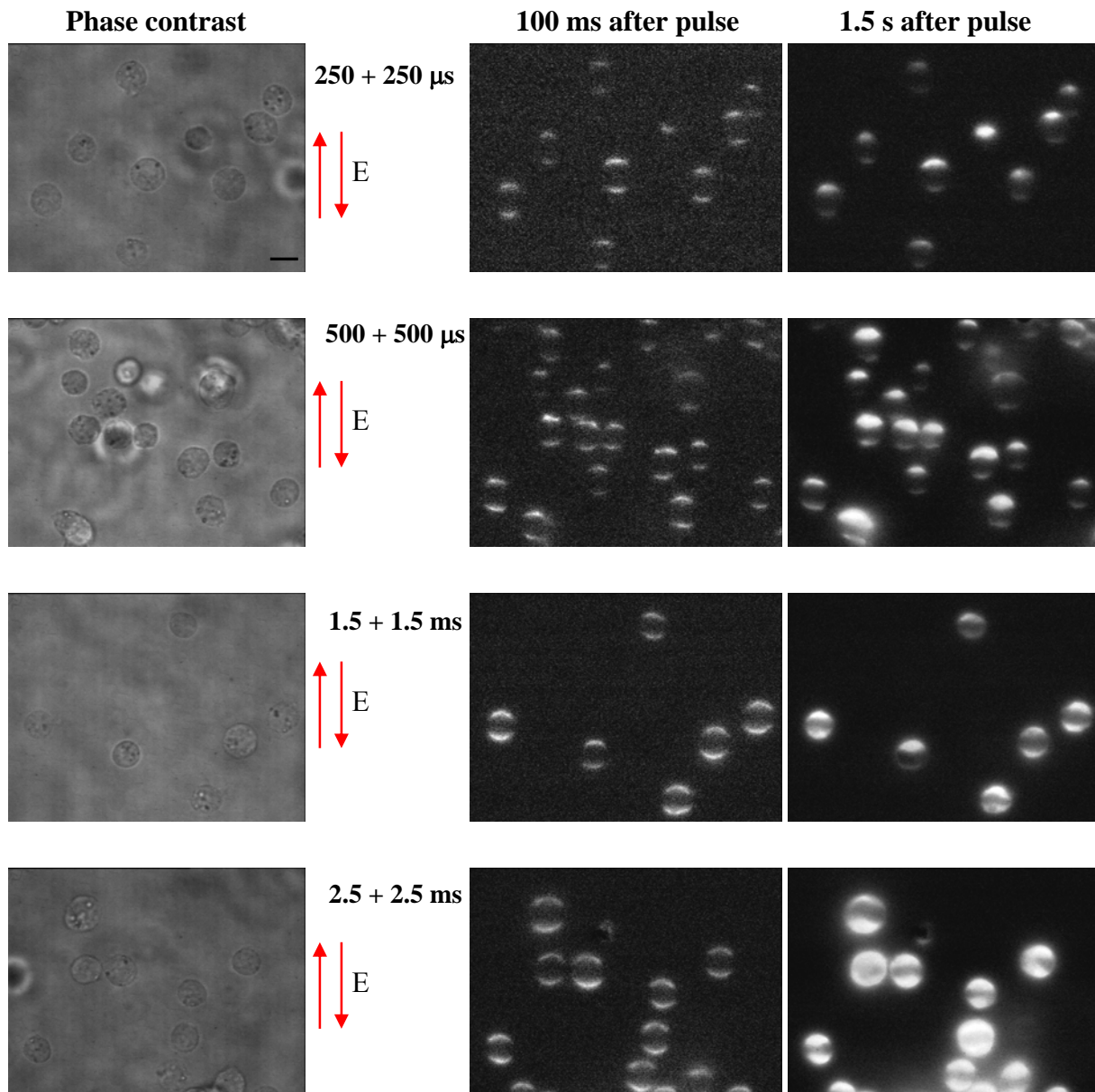


Figure 4.13. Changes in cell fluorescence after electroporation, observed on a time scale of 1.5 s. Cell suspension was permeabilized with 500 V/cm bipolar pulse with durations 250 + 250  $\mu\text{s}$ , 500 + 500  $\mu\text{s}$ , 1.5 + 1.5 ms, and 2.5 + 2.5 ms. The first column shows the phase contrast, the second and the third columns are fluorescence images 100 ms and 1.5 s after the pulse, respectively. The fluorescence image acquired before pulse was subtracted from the fluorescence images. Bar represents 10  $\mu\text{m}$ .

## 4.2 Discussion

The experiments and numerical calculations in this part of the study were performed on isolated spherical cells and dilute cell suspensions. First, induced transmembrane voltage (ITV) was determined on these cells. Then, permeabilization of the same cells on which ITV was measured was monitored by means of fluorescent dye Propidium Iodide. An independent study of the influence of pulse parameters on the course of permeabilization milliseconds and seconds after the pulse delivery was also performed.

Induced transmembrane voltage was measured using the potentiometric fluorescent dye di-8-ANEPPS and the measurements are in good agreement with results of numerical calculations. Substantial noise-like fluctuations of the measured ITV can be observed, but these are characteristic of the dye and are not due to oscillations in ITV on the membrane. The fluctuations could be reduced with ratiometric measurements of the fluorescence, i.e. by excitation of the dye at two wavelengths and measuring the ratio of emissions. However, such a system was not available in our study.

We should note that in the experiments where ITV was measured, cells were exposed to external voltages lower than those required to induce cell membrane permeabilization. According to reports in the literature, permeabilization occurs at critical ITVs ranging from 250 mV to 1000 mV, depending on cell type and experimental conditions (Tsong, 1991; Teissié and Rols, 1993; Bier et al., 1999; Miklavčič et al., 2000). In our experiments, the external pulse amplitude was set to 40 V on the electrodes with 4 mm gap (100 V/cm), which resulted in ITVs below 100 mV. The limitation of the pulse amplitude was necessary to prevent cell movement and the heating of suspension, which would occur as a consequence of relatively long field exposure (100 ms). These problems were also partially overcome by (i) plating the cells on coverglass and performing the experiment 2 to 4 hours later, when the cell shape was still spherical but cells already attached to the coverglass; (ii) using the low conductivity medium to reduce the heating (10 mM K-ZAP, see Materials and Methods Section).

We showed that the response of di-8-ANEPPS to increasing external voltages is linear, meaning that the subcritical ITV (where permeabilization does not occur) for any given external pulse amplitude can be determined by scaling the measured ITV with the corresponding ratio of external pulse amplitudes. For example, at electric field with two times higher amplitude (200 V/cm instead of 100 V/cm) the maximal ITV for the spherical cell shown in Figure 4.1C should be twice as high, around 160 mV. These assumptions are further supported by the reports of other researchers, which found the linear response of the dye in the range from -280 mV to +140 mV (Cheng et al., 1999), as well as from 0 to +250 mV (Lojewska et al., 1989). At the supracritical ITV where electropermeabilization occurs, such an approach is not feasible, because ITV in permeabilized region collapses (Hibino et al., 1991; Hibino et al., 1993). To a certain extent, the scaling can still be used in the

nonpermeabilized regions of the membrane, although the results of ITV obtained in that manner are questionable.

Measured ITV was also compared with numerically calculated ITV and a good agreement was obtained. Numerical calculations were performed on a model of a cell constructed from a sphere with a radius equal to the radius of the cell. The membrane was excluded from the model and was replaced by a boundary condition. Namely, the cell membrane, which is over a thousandfold thinner than the dimensions of a typical cell presents a difficulty in mesh generation. Usually, the thickness of the cell membrane is exaggerated by at least an order of magnitude and this is compensated partly by assigning to the membrane a higher specific conductivity (Huang et al., 2004). In this study we presented a method to replace the membrane in the model of the cell with a boundary condition of the surface between the exterior and interior of the cell (see Materials and Methods Section for details). Such replacement considerably reduces the number of finite elements in the model and the time for solution. More details can be found in **paper 5** in Appendix (Pucihar et al., 2006) where we illustrated how the decrease of membrane thickness from exaggerated values towards realistic ones is accompanied by a rapid increase in the number of elements forming the mesh, and consequently also in the time needed for generating the mesh and solving the problem.

It was shown by many authors that permeabilization occurs in regions of the membrane, where the absolute value of ITV is the highest, that is, in the regions facing the electrodes (Hibino et al., 1991; Tekle et al., 1991; Hibino et al., 1993; Tekle et al., 1994; Gabriel and Teissié, 1998; Gabriel and Teissié, 1999). The observed uptake of molecules through the permeabilized membrane was, however, in most cases asymmetrical, which was suggested to arise from electrophoretic effect of electric field on dye molecules of different size and charge, and due to asymmetry in density and size of structural defects on both sides of the cell. The latter could be attributed to different composition of lipids of the outer and inner layer of the membrane and also due to resting transmembrane voltage. Namely, during field exposure RTV superimposes to the ITV, and the sum of both voltages exceeds the critical threshold value initially on the anode side of the cell.

The asymmetry in the uptake of molecules was also observed in our study where cells were permeabilized with unipolar pulses. The fluorescence from the cells was always observed first on the side of the cell facing the positive electrode, while the opposite side of the cell became fluorescent afterward. As RTV of cells in our study was relatively low in comparison to ITV (see below), we suppose the asymmetrical uptake was mainly due to the electrophoretic effect of the pulse on the fluorescent dye. Propidium Iodide is a positively charged molecule and is therefore electrophoretically dragged towards the negative electrode, which favors the staining of the cell on the side facing the positive electrode. After the pulse, the dye uptake into cells is governed by pure diffusion, which explains the late detection of fluorescence also on the opposite side of the cell. In line with what we stated above, permeabilization with bipolar pulses should, therefore, result in a symmetrical uptake, as the electrophoretic effect

on dye molecules would be the same for both pulse polarities. The results of permeabilization with bipolar pulses, shown in Figures 4.10, 4.11, and 4.13 confirm these assumptions.

However, the electrophoretic force is present only during the application of the external pulse (few milliseconds) and should influence the dye uptake only in that time interval and perhaps a few milliseconds afterwards (due to the inertia of the dye movement). But, asymmetrical fluorescence was still observed even 1.5 second after the pulse delivery, when the dye entrance was governed by diffusion and, more interestingly, even for bipolar pulses. For unipolar pulses, this could be partly explained by the already mentioned asymmetry in density and size of structural defects, which would favor the entrance of dye on one side of the cell. Besides, a small voltage (approximately 7 V) was detected on the output of the pulse generator after the pulse delivery, which could induce a weak electrophoretic force on the dye even after the pulse was delivered. But this was not the case for bipolar pulse generator (Jouan prototype), where no such current existed after pulse delivery. Whether the observed asymmetrical uptake 1.5 s after pulse delivery is a consequence of asymmetric structural changes in the membrane or some other mechanism remains to be elucidated.

One of the aims of our study was to determine the critical value of ITV necessary to induce cell permeabilization from the observations of fluorescence during and after pulse delivery. The critical value of ITV can be calculated from the measurements of the polar angle of fluorescence from the cell by using the following equations (Rols and Teissié, 1990; Gabriel and Teissié, 1997):

$$\cos \varphi_C = \frac{E_c}{E}; \quad E > E_c, \quad (4.1)$$

$$ITV_{c,max} = 1.5 \cdot R \cdot E_c, \quad (4.2)$$

In the above equations,  $\varphi_C$  is the critical angle between the center of the cell and the point of interest on the cell membrane (one half of the polar angle),  $E_C$  is the critical external electric field where electropermeabilization occurs,  $E$  is a given applied field,  $ITV_{C,max}$  is a maximal critical ITV, and  $R$  is the cell radius. By measuring the polar angle ( $2 \times \varphi_C$ ) for a given externally applied electric field  $E$ , we can calculate the critical ITV ( $ITV_C$ ) by using Eq. 4.2. For experiments presented in Figure 4.5 (cell 3,  $R = 5.6 \mu\text{m}$ ), the polar angles of the fluorescence were  $65^\circ$  and  $70^\circ$  ( $\varphi = 32.5^\circ$  and  $35^\circ$  respectively) and  $E$  was 650 V/cm, which yields the maximal calculated value of the critical ITV, 460 mV and 450 mV, respectively. These values are well within reported ranges for critical ITV (Tsong, 1991; Teissié and Rols, 1993; Bier et al., 1999; Miklavčič et al., 2000).

However, as can be seen from Figures 4.6 and 4.7, the polar angle of fluorescence varies with pulse amplitude, pulse duration and time after pulse. While an increase of polar angle with pulse amplitude was expected from Eq. 4.1, and was also experimentally demonstrated

(Hibino et al., 1991), we did not anticipate the changes of angle with increased pulse durations. For example, with durations increasing from 1 ms to 5 ms, the polar angle of fluorescence at the end of investigated time interval increased from  $115^\circ$  to  $155^\circ$  (Figure 4.7). This is probably due to more persistent electrophoretical movement of dye into the cell at longer pulse durations, and also due to the changes in cell size, observed at longer pulse durations (Figure 4.9). An increase in polar angle with time after permeabilization is seeming and occurs due to spreading of the dye upon entering the permeabilized cell. Therefore, calculations of the critical ITV from the measurements of the polar angle should be performed immediately after the pulse and only for short pulse durations and even in that case, the calculations present a rough approximate of the real critical ITV. A better solution would be to directly measure ITV at the supracritical external pulse amplitude. Such measurements were already performed by Hibino and co-workers, showing a considerable decrease of ITV in the permeabilized regions of the membrane (Hibino et al., 1991; Hibino et al., 1993). A fast, sensitive camera is needed to perform such measurements, which was not available in our experiment as already discussed above. In fact, a system consisting of a camera, a calcium indicator (e.g. Fluo 3) and a suitable set of filters, it would be possible to instantaneously measure ITV and monitor the permeabilization of cells (by detecting the inflow of  $\text{Ca}^{2+}$  ions) (Hayashi et al., 1996, Johnson et al., 1999).

## 5 IRREGULARLY SHAPED CELLS

### 5.1 Results

In this part of the study we measured and calculated induced transmembrane voltage (ITV) on single irregularly shaped cells and determined the permeabilized regions of the cell membrane on the same cells. Also, the influence of electric field orientation on the calculated ITV was investigated and the influence of resting transmembrane voltage (RTV) on the total membrane voltage was demonstrated.

The results of measurements and calculations of ITV on irregularly shaped cells are described in detail in **paper 5** in Appendix (Pucihar et al., 2006). In the paper we presented a method for constructing realistic 3D models of irregularly shaped cells and a method to replace the cell membrane in a model with a boundary condition. ITVs calculated on such realistic cell models were then compared with ITV measured on the same cells from which the model was constructed and also with the simplified cell models. In addition, the influence of neighboring cells on ITV was demonstrated.

Because the results in the paper were presented for two cells only, we performed similar measurements and calculations on a few additional irregularly shaped cells. Besides, we included the visualization of permeabilization of these cells, which was not the subject of the paper. For a better demonstration, the results of measured ITV, calculated ITV, a 3D model, and visualization of permeabilization are presented together for each investigated cell. We begin with the treatment of simple, yet irregular cell shapes and then proceed to more complex ones. In addition, for one cell, a detailed analysis of the influence of electric field orientation on the calculated ITV was performed and the influence of RTV on the total membrane voltage was demonstrated.

### 5.1.1 Measurements and calculations of induced transmembrane voltage, and permeabilization of irregularly shaped cells

Measurements of induced transmembrane voltage (ITV) were performed using a potentiometric fluorescent dye di-8-ANEPPS. The changes in fluorescence of dye upon exposure of cell to the electric field are presented in Figure 5.1A and are hardly noticeable. They become visible after subtraction from the control image (without electric field) as shown in Figure 5.1B. In this figure, the side of the cell colored in white represents an increase in fluorescence, and the side of the cell colored in black, a decrease in fluorescence. These changes were transformed to ITV using a calibration curve (see Section Materials and Methods) and are presented with solid curve in Figure 5.1C as a function of the normalized arc length. The results are shown for two opposing orientations of external electric field (100 V/cm). For the first investigated cell (cell I), ITV changes along the cell membrane between approximately 75 mV and -65 mV for electric field directed from left to right and between -80 mV and 55 mV for the opposite direction of the field (Figure 5.1C).

From the fluorescence images of this cell, taken from four different imaging planes, a 3D model of a cell was constructed and placed to the bottom of the cube to model a cell attached to the coverglass. The cube represents the extracellular medium, and two opposing sides colored with grey are the electrodes. A detailed description of the model construction is given in **paper 5** in Appendix (Pucihar et al., 2006). The results of calculations of the electric potential outside and inside the cell model are, for the lowermost layer of the cell, shown in Figure 5.3A. From these values, ITV was calculated as the difference between potentials on both sides of the membrane ( $ITV = V_i - V_o$ , Figure 5.1C - dashed curves). For cell I, the calculated ITV varies between approximately 100 mV and -100 mV.

In the presence of the membrane-impermeant fluorescent dye Propidium Iodide, the same cell was then exposed to a single unipolar rectangular 400 V pulse (1000 V/cm) with 200  $\mu$ s duration. The changes in fluorescence of the cell were observed 100 ms (limitation of the imaging system, see Materials and Methods) after the pulse application on both sides of the membrane, denoting the regions where permeabilization occurred. With time, cell interior becomes more fluorescent indicating continuous dye uptake into cell after permeabilization. The fluorescence regions of the membrane on the first image (100 ms) were compared with calculations of ITV (shown on the surface of the cell model in Figure 5.3B). A good agreement between the observed fluorescence increase and the regions where the absolute value of ITV was the highest was obtained (Figure 5.3C - red denotes the regions where the absolute value of ITV is within arbitrarily chosen range of 15% of its maximal value).

A similar procedure was performed for five irregularly shaped cells with increasing complexity in their shape. Since the results are straightforward, only general observations will be described here, while a thorough discussion on the results will be given in the Discussion part of the study.

For each cell, induced transmembrane voltage was measured, a 3D model was constructed, ITV was calculated, permeabilization was performed and the results were compared. Cells I, II and III were Chinese hamster ovary cells (CHOK1), while cells IV, V, and VI were mouse melanoma cells (B16F1). According to results, measured and calculated ITVs are in a qualitative agreement, while some discrepancies in their amplitudes can be observed. The measured ITV's are generally lower than the calculated ITV's, and the differences seem to be larger for CHO cells than for B16F1 cells. For cell II, the calculations of ITV were performed for the opposite direction of the electric field in order to match the direction of the field during permeabilization (Figures 5.7 and 5.8). The results of permeabilization also show that in most cases, an increase in fluorescence after permeabilization is observed in those regions of the membrane, where the absolute value of the calculated ITV was the highest (see results for cell I, II, III, and IV). However, for cell V, we did not detect any permeabilization (Figure 5.20) while for cell VI, the permeabilization already occurred during the measurements of ITV. The results for all investigated cells are presented in the following pages.

## I. CHO

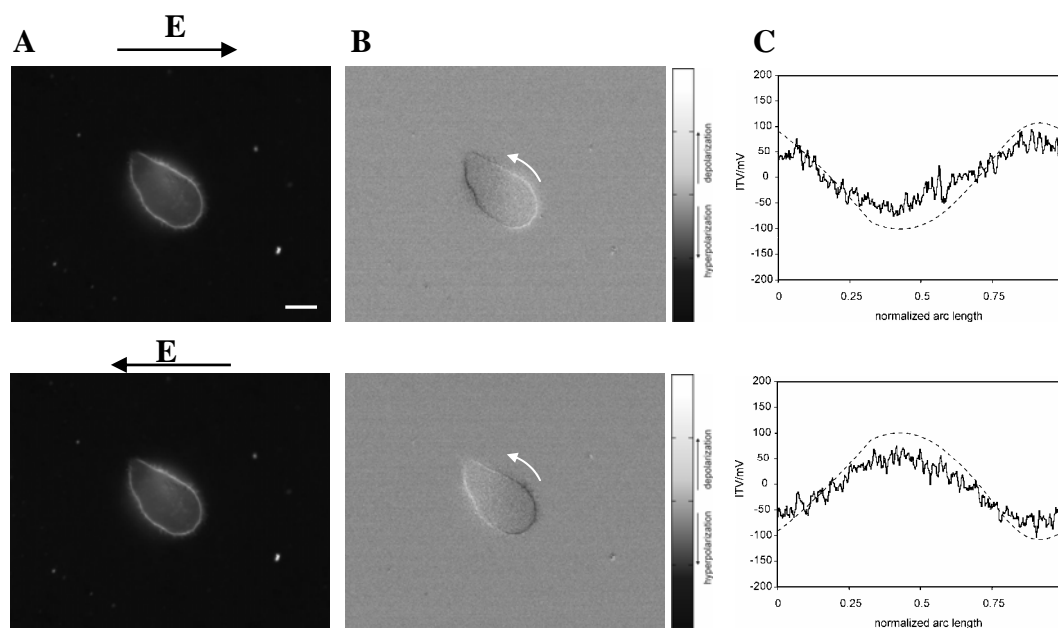


**Figure 5.1.** Measurements of induced transmembrane voltage (ITV) on an irregularly shaped CHO cell. First row shows the results for the electric field  $E$  directed to the right and the second row for the opposite direction. (A) The 8-bit fluorescence images of a cell stained with di-8-ANEPPS and acquired during the exposure to 40 V (100 V/cm), 100 ms rectangular pulse. The brightness of the image was automatically enhanced. Bar represents 10  $\mu\text{m}$ . (B) Changes in fluorescence of cell obtained by subtracting the control image (not shown) from the image with pulse and shifting the grayscale range by 50%. White arrow shows the path along which ITV was measured. The brightness of the image was automatically enhanced. (C) ITV as a function of normalized arc length. Solid curve – measured values, dashed curve – numerically calculated values (see below). The changes in fluorescence were transformed to ITV by using a calibration curve (6 % change in fluorescence corresponding to 100 mV).

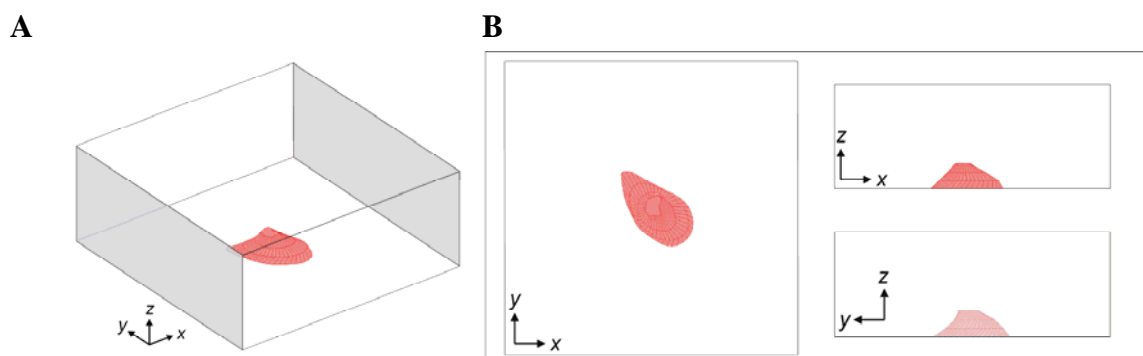


**Figure 5.2.** Numerical model of the irregularly shaped CHO cell shown in Figure 5.1. (A) The three-dimensional geometry of the cell model constructed from four cross-sections (see paper above or Materials and Methods Section for details). The model of a cell is placed to the bottom of the cube to mimic the cell attached to coverglass. The cube with dimensions  $73 \times 73 \times 28 \mu\text{m}$  represents the extracellular medium with conductivity of 0.14 S/m, the gray-shaded faces are the electrodes, one set to 0.73 V and the other to the ground (100 V/cm). The other four faces are insulating. The inside of the cell was assigned a conductivity of 0.3 S/m; the membrane was modeled as a boundary condition. (B) The three side views of the model.

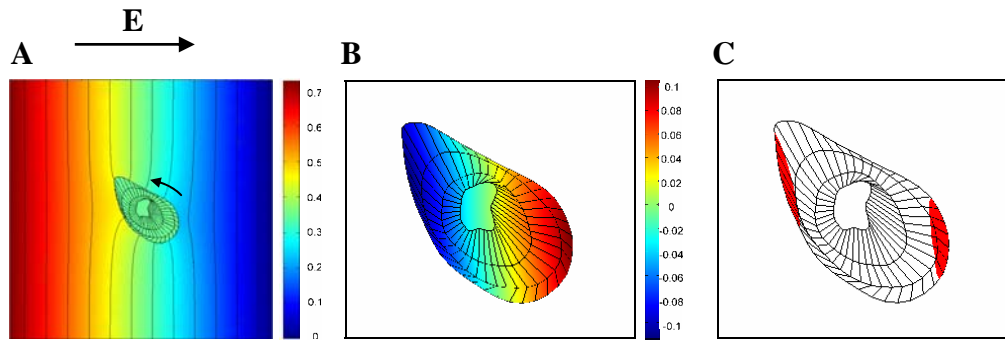


**Figure 5.3.** The calculations of induced transmembrane voltage. (A) The calculated distribution of the electric potential around and inside the cell in the lowermost x-y plane of the cell. The black curves represent the equipotentials and the arrow marks the path along which the potential was measured. The scale is in volts. (B) ITV calculated as a difference between the potentials on both sides of the membrane ( $ITV = V_i - V_o$ ) presented on the surface of the magnified model of the cell. For the lowermost part of the cell, ITV was already presented in Figure 5.1C – dashed curve. The scale is in volts. (C) Regions of the membrane where the absolute value of ITV is the highest (within arbitrarily chosen range (15%) of the maximal value).

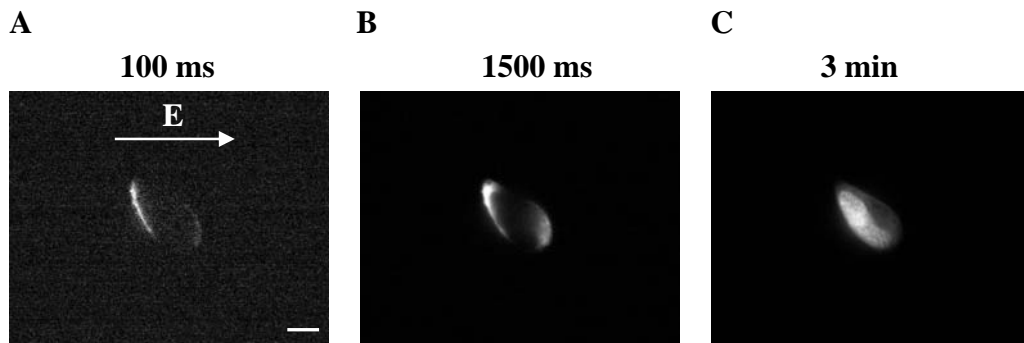


**Figure 5.4** Visualization of cell electroporation. (A) Fluorescence of the cell 100 ms, (B) 1500 ms, and (C) 3 min after pulse delivery. The images were corrected for the background fluorescence and the brightness was automatically enhanced. The cell was exposed to a single 400 V (1000 V/cm) rectangular unipolar pulse (200  $\mu$ s). Propidium Iodide was added to suspension before the pulse was applied to visualize the permeabilized regions. Bar represents 10  $\mu$ m.

## II. CHO

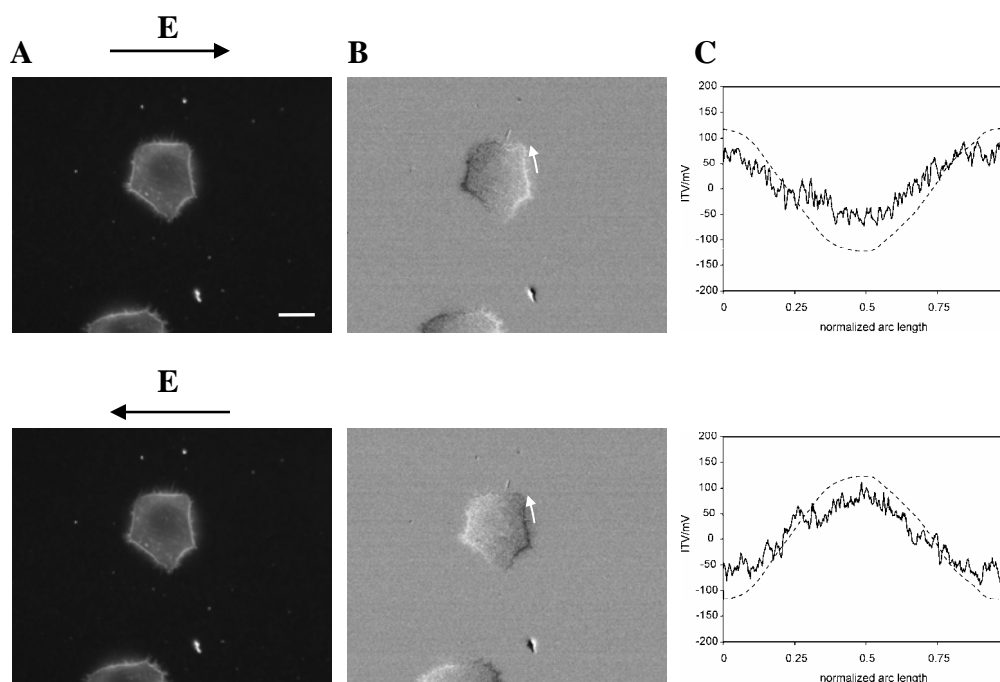


**Figure 5.5.** Measurements of induced transmembrane voltage (ITV) on an irregularly shaped CHO cell. (A) Fluorescence images of a cell acquired during the exposure to 40 V (100 V/cm), 100 ms rectangular pulse. Bar represents 10  $\mu\text{m}$ . (B) Changes in fluorescence of cell. (C) ITV as a function of normalized arc length. Solid curve – measured values, dashed curve – numerically calculated values. See legend of Figure 5.1 for details.

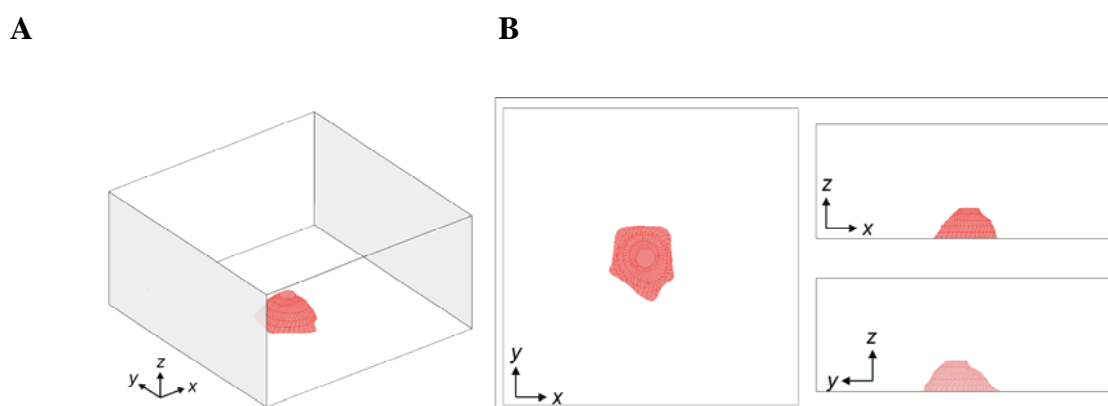


**Figure 5.6.** Numerical model of the irregularly shaped CHO cell shown in Figure 5.5. (A) 3D geometry. The dimensions of the cube were 79 $\times$ 79 $\times$ 38  $\mu\text{m}$ . One electrode was set to 0.73 V and the other to the ground (100 V/cm). (B) The three side views of the model. See legend of Figure 5.2 for details.

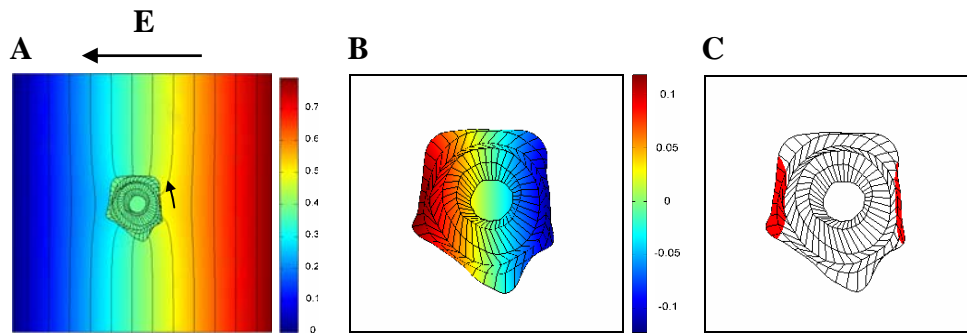


**Figure 5.7.** The calculations of induced transmembrane voltage. (A) Distribution of the electric potential in the x-y plane. (B) ITV on the surface of the magnified model of the cell. (C) Regions of the membrane where the absolute value of ITV is the highest. See legend of Figure 5.3 for details. Note that the calculations are presented for the opposite direction of  $E$  than in the previous experiment, to match the orientation of  $E$  in permeabilization experiment (see Figure 5.8).

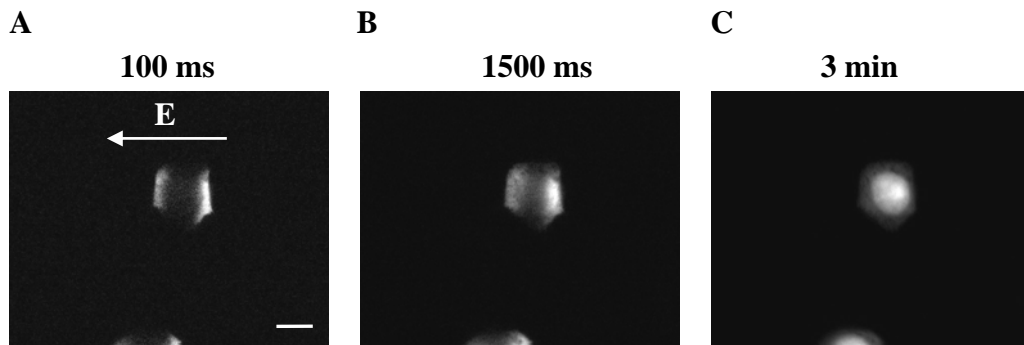


**Figure 5.8.** Visualization of cell electropermeabilization (A) 100 ms, (B) 1500 ms, and (C) 3 min after pulse delivery. The cell was exposed to a single 400 V (1000 V/cm) rectangular unipolar pulse (200  $\mu$ s). See legend of Figure 5.4 for details. Bar represents 10  $\mu$ m.

## III. CHO

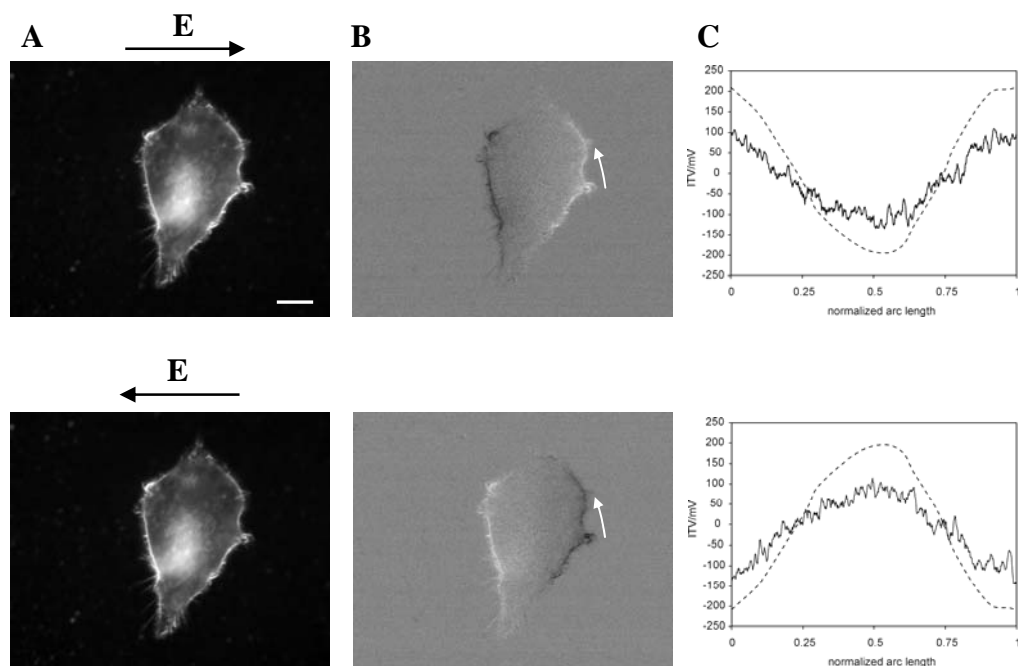


**Figure 5.9.** Measurements of induced transmembrane voltage (ITV) on an irregularly shaped CHO cell. (A) Fluorescence images of a cell acquired during the exposure to 40 V (100 V/cm), 100 ms rectangular pulse. (B) Changes in fluorescence of cell. (C) ITV as a function of normalized arc length. Solid curve – measured values, dashed curve – numerically calculated values. See legend of Figure 5.1 for details. Bar represents 10  $\mu\text{m}$ .

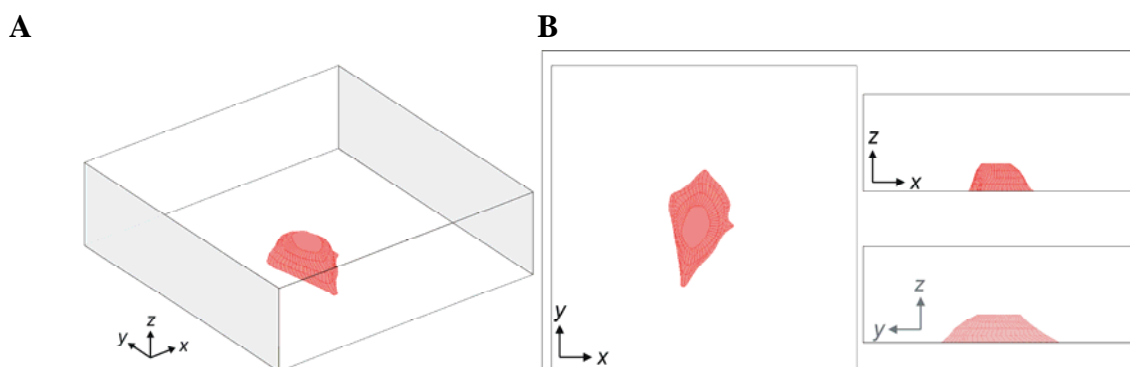


**Figure 5.10.** Numerical model of the irregularly shaped CHO cell shown in Figure 5.9. (A) 3D geometry. The dimensions of the cube were  $130 \times 130 \times 40 \mu\text{m}$ . One electrode was set to 1.3 V and the other to the ground (voltage-to-distance ratio 100 V/cm). (B) The three side views of the model. See legend of Figure 5.2 for details.

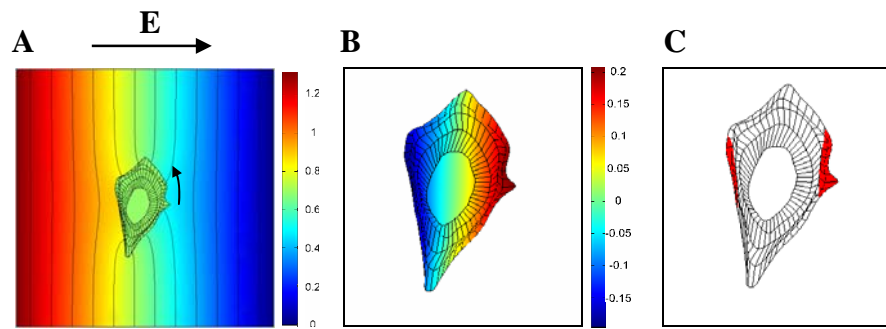


**Figure 5.11.** The calculations of induced transmembrane voltage. (A) Distribution of the electric potential in the x-y plane. (B) ITV on the surface of the magnified model of the cell. (C) Regions of the membrane where the absolute value of ITV is the highest. See legend of Figure 5.3 for details.

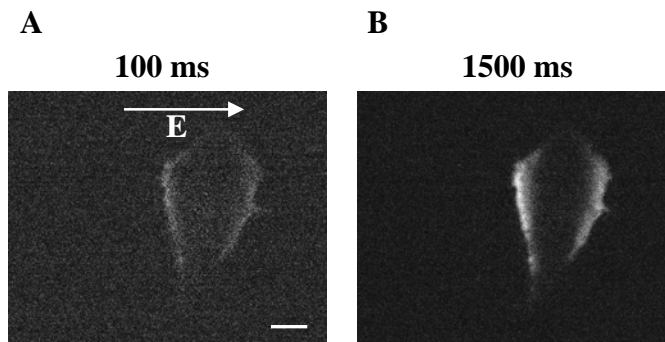


**Figure 5.12.** Visualization of cell electroporation (A) 100 ms, and (B) 1500 ms after pulse delivery. The cell was exposed to a single 400 V (1000 V/cm) rectangular unipolar pulse (200  $\mu$ s). See legend of Figure 5.4 for details. Bar represents 10  $\mu$ m.

## IV. B16F1

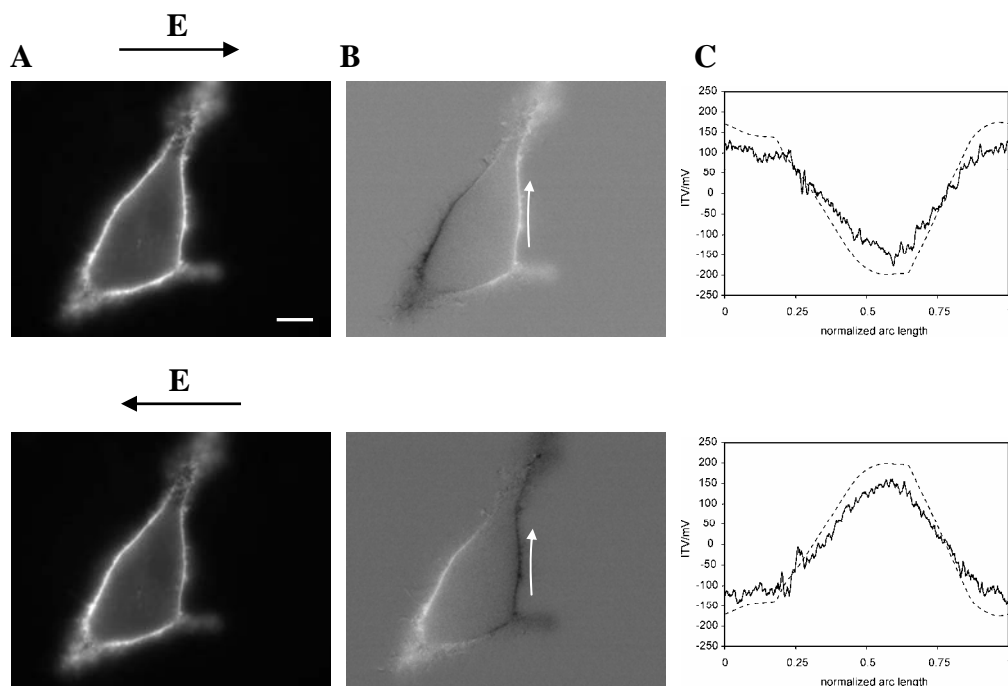


Figure 5.13. Measurements of induced transmembrane voltage (ITV) on an irregularly shaped B16F1 cell. (A) Fluorescence images of a cell acquired during the exposure to 40 V (100 V/cm), 100 ms rectangular pulse. (B) Changes in fluorescence of cell. (C) ITV as a function of normalized arc length. Solid curve – measured values, dashed curve – numerically calculated values. See legend of Figure 5.1 for details. Bar represents 10  $\mu\text{m}$ .

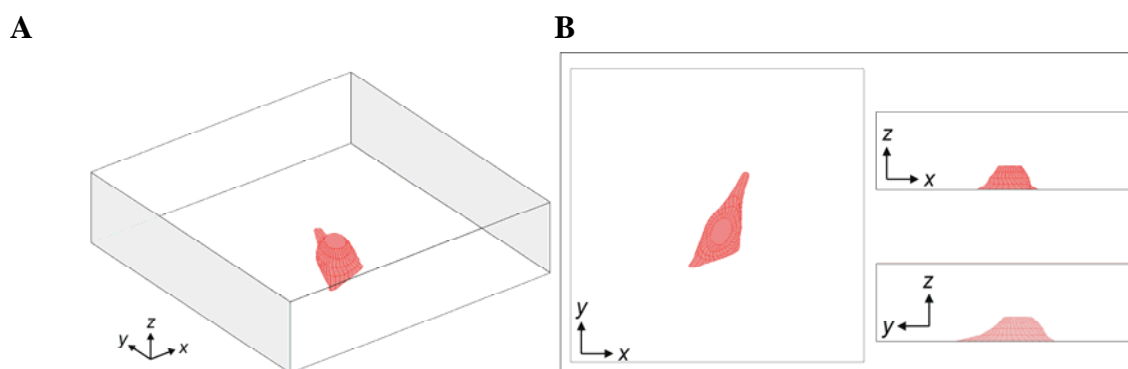
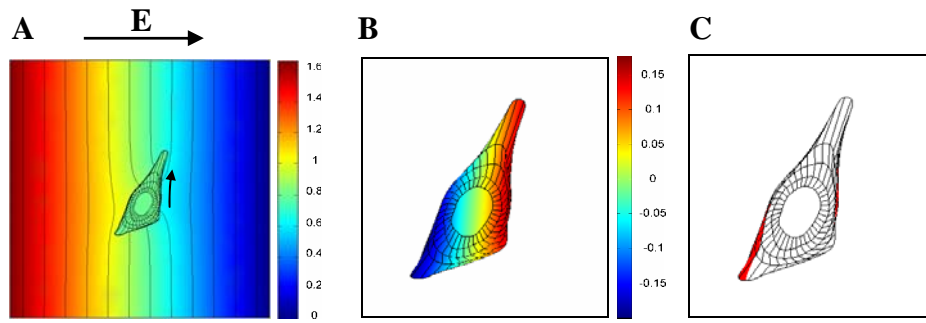
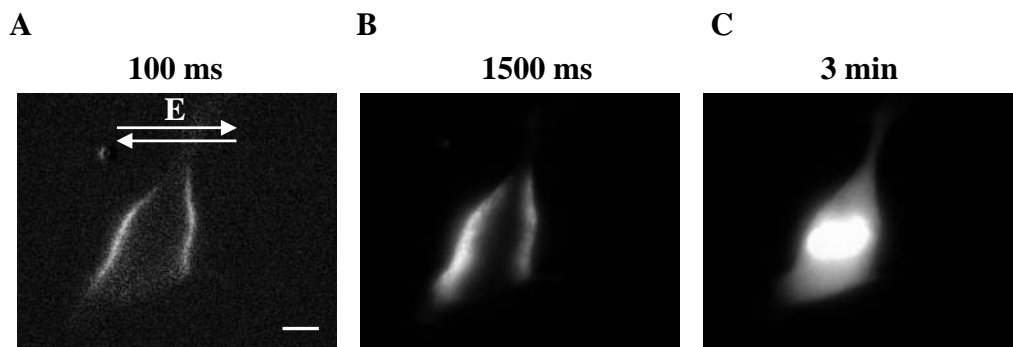


Figure 5.14. Numerical model of the irregularly shaped CHO cell shown in Figure 5.13. (A) 3D geometry. The dimensions of the cube were  $166 \times 166 \times 42 \mu\text{m}$ . One electrode was set to 1.66 V and the other to the ground (100 V/cm). (B) The three side views of the model. See legend of Figure 5.2 for details.



**Figure 5.15.** The calculations of induced transmembrane voltage. (A) Distribution of the electric potential in the x-y plane. (B) ITV on the surface of the magnified model of the cell. (C) Regions of the membrane where the absolute value of ITV is the highest. See legend of Figure 5.3 for details.



**Figure 5.16.** Visualization of cell electroporation (A) 100 ms, (B) 1500 ms, and (C) 3 min after pulse delivery. The cell was exposed to a single 260 V (650 V/cm) rectangular bipolar pulse (750 + 750  $\mu$ s). See legend of Figure 5.4 for details. Bar represents 10  $\mu$ m.

## V. B16F1

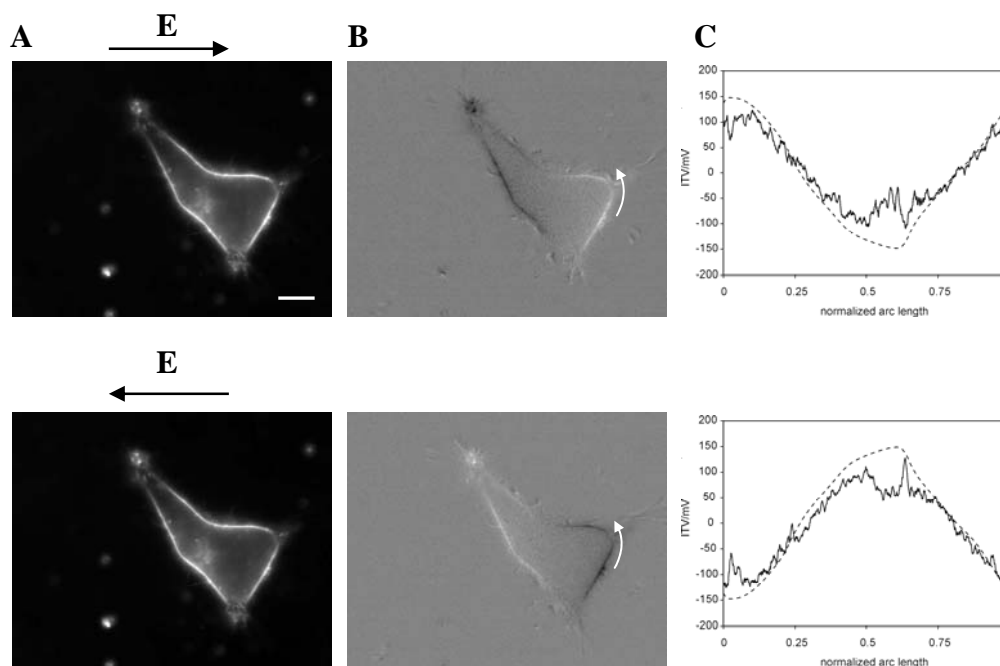


**Figure 5.17.** Measurements of induced transmembrane voltage (ITV) on an irregularly shaped B16F1 cell. (A) Fluorescence images of a cell acquired during the exposure to 30 V (75 V/cm), 100 ms rectangular pulse. (B) Changes in fluorescence of cell. (C) ITV as a function of normalized arc length. Solid curve – measured values, dashed curve – numerically calculated values. See legend of Figure 5.1 for details. Bar represents 10  $\mu\text{m}$ .

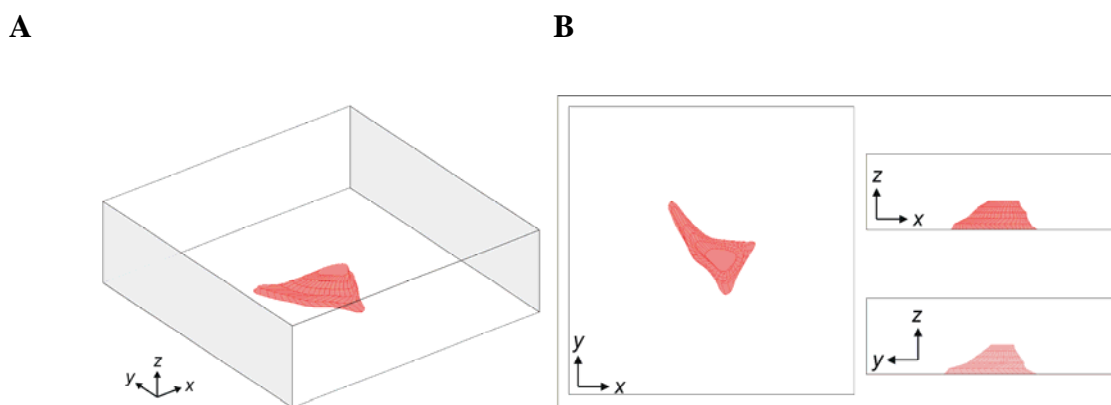


**Figure 5.18.** Numerical model of the irregularly shaped CHO cell shown in Figure 5.17. (A) 3D geometry. The dimensions of the cube were 115 $\times$ 115 $\times$ 38  $\mu\text{m}$ . One electrode was set to 0.86 V and the other to the ground (75 V/cm). (B) The three side views of the model. See legend of Figure 5.2 for details.

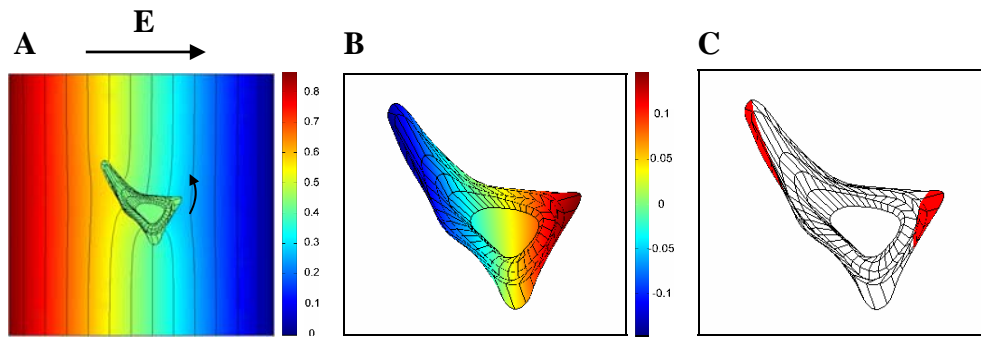


**Figure 5.19.** The calculations of induced transmembrane voltage. (A) Distribution of the electric potential in the x-y plane. (B) ITV on the surface of the magnified model of the cell. (C) Regions of the membrane where the absolute value of ITV is the highest. See legend of Figure 5.3 for details.

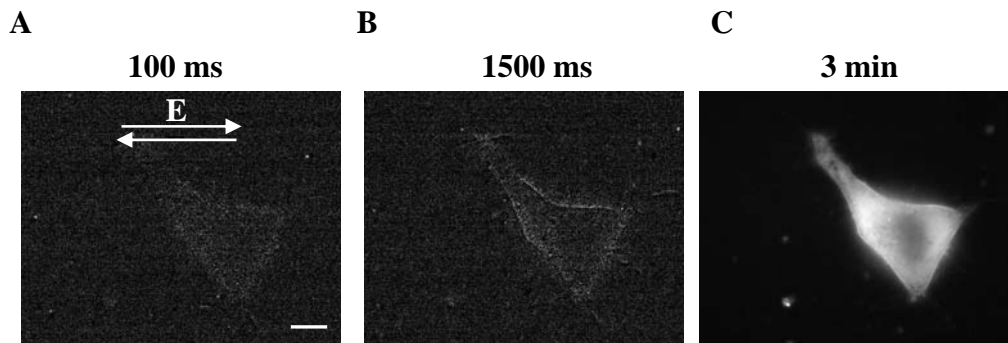


**Figure 5.20.** Visualization of cell electroporation (A) 100 ms, (B) 1500 ms, and (C) 3 min after pulse delivery. The cell was exposed to a single 260 V (650 V/cm) rectangular bipolar pulse (750 + 750  $\mu$ s). No permeabilization was observed (see Discussion Section). See legend of Figure 5.4 for details. Bar represents 10  $\mu$ m.

## VI. B16F1

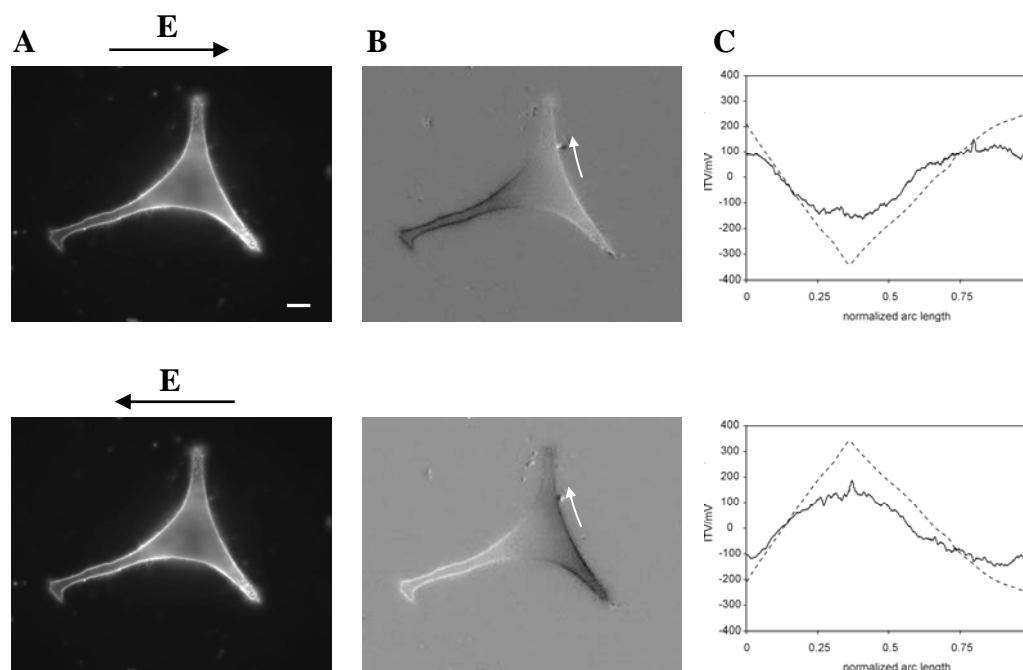


**Figure 5.21.** Measurements of induced transmembrane voltage (ITV) on an irregularly shaped B16F1 cell. (A) Fluorescence images of a cell acquired during the exposure to 30 V (75 V/cm), 100 ms rectangular pulse. (B) Changes in fluorescence of cell. (C) ITV as a function of normalized arc length. Solid curve – measured values, dashed curve – numerically calculated values. See legend of Figure 5.1 for details. Bar represents 10  $\mu\text{m}$ .

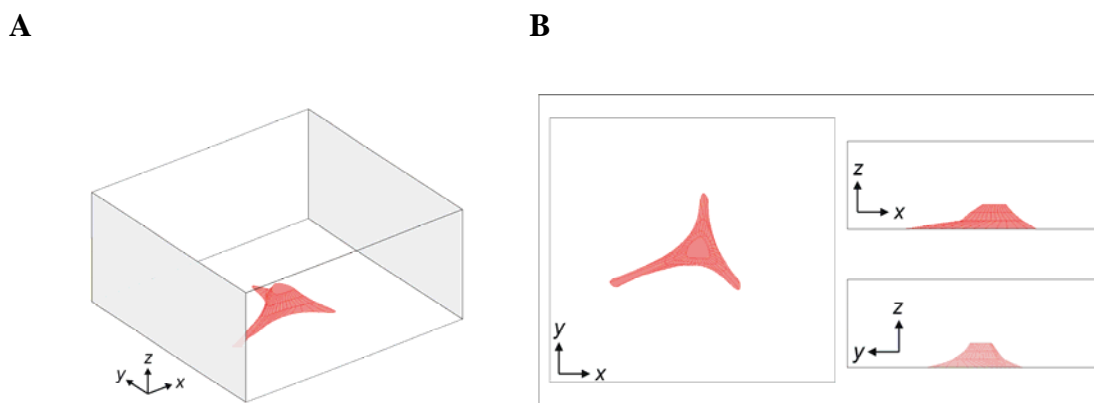


**Figure 5.22.** Numerical model of the irregularly shaped CHO cell shown in Figure 5.21. (A) 3D geometry. The dimensions of the cube were  $187 \times 187 \times 60 \mu\text{m}$ . One electrode was set to 1.4 V and the other to the ground (75 V/cm). (B) The three side views of the model. See legend of Figure 5.2 for details.

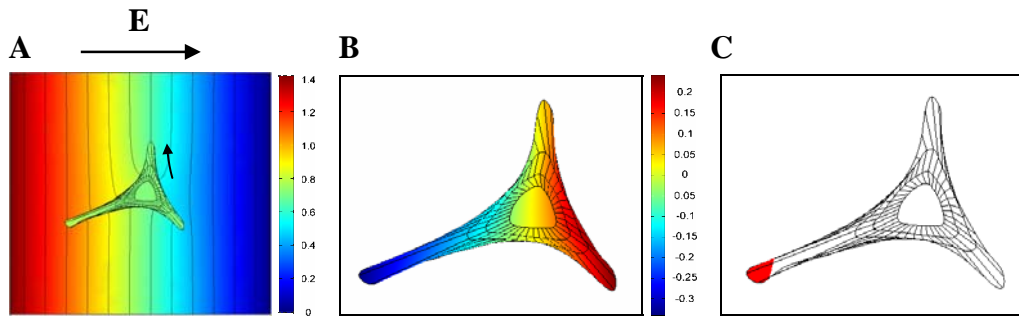
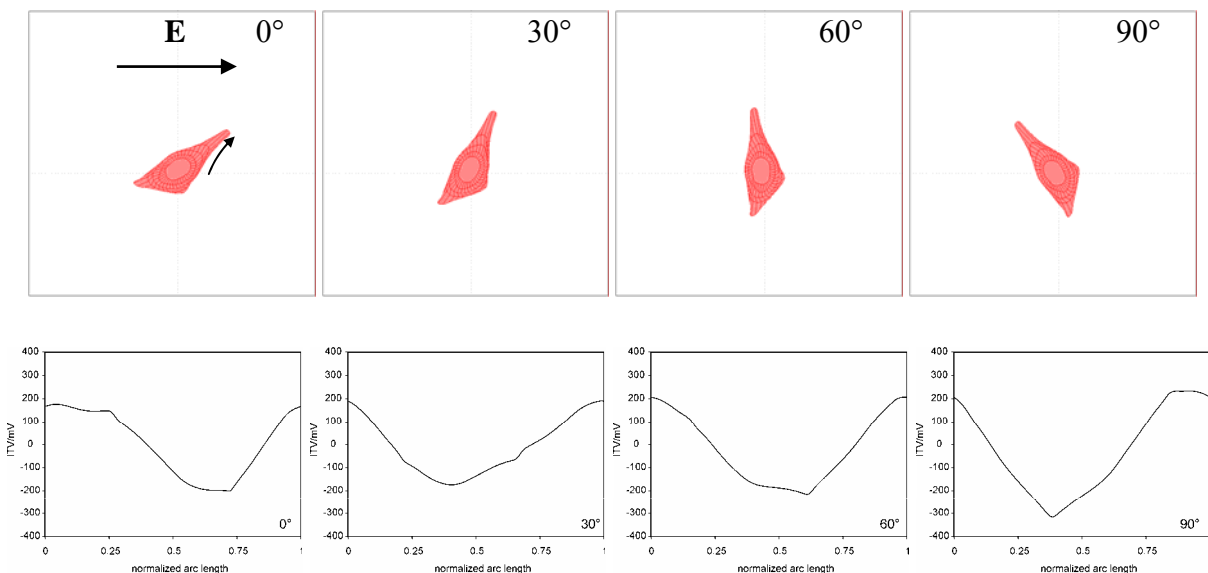


**Figure 5.23.** The calculations of induced transmembrane voltage. (A) Distribution of the electric potential in the x-y plane. (B) ITV on the surface of the magnified model of the cell. (C) Regions of the membrane where the absolute value of ITV is the highest. See legend of Figure 5.3 for details.

### 5.1.2 The influence of electric field orientation on induced transmembrane voltage

Induced transmembrane voltage was calculated for a cell model already shown above (cell IV). Instead of changing the electric field orientation in the model we rather rotated the cell itself and kept a constant direction of the electric field in the model. The cell was rotated counterclockwise around  $z$  - axis in constant steps of  $30^\circ$ . The initial cell orientation ( $0^\circ$ ) is the same as the one shown in Figure 5.14 above. For each cell orientation ITV was calculated and presented as a function of normalized arc length from the same starting point (denoted with a black square and an arrow). The results of calculations presented for the lowermost  $x$ - $y$  plane of the cell show that the course of ITV and its amplitude are affected by the field orientation (Figure 5.24). The largest amplitudes of ITV are obtained, when the cell is oriented with its longer axis parallel to the electric field ( $90^\circ$ ,  $120^\circ$ ,  $150^\circ$ ,  $270^\circ$ ,  $300^\circ$ ,  $330^\circ$ ) and the lowest for the case when the cell is oriented with its longer axis perpendicular to the electric field ( $0^\circ$ ,  $30^\circ$ ,  $60^\circ$ ,  $180^\circ$ ,  $210^\circ$ ,  $240^\circ$ ). For example, for cell rotated by  $120^\circ$  the maximal absolute value of ITV exceeds 300 mV, while for the same cell rotated for  $30^\circ$ , the maximal absolute ITV is below 200 mV (Figure 5.25A). Such variations in ITV could also influence the extent of permeabilization of cells. For example, if the critical value of ITV (where permeabilization occurs) would be 200 mV, the ITV on a cell rotated for  $0^\circ$ ,  $30^\circ$  or  $210^\circ$  would not exceed this critical threshold, while the ITV on the same cell, rotated for  $120^\circ$  would be higher than critical on 20% of the surface of the cell (solid curve in Figure 5.25B).

Experimental measurements of ITV were not performed in this part of the study.



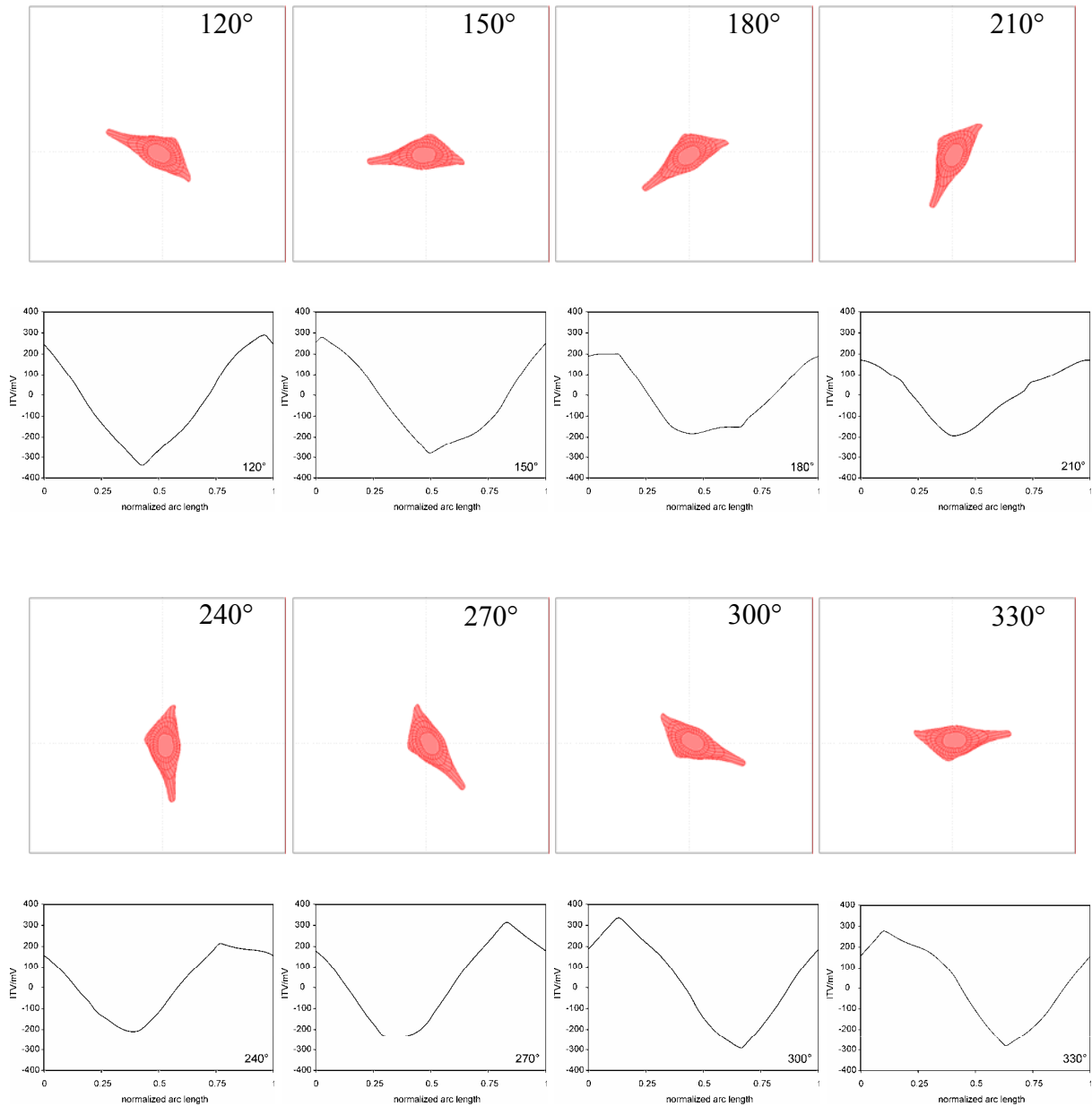


**Figure 5.24.** The influence of the electric field orientation on induced transmembrane voltage. Cell from Figure 5.14 (cell IV) was rotated counterclockwise around z-axis in constant steps of  $30^\circ$  (two perpendicular thin dotted curves in the model denote the axis of rotation). The initial cell orientation ( $0^\circ$ ) is the same as the one shown in Figure 5.14 above. The images are presented in pairs; each cell orientation is accompanied by the calculated ITV for the lowermost x-y plane of the cell. The calculations are presented as a function of normalized arc length from the same starting point (denoted with a black square and an arrow).

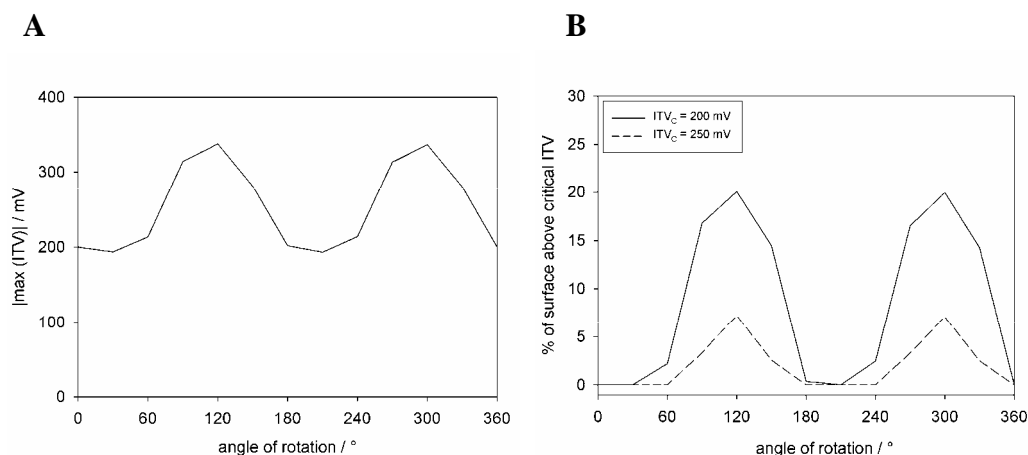


**Figure 5.25.** The influence of electric field orientation on (A) the maximal absolute value of ITV and (B) the % of surface above critical ITV, which was arbitrarily chosen to be 200 mV – solid curve, or 250 mV – dashed curve.

### 5.1.3 The influence of resting transmembrane voltage on the total membrane voltage

So far, ITV was taken as a rough approximate of the total voltage on the membrane and was, as such, compared to the permeabilization results. According to the measurements of RTV presented in Section 3 (Measurements of resting transmembrane voltage), this approximation is reasonable, as in experiments involving permeabilization the RTV is considerably lower than ITV. However, in experiments where RTV considerably exceeds the physiological values (e.g. permeabilization in extremely low conductivity media) or in experiments where external electric fields are lower (e.g. studies of opening and closing of voltage gated channels in membrane) RTV substantially changes the distribution of the total membrane voltage on the membrane and can not be neglected anymore.

In this section the influence of RTV on the total membrane voltage is demonstrated for the case of an irregularly shaped cell I from Figure 5.1. ITV measured and calculated on this cell during the exposure to electric field of 100 V/cm is shown in Figure 5.26A and varies between approximately +100 mV and -100 mV. The mean RTV on attached CHO cells in 10 mM K-ZAP medium was measured to be approximately -25 mV (Figure 5.26B). The total membrane voltage, which is a superposition of ITV and RTV, is presented in Figure 5.26C. Compared to ITV the total membrane voltage is shifted towards more negative values and varies between approximately +75 mV and -125 mV. For illustration, we colored in red the cell surface that would be exposed to critical membrane voltage (e.g. |50 mV|) for the case when ITV is taken as an estimate of the total voltage (RTV is ignored, Figure 5.27A) and the case when total voltage is a superposition of ITV and RTV (Figure 5.27B).

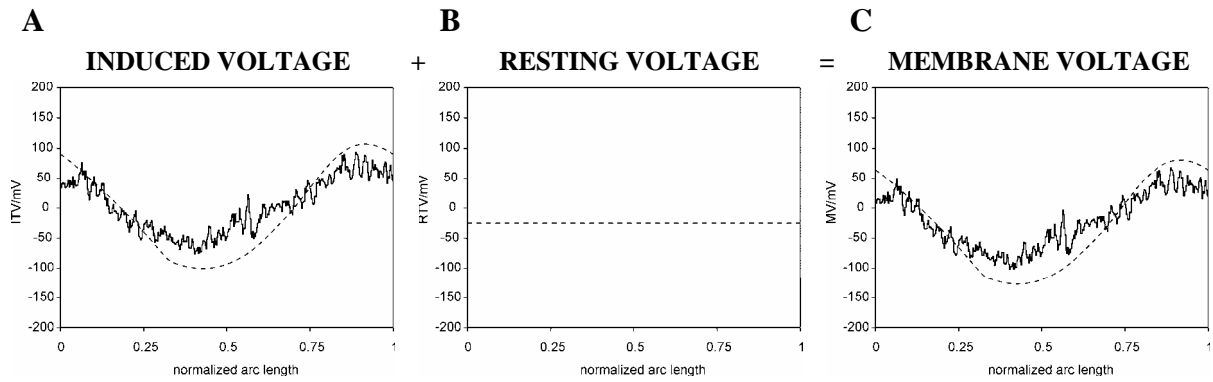


**Figure 5.26.** (A) Measured and calculated distribution of ITV on cell I, exposed to 100 V/cm. (B) The mean measured value of RTV for the attached CHO cell in 10 mM K-ZAP medium. (C) Total membrane voltage obtained by superposition of ITV and RTV.

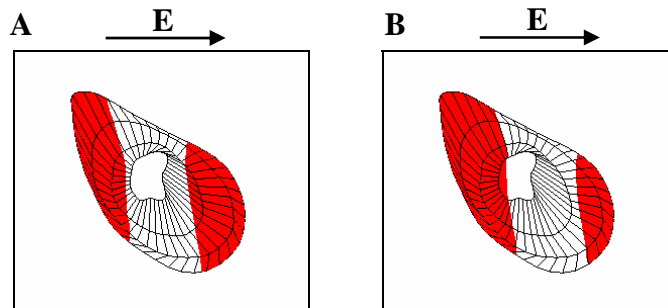


**Figure 5.27.** Regions of the membrane where the total membrane voltage exceeds the critical threshold value, which was chosen to be  $50 \text{ mV}$ . (A) RTV was neglected and ITV was taken as an estimate for the total membrane voltage. (B) The total membrane voltage is a superposition of RTV and ITV.

## 5.2 Discussion

In many applications of electropermeabilization (e.g. DNA electrotransfer) an efficient and at the same time reversible permeabilization is essential. Thus, a careful planning of the experiment, which involves the estimation of the amplitude of ITV leading to cell permeabilization, is required. For simple cell shapes, such as spheres or ellipsoids, ITV can be calculated analytically (Schwan, 1957; Kotnik et al., 1997; Kotnik et al., 2000b; Kotnik and Miklavčič 2000; Gimsa and Wachner, 2001a; Gimsa and Wachner, 2001b). However, since cells are most often complex in shape, the analytical solution is in general not attainable and ITV can be determined only experimentally (Bedlack et al., 1994; Gross et al., 1986; Hassan et al., 2002; Knisley et al., 1993; Loew, 1992; Montana et al., 1989) or numerically (Miller and Henriquez, 1988; Fear and Stuchly, 1998a; Fear and Stuchly, 1998b; Susil et al., 1998; Pavlin et al., 2002; Valič et al., 2003; Gowrishankar and Weaver, 2003; Stewart et al., 2004; Pucihar et al., 2006). This section of the study presented the measurements and numerical calculations of ITV on different irregularly shaped cells and observations of the course of electropermeabilization on the same cells.

While the measured ITV's matched the calculated ITV's in shape, some discrepancies were observed in their amplitudes. Namely, the amplitude of the measured ITV was in most cases lower than calculated and the differences were somewhat higher for CHO cells than for B16F1 cells. The possible reasons for the discrepancies between measured and calculated ITV include the variations of the slope of calibration curve, the differences between the actual and implemented parameters of the model (especially the membrane permeability), and the experimental setup, as already discussed in **paper 5** in Appendix (Pucihar et al., 2006). Most likely, the largest problem is the long exposure of cells to external electric field (100 ms), which could induce changes in membrane permeability, either by changing the configuration of membrane lipids or by opening and closing the voltage gated channels in the membrane, both resulting in a decrease in ITV. This was probably the case for the cell VI shown in Figure 5.21. Because of the star-like shape of this cell, where its parts extend far out from its center, ITV induced by a low amplitude external pulse (75 V/cm induced ITV of approximately 350 mV) with a long duration (100 ms) already provoked electropermeabilization of that cell. This was confirmed by observing a steady increase in fluorescence of the cell after addition of the Propidium Iodide to the solution minutes after the measurements of ITV and before permeabilizing pulses were applied and image was acquired. However, we did not observe such fluorescence increase for other cells, which, however, does not exclude the possibility of the occurrence of transient changes in membrane permeability during the measurements of ITV, when Propidium Iodide was not yet present in the solution.

Often, biological cells are modeled as simple geometrical objects such as spheres or spheroids, and, for more complicated cell shapes, by combining several such objects, such as hemispheres, circular or elliptic cylinders, etc. (Buitengeweg et al., 2003; Fear and Stuchly, 1998a; Fear and Stuchly 1998b; Huang et al., 2004, Kotnik and Miklavčič, 2000a; Valič et al.,

2003). These models can be realistic for cells in suspensions, but cells growing in a dish or in tissues typically have profoundly irregular shapes, and combinations of several simple geometrical objects are not usable anymore. In this study we presented a method for construction of more realistic models of irregularly shaped cells from their cross-section images. We also presented a method to replace a cell membrane in the model with a boundary condition. This efficiently eliminates the number of elements of the mesh and consequently time needed to solve the problem. The details on the construction of the numerical model are presented in **paper 5** in Appendix (Pucihar et al., 2006) where the advantages and disadvantages of such modeling were discussed extensively.

The results of calculations of ITV were then compared with the regions of the membrane where permeabilization occurred. These regions were indicated by the increase in the fluorescence of Propidium Iodide, the otherwise membrane-impermeable fluorescent dye. A good agreement was obtained between the regions of the detected fluorescence increase and the regions where the absolute value of the measured and calculated ITV is the highest. As already stated above (Section 4, Spherical cell), the measurements and calculations of ITV were performed at external electric fields considerably lower than those used in permeabilization experiments. Because ITV is linearly dependent on the external electric field (as confirmed experimentally in this study and also by other authors), we hypothesized that by measuring and computing ITV at subcritical external fields, it would still be possible to predict the regions where permeabilization would occur at supracritical external fields. This was indeed confirmed qualitatively with our measurements as permeabilization always occurred in those regions of the membrane where the measured and numerically calculated ITV's were the highest.

We can estimate the value of the critical ITV needed to provoke permeabilization by locating the points on the graph of ITV that correspond to the edges of fluorescence regions on both sides of the cell. For example, for cell I in Figure 5.1, the highest absolute values of the calculated ITV at these points was 70 mV and 60 mV for left and right side of the cell, respectively, while the measured ITV was approximately 40 mV on both sides of the cell. By scaling these values with the ratio of the external pulse amplitudes used for permeabilization and for ITV measurements (ratio = 400 V / 40 V = 10), we can calculate the corresponding critical absolute values of ITV where permeabilization occurred. Critical ITV's, calculated in this manner, are somewhere between 400 and 700 mV, which is within the reported range of critical ITV's and also close to the critical ITV calculated for a spherical cell in Section 4 (~450 mV). However, for the same reasons as discussed in Section 4 (increase in fluorescence regions with time and pulse duration, questionable assumption on linear scaling above critical ITV) these calculations should be taken only as a rough estimate of the actual critical ITV.

In experiment performed on cell V, we did not observe any permeabilization during the time of acquisition (two seconds), and not even when a second permeabilizing pulse was delivered. However, with time, the cell slowly became fluorescent, indicating that permeabilization did

occur, but the dye entrance was apparently too slow to be detected within the investigated time interval. The amplitude of the pulses was probably too low to obtain an efficient permeabilization of the cell membrane.

We also investigated the influence of electric field orientation on the distribution of ITV calculated on irregularly shaped cell IV. These results clearly indicate that orientation of the electric field (or analogously, the orientation of a cell) considerably affects the distribution and the amplitude of ITV, and consequently the extent of cell permeabilization. Namely, cells oriented with their longer axis parallel to the field are more likely to get permeabilized than cells oriented perpendicular to the field, which is in agreement with experiments and calculations performed by Valič and co-workers (Valič et al., 2003). Our study also demonstrates the advantages of numerical modeling, where relatively simple modifications of the cell model were required to carry out the investigation, while the same study would be difficult to perform experimentally, as the cell is attached to the bottom of the dish and either the electrodes or the dish would have to be rotated.

Finally, we illustrated the influence of resting transmembrane voltage (RTV) on the total membrane voltage. Due to its small value RTV is usually neglected and ITV is taken as a rough estimate of the total membrane voltage. This is a realistic assumption in experiments involving electropermeabilization, because ITV in such cases exceeds few hundred millivolts (see above), while RTV is around -50 mV or, in our case, even less negative (see Section 3, Measurements of resting voltage). However, if experiments are performed in media with extremely low conductivities, RTV can become considerable. Similarly, in experiments where external electric fields are lower, such as in studies of voltage gated channels, the amplitudes of ITV become comparable to amplitudes of RTV. For the accurate interpretation of data and evaluation of the effects of the electric field on cells in these experiments, the superposition of RTV to ITV must be considered as a measure of the total membrane voltage.

## 6 CELL CLUSTERS AND DENSE CELL SUSPENSIONS

### 6.1 Results - Cell Clusters

After having described the experiments on single spherical cells and single irregularly shaped cells, we now proceed to more complex cell assemblies - cell clusters. We measured and calculated induced transmembrane voltage (ITV) on the outermost membrane layer of a cluster and determined the permeabilized regions of the cell membranes in the same cluster. Experiments were performed on six different cell clusters with increasing complexity in their geometry and with increasing number of cells in a cluster. For a better demonstration, the results of measured ITV, calculated ITV, a 3D model, and visualization of permeabilization are again presented together for each investigated cell cluster. We begin our investigation with a treatment of simple clusters comprised of two cells and then proceed to more complex ones comprised of four cells. Cells in clusters were primarily modeled as electrically connected, but we also performed calculations for the case of electrically insulated cells in clusters. The existence of electrical connections between cells was verified by performing a test for gap junctions using a scrape test.

#### 6.1.1 Measurements and calculations of induced transmembrane voltage on cell clusters and visualization of permeabilization

The first investigated cell cluster (cluster I) was composed of two roughly spherical CHO K1 cells with their region of contact nearly perpendicular to external electric field. Induced transmembrane voltage (ITV) was measured by staining the cluster with potentiometric fluorescent dye di-8-ANEPPS and exposing the cluster to a voltage of 40 V delivered to the electrodes at 4 mm distance (electric field 100 V/cm). The fluorescence images acquired during the exposure are shown in the first and second row of Figure 6.1A for two opposing electric field directions, respectively. To visualize changes in fluorescence due to electric field exposure, these images were subtracted from the control image (Figure 6.1B). As the Figure 6.1B shows, one cell in a cluster experienced an increase in fluorescence (white color - depolarization), and the other a decrease (black color - hyperpolarization). The changes of fluorescence were then transformed to values of ITV using a calibration curve (see Section Materials and Methods) and are presented with solid curves in Figure 6.1C as a function of normalized arc length along the outermost membrane of a cluster. The results are shown for two opposing orientations of external electric field (100 V/cm). For the investigated cluster (cluster I), ITV varies along the outer cell membranes between approximately 110 mV and -100 mV for electric field directed from left to right, and between -110 mV and 100 mV for the opposite direction of the field (Figure 6.1C – solid curves).

From fluorescence images of this cluster, taken from three parallel imaging planes, a 3D model was constructed and placed to the bottom of the cube to model a cluster of two cells

attached to the coverglass. The cube represents the extracellular medium, and two grey opposing sides are the electrodes. The contact surface between cells was assigned a higher conductivity than the rest of the membranes of cells, to simulate a connection of two cells with gap junctions. A 1000 times higher conductivity of the contact surface proved to be enough to obtain a roughly constant value of electric potential inside the whole cluster. Higher conductivities yielded essentially the same results, while at lower conductivities, substantial variations of intracellular electric potential was obtained. A computation where such connections between cells were not established (insulated cells) was also performed. In this case, the conductivity of the contact surface was, due to the double thickness of the membrane on the contact, set to half of the conductivity of the rest of the membrane. The results of calculations of the electric potential outside and inside the cluster are, for the lowermost layer, shown in Figure 6.3A. While the potential outside the cluster varies from 0.62 V to 0 V, the potential inside remains on the same value of 0.34 V, reflecting the electrical connection of both cells. For a comparison, when cells in cluster are insulated the potential outside the cell remains the same, while the potential inside the cell is 0.38 V and 0.28 V for the left cell and the right cell in a cluster, respectively (Figure 6.4 A). From the calculated values of electric potential ITV was calculated as a difference between potentials on both sides of the outermost cell membranes of the cluster ( $ITV = V_i - V_o$ ). For cluster I the ITV calculated for the case of electrically connected cells varies between approximately 125 mV and -110 mV and is in good agreement with experimentally measured ITV (Figure 6.1C – black dashed curves). Red dashed curves in the same figure show ITV calculated for the cluster of insulated cells. Because in this case, each cell in a cluster has a different intracellular electric potential (0.38 V for the cell on the left and 0.28 V for the cell on the right), the course of ITV along the outermost membranes is disconnected.

In the presence of membrane-impermeant fluorescent dye Propidium Iodide, the same cluster was then exposed to a single bipolar rectangular 260 V pulse (650 V/cm) with 750  $\mu$ s + 750  $\mu$ s duration. An increase in fluorescence, 100 ms after the pulse application, was observed on both sides of each cell in a cluster, marking the regions where permeabilization occurred (Figure 6.5A). These regions are in agreement with calculations of ITV for electrically insulated cells (Figures 5.4B and C) rather than for electrically connected cells in a cluster (Figures 5.3B and C). It appears that cells in clusters permeabilize individually, which is different than what we expected from ITV measurements, where two cells behaved as one giant cell (Figure 6.1C). Three minutes after pulse delivery the cluster was completely fluorescent, with two bright regions indicating the cell nuclei, where the density of binding sites for the dye is the highest (Figure 6.5C).

A similar procedure was performed for five additional clusters of irregularly shaped cells with increasing complexity in their shape and increasing number of cells in cluster. Since the results are straightforward, only general observations will be described here, while a thorough discussion of the results will be given in the Discussion part of this section.

For each cluster of cells, ITV was measured on cell membranes of the outermost layer of the cluster, a 3D model of electrically connected and electrically insulated cells in a cluster was constructed, ITV was calculated, permeabilization was performed and the results were compared. Clusters I, II and III comprised of two, while clusters IV, V, and VI comprised of four CHO K1 cells. For clusters comprised of two cells, the measured ITV was always in good agreement with ITV calculated on a model of electrically connected cells. However, these calculations were not in agreement with permeabilization results, which show that cells in clusters permeabilize individually, in agreement with the calculations of ITV on the same cluster of insulated cells. In case of a cluster comprised of four cells, ITV measured on the outer membrane layer of a cluster had a similar course as the ITV calculated for connected cells, while the amplitudes were in some cases different (cluster IV and VI). The permeabilization, however, always occurred on each cell in a cluster individually. The results for all investigated cell clusters are presented in the following pages.

### Cluster I

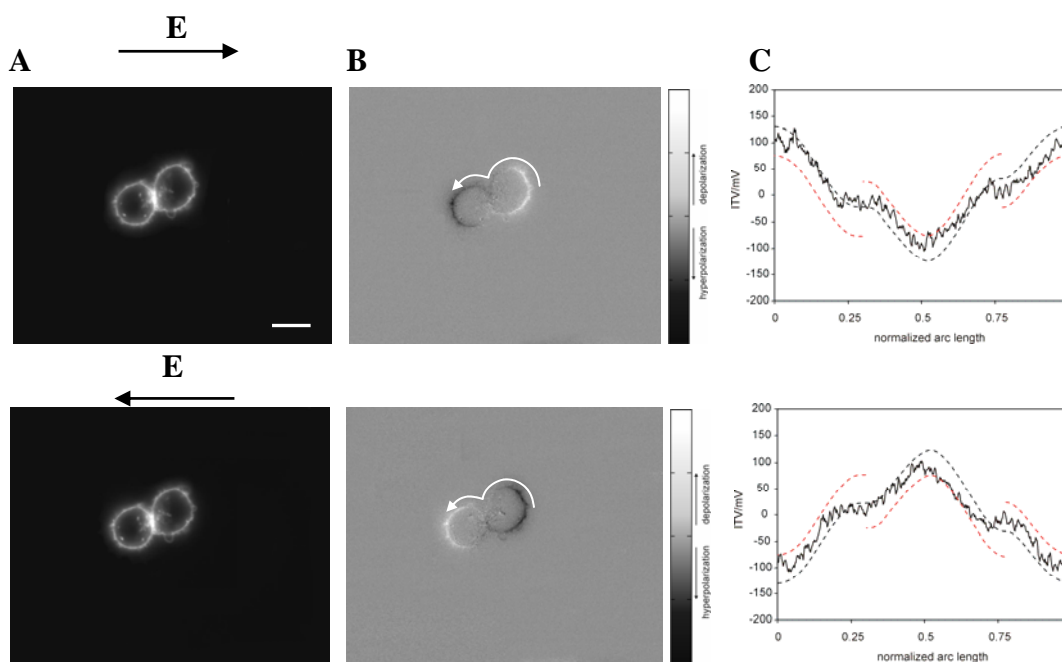


**Figure 6.1.** Measurements of induced transmembrane voltage (ITV) on a cluster of two CHO cells. First row shows the results for the electric field  $E$  directed to the right and the second row for the opposite direction. (A) The 8-bit fluorescence images of a cluster stained with di-8-ANEPPS and acquired during the exposure to 40 V (100 V/cm), 100 ms rectangular pulse. The brightness of the image was automatically enhanced. Bar represents 10  $\mu\text{m}$ . (B) Changes in fluorescence of a cluster obtained by subtracting the control image (not shown) from the image with pulse and shifting the greyscale range by 50%. The brightness of the image was automatically enhanced. White arrow shows the path along which ITV was measured. (C) ITV as a function of normalized arc length measured on the outermost membranes of a cluster. Solid curve – measured values, black dashed curve – numerically calculated values for the case of electrically connected cells, red dashed curve – numerically calculated values for the case of electrically insulated cells (see below). The changes in fluorescence were transformed to ITV by using a calibration curve (6 % change in fluorescence corresponding to 100 mV).

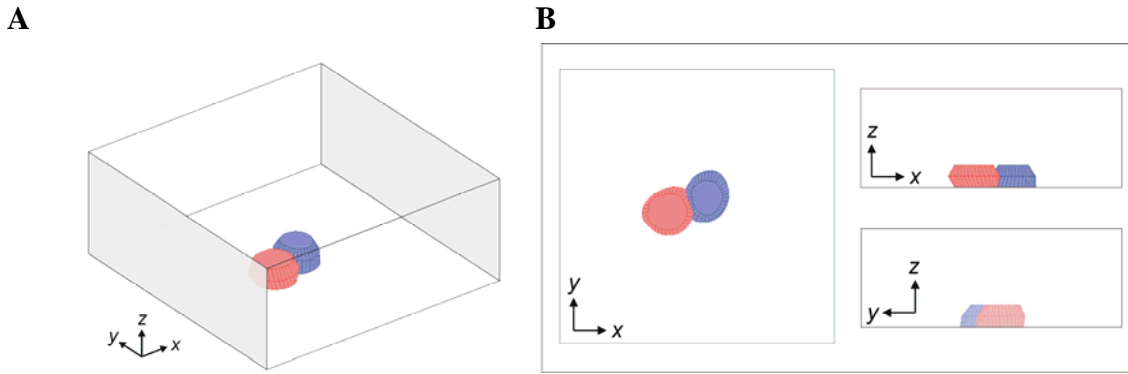


**Figure 6.2.** Numerical model of a cluster of two CHO cells shown in Figure 6.1. (A) The three-dimensional geometry of the model of a cluster constructed from three parallel cross-sections (see Materials and Methods Section for details). The model of a cluster is placed to the bottom of the cube to mimic cells attached to coverglass. The cube with dimensions  $62 \times 62 \times 25 \mu\text{m}$  represents the extracellular medium with conductivity of  $0.14 \text{ S/m}$ , the grey-shaded faces are the electrodes, one set to  $0.62 \text{ V}$  and the other to the ground (electric field  $100 \text{ V/cm}$ ). The other four faces are insulating. The inside of each cell in a cluster was assigned a conductivity of  $0.3 \text{ S/m}$ ; the membranes were modeled as a boundary condition. To model electrically insulated cells in cluster the membrane on the contact was, due to its double thickness, set to half the conductivity of the rest of the membrane. To model electrically connected cells the membrane on a contact was assigned a 1000 times higher conductivity than in case of insulated cells. (B) – The three side views of the model.

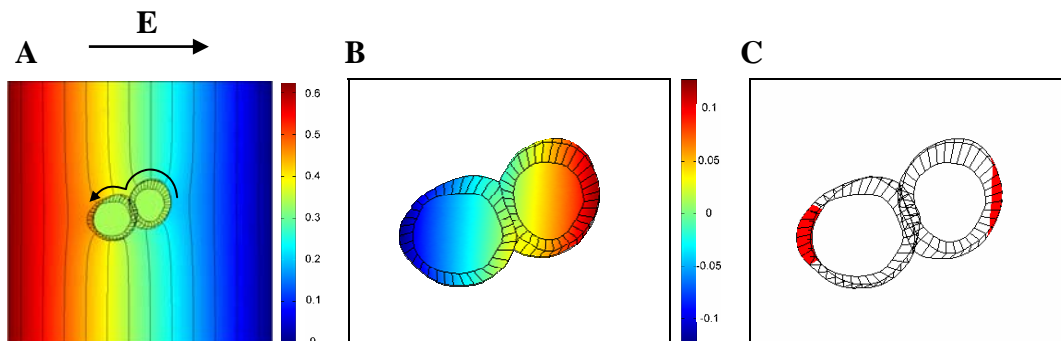


**Figure 6.3.** Calculations of induced transmembrane voltage for electrically connected cells. (A) The calculated distribution of the electric potential around and inside of cell cluster in the  $x$ - $y$  plane through the lowermost part of cluster. Black curves represent the equipotentials and the arrow marks the path along which the potential was measured. The scale is in volts. (B) ITV calculated as a difference between the potentials on both sides of the membrane ( $ITV = V_i - V_o$ ) presented on the surface of the magnified model of the cluster. The scale is in volts. For the lowermost part of the cluster, ITV is presented in Figure 6.1C – black dashed curve. (C) Regions of the membrane where the absolute value of ITV is within 15% of the maximal value.

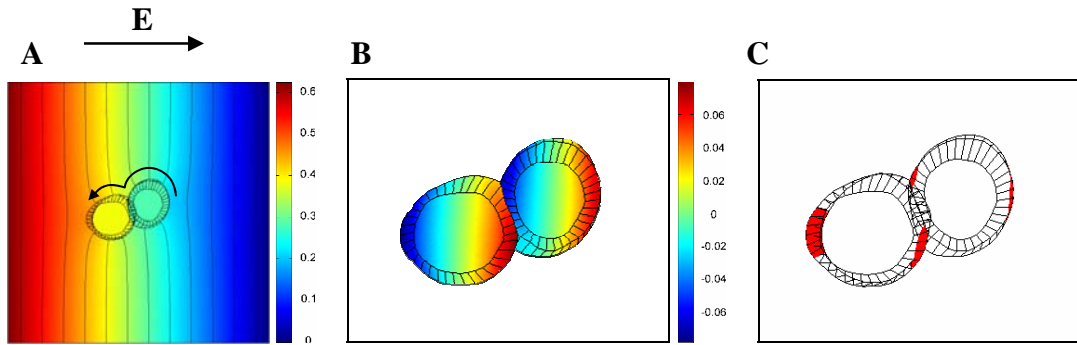


**Figure 6.4.** Calculations of induced transmembrane voltage for electrically insulated cells. (A) The calculated distribution of the electric potential around and inside of cell cluster in the x-y plane through the lowermost part of cluster. Black curves represent the equipotentials and the arrow marks the path along which the potential was measured. The scale is in volts. (B) ITV calculated as a difference between the potentials on both sides of the membrane ( $ITV = V_i - V_o$ ) presented on the surface of the magnified model of the cluster. The scale is in volts. For the lowermost part of the cluster, ITV is presented in Figure 6.1C – red dashed curve. (C) Regions of the membrane where the absolute value of ITV is within 15% of the maximal value.

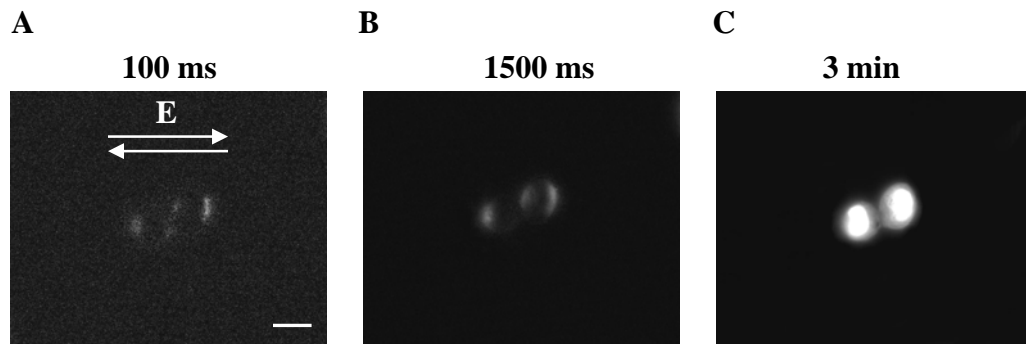


**Figure 6.5.** Visualization of electroporation of the cell cluster shown and modeled in Figure 5.1. (A) Fluorescence from the cluster 100 ms, (B) 1500 ms, and (C) 3 min after pulse delivery. The images are corrected for the background fluorescence and the brightness was automatically enhanced. Cluster was exposed to a single 260 V (650 V/cm) rectangular bipolar pulse (750  $\mu$ s + 750  $\mu$ s). Propidium Iodide was added to suspension before the pulse to visualize the permeabilized regions. Bar represents 10  $\mu$ m.

## Cluster II

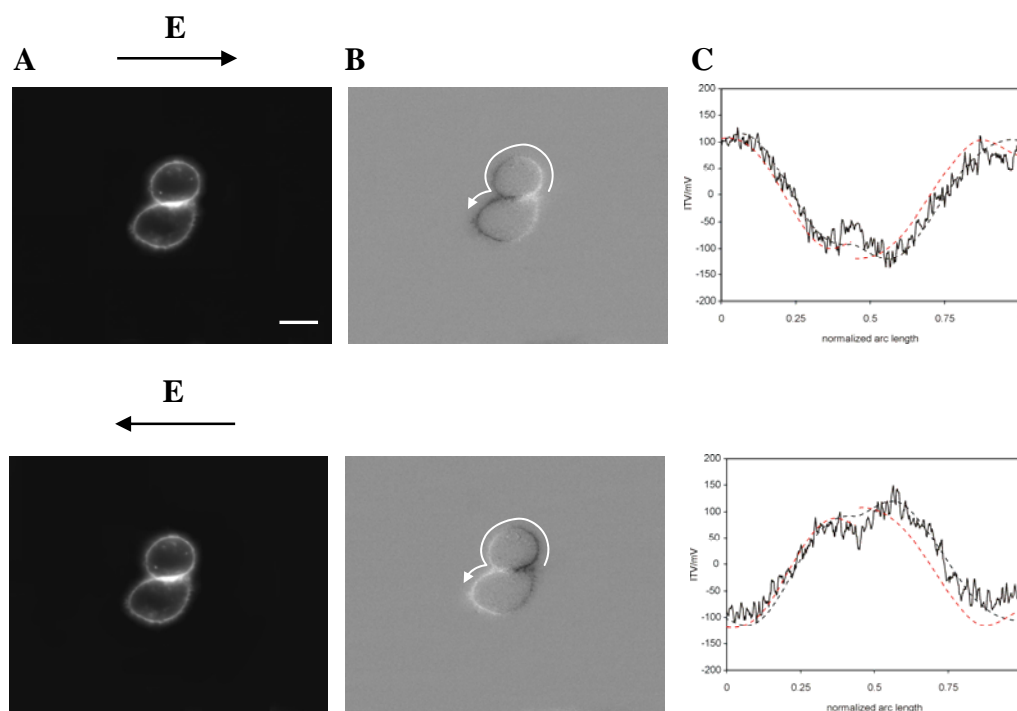


**Figure 6.6.** Measurements of induced transmembrane voltage (ITV) on a cluster of two CHO cells. (A) Fluorescence images of a cluster acquired during the exposure to 40 V (100 V/cm), 100 ms rectangular pulse. Bar represents 10  $\mu\text{m}$ . (B) Changes in fluorescence of a cluster. (C) ITV as a function of normalized arc length. Solid curve – measured values, black dashed curve – numerically calculated values for the case of electrically connected cells, red dashed curve – numerically calculated values for the case of electrically insulated cells. See legend of Figure 6.1 for details.

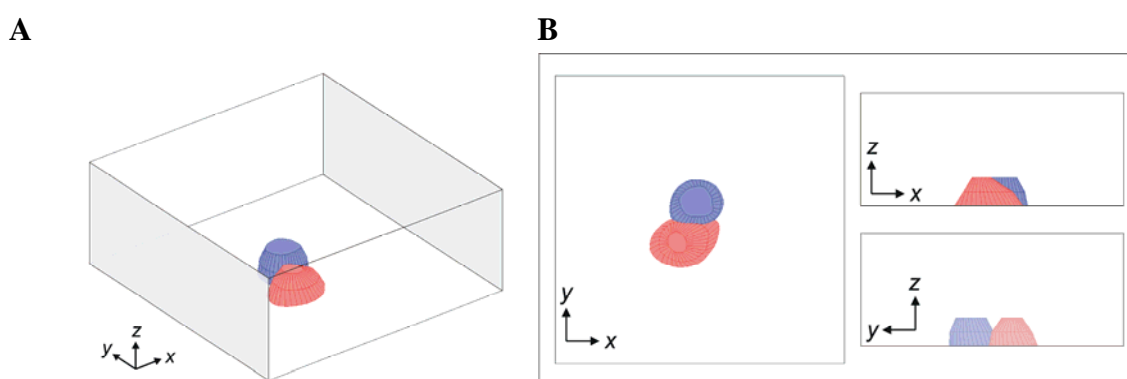


**Figure 6.7.** Numerical model of a cluster of two CHO cells shown in Figure 6.6. (A) 3D geometry. The dimensions of the cube were 67 $\times$ 67 $\times$ 27  $\mu\text{m}$ . One electrode was set to 0.67 V and the other to the ground (electric field 100 V/cm). (B) The three side views of the model. See legend of Figure 6.2 for details.

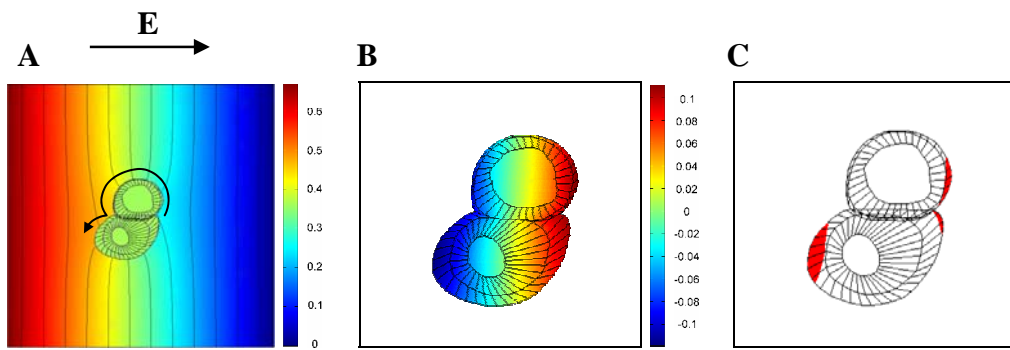


**Figure 6.8.** The calculations of induced transmembrane voltage for electrically connected cells. (A) Distribution of the electric potential in the x-y plane for the lowermost part of the cluster. (B) ITV on a surface of the magnified model. (C) Regions of the membrane where the absolute value of ITV is the highest. See legend of Figure 6.3 for details.

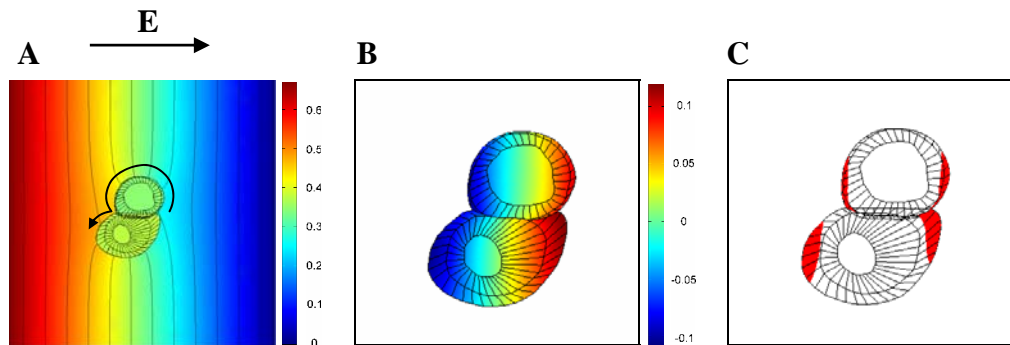


**Figure 6.9.** Calculations of induced transmembrane voltage for electrically insulated cells. (A) Distribution of the electric potential in the x-y plane for the lowermost part of the cluster. (B) ITV on a surface of the magnified model. (C) Regions of the membrane where the absolute value of ITV is the highest. See legend of Figure 6.4 for details

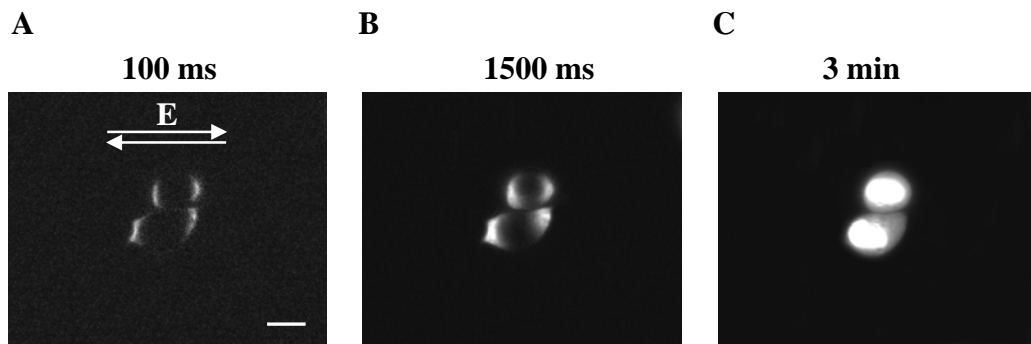


**Figure 6.10.** Visualization of electroporation (A) 100 ms, (B) 1500 ms, and (C) 3 min after pulse delivery. The cluster was exposed to a single 260 V (650 V/cm) rectangular bipolar pulse (750  $\mu$ s + 750  $\mu$ s). See legend of Figure 6.5 for details. Bar represents 10  $\mu$ m.

## Cluster III

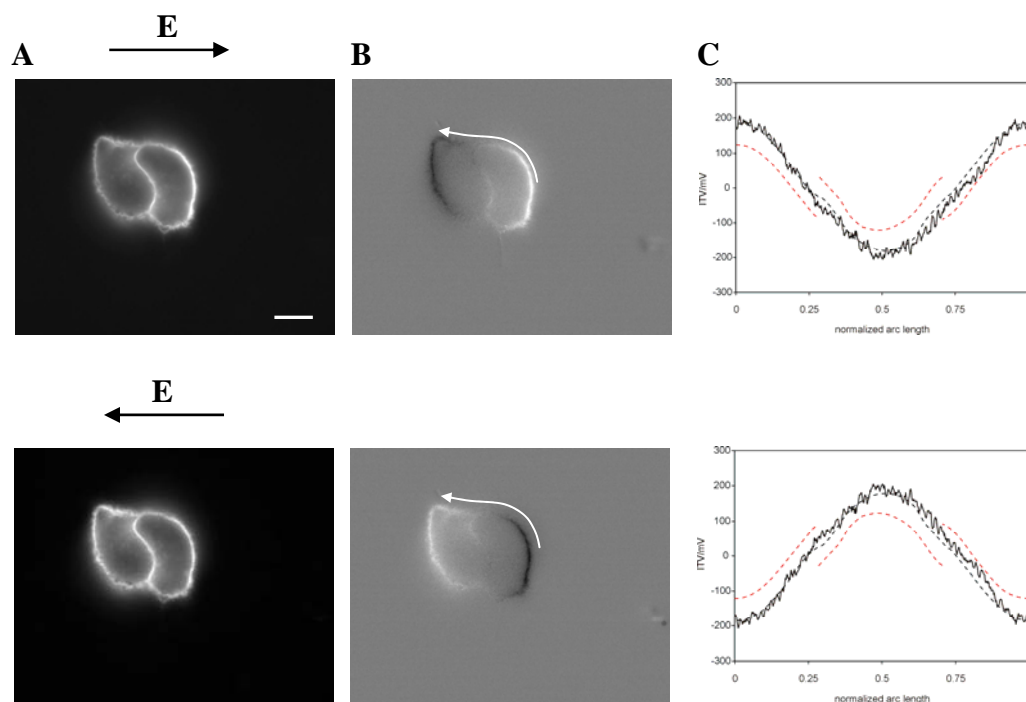


Figure 6.11. Measurements of induced transmembrane voltage (ITV) on a cluster of two CHO cells. (A) Fluorescence images of a cluster acquired during the exposure to 40 V (100 V/cm), 100 ms rectangular pulse. Bar represents 10  $\mu\text{m}$ . (B) Changes in fluorescence of a cluster. (C) ITV as a function of normalized arc length. Solid curve – measured values, black dashed curve – numerically calculated values for the case of electrically connected cells, red dashed curve – numerically calculated values for the case of electrically insulated cells. See legend of Figure 6.1 for details.

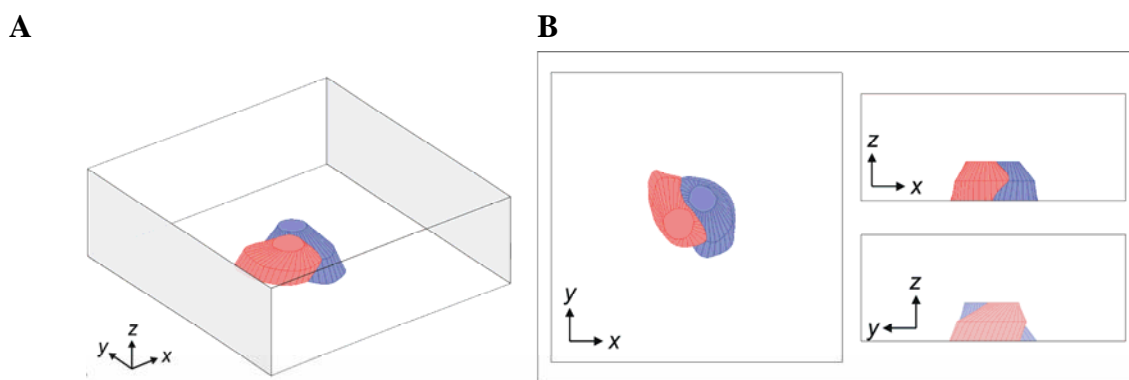
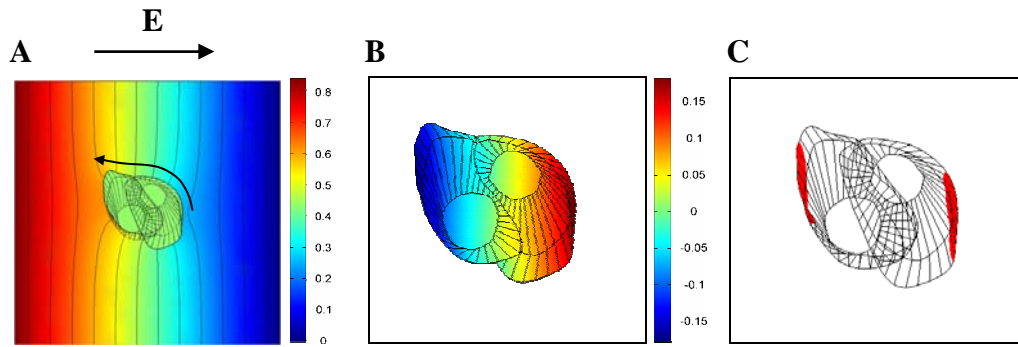
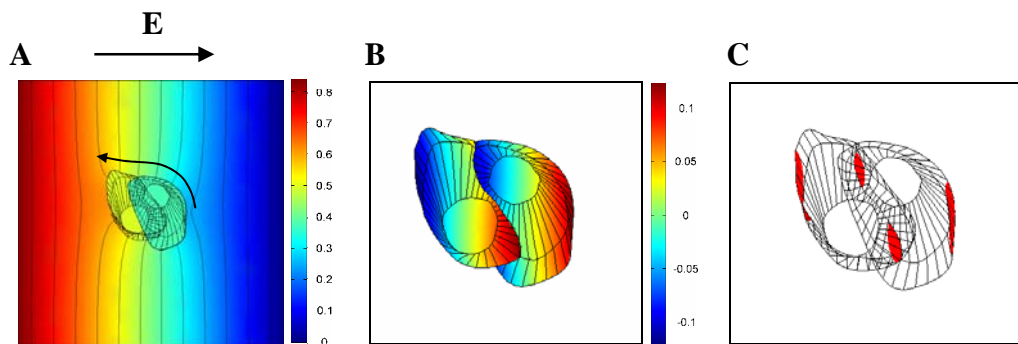


Figure 6.12. Numerical model of a cluster of two CHO cells shown in Figure 6.10. (A) 3D geometry. The dimensions of the cube were  $84 \times 84 \times 27 \mu\text{m}$ . One electrode was set to 0.84 V and the other to the ground (electric field 100 V/cm). (B) The three side views of the model. See legend of Figure 6.2 for details.



**Figure 6.13.** The calculations of induced transmembrane voltage for electrically connected cells. (A) Distribution of the electric potential in the x-y plane for the lowermost part of the cluster. (B) ITV on a surface of the magnified model. (C) Regions of the membrane where the absolute value of ITV is the highest. See legend of Figure 6.3 for details.



**Figure 6.14.** Calculations of induced transmembrane voltage for electrically insulated cells. (A) Distribution of the electric potential in the x-y plane for the lowermost part of the cluster. (B) ITV on a surface of the magnified model. (C) Regions of the membrane where the absolute value of ITV is the highest. See legend of Figure 6.4 for details.

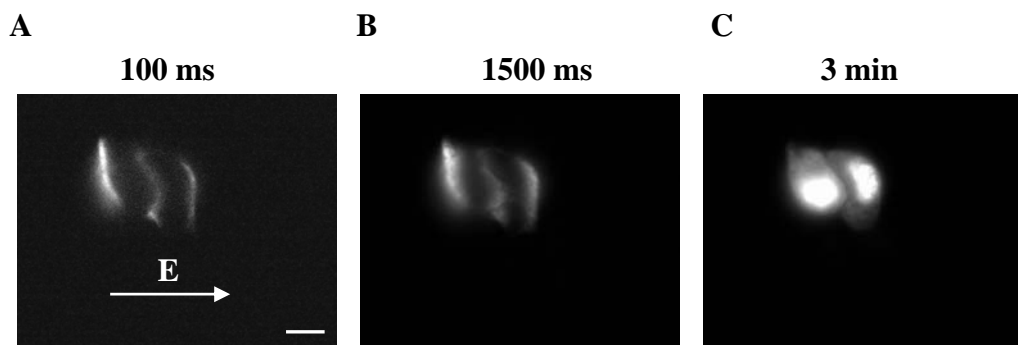


**Figure 6.15.** Visualization of electroporation (A) 100 ms, (B) 1500 ms, and (C) 3 min after pulse delivery. The cluster was exposed to a single 400 V (1000 V/cm) rectangular unipolar pulse (200  $\mu$ s). See legend of Figure 6.5 for details. Bar represents 10  $\mu$ m.

Cluster IV

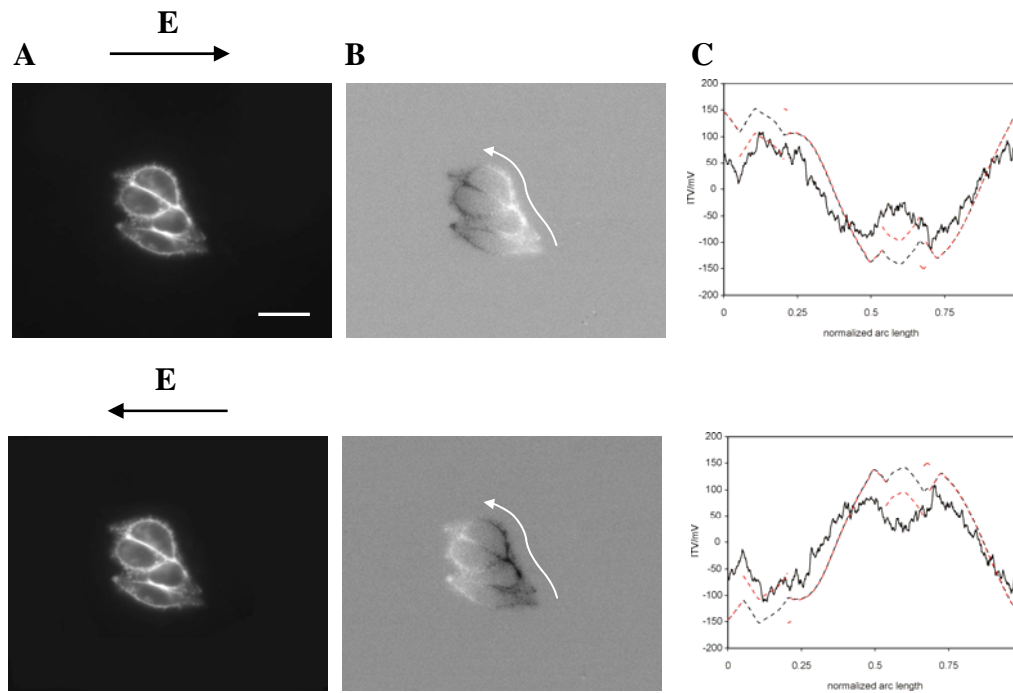


Figure 6.16. Measurements of induced transmembrane voltage (ITV) on a cluster of four CHO cells. (A) Fluorescence images of a cluster acquired during the exposure to 19 V (75 V/cm), 50 ms rectangular pulse. Bar represents 20  $\mu\text{m}$ . (B) Changes in fluorescence of a cluster. (C) ITV as a function of normalized arc length. Solid curve – measured values, black dashed curve – numerically calculated values for the case of electrically connected cells, red dashed curve – numerically calculated values for the case of electrically insulated cells. See legend of Figure 6.1 for details.

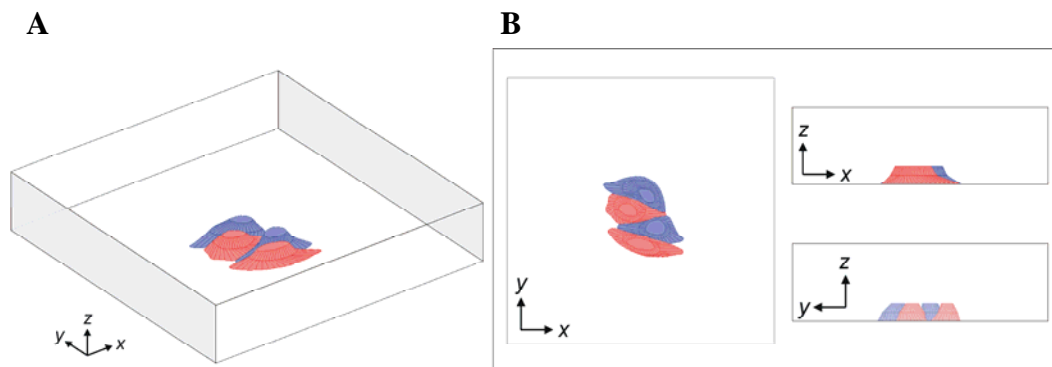


Figure 6.17. Numerical model of a cluster of four CHO cells shown in Figure 6.14. (A) 3D geometry. The dimensions of the cube were 120 $\times$ 120 $\times$ 23  $\mu\text{m}$ . One electrode was set to 0.9 V and the other to the ground (electric field 75 V/cm). (B) The three side views of the model. See legend of Figure 6.2 for details.

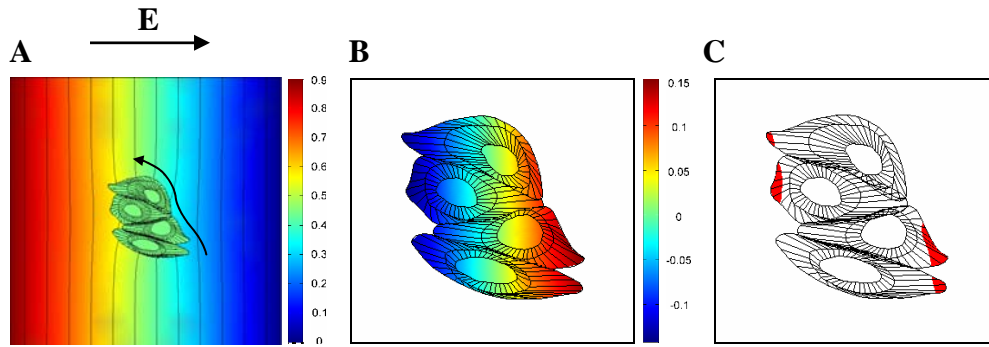


Figure 6.18. Calculations of induced transmembrane voltage for electrically connected cells. (A) Distribution of the electric potential in the x-y plane for the lowermost part of the cluster. (B) ITV on a surface of the magnified model. (C) Regions of the membrane where the absolute value of ITV is the highest. See legend of Figure 6.3 for details.

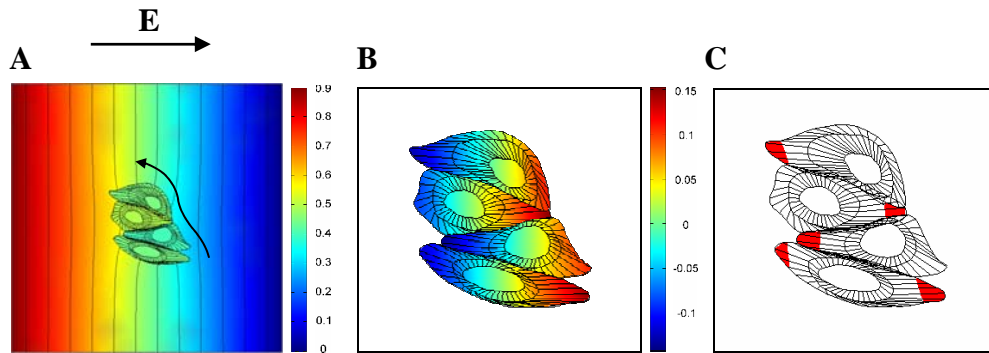


Figure 6.19. Calculations of induced transmembrane voltage for electrically insulated cells. (A) Distribution of the electric potential in the x-y plane for the lowermost part of the cluster. (B) ITV on a surface of the magnified model. (C) Regions of the membrane where the absolute value of ITV is the highest. See legend of Figure 6.4 for details.

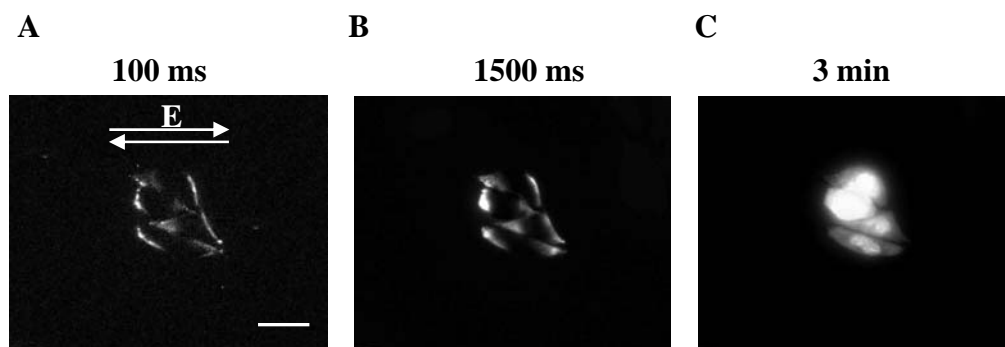


Figure 6.20. Visualization of electroporation (A) 100 ms, (B) 1500 ms, and (C) 3 min after pulse delivery. The cluster was exposed to a single 260 V (1040 V/cm) rectangular bipolar pulse (750  $\mu$ s + 750  $\mu$ s). See legend of Figure 6.4 for details. Bar represents 20  $\mu$ m.

## Cluster V

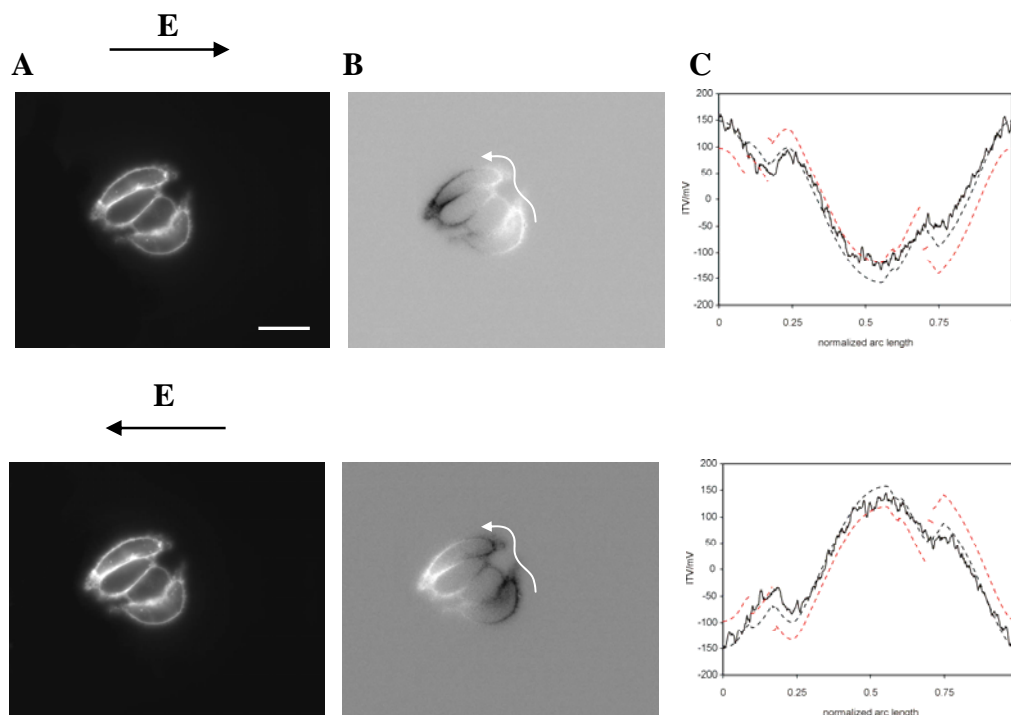


Figure 6.21. Measurements of induced transmembrane voltage (ITV) on a cluster of four CHO cells. (A) Fluorescence images of a cluster acquired during the exposure to 19 V (75 V/cm), 50 ms rectangular pulse. Bar represents 20  $\mu\text{m}$ . (B) Changes in fluorescence of a cluster. (C) ITV as a function of normalized arc length. Solid curve – measured values, black dashed curve – numerically calculated values for the case of electrically connected cells, red dashed curve – numerically calculated values for the case of electrically insulated cells. See legend of Figure 6.1 for details.

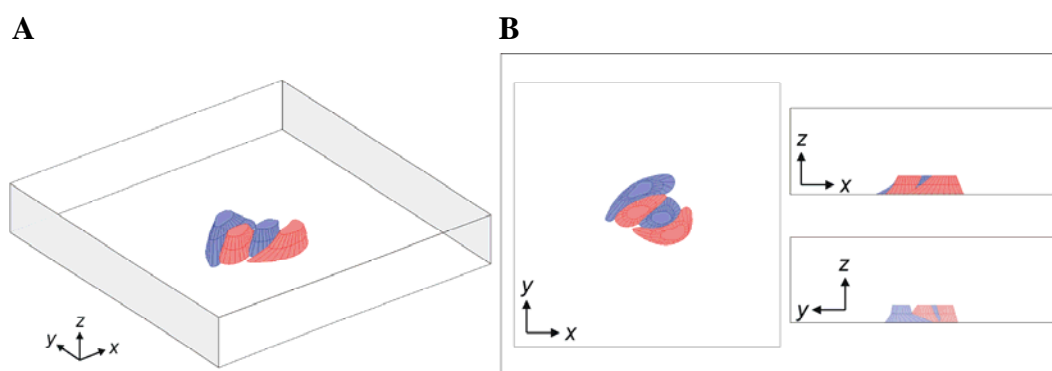
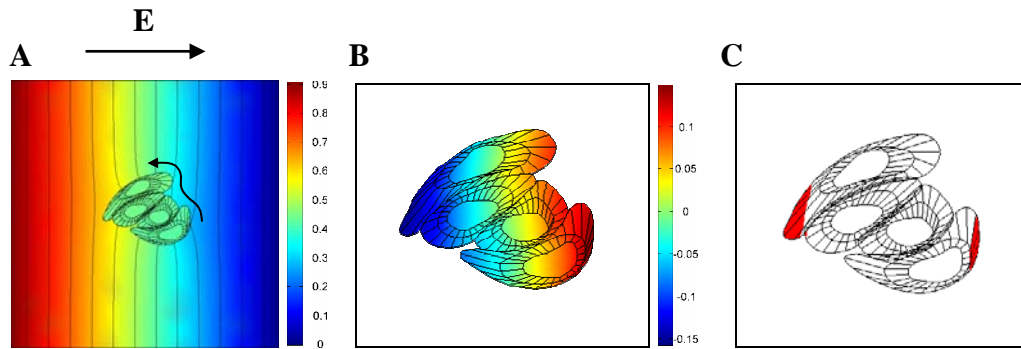
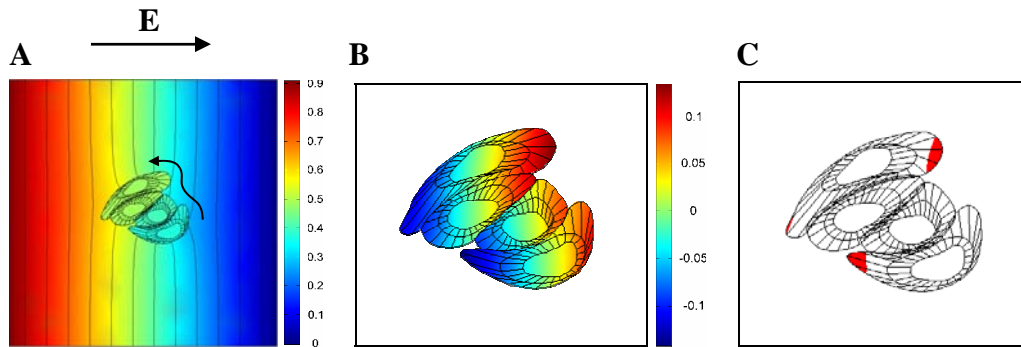


Figure 6.22. Numerical model of a cluster of four CHO cells shown in Figure 6.19. (A) 3D geometry. The dimensions of the cube were  $121 \times 121 \times 35 \mu\text{m}$ . One electrode was set to 0.91 V and the other to the ground (electric field 75 V/cm). (B) The three side views of the model. See legend of Figure 6.2 for details.



**Figure 6.23.** Calculations of induced transmembrane voltage for electrically connected cells. (A) Distribution of the electric potential in the x-y plane for the lowermost part of the cluster. (B) ITV on a surface of the magnified model. (C) Regions of the membrane where the absolute value of ITV is the highest. See legend of Figure 6.3 for details.



**Figure 6.24.** Calculations of induced transmembrane voltage for electrically insulated cells. (A) Distribution of the electric potential in the x-y plane for the lowermost part of the cluster. (B) ITV on a surface of the magnified model. (C) Regions of the membrane where the absolute value of ITV is the highest. See legend of Figure 6.4 for details.

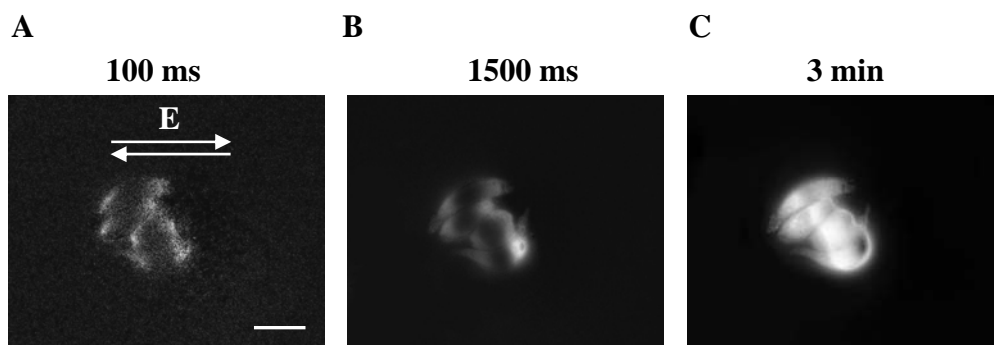


**Figure 6.25.** Visualization of electroporation (A) 100 ms, (B) 1500 ms, and (C) 3 min after pulse delivery. The cluster was exposed to a single 260 V (1040 V/cm) rectangular bipolar pulse (750  $\mu$ s + 750  $\mu$ s). See legend of Figure 6.5 for details. Bar represents 20  $\mu$ m.

## Cluster VI

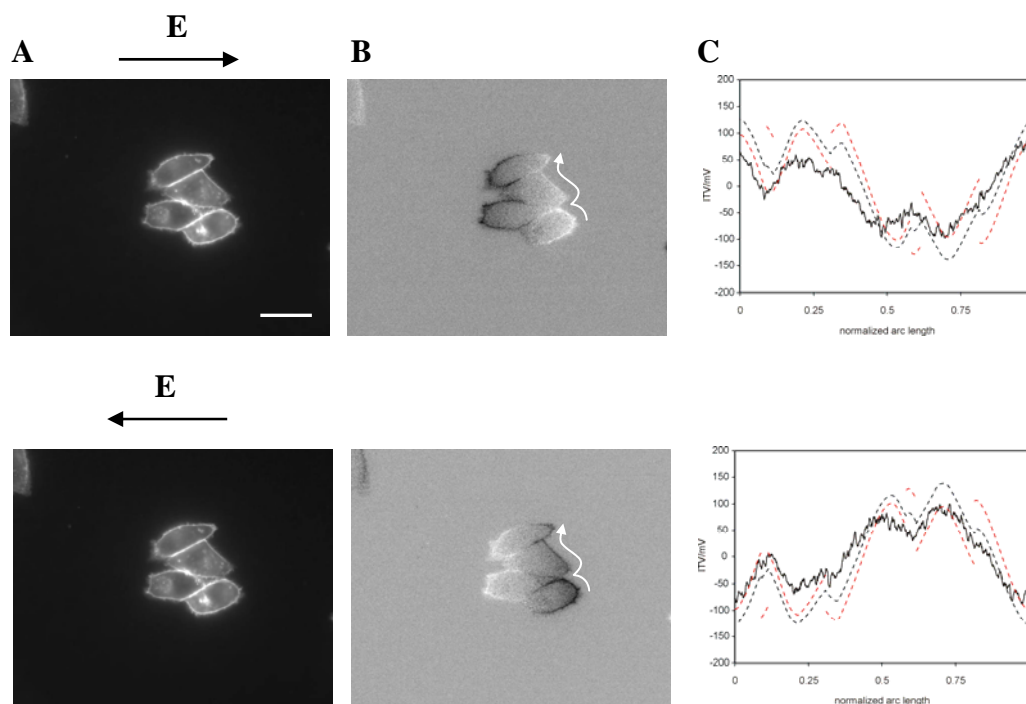


Figure 6.26. Measurements of induced transmembrane voltage (ITV) on a cluster of four CHO cells. (A) Fluorescence images of a cluster acquired during the exposure to 19 V (75 V/cm), 50 ms rectangular pulse. Bar represents 20  $\mu\text{m}$ . (B) Changes in fluorescence of a cluster. (C) ITV as a function of normalized arc length. Solid curve – measured values, black dashed curve – numerically calculated values for the case of electrically connected cells, red dashed curve – numerically calculated values for the case of electrically insulated cells. See legend of Figure 6.1 for details.

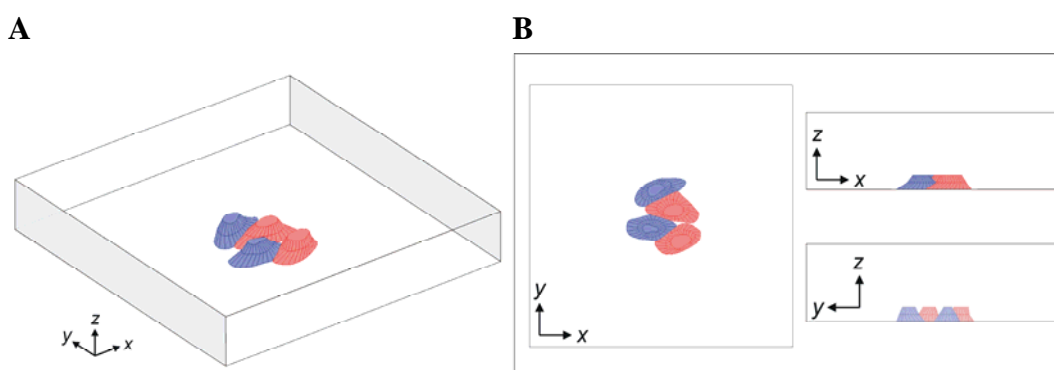


Figure 6.27. Numerical model of a cluster of four CHO cells shown in Figure 6.24. (A) 3D geometry. The dimensions of the cube were 133 $\times$ 133 $\times$ 30  $\mu\text{m}$ . One electrode was set to 1 V and the other to the ground (electric field 75 V/cm). (B) The three side views of the model. See legend of Figure 6.2 for details.

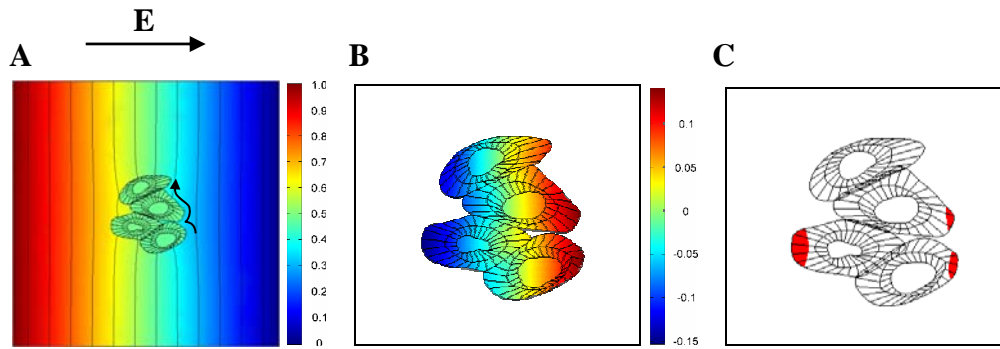


Figure 6.28. Calculations of induced transmembrane voltage for electrically connected cells. (A) Distribution of the electric potential in the x-y plane for the lowermost part of the cluster. (B) ITV on a surface of the magnified model. (C) Regions of the membrane where the absolute value of ITV is the highest. See legend of Figure 6.3 for details.

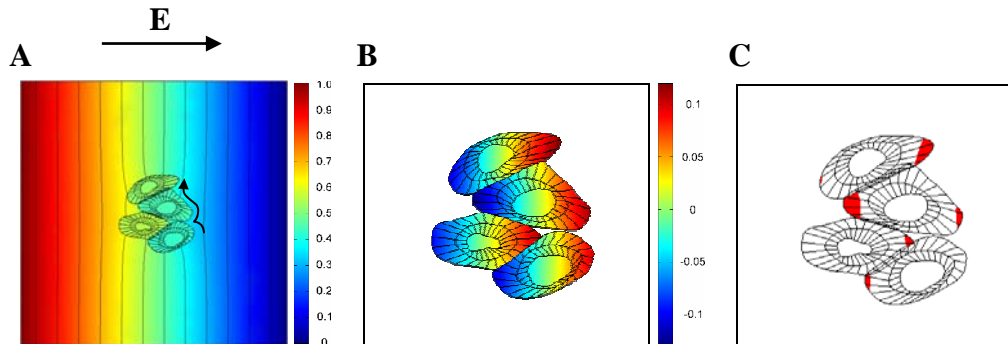


Figure 6.29. Calculations of induced transmembrane voltage for the case of electrically insulated cells. (A) Distribution of the electric potential in the x-y plane for the lowermost part of the cluster. (B) ITV on a surface of the magnified model. (C) Regions of the membrane where the absolute value of ITV is the highest. See legend of Figure 6.4 for details.

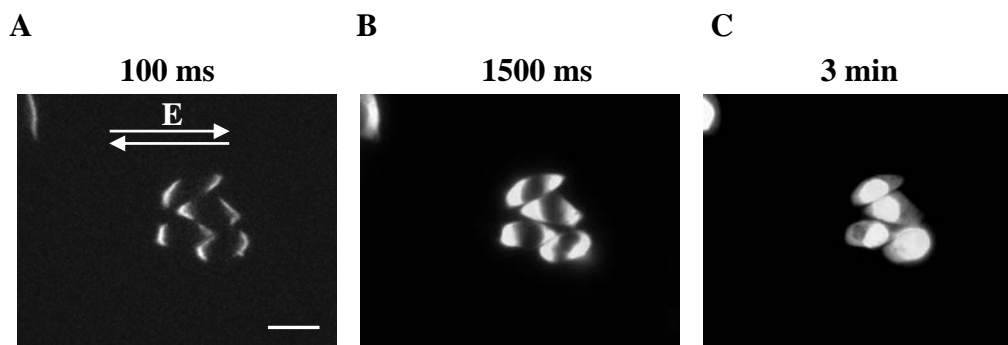
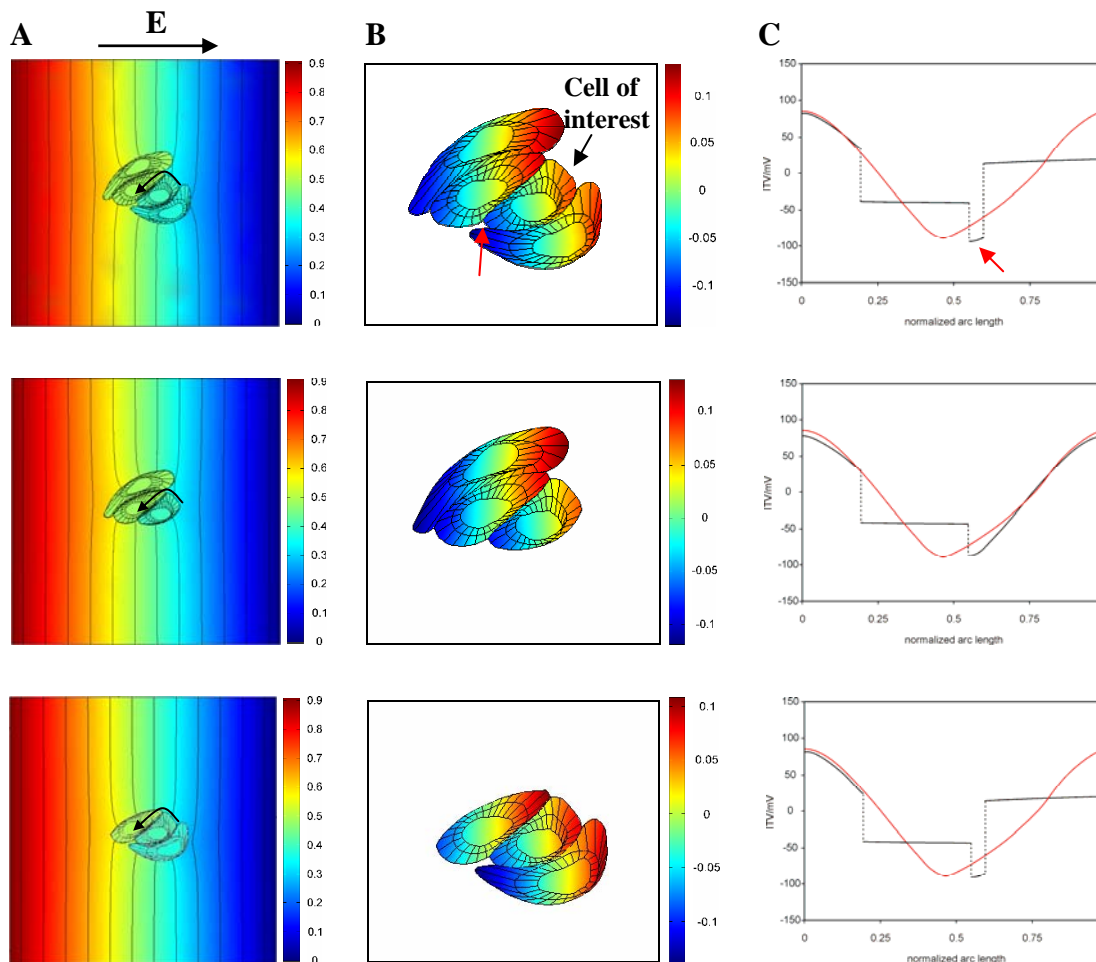
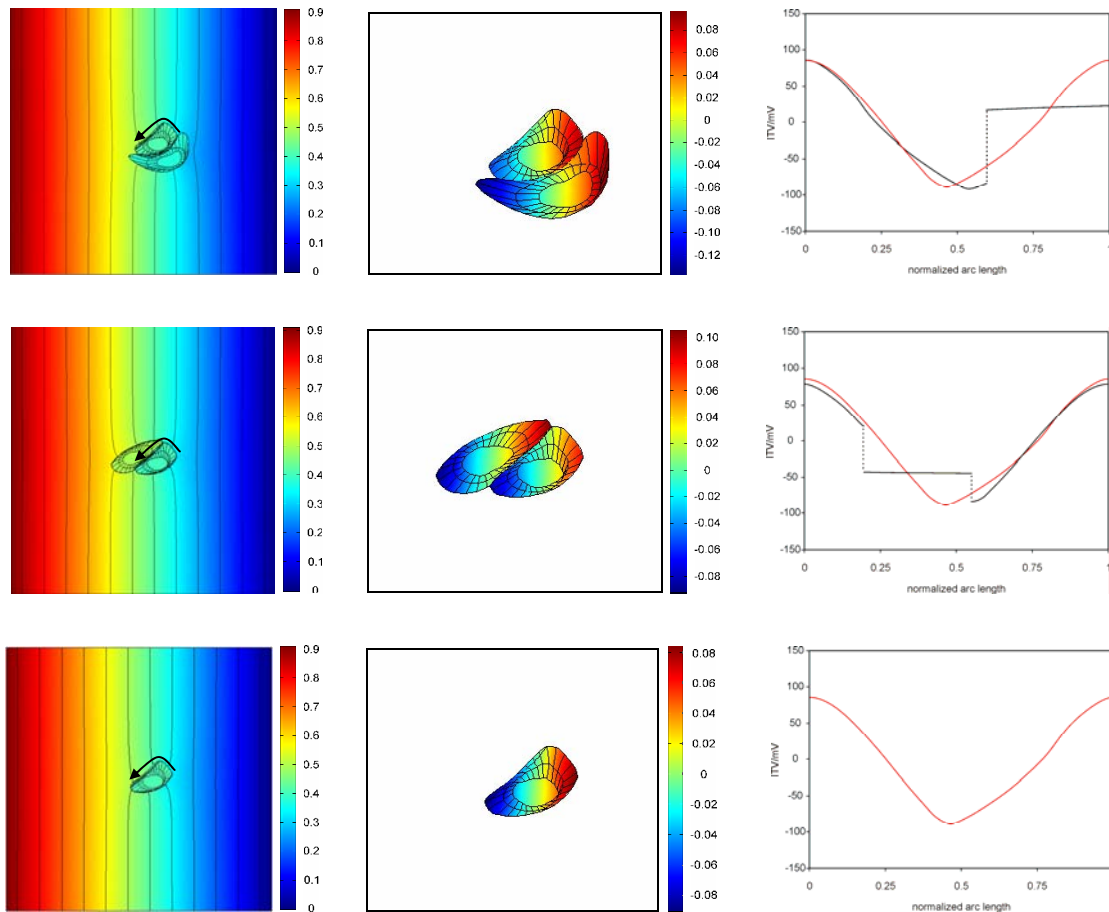


Figure 6.30. Visualization of electroporation (A) 100 ms, (B) 1500 ms, and (C) 3 min after pulse delivery. The cluster was exposed to a single 260 V (1040 V/cm) rectangular bipolar pulse (750  $\mu$ s + 750  $\mu$ s). See legend of Figure 6.5 for details. Bar represents 20  $\mu$ m.

### 6.1.1.1 Induced transmembrane voltage calculated on a cell inside the cluster and on the same cell isolated

A model of a cluster of four electrically insulated cells shown in Figure 6.21(cluster V) was taken and ITV on a cell inside the cluster (third cell from the top) was calculated. Then, one after another, the other cells were removed from the cluster and ITV on the same cell was calculated after each cell removal. Electrical properties of the cell, medium, and external electric field were kept the same as before modification. The calculated electric potential distribution around and inside the modified cell clusters is shown in the first column of Figure 6.31. ITV was determined as a difference of potentials on both sides of the membrane ( $ITV = V_i - V_o$ ) and is presented in the second column of Figure 6.31 on the surface of the cluster. The third column of Figure 6.31 shows the course of ITV for the lowermost cross-section of the cell of interest as a function of normalized arc length (black curve) together with ITV calculated on the same cell isolated (red curve). As the results show, the neighboring cells considerably change the distribution of ITV on the cell membrane. While they provide some screening or shielding of the electric field in the regions of contact, where ITV is almost constant, they can also produce considerable inhomogeneities in distribution of external electric potential, which can lead to substantial deviations of ITV from the values obtained for the isolated cell (marked with a red arrow in Figure 6.31).





**Figure 6.31.** Calculations of ITV on a cell of interest inside the cluster IV (already shown in Figure 6.19). Cells were, one after another, removed from the cluster and ITV on the chosen cell was calculated. (Column A) Distribution of the electric potential in the x-y plane for the lowermost cross-section of the modified cluster. (Column B) ITV on a surface of the magnified model. (Column C) ITV as a function of normalized arc length for the lowermost part of the cell, calculated on the cell of interest – black curve and the same cell isolated – red curve. Black arrow marks the start and direction of the path along which ITV was measured. Red arrow shows the region of membrane where ITV considerably deviates from ITV obtained on the same cell isolated. Bar scale is in volts.

### 6.1.2 Test for gap junctions

To verify if cells from our study were forming connecting pathways between them (gap junctions) we performed a scrape-loading test using a fluorescent dye Lucifer Yellow (El-Fouly et al., 1987). The site where cells were scraped with a sharp blade or a surgical needle is marked with an arrow. After 5 minutes of incubation, a large area of fluorescent cells around the site of damage was observed, clearly indicating the existence of gap junctions. Similar results were obtained for all investigated cell lines. Cells, which were located far from the damaged cells, remained nonfluorescent. Unexpectedly, essentially the same results were observed for cells pre-incubated for 24 - 48 hours in a mixture of culture medium and 25  $\mu\text{M}$  of Lindane, a gap junction inhibitor.

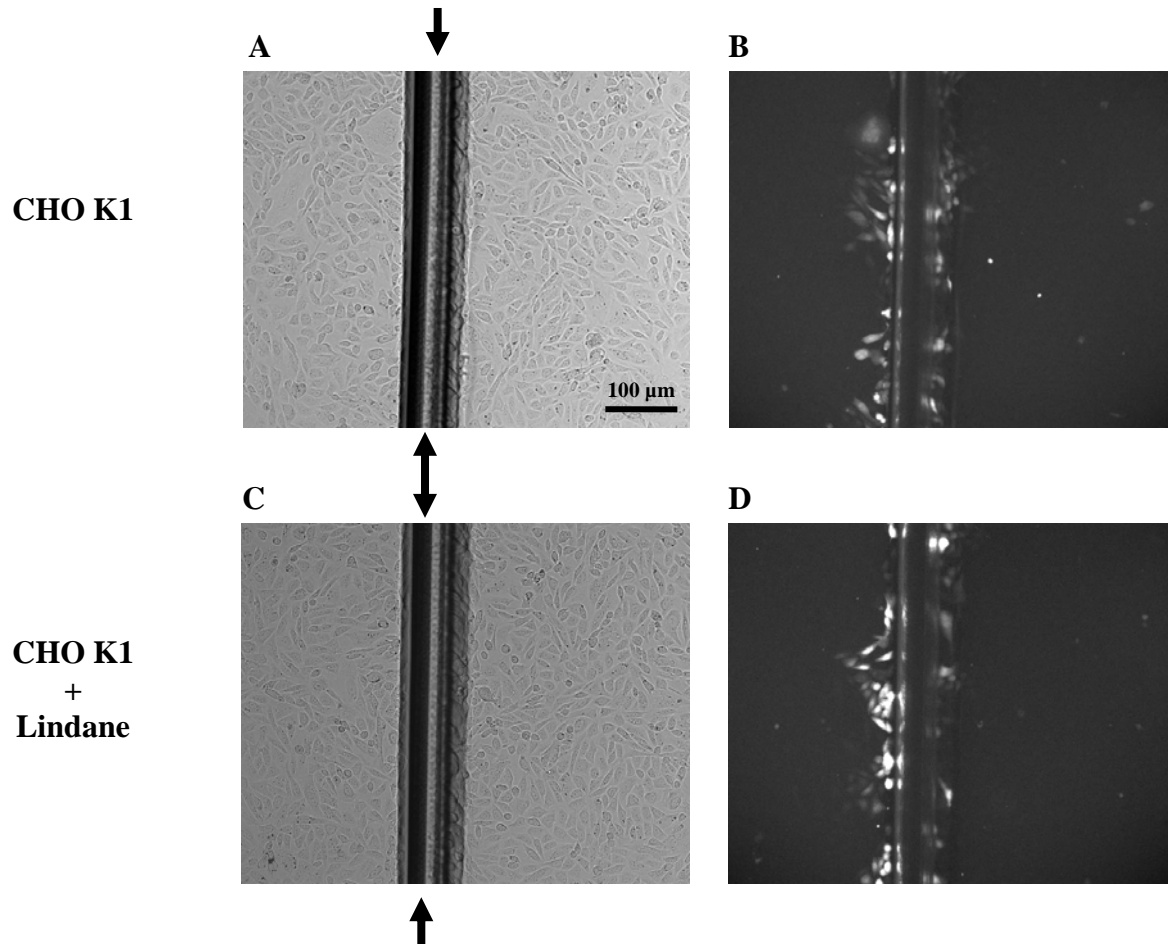


Figure 6.32. Scrap loading test with Lucifer Yellow. Cells (CHO K1) were first scraped with a sharp scalpel or a needle and then incubated for 5 minutes in presence of dye (1 mM). (A) Phase contrast of the monolayer. Black arrow marks the area where cells were scraped. (B) Fluorescence of cells. (C) Same as A except that cells were pre-incubated for 24 - 48 hours with 50  $\mu\text{M}$  Lindane, a gap junction inhibitor. (D) Fluorescence of cells pre-incubated with Lindane.

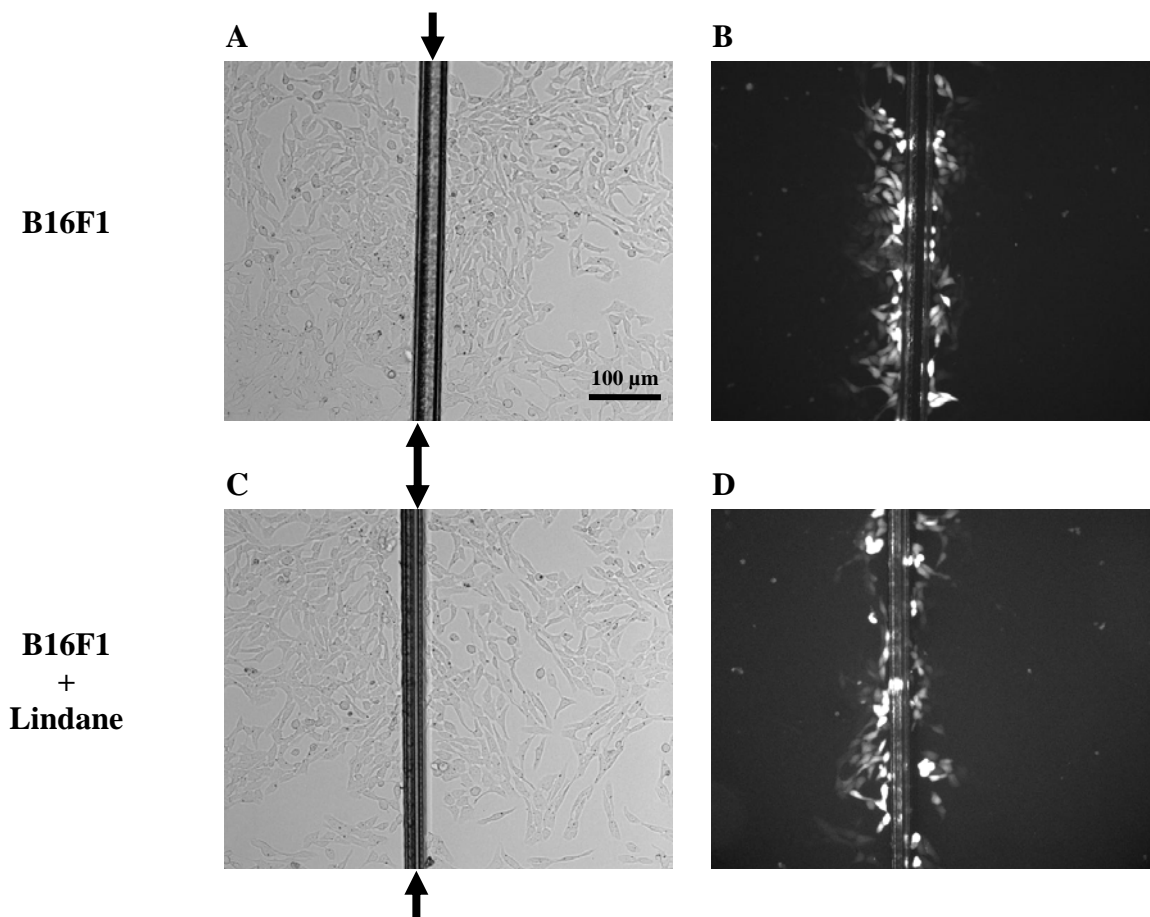


Figure 6.33. Scrap loading test with Lucifer Yellow for B16 cell line. See legend of Figure 6.32 for details.

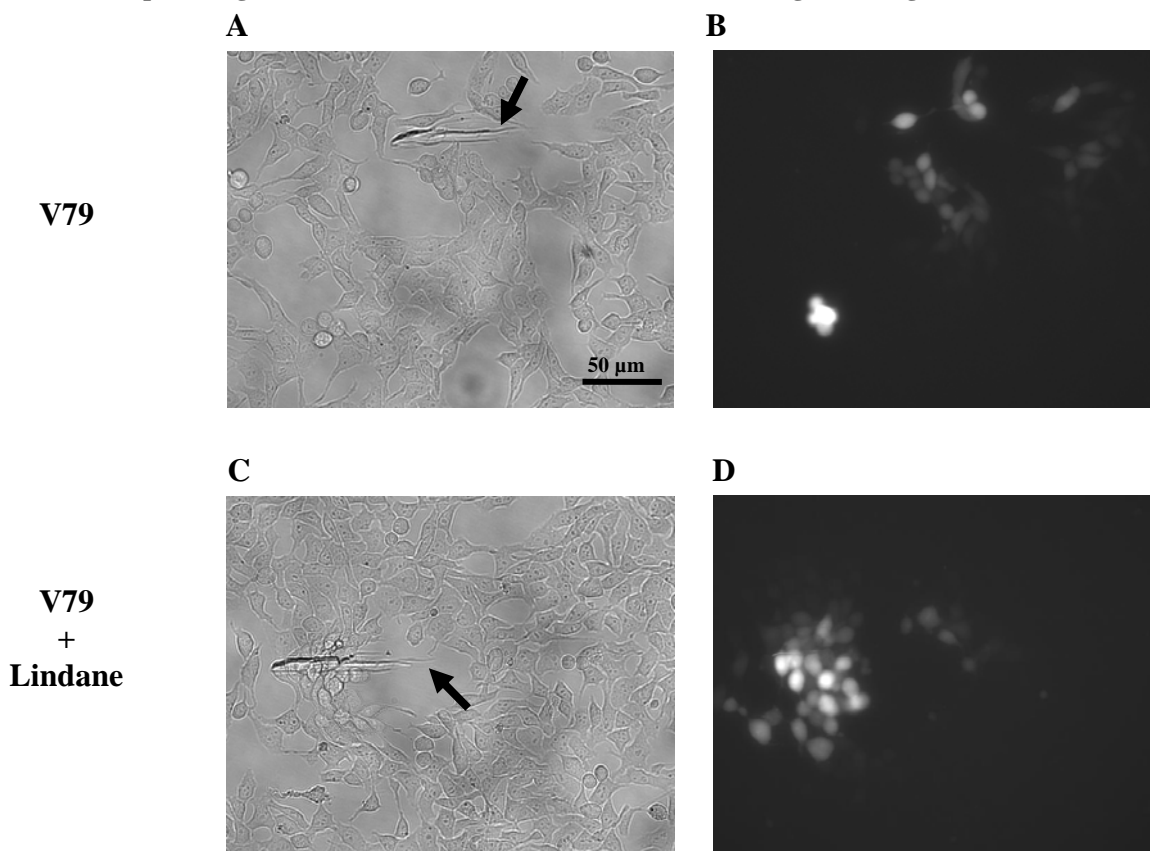


Figure 6.34. Scrap loading test with Lucifer Yellow for V79 cell line. See legend of Figure 6.32 for details.

## 6.2 Results - Dense cell suspensions

### Electropermeabilization of dense cell suspensions

Gorazd Pucihar<sup>1</sup>, Tadej Kotnik<sup>1</sup>, Justin Teissié<sup>2\*</sup>, Damijan Miklavčič<sup>1</sup>

<sup>1</sup> University of Ljubljana, Faculty of Electrical Engineering, Tržaška 25, SI-1000 Ljubljana, Slovenia

<sup>2</sup> IPBS, CNRS, UMR 5089, 205 Route de Narbonne, Toulouse Cedex, France

*(paper 6 in Appendix - manuscript in preparation)*

#### Abstract

We investigated the influence of cell density on cell membrane electropermeabilization. The experiments were performed on dense cell suspensions (up to  $400 \times 10^6$  cells/ml), which represent a simple model for studying electropermeabilization of tissues. Permeabilization was assayed with a fluorescent test using Propidium Iodide to obtain the mean number of permeabilized cells and the mean fluorescence per cell (amount of loaded dye). According to the results, as the cell density increased from  $10 \times 10^6$  to  $400 \times 10^6$  cells/ml, the fraction of permeabilized cells decreased by approximately 50%. We attribute this to the changes in the local electric field, which lead to a decrease in the amplitude of induced transmembrane voltage. To obtain the same fraction of cell permeabilization in suspensions with  $10 \times 10^6$  and  $400 \times 10^6$  cells/ml, the latter suspension had to be permeabilized with higher pulse amplitude, which is in a qualitative agreement with numerical calculations. The electroloading of cells also decreased with cell density and the decrease was considerably larger than expected from the differences in the permeabilized cell fractions. We supposed that the additional decrease in fluorescence was mainly due to cell swelling after permeabilization, which reduced extracellular dye availability to the permeabilized membrane and hindered the dye diffusion into the cells. We also observed that resealing of cells appeared to be slower in dense suspensions, which can be attributed to cell swelling resulting from electropermeabilization.

### 6.3 Kinetics of transmembrane transport of small molecules after electropermeabilization

The transport of small, membrane-impermeant fluorescent molecule Propidium Iodide into CHO WTT cells was followed after the onset of electropermeabilizing pulse. When the dye entered the cytoplasm, its fluorescence increased and the changes in fluorescence were continuously monitored with a photomultiplier tube. Because the tube transforms fluorescence signal into voltage, the results are presented as changes in voltage with time. We studied the influence of pulse amplitude and pulse duration on the kinetics of dye transport into cells in suspension, single spherical cells and confluent cell monolayers. Before these experiments were carried out, the measuring system was analyzed in terms of noise and speed of response (see Materials and Methods Section). Results shown on different time intervals were obtained from different experiments.

#### 6.3.1 Cell suspensions

A single 1 ms pulse with amplitudes ranging from 350 V to 800 V (700 – 1600 V/cm) was applied to the cell suspension and fluorescence was measured. At a given pulse amplitude, fluorescence progressively increased with time, reflecting the dye transport into permeabilized cells (Figure 6.35). Higher pulse amplitudes resulted in faster fluorescence increase and also in higher fluorescence. A sharp increase was observed within the first 10 ms after the onset of a pulse, followed by a moderate additional fluorescence increase (Figure 6.35B). Results measured on a 2 ms time interval are amplified tenfold and show a delay of a few hundred microseconds before the fluorescence starts to increase (Figure 6.35C). In addition, different dynamics of the increase after the offset of the pulse (at time 1 ms) can be observed, demonstrating the electrophoretic effect of the pulse on dye movement (Figure 6.35C).

Similar results were obtained when a single 500 V pulse (1000 V/cm) with durations ranging from 100  $\mu$ s to 3 ms was applied (Figure 6.36). At a given pulse duration, the fluorescence increases with time with different dynamics. Namely, after a delay of approximately 500  $\mu$ s, a sharp increase was observed within the first 10 ms, followed by a more moderate increase in fluorescence. Again, we can observe different dynamics of the increase during and immediately after the pulse, showing the electrophoretic effect of the pulse (Figure 6.36C).

According to the results presented in Figures 6.35C and 6.36C, the increase in fluorescence can be detected between 200  $\mu$ s and 700  $\mu$ s after the onset of pulse, depending on its amplitude and duration. To determine the limit of detection, we increased the sensitivity of the photomultiplier tube, applied a single 800 V, 1 ms pulse to cell suspension containing a ten times higher dye concentration (1 mM instead of 100  $\mu$ M) and monitored the response on a 400  $\mu$ s time interval. The results are shown in Figure 6.37A for three repetitions of the experiment and the average of these responses is presented in Figure 6.37B. According to

these results, an increase in fluorescence, indicating the dye transfer into cells, can be detected approximately 100  $\mu\text{s}$  after the onset of the pulse. Pulse amplitudes higher than 800 V yielded essentially the same results (data not shown).

At the end, we measured the fluorescence of suspension containing different concentrations of Propidium Iodide (10  $\mu\text{M}$ , 100  $\mu\text{M}$ , 1 mM). Permeabilization in higher dye concentration resulted in higher fluorescence at the end of acquisition interval and faster response (Figure 6.38). Eight seconds after pulse application, the fluorescence from suspension with 100  $\mu\text{M}$  and 1 mM dye concentration was approximately 3 times and 12 times higher than in 10  $\mu\text{M}$ , respectively (Figure 6.38A). Again, we observed a fast increase in fluorescence within a few milliseconds after the pulse application, while a further increase was more moderate.

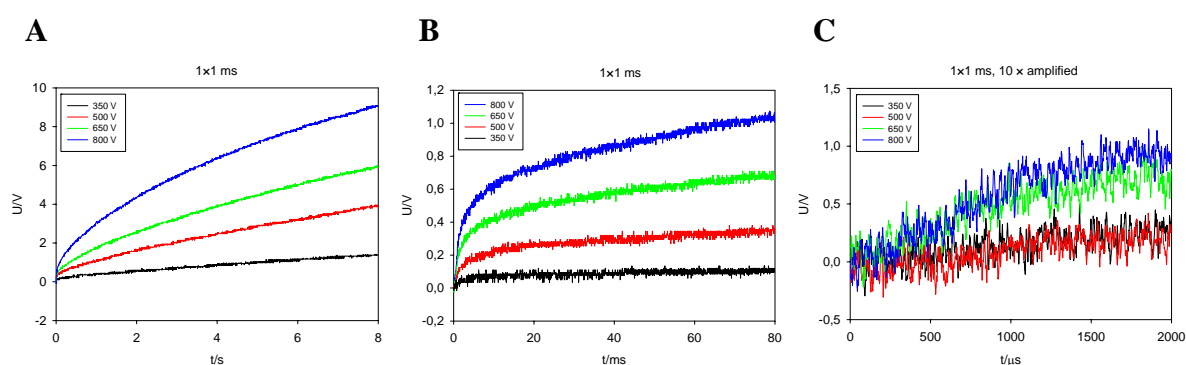


**Figure 6.35.** The influence of pulse amplitudes on the time course of fluorescence after electroporation. (A) 8 s, (B) 80 ms, (C) 2 ms acquisition interval. CHO WTT cells in suspension containing 100  $\mu\text{M}$  of Propidium Iodide were exposed to a single rectangular 1 ms pulse with amplitudes 350, 500, 650, and 800 V (electric field 700, 1000, 1300, 1600 V/cm). Results shown in C are 10 times amplified. Fluorescence was detected with a photomultiplier tube, which transformed fluorescence intensity into voltage.

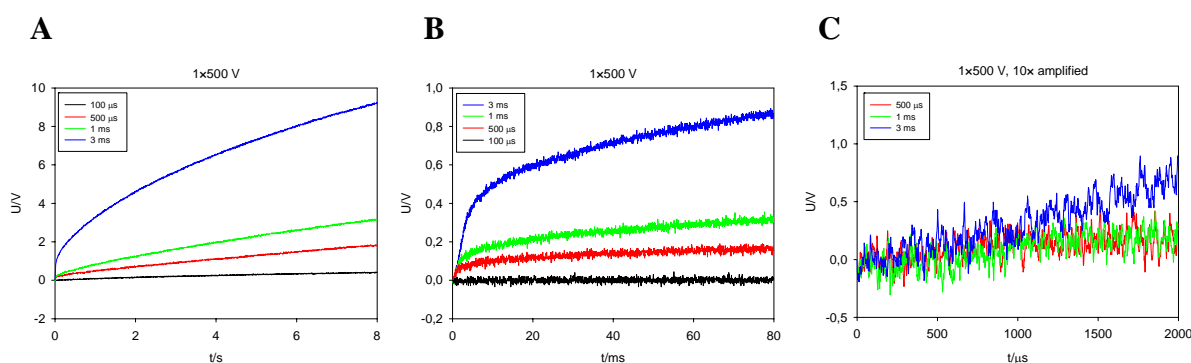


**Figure 6.36.** The influence of pulse durations on the time course of fluorescence after electroporation. (A) 8 s, (B) 80 ms, (C) 2 ms acquisition interval. CHO WTT cells in suspension containing 100  $\mu\text{M}$  of Propidium Iodide were exposed to a single rectangular 500 V (1000 V/cm) pulse with durations 100  $\mu\text{s}$ , 500  $\mu\text{s}$ , 1 ms, and 3 ms. Results shown in C are 10 times amplified. Fluorescence was detected with a photomultiplier tube, which transformed fluorescence intensity into voltage.

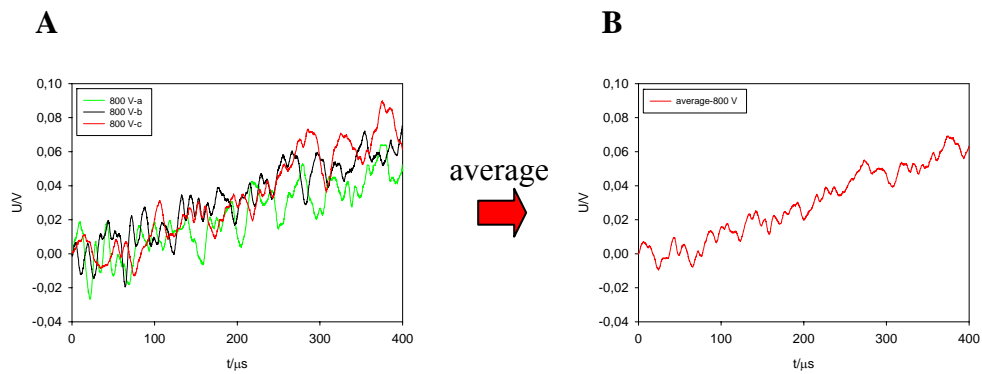


**Figure 6.37.** Time course of fluorescence measured with increased sensitivity of the photomultiplier tube. (A) Results of three repetitions. (B) Average of the three measurements in A. CHO WTT cells in suspension containing 1 mM Propidium Iodide were exposed to a single rectangular 800 V (1600 V/cm), 1 ms pulse.

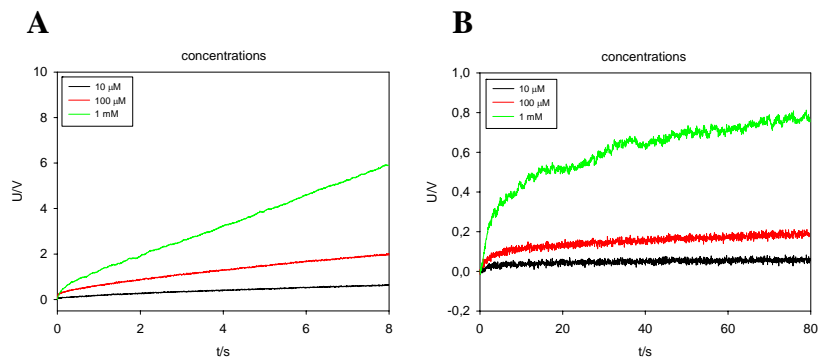


**Figure 6.38.** The influence of dye concentration on the time course of fluorescence after electropermeabilization. (A) 8 s, (B) 80 ms acquisition interval. CHO WTT cells in suspension containing 10  $\mu$ M, 100  $\mu$ M, or 1 mM of Propidium Iodide were exposed to a single rectangular 500 V (1000 V/cm), 1 ms pulse.

### 6.3.2 Single cells

The influence of pulse amplitudes and pulse durations was also investigated on single CHO cells. Time courses of fluorescence increase are presented in Figures 6.39 and 6.40 for different pulse amplitudes and pulse durations, respectively. Compared to results on cell suspensions, the fluorescence increase measured for single cells is more moderate and considerably lower. Due to small changes in fluorescence, these experiments were monitored on 8 s time scale only.

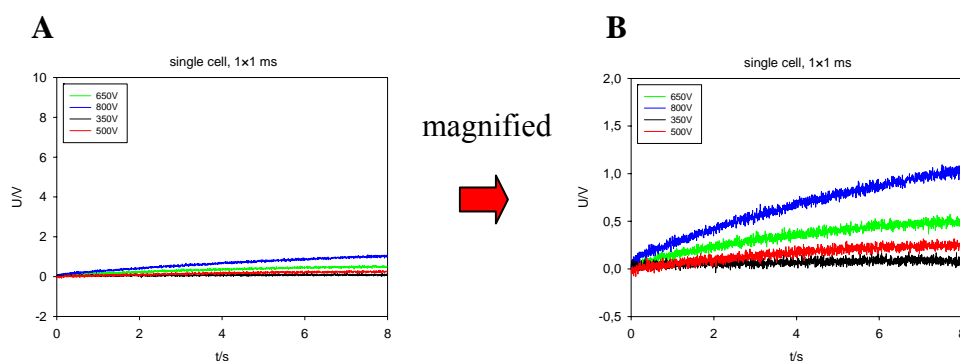


**Figure 6.39.** The influence of pulse amplitudes on time course of fluorescence measured on single cell. (A) Time course of fluorescence. (B) Magnified image of A. CHO WTT cells in dilute suspension containing 100  $\mu\text{M}$  of Propidium Iodide were exposed to a single rectangular 1 ms pulse with amplitudes 350, 500, 650, and 800 V (electric field 700, 1000, 1300, 1600 V/cm). The excitation light was focused on a single cell and fluorescence from this cell was detected with a photomultiplier tube.

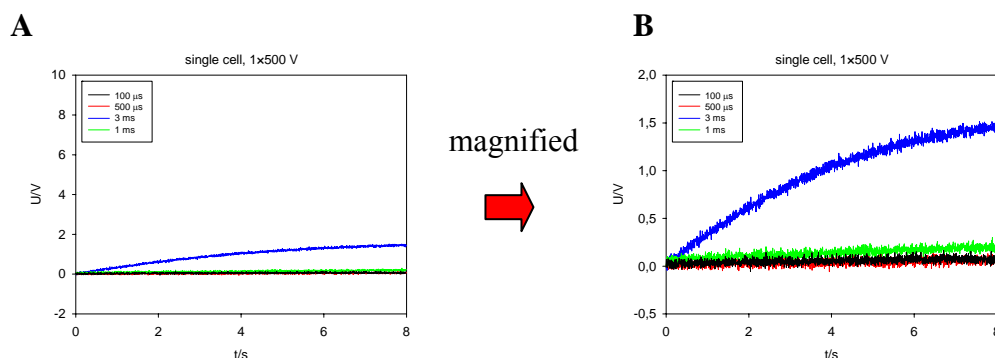


**Figure 6.40.** The influence of pulse durations on time course of fluorescence measured on single cells. (A) Time course of fluorescence. (B) Magnified image of A. CHO WTT cells in dilute suspension containing 100  $\mu\text{M}$  of Propidium Iodide were exposed to a single rectangular 500 V (1000 V/cm) pulse with durations 100  $\mu\text{s}$ , 500  $\mu\text{s}$ , 1 ms, and 3 ms. The excitation light was focused on a single cell and a fluorescence from this cell was detected with a photomultiplier tube.

### 6.3.3 Attached cells

Confluent monolayers of CHO WTT cells were exposed to electric pulses with the same pulse amplitudes and durations as above. Time courses of fluorescence after electropermeabilization with a single 1 ms pulse and amplitudes ranging from 350 to 800 V are presented in Figures 6.41 and 6.42 (black curves). Fluorescence of cells increases with time after permeabilization and with increasing pulse amplitudes. The dynamics of increase is similar to the one observed for suspended cells; a fast increase within 5 to 10 ms after the onset of the pulse is followed by a more moderate increase (Figure 6.42). At each investigated pulse amplitude the fluorescence was lower than in the corresponding case of suspended cells (red curves in Figures 6.41 and 6.42). Note that the y-scale is different than in results obtained under Section 6.3.1, because the measurements were not performed at the same sensitivity of a photomultiplier tube.

Results for permeabilization with a 500 V (1000 V/cm) pulse with durations ranging from 100  $\mu$ s to 3 ms are shown in Figure 6.43. For a comparison, the time course of fluorescence for suspended cells is shown with pink curve but only for 1 ms pulse. Lower fluorescence was observed in case of attached cells while the dynamics of fluorescence is similar for suspended and attached cells (Figures 6.43A and B).

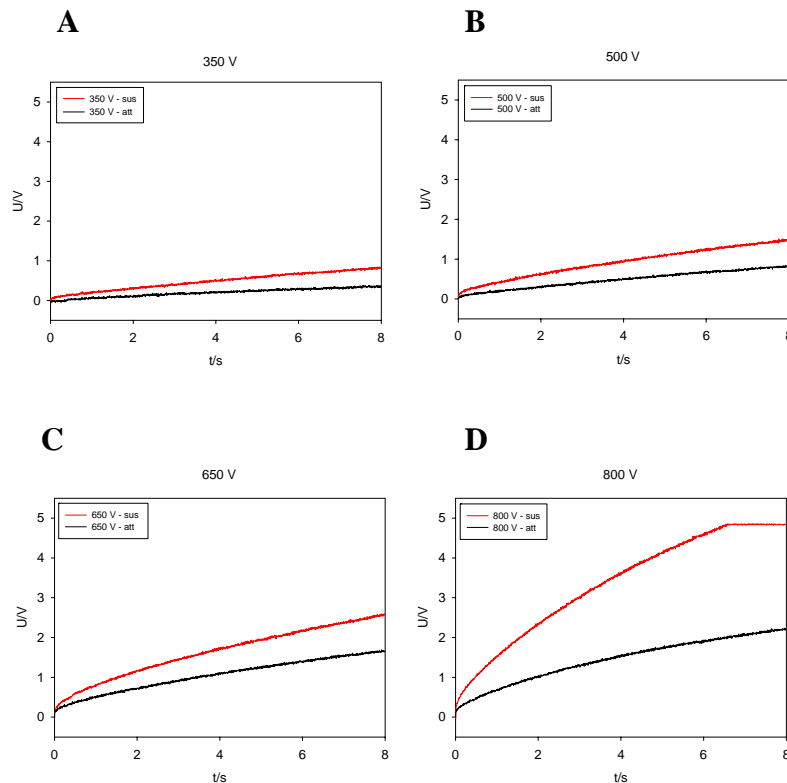


**Figure 6.41.** Comparison of time course of fluorescence from suspended (red curves) and attached cells (black curves) on 8 s time interval. Cells were permeabilized with a single 1 ms pulse with amplitudes (A) 350 V, (B) 500 V, (C) 650 V, and (D) 800 V. The y-scale is different than in results obtained in Section 6.3.1 because the measurements were not performed at same sensitivity of a photomultiplier tube.

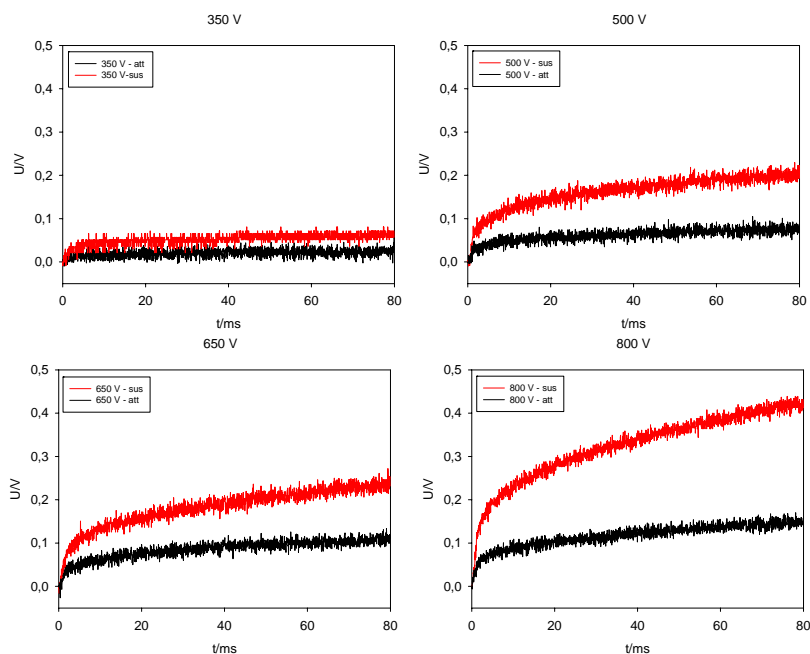


**Figure 6.42.** Comparison of time course of fluorescence from suspended (red curves) and attached cells (black curves) on 80 ms time interval. Cells were permeabilized with a single 1 ms pulse with amplitudes (A) 350 V, (B) 500 V, (C) 650 V, and (D) 800 V. The y-scale is different than in results obtained in Section 6.3.1 because the measurements were not performed at same sensitivity of a photomultiplier tube.

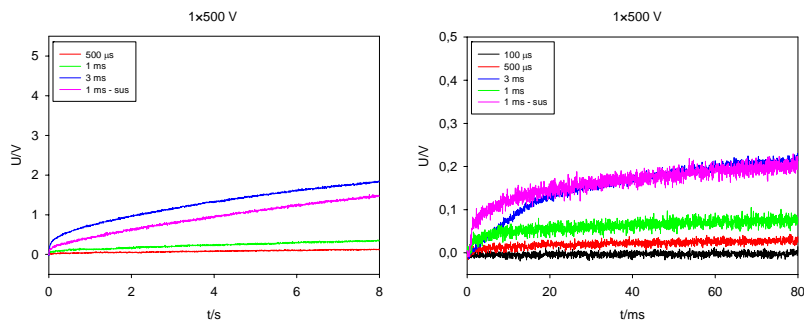


**Figure 6.43.** Comparison of time course of fluorescence from suspended (pink curve) and attached cells on (A) 8 s and (B) 80 ms time interval. Cells were permeabilized with a single 500 V (1000 V/cm) pulse with durations 100  $\mu$ s, 500  $\mu$ s, 1 ms, and 3 ms. The y-scale is different than in results obtained in Section 6.3.1 because the measurements were not performed at same sensitivity of a photomultiplier tube.

## 6.4 Discussion

### 6.4.1 Cell clusters

The experiments described in Sections 4 and 5 were performed on single spherical cells and single irregularly shaped cells. In order to understand how the external electric field interacts with cells in tissues, we needed to proceed to more complex cell assemblies. Namely, cells in tissues have complex geometry, they are sufficiently close to affect the electric field around each other, and they are often interconnected with pathways (gap junctions). The complexity of tissue structure is the main reason why researchers in their studies often use simplified models of tissues, such as cell pellets, multicellular spheroids, or dense cell suspensions (Abidor et al, 1993; Abidor et al., 1994; Susil et al., 1998; Pavlin et al., 2002; Schmeer et al., 2004; Canatella et al., 2004). For the same reason, the numerical models of tissues are often macroscopic, where the average or bulk electric properties (e.g. bulk conductivity or bulk permittivity) are assigned to different types of tissues in the model, while a detailed cell structure is not considered (Šel et al, 2005; Pavšelj et al., 2005). One of the very few numerical studies where cell structure was considered was done by Gowrishankar and Weaver (Gowrishankar and Weaver, 2003). To better understand how the electric field interacts with tissues on a microscopic (single cell) level, which in turn determines the macroscopic behavior of tissue, we decided to perform our study on monolayer clusters of irregularly shaped cells. Regarding the shape, density, and connections between cells, such cell clusters are in their complexity close to tissues and could provide us with findings, which are otherwise not accessible to macroscopic models.

Measurements and calculations of induced transmembrane voltage (ITV) were performed on cell clusters, which differed in complexity and size. In general, a good agreement between measured and calculated ITVs were obtained, especially in case of small clusters composed of two cells, while for large clusters, some differences in the amplitudes of measured and calculated ITVs were observed (e.g. clusters IV and VI). Possible reasons for the discrepancies were already discussed in Sections 3 and 4, and include the slope of calibration curve, experimental setup, and parameters of the model. In addition, the physiological state of cells in clusters could also contribute to differences in measured and calculated ITV. Namely, these cells have already undergone at least one cycle of division and it is probable that at the time when experiment was performed, the individual cells in cluster were in different phases of cell cycle. If the electrical properties of membranes or the connections between cells change during these phases, these changes would affect the distribution of ITV on a cluster. Our numerical model did not account for such changes.

Fluorescence images obtained with di-8-ANEPPS together with measured distribution of ITV on clusters revealed an interesting observation, namely, that during the measurements of ITV, cells in clusters behaved as one giant cell. Specifically, the cell facing the cathode was completely depolarized while the cell facing the anode was completely hyperpolarized (e.g.

Figure 6.1B and 6.11B). These observations are in agreement with numerical calculations of ITV for the case where cells were modeled as electrically connected. To verify whether cells used in our experiments form electrical pathways, such as gap junctions, we performed a scrape-loading test with Lucifer Yellow (El-Fouly et al., 1987), which confirmed our predictions (Figures 6.32B-6.34B). We also planned an experiment on inhibited gap junctions, but unfortunately, the gap junction inhibitor Lindane apparently did not inactivate them as planned (Figures 6.32D-6.34D).

On the contrary, permeabilization results showed that cells in clusters permeabilize individually. Regions of increased fluorescence were observed on both sides of each cell in a cluster, which was not anticipated from measurements of ITV. A better agreement was obtained if cells in clusters were modeled as electrically insulated. In this case the fluorescence regions matched the regions of the model where the absolute values of calculated ITV were the highest (compare e.g. Figure 6.5A with Figures 6.4B and 6.4C). Therefore, two opposing behavior of cells in clusters were observed. During the measurements of ITV, which were performed at long pulse durations and lower pulse amplitudes (50 - 100 ms, 75 - 100 V/cm), cells in clusters behaved as one giant cell, while during electropermeabilization, which was performed at short pulse durations and higher pulse amplitudes (0.2 – 1.5 ms, 650 V/cm – 1040 V/cm) they behaved as individual cells. These observations were attributed to changes in properties of gap junctions as a response to different parameters of electric pulses. Opening and closing of gap junctions is a stochastic process, occurring on a time interval of hundreds of milliseconds to seconds (Brink 1996a; Brink et al., 1996b; Marino et al., 2003). It is therefore likely that the average conductivity of these channels on a shorter time interval (such as during permeabilization) is different than the average conductivity on a longer time interval (such as during measurements of ITV). Besides, higher pulse amplitude in permeabilization experiments could change the structure of gap junctions, by rendering them less conductive. In addition to parameters of electric pulses, the properties of gap junctions can be modified by phosphorylation of connexin protein, elevation of cAMP and cGMP levels, acidification and changes in intracellular  $\text{Ca}^{2+}$  concentration (Bruzzone et al., 1996; Kumar and Gilula, 1996). Regarding the  $\text{Ca}^{2+}$ , it was shown that elevated intracellular concentration of  $\text{Ca}^{2+}$  closes the gap junctions (Loewenstein 1981; Brink and Fan, 1989; Marino et al., 2003) and this could also occur during permeabilization experiments.

The course of permeabilization was also monitored for other cell lines (CHO WTT, B16F1) and the results were essentially the same as those obtained on CHO K1 cells; the permeabilization always occurred on both sides of each individual cell in a cluster (results not shown).

Intuitively, if cells in cluster would behave as a giant cell even at high external voltages, the permeabilization would first occur on the outermost membranes of the cluster facing the electrodes and then proceed to the membranes of internal cells, due to the sudden increase of ITV on the membranes of these cells (a kind of a domino effect). However, we would not be

able to observe the permeabilization of the inner membranes, because the fluorescent dye is present only in extracellular medium. What we would observe would be the entrance of the dye from both outermost sides of the cluster and its diffusion towards the center of the cluster. What we actually observed was the entrance of the dye on both sides of each individual cell in a cluster, which shows that cells permeabilized individually.

The results of ITV presented in this section of the study are in agreement with observations reported by Gross and co-workers on clusters of A-431 nonexcitable human carcinoma cells and with observations of Hassan and co-workers on clusters of excitable bovine adrenal chromaffin cells (Gross et al, 1986; Hassan et al., 2002). Both observed depolarization of one part of a cluster and a complete hyperpolarization of the other part in case of small clusters. For larger clusters, they reported a more complex behavior, where some cells inside the cluster exhibited both hyperpolarization and depolarization. This could be attributed to the fact that their cells did not form gap junctions. The authors presented their results only qualitatively, by mapping the changes in fluorescence of the dye, while in our study we present quantitative measurements of ITV and also complement them by numerical calculations.

Numerical model of a cluster was constructed from cross-section fluorescence images of individual cells in a cluster. However, to avoid difficulties with mesh generation, the model was constructed from three layers only. For the same reason, in case of clusters of four cells (clusters IV, V and VI), we decreased the number of edges of each layer comprising the model from 35 to 25. This resulted in a less realistic model, but did not considerably affect the course of calculated ITV. Nevertheless, the model was still far more realistic than the existing models of irregular cells or cell clusters, which were built by combining several simple geometric shapes, such as hemispheres, hemiellipsoids and cubes (Fear and Stuchly, 1998a; Fear and Stuchly, 1998b; Buitengeweg et al., 2003; Valič et al., 2003). A limitation of such realistic modeling is the number of cells that comprise the cluster. Each additional cell increases the number of finite elements in the model, and by that increases the time for mesh generation and the time for solution. We estimate that using the same computer and software (Femlab 3.1 running on a PC with 2.8 GHz Pentium IV, 1 GB RAM) a cluster of five to six cells would still be possible to build, while more complex clusters would cause problems with mesh generation and calculations.

To model the electrical connections (gap junctions) between cells we would have to incorporate many small channels into the membrane on the contact, which would be, mostly due to the size of the channels, difficult to perform. This was done on a simple model of a cluster by Fear and Stuchly (Fear and Stuchly, 1998a; Fear and Stuchly, 1998b), who investigated the influence of the arrangement and conductivities of gap junctions on ITV. Instead of modeling individual gap junctions and changing their conductivities, we assigned to the contact surface of the membranes a higher average conductivity, which had a similar effect.

### 6.4.2 Kinetics of dye transport

In general, the transport caused by electroporation can be monitored using two techniques, (i) measurements of changes in conductivity of lipid bilayers, single cells, cell suspensions, or cell pellets; or (ii) following the entrance or efflux of fluorescence probes, radioactive labeled dyes or intracellular constituents (Riemann et al., 1975; Kinoshita and Tsong 1977; Benz et al. 1979; Benz and Zimmermann 1980; Chernomordik et al., 1987; Glaser et al., 1988; Mir et al., 1988; Mehrle et al., 1989; Tekle et al., 1991; Hibino et al., 1991; Tekle et al., 1994; Abidor et al., 1994; Prausnitz et al., 1994; Gabriel et al., 1998; Gabriel et al., 1999; Schmeer et al., 2004; Pavlin et al., 2005). By using these techniques, the authors showed that transport of single-atom ions occurs within microseconds after the onset of the electric pulse, while small molecules, due to their size, enter into cells milliseconds after the exposure. Under reversible conditions, the transport continues seconds or even minutes after the exposure, until the membrane is completely resealed. An example of a detailed study of changes of conductivity of a cell suspension during and after electroporation is presented in **paper 7** in Appendix (Pavlin et al., 2005).

While it was evident that transport of single-atom ions occurred during and after the pulse, it was proposed that the same applies to transport of small molecules. However, fluorescence imaging showed that transport of small molecules, such as Propidium Iodide or Ethidium Bromide, start milliseconds after the exposure. With higher amplitudes and longer pulse durations, it was possible to observe transport occurring during the pulse but such pulses, with durations ranging into few milliseconds, are rarely used in electroporation applications. An example of dye transport occurring during a 3 ms pulse was shown in this study in Figure 4.7, Section 4, Spherical cell. The limited sensitivity and especially the low time resolution of imaging cameras are the main reasons why kinetics of molecular transport during the pulse has not been extensively studied until now. The only study of that kind was performed by Prausnitz and co-workers (Prausnitz et al., 1995). They measured the efflux of calcein from erythrocyte ghost membranes during and after electroporation with a 200  $\mu$ s time resolution. Permeabilization was performed by applying an exponentially decaying pulse with a considerable time constant of 3.6 ms. We decided to perform an extensive study of pulse parameters (pulse durations and pulse amplitudes) on the transport of Propidium Iodide on different time intervals ranging from 400  $\mu$ s to 8 s, with time resolutions of 9  $\mu$ s and 100  $\mu$ s, respectively. Measurements at such time resolutions enabled us to compare the transport in presence and absence of the electrophoretic effect of the external field. Instead of an exponentially decaying pulse, which was used in the study of Prausnitz, we used a rectangular pulse, which ensured a constant electrophoretic force on dye molecules during the exposure. Propidium Iodide was used because its fluorescence increases considerably upon entering the cytoplasm, making it easy to detect with a sensitive photomultiplier tube.

Results measured on a long time interval (8 s and 80 ms) show at least two time constants of fluorescence increase after the pulse, one in a millisecond and the other in a second time range. They probably reflect different steps of membrane resealing, first a fast resealing, which occurs immediately after the pulse and then a slow resealing, which occurs seconds to minutes after the pulse (Kinosita and Tsong, 1977; Chernomordik et al., 1983; Glaser et al., 1988; Chang and Reese, 1990; Hibino et al., 1991). Higher pulse amplitudes or longer pulse durations resulted in increased dye transport into cells. This is probably because higher pulse amplitudes increased the permeabilized area of the membrane, while longer pulse durations increased the density of structural changes in membrane, which resulted in larger surface available for the dye transport and slower resealing of cell membrane (Gabriel and Teissié, 1997; Rols and Teissié, 1998; Gabriel and Teissié, 1999).

Results measured on a short time interval (2 ms) revealed different dynamics of fluorescence increase during and after the pulse; the rate of increase of the fluorescence slowed down immediately after the pulse. This can be attributed to different mechanisms of transport of molecules in the presence and absence of the pulse. During the pulse, transport is largely due to electrophoretic force, which drives charged dye molecules into cells, while after the pulse, transport is mainly due to diffusion. These measurements also showed that a transport across permeabilized membrane can be observed between 200  $\mu$ s and 700  $\mu$ s after the onset of the pulse. In fact, by using higher sensitivity of photomultiplier tube and elevated dye concentration, we were able to detect the transport within 100  $\mu$ s after the onset of the pulse. Compared to results obtained by Prausnitz, we detected a transport occurring an order of magnitude faster and with more than 20 times higher temporal resolution (9  $\mu$ s in our study compared to 200  $\mu$ s in the study of Prausnitz).

Transport of small molecules through the permeabilized membrane might occur even before 100  $\mu$ s, but due to limited sensitivity of our measuring system and considerable noise inherent to the electronic setup and excitation light, we were not able to detect it. To a certain extent, the sensitivity of the measuring system could be increased by reducing the noise coming from the excitation source. A reference photomultiplier tube would have to be placed into the excitation beam of the light to compensate for the noise caused by the light fluctuations.

Comparison of molecular transport into confluent cells in monolayers and cell suspensions showed that at the same pulse parameters, transport into monolayers of cells is considerably lower than to suspended cells, at least in the investigated time interval. This is in agreement with our previous observations on irregular cells, cell clusters and especially dense cell suspensions. Namely, proximity of cells and cell orientation considerably affects the amplitude of induced transmembrane voltage and consequently the efficiency of electropermeabilization and by that the amount of dye uptake into cells. Besides, with cells growing in monolayers, the transport is limited to the part of the membrane that is not in contact with the dish or cover glass.

The results of this study can be applied to other molecules of comparable size and net charge. At the same pulse parameters, larger molecules would probably enter into cells at slower rates and the amount of the uptake would be lower. The transport of even larger molecules, such as DNA, would mostly occur during the pulse exposure, when the electrophoretic force acts on the charged molecule.

We also tried to measure the transport of  $\text{Ca}^{2+}$  ions into cells by using fluorescent calcium indicator Fluo3. A similar dynamics of fluorescence response was observed within the first milliseconds after the onset of the pulse, which was followed by a considerable decrease in fluorescence due to photobleaching of the dye (data not shown).

## 7 CONCLUSIONS

Here, we will summarize the most important contributions and findings of the experimental work and numerical calculations presented in our study. In addition, several guidelines will be set for further work.

### 7.1 Measurements of resting transmembrane voltage

Measurements of resting transmembrane voltage (RTV) on different cell lines showed that cells in culture media have negative RTVs of tens of millivolts. Therefore, in experiments involving electropermeabilization RTV can be neglected and induced transmembrane voltage can be used as a rough approximate of the total voltage on the membrane.

RTV in cells in media with progressively decreasing conductivities gradually decreases but the decrease is less pronounced than expected from theoretical calculations. It is possible that the chosen method for measuring RTV, although reported as efficient, was not suitable for these experiments.

### 7.2 Measurements and calculations of induced transmembrane voltage and visualization of permeabilization on spherical cells

Measurements of induced transmembrane voltage (ITV) on spherical cells were in qualitative and quantitative agreement with numerically calculated ITV.

Comparison of measured and numerically calculated ITVs with observations of electropermeabilization confirmed that permeabilization occurs in those regions of the membrane where the absolute value of ITV is the highest, i.e. in the regions facing the electrodes. The fluorescence increase immediately after the pulse delivery was asymmetrical in case of unipolar pulses and symmetrical in case of bipolar pulses. On a longer time scale the asymmetry in fluorescence was observed for both unipolar and bipolar pulses.

Critical value of ITV at which permeabilization occurs was calculated from the polar angle of permeabilization measured immediately after the pulse and was found to be approximately 450 mV. Because the polar angle of permeabilization varies with pulse amplitude, duration and time after the pulse, these calculations present a rough approximate of the real critical ITV. A better solution would be to measure the ITV at supracritical pulse amplitudes.

### **7.3 Measurements and calculations of induced transmembrane voltage and visualization of permeabilization on irregularly shaped cells**

Induced transmembrane voltage (ITV) measured on single attached cells was in qualitative agreement with the results of numerical calculations, while some discrepancies in their amplitudes were observed.

We presented a method for constructing realistic models of irregularly shaped cells from their cross-section images. This provides a possibility to determine ITV on the same cells on which the experiment was carried out and enables a direct comparison of the calculated and experimental results. We also showed how the finite-thickness, nonzero-conductivity membrane can be replaced by a boundary condition in which a specific surface conductivity is assigned to the interface between the cell interior and the exterior. This efficiently reduces the number of elements of the mesh and consequently time needed to solve the problem. Calculations of ITV on simplified models of irregularly shaped cells can lead to considerable deviations from ITV calculated on a more realistic model.

Electropermeabilization always occurred in those regions of the membrane where the absolute value of ITV was the highest, i.e. in the regions facing the electrodes.

Orientation of electric field considerably affects the distribution and the amplitude of ITV and consequently the extent of cell permeabilization. Cells oriented with their longer axis parallel to the field are more likely to be permeabilized than the same cells oriented perpendicularly to the field.

### **7.4 Measurements and calculations of induced transmembrane voltage and visualization of permeabilization on cell clusters**

Measurements of ITV on cell clusters showed that during the measurements performed with long pulses with moderate pulse amplitudes, cells in clusters behaved as one giant cell. One part of the cluster became depolarized while the other part was hyperpolarized. The measurements were in agreement with numerical calculations of ITV if cells in the cluster were modeled as electrically connected.

In contrast, during permeabilization, performed with short pulses with high amplitude, cells in clusters behaved as electrically insulated and were permeabilized individually. Observed fluorescence regions were in agreement with numerical calculations of ITV, but only if cells in clusters were modeled as electrically insulated.

### **7.4.1 Electroporation of dense cell suspensions**

Experiments performed on dense cell suspensions showed that increasing the cell density from  $10 \times 10^6$  cells/ml to  $400 \times 10^6$  cells/ml decreased the fraction of permeabilized cells by approximately 50%. This can largely be attributed to the changes in the local electric field, which lead to a decrease in the amplitude of the induced transmembrane voltage. Fluorescence of cells decreased even more than expected from the differences in the permeabilized cell fractions.

### **7.4.2 Kinetics of transmembrane transport of dye molecules after electroporation**

Electroporation with progressively increasing pulse amplitudes or pulse durations resulted in increased dye transport into cells. A sharp increase was observed milliseconds after the onset of a pulse, followed by a moderate additional fluorescence increase.

The dynamics of fluorescence increase during and after the pulse differed; the rate of increase of the fluorescence slowed down immediately after the pulse. Transport across permeabilized membrane was detected within 100  $\mu$ s after the onset of the pulse. At the same pulse parameters, molecular transport into confluent cells in monolayers was considerably lower than to suspended cells.

## **7.5 Guidelines for future work**

- Verifications of the results of RTV on cells in low conductivity media with measurements performed with other fluorescent dyes (e.g. DiBAC dye) and microelectrodes.
- Measurements of ITV at suprathreshold pulse amplitudes with a faster and more sensitive camera. With such a camera, which recently become available in our laboratory, and a calcium indicator Fluo3AM it would be possible to simultaneously measure the ITV and monitor the course of permeabilization.
- Measurements of ITV and monitoring of permeabilization on cell clusters with inhibited gap junctions. Comparison with results on noninhibited clusters.
- Upgrading the existing monolayer numerical model of a cell cluster to a multilayer model.
- Constructing a time dependent numerical model of voltage induction and permeabilization.
- Comparing the measurements of transport kinetics through permeabilized membrane with the existing theoretical models.



## **8 ORIGINAL SCIENTIFIC CONTRIBUTIONS**

Based on the results presented in this work, the author claims for recognition of the following original scientific contributions to the research area:

### **Measurements of resting transmembrane voltage on cells in different media**

Resting transmembrane voltage (RTV) was measured on different cells lines (CHO, B16F1 and BHK) and extracellular media with decreasing conductivities by using fluorescent dye TMRM. We showed that the amplitude of RTV is low and can be neglected in experiments involving electroporation. Deviations of measured RTV from the theoretically calculated values were found, especially in the case where cells were in low conductivity media.

### **Measurements of induced transmembrane voltage on single irregularly shaped cells and cell clusters**

Quantitative measurements of induced transmembrane voltage (ITV) on irregularly shaped cells and cell clusters are important for understanding the course of electroporation in tissues. So far, ITV was experimentally determined on spherical cells, while on irregularly shaped cells and cell clusters ITV was presented only qualitatively. With the means of potentiometric fluorescent dye di-8-ANEPPS and a system for dynamic cell imaging we were able to quantitatively determine the ITV. Measurements on single irregularly shaped cells showed that the absolute value of ITV is the highest in the regions of the membrane facing the electrodes. Measurements on cell clusters showed that cells in clusters behaved as one giant cell - one part of the cluster became depolarized while the other part was hyperpolarized.

### **Numerical calculations of induced transmembrane voltage on single irregularly shaped cells and cell clusters**

By using the finite element method we numerically calculated ITV on models of irregularly shaped cells and on models of clusters of two or four cells. Realistic models of irregularly shaped cells and clusters were constructed from their cross-section fluorescence images. This provided a possibility to determine the ITV on the same cells on which the experiment was carried out and enabled a direct comparison of the calculated and experimental results. We also showed how the cell membrane in the model can be replaced by a boundary condition, which efficiently reduces the number of elements of the mesh and consequently time needed to solve the problem.

## **Monitoring the course of electropermeabilization on single irregularly shaped cells and cell clusters**

The course of electropermeabilization was monitored by means of fluorescent dye Propidium Iodide on the same cells on which ITV was measured and calculated. In the region of the cell membrane where electropermeabilization occurs, the membrane becomes permeable also to dye molecules. This is indicated by the increase in fluorescence, which is first detected in the surroundings of the permeabilized area of the membrane. Comparison of measured and numerically calculated ITVs with observations of electropermeabilization confirmed that permeabilization occurs in those regions of the membrane where the absolute value of ITV is the highest, i.e. in the regions facing the electrodes. This approach also enabled us to determine the threshold value of ITV where permeabilization occurs. By monitoring the course of permeabilization of cell clusters, we found that cells in clusters behaved as electrically insulated and were permeabilized individually.

---

## 9 LIST OF REFERENCES

- Abidor I. G., Barbul A. I., Zhelev D. V., Doinov P., Bandrina I. N., Osipova E. M., and Sukharev S. I. Electrical properties of cell pellets and cell electrofusion in a centrifuge. *Biochim. Biophys. Acta.* 1152:207-218, 1993.
- Abidor I. G., Li L. H., and Hui S. W. Studies of cell pellets: II. Osmotic properties, electroporation, and related phenomena: membrane interactions. *Biophys. J.* 67:427-435, 1994.
- Alberts B., Bray D., Lewis J., Raff M., Roberts K., and Watson J. D. *Molecular Biology of the Cell*, 3<sup>rd</sup> ed., Garland Publishing, New York, 1994.
- Anderson W. M., Delinck D. L., Benninger L., Wood J. M., Smiley S. T., and Chen L. B. Cytotoxic effect of thiocarbocyanine dyes on human colon carcinoma cells and inhibition of bovine heart mitochondrial NADH-ubiquinone reductase activity via a rotenone-type mechanism by two of the dyes. *Biochem. Pharmacol.* 45:691-696, 1993.
- Babakov A. V., and Ermishkin L. N. Influence of electric field on the capacity of phospholipids membranes. *Nature.* 210:953-955, 1966.
- Baker P. F., Hodgkin A. L., and Ridgeway E. B. Depolarization and calcium entry in squid giant axons. *J. Physiol.* 218:709-755, 1971.
- Barnett A., and Weaver J. C. Electroporation: a unified, quantitative theory of reversible electrical breakdown and rupture. *Bioelectroch. Bioener.* 25:163-182, 1991.
- Bedlack R. S., Wei M. D., and Loew L. M. Localized membrane depolarizations and localized calcium influx during electric field-guided neurite growth. *Neuron.* 9:393-403, 1992.
- Bedlack R. S., Wei M. D., Fox S. H., Gross E., and Loew L. M. Distinct electric potentials in soma and neurite membranes. *Neuron.* 13:1187-1193, 1994.
- Benz R., Beckers F., and Zimmermann U. Reversible electrical breakdown of lipid bilayer membranes - charge-pulse relaxation study. *J. Membrane Biol.* 48:181-204, 1979.
- Benz R., and Zimmermann U. Relaxation studies on cell-membranes and lipid bilayers in the high electric-field range. *Bioelectroch. Bioener.* 7:723-739, 1980.
- Bier M., Hammer S. M., Canaday D. J., and Lee R. C. Kinetics of sealing for transient electropores in isolated mammalian skeletal muscle cells. *Bioelectromagnetics.* 20:194-201, 1999.
- Brink P. R., and Fan S. F. Patch clamp studies from membranes which contain gap junction channels. *Biophys. J.* 56:579-593, 1989.
- Brink P. R. Gap junction channel gating and permselectivity: their roles in co-ordinated tissue function. *Clin. Exp. Pharmacol. P.* 23:1041-1046, 1996.
- Brink P. R., Cronin K., and Ramanan S. V. Gap junctions in excitable cells. *J. Bioenerg. Biomembr.* 28:351-358, 1996.
- Bruzzone R., White T. W., and Paul D. L. Connections with connexins: The molecular basis of direct intercellular signaling. *Eur. J. Biochem.* 238:1-27, 1996.
- Buitenweg J. R., Rutten W. L., and Marani E. Geometry-based finite-element modeling of the electrical contact between a cultured neuron and a microelectrode. *IEEE T. Bio-Med. Eng.* 50:501-509, 2003.
- Canatella P. J., Karr J. F., Petros J. A., and Prausnitz M. R. Quantitative study of electroporation-mediated molecular uptake and cell viability. *Biophys. J.* 80:755-764, 2001.

## 9 REFERENCES

---

- Canatella P. J., Black M. M., Bonnicksen D. M., McKenna C., and Prausnitz M. R. Tissue electroporation: quantification and analysis of heterogeneous transport in multicellular environments. *Biophys. J.* 86:3260-3268, 2004.
- Chang D. C., and Reese T. S. Changes of membrane structure induced by electroporation as revealed by rapid-freezing electron microscopy, *Biophys. J.* 58:1-12, 1990.
- Chen L. B., and Smiley S. T. Probing mitochondrial membrane potential in living cells by a J-aggregate-forming dye. Fluorescent and luminescent probes for biological activity, Mason W. T., Ed., 1993.
- Cheng D. K. L., Tung L., and Sobie E. A. Nonuniform responses of transmembrane potential during electric field stimulation of single cardiac cells. *Am. J. Physiol.* 277:H351-H362, 1999.
- Chernomordik L. V., Sukharev S. I., Abidor I. G., and Chizmadzev Y. A. Breakdown of lipid bilayer membranes in an electric field. *Biochim. Biophys. Acta.* 736:203-213, 1983.
- Chernomordik L. V., Sukharev S. I., Popov S. V., Pastushenko V. F., Sokirko A. I., Abidor I. G., and Chizmadzev Y. A. The electrical breakdown of cell and lipid membranes: the similarity of phenomenologies. *Biochim. Biophys. Acta.* 902:360-373, 1987.
- Chiras D. D. Human biology, Health, Homeostasis, and the Environment, 4<sup>th</sup> ed. Jones and Bartlett Publishers, Boston, USA, 2002.
- Cohen L. B., Salzberg B. M., Davila H. V., Ross W. N., Landowne D., Waggoner A. S., and Wang C. H. Changes in axon fluorescence during activity - molecular probes of membrane-potential. *J. Membrane Biol.* 19: 1-36, 1974.
- Cole, K. Membranes, ions and impulses: A chapter of classical biophysics. Los Angeles, CA. University of California Press, 1968.
- Cone C. D. Jr. Unified theory on the basic mechanism of normal mitotic control and oncogenesis. *J. Theor. Biol.* 30:151-181, 1971.
- Čemažar M., Miklavčič D., Mir L. M., Belehradek J. Jr., Bonnay M., Fourcault D., and Serša G. Electrochemotherapy of tumours resistant to cisplatin: a study in a murine tumour model. *Eur. J. Cancer.* 37: 1166-1172, 2001.
- DeBruin K. A., and Krassowska W. Modeling electroporation in a single cell. II. Effects of ionic concentrations. *Biophys. J.* 77:1225-1233, 1999.
- Denk W., Delaney K. R., Gelperin A., Kleinfeld D., Strowbridge B. W., Tank D. W., and Yuste R. J. Anatomical and functional imaging of neurons using 2-photon laser scanning microscopy. *Neurosci. Methods.* 54:151-162, 1994.
- Djuzenova C. S., Zimmermann U., Frank H., Sukhorukov V. L., Richter E., and Fuhr G. Effect of medium conductivity and composition on the uptake of propidium iodide into electropermeabilized myeloma cells. *Biochim. Biophys. Acta.* 1284:143-152, 1996.
- Dragsten P. R., and Webb W. W. Mechanism of the membrane potential sensitivity of the fluorescent membrane probe merocyanine 540. *Biochemistry.* 17:5228-5240, 1978.
- Ehrenberg B., Farkas D. L., Fluhler E. N., Lojewska Z., and Loew L. M. Membrane-potential induced by external electric-field pulses can be followed with a potentiometric dye. *Biophys. J.* 51:833-837, 1987.
- Ehrenberg B., Montana V., Wei M. D., and Wuskell J. P. Membrane potential can be determined in individual cells from the Nernstian distribution of cationic dyes. *Biophys. J.*, 53:785-794, 1988.
- El-Fouly M., Trosko J. E., and Chang C. C. Scrape-loading and dye transfer. A rapid and simple technique to study gap junctional intercellular communication. *Exp. Cell Res.* 168:422-430, 1987.

- Epps D. E., Wolfe M. L., and Groppi V. Characterization of the steady-state and dynamic fluorescence properties of the potential-sensitive dye bis-(1,3-dibutylbarbituric acid) trimethine oxonol (DiBAC<sub>4</sub>(3)) in model systems and cells. *Chem. Phys. Lipids*. 69:137-150, 1994.
- Farkas D., Wei M., Febroriello P., Carson J. H., and Loew L. M. Simultaneous imaging of cell and mitochondrial membrane potentials. *Biophys. J.*, 56:1053-1069, 1989.
- Fear E. C., and Stuchly M. A. Biological cells with gap junctions in low-frequency electric fields. *IEEE T. Bio-Med. Eng.* 45:856-866, 1998a.
- Fear E. C., and Stuchly M. A. Modeling assemblies of biological cells exposed to electric fields. *IEEE T. Bio-Med. Eng.* 45:1259-1271, 1998b.
- Freeman S. A., Wang M. A., and Weaver J. C. Theory of electroporation for a planar bilayer membrane: predictions of the fractional aqueous area, change in capacitance and pore-pore separation. *Biophys. J.* 67:42-56, 1994.
- Gabriel B., and Teissie J. Direct observation in the milisecond time range of fluorescent molecule asymmetrical interaction with the electropermeabilized cell membrane. *Biophys. J.* 73:2630-2637, 1997.
- Gabriel B., and Teissie J. Fluorescence imaging in the millisecond time range of membrane electropermeabilisation of single cells using a rapid ultra-low-light intensifying detection system. *Eur. Biophys. J.* 27:291-298, 1998.
- Gabriel B., and Teissie J. Time courses of mammalian cell electropermeabilization observed by millisecond imaging of membrane property changes during the pulse. *Biophys. J.* 76:2158-2165, 1999.
- Gamper N., Stockand J. D., and Shapiro M. S. The use of Chinese hamster ovary (CHO) cells in the study of ion channels. *J. Pharmacol. Toxicol. Methods*. 51:177-185, 2005.
- Gascoyne P. R. C., Pethig R., Burt J. P. H., and Becker F. F. Membrane changes accompanying the induced differentiation of Friend murine erythroleukemia cells studied by dielectrophoresis. *Biochim. Biophys. Acta*. 1146:119-126, 1993.
- Gimsa J., and Wachner D. Analytical description of the transmembrane voltage induced on arbitrarily oriented ellipsoidal and cylindrical cells. *Biophys. J.* 81:1888-1896, 2001a.
- Gimsa J., and Wachner D. On the analytical description of transmembrane voltage induced on spheroidal cells with zero membrane conductance. *Eur. Biophys. J.* 30:463-466, 2001b.
- Glaser R. W., Leikin S. L., Chernomordik L. V., Pastushenko V. F., and Sokirko A. V. Reversible electrical breakdown of lipid bilayers: formation and evolution of pores. *Biochim. Biophys. Acta*. 940:275-287, 1988.
- Golzio M., Mora M. P., Raynaud C., Delteil C., Teissie J., and Rols M. P. Control by osmotic pressure of voltage-induced permeabilization and gene transfer in mammalian cells. *Biophys. J.* 74:3015-3022, 1998.
- Golzio M., Mazzolini L., Moller P., Rols M. P., and Teissie J. Inhibition of gene expression in mice muscle by in vivo electrically mediated siRNA delivery. *Gene Ther.* 12:246-251, 2005.
- Gowrishankar T. R., and Weaver J. C. An approach to electrical modeling of single and multiple cells. *Proc. Natl. Acad. Sci. USA*. 100:3203-3208, 2003.
- Grinvald A., Hildesheim R., Farber I. C., and Anglister L. Improved fluorescent-probes for the measurement of rapid changes. *Biophys. J.* 39: 301-308, 1982.
- Grinvald A., Fine A., Farber I. C., and Hildesheim R. Fluorescence monitoring of electrical responses from small neurons and their processes. *Biophys. J.* 42:195-198, 1983.
- Grinvald A., Frostig R. D., Lieke E., and Hildesheim R. Optical imaging of neuronal activity. *Physiol. Rev.* 68:1285-1366, 1988.

## 9 REFERENCES

---

- Gross D., Loew L. M., and Webb W. Optical imaging of cell membrane potential changes induced by applied electric fields. *Biophys. J.* 50:339-348, 1986.
- Hamill O. P., Marty A., Neher E., Sakmann B., and Sigworth F. J. Improved patch-clamp techniques for high-resolution current recording from cells and cell-free membrane patches. *Pflügers Archiv.* 391:85-100, 1981.
- Hamilton W. A., and Sale J. H. Effects of high electric field on microorganisms II. Mechanisms of action of the lethal effect. *Biochim. Biophys. Acta.* 148:789-800, 1967.
- Harris C. M., and Kell D. B. The radio-frequency dielectric properties of yeast cells measured with a rapid, automated, frequency-domain dielectric spectrometer. *Bioelectroch. Bioener.* 11:15-28, 1983.
- Hassan N., Chatterjee I., Publicover N. G., and Craviso G. L.. Mapping membrane-potential perturbations of chromaffin cells exposed to electric fields. *IEEE T. Plasma Sci.* 30:1516-1524, 2002.
- Hayashi Y., Zviman M. M., Brand J. G., Teeter J. H., and Restrepo D. Measurement of membrane potential and  $[Ca^{2+}]_i$  in cell ensembles: Application to the study of glutamate taste buds in mice. *Biophys. J.* 71:1057-1070, 1996.
- Heller R., Gilbert R., and Jaroszeski M. J. Clinical applications of electrochemotherapy. *Adv. Drug. Deliver Rev.* 35:119-129, 1999.
- Hibino M., Shigemori M., Itoh H., Nagayama K., and Kinosita K. Jr. Membrane conductance of an electroporated cell analyzed by submicrosecond imaging of transmembrane potential. *Biophys. J.* 59:209-220, 1991.
- Hibino M., Itoh H., and Kinosita K. Jr. Time courses of cell electroporation as revealed by submicrosecond imaging of transmembrane potential. *Biophys. J.* 64:1789-1800, 1993.
- Hodgkin A. L., and Katz B. The effect of sodium ions on the electrical activity of the giant axon of the squid. *J. Physiol.* 108:37-77, 1949.
- Hodgkin, A. The ionic basis of electrical activity in nerve and muscle. *Biol. Rev.* 26:339-409, 1951.
- Huang, X., Nguyen D., Greve D. W., and Domach M. M. Simulation of microelectrode impedance changes due to cell growth. *IEEE Sensors J.* 4:576-583, 2004.
- Johnson L. V., Walsh M. L., Bockus B. J., and Chen L. B. Monitoring of relative mitochondrial-membrane potential in living cells by fluorescence microscopy. *J. Cell Biol.* 88:526-535, 1981.
- Johnson P. L., Smith W., Baynham T. C., and Knisley S. B. Errors caused by combination of di-4 ANEPPS and Fluo 3/4 for simultaneous measurements of transmembrane potentials and intracellular calcium. *Ann. Biomed. Eng.* 27:563-571, 1999.
- Kakorin S., Stoylov S. P., and Neumann E. Electrooptics of membrane electroporation in diphenylhexatriene-doped lipid bilayer vesicles. *Biophys. Chem.* 58:109-116, 1996.
- Kao W. Y., Davis C. E., Kim Y. I., and Beach J. M. Fluorescence emission spectral shift measurements of membrane potential in single cells. *Biophys. J.* 81:1163-1170, 2001.
- Kasson P. M., and Pande V. S. Molecular dynamics simulation of lipid reorientation at bilayer edges. *Biophys. J.* 86:3744-3749, 2004.
- Kinosita K., and Tsong T. Y. Formation and resealing of pores of controlled sizes in human erythrocyte membrane. *Nature.* 268:438-441, 1977.
- Klenchin V. A., Sukharev S. I., Serov S. M., Chernomordik L. V., and Chizmadzev Y. A. Electrically induced DNA uptake by cells is a fast process involving DNA electrophoresis. *Biophys. J.* 60:804-811, 1991.

- Knisley S. B., Blitchington T. F., Hill B. C., Grant A. O., Smith W. M., Pilkington T. C., and Ideker R. E. Optical measurements of transmembrane potential changes during electric field stimulation of ventricular cells. *Circ. Res.* 72:255-268, 1993.
- Knisley S. B., Justice R. K., Kong W., and Johnson P. L. Ratiometry of transmembrane voltage-sensitive fluorescent dye emission in hearts. *Am. J. Physiol. Heart Circ. Physiol.* 279:1421-1433, 2000.
- Kotnik T., Bobanović F., and Miklavčič D. Sensitivity of transmembrane voltage induced by applied electric fields – a theoretical analysis. *Bioelectroch. Bioener.* 43:285-291, 1997.
- Kotnik T., Miklavčič D., and Slivnik T. Time course of transmembrane voltage induced by time-varying electric fields – a method for theoretical analysis and its application. *Bioelectroch. Bioener.* 45:3-16, 1998.
- Kotnik T., and Miklavčič D. Analytical description of transmembrane voltage induced by electric fields on spheroidal cells. *Biophys. J.* 79:670-679, 2000a.
- Kotnik, T., and Miklavčič D. Second-order model of membrane electric field induced by alternating external electric fields. *IEEE T. Bio-Med. Eng.* 47:1074-1081, 2000b.
- Kotnik T., Mir L. M., Flisar K., Puc M., and Miklavčič D. Cell membrane electropermeabilization by symmetrical bipolar rectangular pulses. Part I. Increased efficiency of permeabilization. *Bioelectrochemistry* 54:83-90, 2001.
- Kotnik T., Pucihar G., Reberšek M., Mir L. M., and Miklavčič D. Role of pulse shape in cell membrane electropermeabilization. *Biochim. Biophys. Acta.* 1614:193–200, 2003.
- Kumar A., Gudi S. R., Gokhale S. M., Bhakuni V., and Gupta C. M. Heat-induced alterations in monkey erythrocyte membrane phospholipid organization and skeletal protein structure and interactions. *Biochim. Biophys. Acta.* 1030:269-278, 1990.
- Kumar N. M., and Gilula N. B. The gap junction communication channel. *Cell.* 84:381-388, 1996.
- Leontiadou H., Mark A. E., and Marrink S. J. Molecular dynamics simulations of hydrophilic pores in lipid bilayers. *Biophys. J.* 86:2156–2164, 2004.
- Lezzi M. Differential gene activation in isolated chromosomes. *Int. Rev. Cytol.* 29:127-168, 1970.
- Ling, G. and R. W. Gerard. The normal membrane potential of frog sartorius fibers. *J. Cell. Comp. Physiol.* 34:383-396, 1949.
- Loew L. M., Bonneville G. W., Scully S., Surow J., Hassner A., and Alexanian V. Design of electrochromic probes of membrane-potential. *Biophys. J.* 21: 206, 1978.
- Loew L. M., Scully S., and Waggoner A. S. Evidence for a charge-shift electrochromic mechanism in a probe of membrane-potential. *Nature.* 281:497-499, 1979.
- Loew L. M., Cohen L. B., Salzberg B. M., Obaid A. L., and Bezanilla F. Charge-shift probes of membrane-potential - characterization of aminostyrylpyridinium dyes on the squid giant-axon. *Biophys. J.* 47: 71-77, 1985.
- Loew L. M. Voltage sensitive dyes: Measurement of membrane potentials induced by DC and AC electric fields. *Bioelectromagnetics.* 1:179-189, 1992.
- Loewenstein W. Junctional intercellular communication: The cell to cell membrane channel. *Physiol. Rev.* 61:829-913, 1981.
- Lojewska Z., Franks D. L., Ehrenberg B., and Loew L. M. Analysis of the effect of medium and membrane conductance on the amplitude and kinetics of membrane potentials induced by externally applied electric fields. *Biophys. J.* 56:121-128, 1989.

## 9 REFERENCES

---

- Marino A. A., Kolomytkin O. V., and Frilot C. Extracellular currents alter gap junction intercellular communication in synovial fibroblasts. *Bioelectromagnetics*. 24:199-205, 2003.
- McDonald T. F., Sachs H. G., and Orr C. W. M. External potassium and baby hamster kidney cells: intracellular ions, ATP, DNA synthesis and membrane potential. *Dev. Biol.* 28:290-303, 1972.
- Mehrle W., Hampp R., and Zimmermann U. Electric pulse induced membrane permeabilization - spatial orientation and kinetics of solute efflux in freely suspended and dielectrophoretically aligned plant mesophyll protoplasts. *Biochim. Biophys. Acta.* 978:267-275, 1989.
- Miklavčič D., Šemrov D., Mekid H., and Mir L. M. A validated model of in vivo electric field distribution in tissues for electrochemotherapy and for DNA electrotransfer for gene therapy. *Biochim. Biophys. Acta.* 1523:73-83, 2000.
- Miklavčič D., Pucihar G., Pavlovec M., Ribarič S., Mali M., Maček-Lebar A., Petkovšek M., Nastran J., Kranjc S., Čemažar M., and Serša G. The effect of high frequency electric pulses on muscle contractions and antitumor efficiency in vivo for a potential use in clinical electrochemotherapy. *Bioelectrochemistry*. 65:121-128, 2005.
- Miller C. E., and Henriquez C. S. Three-dimensional finite element solution for biopotentials: erythrocyte in an applied field. *IEEE T. Bio-Med. Eng.* 35:712-718, 1988.
- Mir L. M., Banoun H., and Paoletti C. Introduction of definite amounts of nonpermeant molecules into living cells after electroporation - direct access to the cytosol. *Exp. Cell Res.* 175:15-25, 1988.
- Mir L. M., Glass L. F., Serša G., Teissié J., Domenge C., Miklavčič D., Jaroszeski M. J., Orłowski S., Reintgen D. S., Rudolf Z., Belehradec M., Gilbert R., Rols M. P., Belehradec J., Bachaud J. M., DeConti R., Štabuc B., Čemažar M., Coninx P., and Heller R. Effective treatment of cutaneous and subcutaneous malignant tumours by electrochemotherapy. *Brit. J. Cancer.* 77: 2336-2342, 1998.
- Mir L. M., and Orłowski S. Mechanisms of electrochemotherapy. *Adv. Drug Deliver Rev.* 35:107-118, 1999.
- Montana V., Farkas D. L., and Loew L. M. Dual-wavelength ratiometric fluorescence measurements of membrane-potential. *Biochemistry* 28:4536-4539, 1989.
- Neher E., and Sakmann B. Single-channel currents recorded from membrane of denervated frog muscle fibres. *Nature.* 260:799-802, 1976.
- Neumann E., and Rosenheck K. Permeability changes induced by electric impulses in vesicular membranes. *J. Membrane Biol.* 10:279-290, 1972.
- Neumann E., Kakorin S., and Toensing K. Fundamentals of electroporative delivery of drugs and genes. *Bioelectroch. Bioener.* 48:3-16, 1999.
- Niemtzow R. C. Transmembrane potentials and characteristics of immune and tumor cells. CRC Press, Florida, USA, 1985.
- Novo D., Perlmutter N. G., Hunt R. H., and Shapiro H. M. Accurate flow cytometric membrane potential measurement in bacteria using diethyloxycarbocyanine and a ratiometric technique. *Cytometry.* 35:55-63, 1999.
- Pavlin M., Pavšelj N., and Miklavčič D. Dependence of induced transmembrane potential on cell density, arrangement, and cell position inside a cell system. *IEEE T. Bio-Med. Eng.* 49:605-612, 2002.
- Pavlin M., Kandušer M., Reberšek M., Pucihar G., Hart F. X., Magjarević R., and Miklavčič D. Effect of cell electroporation on the conductivity of a cell suspension. *Biophys. J.* 88:4378-4390, 2005.
- Pavšelj N., Bregar Z., Cukjati D., Batiuskaite D., Mir L. M., and Miklavčič D. The course of tissue permeabilization studied on a mathematical model of a subcutaneous tumor in small animals. *IEEE T. Bio-Med. Eng.* 52:1373-1381, 2005.
- Potapova T. V., Aslanidi K. B., and Boitzova L. Ju. Energy transfer via cell-to-cell junctions. *FEBS Lett.* 262:67-71, 1990.

- Prausnitz M. R., Milano C. D., Gimm J. A., Langer R., and Weaver J. C. Quantitative study of molecular-transport due to electroporation - uptake of bovine serum-albumin by erythrocyte-ghosts. *Biophys. J.* 66:1522-1530, 1994.
- Pucihar G., Kotnik T., Kandušer M., and Miklavčič D. The influence of medium conductivity on electropermeabilization and survival of cells in vitro. *Bioelectrochemistry.* 54:107-115, 2001.
- Pucihar G., Mir L. M., and Miklavčič D. The effect of pulse repetition frequency on the uptake into electropermeabilized cells in vitro with possible applications in electrochemotherapy. *Bioelectrochemistry.* 57:167-172, 2002.
- Pucihar G., Kotnik T., Valič B., and Miklavčič D. Numerical modeling of induced transmembrane voltage induced on irregularly shaped cells. *Ann. Biomed. Eng.*, 34:642-652, 2006.
- Reers M., Smith T. W., and Chen L. B. J-aggregate formation of a carbocyanine as a quantitative fluorescent indicator of membrane-potential. *Biochemistry.* 30:4480-4486, 1991.
- Remani P., Ostapenko V. V., Akagi K., Bhattathiri V. N., Nair M. K., and Tanaka Y. Relation of transmembrane potential to cell survival following hyperthermia in HeLa cells. *Cancer Lett.* 144:117-123, 1999.
- Riemann F., Zimmermann U., and Pilwat G. Release and uptake of hemoglobin and ions in red blood-cells induced by dielectric-breakdown. *Biochim. Biophys. Acta.* 394:449-462, 1975.
- Rols M. P., and Teissié J. Modulation of electrically induced permeabilization and fusion of Chinese hamster ovary cells by osmotic pressure. *Biochemistry.* 29:4561-4567, 1990.
- Rols M. P., and Teissié J. Experimental evidence for the involvement of the cytoskeleton in mammalian cell electropermeabilization. *Biochim. Biophys. Acta.* 1111:45-50, 1992.
- Rols M. P., Delteil C., Serin G., and Teissié J. Temperature effects on electrotransfection of mammalian cells. *Nucleic Acids Res.* 22:540, 1994.
- Rols M. P., and J. Teissié. Electropermeabilization of mammalian cells to macromolecules: control by pulse duration. *Biophys. J.* 75:1415-1423, 1998.
- Rols M. P., Delteil C., Golzio M., and Teissié J. Control by ATP and ADP of voltage-induced mammalian-cell-membrane permeabilization, gene transfer and resulting expression. *Eur. J. Biochem.* 254:382-388, 1998.
- Sachs H. G., Stambrook P. J., and Ebert J. D. Changes in membrane potential during the cell cycle. *Exp. Cell Res.* 83:362-366, 1974.
- Sale A. J. H., and Hamilton W. A. Effects of high electric fields on microorganisms. I. Killing of bacteria and yeasts. *Biophys. Biochim. Acta.* 148:781-800, 1967.
- Sale J. H., and Hamilton W. A. Effects of high electric field on microorganisms III. Lyses of erythrocytes and protoplasts. *Biophys. Biochim. Acta.* 163:37-43, 1968.
- Scaduto R. C., and Grotyohann L. W. Measurement of mitochondrial membrane potential using fluorescent rhodamine derivatives. *Biophys. J.* 76:469-477, 1999.
- Schmeer M., Seipp T., Pliquett U., Kakorin S., and Neumann E. Mechanism for the conductivity changes caused by membrane electroporation of CHO cell-pellets. *PCCP.* 6:5564-5574, 2004.
- Schwan H. P. Electrical properties of tissue and cell suspensions. *Adv. Biol. Med. Phys.* 5:147-209, 1957.
- Serša G., Štabuc B., Čemažar M., Miklavčič D., and Rudolf Z. Electrochemotherapy with cisplatin: the systemic antitumour effectiveness of cisplatin can be potentiated locally by the application of electric pulses in the treatment of malignant melanoma skin metastases. *Melanoma Res.* 10:381-385, 2000.
- Serša G., Čemažar M., and Rudolf Z. Electrochemotherapy: advantages and drawbacks in treatment of cancer patients. *Cancer Ther.* 1:133-142, 2003.

## 9 REFERENCES

---

- Shapiro H. M. Membrane potential estimation by flow cytometry. *Methods*. 21:271-279, 2000.
- Sims P. J., Waggoner A. S., Wang C. H., and Hoffman J. F. Studies on the mechanism by which cyanine dyes measure membrane potential in red blood cells and phosphatidylcholine vesicles. *Biochemistry*. 13:3315-3330, 1974.
- Smiley S. T., Reers M., Mottolahartshorn C., Lin M., Chen A., Smith T. W., Steele G. D., and Chen L. B. Intracellular heterogeneity in mitochondrial-membrane potentials revealed by a J-aggregate-forming lipophilic cation JC-1. *Proc. Natl. Acad. Sci. USA*. 88:3671-3675, 1991.
- Smith J. C., and Chance B. Kinetics of the potential-sensitive extrinsic probe oxonol VI in beef heart submitochondrial particles. *J. Membrane Biol.* 46:255-282, 1979.
- Somiari S., Malone J. G., Drabick J. J., Gilbert R. A., Heller R., Jaroszeski M. J., and Malone R. W. Theory and in vivo application of electroporative gene delivery. *Mol. Ther.* 2:178-187, 2000.
- Stambrook P. J., Sachs H. G., and Ebert J. D. The effect of potassium on the cell membrane potential and the passage of synchronized cells through the cell cycle. *J. Cell. Physiol.* 85:283-292, 1974.
- Stämpfli R. Reversible electrical breakdown of the excitable membrane of a Ranvier node. *An. Acad. Bras. Scienc.* 30:57-63, 1958.
- Stewart D. A., Gowrishankar T. R., and Weaver J. C. Transport lattice approach to describing cell electroporation: use of a local asymptotic model. *IEEE T. Plasma Sci.* 32:1696-1708, 2004.
- Stillwell W., Wassall S. R., Dumauval A. C., Ehringer W. D., Browning C. W., and Jenks L. J. Use of merocyanine (MC540) in quantifying lipid domains and packing in phospholipid vesicles and tumor cells. *Biochim. Biophys. Acta*. 1146:136-144, 1993.
- Sukharev S. I., Klenchin V. A., Serov S. M., Chernomordik L. V., and Chizmadzhev Y. A. Electroporation and electrophoretic DNA transfer into cells. The effect of DNA interaction with electropores. *Biophys. J.* 63:1320-1327, 1992.
- Susil R., Šemrov D., and Miklavčič D. Electric field induced transmembrane potential depends on cell density and organization. *Electro. Magnetobiol.* 17:391-399, 1998.
- Šatkauskas S., Bureau M. F., Puc M., Mahfoudi A., Scherman D., Miklavčič D., and Mir L. M. Mechanisms of in vitro DNA electrotransfer: Respective combination of cell electroporation and DNA electrophoresis. *Mol. Ther.* 5:1-7, 2002.
- Šatkauskas S., André F., Bureau M. F., Scherman D., Miklavčič D., and Mir L. M. Electrophoretic component of electric pulses determines the efficacy of in vivo DNA electrotransfer. *Hum. Gen. Ther.* 16:1194-1201, 2005.
- Šel D., Cukjati D., Batiuskaite D., Slivnik T., Mir L. M., and Miklavčič D. Sequential finite element model of tissue electroporation. *IEEE T. Bio-Med. Eng.* 52:816-827, 2005.
- Teissié J., and Rols M. P. An experimental evaluation of the critical potential difference inducing cell membrane electroporation. *Biophys. J.* 65:409-413, 1993.
- Teissié J., Eynard N., Gabriel B., and Rols M. P. Electroporation of cell membranes. *Adv. Drug Deliver Rev.* 35:3-19, 1999.
- Tekle E., Astumian R. D., and Chock P. B. Electroporation by using bipolar oscillating electric-field - an improved method for DNA transfection of NIH 3T3 cells. *Proc. Natl. Acad. Sci. USA*. 88:4230-4234, 1991.
- Tekle E., Astumian R. D., and Chock P. B. Selective and asymmetric molecular-transport across electroporated cell-membranes. *Proc. Natl. Acad. Sci. USA*. 91:11512-11516, 1994.
- Tieleman D. P., Leontiadou H., Mark A. E., and Marrink S. J. Simulation of pore formation in lipid bilayer by mechanical stress and electric fields. *J. Am. Chem. Soc.* 125:6382-6383, 2003.

- Tsong, T.Y. Electroporation of cell membranes. *Biophys. J.* 60:297-306, 1991.
- Valič, B., Golzio M., Pavlin M., Schatz A., Faurie C., Gabriel B., Teissié J., Rols M. P., and Miklavčič D. Effect of electric field induced transmembrane potential on spheroidal cells: theory and experiment. *Eur. Biophys. J.* 32:519-528, 2003.
- Valič B., Pavlin M., and Miklavčič D. The effect of resting transmembrane voltage on cell electropermeabilization: a numerical analysis. *Bioelectrochem.* 63:311-315, 2004.
- VanDuijn B., Ypey D. L., and Vandermolen L. G. Electrophysiological properties of dictyostelium derived from membrane-potential measurements with microelectrodes. *J. Membrane Biol.* 106:123-134, 1988.
- Vodovnik L., Miklavčič D., and Serša G. Modified cell proliferation due to electrical currents. *Med. Biol. Eng. Comput.* 30:CE21-CE28, 1992.
- Waggoner A. S. Dye indicators of membrane potential. *Ann. Rev. Biophys. Bioeng.* 8:47-68, 1979.
- Weaver J. C., and Chizmadzhev Y. A. Theory of electroporation: a review. *Bioelectroch. Bioener.* 41:135-160, 1996.
- Weaver J. C., and Mintzer R. A. Decreased bilayer stability due to transmembrane potentials. *Phys Lett.* 86:57-59, 1981.
- Williams J. Origin of transmembrane potentials in non-excitable cells. *J. Theor. Biol.* 28:287-296, 1970.
- Xie T. D., and Tsong T. Y. Study of mechanisms of electric field-induced DNA transfection. III. Electric parameters and other conditions for effective transfection. *Biophys. J.* 63:28-34, 1992.

#### Internet pages

<http://pen2.igc.gulbenkian.pt/cftr/vr/physiology.html>

(microelectrodes)

<http://www.probes.com>

(fluorescent probes)

<http://www.csupomona.edu/~seskandari/Documents/The%20Membrane%20Potential%20-%20Simplified.pdf>

(resting membrane voltage)

<http://www.nervana.montana.edu/academics/100q/biophysics/clamps.pdf>

(voltage and current clamps)

[http://www.warneronline.com/pdf/tutorials/sigworth\\_clamp.pdf](http://www.warneronline.com/pdf/tutorials/sigworth_clamp.pdf)

(voltage nad current clamps)

## 10 APPENDIX

### *Paper 1*

#### **Role of pulse shape in cell membrane electropermeabilization**

T. Kotnik<sup>a</sup>, **G. Pucihar**<sup>a</sup>, M. Reberšek<sup>a</sup>, D. Miklavčič<sup>a</sup>, L.M. Mir<sup>b</sup>

<sup>a</sup> Faculty of Electrical Engineering, University of Ljubljana, SI-1000 Ljubljana, Slovenia

<sup>b</sup> Laboratory of Vectorogy and Gene Transfer, Institute Gustave-Roussy, UMR 8121 CNRS, 39 rue  
C. Desmoulins, F-94805 Villejuif, Cedex, France

#### **Abstract**

The role of the amplitude, number, and duration of unipolar rectangular electric pulses in cell membrane electropermeabilization in vitro has been the subject of several studies. With respect to unipolar rectangular pulses, an improved efficiency has been reported for several modifications of the pulse shape: separate bipolar pulses, continuous bipolar waveforms, and sine-modulated pulses. In this paper, we present the results of a systematic study of the role of pulse shape in permeabilization, cell death, and molecular uptake. We have first compared the efficiency of 1-ms unipolar pulses with rise- and falltimes ranging from 2 to 100 As, observing no statistically significant difference. We then compared the efficiency of triangular, sine, and rectangular bipolar pulses, and finally the efficiency of sine-modulated unipolar pulses with different percentages of modulation. We show that the results of these experiments can be explained on the basis of the time during which the pulse amplitude exceeds a certain critical value.

# Role of pulse shape in cell membrane electroporation

T. Kotnik<sup>a</sup>, G. Pucihar<sup>a</sup>, M. Reberšek<sup>a</sup>, D. Miklavčič<sup>a</sup>, L.M. Mir<sup>b,\*</sup>

<sup>a</sup>Faculty of Electrical Engineering, University of Ljubljana, SI-1000 Ljubljana, Slovenia

<sup>b</sup>Laboratory of Vectorology and Gene Transfer, Institute Gustave-Roussy, UMR 8121 CNRS, 39 rue C. Desmoulins, F-94805 Villejuif, Cedex, France

Received 19 February 2003; received in revised form 20 May 2003; accepted 26 May 2003

## Abstract

The role of the amplitude, number, and duration of unipolar rectangular electric pulses in cell membrane electroporation *in vitro* has been the subject of several studies. With respect to unipolar rectangular pulses, an improved efficiency has been reported for several modifications of the pulse shape: separate bipolar pulses, continuous bipolar waveforms, and sine-modulated pulses. In this paper, we present the results of a systematic study of the role of pulse shape in permeabilization, cell death, and molecular uptake. We have first compared the efficiency of 1-ms unipolar pulses with rise- and falltimes ranging from 2 to 100  $\mu$ s, observing no statistically significant difference. We then compared the efficiency of triangular, sine, and rectangular bipolar pulses, and finally the efficiency of sine-modulated unipolar pulses with different percentages of modulation. We show that the results of these experiments can be explained on the basis of the time during which the pulse amplitude exceeds a certain critical value.

© 2003 Elsevier B.V. All rights reserved.

**Keywords:** Electroporation; Electroporation; Pulse shape; Cell survival; Cell membrane permeability; Molecular uptake

## 1. Introduction

Electroporation (also termed electroporation) is an effective method of internalization of various molecules into biological cells, with an increasing number of applications in oncology [1,2], genetics [3], immunology [4], and cell biology [5,6]. In parallel with the practical use of the method continues the quest for understanding the underlying mechanisms of the phenomenon [3,7–12].

The efficiency of electroporation *in vitro* depends on various physical and chemical parameters, such as the molecular composition of the membrane [13,14] and osmotic pressure [15], but above all, on the parameters of electric pulses. Investigations of the role of the amplitude, number, and duration of unipolar rectangular pulses have been the subject of several comprehensive studies [16–20]. In addition, at least two studies have focused on a comparison of the efficiency of unipolar and bipolar rectangular pulses *in vitro*. Tekle et al. [21] compared continuous unipolar and bipolar 60-kHz rectangular waves of 400  $\mu$ s total duration, and obtained a significantly better DNA

transfection with a bipolar wave. Because electroporation is usually not performed with continuous waves, but with sequences (trains) of separate pulses [18,22–25], our group compared the efficiency of unipolar and symmetrical bipolar rectangular pulses, in both cases delivering eight 1-ms pulses at 1-s intervals [26]. With bipolar pulses, permeabilization was achieved at lower pulse amplitudes and molecular uptake was significantly higher, while the pulse amplitude leading to cell death was practically unaltered. We also demonstrated that electrolytic contamination caused by the release of metal ions from the electrodes can be reduced considerably by the use of bipolar instead of unipolar pulses [27]. Even before these studies were published, bipolar pulses were applied successfully in electrochemotherapy [28], as well as for DNA transfection *in vivo* in mice [29,30].

Unlike the role of the amplitude, number, duration, and polarity of pulses, a hypothetical role of pulse dynamics, or the “pulse shape,” has not yet been a subject to a broader systematic investigation.<sup>1</sup> One of the reasons for this is the absence of commercially available programmable genera-

\* Corresponding author. Tel.: +33-1-42-11-47-92; fax: +33-1-42-11-52-45.

E-mail address: [luismir@igr.fr](mailto:luismir@igr.fr) (L.M. Mir).

<sup>1</sup> Unipolar and bipolar pulses should not be conceived as having different “shapes,” since a bipolar pulse is a sequence of two consecutive, oppositely polarized unipolar pulses.

tors of high-voltage waveforms, which confines these studies to the laboratories with access to custom-designed electronic equipment. Kinoshita and Tsong [31] used linearly increasing electric fields with rates of increase from 12.5 V/cm per microsecond up to 50 V/cm per microsecond for permeabilization of erythrocytes, and concluded that field intensity at which permeabilization occurs is not affected by this rate of increase. Chang et al. reported an improved efficiency of cell permeabilization and fusion [32], as well as gene transfection [33] when a sine wave (40 kHz–1 MHz) was superimposed to a rectangular pulse. Xie and Tsong [34] compared rectangular, sine, and triangular waves with extremely long durations (1–100 s) and relatively low amplitudes (voltage-to-distance ratio 50–200 V/cm), obtaining the most efficient transfection for rectangular, less for sine, and the least for triangular waves. It is, however, uncertain (as the authors themselves agree) whether the transfection was achieved due to permeabilization itself, or rather due to subsequent electrophoresis and electroosmosis caused by the very long pulse duration. Moreover, Šatkauskas et al. [35] recently clearly demonstrated that, even though prior electroporation is necessary, efficiency of DNA-electrotransfer in skeletal muscle depends critically on the electrophoretic component of the pulses.

In this paper, we present the results of a systematic study of the role of pulse shape in cell permeabilization, cell death, and uptake of exogenous molecules. Using custom-designed electronic equipment developed in our laboratory, we compared the efficiency of: (i) unipolar rectangular (trapezoidal) pulses with different rise- and falltimes, (ii) bipolar rectangular, sinusoidal, and triangular pulses, and (iii) unipolar unmodulated and sine-modulated rectangular pulses. Part (i) of the study aimed at an investigation of possible role of the first derivative of the pulse amplitude in electroporation. Parts (ii) and (iii) then focused on the influence of other parameters of the pulse shape, and on the search of a plausible explanation of the obtained results, as well as of the related results published in previous studies [31–34].

## 2. Materials and methods

### 2.1. Cells

DC3F cells, a line of spontaneously transformed Chinese hamster fibroblasts [36], were grown in monolayers at 37 °C and 5% CO<sub>2</sub> (Universal Water Jacketed Incubator, Forma Scientific, Marietta, OH, USA). One hundred fifty-square centimeter flasks were used for general cultivation, and 60-mm petri dishes were used for cloning efficiency assays (both from TPP, Trasadingen, Switzerland). The culture medium consisted of Eagle minimum essential medium EMEM 41090 supplemented with 10% fetal bovine serum (both from Life Technologies, Rockville, MD, USA), 100 U/ml of penicillin and 125 µg/ml of

streptomycin (both from Sarbach/Solvay Pharma, Brussels, Belgium).

### 2.2. Exposure to electric pulses

To allow for comparison with experiments using different electrode distances, the intensity of the pulses was characterized by the voltage-to-distance ratio (VDR), which was calculated as the voltage delivered to the electrodes divided by the distance between them. Since for stainless steel electrodes, the voltage drop at the electrode–electrolyte interface is very small [37], and the dimensions of the droplet in the plane parallel to the electrode plates were several times larger than the distance between the electrodes, the VDR is also a good estimate of the electric field within the droplet.

After trypsination with trypsin–EDTA (Life Technologies), cells were centrifuged for 5 min at 1000 rpm in a C312 centrifuge (Jouan, St. Herblain, France) and resuspended at  $2 \times 10^7$  cells/ml in the electroporation medium. Spinner minimum essential medium SMEM 21385 (Life Technologies) with electrical conductivity of 1.6 S/m was used for trapezoidal (unipolar rectangular with adjustable rise- and falltimes), bipolar rectangular, bipolar sine, and bipolar triangular pulses. These pulses were generated by an AFG 310 programmable function generator (Tektronix, Wilsonville, OR, USA), amplified with a bipolar amplifier built in the Laboratory of Biocybernetics at the Faculty of Electrical Engineering of the University of Ljubljana (the device is described in detail in Ref. [38]). The medium consisting of 250 mM sucrose, 10 mM phosphate buffer, and 1 mM MgCl<sub>2</sub> (made according to Ref. [39]) with electrical conductivity of 0.15 S/m was used for the sine-modulated pulses, which were generated by a custom-designed high-voltage waveform generator built in the same laboratory. In all experiments, the pulses were delivered through a pair of flat stainless steel electrodes 2 mm apart, between which a 50-µl droplet of the cell suspension was placed.

### 2.3. Determination of cell survival

The percentage of surviving cells was determined by their cloning efficiency after pulsation in the electroporation medium. Subsequent to pulsation, the cells were incubated for 10 min at room temperature and then diluted by the addition of 950 µl of SMEM to prevent drying. After additional 30 min, cells were diluted in the culture medium to 100 cells/ml, and 4 ml of suspension was transferred into each 60-mm petri dish where the cells were grown for 5 days. Cells were then fixed for 15 min with 100% ethanol (Carlo Erba Reagenti, Milan, Italy) and consecutively stained for 15 min with 1% crystal violet (Sigma, St. Louis, MO, USA). Clone colonies were counted under a light microscope (Leica, Wetzlar, Germany) and normalized to the control (cells not exposed to electric pulses) to obtain the percentage of surviving cells.

#### 2.4. Determination of cell electropermeabilization

The percentage of electropermeabilized cells was determined by their cloning efficiency after pulsation in the electropermeabilization medium containing 5 nM bleomycin (Laboratoires Roger Bellon, Neuilly-Sur-Seine, France). An intact membrane is impermeable to bleomycin, and while at 5 nM external concentration bleomycin has no effect on nonpermeabilized cells, it causes the death of electropermeabilized cells [40]. This method is highly selective and accurate, as well as affordable.

Subsequent to pulsation, the cells were incubated for 10 min at room temperature and then diluted by the addition of 950  $\mu$ l of SMEM. After additional 30 min, cells were diluted in the culture medium, grown for 5 days and then fixed and stained as described above. Clone colonies were counted and normalized to the control (unpulsed cells, 5 nM bleomycin) to obtain the percentage of cells surviving the exposure to electric pulses in suspension with 5 nM bleomycin. By subtracting this percentage from 100%, the percentage of permeabilized cells was obtained.

#### 2.5. Determination of uptake of exogenous molecules

Uptake of exogenous molecules was determined by the cell fluorescence after pulsation in the electropermeabilization medium containing 1 mM lucifer yellow (Sigma), a nonpermeant fluorescent dye. Subsequent to pulsation, cells were incubated for 10 min at room temperature and then diluted by the addition of 950  $\mu$ l of SMEM. After additional 30 min, cells were diluted in 5 ml of phosphate buffer saline (PBS, Life Technologies), and extracellular lucifer yellow was then washed away by two consecutive centrifugations and resuspensions in PBS. Each centrifugation was performed for 5 min at 1000 rpm, which causes no loss of cell viability. Cells were then broken down by ultrasonication (Sonifier 250, Branson Ultrasonics, Danbury, CT, USA) and fluorescence was measured in arbitrary units on a spectrofluorometer (SFM 25, BioTek, Winooski, VT, USA). Excitation was set at 418 nm wavelength and emission was detected at 525 nm.

At pulse amplitudes which lead to the death of practically all the cells in the population, the detected uptake of lucifer yellow remains somewhat above the background (control) level. This is due to the fact that dead cells are not only those that burst or decompose due to the intense permeabilization, but also those that initially reseal, yet due to the loss of their internal constituents have no ability to form clones. Such “cellular ghosts” retain some lucifer yellow, and this results in an apparent discrepancy between the survival and uptake at high pulse amplitudes (see Figs. 2, 4, and 7).

#### 2.6. Treatment of experimental data

All experiments were repeated three times at intervals of several days or more. For each experimental point, mean

and standard deviation were determined. Voltage-to-distance ratio was used as an estimate of electric field strength of the pulses. The percentages of surviving and permeabilized cells as functions of the applied voltage-to-distance ratio (VDR) were each fitted by a two-parameter sigmoidal curve,

$$y(x) = \frac{100\%}{1 + \exp[(x_c - x)/b]},$$

where  $x$  is the VDR,  $y$  is the percentage of cells,  $x_c$  is the  $x$ -value corresponding to  $y=50\%$ , and  $b$  determines the slope of the sigmoid curve. The VDR leading to the permeabilization of 50% cells was denoted as  $P_{50\%}$ , and the VDR causing the death of 50% cells was denoted by  $D_{50\%}$ .

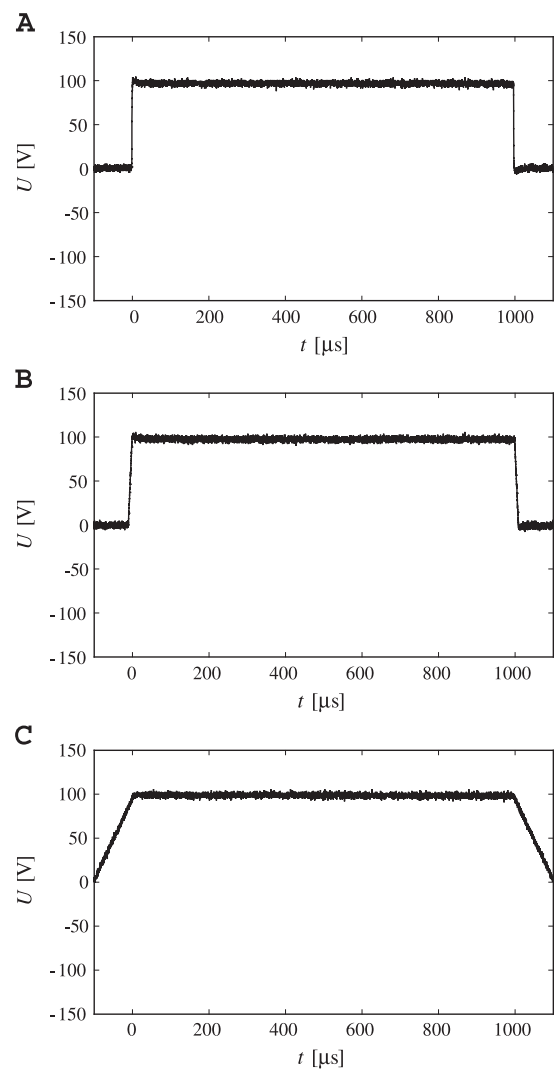


Fig. 1. The time course of a generated unipolar trapezoidal pulse of 1 ms duration, with rise- and falltimes of 2  $\mu$ s (A), 10  $\mu$ s (B), and 100  $\mu$ s (C), and 100 V peak amplitude.

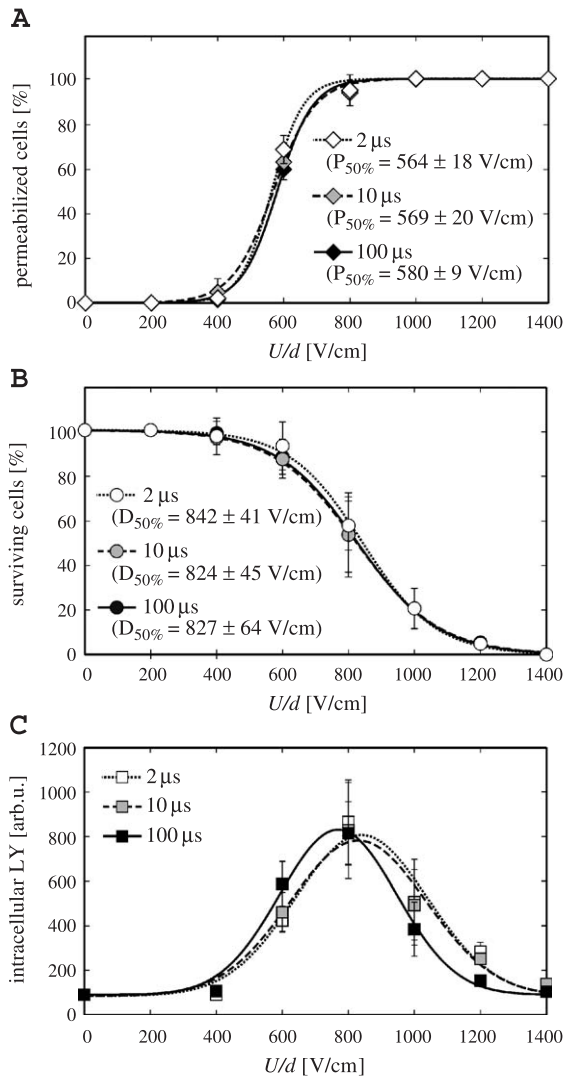


Fig. 2. The efficiency of eight unipolar trapezoidal pulses, 1 ms each, delivered in 1-s intervals, with rise- and falltimes of 2, 10, and 100  $\mu$ s.

The fitting of sigmoidal curves to permeabilization and survival data is widely used, mostly on an empirical ground. However, in a recent theoretical paper [41], we showed that the two-parameter sigmoidal curves as given above are also in good agreement with the permeabilization and survival curves that would correspond to a Gaussian distribution of cell radii.

For the uptake of lucifer yellow, the intensity of fluorescence was fitted by a three-parameter Gaussian peak,

$$y(x) = y_{\max} \exp(-(x_c - x)^2 / 2b^2),$$

where  $x$  is again the VDR,  $y$  is the intracellular concentration of lucifer yellow,  $y_{\max}$  is the maximum intracellular concentration of lucifer yellow in a given experiment,  $x_c$  is the  $x$ -value corresponding to  $y = y_{\max}$ , and  $b$  determines the width of the peak.

All fits were obtained by least-squares nonlinear regression using Sigma Plot 5.05 (SPSS, Richmond, CA, USA).

### 3. Results and discussion

#### 3.1. Unipolar pulses with different rise- and falltimes

Fig. 1 shows the unipolar pulses with rise- and falltimes of 2, 10, and 100  $\mu$ s generated by our setup, and Fig. 2 shows the percentage of electropermeabilized cells (panel A), percentage of surviving cells (panel B), and the internalized lucifer yellow (panel C) obtained with these pulses, each given as a function of voltage-to-distance ratio (VDR). In each case, eight pulses were delivered at intervals of 1 s, each pulse with the maximum VDR lasting for 1 ms (i.e., total pulse duration = risetime + 1 ms + falltime). The results shown in Fig. 2 imply that at least in the investigated range, the risetime and the falltime of the pulse do not play a detectable role in cell membrane permeabilization, which is in agreement with the results of Kinoshita and Tsong [31] on erythrocytes.

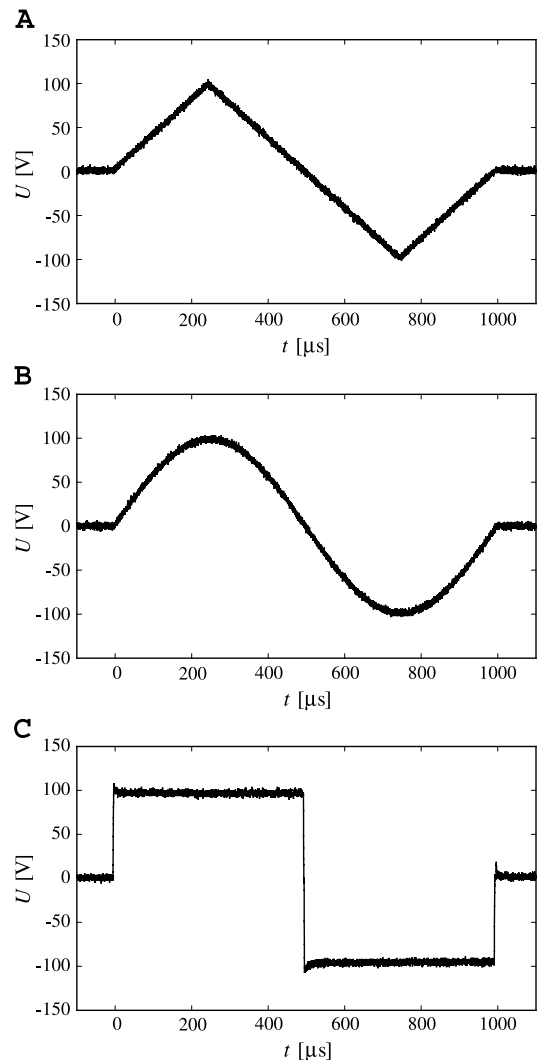


Fig. 3. The time course of a generated bipolar triangular (A), sine (B), and rectangular (C) pulse of 1 ms duration and 100 V peak amplitude.

### 3.2. Bipolar triangular, sine, and rectangular pulses

We previously reported on a significant difference between the efficiency of unipolar and symmetrical bipolar rectangular pulses of the same VDR and total duration [26]. In the present study, we compared the efficiency of bipolar pulses of different shapes: triangular, sine, and rectangular (Fig. 3). The results of this comparison are shown in Fig. 4, which reveals that electroporation, cell death, and the peak of the uptake all occur at the lowest VDR amplitude for rectangular, and at the highest VDR amplitude for triangular pulses. In principle, these results alone could be explained by either different durations of above-critical VDR (i.e., different durations of VDR exceeding a certain critical value), or by different pulse dynamics (i.e., different values of the first derivative of the VDR with respect to time). However, the time

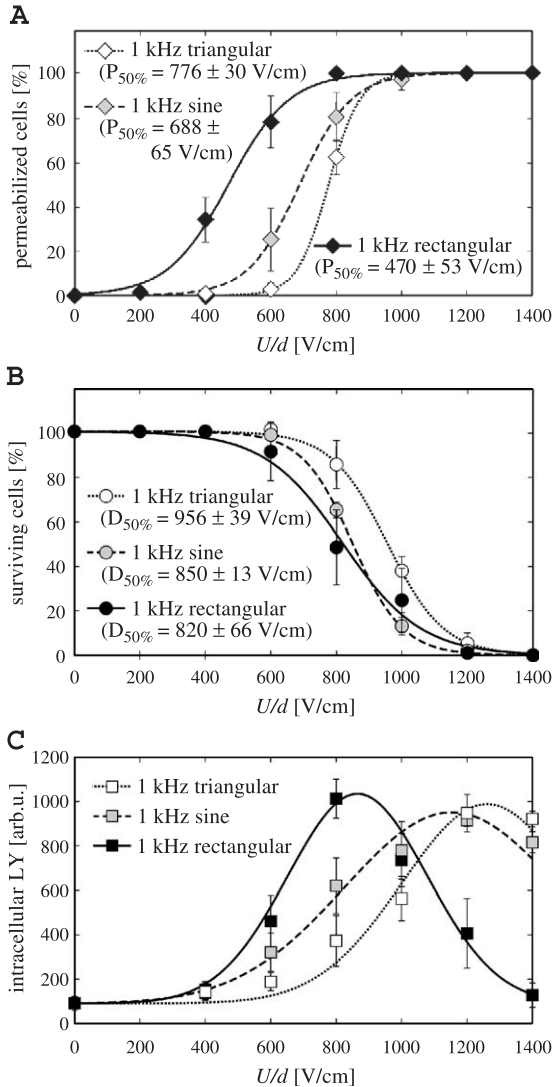


Fig. 4. The efficiency of eight symmetrical bipolar pulses, 1 ms each, delivered in 1-s intervals, for triangular, sine, and rectangular pulse shape.

Table 1

The peak VDR of 1 ms bipolar pulses of various shapes required for VDR of 470 V/cm to be exceeded without interruption for 200 and for 250  $\mu$ s, compared to the experimentally determined values of  $P_{50\%}$

	470 V/cm exceeded for 200 $\mu$ s	470 V/cm exceeded for 250 $\mu$ s	$P_{50\%}$
triangular pulse	783 V/cm	940 V/cm	776 V/cm
sine pulse	581 V/cm	665 V/cm	688 V/cm
rectangular pulse	470 V/cm	470 V/cm	470 V/cm

derivative of VDR was the only variable in the comparison of pulses with different rise- and falltimes (see Unipolar pulses with different rise- and falltimes subsection and Fig. 2), and this comparison shows no statistically significant differences. Consequently, the explanation based on pulse dynamics is unlikely, and it is plausible to attribute the results with different pulse shapes to differences in the duration of above-critical VDR. To an extent, this argument can also be supported quantitatively. In Table 1, the measured values of  $P_{50\%}$  for triangular, sine, and rectangular bipolar pulses are compared to the theoretical values of the peak VDR required for the critical VDR of 470 V/cm to be exceeded without interruption for 200  $\mu$ s and for 250  $\mu$ s (depicted in Fig. 5). Applying durations other than these two does not provide a better agreement between the  $P_{50\%}$  values and the peak VDR values, and this suggests that while the duration of above-critical VDR is indeed important for the efficiency of permeabilization, other parameters also contribute to this efficiency.

The importance of the duration of above-critical VDR is also compatible with the theory of electroporation, which attributes the increase of plasma membrane permeability to the formation of hydrophilic structures (“aqueous pores”) traversing the lipid bilayer and lined with the lipid head-groups [9]. According to this theory, considered by many as a plausible explanation of electroporation, there is a threshold value of transmembrane voltage above which formation of aqueous pores becomes energetically favorable. Since the induced transmembrane voltage is proportional to the electric field [10], and thus practically proportional to the VDR (see Materials and methods section, Exposure to electric pulses subsection), this explains

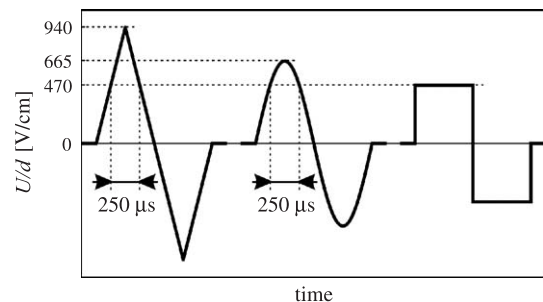


Fig. 5. The peak VDR required for a given value of VDR to be exceeded for a given duration varies with pulse shape. The figure shows the case of symmetric bipolar pulses of 1 ms duration, with VDR of 470 V/cm exceeded during 250  $\mu$ s.

why an above-critical VDR is required for electropermeabilization. In addition, because the formation of aqueous pores is governed by statistical thermodynamics, the probability of formation of individual pores increases with the duration of the above-threshold transmembrane voltage, and thus with the duration of electric pulses.

### 3.3. Unipolar sine-modulated pulses

In the final part of this study, we compared the efficiency of unipolar unmodulated and sine-modulated rectangular pulses, the modulation at 50 kHz representing 10% or 90% of the peak VDR. The modulated pulses are shown in Fig. 6 (the unmodulated pulse is identical to the one shown in Fig. 1A), and the results of this comparison are given in Fig. 7. No statistically significant difference could be detected between an unmodulated and a 10%-modulated pulse, while with the 90%-modulated pulse, both  $P_{50\%}$  and

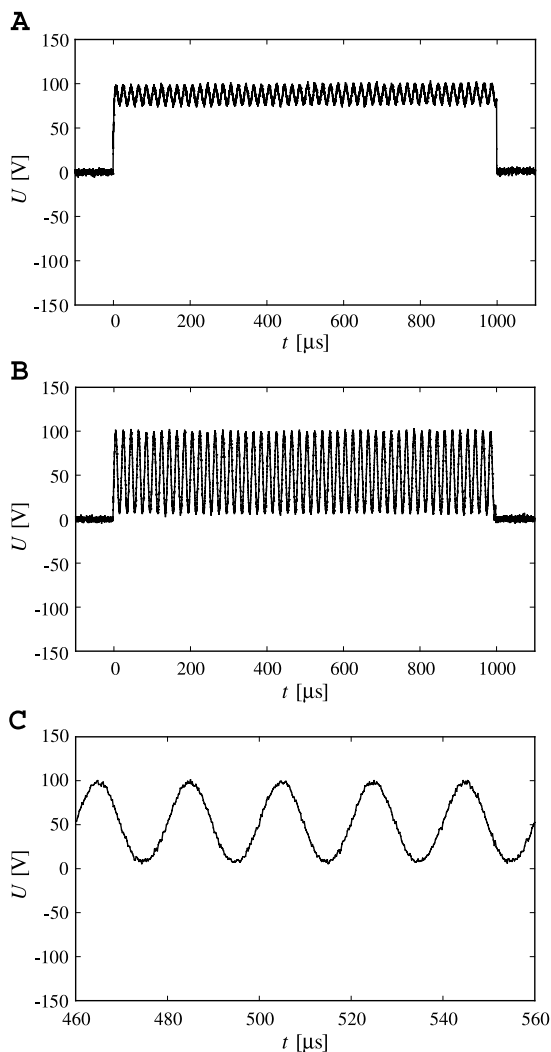


Fig. 6. The time course of a generated unipolar sine-modulated pulse of 1 ms duration and 100 V peak amplitude, with 10% modulation (A) and 90% modulation (B). The modulation frequency was 50 kHz. Panel C shows a part of the 90%-modulated signal in more detail.

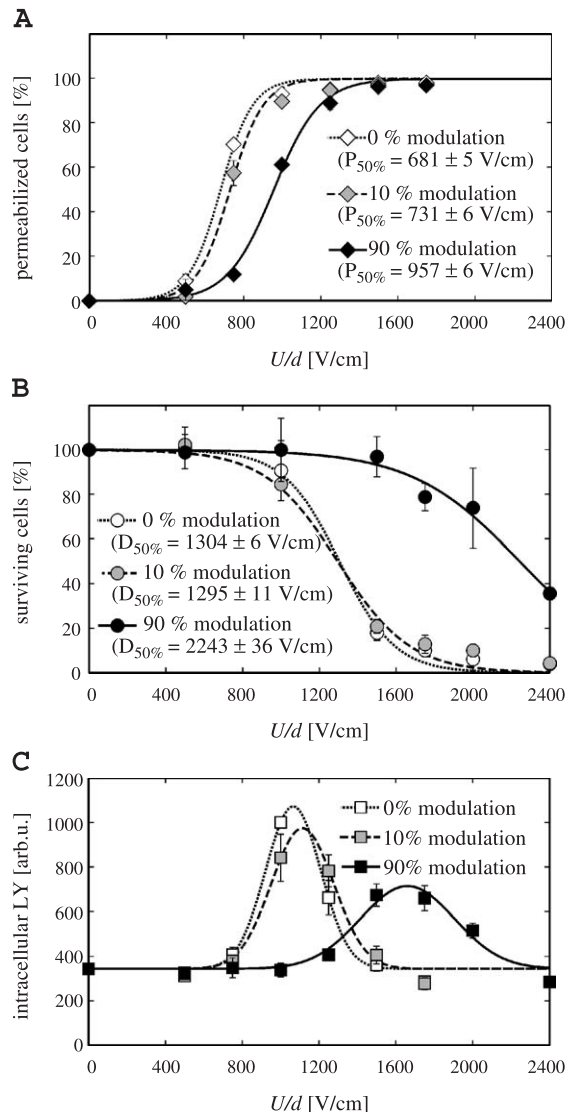


Fig. 7. The efficiency of one unipolar sine-modulated pulse of 1 ms duration, for 0% modulation (unmodulated), 10% modulation, and 90% modulation.

$D_{50\%}$  correspond to significantly higher VDRs than with either unmodulated or 10%-modulated pulse. The peak of the uptake is also rather similar for an unmodulated and a 10%-modulated pulse, while for a 90%-modulated pulse, this peak is much lower, and shifted towards much higher VDRs. These results can be explained by the same argument as the results with different waveforms (see Bipolar triangular, sine, and rectangular pulses)—namely, that the duration of the above-critical VDR has a major role in the efficiency of electropermeabilization. Despite the increase in pulse amplitude, this duration remains short for a 90%-modulated pulse, and consequently the peak of the uptake is rather low. Even at pulse amplitudes where practically all cells are permeabilized, the level of permeabilization is much lower with 90%-modulated pulses than with unmodulated or 10%-modulated pulses, which can also explain why

the value of  $D_{50\%}$  is much higher with 90%-modulated pulses.

#### 4. Conclusions

The results of this study show that among the parameters that describe the pulse shape, the time during which the pulse amplitude exceeds a certain critical value has a major role in the efficiency of electroporation. As described above, this conclusion is in agreement with the theory of electroporation, considered by many as a plausible explanation of electroporation. The differences in the duration of above-critical pulse amplitude can to a large extent explain the differences between various shapes of bipolar pulses, as well as the differences between pulses with different magnitude of modulation. In contrast, the time derivative of the pulse—at least in the range from several volts per microsecond up to several hundred volts per microsecond—has no detectable influence on the efficiency of electroporation. This suggests that pulse generators with sub-microsecond risetimes are not a necessity for successful electroporation.

#### Acknowledgements

This work was supported by CNRS, Institute Gustave-Roussy, University of Paris XI, IGEA Srl (Modena), and the Ministry of Education, Science and Sports of the Republic of Slovenia. Experimental work at Institute Gustave-Roussy was made possible by the Proteus program of scientific, technological and cultural co-operation between France and Slovenia. The high-voltage amplifier has been developed within the Cliniporator project (grant QLK3-1999-00484) under the framework of the 5th PCRD of the European Commission. T.K. was also a recipient of a part-time PhD scholarship of the French Government (CNOUS).

#### References

- [1] L.M. Mir, L.F. Glass, G. Serša, J. Teissié, C. Domenge, D. Miklavčič, M.J. Jaroszeski, S. Orłowski, D.S. Reintgen, Z. Rudolf, M. Belehradec, R. Gilbert, M.P. Rols, J. Belehradec Jr., J.M. Bachaud, R. DeConti, B. Štabuc, M. Čemažar, P. Coninx, R. Heller, Effective treatment of cutaneous and subcutaneous malignant tumors by electrochemotherapy, *Br. J. Cancer* 77 (1998) 2336–2342.
- [2] G. Serša, S. Kranjc, M. Čemažar, Improvement of combined modality therapy with cisplatin and radiation using electroporation of tumors, *Int. J. Radiat. Oncol.* 46 (2000) 1037–1041.
- [3] E. Neumann, S. Kakorin, K. Toensing, Fundamentals of electroporative delivery of drugs and genes, *Bioelectrochem. Bioenerg.* 48 (1999) 3–16.
- [4] J. Lukas, J. Bartek, M. Strauss, Efficient transfer of antibodies into mammalian cells by electroporation, *J. Immunol. Methods* 170 (1994) 255–259.
- [5] Y. Bobiniec, A. Khodyakov, L.M. Mir, C.L. Rieder, B. Eddé, M. Bornens, Centriole disassembly in vivo and its effects on chromosome structure and function in vertebrate cells, *J. Cell Biol.* 143 (1998) 1575–1589.
- [6] F. Bobanović, M.D. Bootman, M.J. Berridge, N.A. Parkinson, P. Lipp, Elementary  $[Ca^{2+}]_i$  signals generated by electroporation functionally mimic those evoked by hormonal stimulation, *FASEB J.* 13 (1999) 365–376.
- [7] T.Y. Tsong, Electroporation of cell membranes, *Biophys. J.* 60 (1991) 297–306.
- [8] M. Hibino, H. Itoh, K. Kinoshita Jr., Time courses of cell electroporation as revealed by submicrosecond imaging of transmembrane potential, *Biophys. J.* 64 (1993) 1789–1800.
- [9] J.C. Weaver, Y.A. Chizmadzhev, Theory of electroporation: a review, *Bioelectrochem. Bioenerg.* 41 (1996) 135–160.
- [10] T. Kotnik, F. Bobanović, D. Miklavčič, Sensitivity of transmembrane voltage induced by applied electric fields—a theoretical analysis, *Bioelectrochem. Bioenerg.* 43 (1997) 285–291.
- [11] E. Neumann, S. Kakorin, Electrooptics of membrane electroporation and vesicle shape deformation, *Curr. Opin. Colloid Interface Sci.* 1 (1996) 790–799.
- [12] B. Gabriel, J. Teissié, Time courses of mammalian cell electroporation observed by millisecond imaging of membrane property changes during the pulse, *Biophys. J.* 76 (1999) 2158–2165.
- [13] S. Raffy, J. Teissié, Control of lipid membrane stability by cholesterol content, *Biophys. J.* 76 (1999) 2072–2080.
- [14] L. Tung, G.C. Troiano, V. Sharma, R.M. Raphael, K.J. Stebe, Changes in electroporation thresholds of lipid membranes by surfactants and peptides, *Ann. N.Y. Acad. Sci.* 888 (1999) 249–265.
- [15] M. Golzio, M.P. Mora, C. Raynaud, C. Delteil, J. Teissié, M.P. Rols, Control by osmotic pressure of voltage-induced permeabilization and gene transfer in mammalian cells, *Biophys. J.* 74 (1998) 3015–3022.
- [16] M.P. Rols, J. Teissié, Electroporation of mammalian cells. Quantitative analysis of the phenomenon, *Biophys. J.* 58 (1990) 1089–1098.
- [17] H. Wolf, M.P. Rols, E. Boldt, E. Neumann, J. Teissié, Control by pulse duration of electric-field mediated gene transfer in mammalian cells, *Biophys. J.* 66 (1994) 524–531.
- [18] M.P. Rols, J. Teissié, Electroporation of mammalian cells to macromolecules: control by pulse duration, *Biophys. J.* 75 (1998) 1415–1423.
- [19] A. Maček-Lebar, N.A. Kopitar, A. Ihan, G. Serša, D. Miklavčič, Significance of treatment energy in cell electroporation, *Electro- Magnetobiol.* 17 (1998) 253–260.
- [20] A. Maček-Lebar, D. Miklavčič, Cell electroporation to small molecules in vitro: control by pulse parameters, *Radiol. Oncol.* 35 (2001) 193–202.
- [21] E. Tekle, R.D. Astumian, P.B. Chock, Electroporation by using bipolar oscillating electric field: an improved method for DNA transfection of NIH 3T3 cells, *Proc. Natl. Acad. Sci. U. S. A.* 88 (1991) 4230–4234.
- [22] S.I. Sukharev, V.A. Klenchin, S.M. Serov, L.V. Chemomordik, Y.A. Chizmadzhev, Electroporation and electrophoretic DNA transfer into cells, *Biophys. J.* 63 (1992) 1320–1327.
- [23] R. Heller, R. Gilbert, M.J. Jaroszeski, Electrochemotherapy: an emerging drug delivery method for the treatment of cancer, *Adv. Drug Deliv. Rev.* 26 (1997) 185–197.
- [24] L.M. Mir, M.F. Bureau, J. Gehl, R. Rangara, D. Rouy, J.M. Caillaud, P. Delaere, D. Branellec, B. Schwartz, D. Scherman, High-efficiency gene transfer into skeletal muscle mediated by electric pulses, *Proc. Natl. Acad. Sci. U. S. A.* 96 (1999) 4262–4267.
- [25] S. Kuriyama, A. Mitoro, H. Tsujinoue, Y. Toyokawa, T. Nakatani, H. Yoshiji, T. Tsujimoto, H. Okuda, S. Nagao, H. Fukui, Electrochemotherapy can eradicate established colorectal carcinoma and leaves a systemic protective memory in mice, *Int. J. Oncol.* 16 (2000) 979–985.
- [26] T. Kotnik, L.M. Mir, K. Flisar, M. Puc, D. Miklavčič, Cell membrane electroporation by symmetrical bipolar rectangular pulses:

- Part I. Increased efficiency of permabilization, *Bioelectrochemistry* 54 (2001) 83–90.
- [27] T. Kotnik, D. Miklavčič, L.M. Mir, Cell membrane electroporation by symmetrical bipolar rectangular pulses: Part II. Increased efficiency of permabilization, *Bioelectrochemistry* 54 (2001) 91–95.
- [28] I. Daskalov, N. Mudrov, E. Peycheva, Exploring new instrumentation parameters for electrochemotherapy. Attacking tumors with bursts of biphasic pulses instead of single pulses, *IEEE Eng. Med. Biol. Mag.* 18 (1999) 62–66.
- [29] I. Mathiesen, Electroporation of skeletal muscle enhances gene transfer in vivo, *Gene Ther.* 6 (1999) 508–514.
- [30] G. Rizzuto, M. Cappelletti, D. Maione, R. Savino, D. Lazzaro, P. Costa, I. Mathiesen, R. Cortese, G. Ciliberto, R. Laufer, N. La Monica, E. Fattori, Efficient and regulated erythropoietin production by naked DNA injection and muscle electroporation, *Proc. Natl. Acad. Sci. U. S. A.* 96 (1999) 6417–6422.
- [31] K. Kinoshita, T.Y. Tsong, Voltage-induced conductance in human erythrocyte membranes, *Biochim. Biophys. Acta* 554 (1979) 479–497.
- [32] D.C. Chang, Cell poration and cell fusion using an oscillating electric field, *Biophys. J.* 56 (1989) 641–652.
- [33] D.C. Chang, P.Q. Gao, B.L. Maxwell, High efficiency gene transfection by electroporation using a radio-frequency electric field, *Biochim. Biophys. Acta* 1092 (1991) 153–160.
- [34] T.D. Xie, T.Y. Tsong, Study of mechanisms of electric field-induced DNA transfection: II. Transfection by low-amplitude, low-frequency alternating electric fields, *Biophys. J.* 58 (1990) 897–903.
- [35] S. Šatkauskas, M.F. Bureau, M. Puc, A. Mahfoudi, D. Scherman, D. Miklavčič, L.M. Mir, Mechanisms of in vivo DNA electrotransfer: respective contributions of cell electroporation and DNA electrophoresis, *Mol. Ther.* 5 (2002) 133–140.
- [36] J.L. Biedler, H. Riehm, Cellular resistance to actinomycin D in Chinese hamster cells in vitro, *Cancer Res.* 30 (1970) 1174–1184.
- [37] F. Loste, N. Eynard, J. Teissié, Direct monitoring of the field strength during electroporation, *Bioelectrochem. Bioenerg.* 47 (1998) 119–127.
- [38] K. Flisar, M. Puc, T. Kotnik, D. Miklavčič, A system for cell membrane electroporation with arbitrary pulse waveforms, *IEEE Eng. Med. Biol.* 22 (2003) 77–81.
- [39] M.P. Rols, J. Teissié, Ionic-strength modulation of electrically induced permeabilization and associated fusion of mammalian cells, *Eur. J. Biochem.* 179 (1989) 109–115.
- [40] T. Kotnik, A. Maček-Lebar, D. Miklavčič, L.M. Mir, Evaluation of cell membrane electroporation by means of a nonpermeant cytotoxic agent, *BioTechniques* 28 (2000) 921–926.
- [41] M. Puc, T. Kotnik, L.M. Mir, D. Miklavčič, Quantitative model of small molecules uptake after in vitro cell electroporation, *Bioelectrochemistry* 60 (2003) (in press).

*Paper 2***The effect of pulse repetition frequency on the uptake into electropermeabilized cells in vitro with possible applications in electrochemotherapy****G. Pucihar<sup>a</sup>, L.M. Mir<sup>b</sup>, D. Miklavčič<sup>a</sup>,**<sup>a</sup>Laboratory of Biocybernetics, Faculty of Electrical Engineering, University of Ljubljana, Tržaška 25, SI-1000 Ljubljana, Slovenia<sup>b</sup>UMR 8532 CNRS, Institute Gustave-Roussy, F-94805 Villejuif, France**Abstract**

Electrochemotherapy is a technique where electric pulses in combination with chemotherapeutic agents are applied to tumor cells. In general, patients find electrochemotherapy tolerable, in spite of unpleasant sensations associated with contraction of muscles located beneath or in the vicinity of the electrodes. These contractions are due to the intensity of the electric pulses required for effective electropermeabilization of tumor cell membranes. Since a train of eight electric pulses with repetition frequency of 1 Hz is usually applied to the tumors, each pulse in the train excites underlying nerves and provokes muscle contractions. Therefore, for patients involved in electrochemotherapy, the use of pulses with repetition frequency higher than the frequency of tetanic contraction would represent reduced number of muscle contractions and associated unpleasant sensations. Our results of the uptake of Lucifer Yellow into electropermeabilized cells in vitro show that with increased repetition frequency the uptake stays at similar levels even at frequencies up to 8.3 kHz. On the basis of these results the possibilities for the clinical use of pulses with high repetition frequency in electrochemotherapy are considered.

# The effect of pulse repetition frequency on the uptake into electropermeabilized cells in vitro with possible applications in electrochemotherapy

G. Pucihar<sup>a</sup>, L.M. Mir<sup>b</sup>, D. Miklavčič<sup>a,\*</sup>

<sup>a</sup>Laboratory of Biocybernetics, Faculty of Electrical Engineering, University of Ljubljana, Trzaska 25, SI-1000 Ljubljana, Slovenia

<sup>b</sup>UMR 8532 CNRS, Institute Gustave-Roussy, F-94805 Villejuif, France

Received 25 October 2001; received in revised form 24 May 2002; accepted 4 June 2002

## Abstract

Electrochemotherapy is a technique where electric pulses in combination with chemotherapeutic agents are applied to tumor cells. In general, patients find electrochemotherapy tolerable, in spite of unpleasant sensations associated with contraction of muscles located beneath or in the vicinity of the electrodes. These contractions are due to the intensity of the electric pulses required for effective electropermeabilization of tumor cell membranes. Since a train of eight electric pulses with repetition frequency of 1 Hz is usually applied to the tumors, each pulse in the train excites underlying nerves and provokes muscle contractions. Therefore, for patients involved in electrochemotherapy, the use of pulses with repetition frequency higher than the frequency of tetanic contraction would represent reduced number of muscle contractions and associated unpleasant sensations. Our results of the uptake of Lucifer Yellow into electropermeabilized cells in vitro show that with increased repetition frequency the uptake stays at similar levels even at frequencies up to 8.3 kHz. On the basis of these results the possibilities for the clinical use of pulses with high repetition frequency in electrochemotherapy are considered.

© 2002 Elsevier Science B.V. All rights reserved.

**Keywords:** Electrochemotherapy; Pulse repetition frequency; Lucifer yellow; Action potential; Muscle contraction

## 1. Introduction

Electropermeabilization is a process where a transient, high-permeability state of cell membrane occurs due to cell exposure to high voltage, short-duration electric pulses. Increased membrane permeability allows ions, small molecules and drugs to cross cell membranes, otherwise impermeable for them [1]. In experiments involving electropermeabilization, a single pulse or a train of rectangular or exponentially decaying pulses is most often used. In case of a train, the repetition frequency of the pulses is usually 1 Hz, which is the frequency probably chosen because of the limitations of commercially available electropulsators. To investigate the effect of higher pulse repetition frequencies on electropermeabilization, some authors have used pulse generators to obtain continuous waveforms of various shapes with frequencies from several hundred Hz to 1

MHz [2–6]. Because of the continuity of these waveforms, change in the frequency always resulted in corresponding change of the duration of the pulses.

In contrast, only few authors have attempted to vary the frequency of the pulses by adjusting only the delay between two consecutive pulses in a train, thus keeping the duration and number of pulses constant. One of these studies was performed by Vernhes and co-workers [7], where the effect of the repetition frequency (ranging from 0.5 to 100 Hz) on cell viability and permeabilization was investigated. This study has shown high permeabilization and survival of the cells can be obtained even at 100 Hz. We decided to investigate the effect of different pulse frequencies on the uptake of exogenous molecules at even higher frequencies. For this purpose, at the University of Ljubljana, we developed an electropulsator, which permits to vary the repetition frequency of the pulses keeping the number and duration of pulses constant [8].

The purpose of our study was to examine the possibilities of using pulses with repetition frequencies higher than 1 Hz in electrochemotherapy. Electrochemotherapy is a technique

\* Corresponding author. Tel.: +386-1-4768-456; fax: +386-1-426-4658.  
E-mail address: damijan@svarun.fe.uni-lj.si (D. Miklavčič).

where electric pulses in combination with chemotherapeutic agents (e.g., bleomycin, cisplatin [9–13]) are applied to tumor cells. This technique was found to be effective in treatment of cutaneous and subcutaneous tumors in patients [14–17]. In the most comprehensive study [14], the results of five different research groups (France, USA, and Slovenia) were summarized and patient responses evaluated. Objective responses (absence of any trace of tumor, complete response, or more than 50% reduction in tumor volume, partial response, for at least 30 days after the treatment) were obtained in 85.3% of the 273 evaluable tumors. Local clinical complete responses were obtained in 56.4% (154) tumors, and partial responses in 28.9% (79) tumors. A high rate of local objective responses was obtained regardless of the histological type of the treated tumors. In general, the patients found electrochemotherapy tolerable, although some complained about unpleasant sensations associated with the delivery of electric pulses. Because of the relatively low repetition frequency of the pulses used (1 Hz), each individual pulse in the train of pulses (usually 4, 6 or 8 pulses) provokes muscle contraction. Since such individual muscle contractions are disagreeable, any reduction of these sensations would be an improvement for the patients. The use of pulses with repetition frequency exceeding the frequency of tetanic contraction (where successive muscle contractions fuse into smooth motion) would already represent an improvement in sense of reducing the pain associated with electrochemotherapy. To study the possibilities for the use of higher pulse repetition frequencies in experiments *in vivo*, the first step is to investigate these conditions *in vitro*. Because electrochemotherapy is based on enhanced uptake of chemotherapeutic agents (e.g., bleomycin, 1500 g/mol) into tumor cells, we examined the effect of repetition frequency of electric pulses on the uptake of Lucifer Yellow, a small nonpermeant hydrophilic molecule (like the bleomycin, but not toxic) into electropermeabilized cells *in vitro*.

## 2. Materials and methods

### 2.1. Cells

DC3F cells—spontaneously transformed Chinese hamster fibroblasts [18]—were grown in Eagle's Minimum Essential Medium (EMEM) with added 10% Fetal bovine serum (both from Life Technologies, USA). After trypsination, cells were centrifuged for 5 min at 1000 rpm at 4 °C and resuspended in Spinner's minimum essential medium (SMEM, Life Technologies, USA) to obtain  $2 \times 10^7$  cells/ml.

To determine the uptake of molecules into the permeabilized cells, the nonpermeant fluorescent dye Lucifer Yellow (MW 522 g/mol, Sigma, USA) was added to the cell suspension before electropermeabilization in quantity that led to 1 mM concentration of Lucifer Yellow in the cell suspension. Because Lucifer Yellow can enter the permeabilized cell and stay inside the cell after pores reseal, the

quantity of Lucifer Yellow taken up by the cell (the uptake) can be determined by measuring the fluorescence. As Lucifer Yellow is not cytotoxic its presence should not affect cell viability.

Cells were kept at 4 °C until electropermeabilization.

### 2.2. Electropermeabilization

A 50- $\mu$ l ( $\pm 0.8\%$ ) droplet of the cells suspended in SMEM ( $\sim 10^6$  cells) was taken and placed between two parallel plate stainless steel electrodes 2 mm ( $\pm 2.5\%$ ) apart. The entrapped droplet was cylindrically shaped with concave sides. In comparison with the cross-section area of the ideal cylinder, the area at the electrode/medium contact was  $\sim 2\%$  larger, while at the narrowest point of the droplet (in the middle between the electrodes), the actual cross-section area was  $\sim 15\%$  smaller. In the first experiment, eight rectangular pulses with each 100- $\mu$ s duration, with amplitudes from 80 to 400 V, and repetition frequencies of 1, 10, 1000, and 2500 Hz were delivered. With our electropulsator, 2500 Hz was the highest frequency that could be generated for 100- $\mu$ s pulses [8]. To obtain higher pulse repetition frequencies, shorter pulses were used. This was a consequence of the limitation of the electropulsator, where the delay between two consecutive pulses is limited by the duration of the pulse (the shortest delay is three times longer than the duration of the pulse). Therefore, in the second experiment, twenty-six 30- $\mu$ s rectangular pulses were delivered, with amplitudes from 80 to 400 V and repetition frequencies of 1 Hz and 8.3 kHz. Twenty-six pulses were used in order to have the same cumulative length of the pulses, thus the product  $N \times T$  of the number  $N$  and duration  $T$  of the pulses was constant in both experiments. After 10 min of incubation at room temperature, 950  $\mu$ l of SMEM was added to prevent drying. After additional 30 min, cells were diluted in 5 ml of phosphate buffer saline (Life Technologies, USA) in order to remove extracellular Lucifer Yellow, and centrifuged at 1000 rpm. The washing procedure was repeated twice, which proved sufficient in preliminary experiments. Cells were then broken down by ultrasonication (Sonifier 250, Branson Ultrasonics, USA) and fluorescence was measured on a spectrofluorometer (SFM 25, BioTek, USA). Excitation was set at 418-nm wavelength and emission was detected at 525 nm. The remnants of the extracellular Lucifer Yellow together with a small amount of Lucifer Yellow taken up by cells with endocytosis represented the background fluorescence, which was measured at 0 V (no pulses). The fluorescence of cell fragments and phosphate buffer saline was considerably lower than the background fluorescence and was thus not taken into consideration.

### 2.3. Data processing

All experiments were repeated at least three times on different days. Due to scattering of the measured fluorescence, the results were normalized to the value of the uptake

at  $8 \times 100 \mu\text{s}$ , 1 Hz,  $U=200$  V in each experiment, which represented 100 arbitrary units of fluorescence. Results from different repetitions of experiments were pooled together and are presented as the mean and standard deviation of the mean (S.D.). On these data, three-parameter Gaussian peaks were fitted,

$$y(u) = y_{\text{max}} \exp(-(u_C - u)^2 / 2b^2) \quad (1)$$

where  $y$  is the uptake,  $u$  is the pulse amplitude,  $y_{\text{max}}$  is the maximum concentration of Lucifer Yellow in cell suspension,  $u_C$  denotes the value of  $u$ , corresponding to  $y=y_{\text{max}}$ , and  $b$  determines the width of the peak. All fits were obtained by least-squares nonlinear regression using Sigma-Plot 5.0.

### 3. Results

The results of the uptake of Lucifer Yellow into electropermeabilized cells as a function of pulse amplitude and repetition frequency of electric pulses are shown in Figs. 1 and 2. As the figures show, increasing the amplitude of the pulses results in an increase of the uptake of Lucifer Yellow, which reaches its maximum value at a certain pulse amplitude. With further increase of the pulse amplitude the uptake decreases. The decrease in the uptake induced by higher amplitudes is a result of irreversible cell electropermeabilization. Cells either disintegrate or do not reseal, therefore allowing the leaking of Lucifer Yellow from the cells after dilution with SMEM (see M&M above).

In the first experiment, where eight 100- $\mu\text{s}$  pulses were used, the highest uptake was obtained at the frequency of 10 Hz, while no significant difference was obtained between the maximum uptake values at 1 Hz, 1 kHz, and 2.5 kHz (Fig. 1). However, higher pulse amplitudes seem to be

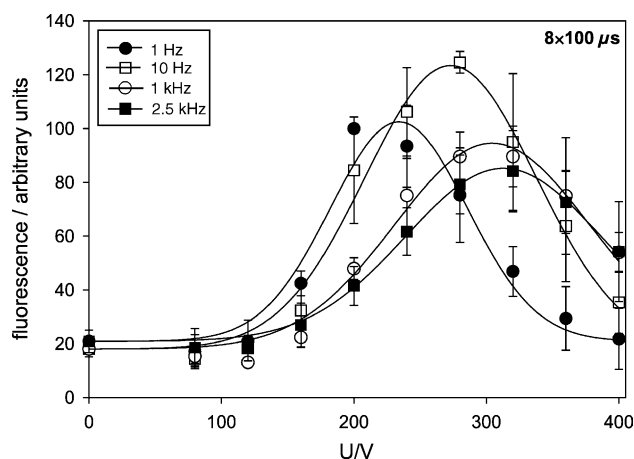


Fig. 1. The uptake of Lucifer Yellow (LY) as a function of pulse amplitude  $U$  at pulse repetition frequencies of 1 Hz (●), 10 Hz (□), 1 kHz (○), and 2.5 kHz (■) (8 pulses of 100- $\mu\text{s}$  duration). Each point on the figure represents the mean of three values  $\pm$  S.D.

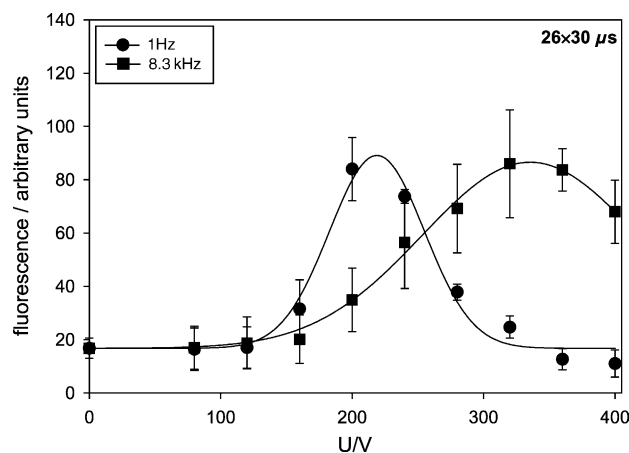


Fig. 2. The uptake of Lucifer Yellow (LY) as a function of pulse amplitude  $U$  at pulse repetition frequencies of 1 Hz (●) and 8.3 kHz (■) (26 pulses of 30- $\mu\text{s}$  duration). Each point on the figure represents the mean of three values  $\pm$  S.D.

required to obtain the maximum uptake with an increase of the repetition frequency of electric pulses. For frequencies 1 Hz, 10 Hz, 1 kHz, and 2.5 kHz, these pulse amplitudes ( $u_C$ ) are 234, 273, 304, and 313 V, respectively. Also, with an increase of the repetition frequency of electric pulses, the uptake peaks are wider.

In the second experiment where 30- $\mu\text{s}$  pulses were used, the maximum uptake at the frequency of 8.3 kHz is comparable with the uptake at 1 Hz (Fig. 2). Again, higher pulse amplitudes are required to obtain maximum uptake values at the higher frequency ( $u_C=219$  V for 1 Hz and  $u_C=335$  V for 8.3 kHz) and the uptake peak is wider at the higher frequency.

### 4. Discussion

#### 4.1. Electropermeabilization in general

Increased efficiency of high frequency unipolar or bipolar waveforms compared to a single rectangular pulse was already reported for fusion and gene transfection by different authors. For example, Tekle and co-workers examined the transfection efficiency of NIH 3T3 cells electropermeabilized by a single rectangular pulse and a high frequency unipolar or bipolar rectangular waves (60 kHz, 250 kHz, 1 MHz) [3]. They reported increased transfection efficiency and also higher survival of the cells with high frequency bipolar and unipolar waves with respect to a single rectangular pulse. Chang studied poration of COS-M6 cells and fusion of human red blood cells by radio frequency (RF) sinusoidal waves (several kHz–1 MHz) superimposed onto a rectangular pulse [4]. He found that pulsed RF field is more efficient in both cell fusion and cell poration than a DC rectangular pulse. He also found that electropermeabilization with RF pulses results in higher percentage of cells surviving the exposure to electric field compared to a DC rectangular pulse. With the

same type of pulses (40-kHz frequency), Chang and co-workers have also reported increased efficiency of gene transfection of COS-M6 cells by electropermeabilization [5].

According to the results of the above-mentioned studies, high-frequency waveforms seem to be more efficient in cell electropermeabilization and also less damaging to the cells than a single rectangular pulse. Because these authors were using amplified signals from common pulse generators, continuous waveforms were generated instead of a train of consecutive pulses that is typically used in electrochemotherapy and electrogenotherapy. This resulted in a frequency-dependent number and duration of the pulses in a train. On the contrary, in our study we varied the frequency of the pulses by changing the delay between two consecutive pulses in a train, thus keeping both the duration and number of pulses constant (except for 8.3 kHz, see below). The effect of different pulse repetition frequencies (from 1 Hz to 8.3 kHz) on the uptake of Lucifer Yellow into electropermeabilized cells was therefore examined. Because 2.5 kHz was the maximum frequency generated by our electropulsator at 100- $\mu$ s pulses, we shortened the duration of the pulses to 30  $\mu$ s, increased the number of pulses (to keep the total cumulative length of the pulses  $N \times T$  constant) and therefore increased the maximum generated frequency to 8.3 kHz.

Our results (Figs. 1 and 2) show that the increase in the repetition frequency of the pulses does not significantly reduce the maximum value of the uptake even at the highest frequencies applied (8.3 kHz), while different voltages correspond to the maximum uptake at a given frequency. The frequency of 10 Hz seems to be the optimum frequency for the maximum uptake, which we are not able to explain at this time.

A study where the duration and the number of consecutive unipolar rectangular pulses in a train were kept constant regardless of the pulse frequency was performed by Vernhes and co-workers [7]. The frequency effect on cell viability and permeabilization of Chinese hamster ovary cells was investigated in the range from 0.5 to 100 Hz. Their results show biphasic dependence of cell viability on pulse frequency, viability increased from 0.5 to 10 Hz and then decreased, while the percentage of permeabilized cells increased with the frequencies above 10 Hz. If we consider that the increasing part of the uptake curves in Fig. 1 corresponds to an increase in the fraction of the permeabilized cells, while the decreasing part corresponds to increased fraction of irreversibly electropermeabilized cells, our results are in agreement with these results, at least up to 10 Hz frequency. In both studies, the 10 Hz frequency seems to be the optimum frequency for the highest viability of the cells (Vernhes), or the highest uptake (our study).

#### 4.2. Prospects of using high frequency pulses in electrochemotherapy

The main purpose of our study was to investigate the possibilities of the use of pulses with higher frequencies in

electrochemotherapy in order to reduce the painful sensations caused by low-frequency (1 Hz) electrochemotherapy. For efficient electrochemotherapy, electric pulses of appropriate amplitude must be delivered to the electrodes. Typically, 1000-V pulses are applied to the electrodes having a distance of 8 mm. Besides electropermeabilization of tumor cell membranes, these pulses also excite the nerve fibers located beneath or in the vicinity of the electrodes. In the form of action potential, the excitation is then carried along the nerve fiber to neuromuscular junctions to cause muscle contraction.

After the first pulse, the membrane of the nerve axon cannot be excited for the refractory period of the axon membrane [19–21]. If a train of pulses is used, with the delay between two consecutive electric pulses shorter than the combined duration of the action potential and the refractory period, each pulse in the train will not be able to initiate a new action potential. In addition, if the duration of the whole train of pulses is shorter than the duration of the action potential including the refractory period, only a single action potential will be generated (Fig. 3). Skeletal muscles are mostly innervated by myelinated nerve fibers for which the maximum frequency of generated action potentials (inverse value of the duration of the action potential and the refractory period) ranges from 400 to 2500 Hz [19–21], depending on the diameter of the nerve axon.

As mentioned above, after excitation of the nerve, the action potential is carried to neuromuscular junctions to provoke muscle contraction, which typically lasts for tens (e.g., ocular muscle) up to hundreds of milliseconds (e.g., soleus). Since the pulse repetition frequency of 1 Hz is most

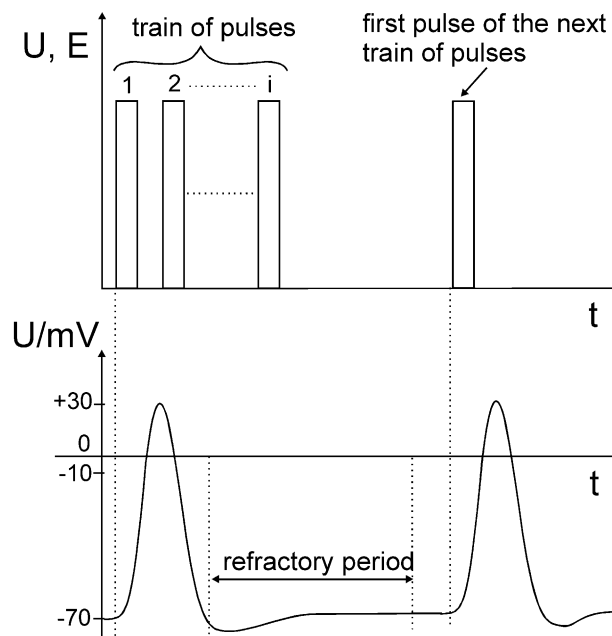


Fig. 3. The duration of the whole train of pulses in comparison with the duration of the action potential considering refractory period.

often used in electrochemotherapy [11–14,22,23], each individual pulse in the train of pulses causes the contraction of muscles innervated by the excited neurons. Increasing the frequency of electric pulses would increase the frequency of generated action potentials in the excited nerve, shorten the delay between two consecutive muscle contractions, and eventually increase the force of muscle contraction (Fig. 4). At a certain frequency of excitation ( $\sim 40$  Hz [19,20]) successive muscle contractions will fuse into smooth motion-tetanic contraction (Fig. 4). Electrochemotherapy with pulse repetition frequencies above the frequency of tetanic contraction would therefore reduce the number of individual muscle contractions but also increase the force of muscle contraction, while at frequencies lower than tetanic, the muscle response to the excitation will not be smooth (Fig. 4).

Suppose the pulses are delivered at the frequency for which the duration of the whole train of pulses is shorter than duration of the action potential with the refractory period (Fig. 3), the response of the muscle to the high frequency of excitation would probably be the same as if the muscle were excited by a single pulse. Considering the train of eight pulses with duration of  $100 \mu\text{s}$ , the repetition frequency of electric pulses generating a single action potential, and thereby a single muscle contraction, is expected to be in the range of a few kHz, but not higher than  $20$  kHz even for the fastest muscles.

Although many electropulsators are unable to generate  $100\text{-}\mu\text{s}$  pulses at this frequencies, the use of pulses with considerably lower repetition frequencies would still result in a decreased muscle response with respect to a typical  $1$

Hz exposure because: (a) the refractory period of the axon membrane consists of the absolute refractory period (during which it is impossible to initiate a new action potential) and the relative refractory period (during which a stronger stimulus can initiate a new action potential). Because the data on the maximum frequency of generated action potentials mentioned above were calculated regarding to the absolute refractory period only, the maximum frequency of generated action potentials considering both refractory periods can be lower; (b) the pulses with repetition frequencies higher than the frequency of tetanic contraction ( $\sim 40$  Hz) will already reduce the number of consecutive muscle contractions and thereby, reduce the number of unpleasant sensations; (c) the pulses with frequencies higher than the maximum frequency of generated action potentials ( $>400$  Hz) will reduce both, the force and the number of muscle contractions, considering finite duration of the train of pulses (filled circles in Fig. 4). For example, the total duration of a pulse train (eight  $100\text{-}\mu\text{s}$  pulses) at  $1$  Hz repetition frequency is  $8$  s, while at  $1$  kHz pulse repetition frequency the total duration of the train is  $8$  ms.

Besides the nerves that innervate the muscles, electric pulses could also excite pain receptors or nerve endings located nearby. An increased pulse repetition frequency could also eliminate these side effects.

In a recent study by Daskalov and co-workers [25], electrochemotherapy with high frequency pulses was performed on basal cell and spin cell carcinoma and on melanoma metastases in patients. They have compared  $8 \times 100 \mu\text{s}$ ,  $8 \times (50 + 50 \mu\text{s})$ , both  $1\text{-Hz}$  rectangular pulses and a burst of eight bipolar rectangular pulses ( $50 + 50 \mu\text{s}$ , pulse repetition frequency  $1$  kHz). No difference between tumor responses on treatment protocols was observed. However, electrochemotherapy with higher pulse frequencies was better accepted by the patients, because of only one electrical excitation instead of eight. Our theoretical considerations are in agreement with these results, while results of our *in vitro* study further substantiate that electrochemotherapy could be effectively performed with higher pulse repetition frequencies. In addition, the total duration of the pulse train is important in the case of treating large tumors with arrays of multiple electrodes, since the total treatment duration can be reduced.

In summary, the uptake at the highest repetition frequencies examined ( $2.5$  kHz for  $100 \mu\text{s}$  and  $8.3$  kHz for  $30\text{-}\mu\text{s}$  pulses) stays at similar levels as the uptake at  $1$  Hz, while different voltages correspond to the maximum value of the uptake at the specific frequency. However, with pulses of longer duration or increased number of pulses, an additional increase in the uptake can be obtained [26,27]. If we refer to the previously mentioned study [14] where muscle contractions and painful sensation were presented as the most disagreeable side effects during electrochemotherapy, on the basis of our theoretical considerations and *in vitro* results, we suggest the use of pulses with higher frequencies as an improvement in a sense of reduced force and number

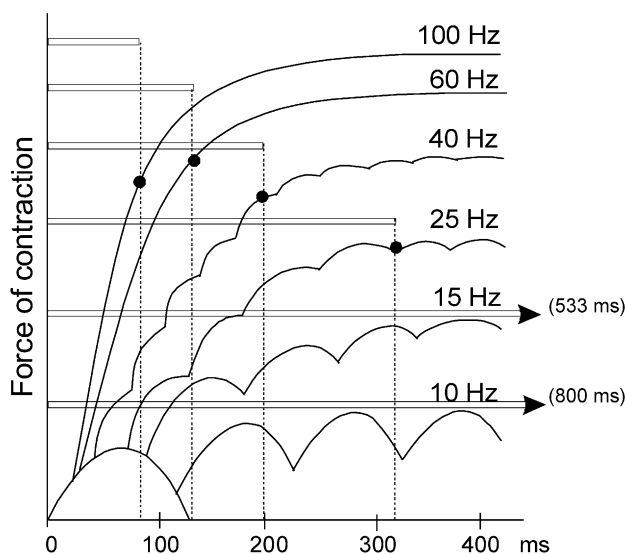


Fig. 4. The dependence of the force of muscle contraction on the pulse repetition frequency and the occurrence of tetanic contraction for continuous muscle stimulation. The filled circles (●) represent the force of contraction due to excitation with a pulse train ( $8 \times 100 \mu\text{s}$ ) at a given frequency (partially adapted from Ref. [24]).  $\longrightarrow$  duration of a pulse train ( $8 \times 100 \mu\text{s}$ ) at a given repetition frequency.

of muscle contractions for the patients. Certainly, before clinical applications, the results obtained in our study in vitro should be verified on animal tumor models in vivo.

### Acknowledgements

G.P. wishes to thank Dr. Tadej Kotnik for valuable help and instructions while the experiments were conducted and for reading the manuscript. This research has been supported through various grants by the Ministry of Education, Science and Sports (MESS) of the Republic of Slovenia. Experimental work at Villejuif (France) has been supported by grants of CNRS and Institut Gustave-Roussy, while visits and stays have been made possible by the Proteus program of scientific, technological and cultural cooperation between CNRS (project no. 5386), France and MESS (Proteus program), Slovenia. G.P. and D.M. would also like to acknowledge the partial support of IGEA Carpi (Modena), Italy.

### References

- [1] E. Neumann, S. Kakorin, Digression on membrane electroporation and electroporative delivery of drugs and genes, *Radiol. Oncol.* 32 (1998) 7–17.
- [2] E. Tekle, R.D. Astumian, P.B. Chock, Electro-permeabilization of cell membranes: effect of the resting membrane potential, *Biochem. Biophys. Res. Commun.* 172 (1990) 282–287.
- [3] E. Tekle, R.D. Astumian, P.B. Chock, Electroporation by using bipolar oscillating electric field: An improved method for DNA transfection of NIH 3T3 cells, *Proc. Natl. Acad. Sci.* 88 (1991) 4230–4234.
- [4] D.C. Chang, Cell poration and cell fusion using an oscillating electric field, *Biophys. J.* 56 (1989) 641–652.
- [5] D.C. Chang, P.Q. Gao, B.L. Maxwell, High efficiency gene transfection by electroporation using a radio-frequency electric field, *Biochim. Biophys. Acta* 1992 (1991) 153–160.
- [6] P. Marszalek, D.S. Liu, T.Y. Tsong, Schwan equation and transmembrane potential induced by alternating electric field, *Biophys. J.* (1990) 1053–1058.
- [7] M.C. Vernhes, P.A. Cabanes, J. Teissié, Chinese hamster ovary cells sensitivity to localized electrical stresses, *Bioelectrochem. Bioenerg.* 48 (1999) 17–25.
- [8] M. Puc, K. Flisar, S. Reberšek, D. Miklavčič, Electroporator for in vitro cell permeabilization, *Radiol. Oncol.* (2001) 203–207.
- [9] B. Poddevin, S. Orłowski, J. Belehradek Jr., L.M. Mir, Very high cytotoxicity of bleomycin introduced into the cytosol of cells in culture, *Biochem. Pharmacol.* 42 (1991) 67–75(suppl.).
- [10] S. Orłowski, J. Belehradek Jr., C. Paoletti, L.M. Mir, Transient electroporation-mediated molecular uptake and cell viability, *Biophys. J.* 80 (2001) 755–764.
- [11] R. Heller, M.J. Jaroszeski, R. Perrot, J. Messina, R. Gilbert, Effective treatment of B16 melanoma by direct delivery of bleomycin using electro-chemotherapy, *Melanoma Res.* 7 (1997) 10–18.
- [12] G. Serša, M. Čemažar, D. Miklavčič, Antitumor effectiveness of electrochemotherapy with *cis*-Diamminedichloroplatinum(II) in mice, *Cancer Res.* 55 (1995) 3450–3455.
- [13] M. Čemažar, D. Miklavčič, L. Vodovnik, T. Jarm, Z. Rudolf, B. Štabuc, T. Čufer, G. Serša, Improved therapeutic effect of electrochemotherapy with cisplatin by intratumoral drug administration and changing of electrode orientation for electroporation on EAT tumor model in mice, *Radiol. Oncol.* 29 (1995) 121–127.
- [14] L.M. Mir, L.F. Glass, G. Serša, J. Teissié, C. Domenge, D. Miklavčič, M.J. Jaroszeski, S. Orłowski, D.S. Reintgen, Z. Rudolf, M. Belehradek, R. Gilbert, M.P. Rols, J. Belehradek Jr., J.M. Bachaud, R. DeConti, B. Štabuc, M. Čemažar, P. Coninx, R. Heller, Effective treatment of cutaneous and subcutaneous malignant tumors by electrochemotherapy, *Br. J. Cancer* 77 (1998) 2336–2342.
- [15] R. Heller, M.J. Jaroszeski, D.S. Reintgen, C.A. Puleo, R.C. DeConti, R.A. Gilbert, L.F. Glass, Treatment of cutaneous and subcutaneous tumors with electrochemotherapy using intralesional bleomycin, *Cancer* 83 (1998) 148–157.
- [16] G. Serša, B. Štabuc, M. Čemažar, D. Miklavčič, Z. Rudolf, Electrochemotherapy with cisplatin: clinical experience in malignant melanoma patients, *Clin. Cancer Res.* 6 (2000) 863–867.
- [17] G. Serša, B. Štabuc, M. Čemažar, D. Miklavčič, Z. Rudolf, Electrochemotherapy with cisplatin: the systemic antitumor effectiveness of cisplatin can be potentiated locally by the application of electric pulses in the treatment of malignant melanoma skin metastases, *Melanoma Res.* 10 (2000) 381–385.
- [18] J.L. Biedler, H. Riehm, Cellular resistance to actinomycin D in Chinese hamster cells in vitro, *Cancer Res.* 30 (1970) 1174–1184.
- [19] A.C. Guyton, J.E. Hall, *Textbook of Medical Physiology*, Saunders, New York, 1996, pp. 57–93.
- [20] A.J. Vander, J.H. Sherman, D.S. Luciano, *Human Physiology: The Mechanisms of Body Function*, McGraw-Hill, New York, 1970.
- [21] S. Deusch, *Models of the Nervous System*, Wiley, New York, 1967, pp. 25–28.
- [22] G. Serša, B. Štabuc, M. Čemažar, B. Jančar, D. Miklavčič, Z. Rudolf, Electrochemotherapy with cisplatin: potentiation of local antitumor effectiveness by application of electric pulses in cancer patients, *Eur. J. Cancer* 34 (1998) 1213–1218.
- [23] L.M. Mir, S. Orłowski, J. Belehradek, J. Teissié, M.P. Rols, G. Serša, D. Miklavčič, R. Gilbert, R. Heller, Biomedical applications of electric pulses with special emphases on antitumor electrochemotherapy, *Bioelectrochem. Bioenerg.* 38 (1995) 203–207.
- [24] L. Vodovnik, *Neurocybernetics*, ZAFE, Ljubljana, Slovenia, 1991 (in Slovenian).
- [25] I. Daskalov, N. Mudrov, E. Peycheva, Exploring new instrumentation. Parameters for electrochemotherapy. Attacking tumors with bursts of biphasic pulses instead of single pulses, *IEEE Eng. Med. Biol.* (1999) 62–66.
- [26] M.P. Rols, J. Teissié, Electroporation-mediated molecular uptake and cell viability, *Biophys. J.* 75 (1998) 1415–1423.
- [27] P.J. Canatella, J.F. Karr, J.A. Petros, M.R. Prausnitz, Quantitative study of electroporation-mediated molecular uptake and cell viability, *Biophys. J.* 80 (2001) 755–764.

*Paper 3*

**The effect of high frequency electric pulses on muscle contractions  
and antitumor efficiency in vivo for a potential use  
in clinical electrochemotherapy**

D. Miklavčič<sup>a</sup>, **G. Pucihar**<sup>a</sup>, M. Pavlovec<sup>a</sup>, S. Ribarič<sup>b</sup>, M. Mali<sup>a</sup>, A. Maček-Lebar<sup>a</sup>,  
M. Petkovšek<sup>a</sup>, J. Nastran<sup>a</sup>, S. Kranjc<sup>c</sup>, M. Čemažar<sup>c</sup>, G. Serša<sup>c</sup>

<sup>a</sup>University of Ljubljana, Faculty of Electrical Engineering, Tržaška 25, SI-1000 Ljubljana, Slovenia

<sup>b</sup>University of Ljubljana, Medical Faculty, Institute of Pathophysiology, Zaloška 4, SI-1000 Ljubljana, Slovenia

<sup>c</sup>Institute of Oncology, Zaloška 2, SI-1000 Ljubljana, Slovenia

**Abstract**

Muscle contractions present the main source of unpleasant sensations for patients undergoing electrochemotherapy. The contractions are a consequence of high voltage pulse delivery. Relatively low repetition frequency of these pulses (1 Hz) results in separate muscle contractions associated with each single pulse that is delivered. It would be possible to reduce the number of unpleasant sensations by increasing the frequency of electric pulses above the frequency of tetanic contraction, provided that the antitumor efficiency of electrochemotherapy remains the same. These assumptions were investigated in the present paper by measuring the muscle torque at different pulse repetition frequencies and at two different pulse amplitudes in rats and studying the antitumor efficiency of electrochemotherapy at different pulse repetition frequencies on tumors in mice. Measurements of muscle torque confirmed that pulse frequencies above the frequency of tetanic contraction (N100 Hz) reduce the number of individual contractions to a single muscle contraction. Regardless of the pulse amplitude, with increasing pulse frequency muscle torque increases up to the frequency of 100 or 200 Hz and then decreases to a value similar to that after application of a 1 Hz pulse train. Electrochemotherapy in vivo with higher repetition frequencies inhibits tumor growth and is efficient at all pulse frequencies examined (1 Hz–5 kHz). These results suggest that there is a considerable potential for clinical use of high frequency pulses in electrochemotherapy.

# The effect of high frequency electric pulses on muscle contractions and antitumor efficiency in vivo for a potential use in clinical electrochemotherapy

Damijan Miklavčič<sup>a,\*</sup>, Gorazd Pucihar<sup>a</sup>, Miran Pavlovec<sup>a</sup>, Samo Ribarič<sup>b</sup>, Marko Mali<sup>a</sup>, Alenka Maček-Lebar<sup>a</sup>, Marko Petkovšek<sup>a</sup>, Janez Nastran<sup>a</sup>, Simona Kranjc<sup>c</sup>, Maja Čemažar<sup>c</sup>, Gregor Serša<sup>c</sup>

<sup>a</sup>University of Ljubljana, Faculty of Electrical Engineering, Tržaška 25, SI-1000 Ljubljana, Slovenia

<sup>b</sup>University of Ljubljana, Medical Faculty, Institute of Pathophysiology, Zaloška 4, SI-1000 Ljubljana, Slovenia

<sup>c</sup>Institute of Oncology, Zaloška 2, SI-1000 Ljubljana, Slovenia

Received 27 November 2003; received in revised form 7 June 2004; accepted 13 July 2004

Available online 10 December 2004

## Abstract

Muscle contractions present the main source of unpleasant sensations for patients undergoing electrochemotherapy. The contractions are a consequence of high voltage pulse delivery. Relatively low repetition frequency of these pulses (1 Hz) results in separate muscle contractions associated with each single pulse that is delivered. It would be possible to reduce the number of unpleasant sensations by increasing the frequency of electric pulses above the frequency of tetanic contraction, provided that the antitumor efficiency of electrochemotherapy remains the same. These assumptions were investigated in the present paper by measuring the muscle torque at different pulse repetition frequencies and at two different pulse amplitudes in rats and studying the antitumor efficiency of electrochemotherapy at different pulse repetition frequencies on tumors in mice. Measurements of muscle torque confirmed that pulse frequencies above the frequency of tetanic contraction (>100 Hz) reduce the number of individual contractions to a single muscle contraction. Regardless of the pulse amplitude, with increasing pulse frequency muscle torque increases up to the frequency of 100 or 200 Hz and then decreases to a value similar to that after application of a 1 Hz pulse train. Electrochemotherapy in vivo with higher repetition frequencies inhibits tumor growth and is efficient at all pulse frequencies examined (1 Hz–5 kHz). These results suggest that there is a considerable potential for clinical use of high frequency pulses in electrochemotherapy.

© 2004 Elsevier B.V. All rights reserved.

**Keywords:** Electrochemotherapy; Pulse frequency; Muscle torque; Pain; Strain gauge

## 1. Introduction

Electrochemotherapy is an efficient local treatment of tumors, which combines the delivery of nonpermeant, cytotoxic chemotherapeutic agent (e.g. bleomycin, cisplatin) and short, high voltage electric pulses. At the appropriate pulse parameters (amplitude, duration and number of pulses) the permeability of tumor cell membranes increases transiently, thereby allowing the chemo-

therapeutic agent to enter the cells, and to exert its cytotoxic action.

Electrochemotherapy was found to be efficient in preclinical studies in mice and rats mostly for the treatment of cutaneous and subcutaneous tumors. Due to the promising results, electrochemotherapy has soon found its way from the laboratory to the clinic. The first clinical trial was performed by Mir and coworkers in Villejuif (France) in 1991 [1] and was soon followed by several clinical trials by other research groups, mostly from USA (Tampa [2,3]), France (besides Villejuif also Toulouse and Reims [4]) and Slovenia (Ljubljana [5]). The tumors under investigation

\* Corresponding author. Tel.: +38 6 1 4768 456; fax: +38 6 1 4264 658.

E-mail address: [damijan@svarun.fe.uni-lj.si](mailto:damijan@svarun.fe.uni-lj.si) (D. Miklavčič).

were head and neck squamous cell carcinoma, basal cell carcinoma, melanoma, and adenocarcinomas. Combined therapy of application of electric pulses to the tumor following intravenous or intratumoral drug injection resulted in objective response rates of the tumors ranging from 62% to 100% [4], while tumors that were exposed only to electric pulses or to a chemotherapeutic drug did not respond. The chemotherapeutic drug administered in the first clinical trials was bleomycin. Bleomycin is a highly cytotoxic drug, which cannot permeate the intact cell membranes, or only in extremely small quantities [6,7]. Concomitant electric pulses that permeabilize tumor cell membranes significantly increase its cytotoxicity. In later clinical trials, another chemotherapeutic drug cisplatin was introduced, which was also demonstrated to be efficient in electrochemotherapy [8–10]. Detailed information on results of clinical application of electrochemotherapy can be found in the latest reviews [11,12].

Despite the success of the therapy, some side effects were reported. They include slight oedema or erythema in the treatment sites, which usually disappeared in less than 24 h after the treatment. In some cases, marks from the electrodes (usually two flat, parallel, stainless steel, plate electrodes with rounded corners) were visible several weeks after treatment, which most probably resulted from the very high local current density that can produce local burns. However, these post-pulse phenomena are not a cause of concern. Most unpleasant or even painful, according to the patients, were the sensations during the pulse delivery, which were mainly attributed to muscle contractions provoked by high amplitude of the pulses. In a great majority of the clinical trials, these pulses were delivered with relatively low pulse repetition frequency (one pulse per second, 1 Hz), which resulted in individual sensations and muscle contractions.

Because a high amplitude of electric pulses is necessary for efficient electroporation of tumor cell membranes it is difficult to eliminate related muscle contractions. On the other hand, it would be possible to at least reduce the number of individual muscle contractions by increasing the frequency of electric pulses above the frequency of tetanic contraction, provided that the efficiency of electrochemotherapy remains the same. In our recent study *in vitro* we already showed that with increasing pulse repetition frequencies, the uptake of nonpermeant molecule remained at a similar level as at the frequency of 1 Hz [13]. We thus proposed that pulses with higher repetition frequencies could reduce the unpleasant sensations associated with muscle contractions during electrochemotherapy without reducing the efficiency of electrochemotherapy. In addition, higher repetition frequencies would also shorten the duration of the treatment, especially in the case where multiple needle electrodes are used (needle electrodes placed equidistantly in a circle, an additional electrode can be located in the center), where pairs of electrodes are activated sequentially [14,15].

In this paper the assumptions that high frequency pulses would reduce the number of individual muscle contractions and decrease the duration of the treatment while preserving the efficiency of electrochemotherapy were investigated further by performing experiments *in vivo*. This was done by measuring muscle torque in rats after electric pulse delivery to the *ischiodic* nerve and by performing electrochemotherapy of a subcutaneous animal tumor model *in vivo* in mice using different pulse repetition frequencies.

## 2. Materials and methods

### 2.1. Measurements of muscle torque in rats

The experiments were performed on 16 male Wistar rats with an average body weight of  $250 \pm 31$  g. The handling of animals was in accordance with the license issued by the Ministry of Agriculture, Republic of Slovenia (license number 326-07-26/98) and consistent with the recommendations of the Panel on Ethics in Biomedical research, Medical Faculty of the University of Ljubljana. Ten minutes before the treatment, the rats were anesthetized with the combination of Rompun, 2% solution (Bayer, Germany) and Ketanest, 10 mg/ml (Parke-Davis, Germany). Anesthesia lasted for 1 h, which proved to be enough for the entire set of measurements. The rats recovered from general anesthesia approximately 30 min after the experiment was finished, which enabled the observation of possible motoric dysfunctions of the stimulated leg. No changes in the motoric function of the leg were observed.

The measurements of muscle response were performed by measuring muscle torque with a strain gauge transducer mounted on a wooden platform [16]. The right hind limb of a rat was stabilized and fastened to aluminium brace equipped with a strain gauge (Fig. 1). The height of the platform was adjustable to keep the leg in plane with the transducer. Muscle contractions rotated the aluminium brace, which induced voltage changes in the strain gauge. Using a BIOPAC MP 100SW data acquisition system (BIOPAC, USA), the analog voltage signal was amplified (BIOPAC, DA 100 amplifier), converted into a digital signal and stored on a computer (Fig. 1). Data acquisition lasted 1 s with a sampling frequency of 1 kHz (i.e. 1000 samples/s).

Electric pulses were generated by an AFG 310 function generator (Sony-Tektronix, Japan). The signal from the function generator was amplified by a power amplifier [17] and delivered to the electrodes (two stainless steel needle electrodes, 0.3 mm in diameter, 10 mm long and 8 mm apart) mounted on a plastic holder to keep the distance constant and reproducible. The electrodes were inserted through the skin into the thigh muscle in the vicinity of the *ischiodic* nerve branches. Synchronization of electric pulses with data acquisition was ensured by a trigger

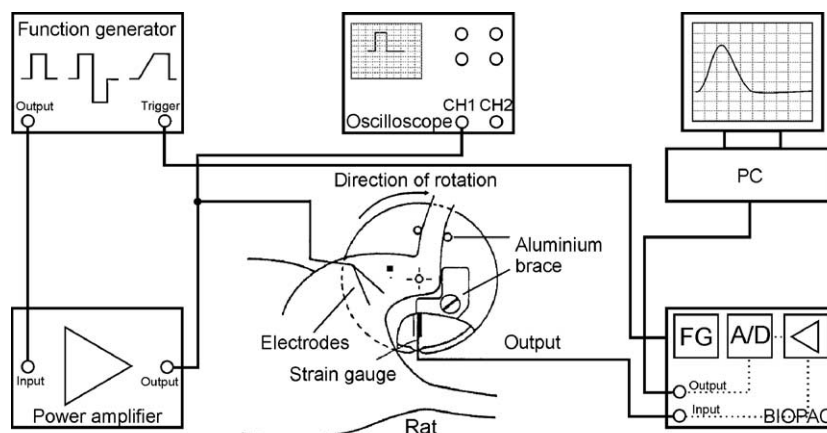


Fig. 1. Setup of the experiment (partly adapted from Ref. [16]). A/D—analogue/digital converter, FG—function generator integrated in a BIOPAC system.

pulse from the BIOPAC system to the function generator (Fig. 1).

Electric pulses were delivered at two different pulse amplitudes. The low pulse amplitude was applied to elicit muscle response locally, while the high pulse amplitude was applied to elicit muscle response at electrochemotherapy conditions. The amplitude of the low voltage pulses was determined before the measurements in the following way. At two repetition frequencies (100 and 200 Hz), where the highest muscle torque was obtained in the preliminary experiments, the pulse amplitude was increased until the plateau of the muscle torque was obtained. At this amplitude the contraction of the hip muscles was not significant. The amplitude which was used for the experiments (70 V) was approximately 20% lower than the amplitude of the plateau. The amplitude of the high voltage pulses was set to a value where the voltage to distance ratio was approximately 1300 V/cm (typical electrochemotherapy value). Because the highest output from our power amplifier was 250 V, the distance between the electrodes was decreased from 8 to 2 mm in order to achieve the appropriate voltage to distance ratio. A numerical calculation of electric field distribution for this experimental application showed that the muscle between the electrodes was exposed to electric fields higher than 1000 V/cm.

The muscle was stimulated with a train of eight 100  $\mu$ s rectangular pulses. At low pulse amplitudes applied (70 V) the measurements were performed at pulse repetition frequencies of 1, 10, 20, 50, 100, 200, 500, 1000, 2000, and 5000 Hz, while at high pulse amplitudes applied (250 V), the measurements were performed at 1, 100, 500, 1000, and 5000 Hz. A shorter range of pulse frequencies in the latter case was used to prevent muscle fatigue, which would occur especially at low pulse frequencies (10, 20, and 50 Hz), and to reduce muscle and nerve injuries due to high local current density. The frequencies were delivered systematically, for half of the animals in an ascending order, and for the other half in a descending order. The repetition frequency ( $f_p$ ) was varied by shortening the delay ( $t_d$ ) between two consecutive pulses while keeping the

number of pulses ( $N=8$ ) and duration of each pulse ( $t_p=100$   $\mu$ s) constant;  $f_p=1/(t_p+t_d)$ .

Muscle contractions in response to a 1 Hz pulse frequency were similar on all eight pulses in a train, for both low and high pulse amplitudes, so we stimulated the muscle with only one pulse, which was repeated at the end of the experiment to verify reproducibility with respect to electrode positions, movement artifacts and muscle fatigue. To prevent muscle fatigue, a 2-min delay was taken between each pulse repetition frequency applied.

To determine whether the muscle was stimulated directly or indirectly through its motor nerve, the muscle torque was measured before and after the denervation. The same amplitude of pulses produced similar amplitude of muscle torque before and after denervation, so we concluded that the muscle was to a large extent stimulated directly.

Statistical analysis was performed with one-way repeated measures analysis of variance (ANOVA) test with Dunnett's method for multiple comparisons versus control group (1 Hz) using SigmaStat 2.0 (Jandel Scientific, San Rafael, CA, USA). The difference was considered as statistically significant for  $P<0.05$ .

## 2.2. Electrochemotherapy of subcutaneous animal tumor model in mice

In the experiments, the inbred A/J mice of both sexes were used, which were purchased from the Institute of Pathology, University of Ljubljana (Ljubljana, Slovenia). Mice were maintained at 21 °C with natural day/night light cycle in a conventional animal colony. Before an experiment, mice were subjected to an adaptation period for at least 10 days. Mice of both sexes in good condition, weighing 20–22 g, without signs of fungal or other infection, 12–14 weeks old, were included in experiments. Treatment protocols were approved by the Department of Agriculture of the Republic of Slovenia No. 323-02-237/01.

The fibrosarcoma SA-1 tumor model (The Jackson Laboratory, Bar Harbor, USA), syngeneic to A/J mice, was used in the study. Tumor cells were obtained from the ascitic form of tumors in mice, serially transplanted every 7 days. Solid subcutaneous tumors, located dorsolaterally in mice, were initiated by an injection of  $5 \times 10^5$  SA-1 cells in 0.1 ml 0.9% NaCl solution. The viability of the cells, as determined by a trypan blue dye exclusion test, was over 95%. Six days after transplantation, when the tumors reached approximately 40 mm<sup>3</sup> in volume, the mice were randomly divided into 12 experimental groups, and subjected to a specific experimental protocol on day 0.

Bleomycin at a dose of 50 µg per animal was injected intravenously. This dose was selected because it usually does not result in complete responses in order to observe only the tumor growth retardation. Electric pulses were delivered by two flat, parallel stainless steel plate electrodes with rounded corners (length=35 mm, width=7 mm, thickness=1 mm, interelectrode distance=8 mm). They were placed at the opposite margins of the tumor in cranial/caudal direction. Good electrical conductance between the electrodes and the skin was assured by applying a conductive gel to the skin. Eight 100 µs rectangular electric pulses with a pulse amplitude of 1040 V and repetition frequencies 1 Hz, 10 Hz, 100 Hz, 1 kHz and 5 kHz were generated by an electropulsator, developed for this purpose at the Faculty of Electrical Engineering, University of Ljubljana [18]. In the combined treatment groups, mice were treated with electric pulses 3 min after bleomycin injection, which was sufficient for the distribution of bleomycin. Mice in the control group and the group subjected to electric pulses only were injected with 0.01 M PBS (pH 7.4) instead of bleomycin. Each treatment group consisted of 6 to 10 mice and the experiment was repeated twice.

Tumor growth was followed by measuring three mutually orthogonal tumor diameters ( $e_1$ ,  $e_2$  and  $e_3$ ) with a caliper on each consecutive day following the day the treatment was performed. Tumor volumes were calculated from the equation  $V = \pi \times e_1 \times e_2 \times e_3 / 6$ . From the measurements, the arithmetic mean and standard error of the mean (SE) were calculated for each experimental group. If the tumor became unpalpable and did not regrow after 100 days, the therapeutic response was classified as a complete response (CR).

### 3. Results

#### 3.1. Measurements of muscle torque in rats

A typical muscle response to low pulse amplitudes (70 V) and different pulse repetition frequencies ranging from 1 Hz to 5 kHz is shown in Fig. 2A. Eight pulses of 100 µs duration were applied at all repetition frequencies except for

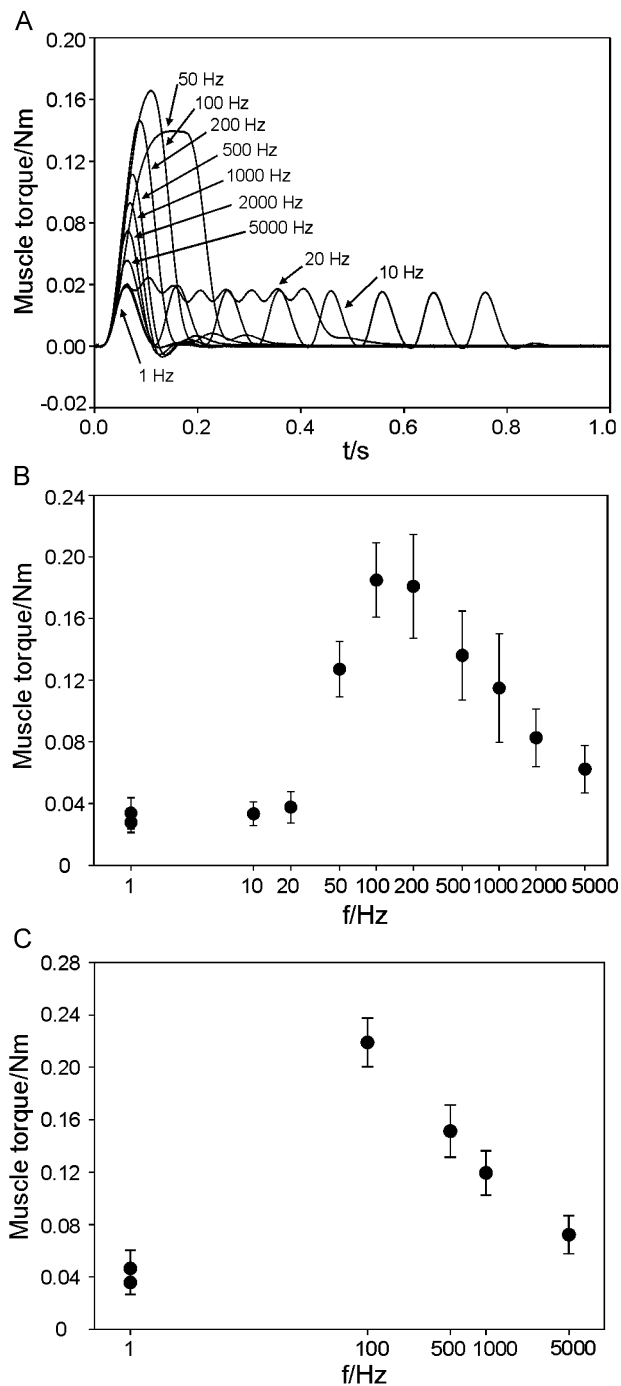


Fig. 2. (A) Time course of a typical muscle response to different pulse repetition frequencies at low pulse amplitudes (70 V, interelectrode distance 8 mm). (B) Muscle torque as a function of pulse repetition frequency at low pulse amplitudes (70 V, interelectrode distance 8 mm) and (C) high pulse amplitudes (250 V, interelectrode distance 2 mm). Each point represents the mean of eight experiments (rats)  $\pm$  S.D. A train of eight pulses was used at all frequencies examined except at 1 Hz where only one pulse was applied.

1 Hz where only one pulse was applied (see Materials and methods). The repetition frequency of the pulses was adjusted by changing the delay between two consecutive pulses in a train. The average muscle torque as a function of pulse frequency is shown in Fig. 2B. With increasing

Table 1

Pulse parameters of muscle response to low pulse amplitudes and different pulse frequencies in rats

f/Hz	$t_{\max} \pm \text{S.D.}$	$t_{\text{delay}} \pm \text{S.D.}$	$t_{\text{rise}} \pm \text{S.D.}$	$t_{50\%} \pm \text{S.D.}$
1	56.4 ± 1.1	23.1 ± 0.8	25.3 ± 1.7	44.4 ± 1.8
50	117.3 ± 23.3	35.4 ± 3.2	52.9 ± 7.2	143.6 ± 5.1
100	104.1 ± 4.1	35.6 ± 2.2	48.3 ± 2.3	79.5 ± 4.1
200	84.3 ± 3.3	32.9 ± 1.9	39.1 ± 1.5	59.1 ± 3.3
500	70.8 ± 1.9	28.9 ± 2.2	32.6 ± 1.4	49.6 ± 1.4
1000	65.6 ± 2.6	26.4 ± 2.9	30.3 ± 2.2	46.9 ± 1.5
2000	61.9 ± 2.2	24.8 ± 2.9 <sup>a</sup>	28.5 ± 1.9	45.8 ± 1.3 <sup>a</sup>
5000	60.9 ± 2.9	23.3 ± 3.7 <sup>a</sup>	28.8 ± 2.7	46.0 ± 1.3 <sup>a</sup>

The values are given as the mean of eight measurements ± S.D. Parameters were determined only at pulse frequencies where tetanic contraction was obtained.  $t_{\max}$ —time at maximum muscle response,  $t_{\text{delay}}$ —time at which 10% of the maximum response is obtained,  $t_{\text{rise}}$ —time between 10% and 90% of the response,  $t_{50\%}$ —time in between 50% of the response. Time is in ms.

<sup>a</sup> No statistically significant difference compared to 1 Hz.

frequency of the pulses, muscle torque increases, reaches a maximum value between 100 and 200 Hz, and then decreases. At frequencies of 50 Hz or higher, muscle response becomes smooth (tetanic contraction). Instead of eight consecutive muscle contractions, only one, tetanic contraction is obtained. At 5 kHz, muscle torque is approximately twice as high as the muscle torque at 1 Hz. Higher repetition frequencies also shorten the duration of the muscle response, at frequencies above 2 kHz the muscle response to a pulse train is similar to the response to a single pulse (Table 1).

The average muscle response to pulses with high amplitudes (250 V) and different pulse repetition frequencies is shown in Fig. 2C. Similar to low amplitude pulses (70 V), with increasing pulse repetition frequency muscle torque first increases, reaches a maximum value at 100 Hz, where a tetanic contraction is obtained, and then decreases. At the highest pulse frequency examined (5 kHz) muscle torque is approximately twice as high as the muscle torque at 1 Hz, but instead of eight consecutive muscle contractions only one muscle contraction is obtained.

The amplitude of muscle torque to a single pulse (1 Hz) before and after the measurements showed no muscle fatigue (Fig. 2B and C).

### 3.2. Electrochemotherapy of subcutaneous tumors in mice

As Fig. 3 shows, electrochemotherapy with bleomycin inhibits tumor growth at all five repetition frequencies of electric pulses investigated in this study (1 Hz, 10 Hz, 100 Hz, 1 kHz, and 5 kHz) (Fig. 3). The antitumor efficiency of electrochemotherapy with different pulse repetition frequencies is also evident in the percentage of complete responses (CR) of the tumors (Table 2). The highest percentage of CR (36.8%) was observed for the “standard” repetition frequency of 1 Hz, and the lowest (9.1%) for repetition

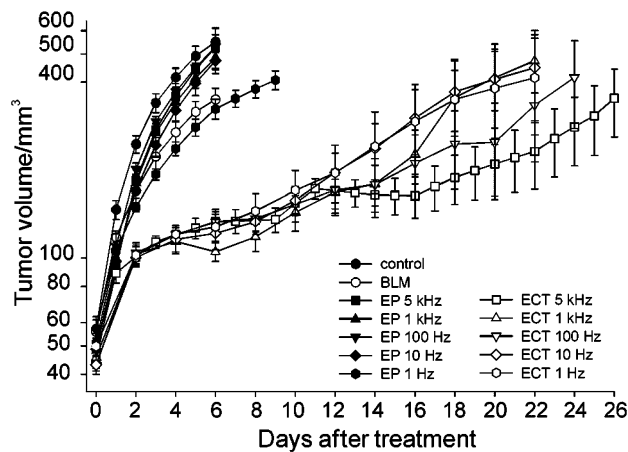


Fig. 3. Electrochemotherapy of tumors in mice with different pulse repetition frequencies. The results are presented as mean ± S.E. of the mean. BLM—bleomycin only, EP—electric pulses only, ECT—electrochemotherapy (BLM+EP).

frequency 1 kHz. Neither electric pulses alone nor bleomycin alone significantly inhibit tumor growth.

## 4. Discussion

Electrochemotherapy is used as an efficient local treatment of cutaneous and subcutaneous tumors in patients [1,4,11,12,19]. The most unpleasant side effects of electrochemotherapy reported so far are the muscle contractions and related sensations during pulse delivery [4,11,19,20]. Although they subside immediately after each pulse, patients find them uncomfortable and sometimes painful. To some extent, it would be possible to reduce these unpleasant sensations by using pulse repetition frequencies higher than tetanic, as an alternative to the ‘standard’ pulse frequency of 1 Hz. However, the efficiency of electrochemotherapy with such pulse frequencies should be preserved. We thus examined the effect of different pulse frequencies on muscle response and the efficiency of electrochemotherapy in vivo.

According to our results, the muscle torque increases with an increase of the repetition frequency of the pulses, reaches a plateau between 100 and 200 Hz and then decreases. At the highest frequency examined (5 kHz) the muscle torque was two times higher than at 1 Hz (Fig. 2B). This bell-shaped dependence of muscle torque on pulse frequency can be explained as follows. At pulse repetition frequencies lower than tetanic, each pulse in the train of pulses provokes an isolated muscle contraction. With increasing frequency of these pulses, consecutive muscle contractions eventually fuse, thereby increasing the muscle torque and reaching a tetanic contraction. In the case of an infinite number of pulses, further increase in pulse frequency eventually results in the same maximum muscle torque regardless of the pulse frequency applied (in time, muscle torque would decrease due to muscle fatigue).

Table 2  
Antitumor efficiency of electrochemotherapy with different pulse repetition frequencies

Therapy	Control	BLM	EP 1 Hz	EP 10 Hz	EP 100 Hz	EP 1 kHz	EP 5 kHz	ECT 1 Hz	ECT 10 Hz	ECT 100 Hz	ECT 1 kHz	ECT 5 kHz
N	16	12	10	13	12	7	13	19	18	17	11	18
CR	0	0	0	0	0	0	0	7	2	5	1	4
(%CR)	(0)	(0)	(0)	(0)	(0)	(0)	(0)	(36.8)	(11.1)	(29.4)	(9.1)	(22.2)

BLM—bleomycin only, EP—electric pulses only, ECT—electrochemotherapy (BLM+EP); N—number of animals in each experimental group; CR—number of complete responses (absence of any trace of tumor at day 100 post-treatment).

However, in the case of a low number of pulses in a train, as in the case of electrochemotherapy (e.g. eight pulses), a further increase in pulse frequency (above 200 Hz) actually decreases muscle torque. This occurs because of a progressively shorter duration of the pulse train compared to the duration of a typical muscle response. For example, at a pulse frequency of 1 kHz, the duration of a train of eight 100  $\mu$ s pulses is 8 ms, while the response of a skeletal muscle, necessary to develop its maximum force of contraction, typically lasts from 40 to 100 ms. Also, at higher pulse repetition frequencies, an increasing number of pulses from the pulse train fails to provoke a muscle contraction because of the latent period of the muscle (during this period the muscle cannot contract and is completely refractory). If, for example, the repetition frequency of the pulses is 1 kHz and the latent period of the muscle is 2 ms, only three out of eight pulses applied will induce muscle contractions, and the cumulative amplitude of muscle response will consequently decrease.

We also examined how the muscle would respond to pulse amplitudes that produce voltage to distance ratios similar to those used in electrochemotherapy (1300 V/cm). Due to limitations of our voltage amplifier, we decreased the interelectrode distance to achieve the appropriate voltage to distance ratio (see Materials and methods). However, different interelectrode distances and consequently different portions of the muscle between the electrodes made quantitative comparison of the amplitude of the muscle response impossible. A numerical calculation of electric field distribution for the case of high pulse amplitudes showed that the muscle between the electrodes was exposed to electric fields higher than 1000 V/cm. Although this value exceeds the reported thresholds for reversible or irreversible electroporation [21–25], the dependence of the muscle response to different pulse repetition frequencies still remains qualitatively similar to the dependence of the muscle response at low pulse amplitudes (Fig. 2B and C). Though we would expect muscle electroporation to have an influence on the muscle response, we did not observe such an influence. This is most probably because at such pulse amplitudes the surrounding muscle groups, which contribute to the muscle response, were excited but were not electroporated.

Despite the fact that at the highest pulse frequencies examined muscle torque remains at values above those at 1 Hz, the number of individual sensations reduces from eight

to a single sensation, which is a significant advantage over the 1 Hz pulse application. These measurements are in agreement with the hypothesis presented in our previous paper [13].

It is reasonable to assume that the dependence of muscle torque on pulse frequency in humans would be similar to that observed in rats. Indeed, we have performed measurements of muscle torque in healthy volunteers and the results, although obtained at low pulse amplitudes, substantiate our assumptions (data not shown). This suggests that pulses with repetition frequencies higher than the frequency of tetanic contraction (approx. 40 Hz for humans) would considerably reduce the number of individual sensations for the patients during electrochemotherapy. Also, pulse frequencies higher than tetanic would eventually decrease the muscle response and consequently the intensity of sensation to a value similar to that after application of a single pulse.

It was shown by several authors that pain sensation depends on pulse parameters such as pulse amplitude, number, duration, frequency, and shape of the pulses [26–31]. With respect to pulse frequency, the authors [29,31] concluded that with increasing pulse frequency the pain sensation decreases and electrical excitation becomes more tolerable. Although sinusoidal pulses were examined in these two studies, the conclusions are in agreement with our results.

Another important benefit from the use of high frequency pulses is a shorter duration of the therapy in case of multiple arrays of electrodes. Usually six to nine electrodes are used in such experiments, and pairs of electrodes are activated sequentially [14,15,19,32,33]. Since more than one pulse can be applied on each pair of electrodes [14,15] important improvement of using high frequency pulses is a significant reduction of the total duration of the treatment.

While we presented the benefits of using higher pulse frequencies, it was also important to determine the antitumor efficiency of electrochemotherapy with each of these frequencies. In experiments *in vitro* it was already shown that the uptake of molecules is comparable for repetition frequencies ranging from 1 Hz up to 8.3 kHz [13]. A step forward was made in the present study, where we demonstrated that electrochemotherapy with higher pulse frequencies can also be successfully performed *in vivo*. According to the results of electrochemotherapy on our

tumor model in mice, electrochemotherapy is efficient regardless of the pulse repetition frequency applied (at least in the investigated range). We should note that the bleomycin dose used in our experiments usually does not result in complete responses. Despite low bleomycin dose, some tumors responded completely to electrochemotherapy at all pulse repetition frequencies examined (Table 2).

In a clinical environment, the efficiency of electrochemotherapy with high frequency pulses still needs to be investigated. Daskalov et al. [34] have demonstrated the antitumor efficiency of electrochemotherapy in patients, but they have only compared pulse frequencies of 1 Hz and 1 kHz. At these two pulse frequencies, they did not observe any difference between tumor responses.

In summary, we demonstrated that pulse frequencies above the frequency of tetanic contraction (above 100 Hz) gradually reduce the number of individual muscle contractions. At pulse frequencies higher than 2000 Hz the muscle torque is similar to that after application of a 1 Hz pulse train (a typical electrochemotherapy protocol), but with an advantage of only one sensation instead of eight. Experiments in vivo in mice demonstrated similar efficiency of electrochemotherapy regardless of the pulse frequency examined. These results suggest that there is a considerable potential for clinical use of high frequency pulses in electrochemotherapy.

## Acknowledgements

The authors wish to thank Tadej Kotnik for reading the manuscript. This work was supported by the Ministry of Education, Science and Sports of the Republic of Slovenia.

## References

- [1] L.M. Mir, M. Belehradec, C. Domenge, S. Orlowski, J. Poddevin Jr., G. Schwab, B. Luboinnski, C. Paoletti, Electrochemotherapy, a novel antitumor treatment: first clinical trial, *C. R. Acad. Sci. Paris* 313 (1991) 613–618.
- [2] R. Heller, Treatment of cutaneous nodules using electrochemotherapy, *J. Fla. Med. Assoc.* 82 (1995) 147–150.
- [3] R. Heller, M.J. Jaroszeski, L.F. Glass, J.L. Messina, D.P. Rapaport, R.C. DeConti, N.A. Fenske, R.A. Gilbert, L.M. Mir, D.S. Reintgen, Phase I/II trial for the treatment of cutaneous and subcutaneous tumors using electrochemotherapy, *Cancer* 77 (1996) 964–971.
- [4] L.M. Mir, L.F. Glass, G. Serša, J. Teissié, C. Domenge, D. Miklavčič, M.J. Jaroszeski, S. Orlowski, D.S. Reintgen, Z. Rudolf, M. Belehradec, R. Gilbert, M.P. Rols, J.J. Belehradec, J.M. Bachaud, R. DeConti, B. Štabuc, M. Čemažar, P. Coninx, R. Heller, Effective treatment of cutaneous and subcutaneous malignant tumors by electrochemotherapy, *Br. J. Cancer* 77 (1998) 2336–2342.
- [5] Z. Rudolf, B. Štabuc, M. Čemažar, D. Miklavčič, L. Vodovnik, G. Serša, Electrochemotherapy with bleomycin. The first clinical experience in malignant melanoma patients, *Radiol. Oncol.* 29 (1995) 229–235.
- [6] L.M. Mir, O. Tounekti, S. Orlowski, Bleomycin: revival of an old drug, *Gen. Pharmacol.* 27 (1996) 745–748.
- [7] M. Čemažar, D. Miklavčič, G. Serša, Intrinsic sensitivity of tumor cells to bleomycin as an indicator of tumor response to electrochemotherapy, *Jpn. J. Cancer Res.* 89 (1998) 328–333.
- [8] G. Serša, B. Štabuc, M. Čemažar, B. Jančar, D. Miklavčič, Z. Rudolf, Electrochemotherapy with cisplatin: potentiation of local cisplatin antitumor effectiveness by application of electric pulses in cancer patients, *Eur. J. Cancer* 34 (1998) 1213–1218.
- [9] G. Serša, B. Štabuc, M. Čemažar, D. Miklavčič, Z. Rudolf, Electrochemotherapy with cisplatin: clinical experience in malignant melanoma patients, *Clin. Cancer Res.* 6 (2000) 863–867.
- [10] M. Reberšek, T. Čufer, Z. Rudolf, G. Serša, Electrochemotherapy with cisplatin of breast cancer tumor nodules in a male patient, *Radiol. Oncol.* 34 (2000) 357–361.
- [11] G. Serša, M. Čemažar, Z. Rudolf, Electrochemotherapy: advantages and drawbacks in treatment of cancer patients, *Cancer Ther.* 1 (2003) 133–142.
- [12] A. Gotheif, L.M. Mir, J. Gehl, Electrochemotherapy: results of cancer treatment using enhanced delivery of bleomycin by electroporation, *Cancer Treat. Rev.* 29 (2003) 371–387.
- [13] G. Pucihar, L.M. Mir, D. Miklavčič, The effect of pulse repetition frequency on the uptake into electroporabilized cells in vitro with possible applications in electrochemotherapy, *Bioelectrochemistry* 57 (2002) 167–172.
- [14] L.M. Mir, P. Devauchelle, F. Quintin-Colonna, F. Delisle, S. Doliger, D. Fradelizi, J. Belehradec Jr., S. Orlowski, First clinical trial of cat soft-tissue sarcomas treatment by electrochemotherapy, *Br. J. Cancer* 76 (1997) 1617–1622.
- [15] L.H. Ramirez, S. Orlowski, D. An, G. Bindoula, R. Dzodic, P. Ardouin, C. Bognel, J. Belehradec, J.N. Munck, L.M. Mir, Electrochemotherapy on liver tumours in rabbits, *Br. J. Cancer* 77 (1998) 2104–2111.
- [16] S. Ribarič, A. Stefanovska, M. Brzin, M. Kogovšek, P. Krošelj, Biochemical, morphological, and functional changes during peripheral nerve regeneration, *Mol. Chem. Neuropathol.* 15 (1991) 143–157.
- [17] K. Flisar, M. Puc, T. Kotnik, D. Miklavčič, Cell membrane electroporation with arbitrary pulse waveforms, *IEEE Eng. Med. Biol. Mag.* 22 (2003) 77–81.
- [18] M. Petkovšek, J. Nastran, D. Vončina, P. Zajec, D. Miklavčič, G. Serša, High voltage pulse generation, *Electron. Lett.* 38 (2002) 680–682.
- [19] R. Heller, R. Gilbert, M.J. Jaroszeski, Clinical applications of electrochemotherapy, *Adv. Drug Deliv. Rev.* 35 (1999) 119–129.
- [20] M.J. Jaroszeski, R. Gilbert, R. Heller, Electrochemotherapy: an emerging drug delivery method for the treatment of cancer, *Adv. Drug Deliv. Rev.* 26 (1997) 185–197.
- [21] D. Miklavčič, K. Beravs, D. Šemrov, M. Čemažar, F. Demšar, G. Serša, The importance of electric field distribution for effective in vivo electroporation of tissues, *Biophys. J.* 74 (1998) 2152–2158.
- [22] D. Šemrov, D. Miklavčič, Calculation of the electrical parameters in electrochemotherapy of solid tumours in mice, *Comput. Biol. Med.* 28 (1998) 439–448.
- [23] J. Gehl, T.H. Sørensen, K. Nielsen, P. Raskmark, S.L. Nielsen, T. Skovsgaard, L.M. Mir, In vivo electroporation of skeletal muscle: threshold, efficacy and relation to electric field distribution, *Biochim. Biophys. Acta* 1428 (1999) 233–240.
- [24] D. Miklavčič, D. Šemrov, H. Mekid, L.M. Mir, A validated model of in vivo electric field distribution in tissues for electrochemotherapy and for DNA electrotransfer for gene therapy, *Biochim. Biophys. Acta* 1523 (2000) 73–83.
- [25] D. Batiškaite, D. Cukjati, L.M. Mir, Comparison of in vivo electroporation of normal and malignant tissue using the Cr-EDTA uptake test, *Biologija* 2 (2003) 45–47.
- [26] B. Bromm, R.D. Treede, Withdrawal reflex, skin resistance reaction and pain ratings due to electrical stimuli in man, *Pain* 9 (1980) 339–354.
- [27] L. Zhang, D.P. Rabussay, Clinical evaluation of safety and human tolerance of electrical sensation induced by electric fields with non-invasive electrodes, *Bioelectrochemistry* 56 (2002) 233–236.

- [28] A.Y.J. Szeto, F.A. Saunders, Electrocutaneous stimulation for sensory communication in rehabilitation engineering, *IEEE Trans. Biomed. Eng.* 29 (1982) 300–308.
- [29] M.R. Prausnitz, The effects of electric current applied to skin: a review for transdermal drug delivery, *Adv. Drug Deliv. Rev.* 18 (1996) 395–425.
- [30] A.R. Ward, V.J. Robertson, Sensory, motor, and pain thresholds for stimulation with medium frequency alternating current, *Arch. Phys. Med. Rehabil.* 79 (1998) 273–278.
- [31] L. Vodovnik, C. Long, E. Regenos, A. Lippay, Pain response to different tetanizing currents, *Arch. Phys. Med. Rehabil.* 46 (1965) 187–192.
- [32] R.A. Gilbert, M.J. Jaroszeski, R. Heller, Novel electrode designs for electrochemotherapy, *Biochim. Biophys. Acta* 1334 (1997) 9–14.
- [33] G.A. Hoffman, S.B. Dev, S. Dimmer, G.S. Nanda, Electroporation therapy: a new approach for the treatment of head and neck cancer, *IEEE Trans. Biomed. Eng.* 46 (1999) 752–759.
- [34] I. Daskalov, N. Mudrov, E. Peycheva, Exploring new instrumentation parameters for electrochemotherapy. Attacking tumors with bursts of biphasic pulses instead of single pulses, *IEEE Eng. Med. Biol. Mag.* 18 (1999) 62–66.

*Paper 4***The influence of medium conductivity on electropermeabilization and survival of cells in vitro****G. Pucihar**, T. Kotnik, M. Kandušer, D. Miklavčič

Laboratory of Biocybernetics, Faculty of Electrical Engineering, University of Ljubljana, Tržaška 25, SI-1000, Ljubljana, Slovenia

**Abstract**

Electropermeabilization and cell death caused by the exposure to high voltage electric pulses depends on the parameters of pulses, as well as the composition of the extracellular medium. We studied the influence of extracellular conductivity on electropermeabilization and survival of cells in vitro. For this purpose, we used a physiological medium with a conductivity of 1.6 S/m and three artificial media with conductivities of 0.14, 0.005, and 0.001 S/m. Measurements of pH, osmolarity, and cell diameter were made to estimate possible side effects of the media on the cells. Our study shows that the percentage of surviving cells increases with the decreasing medium conductivity, while the percentage of electropermeabilized cells remains unaffected. Our results show that cell survival in experiments involving electropermeabilization can be improved by decreasing the medium conductivity. To provide an interpretation of experimental results, we have theoretically estimated the resting transmembrane voltage, the induced transmembrane voltage, the time constant of the voltage inducement, and heating of the cell suspension for each of the media used. These calculations imply that for accurate interpretation of experimental results, both the induced and the resting transmembrane voltage must be considered, taking into account the conductivity and the ionic composition of the extracellular medium.

# The influence of medium conductivity on electropermeabilization and survival of cells in vitro

Gorazd Pucihar, Tadej Kotnik, Maša Kandušer, Damijan Miklavčič\*

Laboratory of Biocybernetics, Faculty of Electrical Engineering, University of Ljubljana, Tržaška 25, SI-1000, Ljubljana, Slovenia

Received 27 April 2001; received in revised form 25 May 2001; accepted 31 May 2001

## Abstract

Electropermeabilization and cell death caused by the exposure to high voltage electric pulses depends on the parameters of pulses, as well as the composition of the extracellular medium. We studied the influence of extracellular conductivity on electropermeabilization and survival of cells in vitro. For this purpose, we used a physiological medium with a conductivity of 1.6 S/m and three artificial media with conductivities of 0.14, 0.005, and 0.001 S/m. Measurements of pH, osmolarity, and cell diameter were made to estimate possible side effects of the media on the cells. Our study shows that the percentage of surviving cells increases with the decreasing medium conductivity, while the percentage of electropermeabilized cells remains unaffected. Our results show that cell survival in experiments involving electropermeabilization can be improved by decreasing the medium conductivity. To provide an interpretation of experimental results, we have theoretically estimated the resting transmembrane voltage, the induced transmembrane voltage, the time constant of the voltage inducement, and heating of the cell suspension for each of the media used. These calculations imply that for accurate interpretation of experimental results, both the induced and the resting transmembrane voltage must be considered, taking into account the conductivity and the ionic composition of the extracellular medium. © 2001 Elsevier Science B.V. All rights reserved.

**Keywords:** Electropermeabilization; Induced transmembrane voltage; Resting transmembrane voltage; Medium conductivity; Bleomycin; DC3F cells

## 1. Introduction

Application of electric pulses to cells induces a voltage across cell membrane, termed the induced transmembrane voltage. This voltage combines with the resting transmembrane voltage, which is permanently present on cell membrane. Due to the induced component, which is proportional to the pulse amplitude, the total transmembrane voltage can significantly exceed its physiological range, and above a certain critical value in the range from 200 to 1000 mV [1,2], a large increase in membrane permeability is observed. The occurrence of transient high-permeability state of the cell membrane due to high-voltage electric pulses is called electropermeabilization. The ability to influence membrane permeability by application of electric pulses has opened a variety of applications in oncology [3–7], genetics [8–10], and cell biology [11,12].

To date, only few studies have experimentally investigated the effect of medium conductivity on electropermeabilization in vitro. Rols and Teissié [13] have shown that the threshold value for permeabilization of Chinese hamster ovary cells was independent of the ionic strength of the pulsing medium. The conductivities were not given, but on the basis of the media composition, it follows that they were above 0.1 S/m. Neumann [14] has shown that the percentage of permeabilized green algae cells (*Chlamydomonas reinhardtii*) decreases if the medium conductivity decreases (the interval of conductivities was from 0.0056 to 0.035 S/m). Djuzenova et al. [15] have shown that decreasing the extracellular conductivity results in lower viability of the murine myeloma cells while the PI-uptake increases, but the investigated interval of conductivities was quite narrow (0.08–0.37 S/m). Lojewska et al. [16] confirmed the theoretical predictions that the charging time of the membrane decreases with increasing medium conductivity, but this study was performed on lipid bilayers, and only in a range of very low conductivities (up to 0.005 S/m).

In summary, each of the studies mentioned above investigated the effect of the medium conductivity on electrop-

\* Corresponding author. Tel.: +38-61-4768-456; fax: +38-61-4264-658.

E-mail address: damijan@svarun.fe.uni-lj.si (D. Miklavčič).

ermeabilization on cells and lipid bilayers at a specific, narrow interval of conductivities, with partially different observations. Therefore, we decided to investigate the influence of extracellular media on permeabilization and survival of the cells on a wider interval of conductivities ( $\sim 0.001$  to  $\sim 1.5$  S/m). In order to theoretically explain the experimental results, resting transmembrane voltage  $U_{TR}$ , time constant  $\tau$ , and function  $f_S$  were calculated and their influence on the permeabilization and survival of the cells in different media was estimated. To determine the influence of the extracellular conductivity on physiological parameters of media and cells, measurements of pH, osmolarity, and cell diameter have been performed, and heating of cell suspension was estimated.

## 2. Materials and methods

### 2.1. Extracellular media

Cell line DC3F—spontaneously transformed Chinese hamster fibroblasts [17]—were grown in Eagle's Minimum Essential Medium (EMEM) with added 10% fetal bovine serum—FCS (both from Sigma, USA). Electroporation was performed in four different media with conductivities in range of three orders of magnitude ( $\sim 0.001$  to  $\sim 1$  S/m). Medium 1 was prepared according to the specifications of the research group of Rols and Teissié [18]. Because mediums 2 and 3 were prepared by dilution of medium 1 with isoosmotic solution of distilled water and sucrose (medium 2: distilled water/medium 1, 100:3; medium 3: distilled water/medium 1, 100:0.45), medium 1 represented our reference point. For the last medium, we used Spinner Minimum Essential Medium (SMEM, Gibco, Life Technologies, USA), which is a  $Ca^{2+}$ -depleted version of EMEM, and has approximately 10 times higher conductivity than medium 1. The basic components of the electroporative media used are presented in Table 1.

Table 1  
Composition of media used

	SMEM <sup>a</sup> (mg/l)	m1 (mg/l)	m2 (mg/l)	m3 (mg/l)
NaCl	6800	–	–	–
KCl	400	–	–	–
NaHCO <sub>3</sub>	2200	–	–	–
NaH <sub>2</sub> PO <sub>4</sub>	1580	–	–	–
Na <sub>2</sub> HPO <sub>4</sub>	–	1125	33.75	4.95
KH <sub>2</sub> PO <sub>4</sub>	–	283	8.49	1.244
MgCl <sub>2</sub>	–	95	2.85	0.418
MgSO <sub>4</sub>	200	–	–	–
Sucrose	–	85580	85580	85580
Glucose	1000	–	–	–

m1—medium 1, m2—medium 2, m3—medium 3.

<sup>a</sup>Besides the components given in the table, SMEM also contains amino acids, vitamins, and Phenol Red. More detailed information on composition can be found in Gibco catalog under Catalog no. 21385.

### 2.2. Measurements of specific conductivity, osmolarity and pH of the media

Conductometer MA 5950 (Metrel, Slovenia) was used to determine the specific conductivity of the media. Values for osmolarity were determined with an osmometer—Vapour Pressure Osmometer 5500 (Wascor). pH was measured using pH-meter MA 5750 (Metrel). All results are values corresponding to the temperature of 25 °C. Mean values for all parameters were determined from at least three measurements.

### 2.3. Measurements of cell diameter

Measurements were performed with DP 10 camera fixed on CK 40 microscope (both Olympus, Germany) at 200× magnification. Cell diameters were measured on three samples of cells ( $\sim 15$  cells in each sample) from cell suspension not exposed to electric pulses. Measurements were performed in each of the media used and also in the presence of bleomycin.

### 2.4. Electroporation

To generate square pulses, prototype Electroporator was used (rise time and fall time:  $< 1$   $\mu$ s, pulse width: 5  $\mu$ s–5 ms, pulse amplitude: 25–500 V, number of pulses: 1–128), made in our laboratory at the Faculty of Electrical Engineering, University of Ljubljana, Slovenia. A train of eight rectangular pulses, duration: 100  $\mu$ s, repetition frequency: 1 Hz, was used for electroporation.

### 2.5. Experiment

After trypsination, cells were centrifuged for 5 min at 1000 rpm ( $180 \times g$ ) at 4 °C, resuspended in specific extracellular medium within minutes after centrifugation, and centrifuged again at the same conditions. For mediums 2 and 3, a third centrifugation was needed. Although additional centrifugation could increase the mechanical damage to the cells and reduce the survival of the cells in these two media, it was necessary in order to wash away the remains of EMEM. The high conductivity of EMEM could otherwise increase the desired low conductivity of extracellular media. However, as the absolute plating efficiency did not change significantly for any of the investigated medium, we can conclude that the cell survival in mediums 2 and 3 was not affected by the additional centrifugation (data not shown). Cells were then diluted in the specific extracellular medium to obtain  $2 \times 10^7$  cells/ml and kept at 4 °C until electroporation. Cells were never kept in suspension longer than 30 min, because otherwise, the viability of cells was affected (especially in medium 3). A 50- $\mu$ l droplet of cell suspension

was put between two parallel plate stainless steel electrodes. Trains of eight rectangular pulses with amplitudes from 0 to 400 V (voltage kept constant for all the pulses in the train, voltage drop over the duration of the pulse < 1%) were applied. All experiments were performed at 25 °C. After 10 min of incubation at this temperature, SMEM was added to prevent drying. After additional 30 min, cells were diluted with EMEM with 10% FCS to obtain 50 cells/ml. Due to its content of Ca<sup>2+</sup>, EMEM was found to have a harmful effect on permeabilized cells. However, 40 min of incubation were sufficient to prevent this effect. Cell suspension was put in petri dishes (4 ml/dish) and stored in an incubator (37 °C, 5% CO<sub>2</sub>) for plating efficiency.

After 5 days, cells were fixed with methanol (Merck, Germany) and stained with 1% crystal violet (Sigma). Colonies were then counted and normalized to the control (cells subjected to exactly the same procedures for each medium except of exposure to electric pulses) to obtain the fraction of surviving cells in this medium.

To determine the percentage of electropermeabilized cells, the cells (2 × 10<sup>7</sup> cells/ml) were exposed to electric pulses in presence of 5 nM concentration of cytotoxic agent bleomycin, as described in detail in Ref. [19]. An intact membrane is impermeable to bleomycin, and while at 5 nM external concentration bleomycin has no effect on nonpermeabilized cells, it causes the death of permeabilized cells. The protocol of cell handling after electropermeabilization, including fixation and staining, was the same as for survival. Colonies were counted and normalized to the control (unpulsed cells, 5 nM bleomycin) and the fraction of cells surviving the exposure of electric pulses with added bleomycin was subtracted from 100% to obtain the fraction of permeabilized cells.

## 2.6. Data processing

All experiments were repeated at least three times on different days. Results from different repetitions of experiments were pooled together and are presented as mean and standard error of the mean (S.E.). On the fraction of permeabilized and surviving cells, a two-parameter sigmoid was fitted,

$$y(u) = \frac{100\%}{1 + e^{\frac{u_c - u}{b}}}, \quad (1)$$

where  $y$  is the fraction of cells,  $u$  is the pulse amplitude,  $u_c$  denotes the value of pulse amplitude corresponding to electropermeabilization or survival of 50% of the cells, and  $b$  determines the slope of the sigmoid curve. All fits were obtained by least-squares nonlinear regression using SigmaPlot 5.0.

Statistical analysis was performed with Kruskal–Wallis one-way analysis of variance on ranks (ANOVA) test using SigmaStat 2.0.

## 3. Results

### 3.1. Theoretical considerations

For a spherical cell with radius  $r$  and no surface charge, the induced transmembrane voltage ( $U_{TI}$ ) can be calculated using the equation [20,21]

$$U_{TI} = f_S r E \cos \varphi (1 - \exp(-t/\tau)) \quad (2)$$

where  $\varphi$  is the angle between the direction of the applied electric field  $E$  and the normal from the center of the cell to the point of interest on cell surface,  $t$  denotes time from the onset of the electric field, while the function  $f_S$  and the time constant  $\tau$  are given by

$$f_S = \frac{3\lambda_o(3dr^2\lambda_i + (3d^2r - d^3)(\lambda_m - \lambda_i))}{2r^3(\lambda_m + 2\lambda_o)(\lambda_m + 0.5\lambda_i) - 2(r-d)^3(\lambda_o - \lambda_m)(\lambda_i - \lambda_m)} \quad (3)$$

$$\tau = \frac{rC_m}{\frac{2\lambda_o\lambda_i}{2\lambda_o + \lambda_i} + \frac{r}{d}\lambda_m}, \quad (4)$$

with  $C_m$ , the membrane capacitance,  $d$ , the membrane thickness and  $\lambda_i$ ,  $\lambda_m$ ,  $\lambda_o$ , the conductivities of the cytoplasm, cell membrane and extracellular medium, respectively. All symbols are also presented in Fig. 1, and their typical values are given in the Appendix A.

Under physiological conditions, where  $\lambda_m \ll \lambda_i$ ,  $\lambda_o$ , the function  $f_S$  is reduced to a constant,  $f_S = 1.5$ , and the

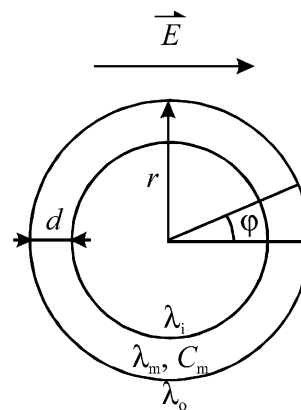


Fig. 1. Model of the cell. ( $E$ —electric field,  $r$ —cell diameter,  $d$ —membrane thickness,  $\varphi$ —the angle between the direction of  $E$  and a point on cell membrane,  $\lambda_i$ ,  $\lambda_o$ ,  $\lambda_m$ —intracellular, extracellular, and membrane conductivity, respectively,  $C_m$ —membrane capacitance).

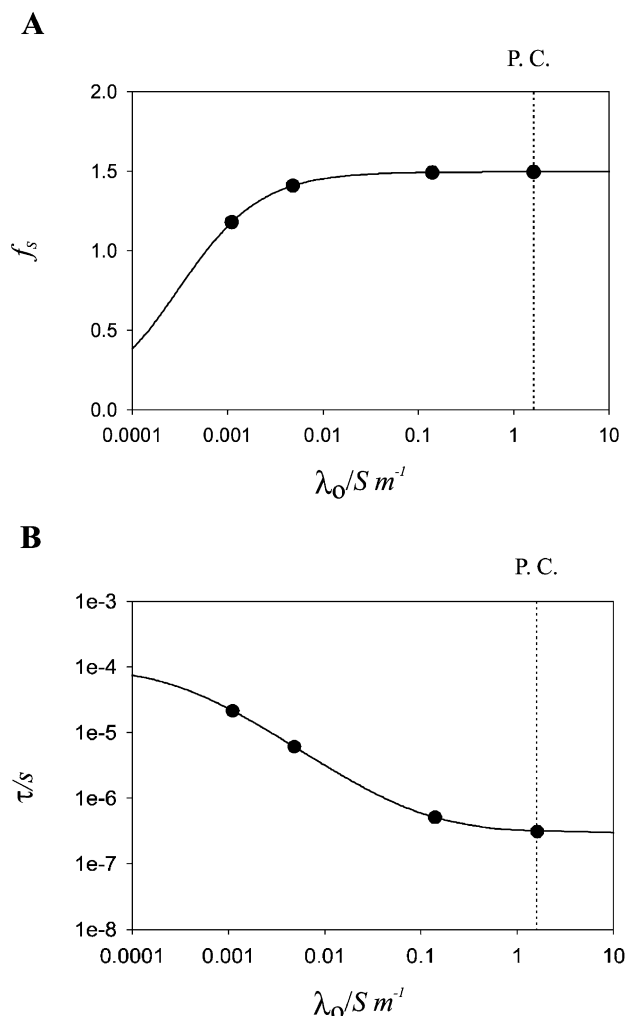


Fig. 2. The influence of extracellular conductivity on (A) the value of the function  $f_s$ , (B) the time constant  $\tau$ . The symbols represent the values of conductivities of media used in our study (values of parameters used:  $r = 5.94 \mu\text{m}$ ,  $E = 1000 \text{ V/cm}$ ,  $\lambda_m = 5 \times 10^{-7} \text{ S/m}$ ,  $\lambda_i = 0.2 \text{ S/m}$ ,  $d = 5 \text{ nm}$ ,  $C_m = 0.01 \text{ F/m}^2$ ). P.C.—physiological conditions.

time constant  $\tau$  takes values in the range of several microseconds, which is considerably shorter than pulse durations typically used in electroporation. With these simplifications, Eq. (2) transforms into

$$U_{\text{TI}} = 1.5rE \cos \varphi. \quad (5)$$

If the cell suspension is placed between parallel plate electrodes with dimensions much larger than the distance between them, we can assume that the electric field is homogeneous and can be calculated as  $U/h$ , where  $U$  is the applied voltage and  $h$  is the distance between electrodes.

While Eq. (5) holds under physiological conditions, artificial extracellular media with a reduced conductivity are often used in electroporation experiments, mostly to decrease the heating [22]. In addition, certain other applications of electric pulses on cells (e.g. electrofu-

sion, electrorotation) require the conductivity of the extracellular medium to be reduced even further, e.g. by several orders of magnitude with respect to physiological conditions. A comparison of the values of the induced transmembrane voltage obtained using Eqs. (2) and (5) shows that under such conditions, the results given by the latter are incorrect. With the decrease of the medium conductivity, the value of the function  $f_s$  starts to decrease (from the asymptotic value of 1.5), and the value of the time constant  $\tau$  increases (Fig. 2). As this figure shows, the dependence of  $f_s$  only becomes important with the decrease of the medium conductivity exceeding two orders of magnitude with respect to the physiological value, while  $\tau$  is sensitive to smaller variations of the medium conductivity.

Besides the induced voltage, the resting transmembrane voltage ( $U_{\text{TR}}$ ) is also present on cell membrane, but due to its relatively small value ( $\sim -70 \text{ mV}$ ), it is often neglected in determination of the total transmembrane voltage. The resting transmembrane voltage is affected by extracellular conductivity, and since media of different ionic compositions have, in general, different conductivities, consequently, the resting transmembrane voltages of the cells suspended in different media are also different. In low conductivity media, the resting voltage can take values considerably higher than in physiological case and should not be neglected in determination of the total transmembrane voltage

$$U_{\text{T}} = U_{\text{TI}} + U_{\text{TR}}. \quad (6)$$

### 3.2. Calculations

#### 3.2.1. Values for function $f_s$ , time constant $\tau$ , and resting transmembrane voltage $U_{\text{TR}}$

Values for function  $f_s$ , and time constant  $\tau$  were calculated using Eqs. (3) and (4), respectively, while the resting transmembrane voltage  $U_{\text{TR}}$  was calculated using Goldman's equation [23,24]. All values are shown in Table 2. Function  $f_s$  decreases considerably only in medium 3. Time constant increases with decrease of the medium conductivity and for media 2 and 3, it takes values consid-

Table 2

Calculated values for function  $f_s$ , time constant  $\tau$ , and resting transmembrane voltage  $U_{\text{TR}}$

	SMEM	m1	m2	m3
$f_s$	1.495	1.492	1.409	1.18
$\tau$ ( $\mu\text{s}$ )	0.31	0.51	6.1	21.4
$U_{\text{TR}}$ (mV)	-78	-68	-159 <sup>a</sup>	-209 <sup>a</sup>

m1—medium 1, m2—medium 2, m3—medium 3.

<sup>a</sup>Because the resting transmembrane voltage was calculated under a questionable assumption of unchanged intracellular ionic concentration regardless of the extracellular ionic concentration, the calculated values might not reflect the actual situation (see Section 4 for details).

Table 3

Calculated values for resistivity of cell suspension  $R$ , temperature rise after one pulse  $\Delta T_1$  and after train of eight pulses  $\Delta T_8$ , calculated at the highest voltage applied—400 V

	SMEM	m1	m2	m3
$R$ ( $\Omega$ )	51	587	17.1 k	72.9 k
$\Delta T_1$ ( $^\circ\text{C}$ )	1.5	0.13	0.0045	0.0011
$\Delta T_8$ ( $^\circ\text{C}$ )	12	1.04	0.036	0.0084

m1—medium 1, m2—medium 2, m3—medium 3.

erably higher than in the physiological case. Resting transmembrane voltage varies with decrease of the medium conductivity and may have an effect on the total transmembrane voltage.

### 3.2.2. Heating of cell suspension

Because during electroporation, cell suspension is exposed to high-voltage pulses (up to 400 V), electric currents can take values up to several A (depending on medium conductivity) and the heating of cell suspension could influence cell survival. If we assume that electric energy from the pulse of amplitude  $U$  and duration  $t$  transmitted to cell suspension transforms into heat without loss and heat dissipation to the electrodes and the surrounding air, the change in temperature of the suspension  $\Delta T$  can be estimated as

$$\Delta T = \frac{U^2 t}{R \rho V c_p} \quad (7)$$

with  $R$ , resistivity of cell suspension ( $R = h^2 / \lambda V$ );  $h$ , distance between electrodes;  $\rho$ , specific density;  $V$ , volume; and  $c_p$ , the specific heat of droplet of cell suspension. Furthermore, the specific conductivity of cell suspension can be calculated as [24]

$$\lambda = \lambda_o \frac{1 - f}{1 + 0.5f} \quad (8)$$

with  $\lambda_o$ , the specific conductivity of the pure medium;  $f$ , the volume fraction occupied by the cells in suspension. Introducing Eq. (8) into Eq. (7), the maximum heating can be calculated (i.e., the heating for the highest voltage applied and after a train of eight pulses where no thermal dissipation between pulses is assumed). The results are shown in Table 3. The values of parameters used in calculations are shown in Appendix A.

Calculated values show a noticeable temperature rise of up to 12  $^\circ\text{C}$  in SMEM, while the temperature rise in other media is less than 1.04  $^\circ\text{C}$ . Because the cells were kept at 4  $^\circ\text{C}$  before the exposure to electric pulses, even the highest temperature rise due to heating (at highest voltage amplitudes) is too small to affect cell survival in any of the media used. This was verified using a water bath where cell suspension was heated from 4 to 30  $^\circ\text{C}$  and cooled back to 4  $^\circ\text{C}$ . The procedure was repeated twice. The cells were taken from the cell suspension before, during, and at the end of the experiment. The clonogenic test has shown that the cell survival remained unaffected.

## 3.3. Experimental results

### 3.3.1. Specific conductivity, osmolarity and pH of media used

Measured values for all parameters are shown in Table 4. Specific conductivities span three orders of magnitude which is sufficient for an observable change in induced transmembrane voltage, according to Eq. (2). Osmolarity results are within physiological values obtained from the literature (260–320 mOsm/kg  $\text{H}_2\text{O}$ ) [25], which according to a study by Golzio et al. [26] should not affect cell electroporation. Measured values for pH were within physiological values as well ( $\text{pH}_{\text{phys.}} = 7.4$ ) [27]. Therefore, the effect of the variations of osmolarities and pH can be excluded from further examination.

### 3.3.2. Cell diameter

ANOVA test has shown no statistically significant difference between cell diameters in different media used. Therefore, all results were pooled and the median diameter was calculated to be 11.877  $\mu\text{m}$  on measured population of 545 cells. The value of cell diameter did not change significantly during the experiment.

### 3.3.3. Survival and electroporation of the cells

Experimental results for survival and electroporation of the cells as a function of pulse amplitude are shown in Fig. 3A,B. Survival results show that cells in SMEM have the lowest 50% survival threshold (267 V), followed by other media in descending order of conductivities. According to the experimental results, electroporation

Table 4

Measured values for specific conductivity, osmolarity and pH of media used

	SMEM	m1	m2	m3
Specific conductivity ( $\text{S m}^{-1}$ )	$1.61 \pm 0.5\%$	$0.14 \pm 0.5\%$	$0.0048 \pm 0.5\%$	$0.0011 \pm 1\%$
Osmolarity (mOsm $\text{kg}^{-1}$ $\text{H}_2\text{O}$ )	$299 \pm 1\%$	$286 \pm 1\%$	$269 \pm 1\%$	$259 \pm 1\%$
pH	$7.11 \pm 0.01$	$7.40 \pm 0.01$	$7.30 \pm 0.01$	$7.12 \pm 0.01$

m1—medium 1, m2—medium 2, m3—medium 3.

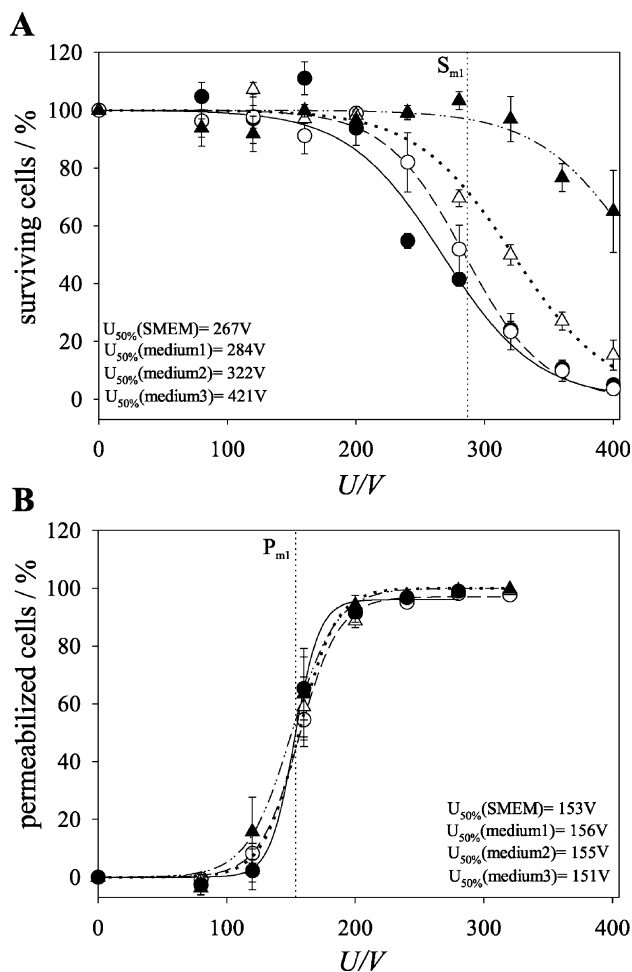


Fig. 3. Experimentally determined results for (A) survival and (B) permeabilization of the cells plotted as a function of pulse amplitude. Train of eight 100- $\mu\text{s}$  rectangular pulses, repetition frequency 1 Hz was used for pulsation. Each point on the figure represents the mean of three values  $\pm$  S.E. Conductivities of media used: SMEM ( $\bullet$ ): 1.61 S/m, medium 1 ( $\circ$ ): 0.14 S/m, medium 2 ( $\triangle$ ): 0.0048 S/m, medium 3 ( $\blacktriangle$ ): 0.0011 S/m.  $S_{m1}$  denotes the pulse amplitude causing the death of 50% of the cells in medium 1.  $P_{m1}$  denotes the pulse amplitude needed for permeabilization of 50% of the cells in medium 1.

abilization of the cells is not affected by the conductivity of the medium.

#### 4. Discussion

According to the experimental results (Fig. 3A,B), by decreasing the medium conductivity, we observed an influence on survival of the cells, but no effect was obtained on permeabilization of the cells. To explain why survival was affected by reduced medium conductivity while permeabilization remained unaffected, the influence of the reduction of the medium conductivity on the physiological parameters of the media and cells must be estimated.

The measurements have shown that the values of pH and osmolarity of the media are within physiological values, and cell diameter is unaffected by different media

used. Moreover, estimated heating of cell suspension could not affect cell survival even at the highest voltages applied in the medium having the highest conductivity (this was verified experimentally by using water bath).

However, according to Eq. (2) and Goldman's equation [23,24], the induced and the resting transmembrane voltage both depend on the medium conductivity. Different values of these two voltages in different media could explain the experimentally obtained results for survival and permeabilization of the cells. To illustrate the influence of different medium conductivities on the induced and the resting transmembrane voltage at different pulse amplitudes in steady-state conditions, the total transmembrane voltage (Eq. (6)) is plotted as a function of pulse amplitude. It is therefore represented as a straight line with slope determined by the function  $f_s$  and the initial value determined by the resting transmembrane voltage ( $U_{\text{TR}}$ —absolute value). The total transmembrane voltages for different media have slopes and initial values corresponding to the conductivity of the specific medium (Table 2) (Fig. 4).

According to Fig. 4, at the pulse amplitudes between 100 and 200 V, the differences between the total transmembrane voltages of the cells in media with different conductivities are insignificant. If we consider that the value of the total transmembrane voltage determines the degree of permeabilization of the cell, cells exposed to pulses with amplitudes below 200 V should have the same degree of permeabilization independent of the media conductivity. This is in agreement with our experimentally obtained results for survival and permeabilization of the cells at mentioned pulse amplitudes (Fig. 3A,B).

At pulse amplitudes higher than 200 V, the difference between the calculated total transmembrane voltages for

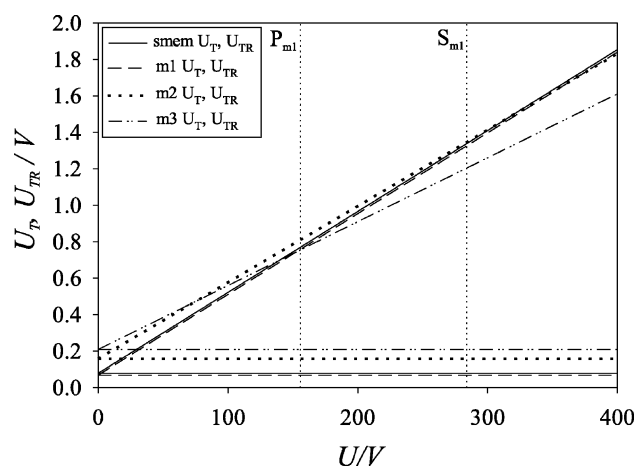


Fig. 4. The total transmembrane voltage ( $U_T$ , at  $\varphi = 0^\circ$ , steady-state conditions) and the resting transmembrane voltage ( $U_{\text{TR}}$ ) as a function of pulse amplitude ( $U$ ) for each of the media used. The slope of  $U_T$  is determined by the value of the function  $f_s$ , while the initial value is determined by the value of the resting transmembrane voltage ( $U_{\text{TR}}$ —absolute value).  $S_{m1}$  denotes the pulse amplitude causing the death of 50% of the cells in medium 1.  $P_{m1}$  denotes the pulse amplitude needed for permeabilization of 50% of the cells in medium 1.

SMEM, medium 1, and medium 2 remains insignificant, while the total transmembrane voltage for medium 3 is significantly lower. Based on these theoretical considerations, for pulse amplitudes above 200 V, one would expect a similar degree of permeabilization and consequently, cell survival in SMEM and media 1 and 2, but a considerably lower degree of permeabilization and higher cell survival in medium 3. Experimental results confirm that at each given pulse amplitude, cell survival is much higher in medium 3 than in SMEM, medium 1, and medium 2, but they suggest that there are also differences between the latter three media (Fig. 3A).

Although our theoretical predictions for survival and permeabilization of the cells on the basis of the total transmembrane voltages are in a qualitative agreement with experimental results, the difference between the total transmembrane voltage for medium 3 and the other three media would suggest a smaller difference in cell survival of the cells than obtained by the experiments. Two plausible explanations for this can be stated.

In our calculations, the value of the resting transmembrane voltage was determined under the assumption of unchanged internal ionic concentration ( $[K^+]_i = 140$  mM,  $[Na^+]_i = 5$  mM) regardless of external ionic concentration (e.g.:  $[K^+]_o = 0.044$  mM in medium 3). Because of the high ionic concentration difference, especially when low conductivity media are used, it is likely that ionic flux occurs (mostly  $K^+$  efflux) which decreases the resting transmembrane voltage [15,28,29]. Moreover, a living cell will pump ions as long as ATP is present and it is improbable that the resting potential of the living cell could change as dramatically as the calculations suggest (from  $-78$  to  $-209$  mV). Taking this into account, reducing the resting transmembrane voltage would shift the straight lines of the total transmembrane voltages towards lower values (Fig. 4), thus increasing the survival of the cells in low conductivity media. Reduction of the resting transmembrane voltage due to ionic flux is more emphasized with higher pulse amplitudes and during the pulses subsequent to electropermeabilization.

Perhaps the most plausible explanation for the disagreement between theoretically predicted and experimentally obtained survival of the cells in medium 3 is the dynamics of permeabilization, which was not accounted for in Fig. 4. Because of the large value of time constant  $\tau$  in low conductivity media (Table 2), the membrane becomes permeabilized before the total transmembrane voltage reaches the maximum value predicted by Eq. (2) (Fig. 5A, phase 2). A substantial increase of membrane permeability results in an increase of its conductivity  $\lambda_m$ , and consequently, in the decrease of the function  $f_s$  (Fig. 5B). This hinders further increase of the total transmembrane voltage, which then even slightly decreases, as confirmed by experimental observations made by Hibino et al. [30] on sea urchin eggs, and by the modeling study made by DeBruin and Krassowska [31] (Fig. 5A, phase 3).

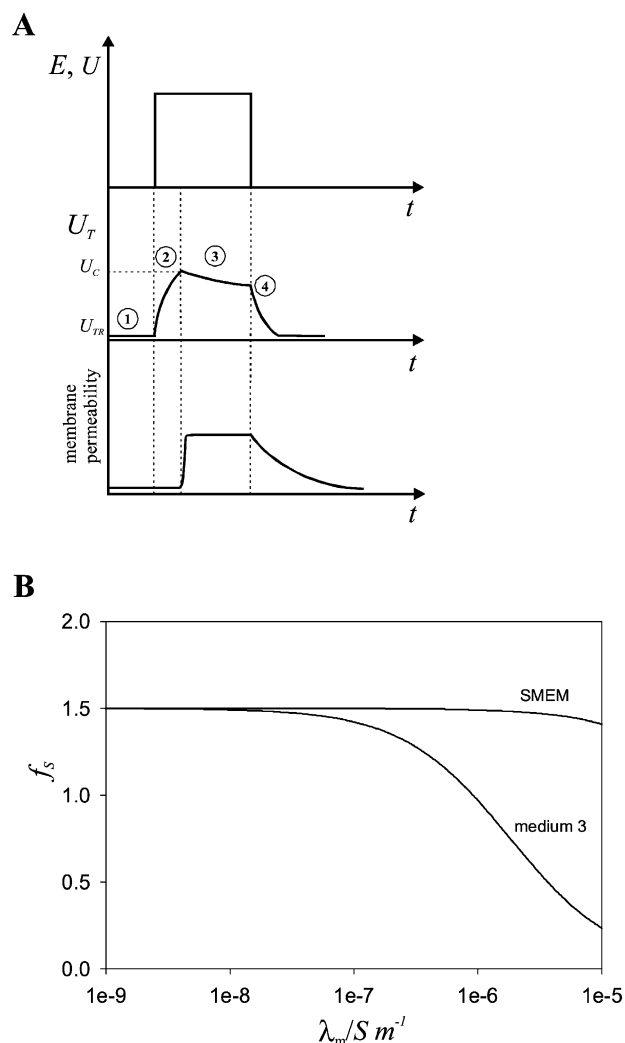


Fig. 5. (A) schematic presentation of electropermeabilization dynamics. (1)  $U_T = U_{TR}$ , membrane permeability is low; (2)  $U_T = U_{TR} + U_{TI}$ , and  $U_{TI}$  increases with time constant  $\tau$ ; (3) when  $U_T$  exceeds a critical value  $U_C$ , the permeability of the membrane rapidly increases and prevents further increase of  $U_T$ , which then even slightly decreases; (4) after the end of the pulse,  $U_T$  returns to  $U_{TR}$  with time constant  $\tau$ , while membrane permeability decreases with a time constant in the range of seconds or even minutes. ( $U_{TR}$ —resting transmembrane voltage,  $U_{TI}$ —induced transmembrane voltage,  $U_T$ —total transmembrane voltage) (B) The dependence of function  $f_s$  on membrane conductivity  $\lambda_m$  for two media (SMEM: 1.61 S/m, medium 3: 0.0011 S/m).

In contrast to cell survival, the fraction of permeabilized cells seems to be unaffected by the time constant of voltage inducement, as long as the pulse duration exceeds this time constant considerably. We should note that the method used for detection of permeabilization, although very precise in determining the threshold of permeabilization, does not evaluate the quantity of molecules taken up per cell. Therefore, our results do not exclude the possibility that the amount of the uptake depends on medium conductivity.

A detailed study on the effect of ionic composition and medium conductivity on viability and PI-uptake of the

cells was made by Djuzenova et al. [15]. This study implies that reducing the medium conductivity results in lower viability of the cells in this medium, which is in disagreement with our experimental results, where reducing the medium conductivity resulted in higher cell survival (see Fig. 3A). However, the range of media conductivities investigated by Djuzenova et al. [15] was between 0.08 and 0.37 S/m, whereas we investigated a much broader range of conductivities between 0.0011 and 1.61 S/m.

In summary, our study has shown that medium conductivity influences the survival of the cells while no detectable effect was obtained on electroporation of the cells. To interpret the experimental results, we have analyzed the influence of the medium conductivity on the induced and the resting transmembrane voltage. This analysis suggests that different values of these two voltages in media with different conductivities are the main reason for the experimentally obtained results, taking into account the time constant of the voltage inducement. Some practical guidelines for experiments involving electroporation can also be made from our study. Use of extracellular media with lower conductivities reduces the electric current and consequently, the heating of cell suspension is reduced. Moreover, because of the lower electric current, less power is required of the electropulsator. Nevertheless, the reduction of the medium conductivity should be moderate, because in the opposite case, the time constant of voltage inducement  $\tau$  increases and the function  $f_S$  decreases, and this increases the pulse duration and the amplitude required for successful electroporation.

### Acknowledgements

The osmolarity measurements were performed in the Department of Solid Physics, Jožef Stefan Institute, Ljubljana, Slovenia. Electroporation experiments could not have been performed without the equipment built by Marko Puc and Karel Flisar in our laboratory. This research was supported by the Ministry of Science and Technology of the Republic of Slovenia and in part by IGEA s.r.l. Carpi (Modena), Italy.

### Appendix A

Symbol	Description	Value
$C_m^*$	Membrane capacitance	$1 \times 10^{-2} \text{ F/m}^2$
$d^*$	Membrane thickness	5 nm
$\lambda_i^*$	Cytoplasmic conductivity	0.2 S/m
$\lambda_m^*$	Membrane conductivity	$5 \times 10^{-7} \text{ S/m}$
$r$	Cell radius	5.94 $\mu\text{m}$
$t$	Pulse duration	100 $\mu\text{s}$
$h$	Distance between the electrodes	2 mm

$U$	Applied voltage	400 V
$R$	Gas constant	8.3 J/mol K
$T$	Temperature	300 K
$F$	Faraday constant	$9.6 \times 10^4 \text{ As}$
$[\text{Na}^+]_i^\#$	Concentration of $\text{Na}^+$ ions inside the cell	5 mM
$[\text{K}^+]_i^\#$	Concentration of $\text{K}^+$ ions inside the cell	140 mM
$c_p$	Specific heating	4.18 J/kg K
$V$	Volume of droplet	50 $\mu\text{l}$
$\rho$	Specific density	1 g/cm <sup>3</sup>
$N$	Number of cells	$10^6$ cells
$V_C$	Volume of cell	$8.77 \times 10^{-16} \text{ m}^3$
$f$	The volume fraction occupied by the cells in suspension	0.0018
$q^{**}$	The permeability ratio ( $P_{\text{Na}}/P_{\text{K}}$ )	0.01

\* Values taken from Ref. [32].

\*\* Values taken from Ref. [24].

# Values taken from Ref. [27].

### References

- [1] J. Teissié, M.P. Rols, An experimental evaluation of the critical potential difference inducing cell membrane electroporation, *Biophys. J.* 65 (1993) 409–413.
- [2] T.Y. Tsong, Electroporation of cell membranes, *Biophys. J.* 60 (1991) 297–306.
- [3] M. Okino, H. Mohri, Effects of a high-voltage electric impulse and an anticancer drug on in vivo growing tumors, *Jpn. J. Cancer Res.* 78 (1987) 1319–1321.
- [4] L.M. Mir, L.F. Glass, G. Serša, J. Teissié, C. Domenge, D. Miklavčič, M.J. Jaroszeski, S. Orłowski, D.S. Reintgen, Z. Rudolf, M. Belehradek, R. Gilbert, M.P. Rols, J. Belehradek Jr., J.M. Bachaud, R. DeConti, B. Štabuc, M. Čemažar, P. Coninx, R. Heller, Effective treatment of cutaneous and subcutaneous malignant tumors by electrochemotherapy, *Br. J. Cancer* 77 (1998) 2336–2342.
- [5] G. Serša, B. Štabuc, M. Čemažar, D. Miklavčič, Z. Rudolf, Electrochemotherapy with cisplatin: the systemic antitumor effectiveness of cisplatin can be potentiated locally by the application of electric pulses in the treatment of malignant melanoma skin metastases, *Melanoma Res.* 10 (2000) 381–385.
- [6] G. Serša, T. Čufer, M. Čemažar, M. Reberšek, Z. Rudolf, Electrochemotherapy with bleomycin in the treatment of hypernephroma metastasis: case report and literature review, *Tumori* 86 (2000) 163–165.
- [7] G. Serša, S. Kranjc, M. Čemažar, Improvement of combined modality therapy with cisplatin and radiation using electroporation of tumors, *Int. J. Radiat. Oncol.* 46 (2000) 1037–1041.
- [8] T.K. Wong, E. Neumann, Electric field mediated gene transfer, *Biochem. Biophys. Res. Co.* 107 (1982) 584–587.
- [9] E. Neumann, S. Kakorin, K. Toensing, Fundamentals of electroporative delivery of drugs and genes, *Bioelectrochem. Bioenerg.* 48 (1999) 3–16.
- [10] S. Somiari, J. Glasspool-Malone, J.J. Drabick, R.A. Gilbert, R. Heller, M.J. Jaroszeski, R.W. Malone, Theory and in vivo application of electroporative gene delivery, *Mol. Ther.* 2 (2000) 178–187.
- [11] D.C. Chang, B.N. Chassy, J.A. Saunders, A.E. Sowers (Eds.), *Guide to Electroporation and Electrofusion*, Academic Press, New York, 1992.

- [12] F. Bobanovič, M.D. Bootman, M.J. Berridge, N.A. Parkinson, P. Lipp, Elementary  $[Ca^{2+}]_i$  signals generated by electroporation functionally mimic those evoked by hormonal stimulation, *FASEB J.* 13 (1999) 365–376.
- [13] M.P. Rols, J. Teissié, Ionic-strength modulation of electrically induced permeabilization and associated fusion of mammalian cells, *Eur. J. Biochem.* 179 (1989) 109–115.
- [14] E. Neumann, Membrane electroporation and direct gene transfer, *Bioelectrochem. Bioenerg.* 28 (1992) 247–267.
- [15] C.S. Djuzenova, U. Zimmermann, H. Frank, V.L. Sukhorukov, E. Richter, G. Fuhr, Effect of medium conductivity and composition on the uptake of propidium iodide into electroporated myeloma cells, *Biochim. Biophys. Acta* 1284 (1996) 143–152.
- [16] Z. Lojewska, D.L. Franks, B. Ehrenberg, M. Loew, Analysis of the effect of medium and membrane conductance on the amplitude and kinetics of membrane potentials induced by externally applied electric fields, *Biophys. J.* 56 (1989) 121–128.
- [17] J.L. Biedler, H. Riehm, Cellular resistance to actinomycin D in Chinese hamster cells in vitro, *Cancer Res.* 30 (1970) 1174–1184.
- [18] M.P. Rols, J. Teissié, Ionic strength modulation of electrically induced permeabilization and associated fusion of mammalian cells, *Eur. J. Biochem.* 179 (1989) 109–115.
- [19] T. Kotnik, A. Maček-Lebar, D. Miklavčič, L.M. Mir, Evaluation of cell membrane electroporation by means of a nonpermeant cytotoxic agent, *Biotechniques* 28 (2000) 921–926.
- [20] H.P. Schwan, Electrical properties of tissue and cell suspensions, *Adv. Biol. Med. Phys.* 5 (1957) 147–209.
- [21] T. Kotnik, D. Miklavčič, T. Slivnik, Time course of transmembrane voltage induced by time-varying electric fields—a method for theoretical analysis and its application, *Bioelectrochem. Bioenerg.* 45 (1998) 3–16.
- [22] B. Gabriel, J. Teissié, Control by electrical parameters of short- and long-term cell death resulting from electroporation of Chinese hamster ovary cells, *Biochim. Biophys. Acta* 1266 (1995) 171–178.
- [23] D.E. Goldman, Potential, impedance, and rectification in membranes, *J. Gen. Physiol.* 27 (1943) 37–60.
- [24] J.D. Bronzino, *The Biomedical Engineering Handbook*, CRC Press, Connecticut, 1995, pp. 127–128.
- [25] R.I. Freshney, *Culture of Animal Cells*, 3rd edn., Garland Publishing, New York, 1994, pp. 83–84.
- [26] M. Golzio, M.P. Mora, C. Raynaud, C. Delteil, J. Teissié, M.P. Rols, Control by osmotic pressure of voltage-induced permeabilization and gene transfer in mammalian cells, *Biophys. J.* 74 (1998) 3015–3022.
- [27] B. Alberts, D. Bray, J. Lewis, M. Raff, K. Roberts, J.D. Watson, *Molecular Biology of the Cell*, 3rd edn., Garland Publishing, New York, 1994.
- [28] E. Neumann, S. Kakorin, Digression on membrane electroporation and electroporative delivery of drugs and genes, *Radiol. Oncol.* 32 (1998) 7–17.
- [29] G. Saulis, Pore disappearance in a cell after electroporation: theoretical simulation and comparison with experiments, *Biophys. J.* 73 (1997) 1299–1309.
- [30] M. Hibino, H. Itoh, K. Kinoshita Jr., Time courses of cell electroporation as revealed by submicrosecond imaging of transmembrane potential, *Biophys. J.* 64 (1993) 1789–1800.
- [31] K.A. DeBruin, W. Krassowska, Modeling electroporation in a single cell I. Effects of field strength and rest potential, *Biophys. J.* 77 (1999) 1213–1224.
- [32] T. Kotnik, F. Bobanovič, D. Miklavčič, Sensitivity of transmembrane voltage induced by applied electric fields—a theoretical analysis, *Bioelectrochem. Bioenerg.* 43 (1997) 285–291.

*Paper 5***Numerical Determination of Transmembrane Voltage Induced  
on Irregularly Shaped Cells****G. Pucihar**, T. Kotnik, B. Valič, D. Miklavčič

Faculty of Electrical Engineering, University of Ljubljana, Ljubljana, Slovenia

**Abstract**

The paper presents an approach that reduces several difficulties related to the determination of induced transmembrane voltage (ITV) on irregularly shaped cells. We first describe a method for constructing realistic models of irregularly shaped cells based on microscopic imaging. This provides a possibility to determine the ITV on the same cells on which an experiment is carried out, and can be of considerable importance in understanding and interpretation of the data. We also show how the finite-thickness, nonzero-conductivity membrane can be replaced by a boundary condition in which a specific surface conductivity is assigned to the interface between the cell interior (the cytoplasm) and the exterior. We verify the results obtained using this method by a comparison with the analytical solution for an isolated spherical cell and a tilted oblate spheroidal cell, obtaining a very good agreement in both cases. In addition, we compare the ITV computed for a model of two irregularly shaped CHO cells with the ITV measured on the same two cells by means of a potentiometric fluorescent dye, and also with the ITV computed for a simplified model of these two cells.

# Numerical Determination of Transmembrane Voltage Induced on Irregularly Shaped Cells

G. PUCIHAR, T. KOTNIK, B. VALIČ, and D. MIKLAVČIČ

Faculty of Electrical Engineering, University of Ljubljana, Ljubljana, Slovenia

(Received 03 May 2005; accepted 23 December 2005; published online: 18 March 2006)

**Abstract**—The paper presents an approach that reduces several difficulties related to the determination of induced transmembrane voltage (ITV) on irregularly shaped cells. We first describe a method for constructing realistic models of irregularly shaped cells based on microscopic imaging. This provides a possibility to determine the ITV on the same cells on which an experiment is carried out, and can be of considerable importance in understanding and interpretation of the data. We also show how the finite-thickness, nonzero-conductivity membrane can be replaced by a boundary condition in which a specific surface conductivity is assigned to the interface between the cell interior (the cytoplasm) and the exterior. We verify the results obtained using this method by a comparison with the analytical solution for an isolated spherical cell and a tilted oblate spheroidal cell, obtaining a very good agreement in both cases. In addition, we compare the ITV computed for a model of two irregularly shaped CHO cells with the ITV measured on the same two cells by means of a potentiometric fluorescent dye, and also with the ITV computed for a simplified model of these two cells.

**Key words**—Finite elements modeling, Induced transmembrane voltage, Di-8-ANEPPS, Electroporation, Electroporabilization.

## INTRODUCTION

When a biological cell is exposed to an external electric field, the induced transmembrane voltage (ITV) forms on its membrane.<sup>17,18,35</sup> The amplitude of the ITV is proportional to the amplitude of the applied electric field, and with a sufficiently strong field, this leads to a strong increase in membrane permeability. As a result, molecules for which the membrane is otherwise impermeable can be transported across the membrane. With appropriate duration and amplitude of the field, the phenomenon (termed electroporation or electroporabilization) is reversible and holds great potential for application in biochemistry, molecular biology, and many fields of medicine.<sup>31,43</sup> It has already become an established method in oncology (electrochemotherapy

of tumors)<sup>16,27,29,36</sup> and holds great promises in gene therapy.<sup>11,37,40</sup>

Increased permeability is localized to the regions of the cell membrane where the ITV exceeds a certain critical threshold, which is in the range of 200–1000 mV, depending on the cell type.<sup>42,44</sup> In order to obtain an efficient cell permeabilization it is therefore important to determine the distribution of the ITV on the cell membrane. The ITV varies with the position on the cell membrane, is proportional to the electric field, and is influenced by cell geometry and physiological characteristics of the medium surrounding the cell.<sup>7,21,26,33,35</sup> For an isolated cell of a simple shape, such as a cylinder, a sphere, or an ellipsoid, the ITV can be described analytically.<sup>9,10,21–23,35</sup> If the cell geometry is more complicated, or when cells are close enough to affect the electric field around each other, an analytical description is in general not attainable, and the ITV can be determined either experimentally (e.g. with potentiometric fluorescence dyes)<sup>2,13,15,20,25,30</sup> or numerically (e.g. using finite elements modeling<sup>5,6,28,32,39,45</sup> or resistive-capacitive [RC] transport lattices).<sup>12,38</sup>

In tissues, both complicated geometry and dense cell distribution are commonly the case. The experimental approach, which is simple and efficient with suspended cells or with cells growing in monolayers, is of limited use in tissues, where only the surface and a thin layer beneath it are directly accessible to standard microscopy techniques. For determination of the ITV on cells in tissues, the numerical methods are thus often the only feasible approach. The main problems of these methods are related to realistic modeling of a cell and—perhaps even more importantly—of its membrane. First, the models in which the cell is built with simple geometric shape or by combining several simple geometric shapes are usually only rough approximations of the actual cell shape.<sup>3,5,6,45</sup> Second, as the cell membrane is over a thousandfold thinner than the dimensions of a typical cell, even in models that use an adaptive mesh size, the thickness of the cell membrane is usually exaggerated by at least an order of magnitude.<sup>19</sup> This can be compensated partly by assigning to the membrane a higher specific conductivity,

Address correspondence to D. Miklavčič, Faculty of Electrical Engineering, University of Ljubljana, Tržaška 25, SI-1000 Ljubljana, Slovenia. Electronic mail: damijan@svarun.fe.uni-lj.si

but the resulting error is difficult to estimate. And third, the uniform thickness of the membrane is a realistic condition that is very hard to meet in building a finite-elements model of an irregularly shaped cell.

In this paper, we describe an approach that reduces the difficulties mentioned above, allowing for determination of the ITV on irregularly shaped single cells, as well as cells in tissues. We describe a method for constructing realistic

models of irregularly shaped cells based on microscopic imaging. This provides a possibility to determine the ITV on the same cells on which an experiment was carried out, which can be of considerable importance in understanding and interpretation of the data. We also show how the finite-thickness, nonzero-conductivity membrane can be replaced by a boundary condition assigned to the interface between the cell interior (the cytoplasm) and the exterior.

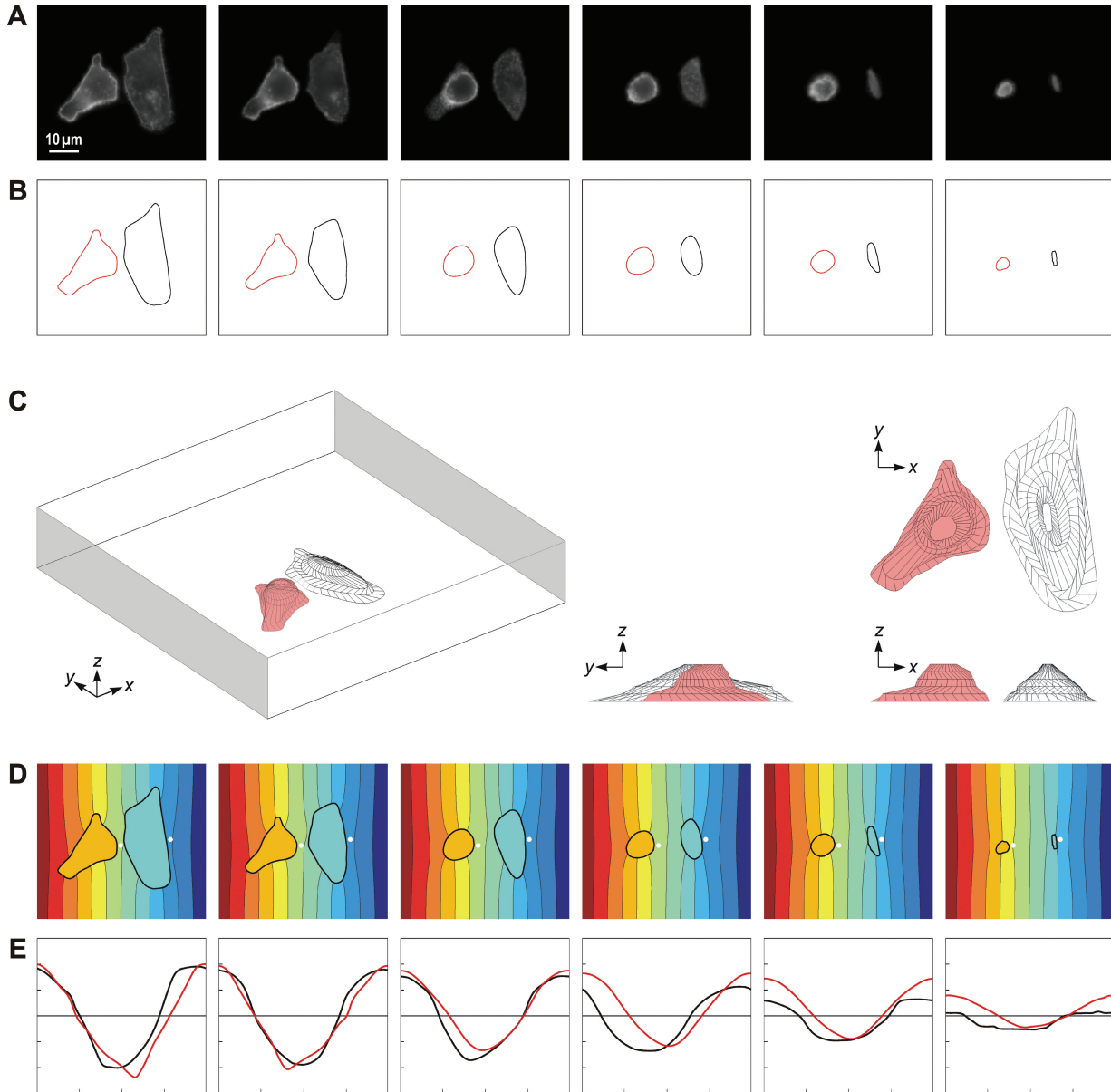


**FIGURE 1.** (A) Fluorescence images (8 bit) of two irregularly shaped CHO cells stained with di-8-ANEPPS. The images represent six cross-sections of the cells, acquired from the bottom to the top of the cells in  $1 \mu\text{m}$  steps. (B) The corresponding contours of the cell edges for a given cross-section. (C) The three-dimensional geometry of the cell models constructed from the cross-sections. The interior of the rectangular block represents the extracellular medium, the gray-shaded faces are the electrodes, and the other four faces are insulating. (D) The computed distribution of the electric potential for each of the six cross-sections. The black curves represent the equipotentials, and the white circles mark the start of the path along which the normalized arc length is measured counterclockwise. The contours separating the colors correspond, from left to right, to electric potential decrements of 50 mV. (E) The calculated ITV for the left (red) and the right cell (black). The plot ranges are identical to those shown in more detail in Figs. 5–7, with the horizontal ticks marking 0.25 increments of the relative arc length, and vertical ticks marking 50 mV increments of the ITV.

This efficiently eliminates the problems related to the modeling of a realistic cell membrane.

## METHODS

### *Construction of the Model*

The three-dimensional model of an irregularly shaped biological cell was constructed from a sequence of microscopic fluorescence images representing cross-sections of a Chinese hamster ovary (CHO) cell attached to the cover glass. The fluorescence images were obtained by staining the cell with fluorescent dye di-8-ANEPPS. The dye emits a strong fluorescence when it binds to the membrane, thereby making the cell edges visible. Besides, its fluorescence is linearly proportional to the voltage on the membrane, and can therefore be used for the measurements of the ITV (see later for details). The cross-sections were obtained by shifting the focus on a fluorescence microscope (Zeiss AxioVert 200, objective  $\times 100$ , oil immersion, Zeiss, Germany) in constant steps of  $1 \mu\text{m}$  from the bottom to the top of the cell Fig. 1a. The images were acquired using a cooled CCD camera (VisiCam 1280, Visitron, Germany) and MetaMorph 5.0 software (Visitron, Germany), and converted from grayscale (8 bit) to black and white (1 bit) in Corel PhotoPaint 11.0 (Corel Corp., Ottawa, Canada). Subsequent processing was performed on a PC equipped with a 2.8 GHz Pentium IV processor and 1 GB RAM. Using FEMLAB 3.1 package (COMSOL Inc., Burlington, MA) with MATLAB 6.5 (MathWorks Inc., Natick, MA, USA), the contours of the cell were detected using *flim 2 curve* (Fig. 1b), transformed to solid planes with 35 edges with *solid 2*, and the planes were connected into a 3D object using *loft* to obtain the model of the cell. This model was then imported to the FEMLAB workspace, where it was positioned at the bottom of a rectangular block, thereby mimicking the cell attached with its bottom to the cover glass (Fig. 1c). To construct a model of several cells, this procedure was repeated for each cell separately (in this paper we illustrate this for the case of two cells).

As discussed in the Introduction, direct incorporation of a realistic cell membrane (i.e. a very thin layer of very small, yet non-zero thickness surrounding the cell) into the model is technically very problematic. Unless the distribution of the electric field, current density, and/or electric potential *within the membrane* is of interest, this can be avoided. Namely, the effect of the membrane on these electric quantities in the cell interior and exterior is equivalent to the effect of a corresponding surface conductivity assigned to the interface between the interior and the exterior. More precisely, as the specific conductivity of the membrane—typically about  $5 \times 10^{-7} \text{ S/m}^8$ —is at least five orders of magnitude lower than the specific conductivities of the aqueous media surrounding it, the current flows through the membrane practically orthogonally to its surface. Consequently, in the membrane the total current density is vir-

tually equal to its normal component alone ( $J$ ), which is given by

$$J = \frac{\sigma_m(V_o - V_i)}{d}, \quad (1)$$

where  $\sigma_m$  is the specific membrane conductivity,  $d$  is the membrane thickness and  $V_o, V_i$  are the electric potentials at the outer and inner surface of the membrane, respectively. Here  $J, V_o$ , and  $V_i$  are functions varying with the position on the membrane, while  $\sigma_m$  and  $d$  are constants. For the purpose of determining the induced transmembrane voltage, the events inside the membrane layer are not relevant, and the ratio  $\sigma_m/d$  can be treated as a single entity—the specific surface conductivity,  $\kappa_m = \sigma_m/d$ . The interface between the cell interior (the cytoplasm) and the cell exterior is then characterized by

$$J = \kappa_m(V_o - V_i). \quad (2)$$

Despite the membrane as such being absent from the model, the drop of electric potential at such an interface is equivalent to the transmembrane voltage induced on a membrane with a specific conductivity  $\sigma_m$  and thickness  $d$ . In models constructed in this way, the mesh of finite elements is generated without difficulty, as very small (and possibly very irregularly shaped) elements corresponding to the membrane itself are avoided.

The computation of the functions  $J, V_o$ , and  $V_i$  was performed in FEMLAB by introducing two application modes, cell exterior (extracellular medium) being active in the first, and the cell interior (cytoplasm) in the second mode. Both application modes were of a static current density type. For models containing several cells, an additional application mode active in the cytoplasm of each cell was introduced, and the functions  $J_1, J_2, \dots$  and  $V_o, V_{i1}, V_{i2}, \dots$  were computed.

The specific conductivity of the cell interior was set to 0.2 S/m, a typical conductivity of the cell cytoplasm,<sup>14</sup> and the specific conductivity of the rest of the block (the cell exterior) was set to 0.15 S/m, which is a typical value of the low conductivity extracellular medium.<sup>34</sup> Two of the opposite vertical faces of the block were modeled as electrodes, which was done by assigning fixed electric potentials; 1 V to one electrode, and 0 V to the other (ground). The electrodes were positioned 0.01 cm apart to obtain the voltage-to-distance ratio of 100 V/cm. The remaining four faces of the block were modeled as insulating surfaces, the bottom one representing the cover glass. At the boundary surface between the cell interior and exterior, the normal component of the current density was set corresponding to Eq. (2) with a negative sign ( $-J$ ) in the mode corresponding to the cell exterior, and with a positive sign in the mode corresponding to the cytoplasm (or, with several cells, in all such modes). The specific surface conductivity was set at  $\kappa_m = 100 \text{ S/m}$ ,<sup>2</sup> which is the ratio between a specific

membrane conductivity of  $5 \times 10^{-7}$  S/m<sup>8</sup> and a membrane thickness of 5 nm.<sup>1</sup>

After the mesh was generated, the electric potential was computed using FEMLAB's stationary nonlinear *Conjugate gradients* solver with *Algebraic multigrid* preconditioner Fig. (1d). The induced transmembrane voltage (ITV) was calculated as the difference between electric potentials on the two sides of the boundary surface separating the inside and outside of the cell, i.e. as  $ITV = V_i - V_o$ . The ITV was then plotted as a function of relative arc length Fig. (1e).

#### Potentiometric Fluorescence Measurements

To experimentally determine the ITV on cells of irregular shape, we used di-8-ANEPPS, a fast potentiometric fluorescence dye which binds to the cell membrane, its fluorescence intensity varying linearly with the change in the ITV.<sup>2, 13, 15, 30</sup> The linear response of the dye was found for voltages ranging from  $-280$  mV to  $+140$  mV,<sup>4</sup> as well as from 0 to  $+250$  mV.<sup>26</sup>

CHO cells were grown on a cover glass in the culture medium (HAM-F12, Sigma-Aldrich, Steinheim, Germany). When cells attached to the glass (usually after 5–7 h), the culture medium was replaced with SMEM medium (Spinner's modification of the MEM, Gibco, USA) containing  $30 \mu\text{M}$  of di-8-ANEPPS and 0.05% of Pluronic (both Molecular Probes, Leiden, Netherlands). After staining for 12 min at  $4^\circ\text{C}$ , the cells were washed thoroughly with pure SMEM to remove the excess dye. Before the experiments, SMEM was replaced with an iso-osmotic buffer consisting of 10 mM potassium phosphate buffer (pH 7.4), 250 mM sucrose, and 1 mM  $\text{MgCl}_2$ . First, the cross-section fluorescence images of the cells were acquired (excitation 490 nm, emission 605 nm) as described in the previous section. Then, the same cells were exposed to a 40 V of voltage applied for a duration of 150 ms on two parallel electrodes with a 4 mm distance between them (voltage-to-distance ratio 100 V/cm). During the pulse, the fluorescence image of the lowermost level of the cell was acquired (excitation 490 nm, emission 605 nm). Five consecutive pulses of 150 ms duration were applied with a delay of 4 s and during each pulse the image was acquired. The control image, which was acquired before the train of pulses was delivered, was subtracted from these images and the corrected images were then averaged to increase the signal-to-noise ratio. The changes in the fluorescence of the dye in the membrane were quantified by measurements of gray levels of the region of interest, which was a line encircling the cell at the site of the membrane. Using a calibration curve obtained in a separate experiment (see below), the fluorescence changes were transformed to the values of the ITV, which were plotted on a graph as a function of the relative arc length. The images were acquired and processed

with the same imaging system as described in the previous section.

#### Calibration of the Fluorescent Dye

CHO cells were grown and stained with di-8-ANEPPS as described above. After washing, the SMEM was replaced with the calibrating medium consisting of 10 mM Hepes buffer (pH 7.5, Merck, Darmstadt, Germany), 140 mM NaCl/KCl and  $1 \mu\text{M}$  valinomycin (Sigma-Aldrich, Steinheim, Germany). The concentrations of NaCl and KCl were adjusted to obtain 3, 10, 50, and 140 mM concentrations of KCl, corresponding to membrane voltages of  $-99$ ,  $-68$ ,  $-27$ , and 0 mV, respectively. The voltages were obtained using the Nernst equation, assuming the intracellular  $\text{K}^+$  concentration of  $140 \text{ mM}$ <sup>1</sup> and considering that the membrane voltage corresponds to  $\text{K}^+$  equilibrium in the presence of valinomycin. After 4 min of incubation in the calibration medium with the lowest KCl concentration (3 mM), the image was acquired and the medium was replaced with the one with higher KCl concentration. This procedure was repeated until 140 mM concentration was reached. The average gray value of the whole line (region of interest) encircling the cell was determined for each image acquired. These values were then transformed to relative changes of the di-8-ANEPPS fluorescence and were plotted versus the voltage. The measurements were performed on three cells and the results are presented in the Fig. 2 as the mean  $\pm$  SD. Linear regression was performed on the measured values to obtain the calibration curve with a slope of 6%/100 mV. Despite the linear response of the dye, the error margins in the calibration curve suggest that the measured ITV values obtained from this curve can deviate considerably from the actual ITV. Also empirically, the ITV measurements with di-8-ANEPPS are characterized by extreme

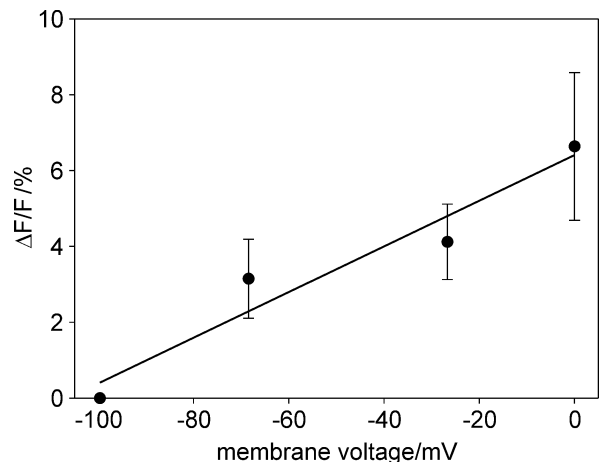


**FIGURE 2.** Calibration curve for di-8-ANEPPS. The measurements represent the mean of the relative changes in the fluorescence ( $\Delta F/F$ )  $\pm$  SD ( $n = 3$ ). The slope of the calibration curve (6%/100 mV) was determined from the linear regression curve.

sensitivity of the dye fluorescence to the environment<sup>30</sup> and intense noise-like spatial fluctuations (see e.g. Ref.<sup>24</sup>). To a certain extent, with a faster imaging system these errors can be reduced using ratiometric measurements,<sup>30</sup> but such a system was not available in our experiments. The images were acquired and processed with the same imaging system as described in the Construction of the Model section.

### NUMERICAL COMPUTATION OF THE ITV AND COMPARISON WITH OTHER METHODS

Reliability of a numerically determined ITV is in general open to doubt, as there are several steps in the modeling and subsequent computation where errors could potentially arise. The results obtained by the method introduced in Construction of the Model section were therefore verified by comparing it with the analytically derived ITV for a spherical cell and a tilted oblate spheroidal cell. In addition, the ITV computed for a model of two irregularly shaped CHO cells photographed under a microscope was compared with the ITV measured on these two cells by means of a potentiometric fluorescent dye, and also with the ITV computed for a simplified model of the same two cells each represented as a hemiellipsoid.

#### Validation by Comparison with two Analytical Solutions

##### A Spherical Cell

Under physiological conditions, the transmembrane voltage (ITV) induced by an electric field  $E$  on a spherical cell with outer radius  $R$  is given by Schwan's equation<sup>35</sup>

$$\text{ITV} = f_s E R \cos \varphi \quad (3)$$

where  $\varphi$  is the angle between the direction of the field and the line connecting the center of the cell to the point of interest and  $f_s$  is a function reflecting the electric and dimensional properties of the cell and the surrounding medium.<sup>21</sup>

$$f_s = \frac{3\lambda_o [3dR^2\lambda_i + (3d^2R - d^3)(\lambda_m - \lambda_i)]}{2R^3(\lambda_m + 2\lambda_o)(\lambda_m + \frac{1}{2}\lambda_i) - 2(R-d)^3(\lambda_o - \lambda_m)(\lambda_i - \lambda_m)} \quad (4)$$

In Eq. (4),  $\lambda_o$ ,  $\lambda_i$ , and  $\lambda_m$  are the specific conductivities of the extracellular medium, cytoplasm and the membrane, respectively, and  $d$  is the thickness of the membrane. Under physiological conditions, where  $\lambda_m$  is at least five orders of magnitude smaller than both  $\lambda_o$  and  $\lambda_i$ ,  $f_s$  is very close to the value of  $3/2$ , and the Schwan's equation is sometimes also written with  $f_s$  replaced by this explicit constant.

Schwan's equation provides a precise description of the ITV on a single spherical cell, and was as such used as the first test of the method of numerical determination of the ITV described in this paper. Figure 3b shows the ITV

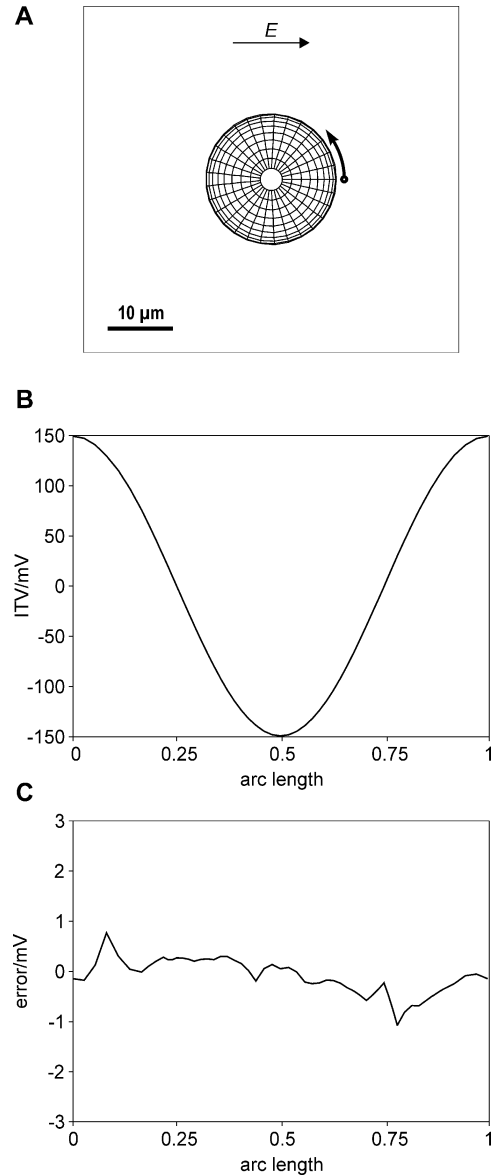


**FIGURE 3. (A) Geometry of a spherical cell. The arrow denotes the start and the direction of the path along which the normalized arc length is measured. (B) Computed ITV for a spherical cell with a membrane modeled as a boundary condition. (C) The difference between the computed and analytically derived ITV. The calculations were performed for a spherical cell with  $R = 10 \mu\text{m}$ ,  $\lambda_o = 1 \text{ S/m}$ ,  $\lambda_i = 0.2 \text{ S/m}$ ,  $\lambda_m = 5 \times 10^{-7} \text{ S/m}$ ,  $d = 5 \text{ nm}$ , and  $E = 100 \text{ V/cm}$ .**

computed using this method and Fig. 3c shows the error with respect to Schwan's equation (note that the y-scale is much smaller than in Fig. 3b). Both the analytical and the numerical solution were determined for a spherical cell with  $R = 10 \mu\text{m}$ ,  $\lambda_o = 1 \text{ S/m}$ ,  $\lambda_i = 0.2 \text{ S/m}$ ,  $\lambda_m = 5 \times 10^{-7} \text{ S/m}$ , and  $d = 5 \text{ nm}$ . The cell was exposed to an electric field of  $100 \text{ V/cm}$ , which was, in the numerical solution, generated by applying  $1 \text{ V}$  to a pair of rectangular parallel plate electrodes  $0.01 \text{ cm}$  apart. The cell was

centered between them, occupying a region in which the inhomogeneity of the field was everywhere below 1%.

The comparison with Schwan's equation shows that the error due to numerical computation varies with the position, but remains in the range between  $-1.07$  and  $0.77$  mV (less than 0.72% of the maximum value of the ITV, Fig. 3c), sufficiently accurate for any practical purpose. This error is mostly due to the finite size of the modeled electrodes and the space between them, and to some extent also due to nonzero size of the elements. This was verified by computing the ITV: (i) on the model of a spherical cell where the mesh was constructed from smaller finite elements (18,168 elements instead of 3746); (ii) on the same model of a spherical cell with electrodes larger (2.25 times the original surface) and further apart (1.5 times the original distance). In the first case (finer mesh), the maximum error between the computed and analytically derived ITV decreased from 0.72 to 0.46%, while in the second case (larger electrodes) the error decreased from 0.72% to 0.53%.

The main advantage of replacing the cell membrane with a boundary condition is that the mesh elements corresponding to the membrane are avoided. As described in the Introduction, if the membrane is instead modeled explicitly (i.e. built from mesh elements), its thickness must typically be exaggerated by an order of magnitude or more, otherwise the number of mesh elements is far too large to be handled by a computer. To compensate for this, the membrane can be assigned a correspondingly higher specific conductivity  $\lambda_m' = (d'/d) \times \lambda_m$ . Table 1 illustrates how the decrease of membrane thickness from exaggerated values towards realistic ones is accompanied by a rapid increase in the number of elements forming the mesh, and consequently also in the time needed for generating the mesh and solving the problem. With the PC and the FEMLAB software used in this study (see Construction of the Model section), the calculation of the solution was not possible for a membrane thinner than  $0.3 \mu\text{m}$ .

### An Oblate Spheroidal Cell

An example of a more complex geometry for which the analytical solution is still attainable is that of a spheroidal cell. The generalizations of Schwan's equation for these cases can be found in the literature.<sup>9,10,22,45</sup> Figure 4a shows an oblate spheroidal (disc-shaped) cell with its axis of rotational symmetry tilted by  $45^\circ$  with respect to the direction of the field. The ITV computed using our method is shown in Fig. 4b, and the error with respect to the analytical solution in Fig. 4c. The radii of the spheroidal cell were 2, 10, and  $10 \mu\text{m}$ , while the other parameters were the same as in the case of the spherical cell described in the preceding subsection. The error in the numerical computation ranged from  $-0.94$  mV to  $1.98$  mV, which is less than 2% of the maximum value of the ITV. Also in this case, the error was reduced further by using smaller finite elements (to 0.41% by using 69,772 elements instead of 9870). Thus, despite less symmetry in cell shape than in the case of a spherical cell, and despite the lack of symmetry in the position of the cell with respect to the field, the method again yields results with sufficient accuracy for any practical purpose.

### Comparison with Fluorescence Measurements

The model of two irregularly shaped cells was constructed from six cross-sections of the cells photographed under a microscope, as described in detail in the Methods section (Figs. 1a–c). The electric potential was computed on the finite-elements rendering of this model, as shown in Fig. 1d, and the ITV for each cell was then calculated as the difference between the electric potentials in the cell interior and exterior. Figure 1e shows the computed ITV for each of the six cross-sections (counted from the bottom of the cells) for the left cell (red curve) and the right cell (black curve), respectively. Towards the top of the cells the cross-sections become smaller, and so does their effect on the external field. As a consequence, the amplitudes of the ITV gradually decrease, and in the topmost cross-section

**TABLE 1. The influence of the membrane thickness on the number of mesh elements, the time required for mesh generation, and the time required for solution (i.e., determination of the electric potential) for a spherical cell.**

Numerical model	No. of mesh elements	Time for mesh	Time for solution
Membrane modeled implicitly through the boundary condition			
$d = 5 \text{ nm}, \lambda_m = 5 \times 10^{-7} \text{ S/m}$	3746	< 1 s	2,6 s
Membrane modeled explicitly			
$d' = 1.5 \mu\text{m}, \lambda_m' = 1.5 \times 10^{-4} \text{ S/m}$	9738	< 1 s	7 s
$d' = 1 \mu\text{m}, \lambda_m' = 1 \times 10^{-4} \text{ S/m}$	18376	2 s	13 s
$d' = 0.5 \mu\text{m}, \lambda_m' = 0.5 \times 10^{-4} \text{ S/m}$	73305	15 s	60 s
$d' = 0.3 \mu\text{m}, \lambda_m' = 0.3 \times 10^{-4} \text{ S/m}$	198895	45 s	179 s
$d' = 0.2 \mu\text{m}, \lambda_m' = 0.2 \times 10^{-4} \text{ S/m}$	410502	400 s	Out of memory

*Note.*  $d$  and  $\lambda_m$  are the thickness and the conductivity of the implicitly modeled membrane, respectively, which are incorporated in the boundary condition of surface conductivity, while  $d'$  is the thickness of the explicitly modeled membrane, for which the conductivity is chosen as  $\lambda_m' = (d'/d) \times \lambda_m$

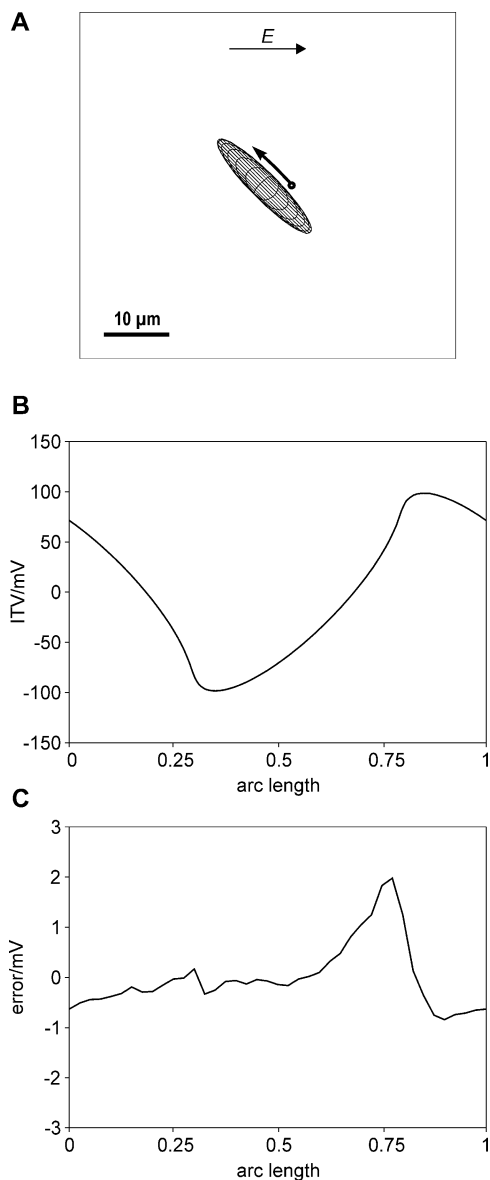


**FIGURE 4.** (A) Geometry of an oblate spheroidal cell. The arrow denotes the start and the direction of the path along which the normalized arc length is measured. (B) Computed ITV for this cell with a membrane modeled as a boundary condition. (C) The difference between the computed and analytically derived ITV. The calculations were performed for a cell with radii of 10, 10, and 2  $\mu\text{m}$ , and the other parameters are as in Fig. 3.

they are only 30 and 18% of the amplitudes at the bottom level of the left and the right cell, respectively (Fig. 1e).

The computed values of the ITV for the left and the right cell at the level of the lowermost surface were than compared to the experimentally measured ITV for the same two cells, by using di-8-ANEPPS. The dye binds to the membrane, and within the linear range a 6% change in fluorescence intensity corresponds to approximately 100 mV change in transmembrane voltage (Fig. 2). The results presented in Figs. 5b and 5c show that for each

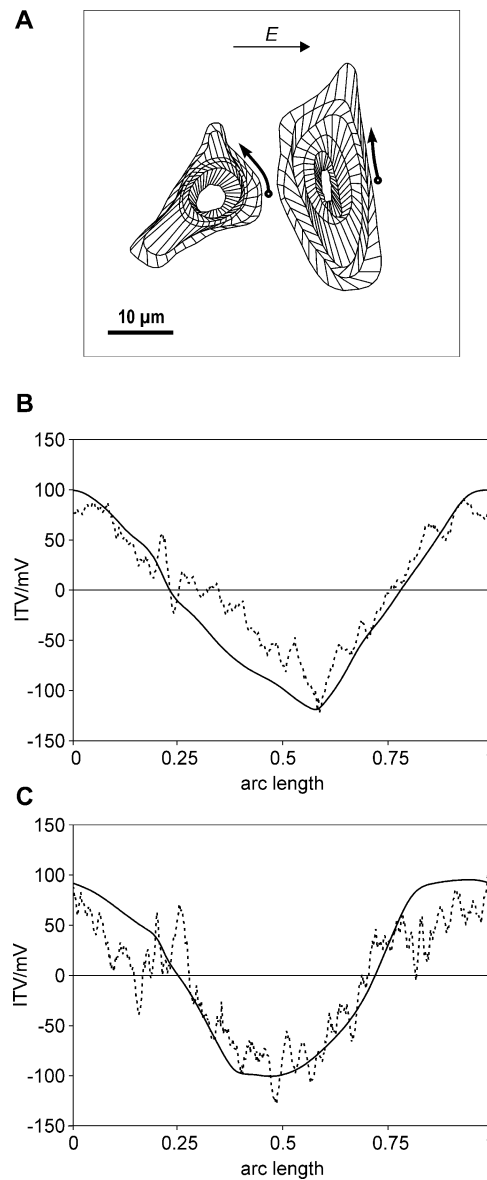


**FIGURE 5.** (A) Geometry of the two irregularly shaped cells (see also Fig. 1). The arrow denotes the start and the direction of the path along which the normalized arc length is measured. (B) Comparison of the ITV determined numerically (solid) and experimentally (dashed) for the lowermost cross-section of the cell on the left. (C) Same as in B, but for the cell on the right. The measured ITV was obtained by staining CHO cells with di-8-ANEPPS (excitation 490 nm, emission 605 nm), and exposing them for 100 ms to 40 V applied to a pair of flat parallel stainless-steel electrodes 4 mm apart.

cell, the experimental ITV curve (dashed) is similar in large-scale shape and amplitude to the corresponding computed ITV curve (solid).

#### *Comparison with Simplified Cell Shapes*

To evaluate how a simplification of the geometry affects the computed ITV, the irregularly shaped cells treated in

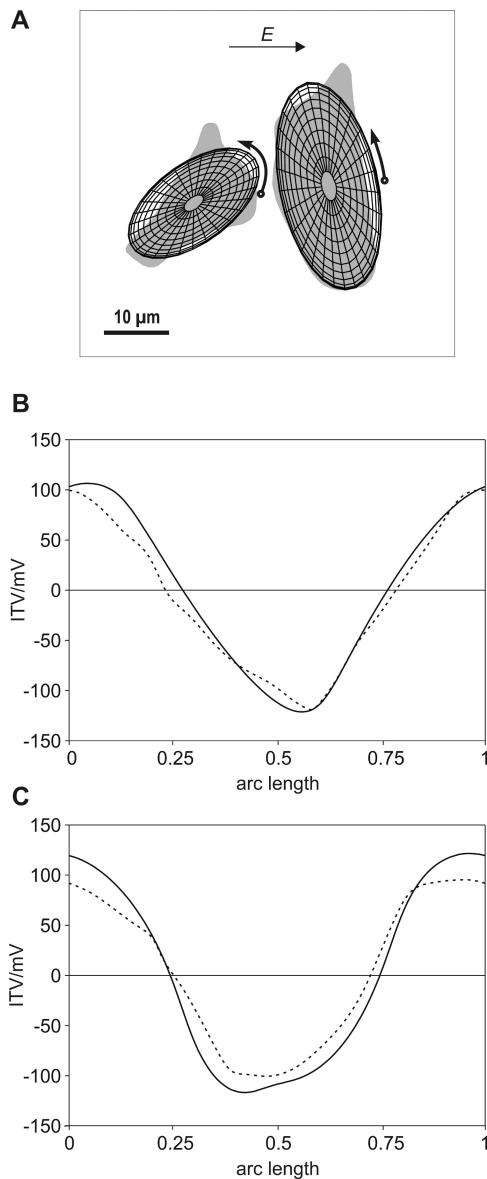


**FIGURE 6.** Comparison of the model of two irregularly shaped cells from Fig. 5 with a simpler model of the same two cells represented by hemiellipsoids. (A) The geometry and the position of the hemiellipsoids with respect to the realistic model. The left hemiellipsoid had horizontal semi-axes  $11.5 \mu\text{m}$  and  $6 \mu\text{m}$ , the right one  $16$  and  $7.5 \mu\text{m}$ , and vertical semi-axes of both were  $6 \mu\text{m}$ . The arrows represent the start and the direction of the path along which the normalized arc length is measured. (B) The comparison of the ITV determined on the hemiellipsoid (solid line) with the more realistic model (dashed line) for the cell on the left. (C) Same as in B, but for the cell on the right. The computed ITV curves are for the lowermost cross-section.

Comparison with Fluorescence Measurement section were replaced by hemiellipsoids of the same height, with the other two dimensions and the position adjusted to resemble those of the original irregularly shaped cells (Fig. 6a). The membrane was again included as a boundary condition, and the electrical parameters were as in preceding subsec-

tions. The computed ITV for the lowermost level of the hemiellipsoids is shown with solid curves in Figs. 6b and 6c for the hemiellipsoid on the left and the hemiellipsoid on the right, respectively. The dashed curves give the ITV on the corresponding irregularly shaped cells. These results show that the differences in the ITV computed with simplified geometry when compared to the more realistic geometry are considerable. More precisely, the largest differences with respect to the maximum ITV are approximately 25 and 30% for the cell on the left and the cell on the right, respectively, and the average differences are approximately 10 and 17%, respectively. These deviations, although considerable, are still smaller than the noise inherent to experimental measurements of ITV such as those shown in Fig. 5.

## DISCUSSION

The distribution of the voltage induced on the cell membrane (the ITV) can be of interest in many theoretical and experimental settings, such as activation of voltage-dependent membrane channels and cell membrane electroporation. With cells of simple geometrical shapes, this distribution can be determined analytically<sup>9, 10, 21–23, 35</sup> but with irregularly shaped cells this can only be achieved experimentally<sup>2, 13, 15, 20, 25, 30</sup> or numerically<sup>5, 6, 12, 28, 32, 38, 39, 45</sup>. Frequently biological cells are modeled as simple geometrical objects (spheres, spheroids. . .) and, for more complicated cell shapes, by combining several such objects (e.g. hemispheres, circular or elliptic cylinders, etc.).<sup>3, 5, 6, 19, 22, 32, 45</sup> These models can be realistic for cells in suspensions, but cells growing in a dish or in tissues have markedly irregular shapes, and combinations of several simple geometrical objects are only rough approximations of their real shapes. In this paper we presented a method for construction of more realistic models of such cells from their cross-section images. In our case, each cell model was composed of six cross-sections transformed to solid planes with 35 edges, which is sufficient for a reasonably faithful representation of the real cell. In FEMLAB 3.1, all the planes from which the solid object is generated must have the same number of edges, and the object always has a flat top. Increasing the number of planes or the number of edges yields a more detailed model, but if carried out too far, this eventually results in difficulties in mesh generation. Because we were not using the confocal microscope, our images contained a considerable amount of the out-of-focus fluorescence, so performing the transformation of these images to 1-bit (black and white) images occasionally required manual correction of one or several edges of the cell.

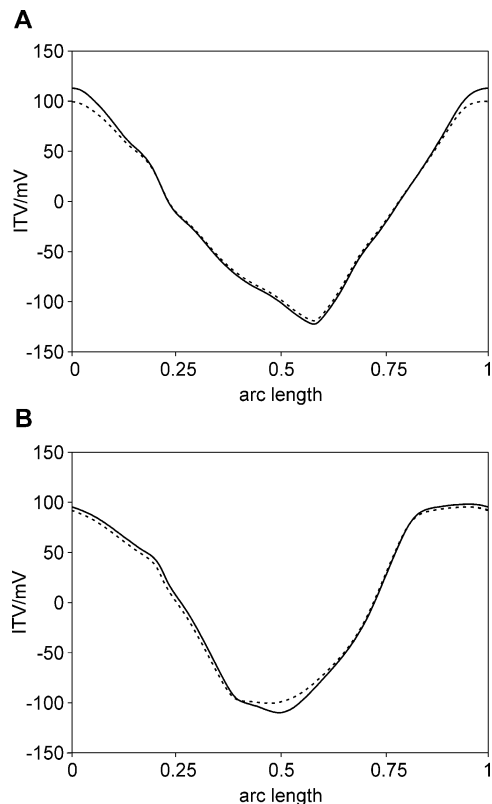
The ITV is the difference between the potentials on both sides of the membrane. Therefore in computing the ITV, the model of the cell cannot be a homogeneous solid with a low conductivity (which would suffice for determination of the external potential distribution, for example), but must have a conductive interior corresponding to the cytoplasm. As

Table 1 shows, it is practically impossible to incorporate a cell membrane of a realistic thickness into a finite-elements model of the cell. Furthermore, even if this thickness is exaggerated, it is problematic to make it uniform, particularly at the protrusions and edges of the cell, and pronounced nonuniformities can affect the calculation of the ITV considerably.<sup>22</sup> The method we present in this paper resolves these difficulties by replacing the membrane with a specific surface conductivity assigned to the interface between the cell interior and the exterior, whereby the conditions corresponding to the uniform thickness are automatically met. An additional advantage is that the model in which the explicit membrane is replaced by a boundary condition consists of a considerably lower number of mesh elements, and the solution is also obtained faster. To validate this method, the ITV computed using this method was compared with the analytical expression describing the ITV for the same cell (a sphere or a tilted spheroid), showing a very good agreement between both solutions (Figs. 3b and 3c, 4b and 4c).

The construction of a 3D model from the cross-section images and the replacement of an explicit membrane with a boundary condition were used to build a model of two irregularly shaped cells and to calculate the ITV on them. Because the model was built from the cross-sections of the same cells on which the experimental measurements of the ITV were performed, it was possible to compare the computed and the experimental results. As the errors of the presented method with respect to the analytical solution for a spherical and a tilted oblate spheroidal cell are very small (Figs. 3c and 4c), this can be considered as evidence that this method is a reliable and accurate one.

We found some discrepancies in the amplitudes of the computed and experimentally obtained ITV, mostly attributable to the calibration which was not performed on the same cells on which the experiment was carried. The obtained calibration slope of  $\sim 6\%$  was also lower than the slope obtained by other authors ( $\sim 9\%/100$  mV),<sup>13,30</sup> perhaps due to our selection of excitation and emission filters that were probably not perfect for the best response fluorescence with the chosen dye. To perform an experimental determination of the ITV at levels other than the lowermost one, one would have to use a confocal microscope, as on other microscopes higher levels contain the out-of-focus fluorescence from the regions above and below the observed one, which affects the measurements of the fluorescence. In contrast, the ITV can easily be investigated at any level using numerical methods including the one described in this paper.

Finally, in Comparison with Simplified Cell Shapes section we compared the ITV calculated on our detailed model and on a simplified model composed of two semiellipsoids. This comparison demonstrates that for cell shapes deviating significantly from a regular geometric object, computation of the ITV on the latter object can lead to deviations ranging into tens of percents (Fig. 6). Thus for cells with a com-



**FIGURE 7.** The effect of the mutual electrical screening of the cells on the ITV. (A) The ITV for the left cell in Fig. 5 with the right cell absent (solid line) and with the right cell present (dashed line). (B) The ITV for the right cell with the left cell absent (solid line) and with the left cell present (dashed line).

plicated shape, such as neurons, computations on the more realistic model can provide a better understanding of the response of the cells to an electric field. The construction of a model of such cells along the lines described in this paper is rather simple, and is probably worth the effort. In contrast, for cells having a simple shape, such as bacilli (approximated by prolate spheroids) or erythrocytes (oblate spheroids), computation of the ITV on a regular geometric object would suffice. In addition, if the only purpose of computing the ITV is to compare it to potentiometric experimental data that contain oscillations similar to those shown in Fig. 5, the ITV computed with either a simplified or a more realistic geometry will likely be within these oscillations, showing a similar degree of agreement.

The results presented above demonstrate that the computational approach to ITV determination is a useful technique either by itself or as a complement to experimental studies. Moreover, it can provide insights that would be rather difficult to obtain in the actual experimental environment. As an example, Figs. 7a and 7b show, in solid curves, the computed ITV for the left and the right cell from Fig. 5, respectively, but this time with the other cell absent; for comparison, the dashed curves give the computed ITV

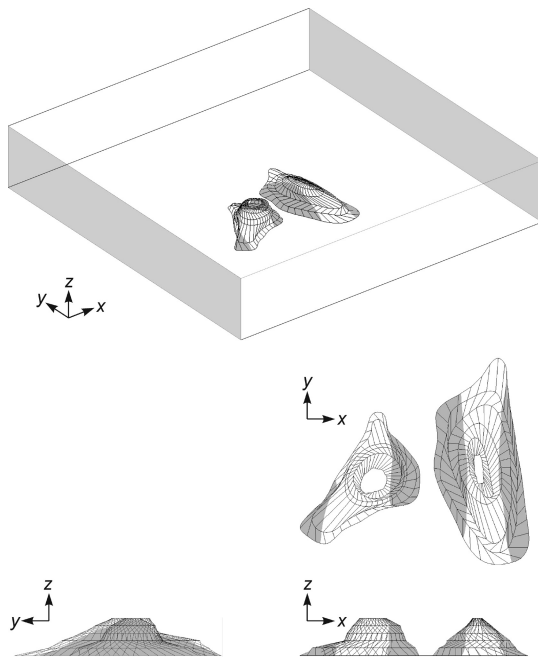


**FIGURE 8.** The permeabilized regions of the cell membrane. A voltage of 3 V was applied to the electrodes of the same model of two irregular cells as shown in Figs. 1 and 5. The permeabilized parts of the membrane are colored gray and represent the regions where the ITV exceeds 250 mV.

when both cells are present. In a finite-elements model, this is an elementary modification of the earlier analysis, as the object corresponding to one of the cells is simply removed from the rectangular block representing the extracellular medium. In the case shown here, the differences are not large, but they are detectable, reflecting the mutual electrical shielding of one cell by the other. This is an illustration of the often-neglected fact that even when not in direct physical contact, the neighboring cells affect the ITV of each other (for a detailed treatment of the case of spherical cells, see e.g. Refs.<sup>32,39</sup>).

Another example of a potentially useful application of the described method is the investigation of cell membrane electropermeabilization. As mentioned in the Introduction, this phenomenon occurs in those regions of the cell membrane where the ITV exceeds a certain threshold value, typically ranging from 250 to 1000 mV.<sup>42,44</sup> The regions permeabilized by an exposure to electric pulses of given amplitude can easily be determined with our method, by marking in the model the areas where the ITV is above the chosen threshold value. In Fig. 8, a voltage of 3 V is applied to the electrodes of the same model of two irregular cells treated in the preceding sections of the paper, and assuming the threshold ITV of 250 mV, the permeabilized membrane regions are shown in gray. The same approach is applicable in investigating the location of the open and closed voltage-gated membrane channels. Since the presented model treats the membrane as electrically passive (i.e., having

a constant electric conductivity), it cannot predict the ITV modification caused by opening or closing of voltage-gated channels or forming of electropores, since these events alter the conductivity of the membrane.<sup>1</sup>

The computations presented in the paper are based on the conditions occurring in an exposure to a time-constant (DC) field. Since the charging time of the membrane is in the order of microseconds, the method is also applicable for computing the ITV induced at any given moment by fields that vary sufficiently slowly, e.g. alternating (AC) fields below 100 kHz. It cannot, however, be used for computation of the transients.

Finally, the presented methods of model construction from cross-section images and replacement of the membrane by a boundary condition can also be used to study more complicated cell geometries, such as several cells in contact, which represent a simple model of a tissue.

## ACKNOWLEDGMENTS

This work was supported by the Ministry of Higher Education, Science and Technology of the Republic of Slovenia. The authors wish to thank Dr Marko Puc for building the switcher device for delivery of electric pulses in the experiments.

## REFERENCES

- <sup>1</sup>Alberts, B., D. Bray, J. Lewis, M. Raff, K. Roberts, and J. D. Watson. *Molecular Biology of the Cell*, 3rd edn., New York: Garland, 1994.
- <sup>2</sup>Bedlack, R. S., M. Wei, S. H. Fox, E. Gross, and L. M. Loew. Distinct electric potentials in soma and neurite membranes. *Neuron* 13:1187–1193, 1994.
- <sup>3</sup>Buitenweg, J. R., W. L. Rutten, and E. Marani. Geometry-based finite-element modeling of the electrical contact between a cultured neuron and a microelectrode. *IEEE Trans. Biomed. Eng.* 50:501–509, 2003.
- <sup>4</sup>Cheng, D. K. L., L. Tung, and E. A. Sobie. Nonuniform responses of transmembrane potential during electric field stimulation of single cardiac cells. *Am. J. Physiol.* 277:H351–H362, 1999.
- <sup>5</sup>Fear, E. C., and M. A. Stuchly. Biological cells with gap junctions in low-frequency electric fields. *IEEE Trans. Biomed. Eng.* 45:856–866, 1998.
- <sup>6</sup>Fear, E. C., and M. A. Stuchly. Modeling assemblies of biological cells exposed to electric fields. *IEEE Trans. Biomed. Eng.* 45:1259–1271, 1998.
- <sup>7</sup>Gabriel, B., and J. Teissié. Fluorescence imaging in the millisecond time range of membrane electropermeabilization of single cell using a rapid ultra-low-light intensifying detection system. *Eur. Biophys. J.* 27:291–298, 1998.

<sup>1</sup> This could be addressed by sequentially modifying the electric properties of the membrane and recomputing the potential distribution. An example of such modification for a tissue exposed to an electric field can be found in Ref.<sup>41</sup>

- <sup>8</sup>Gascoyne, P. R. C., R. Pethig, J. P. H. Burt, and F. F. Becker. Membrane changes accompanying the induced differentiation of Friend murine erythroleukemia cells studied by dielectrophoresis. *Biochim. Biophys. Acta.* 1146:119–126, 1993.
- <sup>9</sup>Gimsa, J., and D. Wachner. Analytical description of the transmembrane voltage induced on arbitrarily oriented ellipsoidal and cylindrical cells. *Biophys. J.* 81:1888–1896, 2001.
- <sup>10</sup>Gimsa, J., and D. Wachner. On the analytical description of transmembrane voltage induced on spheroidal cells with zero membrane conductance. *Eur. Biophys. J.* 30:463–466, 2001.
- <sup>11</sup>Golzio, M., L. Mazzolini, P. Moller, M. P. Rols, and J. Teissie. Inhibition of gene expression in mice muscle by in vivo electrically mediated siRNA delivery. *Gene Therapy* 12:246–251, 2005.
- <sup>12</sup>Gowrishankar, T. R., and J. C. Weaver. An approach to electrical modeling of single and multiple cells. *Proc. Natl. Acad. Sci. U.S.A.* 100:3203–3208, 2003.
- <sup>13</sup>Gross, D., L. M. Loew, and W. Webb. Optical imaging of cell membrane potential changes induced by applied electric fields. *Biophys. J.* 50:339–348, 1986.
- <sup>14</sup>Harris, C. M., and D. B. Kell. The radio-frequency dielectric properties of yeast cells measured with a rapid, automated, frequency-domain dielectric spectrometer. *Bioelectrochem. Bioenerg.* 11:15–28, 1983.
- <sup>15</sup>Hassan, N., I. Chatterjee, N. G. Publicover, and G. L. Craviso. Mapping membrane-potential perturbations of chromaffin cells exposed to electric fields. *IEEE Trans. Plasma Sci.* 30:1516–1524, 2002.
- <sup>16</sup>Heller, R., R. Gilbert, and M. J. Jaroszeski. Clinical applications of electrochemotherapy. *Adv. Drug. Deliv. Rev.* 35:119–129, 1999.
- <sup>17</sup>Hibino, M., H. Itoh, and K. Kinoshita. Time courses of cell electroporation as revealed by submicrosecond imaging of transmembrane potential. *Biophys. J.* 64:1789–1800, 1993.
- <sup>18</sup>Hibino, M., M. Shigemori, H. Itoh, K. Nagayama, and K. Kinoshita. Membrane conductance of an electroporated cell analyzed by submicrosecond imaging of transmembrane potential. *Biophys. J.* 59:209–220, 1991.
- <sup>19</sup>Huang, X., D. Nguyen, D. W. Greve, and M. M. Domach. Simulation of microelectrode impedance changes due to cell growth. *IEEE Sensors J.* 4:576–583, 2004.
- <sup>20</sup>Knisley, S. B., T. F. Blitchington, B. C. Hill, A. O. Grant, W. M. Smith, T. C. Pilkington, and R. E. Ideker. Optical measurements of transmembrane potential changes during electric field stimulation of ventricular cells. *Circ. Res.* 72:255–268, 1993.
- <sup>21</sup>Kotnik, T., F. Bobanovič, and D. Miklavčič. Sensitivity of transmembrane voltage induced by applied electric fields – a theoretical analysis. *Bioelectrochem. Bioenerg.* 43:285–291, 1997.
- <sup>22</sup>Kotnik, T., and D. Miklavčič. Analytical description of transmembrane voltage induced by electric fields on spheroidal cells. *Biophys. J.* 79:670–679, 2000.
- <sup>23</sup>Kotnik, T., and D. Miklavčič. Second-order model of membrane electric field induced by alternating external electric fields. *IEEE Trans. Biomed. Eng.* 47:1074–1081, 2000.
- <sup>24</sup>Lee, D. C., and W. M. Grill. Polarization of a spherical cell in a nonuniform extracellular electric field. *Anal. Biomed. Eng.* 33:603–615, 2005.
- <sup>25</sup>Loew, L. M. Voltage sensitive dyes: Measurement of membrane potentials induced by DC and AC electric fields. *Bioelectromagnetics Suppl.* 1:179–189, 1992.
- <sup>26</sup>Lojewska, Z., D. L. Franks, B. Ehrenberg, and L. M. Loew. Analysis of the effect of medium and membrane conductance on the amplitude and kinetics of membrane potentials induced by externally applied electric fields. *Biophys. J.* 56:121–128, 1989.
- <sup>27</sup>Miklavčič, D., G. Pucihar, M. Pavlovec, S. Ribarič, M. Mali, A. Maček-Lebar, M. Petkovšek, J. Nastran, S. Kranjc, M. Čemažar, and G. Serša. The effect of high frequency electric pulses on muscle contractions and antitumor efficiency in vivo for a potential use in clinical electrochemotherapy. *Bioelectrochemistry* 65:121–128, 2005.
- <sup>28</sup>Miller, C. E., and C. S. Henriquez. Three-dimensional finite element solution for biopotentials: Erythrocyte in an applied field. *IEEE Trans. Biomed. Eng.* 35:712–718, 1988.
- <sup>29</sup>Mir, L. M., and S. Orłowski. Mechanisms of electrochemotherapy. *Adv. Drug Deliv. Rev.* 35:107–118, 1999.
- <sup>30</sup>Montana, V., D. L. Farkas, and L. M. Loew. Dual-wavelength ratiometric fluorescence measurements of membrane-potential. *Biochemistry* 28:4536–4539, 1989.
- <sup>31</sup>Neumann, E., S. Kakorin, and K. Toensing. Fundamentals of electroporative delivery of drugs and genes. *Bioelectrochem. Bioenerg.* 48:3–16, 1999.
- <sup>32</sup>Pavlin, M., N. Pavšelj, and D. Miklavčič. Dependence of induced transmembrane potential on cell density, arrangement, and cell position inside a cell system. *IEEE Trans. Biomed. Eng.* 49:605–612, 2002.
- <sup>33</sup>Pucihar, G., T. Kotnik, M. Kandušer, and D. Miklavčič. The influence of medium conductivity on electroporation and survival of cells in vitro. *Bioelectrochemistry* 54:107–115, 2001.
- <sup>34</sup>Rols, M. P., C. Delteil, M. Golzio, and J. Teissie. Control by ATP and ADP of voltage-induced mammalian-cell-membrane permeabilization, gene transfer and resulting expression. *Eur. J. Biochem.* 254:382–388, 1998.
- <sup>35</sup>Schwan, H. P. Electrical properties of tissue and cell suspensions. *Adv. Biol. Med. Phys.* 5:147–209, 1957.
- <sup>36</sup>Serša, G., M. Čemažar, and Z. Rudolf. Electrochemotherapy: advantages and drawbacks in treatment of cancer patients. *Cancer Ther.* 1:133–142, 2003.
- <sup>37</sup>Somiari, S., J. G. Malone, J. J. Drabick, R. A. Gilbert, R. Heller, M. J. Jaroszeski, and R. W. Malone. Theory and in vivo application of electroporative gene delivery. *Mol. Ther.* 2:178–187, 2000.
- <sup>38</sup>Stewart, D. A., T. R. Gowrishankar, and J. C. Weaver. Transport lattice approach to describing cell electroporation: use of a local asymptotic model. *IEEE Trans. Plasma Sci.* 32:1696–1708, 2004.
- <sup>39</sup>Susil, R., D. Šemrov, and D. Miklavčič. Electric field induced transmembrane potential depends on cell density and organization. *Electro. Magnetobiol.* 17:391–399, 1998.
- <sup>40</sup>Šatkauskas, S., M. F. Bureau, M. Puc, A. Mahfoudi, D. Scherman, D. Miklavčič, and L. M. Mir. Mechanisms of in vivo DNA electrotransfer: respective contributions of cell electroporation and DNA electrophoresis. *Mol. Ther.* 5:133–140, 2002.
- <sup>41</sup>Šel, D., D. Cukjati, D. Batiškaite, T. Slivnik, L. M. Mir, and D. Miklavčič. Sequential finite element model of tissue electroporation. *IEEE Trans. Biomed. Eng.* 52:816–827, 2005.
- <sup>42</sup>Teissie, J., and M. P. Rols. An experimental evaluation of the critical potential difference inducing cell membrane electroporation. *Biophys. J.* 65:409–413, 1993.
- <sup>43</sup>Teissie, J., N. Eynard, B. Gabriel, and M. P. Rols. Electroporation of cell membranes. *Adv. Drug Deliver Rev.* 35:3–19, 1999.
- <sup>44</sup>Tsong, T. Y. Electroporation of cell membranes. *Biophys. J.* 60:297–306, 1991.
- <sup>45</sup>Valič, B., M. Golzio, M. Pavlin, A. Schatz, C. Faurie, B. Gabriel, J. Teissie, M. P. Rols, and D. Miklavčič. Effect of electric field induced transmembrane potential on spheroidal cells: theory and experiment. *Eur. Biophys. J.* 32:519–528, 2003.

*Paper 6***Electropermeabilization of dense cell suspensions****G. Pucihar**<sup>1</sup>, T. Kotnik<sup>1</sup>, J. Teissié<sup>2</sup>, D. Miklavčič<sup>1</sup><sup>1</sup> University of Ljubljana, Faculty of Electrical Engineering, Tržaška 25, SI-1000 Ljubljana, Slovenia<sup>2</sup> IPBS, CNRS, UMR 5089, 205 Route de Narbonne, Toulouse Cedex, France*(manuscript in preparation)***Abstract**

This paper investigates the influence of cell density on cell membrane electropermeabilization. The experiments were performed on dense cell suspensions (up to  $400 \times 10^6$  cells/ml), which represent a simple model for studying electropermeabilization of tissues. Permeabilization was assayed with a fluorescent test using Propidium iodide to obtain the mean number of permeabilized cells (i.e. fluorescence positive) and the mean fluorescence per cell (amount of loaded dye). In our study, as the cell density increased from  $10 \times 10^6$  to  $400 \times 10^6$  cells/ml, the fraction of permeabilized cells decreased by approximately 50%. We attribute this to the changes in the local electric field, which lead to a decrease in the amplitude of the induced transmembrane voltage. To obtain the same fraction of cell permeabilization in suspensions with  $10 \times 10^6$  and  $400 \times 10^6$  cells/ml, the latter suspension had to be permeabilized with higher pulse amplitude, which is in a qualitative agreement with numerical computations. The electroloading of the cells also decreased with cell density. The decrease was considerably larger than expected from the differences in the permeabilized cell fractions. The additional decrease in fluorescence was mainly due to cell swelling after permeabilization, which reduced extracellular dye availability to the permeabilized membrane and hindered the dye diffusion into the cells. We also observed that resealing of cells appeared to be slower in dense suspensions, which can be attributed to cell swelling resulting from electropermeabilization.

# Electropermeabilization of dense cell suspensions

Gorazd Pucihar · Tadej Kotnik · Justin Teissié ·  
Damijan Miklavčič

Received: 24 August 2006 / Revised: 8 November 2006 / Accepted: 17 November 2006 / Published online: 9 February 2007  
© EBSA 2007

**Abstract** This paper investigates the influence of cell density on cell membrane electropermeabilization. The experiments were performed on dense cell suspensions (up to  $400 \times 10^6$  cells/ml), which represent a simple model for studying electropermeabilization of tissues. Permeabilization was assayed with a fluorescence test using Propidium iodide to obtain the mean number of permeabilized cells (i.e. fluorescence positive) and the mean fluorescence per cell (amount of loaded dye). In our study, as the cell density increased from  $10 \times 10^6$  to  $400 \times 10^6$  cells/ml, the fraction of permeabilized cells decreased by approximately 50%. We attributed this to the changes in the local electric field, which led to a decrease in the amplitude of the induced transmembrane voltage. To obtain the same fraction of cell permeabilization in suspensions with  $10 \times 10^6$  and  $400 \times 10^6$  cells/ml, the latter suspension had to be permeabilized with higher pulse amplitude, which is in qualitative agreement with numerical computations. The electroloading of the cells also decreased with cell density. The decrease was considerably larger than expected from the differences in the permeabilized cell fractions alone. The additional decrease in fluorescence was mainly due to cell swelling after permeabilization, which reduced extracellular dye availability to

the permeabilized membrane and hindered the dye diffusion into the cells. We also observed that resealing of cells appeared to be slower in dense suspensions, which can be attributed to cell swelling resulting from electropermeabilization.

**Keywords** Electroporation · Cell pellets · Propidium iodide · Membrane resealing

## List of symbols

$\Delta\psi$	induced transmembrane voltage, V
$R$	cell radius, m
$E$	applied electric field, V/m
$\varphi$	angle between $E$ and the normal vector to the membrane, $^\circ$
$\varphi_c$	critical angle where permeabilization occurs, $^\circ$
$E_S$	critical amplitude of the electric field, V/m
$A_{\text{perm}}$	permeabilized surface of the membrane, $\text{m}^2$
$A_{\text{tot}}$	total area of the membrane, $\text{m}^2$
$\alpha$	angle, $^\circ$
$\Phi$	flow of molecules, mol/s
$P$	permeability coefficient, m/s
$\Delta S$	concentration difference of the molecule $S$ , $\text{mol}/\text{m}^3$
$F(t)$	fraction of membrane defects in the permeabilized region, –
$F^*(N, T)$	fraction of membrane defects immediately after the onset of permeabilizing pulse, –
$t$	time, s
$N$	number of pulses, –
$T$	pulse duration, s
$k$	resealing rate, 1/s
$F_{\text{NC}}$	fraction of permeabilized surface where cell contacts are not present, –

G. Pucihar · T. Kotnik · D. Miklavčič  
Faculty of Electrical Engineering, University of Ljubljana,  
Tržaška 25, 1000 Ljubljana, Slovenia

J. Teissié (✉)  
IPBS, CNRS, UMR 5089, 205 Route de Narbonne,  
Toulouse Cedex, France  
e-mail: justin.teissie@ipbs.fr

$c$	total concentration of PI after permeabilization (cells + external medium), mol/m <sup>3</sup>
$c_1$	concentration of PI in external medium, mol/m <sup>3</sup>
$V$	total volume (cells + external medium), m <sup>3</sup>
$V_1$	volume of external medium, m <sup>3</sup>
EMEM	eagle's minimum essential medium, –
PI	propidium iodide, –
CHO	Chinese hamster ovary cells, –

## Introduction

Exposure of cells to an electric field of sufficient amplitude leads to an increased permeability of cell membranes, a phenomenon termed electroporation (Tsong 1991; Barnett and Weaver 1991; Weaver and Chizmadzhev 1996; Teissié et al. 1999; Neumann et al. 1999). Electroporation occurs in the regions of the membrane where the transmembrane voltage, induced by the external electric field, exceeds a certain threshold characteristic for each cell line. Provided that the amplitude of the field is not too high and the duration not too long, the increase in permeability is reversible, and cells return to their initial state after the exposure.

During the state of high permeability it is possible to deliver membrane-impermeant ions and molecules (e.g. various drugs, DNA) into cells. With a reversible permeabilization and sufficiently rapid resealing of the membrane, this method is very efficient, and during the last two decades it has found an increasing use in drug delivery to tumor cells—electrochemotherapy (Okino and Mohri 1987; Serša et al. 1995; Mir and Orlowski 1999; Gothelf et al. 2003; Šatkauskas et al. 2005) and gene delivery to cells—electrogenotherapy (Neumann et al. 1982; Šatkauskas et al. 2002; Čemažar et al. 2003; Fattori et al. 2005).

Despite the increasing use of electroporation, the events on the molecular scale that result in the increase in membrane permeability are not completely understood even in such simplified membrane models as pure lipid bilayers. For biological cells, the mechanisms of electroporation are better understood in diluted cell suspensions than in tissues, where irregular shapes of the cells, their mutual electric shielding, and perhaps connections between them (e.g. gap junctions) play a role. As a consequence, it is more difficult to plan, without prior experiments, an efficient and safe electroporation protocol for cells in tissues than for suspensions. For one reason, the

induced transmembrane voltage for cells in suspension can be calculated analytically, while for cells in tissues, which are irregularly shaped, numerical computing is required (see e.g. Pucihar et al. 2006). To gain understanding of tissue electroporation, the researchers often use—both in theoretical analysis and in experiments—simple models of tissues, such as dense cell suspensions, cell pellets or multicellular spheroids (Abidor et al. 1993, 1994; Susil et al. 1998; Schmeer et al. 2004; Pavlin et al. 2002; Canatella et al. 2004). Here and throughout this paper, “cell density” should be understood as the volume fraction that the cells occupy in the suspension and a “dense suspension” is a suspension in which the cell density is considerable. These studies suggest that if cells are relatively close to each other, they respond to the electric field differently from isolated cells. Condensation of cells changes their response to electroporation. Indeed, in two recent theoretical studies the authors showed that the amplitude of transmembrane voltage induced on spherical cells progressively decreases when cells are brought closer together (Susil et al. 1998; Pavlin et al. 2002). Because permeabilization is observed in the regions of the membrane where the induced transmembrane voltage exceeds a threshold value, the increased cell density should, according to these theoretical studies, lead to a decrease in cell permeabilization. In addition, an experimental study on multicellular spheroids showed that the uptake of molecules to cells after permeabilization is lower and spatially more heterogeneous in such spheroids than in isolated cells (Canatella et al. 2004). The observed differences in uptake were attributed to cell size distribution (cells in the interior of the spheroids were smaller than cells on the periphery), slow diffusion of the dye to the cells inside the spheroids, limited extracellular solute reservoir, and heterogeneous field strength due to influence of neighbouring cells.

The purpose of the study presented in this paper was to investigate the effect of the mutual electrical shielding of cells on the process of cell electroporation. The experiments were performed on cell suspensions, because they presented an easy and controlled system, which could also be treated theoretically. Besides, the cell size distribution was uniform over the whole suspension and the dye distribution in suspension was homogeneous. This enabled the observation of the changes in cell permeabilization, resulting only from the electrical shielding of cells. Together with numerical computations of the induced transmembrane voltage, the results of our study provide a complement to the theoretical and experimental studies presented before.

## Materials and methods

### Cells

The experiments were performed on Chinese hamster ovary cells (CHO cells, WTT clone), which were grown in EMEM medium (MEM 0111, Eurobio, France) with added fetal calf serum (8%, Boehringer, Germany), antibiotics (penicillin 100 units/ml, streptomycin 100 µg/ml) and L-glutamine (1.16 mg/ml). The cells were kept in suspension by gentle, continuous agitation (100 rpm) in spinner flasks at 37°C. The key advantage of the WTT clone of CHO cells is that the cells are growing in suspension, so no trypsin treatment is needed and the extracellular matrix remains intact. Light scattering studies by flow cytometry did not show considerable cell clustering resulting from spinning of suspension. Prior to the experiments, part of the suspension was taken from the spinner to determine the cell density (usually  $1.5 \times 10^6$  cells/ml), and then the suspension (4 × 50 ml) was centrifuged (200×g, 5 min, Jouan C 500 centrifuge, France). After centrifugation, the supernatant was replaced with pulsing buffer (10 mM  $\text{KH}_2\text{PO}_4/\text{K}_2\text{HPO}_4$ , 250 mM sucrose, 1 mM  $\text{MgCl}_2$ ), which contained 100 µM of fluorescent dye propidium iodide (PI, Sigma, St Louis, USA), to obtain cell density of  $400 \times 10^6$  cells/ml. When the buffer was added, the volume of the pellet was taken into account and was thus subtracted from the calculated volume. The suspension was gently pipetted a few times with a large tip pipet to obtain a homogenous dye distribution. We should note that  $400 \times 10^6$  cells/ml results in a very dense but still liquid suspension. A part of the suspension with  $400 \times 10^6$  cells/ml was then further diluted with the same dye-containing buffer to obtain cell densities of  $200 \times 10^6$  and  $10 \times 10^6$  cells/ml. The volume fractions of cells in these cell densities were approximately 36, 18, and 1%, respectively [the average radii of CHO cell is about 6 µm (Golzio et al. 1998)]. Cells were kept at 4°C before exposure to electric pulses. Only limited cell damages were associated to these manipulations.

### Electroporation

Cell suspension (100 µl) was placed between two parallel, flat, stainless steel electrodes placed 5 mm apart. The electrodes were connected to a Jouan electropulsator (Jouan, St Herblain, France) and to an oscilloscope (Enertec, St Etienne, France), where pulse delivery was continuously monitored. Two different pulse protocols were used:  $8 \times 100$  µs rectangular pulses (short pulses), a typical electroporation

protocol, and a  $10 \times 5$  ms rectangular pulses (long pulses), a protocol, which induces membrane perturbations supporting gene transfer. In both protocols, the pulses were delivered with 1 Hz repetition frequency. After electroporation cells were incubated for 7 min at 25°C and then resuspended in 1 ml of D-PBS (Gibco, USA).

### Detection of electroporation

Cells were pulsed in the presence of PI, a non-permeant fluorescent dye, which emits strong fluorescence after entering the permeabilized or damaged cells. The percentage of permeabilized cells and the mean fluorescence intensity of the cells were determined from the histograms obtained by flow cytometry (FACscan, Becton-Dickinson, USA) as shown in Fig. 1a, b. On the histogram of the pulsed sample (cells exposed to electric pulses), the position of two markers (M1 and M2) was selected at the apparent boundary between the population of nonpermeabilized (M1) and permeabilized cells (M2) as shown in Fig. 1b. The fraction of permeabilized cells was then given by the percentage of cells in the M2 window, while the fluorescence of the cells was represented by the mean fluorescence of the whole sample (M1 and M2). The position of the markers was kept the same for all investigated parameters within one experiment. Intact cells of the control sample (85% of the population) were in the M1 section (Fig. 1a).

### Resealing of cells after electroporation

The cells were prepared as described above, except that propidium iodide was mixed into cell suspension

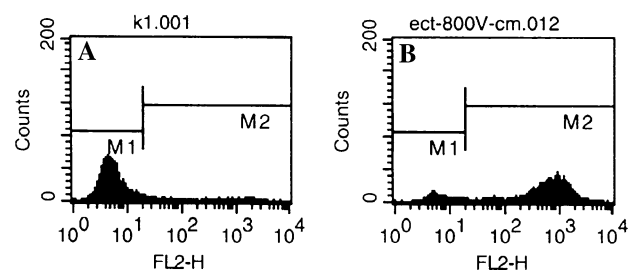


**Fig. 1** The histogram of the fluorescence of the cells. M1 and M2 mark the nonpermeabilized and permeabilized cells, respectively, for **a** the control sample, and **b** electroporation with 800 V/cm,  $8 \times 100$  µs pulses. The fraction of permeabilized cells was given by the percentage of cells within the range of M2. The fluorescence of the cells was represented by the mean fluorescence of the whole sample (M1 and M2)

at specific times after the pulse delivery. The experiments were first performed in  $10 \times 10^6$  cells/ml suspension, where the dye was added 0, 10, 30 s, 1, 3, 5, and 7 min after permeabilization. Specifically, at a given time, 100  $\mu$ l of dye in pulsing buffer was added to 100  $\mu$ l of cell suspension to obtain 100  $\mu$ M final concentration of the dye in cell suspension. From the results, the times at which roughly 0, 50, and 100% of the cells resealed were determined and at these specific times, the resealing of cells in  $400 \times 10^6$  cells/ml suspension was then measured. The dye was added in the same manner as described for dilute suspensions. In experiments where the dense suspension was diluted after permeabilization with 900  $\mu$ l of the pulsing buffer, 100  $\mu$ l of 1.1 mM PI was added at specific times after permeabilization to obtain 100  $\mu$ M final concentration of the dye in suspension. In all cases, the suspensions were carefully pipetted a few times with a large tip pipet to obtain homogenous distribution of the dye in suspension. In dense suspension, the resealing was measured only at three specific times because a large number of cells would be required to perform the same experiment with dilute and dense cell suspension. The resealing is known to obey first-order kinetics (Rols and Teissié 1990; Neumann et al. 1998).

After permeabilization, the cells were incubated for 7 min at 25°C, except for the cells to which the dye was added 7 min after pulsation, which were incubated for two additional minutes. The subsequent cell handling and the detection of permeabilization were the same as described above.

## Theoretical background

Isolated cells, cells in dilute suspensions

When a cell is exposed to an external electric field  $E$ , a transmembrane voltage  $\Delta\Psi$  is induced across its membrane. For an isolated spherical cell in physiological conditions, this voltage can be calculated from the following equation (Schwan 1957; Pauly and Schwan 1959; Grosse and Schwan 1992; Kotnik et al. 1997):

$$\Delta\Psi = 1.5 \cdot R \cdot E \cdot \cos \varphi, \quad (1)$$

where  $R$  is the cell radius and  $\varphi$  is the angle between the electric field and the normal vector to the membrane. At certain amplitude of the external electric field ( $E_S$ ), the transmembrane voltage reaches critical amplitude and electropermeabilization is detected. Because  $\Delta\Psi$  varies with the position on the cell membrane, the permeabilization first occurs in the regions of the

membrane facing the electrodes ( $|\cos \varphi| = 1$ ). For  $E > E_S$ , the relation between  $E$  and  $E_S$  can be written as (Rols and Teissié 1990):

$$E_S = E \cdot \cos \varphi_c, \quad (2)$$

where  $\varphi_c$  is the angle characterizing the permeabilized cap of the membrane ( $A_{\text{perm}}$ ). This region can be calculated by integrating the equation:

$$dA_{\text{perm}} = R \cdot d\alpha \cdot 2\pi \cdot R \cdot \sin \alpha, \quad (3)$$

where  $\alpha$  varies from 0 to  $\varphi_c$ , and introducing the total area of the membrane ( $A_{\text{tot}}$ ):

$$A_{\text{perm}} = 1/2 \cdot A_{\text{tot}} \cdot (1 - E_S/E); \quad \text{for } E > E_S. \quad (4)$$

Membrane-impermeable ions and molecules can enter the cell through the permeabilized region of the membrane ( $A_{\text{perm}}$ ) with the flow ( $\Phi$ ), which can be described by using the modified First law of Fick:

$$\Phi = P \cdot F \cdot A_{\text{perm}} \cdot \Delta S. \quad (5)$$

In this equation,  $P$  denotes the permeability coefficient in the defects of the membrane for molecule  $S$ ,  $F$  is a fraction of defects in the permeabilized region and  $\Delta S$  is the concentration difference of the molecule between cell interior and exterior. Taking into account the above equations and under the assumption that the extracellular volume is an infinite reservoir compared to the cytoplasmic volumes, the flux of the molecule  $S$  at time  $t$  after the pulse can therefore be expressed as:

$$\Phi(S, t) = 1/2 \cdot P \cdot \Delta S(t) \cdot F(t) \cdot A_{\text{tot}} \cdot (1 - E_S/E), \quad (6)$$

where  $\Delta S(t)$  is the concentration difference of the molecule  $S$  at time  $t$ . The fraction of defects in the permeabilized region,  $F(t)$ , can be written as:

$$F(t) = F^*(T, N) \cdot e^{-k \cdot t} \quad (7)$$

where  $F^*$ , the density of defects instantaneously resulting from the pulses, is a function of only the pulse duration ( $T$ ) and the number of pulses ( $N$ ), (resealing is not present if the frequency of pulses is high enough as in our experimental conditions),  $k$ , the resealing rate, is a function of pulse duration ( $T$ ), number of pulses ( $N$ ) (Rols and Teissié 1990, 1998) and osmotic conditions (Golzio et al. 1998) and  $t$  is the time elapsed after electropermeabilization. Electroloading is obtained by the integral of  $\Phi(S, t)$  during the permeabilized lifetime. Under these conditions, at given  $E$ ,  $T$ ,  $N$ , cell size and  $\Delta S(0)$ , electroloading is controlled by  $k$ .

## Cells in dense suspensions

When a cell is in a dense suspension it is close to its neighbouring cells, which alter the local electric field around it. As a consequence, the amplitude of  $\Delta\Psi$  decreases and its spatial distribution changes, so that it becomes flatter in the regions of the cell facing the electrodes (Susil et al. 1998; Pavlin et al. 2002). The analytical solution for  $\Delta\Psi$  obtained for an isolated cell (Eq. 1) is therefore not valid anymore and  $\Delta\Psi$  in dense suspensions can be calculated only numerically (Susil et al. 1998; Pavlin et al. 2002). Also, the extracellular volume cannot be considered as an infinite reservoir compared to the cytoplasmic volumes anymore. The change in  $\Delta S(t)$  after permeabilization may be affected.

### Numerical calculations of $\Delta\Psi$ on cells in dense suspensions

The influence of volume fraction of cells and their arrangements in suspension on  $\Delta\Psi$  was studied in a paper published by Pavlin et al. (2002). Here, we computed  $\Delta\Psi$  for the specific experimental conditions and volume fractions of cells used in our study (1, 18, and 36%). Although the arrangement of cells in suspension is random, on a large scale it can be approximated by a face-centered cubic lattice, where cells are located in the corners and in faces of a cube (Fig. 2a). Detailed information on the methodology of the computation of the induced transmembrane voltage on cubic lattices can be found in (Susil et al. 1998; Pavlin et al. 2002). Numerical computations were performed with finite elements modeling software Femlab 3.1 (COMSOL Inc., Burlington, MA, USA) using DC

application mode. As the results in Fig. 2b show, the maximum amplitude of  $\Delta\Psi$  normalized to the radius  $R$  and electric field  $E$  decreases from the value of 1.5 for an isolated cell to 1.493, 1.39, and 1.32, for 1% (solid line), 18% (dotted line), and 36% (dashed line) volume fractions of cells in suspension, respectively.

The flow of molecules ( $\Phi$ ) through the permeabilized cell membrane can be derived from Eq. 5. The permeabilized surface ( $A_{\text{perm}}$ ) in this case can be calculated numerically, by integration over the part of the cell surface where  $\Delta\Psi$  is above the critical value. Because cells are in close contact, (due to the high density of suspension or due to cell swelling after permeabilization), the flow mostly occurs on the fraction of the permeabilized surface where such contacts are not present ( $F_{\text{NC}}$ ):

$$\Phi(S, t) = P \cdot \Delta S \cdot F_{\text{NC}} \cdot F \cdot A_{\text{perm}}. \quad (8)$$

Compared to isolated cells or dilute cell suspensions, the flow of molecules and the resulting electroloading are decreased, because  $A_{\text{perm}}$  is smaller (due to lower  $\Delta\Psi$ ) and also because  $F_{\text{NC}} < 1$ .

## Results

### Determination of pulse amplitudes for electropermeabilization

To investigate the efficiency of electropermeabilization as a function of cell density we first determined the pulse amplitude that led to a detectable electropermeabilization of cells in these suspensions. For this

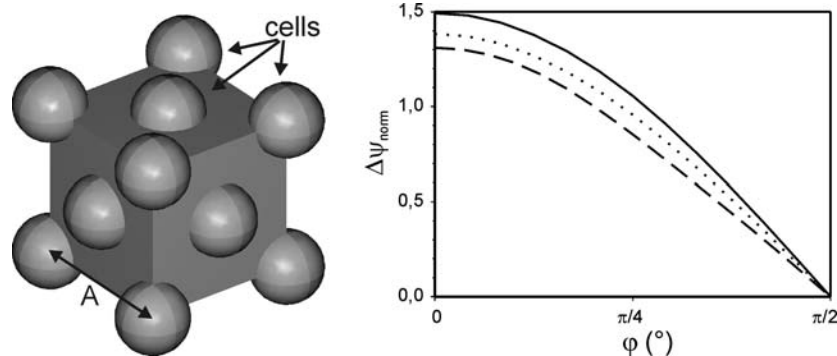


**Fig. 2** **a** Model of cell suspension with cells arranged in a face-centered cubic lattice.  $A$  is the length of the side of the cube. The cube represents the extracellular medium with specific conductivity 0.14 S/m (Rols et al. 1998), while the cells were modeled as nonconductive solid spheres. The remaining sides of the cube were insulating, to model the infinite lattice of cells. **b**  $\Delta\Psi$  on

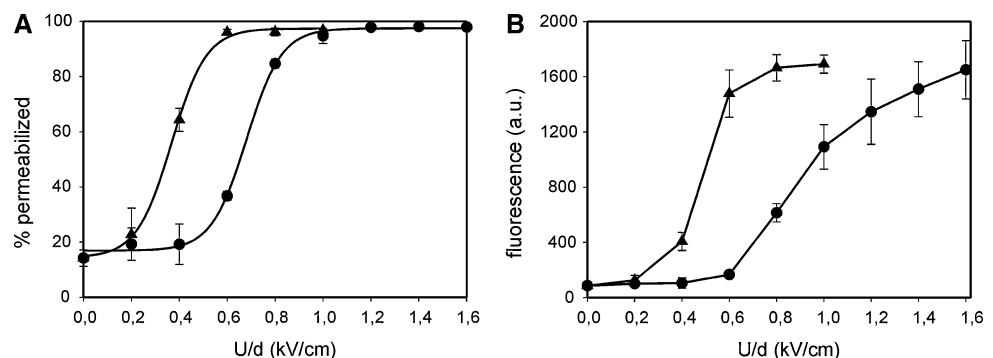
cells arranged in the lattice for volume fractions of 1% *solid line*, 18% *dotted line*, and 36% *dashed line*.  $\Delta\Psi$  was normalized to the cell radius and the electric field. Due to symmetry, only one quarter of the distribution of  $\Delta\Psi$  is shown. The values of  $\Delta\Psi$  were calculated in steps smaller than  $0.5^\circ$ , points were connected with a smooth curve

purpose we performed the measurements of cell permeabilization as a function of the pulse amplitude (expressed by the ratio of the voltage applied to the electrodes and the distance between them). Since an increase in cell density can generally be expected to reduce the level of electroporation (see [Introduction](#)), we performed these initial experiments on a suspension with the lowest cell density ( $10 \times 10^6$  cells/ml). The results of electroporation as a function of the pulse amplitude for  $8 \times 100 \mu\text{s}$  (short pulses) and  $10 \times 5 \text{ ms}$  (long pulses) are shown in Fig. 3a. Two typical electroporation curves were obtained, showing almost no change from the control up to certain amplitudes, then a relatively sharp increase in the fraction of permeabilized cells, and finally a plateau where practically all cells were permeabilized. Compared to the electroporation curve for short pulses, the curve for long pulses is shifted towards lower pulse amplitudes, reflecting the effect of longer pulse duration (Rols and Teissie 1998). From these two curves, the pulse amplitudes that caused the permeabilization of  $\sim 70\%$  of the cells were estimated. For short and long pulses these voltage-to-distance amplitudes were approximately 700 and 400 V/cm, respectively.

Applying the same amplitudes on denser cell suspensions would allow detecting expected reduction in electroporation resulting from an increase in cell density.

Fig. 3b shows the fluorescence of the cells as a function of the pulse amplitude. Similar to the permeabilization curves, we detected almost no increase in fluorescence at low pulse amplitudes, where cells are not yet permeabilized. As the amplitude increases, so does the fluorescence, until reaching a plateau that reflects the maximum level of permeabilization and the occupation of binding sites for the fluorescence dye. Similar limiting fluorescence was observed on the plateau conditions, whatever the pulse duration, suggesting the same loading of PI (Fig. 3b).

**Fig. 3** **a** Electroporation, and **b** fluorescence as a function of voltage-to-distance ratio for  $8 \times 100 \mu\text{s}$  (black circles) and  $10 \times 5 \text{ ms}$  pulse protocol (black triangles). The density of cell suspension is  $10 \times 10^6$  cells/ml. Each point in the figure represents the mean  $\pm$  SD ( $n = 3$ )



Electroporation as a function of cell density

### Initial experiments

Suspensions with three different cell densities, containing  $10 \times 10^6$ ,  $200 \times 10^6$ , and  $400 \times 10^6$  cells/ml, were exposed to electric pulses with the amplitudes yielding permeabilization of  $\sim 70\%$  of the diluted cells for each of the two protocols (400 and 700 V/cm, see the preceding section). The fraction of permeabilized cells as a function of cell density for the two protocols is shown in Fig. 4a, b. The relation between cell density and permeabilization was similar for both pulse protocols, namely an increase in cell density corresponding to a significant decrease in the fraction of permeabilized cells at the same pulse amplitude. More precisely, with an increase in cell density from  $10 \times 10^6$  to  $400 \times 10^6$  cells/ml, the fraction of permeabilized cells is reduced from 81 to 42% in the case of short 700 V/cm pulses, and from 65 to 24% in the case of long 400 V/cm pulses. The permeabilization in the control sample ( $10 \times 10^6$  cells/ml, 15%) reflects the cells that were damaged or lost their viability during the preparation.

Figure 4c, d show the fluorescence of permeabilized cells as a function of cell density. For both pulse protocols, the fluorescence was the strongest in the suspension containing  $10 \times 10^6$  cells/ml, and the weakest in the suspension with  $400 \times 10^6$  cells/ml.

In addition, experiments with short pulses were also performed with 1 mM concentration of PI, to verify if the extracellular reservoir of the dye affects the measurements. The results presented in Fig. 5 show the same tendency as those obtained with a 100  $\mu\text{M}$  concentration. The fraction of cell permeabilization and the fluorescence both decrease with an increase in cell density, and the decrease is similar to the one observed with low PI concentration (100  $\mu\text{M}$ , Fig. 5a, b). With 1 mM dye, the 40% of cells detected as permeabilized in the control group is due to the diffusion through

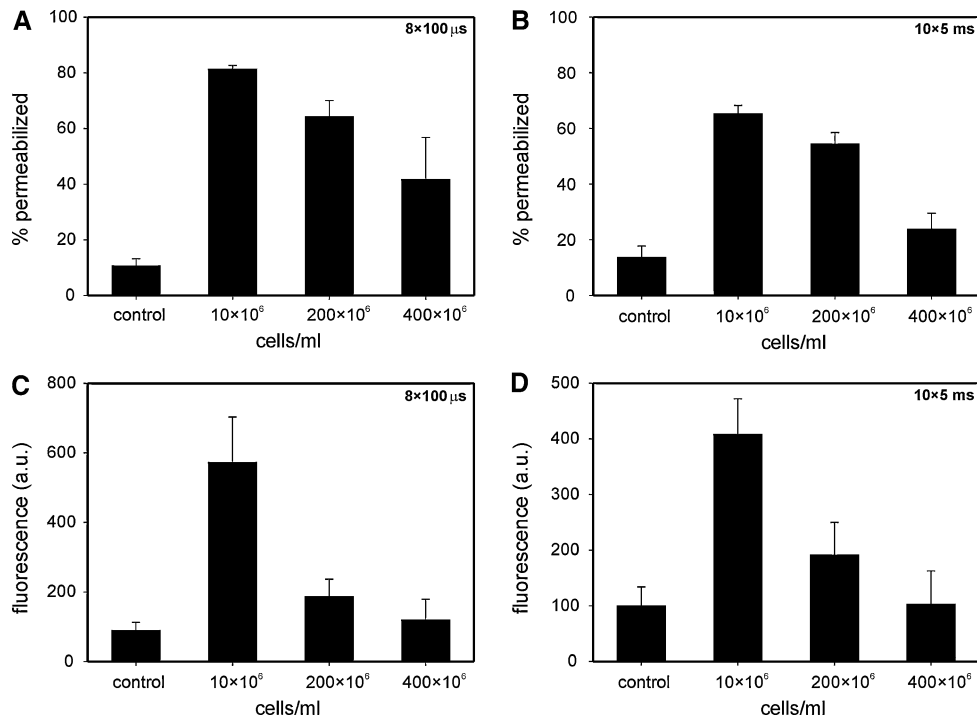


**Fig. 4** Electropermeabilization as a function of cell density for a  $8 \times 100 \mu\text{s}$  (700 V/cm) and **b**  $10 \times 5 \text{ ms}$  (400 V/cm) pulse protocol. Fluorescence as a function of cell density for **c**  $8 \times 100 \mu\text{s}$

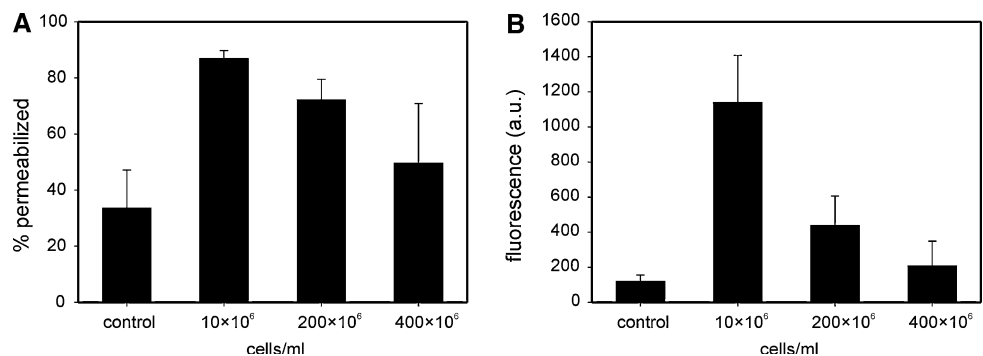
(700 V/cm) and **d**  $10 \times 5 \text{ ms}$  (400 V/cm) pulse protocol. Each column represents the mean  $\pm$  SD ( $n = 3$ )

intact membranes, which becomes pronounced due to the very high dye concentration. Because of higher dye concentration and consequently higher fluorescence intensity, the parameters of the flow cytometer and the markers on the histogram (see [Materials and methods](#)) were adjusted.

A closer examination of the fluorescence in cell suspensions with different densities and comparison with permeabilization results show that the decrease in the fluorescence is more pronounced than would be expected from the differences in the fractions of permeabilized cells. This can be observed in the

experiment with 100  $\mu\text{M}$  and 1 mM dye concentration. Namely, as seen in Fig. 4a for example, the fractions of permeabilized cells in suspensions containing  $200 \times 10^6$  and  $400 \times 10^6$  cells/ml were approximately 80 and 50% of the fraction of permeabilized cells in the suspension with  $10 \times 10^6$  cells/ml. Therefore, we would expect that the fluorescence in dense suspensions (200 and  $400 \times 10^6$  cells/ml) would also decrease to roughly 80 and 50%, respectively, of the fluorescence in suspension with  $10 \times 10^6$  cells/ml, but the observed fluorescence decrease was significantly larger (down to approximately 30 and 20%).

**Fig. 5 a** Electropermeabilization, and **b** fluorescence as a function of cell density for  $8 \times 100 \mu\text{s}$  (700 V/cm) pulse protocol and higher dye concentration (1 mM). Each column represents the mean  $\pm$  SD ( $n = 3$ )



Two plausible explanations may be suggested for the observed fluorescence decrease. One is the dilution of the dye after permeabilization. Namely, in dense suspensions, cells represent a considerable part of the total volume of the suspension (e.g. 36% for  $400 \times 10^6$  cells/ml), which means that the extracellular volume cannot be considered as an infinite reservoir of the dye anymore. Permeabilization allows the dye to enter the cells, which results in a decrease in the dye concentration outside the cell by an amount corresponding to the volume fraction represented by the cells. This dilution effect is negligible for the  $10 \times 10^6$  cells/ml suspension, as the cells represent only 1% of the total volume of the suspension, but not for the  $400 \times 10^6$  cells/ml suspension, where the volume fraction of cells is approximately 36%. The second possible explanation for the decrease in the fluorescence in dense suspensions could be cell swelling after electroporation (Abidor et al. 1993, 1994; Canatella et al. 2004; Kinoshita and Tsong 1977). After electroporation in a sufficiently dense suspension, the volume represented by the cells could increase to a value where the cells come into close contact (similar to the situation in tissues), which would then limit the part of the permeabilized cell surface available for the transfer of PI, resulting in lower fluorescence (as explained in the theoretical background section).

We investigate these two plausible explanations in subsequent sections of this paper. Because the largest differences in the fraction of cell permeabilization and the fluorescence were observed between suspensions with  $10 \times 10^6$  and  $400 \times 10^6$  cells/ml, these investigations were performed only with these two suspensions. Also, to avoid the decrease in the fluorescence in dense suspension resulting from the decrease in the fraction of cell permeabilization in this suspension, we adjusted the pulse amplitudes to obtain roughly the same fraction of permeabilized cells in both cell density suspensions.

#### *Compensation for dye dilution*

Cells were permeabilized with pulse amplitudes yielding roughly the same fraction of permeabilization in the dilute and in the dense cell suspension. This was obtained from our experimental observations. In this manner, with short pulses the amplitude was 700 V/cm for  $10 \times 10^6$  cells/ml, and 900 V/cm for  $400 \times 10^6$  cells/ml. Similarly, with long pulses the amplitude was 400 V/cm for  $10 \times 10^6$  cells/ml, and 540 V/cm for  $400 \times 10^6$  cells/ml. Also, the concentration of the dye ( $c_I$ ) in dense suspension was increased to 156  $\mu\text{M}$ , to

account for the decrease in external volume outside of the cells (from 99 down to 64%) ( $c_I \times V_I = c \times V$ ;  $c_I = 100 \mu\text{M} \times 1/0.64$ ). Namely, increasing the concentration of PI in dense suspension from 100 to 156  $\mu\text{M}$  provided the final concentration of the dye after permeabilization (that is in extracellular and intracellular volume) equal to the concentration of the dye in dilute suspension (100  $\mu\text{M}$ ). The dilution of the dye in  $10 \times 10^6$  cells/ml suspension was neglected due to the small volume fraction of cells in this suspension (1%).

As shown in Fig. 6, the modifications (increased pulse amplitude and compensation for the dye dilution) result in similar permeabilization of the population, but have a limited effect on the fluorescence in dense suspension. It remains considerably lower than the fluorescence in dilute suspension for both pulse protocols (e.g. compare the fluorescence of  $400 \times 10^6$  cells/ml suspension in Fig. 6c, black column and grey columns).

#### *Compensation for possible cell swelling*

This experiment was similar to the one described in the previous subsection, except that immediately after electroporation, the cell suspension (100  $\mu\text{l}$ ) was resuspended in 900  $\mu\text{l}$  of pulsing medium with 100  $\mu\text{M}$  dye concentration. If we assume that cells after permeabilization increase in their size, this results in a dramatic effect in case of dense suspensions, where the volume represented by the cells could increase to a value where the cells are in close contact. By dilution after the pulses we can avoid a long duration of these induced intercellular contacts.

The experiments were performed only for short pulses and the results (Fig. 7) are in agreement with our hypothesis. If the pulse amplitude was adjusted to achieve roughly the same fraction of cell permeabilization in suspensions with  $10 \times 10^6$  and  $400 \times 10^6$  cells/ml, the fluorescence of dense suspension diluted after permeabilization (denoted with letter D in superscript, grey hatched column in Fig. 7b), increased and approached the fluorescence of  $10 \times 10^6$  cells/ml suspension (black hatched column in Fig. 7b). The fluorescence of dense cell suspension, which was not diluted after permeabilization, remained low (Fig. 7b, grey column). The fraction of cells detected as permeabilized in the dense suspension was slightly increased with dilution (Fig. 7a), which may result from a facilitated dye uptake. The remaining difference in fluorescence between the suspensions could be attributed to the slower resealing of cells after permeabilization.

**Fig. 6** Permeabilization of the cells in dilute ( $10 \times 10^6$  cells/ml, *black columns*) and dense suspension ( $400 \times 10^6$  cells/ml, *grey columns*) for **a**  $8 \times 100 \mu\text{s}$ , and **b**  $10 \times 5 \text{ ms}$  pulse protocol, after adjustment of the pulse amplitude to achieve roughly the same fraction of cell permeabilization and after increasing the dye concentration ( $100 \mu\text{M}$  in dilute and  $156 \mu\text{M}$  in dense cell suspension) to account for the volume occupied by the cells. Fluorescence of the cells for **c**  $8 \times 100 \mu\text{s}$  and **d**  $10 \times 5 \text{ ms}$  pulse protocol, for the same pulse parameters and dye concentrations as in **a** and **b**. Each column represents the mean  $\pm$  SD ( $n = 3$ )

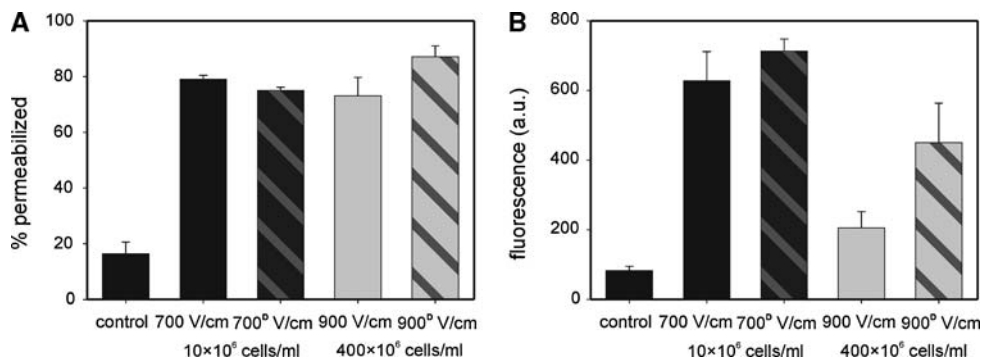
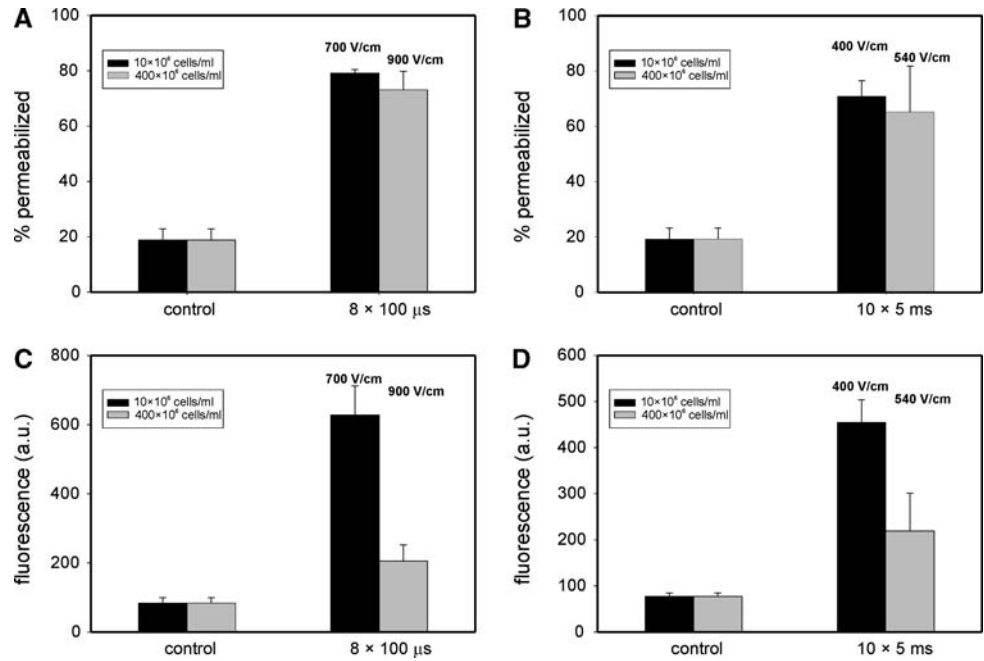


**Fig. 7** The influence of the dilution of cell suspension immediately after electroporation. **a** Permeabilization, and **b** fluorescence of the cells in  $10 \times 10^6$  cells/ml suspension (700 V/cm, *black columns*) and  $400 \times 10^6$  cells/ml suspension (900 V/cm, *grey columns*) for  $8 \times 100 \mu\text{s}$  pulse protocol. *Hatched columns*

represent permeabilization and the fluorescence of the cells that were diluted in 1 ml of pulsing buffer immediately after permeabilization (also denoted with letter D in superscript). Each column represents the mean  $\pm$  SD ( $n = 3$ )

### Resealing after electroporation

The experiment was performed at  $25^\circ\text{C}$  by addition of PI at different times after permeabilization.

First, the resealing of the cells in  $10 \times 10^6$  cells/ml suspension was determined (black columns in Fig. 8a, b). The fraction of permeabilized cells gradually decreases with time, drops to 50% of the initial value approximately 3 min after permeabilization, and returns to the control value (complete resealing) 7 min after permeabilization (Fig. 8a, b). The fluorescence, on the other hand, decreases sharply in the first 10 s after permeabilization, while the following decrease in

the fluorescence is more moderate (Fig. 8c, d). The same trend was observed for both pulse protocols (short or long pulse duration).

Second, the resealing of cells in  $400 \times 10^6$  cells/ml suspension was determined and compared with resealing in  $10 \times 10^6$  cells/ml suspension. The resealing was measured at three specific times after permeabilization (0 s, 3, and 7 min), at which approximately 0, 50 and 100% of cells in  $10 \times 10^6$  cells/ml suspension were detected as resealed, respectively. According to the results shown in Fig. 8, the fraction of permeabilized cells in  $400 \times 10^6$  cells/ml suspension decreases with time more slowly than in  $10 \times 10^6$  cells/ml suspension.

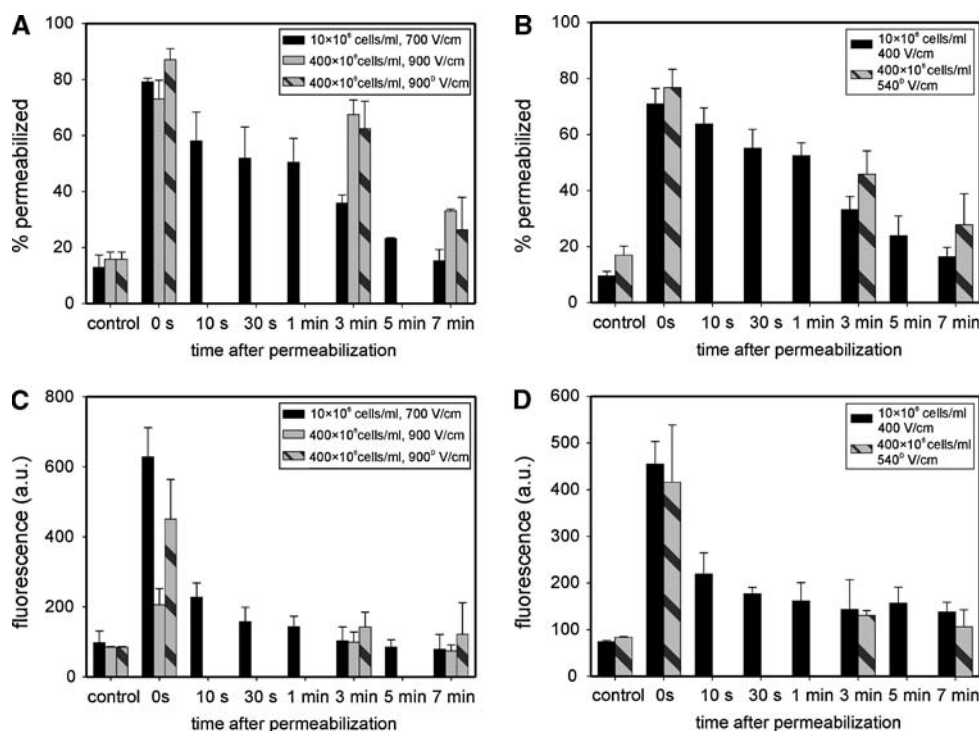


**Fig. 8** Resealing after permeabilization. **a** Permeabilization of cells at different times after pulse delivery for  $8 \times 100 \mu\text{s}$  pulse protocol, and **b** for  $10 \times 5 \text{ ms}$  pulse protocol. *Black columns*, suspension with  $10 \times 10^6$  cells/ml; *grey columns*, suspension with  $400 \times 10^6$  cells/ml. **c** Fluorescence of the cells by adding the dye at different times after pulse delivery for  $8 \times 100 \mu\text{s}$  pulse protocol, and **d** for  $10 \times 5 \text{ ms}$  pulse protocol. The pulse

This effect is more pronounced for short pulses where, for example, the fraction of permeabilized cells in  $400 \times 10^6$  cells/ml suspension 3 min after permeabilization is approximately 60% in comparison with 35% for cells in  $10 \times 10^6$  cells/ml suspension. The dilution of the  $400 \times 10^6$  cells/ml suspension after permeabilization does not considerably influence the detected level of permeabilization (compare the grey and hatched columns in Fig. 8a). The fluorescence of  $400 \times 10^6$  cells/ml suspension, which was diluted after permeabilization, decreases with time (Fig. 8c, d). Without dilution after permeabilization (grey columns in Fig. 8c), the fluorescence also decreases with time, but from a considerably lower initial value. Three minutes after permeabilization the fluorescence in  $10 \times 10^6$  and  $400 \times 10^6$  cells/ml suspension is similar to the fluorescence detected in the control sample.

## Discussion

Numerical computations indicated that the transmembrane voltage induced on suspended cells depends

amplitudes and the dye concentrations were the same as in the experiment shown in Fig. 7. Hatched columns represent permeabilization and fluorescence of the cells that were diluted in 1 ml of pulsing buffer immediately after permeabilization (also denoted with letter D in superscript). Each column represents the mean  $\pm$  SD ( $n = 3$ )

on their density in the suspension (Susil et al. 1998; Pavlin et al. 2002). More specifically, as cell density increases, this modifies the peak amplitude of the transmembrane voltage as well as its spatial distribution (Susil et al. 1998; Pavlin et al. 2002). While the deformation of the cosine dependence becomes significant only when the volume fraction of cells exceeds 50% (which is an extreme for suspensions, but a realistic value for cell aggregates or tissues), the decrease in the peak value of the induced transmembrane voltage becomes detectable at volume fractions as low as 10% (Pavlin et al. 2002). Because in our experiments, the volume fractions of cells in suspensions with  $10 \times 10^6$ ,  $200 \times 10^6$ , and  $400 \times 10^6$  cells/ml were approximately 1, 18, and 36%, respectively, we predicted that it was mostly the peak value of the induced transmembrane voltage that was affected by the differences in cell density.

Assuming as usually that the induced transmembrane voltage determines the regions of the cell membrane where electropermeabilization occurs, the increased cell density should, due to lower peak value of the transmembrane voltage, reduce the area of the

permeabilized regions. For cells in suspension, for which the radii are roughly normally distributed [the mean radii being about 6  $\mu\text{m}$  for CHO cells (Golzio et al. 1998)], it would mean that if cell density is increased considerably, some cells may not be permeabilized at all, and those that do will be permeabilized to a smaller geometric extent. The prediction is that the permeabilization of the whole cell suspension assayed both by the percentage of permeabilized cells in the pulsed population and by the extent of electroloading will decrease. Our experimental results of permeabilization as a function of cell density indeed show that the fraction of cell permeabilization and the fluorescence decrease as the cell density increases (Figs. 4a, b; 5a, b), thereby supporting the numerical assumptions qualitatively. Moreover, higher pulse amplitudes were needed to achieve the same fraction of cell permeabilization in dense than in dilute cell suspensions. However, if reduced transmembrane voltage at high cell densities would be the only factor influencing permeabilization, the pulse amplitude achieving the same fraction of permeabilized cells with  $400 \times 10^6$  cells/ml would have to be by a factor of  $\sim 1.13$  higher than with  $10 \times 10^6$  cells/ml (see Fig. 2b). In fact, the ratio between the amplitudes yielding the same permeabilized fractions in our experiments was  $\sim 1.29$  for  $8 \times 100 \mu\text{s}$  pulses (900 and 700 V/cm), and  $\sim 1.35$  for  $10 \times 5 \text{ ms}$  pulses (540 and 400 V/cm). One of the possible reasons for the discrepancy between the numerical and experimental results could be the arrangement of cells in the numerical model of cell suspension (Fig. 2a). Besides the face-centered cubic lattice, other arrangements, such as body cubic or body-centered cubic can be used to model the cell suspension (Pavlin et al. 2002). Computations with these arrangements yield considerably higher decrease in the transmembrane voltages than shown in Fig. 2b. Also, the influence of external cell matrix on the distortion of the electric field around the cells was not taken into account in the calculations. The reduced transmembrane voltage appears not to be the only factor contributing to the reduced permeabilization in dense suspensions, the other factors remain to be elucidated.

The fluorescence results were also affected more than would be expected on the basis of the decreased fraction of permeabilized cells. The fluorescence was thus lower in the dense cell suspension than in the dilute one, even if the pulse amplitudes were chosen to yield roughly the same fraction of permeabilized cells in the two suspensions, and the dye dilution effect was compensated by a higher dye concentration in dense suspension (156  $\mu\text{M}$ ) (Fig. 6a–d). We showed with additional experiments that the detected decrease in

the fluorescence of dense suspensions was most probably due to cell swelling associated to electropermeabilization (Fig. 7). It has been shown by many authors, including our group on the same CHO strain as used in this paper, that after permeabilization cell size increased (Abidor et al. 1993, 1994; Golzio et al. 1998; Kinoshita and Tsong 1977). This occurred even if the pulsing medium was isotonic, and it played a significant role in the dye diffusion into the cells. If the suspension was sufficiently dense, an increase in cell size could bring the cells in such suspension into close contact, thereby reducing the free access of dye from extracellular space to the cell membrane and hindering the dye diffusion into the cells (see Eq. 8, Fig. 9). A direct video assay under the microscope showed that the volume of CHO cells (the same WTT clone) can increase by more than 100% during a 10 s permeabilizing pulse train, and cells remain swollen for a few minutes after the pulse (Golzio et al. 1998). This makes it reasonable to believe that our initial volume fraction of cells (36%) could have increased to a limiting value ( $\sim 75\%$ , Pavlin et al. 2002), where cells are in close contact with each other. The external volume in this case would reduce to 25%. Cell swelling was probably also the main reason for the decrease in electrical conductivity after permeabilization, observed in cell pellets and dense cell suspensions (Abidor et al. 1994; Pavlin et al. 2005).

Recently Canatella et al. (2004) used multicellular spheroids as a simple model of tissue, showing that the uptake of molecules into the cells in the spheroid was lower than the uptake into the same cells when suspended (Canatella et al.). Canatella attributed this to slow diffusion of the dye into the cells in the interior of the spheroid, limited extracellular reservoir and heterogeneous electric field strength. However, our study on dense cell suspensions presented in this paper shows that even if all these effects are accounted for, the dye uptake is still lower in dense suspensions than in dilute ones, and that cell swelling is also a contributing factor. Cell swelling after electropermeabilization could perhaps also occur in tissues and contribute to the reduced uptake.

Our experiments show that the resealing of cells after permeabilization also depends on the density of the suspension. Namely, the cells in dense suspensions resealed more slowly than cells in dilute suspensions (Fig. 8). A possible explanation for slower resealing of cells in dense suspensions is the stress experienced during the addition of the dye (see [Materials and methods](#)), because repeated pipetting was needed to homogenize the dye distribution in dense cell suspension. Nevertheless, our protocol was not observed to

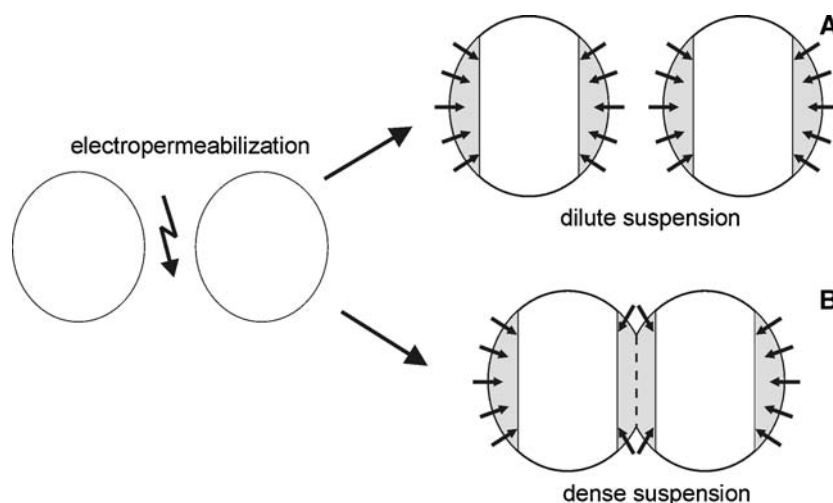


**Fig. 9** Cell swelling after permeabilization in **a** dilute suspensions, **b** dense suspensions. Cells after permeabilization increase in their size (cell swelling) due to the fast inflow of water and ions. In contrast, inflow of exogenous molecules, like PI is rather slow. If suspension is sufficiently dense, cells could come into

close contact, thereby reducing the free access of dye in extracellular space to the cell membrane and hindering the dye diffusion into the cells (arrows). Permeabilized regions of the membranes are marked in grey

damage the cells, as no lysis was detected in the long term. Li et al. (1999) suggested that at high cell densities, the restriction of nutrients supply should slow cell recovery and induce a decrease in viability. Such an interpretation did not seem to apply in our case, as resealing was fast and we observed that the exchange across the membrane was decreased. This implies that ATP cytoplasmic level was not affected significantly (and should not affect the resealing process as reported for starved cells) (Rols et al. 1998). Osmotic effects appeared more relevant. It was observed that under hyperosmolar conditions the membrane resealing after electropermeabilization is slower than under isoosmolar conditions (Rols et al. 1990). In the present experiments, swelling was a fast process, meaning that the water inflow was rapid. In contrast, inflow of exogenous molecules (sucrose, PI) was shown to be rather slow (minutes after permeabilization) (Sixou and Teissié 1993). As a conclusion, permeabilization by inducing cell swelling changed the osmotic pressure of the extracellular buffer. This means that cells in dense suspensions were pulsed in a buffer with an increasing osmolarity during the pulse train. Hyperosmolarity was therefore present and should support the observation of a slower resealing. Such an explanation is further supported by our previous observations of a lower extent of permeabilization and of electroloading (mean fluorescence) in hyperosmolar pulsing buffers (Rols et al. 1990).

Experiments in this study were performed with propidium iodide, a small molecule that enters the cell

largely by diffusion. For molecules of similar size the results are predicted to be similar (Sixou and Teissié 1993). For larger molecules, such as DNA, which enter the cells by a different process than diffusion, the uptake would probably be affected at the level of the diffusion in the bulk (Golzio et al. 2002).

In summary, our results show that cell permeabilization in dense suspensions differs considerably from that in dilute suspensions. The differences mostly arise as a consequence of mutual electrical shielding of cells, which causes a decrease in the amplitude of transmembrane voltage on such cells. These observations provide the experimental support for previous theoretical studies. The findings obtained on dense suspensions could contribute to a better understanding of the mechanisms of tissue electropermeabilization, where mutual shielding of cells (cells in tissues are in close contact) is one of the important factors influencing the permeabilization of cells. In this aspect, dense cell suspensions with an intact extracellular matrix (such as the CHO cells used in this study) are in their properties closer to tissues than dilute suspensions, and as such present a suitable model for tissues exhibiting isotropic characteristics. However, tissues showing anisotropic characteristics (e.g. muscles), or tissues which are a complex assembly of cells considerably different in shape from those in suspensions, cannot be modeled with dense suspensions of spherical cells. The second conclusion is that cell swelling is cross-reacting with electropermeabilization and this phenomenon should be present also in tissues.

**Acknowledgments** The author (G. P.) would like to thank Dr. M. Golzio, Dr. M. P. Rols and Dr. B. Gabriel for their valuable discussions during the experiments, and Ms. C. Millot for her help with cell cultures. This work was supported by the Ministry of the Higher Education and Science of the Republic of Slovenia. G. P. was also a recipient of a scholarship from the French government. The two institutes are partners in a Slovenian-French CNRS PICS program.

## References

- Abidor IG, Barbul AI, Zhelev DV, Doinov P, Bandrina IN, Osipova EM, Sukharev SI (1993) Electrical properties of cell pellets and cell electrofusion in a centrifuge. *Biochim Biophys Acta* 1152:207–218
- Abidor IG, Li LH, Hui SW (1994) Studies of cell pellets: II. Osmotic properties, electroporation, and related phenomena: membrane interactions. *Biophys J* 67:427–435
- Barnett A, Weaver JC (1991) Electroporation: a unified, quantitative theory of reversible electrical breakdown and rupture. *Bioelectrochem Bioenerg* 25:163–182
- Canatella PJ, Black MM, Bonnicksen DM, McKenna C, Prausnitz MR (2004) Tissue electroporation: quantification and analysis of heterogeneous transport in multicellular environments. *Biophys J* 86:3260–3268
- Čemažar M, Grošel A, Glavač D, Kotnik V, Škobrne M, Kranjc S, Mir LM, Andre F, Opolon P, Serša G (2003) Effects of electrogenetherapy with p53wt combined with cisplatin on survival of human tumor cell lines with different p53 status. *DNA Cell Biol* 22:765–775
- Fattori E, Cappelletti M, Zampaglione I, Mennuni C, Calvaruso F, Arcuri M, Rizzuto G, Costa P, Perretta G, Ciliberto G, La Monica N (2005) Gene electro-transfer of an improved erythropoietin plasmid in mice and non-human primates. *J Gene Med* 7:228–236
- Golzio M, Mora MP, Raynaud C, Delteil C, Teissié J, Rols MP (1998) Control by osmotic pressure of voltage-induced permeabilization and gene transfer in mammalian cells. *Biophys J* 74:3015–3022
- Golzio M, Teissié J, Rols MP (2002) Direct visualization at the single-cell level of electrically mediated gene delivery. *Proc Natl Acad Sci* 99:1292–1297
- Gothelf A, Mir LM, Gehl J (2003) Electrochemotherapy: results of cancer treatment using enhanced delivery of bleomycin by electroporation. *Cancer Treat Rev* 29:371–387
- Grosse C, Schwan HP (1992) Cellular membrane potentials induced by alternating fields. *Biophys J* 63:1632–1642
- Kinosita K, Tsong TY (1977) Formation and resealing of pores of controlled sizes in human erythrocyte membrane. *Nature* 268:438–441
- Kotnik T, Bobanović F, Miklavčič D (1997) Sensitivity of transmembrane voltage induced by applied electric fields—a theoretical analysis. *Bioelectrochem Bioenerg* 43:285–291
- Li LH, Ross P, Hui SW (1999) Improving electrotransfection efficiency by post pulse centrifugation. *Gene Ther* 6:364–372
- Mir LM, Orlowski S (1999) Mechanisms of electrochemotherapy. *Adv Drug Deliver Rev* 35:107–118
- Neumann E, Ridder MS, Wang Y, Hofschneider PH (1982) Gene transfer into mouse lyoma cells by electroporation in high electric fields. *EMBO J* 1:841–845
- Neumann E, Toensing K, Kakorin S, Budde P, Frey J (1998) Mechanism of electroporative dye uptake by mouse B cells. *Biophys J* 74:98–108
- Neumann E, Kakorin S, Toensing K (1999) Fundamentals of electroporative delivery of drugs and genes. *Bioelectrochem Bioenerg* 48:3–16
- Okino M, Mohri H (1987) Effects of high-voltage electrical impulse and an anticancer drug on in vivo growing tumors. *Jpn J Cancer Res* 78:1319–1321
- Pauly H, Schwan HP (1959) Über die impedanz einer suspension von kugelförmigen teilchen mit einer schale. *Z Naturforsch* 14B:125–131
- Pavlin M, Pavšelj N, Miklavčič D (2002) Dependence of induced transmembrane potential on cell density, arrangement, and cell position inside a cell system. *IEEE Trans Biomed Eng* 49:605–612
- Pavlin M, Kandušer M, Reberšek M, Pucihar G, Hart FX, Magjarevič R, Miklavčič D (2005) Effect of cell electroporation on the conductivity of a cell suspension. *Biophys J* 88:4378–4390
- Pucihar G, Kotnik T, Valič B, Miklavčič D (2006) Numerical determination of transmembrane voltage induced on irregularly shaped cells. *Annals Biomed Eng* 34:642–652
- Rols MP, Teissié J (1990) Electroporability of mammalian cells: quantitative analysis of the phenomenon. *Biophys J* 58:1089–1098
- Rols MP, Teissié J (1998) Electroporability of mammalian cells to macromolecules: control by pulse duration. *Biophys J* 75:1415–1423
- Rols MP, Dahhou F, Mishra KP, Teissie J (1990) Control of electric field induced cell membrane permeabilization by membrane order. *Biochemistry* 29:2960–2966
- Rols MP, Delteil C, Golzio M, Teissié J (1998) Control by ATP and ADP of voltage-induced mammalian-cell-membrane permeabilization, gene transfer and resulting expression. *Eur J Biochem* 254:382–388
- Šatkauskas S, Bureau MF, Puc M, Mahfoudi A, Scherman D, Miklavčič D, Mir LM (2002) Mechanisms of in vivo DNA electrotransfer: respective contributions of cell electroporability and DNA electrophoresis. *Mol Ther* 5:133–140
- Šatkauskas S, Batiškaite D, Šalomskaitė-Davalgiene S, Venšauskas MS (2005) Effectiveness of tumor electrochemotherapy as a function of electric pulse strength and duration. *Bioelectrochemistry* 65:105–111
- Schmeer M, Seipp T, Pliquett U, Kakorin S, Neumann E (2004) Mechanism for the conductivity changes caused by membrane electroporation of CHO cell-pellets. *PCCP* 6:5564–5574
- Schwan HP (1957) Electrical properties of tissue and cell suspensions. *Adv Biol Med Phys* 5:147–209
- Serša G, Čemažar M, Miklavčič D (1995) Antitumor effectiveness of electrochemotherapy with cis-diamminodichloroplatinum(II) in mice. *Cancer Res* 55:3450–3455
- Sixou S, Teissié J (1993) Exogeneous uptake and release of molecules by electroloaded cells: a digitized videomicroscopy study. *Bioelectrochem Bioenerg* 31:237–257
- Susil R, Šemrov D, Miklavčič D (1998). Electric field induced transmembrane potential depends on cell density and organization. *Electro Magnetobiol* 17:391–399
- Teissié J, Eynard N, Gabriel B, Rols MP (1999) Electroporability of cell membranes. *Adv Drug Deliver Rev* 35:3–19
- Tsong TY (1991) Electroporation of cell membranes. *Biophys J* 60:297–306
- Weaver JC, Chizmadzhev YA (1996) Theory of electroporation: a review. *Bioelectrochem Bioenerg* 41:135–160

*Paper 7***Effect of Cell Electroporation on the Conductivity of a Cell Suspension**

M. Pavlin<sup>1</sup>, M. Kandušer<sup>1</sup>, M. Reberšek<sup>1</sup>, **G. Pucihar<sup>1</sup>**, F. X. Hart<sup>2</sup>,  
R. Magjarević<sup>3</sup>, D. Miklavčič<sup>1</sup>

<sup>1</sup>University of Ljubljana, Faculty of Electrical Engineering, Ljubljana, Slovenia

<sup>2</sup>University of the South, Sewanee, Tennessee

<sup>3</sup>University of Zagreb, Faculty of Electrical Engineering and Computing, Zagreb, Croatia

**Abstract**

An increased permeability of a cell membrane during the application of high-voltage pulses results in increased transmembrane transport of molecules that otherwise cannot enter the cell. Increased permeability of a cell membrane is accompanied by increased membrane conductivity; thus, by measuring electric conductivity the extent of permeabilized tissue could be monitored in real time. In this article the effect of cell electroporation caused by high-voltage pulses on the conductivity of a cell suspension was studied by current-voltage measurements during and impedance measurement before and after the pulse application. At the same time the percentage of permeabilized and survived cells was determined and the extent of osmotic swelling measured. For a train of eight pulses a transient increase in conductivity of a cell suspension was obtained above permeabilization threshold in low- and high-conductive medium with complete relaxation in ,1 s. Total conductivity changes and impedance measurements showed substantial changes in conductivity due to the ion efflux in low-conductive medium and colloid-osmotic swelling in both media. Our results show that by measuring electric conductivity during the pulses we can detect limit permeabilization threshold but not directly permeabilization level, whereas impedance measurements in seconds after the pulse application are not suitable.

## Effect of Cell Electroporation on the Conductivity of a Cell Suspension

Mojca Pavlin,\* Maša Kandušer,\* Matej Reberšek,\* Gorazd Pucihar,\* Francis X. Hart,<sup>†</sup> Ratko Magjarević,<sup>‡</sup> and Damijan Miklavčič\*

\*University of Ljubljana, Faculty of Electrical Engineering, Ljubljana, Slovenia; <sup>†</sup>University of the South, Sewanee, Tennessee; and <sup>‡</sup>University of Zagreb, Faculty of Electrical Engineering and Computing, Zagreb, Croatia

**ABSTRACT** An increased permeability of a cell membrane during the application of high-voltage pulses results in increased transmembrane transport of molecules that otherwise cannot enter the cell. Increased permeability of a cell membrane is accompanied by increased membrane conductivity; thus, by measuring electric conductivity the extent of permeabilized tissue could be monitored in real time. In this article the effect of cell electroporation caused by high-voltage pulses on the conductivity of a cell suspension was studied by current-voltage measurements during and impedance measurement before and after the pulse application. At the same time the percentage of permeabilized and survived cells was determined and the extent of osmotic swelling measured. For a train of eight pulses a transient increase in conductivity of a cell suspension was obtained above permeabilization threshold in low- and high-conductive medium with complete relaxation in <1 s. Total conductivity changes and impedance measurements showed substantial changes in conductivity due to the ion efflux in low-conductive medium and colloid-osmotic swelling in both media. Our results show that by measuring electric conductivity during the pulses we can detect limit permeabilization threshold but not directly permeabilization level, whereas impedance measurements in seconds after the pulse application are not suitable.

### INTRODUCTION

A cell membrane represents a barrier to the transport of the majority of water-soluble molecules due to the hydrophobic nature of the inner part of the lipid bilayer. When a strong electric field is applied the cell membrane becomes more permeable thus enabling entrance of various molecules, which can be used as a method for introducing certain drugs or genes into the cell. The process was named electroporation because it is believed that pores are formed in the membrane due to the induced transmembrane voltage above some critical voltage (between 0.2 and 1 V), but the term electropermeabilization is used as well to stress that increased membrane permeability is observed (Neumann and Rosenheck, 1972; Zimmermann, 1982; Neumann et al., 1989; Tsong, 1991; Weaver and Chizmadzhev, 1996). After application of electric pulses the membrane completely reseals for proper selection of pulse parameters. The process of resealing takes several minutes thus allowing transport of molecules from the exterior into the cell. When the electric field is too high, for a given duration and number of pulses, physiological changes of the cell become too large to be repaired; a cell either loses too much of its content or it swells too much, which ultimately leads to cell death.

In the last decade it was shown that electroporation can be successfully used on patients, as a part of electrochemotherapy (Okino and Mohri, 1987; Mir et al., 1991; Jaroszeski et al., 1997; Mir, 2000; Serša et al., 2000) where electric pulses are used to increase locally the uptake of

cytostatic drugs. In parallel it was shown that electroporation can be successfully used also for gene transfection (Wong and Neumann, 1982; Neumann et al., 1982, 1989; Sukharev et al., 1992). Electric field mediated gene transfection uses locally delivered electric pulses to transfer DNA into the cell. In contrast to more frequently used viral transfection, which has been proved to have severe side effects in some cases of *in vivo* gene therapy on animals and humans, electroporation presents a safer alternative method, as it does not use viral vectors (Ferber, 2001; Nebeker, 2002). Although being already an established method for *in vitro* gene transfection, electroporation is currently being extensively studied on animal models *in vivo* (Jaroszeski et al., 1999; Mir, 2000).

Until now the rate of permeabilization, survival of cells, and related efficiency of the electropermeabilization could be determined only after the application of pulses by various time-consuming methods. However, the possibility of monitoring the extent of permeabilized tissue in real time is of great importance for practical clinical use of electrochemotherapy or gene therapy. Under an assumption that the increased conductivity, which is observed in single cells, cell pellets, and cell suspensions, correlates with the extent of permeabilization, measuring electrical properties could enable observation of cell permeabilization (Kinosita and Tsong, 1977a,b, 1979; Abidor et al., 1993, 1994). Nevertheless, the complex structure of a tissue makes the interpretation of such measurements difficult. For these reasons it is important to verify this hypothesis on a dense suspension of cells, which represent a more controllable and homogeneous sample than tissue.

Only a few studies have been performed to assess changes of the electrical properties of cells in suspensions or pellets

*Submitted July 5, 2004, and accepted for publication January 24, 2005.*

Address reprint requests to Prof. Dr. Damijan Miklavčič, University of Ljubljana, Faculty of Electrical Engineering, Trzaska 25, 1000 Ljubljana, Slovenia. Tel.: 386-1-4768-456; Fax: 386-1-4264-658; E-mail: damijan@svarun.fe.uni-lj.si.

© 2005 by the Biophysical Society

0006-3495/05/06/4378/13 \$2.00

doi: 10.1529/biophysj.104.048975

due to electroporation. The first measurements of the electrical properties were done on erythrocytes 20 years ago (Kinosita and Tsong, 1977a,b, 1979). Increased conductivity was observed above the threshold electric field, which after the pulse returned to its initial value. On a longer timescale, however, conductivity of a cell suspension was increased due to the ion efflux. The observed increase in conductivity correlated with the hemolysis of the cells. These observations were confirmed on pellets of different cell lines by Abidor and co-workers as well (Abidor et al., 1993, 1994), where a similar nonlinear current voltage relationship and fast resealing after the pulse was observed. In another study (Hibino et al., 1991, 1993) a decrease of the induced transmembrane voltage was detected on a part of the cell indicating increased membrane permeability for ions in that region of the membrane. Using microsecond and nanosecond pulses also increased conductivity was observed (Garner et al., 2004). Recently it was suggested (Davalos et al., 2000, 2002; Pliquett et al., 2004) that measurement of conductivity could enable online observation and control of tissue electroporation.

In this article we present measurements of electrical conductivity of a dense cell suspension in typical electroporation experiments. Conductivity of cells in a suspension was measured by current-voltage measurements during and impedance measurement before and after the application of high-voltage pulses. In parallel we determined the percentage of permeabilized and survived cells, and extent of osmotic swelling. The effect of different parameters (e.g., cell volume fraction, number of pulse, medium conductivity, . . .) on the conductivity of a cell suspension was studied and measured changes were compared to theoretical estimates. Previous studies focused on experiments with one or two pulses at most, however, for more efficient permeabilization several pulses have been proved to be more successful (Kotnik et al., 2000; Canatella et al., 2001). Thus, our interest was to also determine conductivity changes during a train of successive pulses. We analyzed how conductivity changes are related to the percentage of permeabilized cells in view of possible application of such measurements for online monitor of cell electroporation. Finally, we discuss how our observations agree with the current theoretical models of electroporation and which processes might contribute to the observed increase of bulk conductivity of a cell suspension.

## MATERIALS AND METHODS

### Current-voltage and impedance measurements

The experimental setup for current-voltage and impedance measurements is shown in Fig. 1. To generate high-voltage square pulses a high-voltage generator (prototype developed at the Laboratory of Biocybernetics, Faculty of Electrical Engineering, University of Ljubljana) was used. Impedance amplitude  $|Z|$  and phase angle  $\varphi$  before and after pulses were measured with impedance meter (HP4274A, Houston, TX). For every sample first impedance was measured after which the system switched electrodes to the high-voltage pulse generator and pulses were delivered. The second

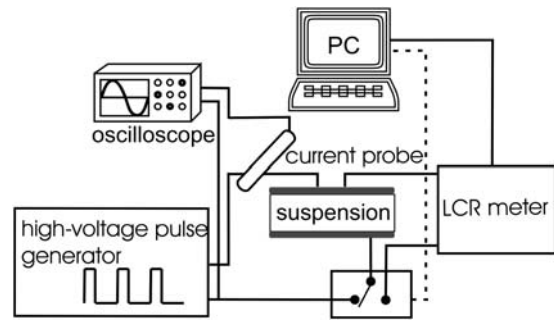


FIGURE 1 A schematic diagram of the system for electroporation and current-voltage and impedance measurements. The cell suspension ( $100 \mu\text{l}$ ) was placed between the electrodes. First, impedance was measured then the system switched electrodes to the high-voltage pulse generator and pulses were delivered. Two to three seconds after the pulses, impedance was measured for the second time and after another 10 s for the third time. For each pulse application, voltage, and current were traced on oscilloscope and stored for further analysis.

impedance measurement was carried out 2–3 s after the train of pulses and the third measurement 10 s after the second measurement. Impedance was measured at 10 different frequencies from 100 Hz to 100 kHz and altogether lasted 4 s.

During the pulses the electric current was measured with a current probe (LeCroy AP015, New York, NY) and both current and voltage were measured and stored on the oscilloscope (LeCroy 9310 C Dual, 400 MHz). Pulse amplitudes were varied to produce applied electric field  $E_0$  between 0.4 and 1.8 kV/cm. We used a train of eight square pulses of  $100\text{-}\mu\text{s}$  duration with 1 Hz repetition frequency except where stated otherwise. The memory segmentation function was used to obtain high time resolution during the pulses and only  $100 \mu\text{s}$  after the pulses were recorded. Parallel aluminum plate electrodes (Eppendorf cuvettes) with 2-mm distances between the electrodes when the whole range of amplitude were used and 4-mm distances in experiments where two volume fractions of cells were used. For every set of parameters a reference measurement on medium with no cells was also performed.

### Cells and medium

Mouse melanoma cell line, B16F1, was used in experiments. Cells were grown in Eagle's minimum essential medium supplemented with 10% fetal bovine serum (Sigma-Aldrich Chemie GmbH, Deisenhofen, Germany) at  $37^\circ\text{C}$  in a humidified 5%  $\text{CO}_2$  atmosphere in the incubator (WTB Binder, Labortechnik GmbH, Seelbach, Germany). For all experiments the cell suspension was prepared from confluent cultures with 0.05% trypsin solution containing 0.02% EDTA (Sigma-Aldrich Chemie GmbH). From the obtained cell suspension trypsin and growth medium were removed by centrifugation at 1000 rpm at  $4^\circ\text{C}$  (Sigma-Aldrich Chemie GmbH) and the resulting pellet was resuspended in medium and again centrifuged. Two media were used for electroporation: a high-conductive medium Spinner's modification of Eagle's minimum essential medium (SMEM) (Life Technologies, Paisley, UK) having conductivity  $\sigma_0$  ( $25^\circ\text{C}$ ) = 1.58 S/m that does not contain calcium and a low-conductive medium that contained phosphate buffer with 250 mM sucrose, PB  $\sigma_0$  ( $25^\circ\text{C}$ ) = 0.127 S/m. Cell suspensions having cell volume fractions  $f = 0.15$  ( $5 \times 10^7$  cells/ml) and  $f = 0.3$  ( $1 \times 10^8$  cells/ml) were used in the experiments.

### Permeabilization and viability experiments

Cell permeabilization was determined by the uptake of the cytostatic drug bleomycin and cell survival by the cell ability to survive the application of

electric pulses. It was shown that bleomycin at 5 nM external concentration penetrates only the permeabilized cells thus it can be used as an indicator of membrane permeabilization. The method is described in detail by Kotnik and co-workers (Kotnik et al., 2000). A 100- $\mu$ l droplet of a cell suspension was placed between electrodes. Bleomycin was added (5 nM external concentration) immediately after pulse application (never >60 s after the end of pulse application) to determine permeabilization. We used two amplitudes of the applied electric pulses, under permeabilization threshold (0.4 kV/cm) and above the threshold (0.94 kV/cm) for cells suspended in SMEM medium, and one amplitude for PB medium (0.94 kV/cm) for which two different volume fractions were used. For each pulse amplitude, a train of eight rectangular pulses with duration of 100  $\mu$ s and repetition frequency 1 Hz was applied and a control consisting of cells that were not exposed to an electric field was prepared. All cells were incubated at room temperature for 30 min to allow resealing of membrane and were plated at a concentration of 250 cells per petri dish for clonogenic assay. Colonies were grown in the same conditions as described above for cell culturing and after five days colonies were fixed with methanol (Merck KGaA, Darmstadt, Germany) and stained with crystal violet (Sigma-Aldrich Chemie GmbH). Visible colonies were counted and results were normalized to the control (cells with added 5 nM bleomycin not exposed to electric field). The percentage of survived colonies was subtracted from 100 percent to obtain the percentage of bleomycin uptake. Three different sample data were pooled together to obtain average and standard deviation. Each experiment was repeated twice on two separate days. Cell survival was determined as described above for the cell permeabilization but without addition of bleomycin. Results were expressed as a percentage of the cell survival.

Both results of permeabilization and survival were compared to the results obtained with the same procedure in similar conditions but with lower cell density ( $2 \times 10^7$ /ml) obtained from our previous study. Results are plotted against the local electric field  $E$  rather than applied electric field  $E_0 = U/d$  because for a high density of cells the local field experienced by each cell is smaller than the applied field due to the interaction between the cells (Susil et al., 1998; Canatella et al., 2001; Pavlin et al., 2002a). The scaling factor  $E/E_0$  was taken from our previous study (Pavlin et al., 2002a), where the decrease of the field (and induced transmembrane voltage) due to the neighboring cells was calculated to be 1% for  $f = 0.05$  and 9% for  $f = 0.3$ .

## Measurements of cells swelling

In separate experiments we exposed cells to pulses ( $E_0 = 0.4, 0.95, 1.43$  kV/cm) in an observation chamber under the inverted phase contrast microscope (Zeiss 200, Axiovert, Jena, Germany). As in other measurements a train of eight 100- $\mu$ s pulses with 1-Hz repetition frequency was used. The images were recorded (MetaMorph imaging system, Visitron, Puchheim, Germany) during the train of pulses and after the pulses up to 600 s after the first pulse. Three experiments for each, SMEM and PB medium, were made on three different days. For every parameter the area of five cells was measured from which an average was obtained. From this the changes in cells volume fraction was determined.

## Theoretical analysis: calculation of the conductivity of a suspension of permeabilized cells

For theoretical analysis we used an analytical model that relates the change in the membrane conductivity with the change of the effective conductivity of a cell suspension (Pavlin and Miklavčič, 2003). The induced transmembrane voltage for a nonpermeabilized spherical cell exposed to the external electrical field  $E$  can be derived from the Laplace equation. Except in very low-conductive medium, the solution can be approximated with

$$U_m = 1.5 ER \cos \theta, \quad (1)$$

where we assume that the cell membrane is almost nonconductive compared to the external medium.  $R$  is the cell radius and  $\theta$  is the angle between direction of the electric field and the point vector on the membrane.

When the induced transmembrane voltage exceeds the threshold voltage, the part of the cell membrane where  $U_m$  exceeds  $U_c$  is permeabilized. The permeabilized part of the cell membrane can be therefore defined by the critical angle  $\theta_c$ , where  $U_c = 1.5 ER \cos \theta_c$ . This permeabilized part of the cell membrane is in the model described by the increased membrane conductivity  $\sigma_m$ , whereas other parts of the cell membrane have zero conductivity. The potential around such permeabilized cell oriented parallel to the electric field is calculated with the Laplace equation and by using a dipole approximation the equivalent conductivity  $\sigma_p$  of a single cell is calculated. From this, using the Maxwell equation (Maxwell, 1873; Pavlin et al., 2002b)

$$\frac{\sigma_e - \sigma}{2\sigma_e + \sigma} = f \frac{\sigma_e - \sigma_p}{2\sigma_e + \sigma_p}, \quad (2)$$

the effective conductivity  $\sigma$  of a suspension of permeabilized cells is obtained, where  $f$  is the volume fraction of the cells and  $\sigma_e$  the conductivity of the external medium. The model takes into account the anisotropic nature of permeabilization, i.e., that only part of the membrane is permeabilized, and incorporates this in the calculation of the effective conductivity. The model allows calculation of the change of the effective conductivity ( $\sigma - \sigma_0$ ), which depends on different parameters: the cell volume fraction  $f$ , average membrane conductivity of the permeabilized area  $\sigma_m$ , critical angle of permeabilized area  $\theta_c$ , and conductivities of the external medium and cytoplasm,  $\sigma_e$  and  $\sigma_i$ , respectively. A more detailed description of the model is described in our previous article (Pavlin and Miklavčič, 2003).

## RESULTS

In the presented study we performed experiments where conductivity of a cell suspension was measured in parallel with the extent of cell permeabilization and cell survival. We used low-conductive medium typically used in in vitro conditions and high-conductive medium that is more representative for in vivo conditions. In addition, different volume fractions and pulse repetition frequencies were used to establish their effect on the conductivity changes.

Measured data were analyzed in terms of “instant” conductivity  $\sigma(t) = I(t)/U(t) d/S$ , the ratio between current and voltage at a given time point, where  $d$  is the distance between the electrodes, and  $S$  the surface of the sample volume at the electrodes. We obtained time-dependent conductivity of cell suspension  $\sigma$  for a train of eight 100- $\mu$ s pulses and applied electric field between 0.4 and 1.8 kV/cm, as shown in Fig. 2. Because our goal was to determine the difference in the conductivity of permeabilized and non-permeabilized cells, only the difference in the initial and final level was analyzed and not the dynamic behavior. The initial value of conductivity at the start of each pulse  $\sigma_0^N$  was determined 3  $\mu$ s after the start of the pulse, so that transient effects were not taken into account. The conductivity at the end of each pulse  $\sigma^N$  was determined and from this the change in the conductivity during the  $N^{\text{th}}$  pulse was obtained:  $\Delta\sigma^N = \sigma^N - \sigma_0^N$ . With  $\sigma_0$  we denote the initial conductivity at the start of the first pulse  $\sigma_0 = \sigma_0^1$ .

Fig. 3 represents conductivity changes  $\Delta\sigma^1/\sigma_0$  during the first 100- $\mu$ s pulse for cells in SMEM medium (a) and cells in

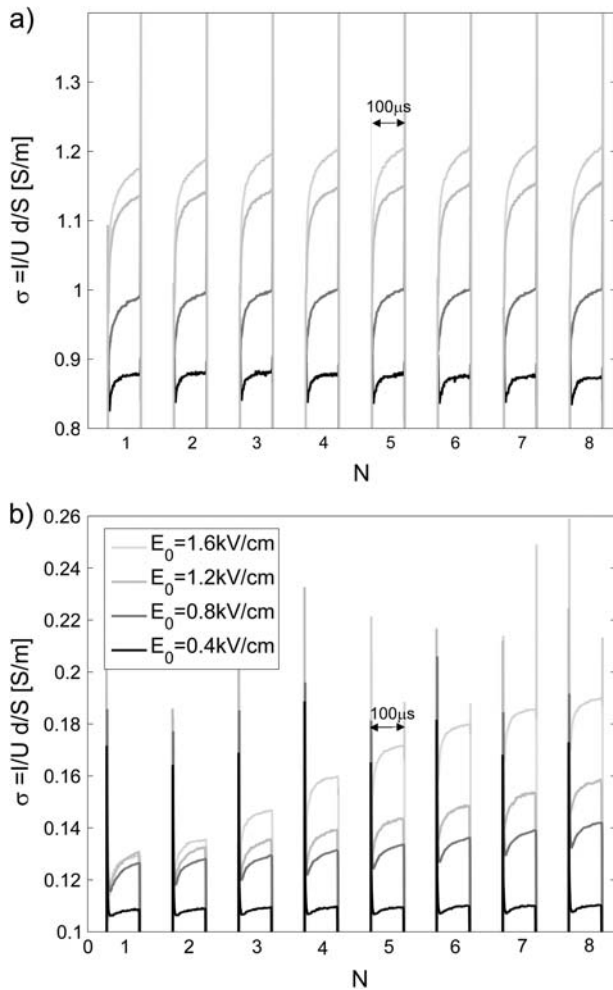


FIGURE 2 Measured time-dependent conductivity  $\sigma(t) = I(t)/U(t) d/S$  during a train of eight  $100\text{-}\mu\text{s}$  pulses, 1-Hz repetition frequency for (a) cells in high-conductive SMEM medium and (b) cells in low-conductive PB medium for different applied electric fields  $E_0 = U/d$ . The memory segmentation function of the oscilloscope was used to obtain high time resolution during the pulses, and only  $100\ \mu\text{s}$  after the pulse were recorded. Legend in panel b applies also to panel a.

PB medium (b) for  $E_0 = U/d = [0.4\text{--}1.8]$  kV/cm, electrode distance was 2 mm. In analysis all data are represented for the local electric field  $E$  obtained from the applied electric field  $E_0$  by taking into account the decrease of the electric field due to the neighboring cells.

For cells in both media, an increase in conductivity change during first pulse  $\Delta\sigma^1/\sigma_0$  is observed for  $E$  above 0.5 kV/cm, which reaches the maximum (12%) around 1 kV/cm in SMEM medium and at 1.4 kV/cm (25%) in PB medium. Very similar field dependence is obtained for all pulses in both media, where a dramatic increase in conductivity is observed above 0.5 kV/cm. The reference measurements in pure SMEM and PB media show constant  $\Delta\sigma^1/\sigma_0$  that can be attributed to electrode processes and Joule heating. Conductivity changes  $\Delta\sigma^N/\sigma_0$  during consecutive pulses in PB (see Fig. 8 b) and SMEM media are approximately constant at

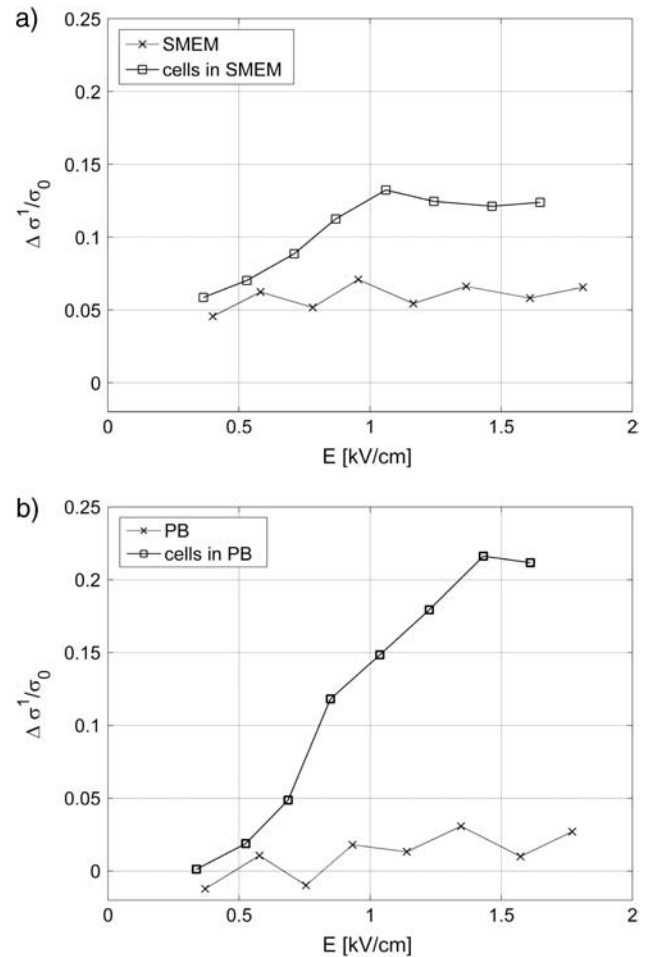


FIGURE 3 Conductivity change after the first pulse of the train of  $8 \times 100\text{-}\mu\text{s}$  pulses  $\Delta\sigma^1$  normalized to initial conductivity in (a) cells in SMEM medium and (b) cells in PB medium, cells in medium (solid line), reference measurement on medium without the cells (dotted line). The results are shown for local electric field  $E$ , where  $E/E_0 = 0.91$  ( $f = 0.3$ ).

1-Hz repetition frequency and even when a train of 24 pulses was applied, the increase in the conductivity during the pulses surprisingly remained constant.

In Fig. 4 percentage of permeabilized and survived cells in SMEM medium after application of  $8 \times 100\ \mu\text{s}$  pulses ( $E = 0.84$  kV/cm) is shown. Results in dense suspensions ( $f = 0.3$ ) are compared to previous measurements performed using the same experimental protocol but with lower cell density ( $f = 0.05$ ). We can see good agreement with the permeabilization curve for a lower density of cells. The permeabilization curve for PB medium is similar to the curve for SMEM medium because we have shown previously that permeabilization curves for SMEM and PB medium are similar (Pucihar et al., 2001). Similar agreement of measurements for high density with results for lower density of cells was obtained also for PB medium where at  $E = 0.84$  kV/cm 92% of permeabilization is achieved with survival being 100%.

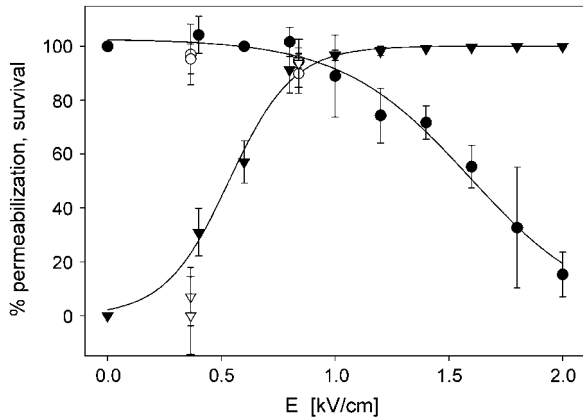


FIGURE 4 Permeabilization ( $\blacktriangledown$ ) and survival rate ( $\bullet$ ) of B16F1 cells in SMEM medium for electroporation experiments with  $8 \times 100\text{-}\mu\text{s}$  pulses, 1-Hz repetition frequency (lines show fitted sigmoid function). Experiments where high density of cells  $f = 0.3$  (open symbols) are compared with the permeabilization and survival curves obtained in experiments with lower cell density  $f = 0.05$  (solid symbols).

Comparing Figs. 3 and 4 it can be seen that transient conductivity changes  $\Delta\sigma^1/\sigma_0$  increase above 0.5 kV/cm agrees with permeabilization curve shown in Fig. 4. Percentage of permeabilized cells reaches maximum at 1 kV/cm similarly as conductivity changes in SMEM, whereas in PB medium maximum conductivity increase is obtained at 1.4 kV/cm.

In Fig. 5 relative changes of the initial level of conductivity  $(\sigma_0^N - \sigma_0)/\sigma_0$  in PB medium for consecutive pulses are shown. It can be seen that the initial level starts to increase again for  $E > 0.5$  kV/cm, which can be explained with the efflux of ions (mostly  $K^+$  ions) from the cytoplasm into the medium through membrane pores due to the concentration gradient, indicating that the cell membrane is permeabilized above 0.5 kV/cm. In high-conductive SMEM medium the

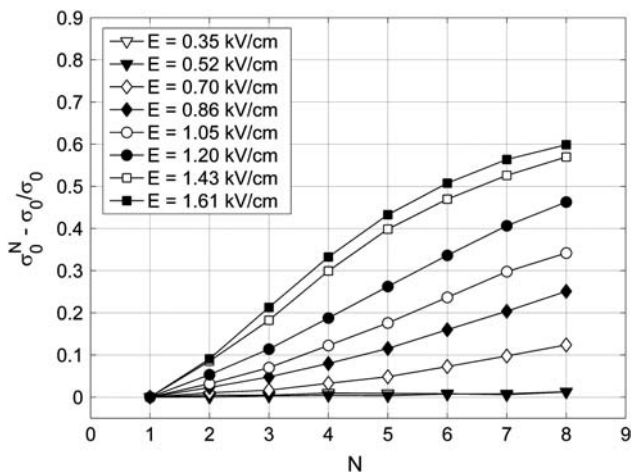


FIGURE 5 The relative change of the initial level of conductivity in PB medium for consecutive pulses:  $(\sigma_0^N - \sigma_0)/\sigma_0$ , where  $\sigma_0^N$  is the initial level at the start of the  $N^{\text{th}}$  pulse is shown.

increase of the initial conductivity  $(\sigma_0^N - \sigma_0)/\sigma_0$  is solely due to Joule heating as almost the same values are obtained for medium alone (results not shown). For higher electric fields the efflux of ions in PB increases up to 1.4 kV/cm where it reaches maximum, similarly as transient conductivity changes during a single pulse. Up to  $E = 1.0$  kV/cm the conductivity increases approximately linearly with time but starts to reach saturation level at higher electric field due to a decrease of the concentration gradient of the ions. This is expected because the total duration of the train of eight pulses at 1 Hz is 7 s and the time constant for diffusion of ions is few seconds. In Appendix B we theoretically analyzed the efflux of ions through the permeabilized membrane and obtained an exponential rise to a maximum. Deviation from this behavior is due to different simplifications of the model and statistical variation of cell sizes that are consequently permeabilized above different critical electric fields.

Another interesting parameter is the total conductivity change  $\Delta\sigma_{\text{tot}} = \sigma^8 - \sigma_0$ , which we define as the difference between the final conductivity at the end of the eight pulse and the initial conductivity. In Fig. 6 the total conductivity changes after the application of a train of eight 100- $\mu\text{s}$  pulses are presented for the same experiments as shown in Fig. 3. For the low-conductive medium a steady increase of the total conductivity change is observed above 0.5 kV/cm, corresponding to both ion efflux from the cell interior and the increased conductivity. The conductivity changes in low-conductive medium without cells are negligible.

In contrast, in high-conductive medium the difference between the total change in conductivity for cells in a suspension and the total conductivity change for pure medium is less pronounced. This can be attributed to substantial Joule heating during  $8 \times 100\text{-}\mu\text{s}$  pulses, which can be calculated theoretically when neglecting the heat dissipation:

$$\frac{\Delta\sigma_{\text{temp}}}{\sigma_0} = \alpha\Delta T, \quad \Delta T = N t_E E_0^2 \frac{\sigma}{\rho c_p}, \quad (3)$$

where  $T$  is temperature of the suspension,  $\alpha$  is constant of the conductivity temperature dependence,  $t_E$  is length of the pulse,  $\rho$  the density,  $c_p$  specific heat capacity of the suspension, and  $N$  number of pulses. The above equation gives for  $\alpha = 0.017/^\circ\text{C}$  (SMEM medium) a temperature increase of  $\sim 3^\circ\text{C}$  after eight pulses for  $E_0 = 1$  kV/cm. From this theoretical calculation of the conductivity change due to Joule heating for  $8 \times 100\text{-}\mu\text{s}$  pulses gives  $\Delta\sigma_{\text{temp}}^8/\sigma_0 \cong 0.048$  ( $\Delta\sigma_{\text{temp}}^1/\sigma_0 \cong 0.006$ ). But during a single 100- $\mu\text{s}$  pulse in pure medium a change of  $\Delta\sigma^1/\sigma_0 \cong 0.04$  is observed (see Fig. 3 a), which is evidently not only due to Joule heating but also due to some other effects (electrode processes, anomalous heating), which has been observed by other authors (Pliquett et al., 1996).

Another important process that significantly affects mainly the results obtained in high-conductive medium (because the total changes are smaller) is colloid-osmotic swelling of cells, which increases the effective volume fraction of the cells and

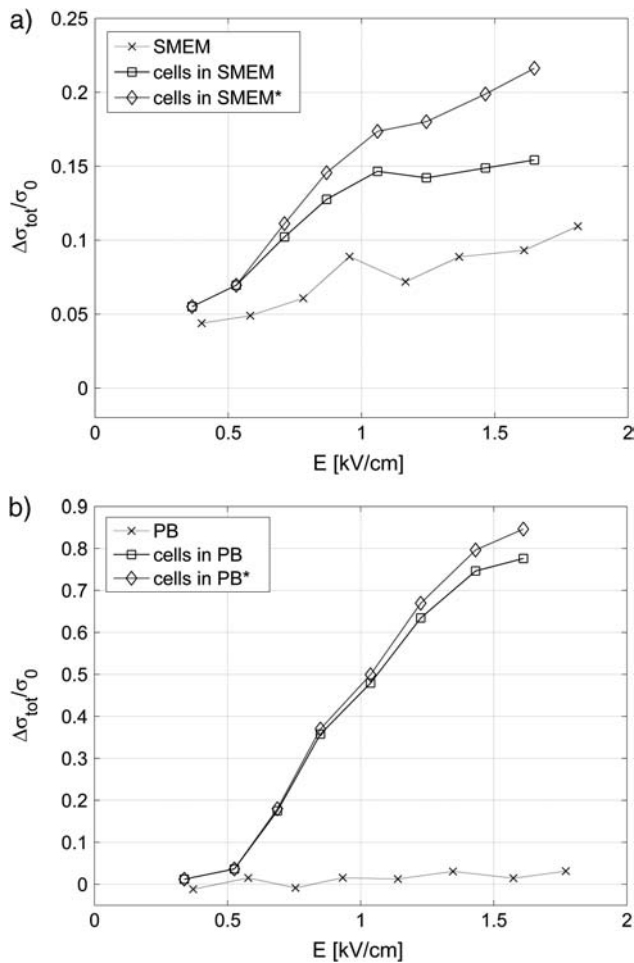


FIGURE 6 The total conductivity change  $\Delta\sigma_{\text{tot}} = \sigma^8 - \sigma_0$  after the application of  $8 \times 100\text{-}\mu\text{s}$  pulses (same experiment as in Fig. 3) in (a) cells in SMEM medium and (b) cells in PB medium, cells in medium (solid line), reference measurement (dotted line) on pure medium ( $\times$ ). Note the difference in scale between panels a and b. In Fig. 6 a measured total conductivity change ( $\square$ ) and total conductivity change corrected for the increased cell size due to the colloid-osmotic swelling ( $\diamond$ )  $\Delta\sigma'_{\text{tot}}/\sigma_0 = \Delta\sigma_{\text{tot}}/\sigma_0 - \Delta\sigma_{\text{swell}}/\sigma_0$  is shown.

consequently decreases the conductivity (see Fig. 7). In Fig. 6 a we compare the total conductivity changes (open squares) and total conductivity changes corrected for the increased cell size due to the colloid-osmotic swelling (\*)  $\Delta\sigma'_{\text{tot}}/\sigma_0 = \Delta\sigma_{\text{tot}}/\sigma_0 - \Delta\sigma_{\text{swell}}/\sigma_0$ . We can see that when the increase in cell size is taken into account the total change after the eight pulses shows a similar strong increase above the threshold field as in the low-conductive medium.

### Measurements of colloid-osmotic swelling

It was shown in several experiments that cells swell during electroporation and consequently a drop in the conductivity of the cell suspensions and pellets after the pulses was observed (Kinosita and Tsong, 1977b; Abidor et al., 1993,

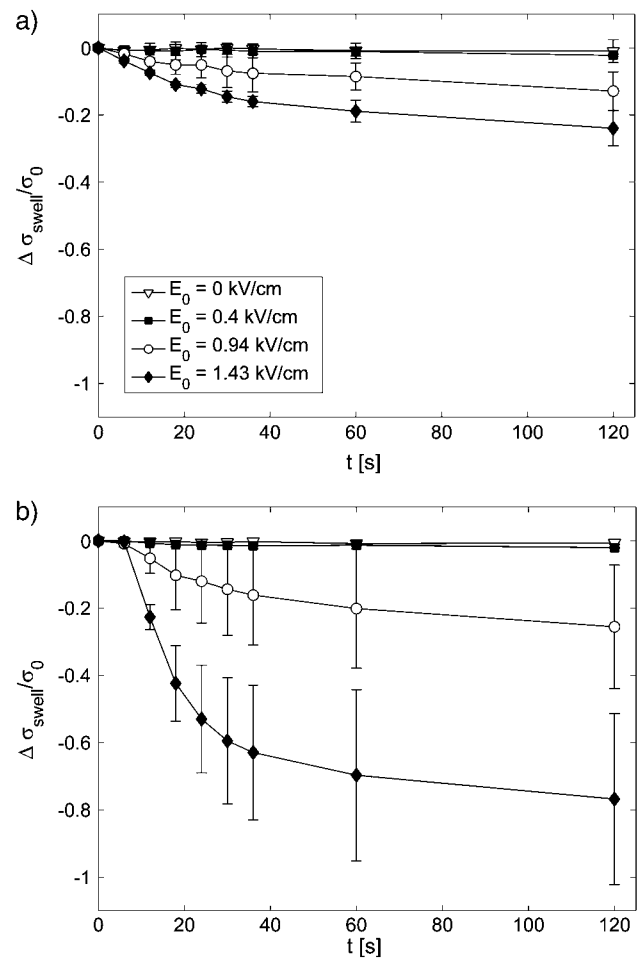


FIGURE 7 The effect of colloid-osmotic swelling on the bulk conductivity for different applied electric field strengths  $E_0$  and control ( $E_0 = 0$  kV/cm); time  $t = 0$  s, start of the first pulse;  $t = 7$  s, end of the pulsation. The changes of cells volume fractions due to the increased cell sizes were transformed into the conductivity change  $\Delta\sigma_{\text{swell}}/\sigma_0$  in (a) SMEM and (b) PB medium.

1994). Swelling of permeabilized cells is caused due to the difference in the permeabilities of ions and larger molecules (macromolecules) inside the cell, which results in an osmotic pressure that drives water into the cells and leads to cell swelling.

To determine the dynamics and the extent of cell swelling for our experimental conditions we made additional experiments where images of cells during and after pulse application were recorded. The results of the measurements of the cell sizes during and after the pulses are shown in Fig. 7 where the changes in the volume fraction were transformed into changes of conductivity  $\Delta\sigma_{\text{swell}}/\sigma_0(\Delta f)$  according to Eq. 2. The corrected curve in Fig. 6 a was obtained by extracting the  $\Delta\sigma_{\text{swell}}/\sigma_0$  due to cell swelling at  $t = 7$  s, which corresponds to the time point at the end of the eight pulse.

The time constant of colloid-osmotic swelling is a few tens of seconds; this is in agreement with the time constant for efflux of ions, which is between 10 and 20 s (see Fig. 5).

### Impedance measurements

From impedance measurements before and after application of pulses, the change of the real part of the impedance was calculated. From the impedance spectrum only the results at 100-kHz frequency were used due to the large scattering of data at lower frequencies. From the real part of the impedance we calculated bulk conductivity:  $\sigma = 1/\text{Re}(Z) d/S$ . For each sample we present values of the conductivity change  $\Delta\sigma/\sigma_0$  at the two time points:  $t_1 = 14$  s and  $t_2 = 28$  s after the first pulse.

Impedance measurements in all experiments showed reproducibly decrease in conductivity in SMEM medium above permeabilization threshold and increase in conductivity in PB medium. Results of the experiments with the  $8 \times 100\text{-}\mu\text{s}$  pulses for  $E = 0.35\text{--}1.6$  kV/cm are given in Table 1. We can observe steady increase in conductivity in PB medium for higher fields whereas in SMEM medium conductivity is decreased after the pulses. We can explain these values by considering all the effects that contribute to post-pulse conductivity: efflux of ions in PB medium, Joule heating in SMEM medium, and osmotic swelling:  $\Delta\sigma_{\text{imp}}/\sigma_0 = \Delta\sigma_{\text{efflux}}/\sigma_0 + \Delta\sigma_{\text{swell}}/\sigma_0 + \Delta\sigma_{\text{temp}}/\sigma_0$ . For example, in PB medium at 1 kV/cm is  $\Delta\sigma_{\text{imp}}/\sigma_0$  (14 s) = 0.47, which can be obtained from extrapolating the values of the initial conductivity changes from Fig. 5 at  $t = 7$  s ( $N = 8$ ) to  $t = 14$  s, which gives approximately  $\Delta\sigma_{\text{efflux}}/\sigma_0 + \Delta\sigma_{\text{swell}}/\sigma_0 \cong 0.5$ . Here the first term efflux of ions dominates because from Fig. 7 b we obtain  $\Delta\sigma_{\text{swell}}/\sigma_0$  (14 s)  $\cong -0.05$ . At higher fields osmotic swelling drastically decreases conductivity up to  $-0.4$ , however, the efflux of ions in PB is so large that after the pulse  $\Delta\sigma_{\text{imp}}/\sigma_0$  (14 s) increases up to  $+0.7$ , which is also the saturation level of the changes of the initial level. On the other hand in SMEM medium there is no net efflux of ions, therefore, mostly osmotic swelling contributes to reducing of bulk conductivity, which results in negative values of  $\Delta\sigma_{\text{imp}}/\sigma_0$ ; e.g., at 1 kV/cm we obtain  $\Delta\sigma_{\text{imp}}/\sigma_0$  (28 s) =  $-0.04$ , which can be explained by contributions of cell swelling  $\Delta\sigma_{\text{swell}}/\sigma_0 \cong -0.07$  (see Fig. 7 a) and Joule heating  $\Delta\sigma_{\text{temp}}/\sigma_0 \cong +0.035$  whereas efflux of ions in high-conductive SMEM medium is negligible.

### The effect of the repetition frequency on the measured increase in conductivity

Fig. 8 summarizes the effect of the repetition frequency on the conductivity changes in low-conductive PB medium. In Fig. 8 a the initial level of conductivity is shown for consecutive pulses and it can be seen that for frequencies above 10 Hz (100-ms pause between the pulses) very small changes of the initial level are obtained, which agrees with previous observation that the diffusion time constant is around a few seconds. In Fig. 8 b absolute changes of conductivity  $\Delta\sigma(t)$  during the first, third, and the fifth pulse are compared for different frequencies.

We can observe that for 1 Hz the consecutive pulses are almost identical and that relaxation of the conductivity is complete in one second, however, for higher frequencies each consecutive pulse is smaller than the previous pulse and the time course of the second part of the pulse is different. This indicates that relaxation in milliseconds after the pulse is not complete and that the conductivity does not relax to its initial level but constantly increases. In SMEM medium (results not shown) we also obtained complete relaxation at 1 Hz and difference in pulse shapes for consecutive pulses at 1 kHz. The initial level of conductivity increased between the pulses almost twice as in pure medium at 1 kHz, whereas at 1 Hz no difference between pure medium and cells was observed, which similarly as in PB medium shows that time constant of conductivity relaxation is in the millisecond range.

In Fig. 9 changes of conductivity after the first pulse  $\Delta\sigma^1$  for two volume fractions are shown at  $E = 0.84$  kV/cm, electrode distance was 4 mm. The measured values for cells in SMEM medium are corrected for the changes in the medium alone. The lines represent results of the theoretical model described in the Materials and Methods section. Membrane conductivity was fitted to the measured data in high- and low-conductive medium to obtain the equivalent conductivity  $\sigma_p = 0.0495$  and  $0.0209$  S/m, respectively. Then the dependence of the relative changes on the electric field were obtained from finite elements models of permeabilized cells for different critical angles and by this a scaling factor was determined between equivalent conductivity  $\sigma_p$  when  $\theta_c = 54^\circ$  (at 0.84 kV/cm) and  $\sigma'_p$  when  $\theta_c = 90^\circ$ . From the equivalent conductivity  $\sigma'_p$  [0.053 S/m, 0.0226 S/m] of a single cell  $\sigma_m$  for  $\theta_c = 90^\circ$  can be obtained from the Pauly-Schwan equation:

**TABLE 1** The changes of the real part of the impedance 14 and 28 s after the first pulse transformed into the conductivity change  $\Delta\sigma_{\text{imp}}/\sigma_0$  for cells in SMEM and PB medium

$\Delta\sigma_{\text{imp}}/\sigma_0$	$E = 0.35$ kV/cm	$E = 0.52$ kV/cm	$E = 0.7$ kV/cm	$E = 0.86$ kV/cm	$E = 1.05$ kV/cm	$E = 1.2$ kV/cm	$E = 1.43$ kV/cm	$E = 1.61$ kV/cm
SMEM $t_1 = 14$ s	-0.002	-0.025	-0.010	-0.0136	-0.026	-0.030	-0.023	-0.032
SMEM $t_2 = 28$ s	0.000	-0.061	-0.017	-0.022	-0.040	-0.043	-0.033	-0.042
PB $t_1 = 14$ s	0.010	0.027	0.24	0.40	0.47	0.58	0.66	0.70
PB $t_2 = 28$ s	0.015	0.041	0.33	0.48	0.54	0.63	0.70	0.73

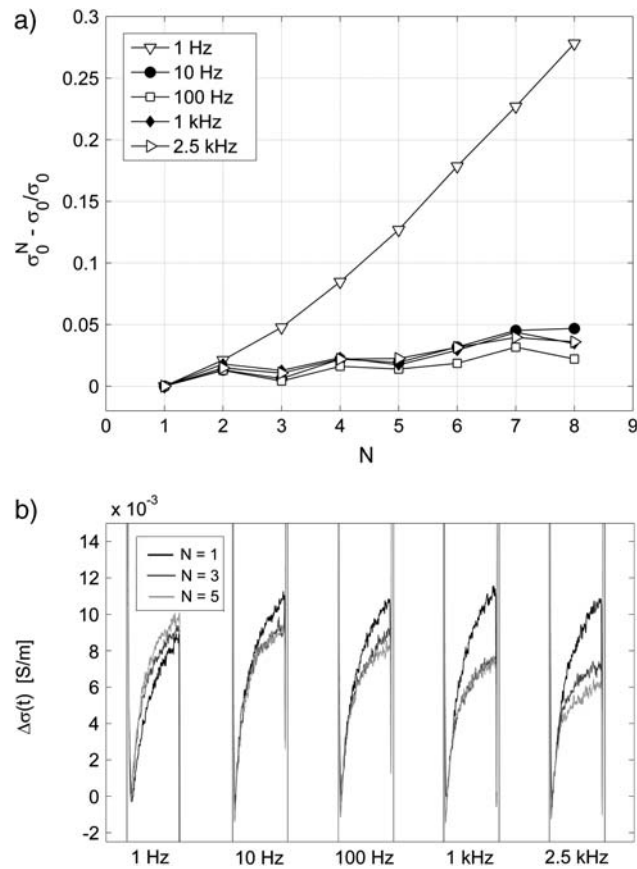


FIGURE 8 Effect of the repetition frequency on the conductivity changes in PB medium. Pulses  $8 \times 100 \mu\text{s}$  with repetition frequencies from 1 Hz to 2.5 kHz were used,  $E = 0.84 \text{ kV/cm}$ . (a) Relative change of the initial level of the conductivity  $\sigma_0^N$  is shown. (b) The time-dependent conductivity changes  $\Delta\sigma(t)$  of the first, third, and fifth pulse with respect to the first pulse (all initial levels are set to zero) are compared for different frequencies.

$$\sigma'_p = \sigma_m \frac{2(1 - \nu)\sigma_m + (1 + 2\nu)\sigma_i}{(2 + \nu)\sigma_m + (1 - \nu)\sigma_i} \quad \nu = (1 - d/R)^3, \quad (4)$$

where  $R$  is the cell radius and  $d$  the thickness of the membrane. In this way we obtained average membrane conductivity of the permeabilized part to be  $\sigma_m = 3.5 \times 10^{-5} \text{ S/m}$  (SMEM) and  $\sigma_m = 1.4 \times 10^{-5} \text{ S/m}$  (PB).

Under the assumption that the number and size of the pores remain constant for different electric field strengths, the average membrane conductivity of the permeabilized area  $\sigma_m$  does not depend on  $E$ . Therefore,  $E$  governs only the area of the permeabilized surface given by (Schwister and Deuticke, 1985)

$$S_c = S_0(1 - E_c/E), \quad (5)$$

and by this the dependency of the cell equivalent conductivity on  $E$ .

In Fig. 10 the theoretical curve of the dependency of the conductivity increase due to the increased surface of per-

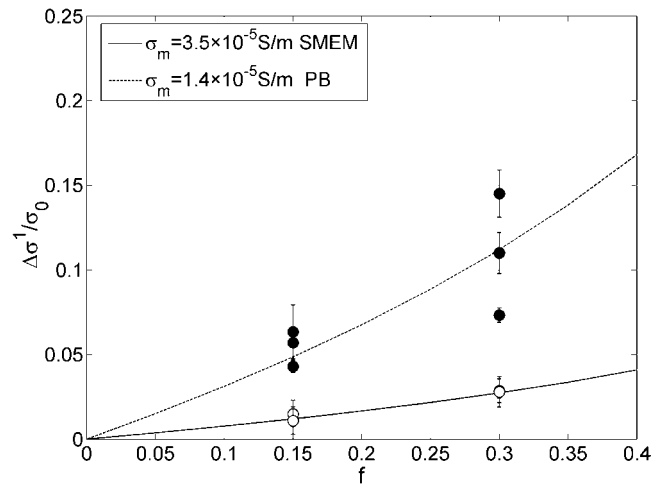


FIGURE 9 Absolute change in conductivity during the first pulse  $\Delta\sigma^1$  is shown. Each error bar represents three sample data pooled together, obtained for a train of eight  $100\text{-}\mu\text{s}$  pulses of  $0.84 \text{ kV/cm}$  in SMEM medium ( $\circ$ ) and PB medium ( $\bullet$ ). The conductivity changes in pure SMEM medium were subtracted from the measured value obtained for cells in SMEM. The lines represent values of the theoretical model (see the Materials and Methods section) where membrane conductivity was fitted to obtain the best agreement with measured data.

meabilized area for different  $E$  is shown where the critical angle  $\theta_c$  is defined by the applied electric field and the critical voltage  $U_c$ . We numerically calculated the equivalent conductivity of a single cell  $\sigma_p(\theta_c)$  and the bulk conductivity of a suspension of permeabilized cells for different critical angles as described in our previous work (Pavlin and Miklavčič, 2003) and in Materials and Methods. From this field-dependent conductivity changes  $\Delta\sigma/\sigma_0(E)$  were calculated for constant membrane conductivity or taking into account the nonohmic behavior of the conductivity inside the pore using Eq. A.7, as shown in Fig. 10. Values of membrane conductivity were obtained from fitted values of our experimental data shown in Fig. 9. Critical electric field strength in both media was set to  $0.5 \text{ kV/cm}$  according to our experimental results (see Figs. 3 and 4).

## DISCUSSION

The aim of our study was to analyze the effect of high-voltage pulses on the electrical properties of cells in a suspension and to analyze how these changes correspond to the level of membrane permeabilization. We performed current and voltage measurements during the train of eight high-voltage pulses and impedance measurements before and after the application of pulses in a dense suspension of cells. At the same time we determined the percentage of permeabilized cells and cell survival. In additional experiments the extent of colloid-osmotic swelling was also determined.

We observed a transient increase in conductivity during electric pulses for electric fields above  $0.5 \text{ kV/cm}$  ( $U_m = 450$

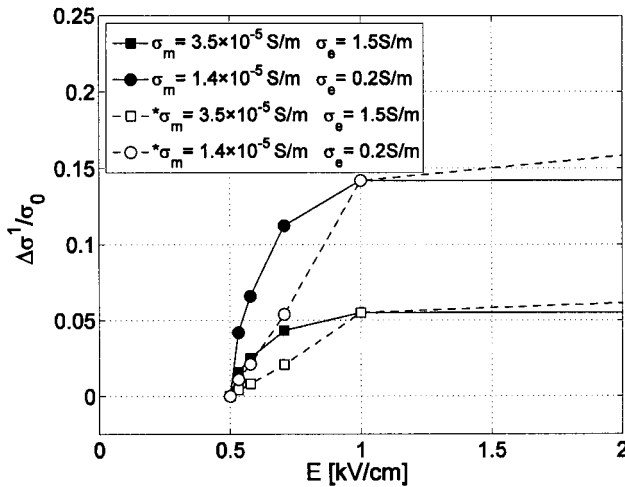


FIGURE 10 The theoretical curve of the dependency of the conductivity increase on the electric field due to the increased permeabilized surface area according to the theoretical model (see Appendix). Field-dependent conductivity change calculated theoretically for high conductive medium (squares) and low conductive medium (circles),  $f = 0.3$ , under an assumption of constant membrane conductivity of the permeabilized area (solid line) or \*taking into account the nonohmic behavior of the conductivity inside the pore using Eq. A.7 (dashed line) is shown. Values for membrane conductivity  $\sigma_m$  were chosen as obtained from experiments shown in Fig. 9 at  $E = 0.84$  kV/cm, threshold electric field in both cases was set to 0.5 kV/cm according to our experimental results.

mV) both in low- and high-conductive medium after which the pulse conductivity relaxed almost to the initial level. Our results are in agreement with the results of other groups obtained on single cells (Chernomordik et al., 1987; Ryttsen et al., 2000), cell suspensions (Kinosita and Tsong, 1977a,b; 1979), and cell pellets (Abidor et al., 1993; 1994) where also a transient increase in conductivity above a threshold electric field was observed. The threshold electric field at which the increased conductivity is observed in our experiments corresponds to the permeabilization threshold for the uptake of molecules for both media for several pulses. We obtained similar results for dense and dilute suspensions for permeabilization and survival, in agreement with Canatella et al. (2001) where it has been shown that the cell density itself does influence permeabilization only by affecting the local electric field. For tissue electroporation in general, however, there are several effects that contribute to non-homogeneous molecules uptake due to differences in cell state, solute concentration, and local electric field (Canatella et al., 2004).

The saturation of the conductivity in high-conductive medium, which is reached at the same electric field (around 1 kV/cm) as the permeabilization level (see Figs. 3 and 4) for eight pulses, agrees with the theoretical model where the field strength determines the permeabilized area and the membrane conductivity is assumed to be constant or having conductivity of the pore dependent on the electric field (see

Appendix A) as shown in Fig. 10. In low-conductive medium maximum increase in conductivity is reached at higher electric field as permeabilization (and as described by the theoretical model) indicating that conductivity of permeabilized area is also increased due to increase in number or size of the pores, as has been suggested in some theoretical descriptions of pore evolution during the electric pulses (Chernomordik et al., 1987; Glaser et al., 1988). The changes of the initial level of conductivity obtained in the low-conductive medium (see Fig. 5) clearly show an increase of the overall level of the conductivity above 0.5 kV/cm, as well as saturation of conductivity increase at 1.4 kV/cm indicating that permeable structures in the membrane are present, which enable ions to leak from the cytoplasm into the external medium.

When analyzing the total increase in conductivity after the eight pulses (see Fig. 6) and the impedance several seconds after the pulses, we obtained that the change in conductivity consists of several contributions: i), a transient increase in conductivity during each pulse, which is observed above the threshold electric field and drops back to the initial level in less than a second; ii), a decrease in conductivity caused by colloid-osmotic swelling due to osmotic imbalance when the cell membrane is permeabilized, which is again observed only above the threshold field; swelling decreases the relative conductivity for a few percent in seconds after the application of pulses and up to 80% on the order of minutes; iii), increase in conductivity due to Joule heating by a few percent in high-conductive medium; and iv), efflux of ions from the cell interior, which is observed in low-conductive medium above the threshold electric field. All these contributions have to be taken into account when measuring the conductivity in cell suspensions as well as in tissue, where except for the efflux of ions, both the Joule heating and swelling of cells could affect the results considerably. Altogether our experiments on cell suspensions indicate that only measurements during the pulses or very shortly after the pulses relate to permeabilization, whereas impedance measurements several seconds later detect predominantly other effects. Because of higher density of cells in tissue and consequently lesser cell swelling due to cell-cell contacts (Abidor et al., 1993; 1994) the impedance measurements in tissue could give more information compared to measurements in cell suspensions.

Fitting the measured values of the conductivity changes to our theoretical model gives us an approximate membrane conductivity at the end of the 100- $\mu$ s pulse  $\sigma_m = [1.4-3.5] \times 10^{-5}$  S/m, which is smaller than the membrane conductivity determined on sea urchin eggs  $\sigma_m = [1-4] \times 10^{-4}$  S/m (Hibino et al., 1991) or a magnitude lower than the values obtained on erythrocytes by Kinosita and Tsong (1977a, 1979) ( $\sigma_m = 5 \times 10^{-4} - 5 \times 10^{-3}$  S/m). This discrepancy can be explained by different experimental procedures and differences between the cell types. Comparison of theoretical curves in Fig. 10 and permeabilization

dependence on the electric field suggest that electric field affects mostly the surface of the permeabilized area and consequently increased conductivity as well as fraction of permeabilized cells. Of course, the surface area of the permeabilized part of the cell membrane depend on the number as well as on the size of the pores, which both are time dependent. But in this article we limited our analysis only on the change of the conductivity and surface area of pores at the end of one pulse. A complementary theoretical analysis of the conductivity changes caused by membrane electroporation on CHO cell pellets was published recently (Schmeer et al., 2004). Authors analyze also the dynamic behavior and the size of the pores and obtain similarly that the conductivity changes during the pulses are transient whereas the conductivity increase between the pulses in a low conductive medium is due to the ion efflux.

In Appendix A, we estimate the fraction of surface area of the pores  $f_p = S_{\text{por}}/S_0$  from obtained membrane conductivity that gives us  $f_p \approx 10^{-5}$ – $10^{-4}$ . This is substantially less than the values obtained on sea urchin eggs (Hibino et al., 1991)  $f_p \approx 10^{-4}$ – $10^{-3}$  and CHO cells  $f_p \approx 10^{-4}$  (Neumann et al., 1998) or values that were obtained by electrooptical measurements on vesicles  $f_p \approx 10^{-4}$  (Tönsing et al., 1997). We further estimated fraction of pores from ion efflux between the pulses in low-conductive medium (see Appendix B) and obtained  $f_p \approx 10^{-7}$ – $10^{-6}$  that is approximately two orders of magnitude lower than the fraction of pores calculated from the membrane conductivity during the pulses.

Our results are in agreement with fast relaxation of the conductivity and with results of other authors (Kinosita and Tsong, 1977a, 1979; Hibino et al., 1991, 1993) where the conductivity of the membrane dropped for an order of magnitude in the millisecond range. The results support the hypothesis of the existence of two types of pores: short-lived pores, which are created during the pulse and transiently increase conductivity, and long-lived pores that contribute to increased permeability for ions and molecules in minutes after the pulses.

The results obtained in both low-conductive and high-conductive medium show that the conductivity changes during each pulse do not “remember” previous pulses for 1-Hz repetition frequency, similarly as observed by other authors on planar bilayer membranes (Chernomordik et al., 1987; Macek-Lebar et al., 2002a) and cells (Chernomordik et al., 1987; Kinosita and Tsong, 1979), where for a 1-s pause between the pulses the second pulse started from the same level as the first one. When repetition frequency is increased above 1 kHz, relaxation is not complete and the initial level of conductivity for consecutive pulses increases. This is in agreement with the results of other authors where at 1-kHz repetition frequency the second pulse started from much higher level (Chernomordik et al., 1987; Kinosita and Tsong, 1979), except for slightly faster relaxation in our experiments. It is also interesting to note that even after application of three series of 24 pulses of 1 Hz in low-

conducting medium the dynamic behavior and conductivity change during each pulse remained the same.

One possible explanation for fast relaxation of conductivity is that the number and diameter of short-lived conductive pores is decreased to a level where their contribution to the conductivity is negligible, whereas some of them are still present and can later participate in formation of the long-lived transport pores that have long resealing time and are large enough to facilitate transport of molecules. Only a few long-lived pores could suffice for a substantial uptake of molecules, however, their contribution to the increase in conductivity would be negligible; e.g., from our data for the efflux of ions the membrane conductivity  $10^{-6}$  S/m gives an increase in conductivity on the order of 0.1%, which is not measurable, but the corresponding fraction of pores gives approximately  $N = 100$  pores having a radius of 1 nm (from the literature approximately the size of a hydrophilic metastable pore) and large enough for the transport of molecules of a few kilodaltons such as bleomycin (1.5 kDa).

This is in accordance with the theoretical predictions of the electroporation theory that the size distribution of the pores is changed after the pulse (Weaver and Chizmadzhev, 1996) due to the resealing of smaller pores while a small number of larger long-lived pores remain in the membrane. Long-lived permeable state of the cell membrane is not yet fully explained even though several hypotheses exist such as existence of metastable hydrophilic pores (Weaver and Chizmadzhev, 1996; Neumann et al., 1989; Smith et al., 2004; Leontiadou et al., 2004), coalescence of pores (Sugar and Neumann, 1984), or presence of small defects in the lipid bilayer (Teissie and Ramos, 1998). Also specific cell structures could be important for the creation of long-lived permeable structures and could lead to difference in resealing dynamics between lipid bilayers and cells like involvement of cytoskeletal network (Rols and Teissie, 1992; Teissie and Rols, 1994), membrane proteins (Weaver and Chizmadzhev, 1996), or anisotropic inclusions in the membrane (Fošnarič et al., 2003; Kandušer et al., 2003).

Another possible explanation of the fast relaxation of conductivity could be, that only a smaller part of the increased conductivity can be attributed to the conductive pores and that the larger part is a result of some related process (e.g., release of bound charges in the vicinity of a pore due to the very strong local electric field) with relaxation around 1 ms. This process remains, however, to be identified and explained.

When analyzing if transient conductivity changes reflect the level of permeabilization we identified the major discrepancy between permeabilization and conductivity changes when a train of pulses was analyzed, which has not been studied in previous reports. Our results indicate that the increase in conductivity is observed above the threshold electric field for permeabilization. This on one hand suggests that permeabilization could be detected with measurements of conductivity. On the other hand, almost identical transient

conductivity changes for consecutive pulses are observed, indicating that the conductivity increase is not necessarily related to the formation of the long-lived “transport” pores. The results further show that conductivity changes and the conductivity threshold do not depend on number of pulses, in contrast to cell permeabilization (detected usually as a transport of certain molecules), which depends on the duration and the number of pulses (Rols and Teissie, 1990; Kotnik et al., 2000; Canatella et al., 2001; Macek-Lebar et al., 2002b). This can be partially explained by the fact that electric current depends on different ion properties (mobility, concentration, and charge) and is governed by the electric field, whereas for small and especially noncharged molecules transport is governed mostly by diffusion (Puc et al., 2003). Hence, increased conductivity and permeabilization are not necessarily directly linked. It was also shown (Rols and Teissie, 1990) that when the number of pulses (or pulse duration) is increased, the threshold level reaches a certain limit threshold that cannot be decreased any further. So it is possible that with conductivity measurements we actually detect this limit threshold, which then explains why the conductivity threshold is equal for one or several pulses.

To summarize, conductivity measurements during the pulses give information about increased membrane permeability whereas impedance measurements several seconds after pulse application are not suitable due to fast relaxation of conductivity changes, colloid-osmotic swelling, and ions leakage. By measuring electric conductivity we can detect limit permeabilization threshold above which the electro-poration process (uptake) occurs. However, conductivity changes are similar for a single or several pulses in contrast to considerable increase in permeabilization for several pulses, thus the transient conductivity changes, i.e., short-lived pores are related to permeabilization (long-lived pores) only indirectly and the relationship between the transient pores and long-lived permeable structures in the membrane remains to be explained. So, our results suggest that conductivity measurements can be used to optimize the voltage but not to control cell permeabilization in vitro in general, e.g., varying all pulse parameters. For application of conductivity measurements for online monitoring of cell electroporation relationship between permeabilization for a single and several pulses should be known, which is feasible because usually a certain protocol is chosen with constant number of pulses, and only the electric field is varied to achieve optimum efficiency. In such case the use of conductivity measurements for online control of the electroporation could be readily applied.

## APPENDIX A: CALCULATION OF THE FRACTION OF SURFACE AREA OF PORES

Here we present the estimation of the fraction of the surface area of pores in the cell membrane from the increased membrane conductivity (similar derivation was first presented by Hibino). We assume that the specific conductance of the permeabilized area of a cell is approximately the sum of the conductance of  $N_p$  pores having radius  $r_p$ :

$$G_p = N_p \pi r_p^2 \frac{\sigma_{\text{por}}}{d} = S_{\text{por}} \frac{\sigma_{\text{por}}}{d}, \quad (\text{A.1})$$

where we neglect the very small conductance of nonpermeabilized cell membrane,  $S_{\text{por}}$  represents the surface of all conducting pores. On the other hand this conductance is equal to the average membrane conductance of the permeabilized area as obtained from our measurement and from the theoretical model:

$$G_p = \bar{G}, \quad (\text{A.2})$$

thus

$$S_{\text{por}} \frac{\sigma_{\text{por}}}{d} = S_c \frac{\sigma_m}{d}, \quad (\text{A.3})$$

where  $S_c$  represents the total permeabilized surface of one cell (the area exposed to above-threshold transmembrane voltage), which is described by Eq. 5 and  $\sigma_m$  the average membrane conductivity of permeabilized area as defined in the theoretical model.

Conductance of the pore in a 1:1 electrolyte is given by (Glaser et al., 1988)

$$G_{\text{por}} = G_0 \frac{\exp(\beta U_m) - 1}{\int_0^d \exp[\beta U_m \frac{d-x}{d} + w(x)] dx} = G_0 \rho, \quad (\text{A.4})$$

$$G_0 = N_p \pi r_p^2 \frac{\sigma_{0\text{por}}}{d},$$

where  $\beta = e / kT$  and  $w(x) = W(x) / kT$  where  $e$  is the electron charge,  $U_m$  is the transmembrane voltage, and  $W(x)$  the energy of an ion inside the pore due to the interactions of the ion with the pore walls (Parsegian, 1969; Glaser et al., 1988). Parameter  $\rho$  is a scaling factor, which reduces the conductivity of the ions inside the pores ( $\sigma_{\text{por}}$ ), compared to the bulk approximation  $\sigma_{0\text{por}} \approx (\sigma_e + \sigma_i)/2$  in the limit of very large pores when interactions are negligible. For a trapezoid shape of  $w(x)$  we obtain from Eq. A.4 that when the transmembrane voltage is small  $n\beta U_m \ll w_0$

$$\rho = \exp[-0.43(w_0 - n\beta U_m)], \quad (\text{A.5})$$

and when the transmembrane voltage is large, e.g., for  $\beta U_m \gg w_0$  ( $U_m \gg 25\text{mV}$ ) we get

$$\rho = \frac{1}{\left(1 + \frac{n\beta U_m}{w_0 - n\beta U_m}\right) \exp(w_0 - n\beta U_m) - \frac{n\beta U_m}{w_0 - n\beta U_m}}, \quad (\text{A.6})$$

where  $n$  is the relative size of the entrance region of the pore, and was estimated to be  $\sim 0.15$  (Glaser et al., 1988).  $W_0$  is the energy of an ion inside

**TABLE 2** Values of used parameters

$n$	$e/kT$	$\sigma_i$	$U_m$	$R$	$d$
0.15	40 V <sup>-1</sup>	0.5 S/m	900 mV	9.5 μm	5 nm
$E$	$E_c$	$w_0$	$\rho$	$\sigma_m$	$D$
0.84 kV/cm	0.5 kV/cm	2.5–5	0.22–0.57	1.4–3.5 × 10 <sup>-5</sup> S/m	2.5 × 10 <sup>-5</sup> cm <sup>2</sup> /s

center of a pore and was estimated to be a few  $kT$  (Glaser et al., 1988). Thus, the fraction of pores  $f_p$  of the total membrane surface is approximately:

$$f_p = \frac{S_{\text{por}}}{S_0} = \frac{(1 - E_c/E)S_{\text{por}}}{S_c} \approx \frac{(1 - E_c/E)\sigma_m}{\sigma_{\text{por}}} \approx \frac{(1 - E_c/E)\sigma_m}{\rho\sigma_{0\text{por}}}, \quad (\text{A.7})$$

where  $\rho$  is obtained from Eq. A.4. To estimate fraction of pores in our case for the membrane conductivity  $\sigma_m = [1.4-3.5] \times 10^{-5}$  at  $E = 0.84$  kV/cm we can use approximation Eq. A.6 because  $U_m \gg 450$  mV. Inserting values of parameters (see Table 2) into Eq. A.7 ( $1 - E_c/E = 0.404$  and Eq. A.6  $w_0 = 2.5-5$  we obtain for fraction of pores after 100- $\mu$ s pulse being  $f_p = 10^{-5}-10^{-4}$ .

## APPENDIX B: EFFLUX OF IONS

From the efflux of ions in the low conductivity medium (see Fig. 5) the fraction of the surface area of pores can be estimated. Here we assume that all conductivity increase on the order of seconds can be attributed to the efflux of ions (also some other process could be involved). Because by far the largest concentration difference between internal and external concentration is for  $K^+$  ions ( $c_e \approx 0$  mM,  $c_i = 142$  mM) only this ion will be considered in the following analysis and their contribution to the external conductivity.

The diffusion of ions through the membrane is governed by Nernst-Planck equation

$$\frac{dn_e(x, t)}{dt} = -D S \frac{dc(x, t)}{dx} - \frac{zF}{RT} D S c(x, t) \frac{d\Psi(x, t)}{dx}, \quad (\text{A.8})$$

where  $n_e$  is the number of mol in the external medium,  $D$  is the diffusion constant ( $2 \times 10^{-5}$  cm<sup>2</sup>/s),  $c$  the molar concentration,  $S$  the total transport surface  $S = N S_{\text{por}}$  of  $N$  permeabilized cells, and  $\Psi$  the electric potential. In general  $D$  and  $S$  depend on time, electric field strength, and number of pulses, but here we will assume that they are approximately constant. The diffusion of ions is a slow process compared to the duration of the electric pulses, thus we can assume that the major contribution to efflux of ions occurs without the presence of the electric field. When there is no external electric field present,  $\Delta\Psi$  is small (around 20 mV) because only the imbalance of the electric charges due to concentration gradient contributes (i.e., the reversal potential); therefore, the second term in Eq. A.8 can be neglected. By replacing the concentration gradient with  $(c_e - c_i)/d$  we obtain:

$$\frac{dc_e(t)}{dt} = -\frac{DS}{dV_e} [c_e(t) - c_i(t)], \quad (\text{A.9})$$

where  $V_e$  represent the external volume. In the above equation, we neglect spatial changes of the concentration and assume that they are approximately constant. We further neglect the volume fraction changes during the pulses and by taking into account that the sum of ions inside and outside remains constant, the equation further simplifies:

$$\frac{dc_e(t)}{dt} = -\frac{DS}{dVf(1-f)} (c_e(t) - fc_i^0), \quad (\text{A.10})$$

where  $c_i^0$  is the initial internal concentration of  $K^+$  ions. Solution of the above equation is an exponential increase to maximum  $c_e^k = fc_i^0$

$$c_e(t) = c_e^k \left[ 1 - \exp\left(-\frac{t}{\tau}\right) \right], \quad (\text{A.11})$$

with a time constant

$$\tau = \frac{S_p}{S_0} \frac{3D}{dRf(1-f)}. \quad (\text{A.12})$$

From the time constant  $\tau$  the fraction of pores can be estimated:

$$f_p \approx \frac{1}{\tau} \frac{dRf(1-f)}{3D'}, \quad D' = D \exp(-0.43 w_0), \quad (\text{A.13})$$

where we again take into account that the effective diffusion constant  $D'$  of  $K^+$  ions inside the pore differs from that in bulk. From Fig. 5 we obtain that for  $E = 0.84$  kV/cm the time constant for conductivity changes is  $\approx 22$  s. Using Eq. A.12 for  $w_0 = 2.5-5$  we obtain for diffusion time constants being between 8 s ( $E = 1.6$  kV/cm) and 42 s ( $E = 0.7$  kV/cm) fraction of the pores in PB medium  $f_p = 10^{-7}-10^{-6}$ .

The authors thank D. Kovačić (Faculty of Electrical Engineering and Computer Science, University of Zagreb), M. Puc, and K. Flisar (both Faculty of Electrical Engineering, University of Ljubljana) who developed the measuring system that enabled us this research and Prof. J. Trontelj (Faculty of Electrical Engineering, University of Ljubljana) who kindly borrowed the LCR meter. M. Pavlin also thanks B. Valič (Faculty of Electrical Engineering, University of Ljubljana) for his help and V. B. Bregar for his valuable suggestions and comments.

This research was supported by the Ministry of Education, Science and Sports of the Republic of Slovenia under the grants Z2-6503 and SLO-CRO grant Monitoring of the Efficiency of Electrochemotherapy by Means of Bioimpedance Measurements, and the European Commission under the grant Cliniporator QLK3-99-00484 within the fifth framework.

## REFERENCES

- Abidor, I. G., A. I. Barbul, D. V. Zhelev, P. Doinov, I. N. Bandarina, E. M. Osipova, and S. I. Sukharev. 1993. Electrical properties of cell pellets and cell fusion in a centrifuge. *Biochim. Biophys. Acta.* 1152:207–218.
- Abidor, I. G., L.-H. Li, and S. W. Hui. 1994. Studies of cell pellets. II. Osmotic properties, electroporation, and related phenomena: membrane interactions. *Biophys. J.* 67:427–435.
- Canatella, P. J., M. M. Black, D. M. Bonnichsen, C. McKenna, and M. R. Prausnitz. 2004. Tissue electroporation: quantification and analysis of heterogeneous transport in multicellular environments. *Biophys. J.* 86: 3260–3268.
- Canatella, P. J., J. F. Karr, J. A. Petros, and M. R. Prausnitz. 2001. Quantitative study of electroporation-mediated molecular uptake and cell viability. *Biophys. J.* 80:755–764.
- Chernomordik, L. V., S. I. Sukarev, S. V. Popov, V. F. Pastushenko, A. V. Sokirko, I. G. Abidor, and Y. A. Chizmadzev. 1987. The electrical breakdown of cell and lipid membranes: the similarity of phenomenologies. *Biochim. Biophys. Acta.* 902:360–373.
- Davalos, R. V., Y. Huang, and B. Rubinsky. 2000. Electroporation: bio-electrochemical mass transfer at the nano scale. *Microscale Thermophys. Eng.* 4:147–159.
- Davalos, R. V., B. Rubinsky, and D. M. Otten. 2002. A feasibility study for electrical impedance tomography as a means to monitor tissue electroporation for molecular medicine. *IEEE Trans. Biomed. Eng.* 49:400–403.
- Ferber, D. 2001. Gene therapy: safer and virus-free? *Science.* 294:1638–1642.
- Fošnarič, M., V. Kralj-Iglič, K. Bohinc, A. Iglič, and S. May. 2003. Stabilization of pores in lipid bilayers by anisotropic inclusions. *J. Phys. Chem. B.* 107:12519–12526.
- Garner, A. L., N. Y. Chen, J. Yang, J. Kolb, R. J. Swanson, K. C. Loftin, S. J. Beebe, R. P. Joshi, and K. H. Schoenbach. 2004. Time domain dielectric spectroscopy measurements of HL-60 cell suspensions after microsecond and nanosecond electrical pulses. *IEEE Trans. Plasma. Sci.* 32:2073–2084.
- Glaser, R. W., S. L. Leikin, L. V. Chernomordik, V. F. Pastushenko, and A. V. Sokirko. 1988. Reversible electrical breakdown of lipid bilayers: formation and evolution of pores. *Biochim. Biophys. Acta.* 940:275–287.

- Hibino, M., H. Itoh, and K. Jr. Kinoshita. 1993. Time courses of cell electroporation as revealed by submicrosecond imaging of transmembrane potential. *Biophys. J.* 64:1789–1800.
- Hibino, M., M. Shigemori, H. Itoh, K. Nagayama, and K. Jr. Kinoshita. 1991. Membrane conductance of an electroporated cell analyzed by submicrosecond imaging of transmembrane potential. *Biophys. J.* 59:209–220.
- Jaroszkeski, M. J., R. Gilbert, and R. Heller. 1997. Electrochemotherapy: an emerging drug delivery method for the treatment of cancer. *Adv. Drug Deliv. Rev.* 26:185–197.
- Jaroszkeski, M. J., R. Heller, and R. Gilbert. 1999. Electrochemotherapy, Electrogenotherapy and Transdermal Drug Delivery: Electrically Mediated Delivery of Molecules to Cells. Humana Press, Totowa, NJ.
- Kandušer, M., M. Fošnarčič, M. Šentjurc, V. Kralj-Iglič, H. Hägerstrand, A. Iglič, and D. Miklavčič. 2003. Effect of surfactant polyoxyethylene glycol (C12E8) on electroporation of cell line DC3F. *Colloids Surf. A.* 214:205–217.
- Kinoshita, K., and T. Y. Tsong. 1977a. Voltage-induced pore formation and hemolysis of human erythrocytes. *Biochim. Biophys. Acta.* 471:227–242.
- Kinoshita, K., and T. Y. Tsong. 1977b. Formation and resealing of pores of controlled sizes in human erythrocyte membrane. *Nature.* 268:438–441.
- Kinoshita, K., and T. Y. Tsong. 1979. Voltage-induced conductance in human erythrocyte. *Biochim. Biophys. Acta.* 554:479–497.
- Kotnik, T., A. Maček-Lebar, D. Miklavčič, and L. M. Mir. 2000. Evaluation of cell membrane electroporation by means of a non-permeant cytotoxic agent. *Biotechniques.* 28:921–926.
- Leontiadou, H., A. E. Mark, and S. J. Marrink. 2004. Molecular dynamics simulations of hydrophilic pores in lipid bilayers. *Biophys. J.* 86:2156–2164.
- Macek-Lebar, A., G. Sersa, S. Kranjc, A. Groselj, and D. Miklavcic. 2002b. Optimisation of pulse parameters in vitro for in vivo electrochemotherapy. *Anticancer Res.* 22:1731–1736.
- Macek-Lebar, A., G. C. Troiano, L. Tung, and D. Miklavčič. 2002a. Inter-pulse interval between rectangular voltage pulses affects electroporation threshold of artificial lipid bilayers. *IEEE Trans. Nanobiosc.* 1:116–120.
- Maxwell, J. C. 1873. Treatise on Electricity and Magnetism. Oxford University Press, London, UK.
- Mir, L. M. 2000. Therapeutic perspectives of in vivo cell electroporation. *Bioelectrochemistry.* 53:1–10.
- Mir, L. M., S. Orłowski, J. Belehradek, Jr., and C. Paoletti. 1991. Electrochemotherapy potentiation of antitumour effect of bleomycin by local electric pulses. *Eur. J. Cancer.* 27:68–72.
- Nebeker, F. 2002. Golden accomplishments in biomedical engineering, 50 years of the IEEE EMBS and the emergence of a new discipline. *IEEE Eng. Med. Biol. Mag.* 21:17–47.
- Neumann, E., and K. Rosenheck. 1972. Permeability changes induced by electric impulses in vesicular membranes. *J. Membr. Biol.* 10:279–290.
- Neumann, E., M. Schaefer-Ridder, Y. Wang, and P. H. Hofschneider. 1982. Gene transfer into mouse lymphoma cells by electroporation in high electric fields. *EMBO J.* 1:841–845.
- Neumann, E., A. E. Sowers, and C. A. Jordan. 1989. Electroporation and Electrofusion in Cell Biology. Plenum Press, New York, NY.
- Neumann, E., K. Toensing, S. Kakorin, P. Budde, and J. Frey. 1998. Mechanism of electroporative dye uptake by mouse B cells. *Biophys. J.* 74:98–108.
- Okino, M., and H. Mohri. 1987. Effects of a high-voltage electrical impulse and an anticancer drug on in vivo growing tumors. *Jpn. J. Cancer Res.* 78:1319–1321.
- Parsegian, A. 1969. Energy of an ion crossing a low dielectric membrane: solutions to four relevant electrostatic problems. *Nature.* 221:844–846.
- Pavlin, M., and D. Miklavčič. 2003. Effective conductivity of a suspension of permeabilized cells: a theoretical analysis. *Biophys. J.* 85:719–729.
- Pavlin, M., N. Pavšelj, and D. Miklavčič. 2002a. Dependence of induced transmembrane potential on cell density, arrangement and cell position inside a cell system. *IEEE Trans. Biomed. Eng.* 49:605–612.
- Pavlin, M., T. Slivnik, and D. Miklavčič. 2002b. Effective conductivity of cell suspensions. *IEEE Trans. Biomed. Eng.* 49:77–80.
- Pliquett, U., R. Elez, A. Piiper, and E. Neumann. 2004. Electroporation of subcutaneous mouse tumors by rectangular and trapezium high voltage pulses. *Bioelectrochemistry.* 62:83–93.
- Pliquett, U., E. A. Gift, and J. C. Weaver. 1996. Determination of the electric field and anomalous heating caused by exponential pulses with aluminum electrodes in electroporation experiments. *Bioelectrochem. Bioenerg.* 39:39–53.
- Puc, M., T. Kotnik, L. M. Mir, and D. Miklavčič. 2003. Quantitative model of small molecules uptake after in vitro cell electroporation. *Bioelectrochemistry.* 60:1–10.
- Pucihar, G., T. Kotnik, M. Kanduser, and D. Miklavčič. 2001. The influence of medium conductivity on electroporation and survival of cells in vitro. *Bioelectrochemistry.* 54:107–115.
- Rols, M. P., and J. Teissie. 1990. Electroporation of mammalian cells: quantitative analysis of the phenomenon. *Biophys. J.* 58:1089–1098.
- Rols, M. P., and J. Teissie. 1992. Experimental evidence for the involvement of the cytoskeleton in mammalian cell electroporation. *Biophys. J.* 1111:45–50.
- Ryttsen, F., C. Farre, C. Brennan, S. G. Weber, K. Nolkranz, K. Jardemark, D. T. Chiu, and O. Orwar. 2000. Characterization of single-cell electroporation by using patch-clamp and fluorescence microscopy. *Biophys. J.* 79:1993–2001.
- Schmeer, M., T. Seipp, U. Pliquett, S. Kakorin, and E. Neumann. 2004. Mechanism for the conductivity changes caused by membrane electroporation of CHO cell-pellets. *Phys. Chem. Chem. Phys.* 6:5564–5574.
- Schwister, K., and B. Deuticke. 1985. Formation and properties of aqueous leaks induced in human erythrocytes by electrical breakdown. *Biochim. Biophys. Acta.* 816:332–348.
- Serša, G., T. Čufer, M. Čemazar, M. Reberšek, and Z. Rudolf. 2000. Electrochemotherapy with bleomycin in the treatment of hypernephroma metastasis: case report and literature review. *Tumori.* 86:163–165.
- Smith, K. C., J. C. Neu, and W. Krassowska. 2004. Model of creation and evolution of stable electropores for DNA delivery. *Biophys. J.* 86:2813–2826.
- Sugar, I. P., and E. Neumann. 1984. Stochastic model for electric field-induced membrane pores electroporation. *Biophys. Chem.* 19:211–225.
- Sukharev, S. I., V. A. Klenchin, S. M. Serov, L. V. Chernomordik, and Y. A. Chizmadzhev. 1992. Electroporation and electrophoretic DNA transfer into cells. The effect of DNA interaction with electropores. *Biophys. J.* 63:1320–1327.
- Susil, R., D. Šemrov, and D. Miklavčič. 1998. Electric field-induced transmembrane potential depends on cell density and organization. *Electro. Magnetobiol.* 17:391–399.
- Teissie, J., and C. Ramos. 1998. Correlation between electric field pulse induced long-lived permeabilization and fusogenicity in cell membranes. *Biophys. J.* 74:1889–1898.
- Teissie, J., and M. P. Rols. 1994. Manipulation of cell cytoskeleton affects the lifetime of cell-membrane electroporation. *Ann. N. Y. Acad. Sci.* 720:98–110.
- Tönsing, K., S. Kakorin, E. Neumann, S. Liemann, and R. Huber. 1997. Annexin V and vesicle membrane electroporation. *Eur. Biophys. J.* 26:307–318.
- Tsong, T. Y. 1991. Electroporation of cell membranes. *Biophys. J.* 60:297–306.
- Weaver, J. C., and Y. A. Chizmadzhev. 1996. Theory of electroporation: a review. *Bioelectrochem. Bioenerg.* 41:135–160.
- Wong, T. K., and E. Neumann. 1982. Electric field mediated gene transfer. *Biochem. Biophys. Res. Commun.* 107:584–587.
- Zimmermann, U. 1982. Electric field-mediated fusion and related electrical phenomena. *Biochim. Biophys. Acta.* 694:227–277.